AD-A081 380 WESTINGHOUSE ELECTRIC CORP PITTSBURGH PA ADVANCED ENE--ETC F/G 20/13
COMPACT CLOSED CYCLE BRAYTON SYSTEM FEASIBILITY STUDY, VOLUME I--ETC(U)
AUG 79 R E THOMPSON, R L AMMON, R CALVO N00014-76-C-0706
UNCLASSIFIED WAES-TNR-237-VOL-2 NL

1 OF 6
AD A081380

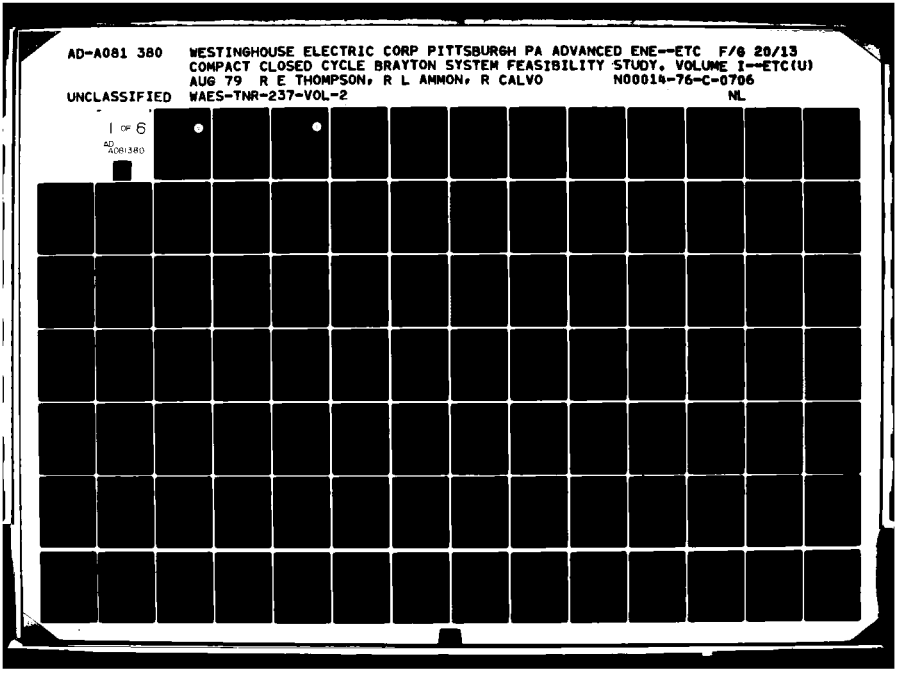

WAES-TNR-237
August,1979

Advanced Energy Systems Division

COMPACT CLOSED CYCLE BRAYTON SYSTEM FEASIBILITY STUDY

FINAL REPORT

Volume II

Research Sponsored by Office of Naval Research
Arlington, Virginia 22217

Under Contract N00014-76-C-0706

Westinghouse Electric Corporation
Advanced Energy Systems Division
P.O. Box 10864
Pittsburgh,Pennsylvania 15236

WAES-TNR-237
Aug[illegible]79

Advanced Energy Systems Division

COMPACT CLOSED CYCLE BRAYTON SYSTEM FEASIBILITY STUDY

~~FINAL REPORT~~

Volume II

Research Sponsored by Office of Naval Research
Arlington, Virginia 22217

Under Contract N00014-76-C-0706

Westinghouse Electric Corporation
Advanced Energy Systems Division
P.O. Box 10864
Pittsburgh, Pennsylvania 15236

"UNCLASSIFIED"

SECURITY CLASSIFICATION OF THIS PAGE (When Data Entered)

REPORT DOCUMENTATION PAGE		READ INSTRUCTIONS BEFORE COMPLETING FORM
1. REPORT NUMBER WAES-TNR-237	2. GOVT ACCESSION NO.	3. RECIPIENT'S CATALOG NUMBER
4. TITLE (and Subtitle)		5. TYPE OF REPORT & PERIOD COVERED FINAL 20 May 1976 to 20 June 1979
		6. PERFORMING ORG. REPORT NUMBER WAES-TNR-237
7. AUTHOR(s) R. E. Thompson, R. L. Ammon, R. Calvo L. R. Eisenstatt, F. R. Spurrier, B. L. Pierce G. O. Yatsko of Westinghouse and A. Pietsch and B. B. Heath of AiResearch		8. CONTRACT OR GRANT NUMBER(s) N00014-76-C-0706
9. PERFORMING ORGANIZATION NAME AND ADDRESS Westinghouse Electric Corporation Advanced Energy Systems Division P. O. Box 10864 Pittsburgh, Pennsylvania 15236		10. PROGRAM ELEMENT, PROJECT, TASK AREA & WORK UNIT NUMBERS
11. CONTROLLING OFFICE NAME AND ADDRESS Office of Naval Research 800 North Quincy Street Arlington, Virginia 22217		12. REPORT DATE August 1979
		13. NUMBER OF PAGES 675
14. MONITORING AGENCY NAME & ADDRESS(if different from Controlling Office)		15. SECURITY CLASS. (of this report) "UNCLASSIFIED"
		15a. DECLASSIFICATION/DOWNGRADING SCHEDULE

16. DISTRIBUTION STATEMENT (of this Report)

Approved for public release; distribution unlimited. Reproduction in whole or in part is permitted for any purpose of the United States government.

17. DISTRIBUTION STATEMENT (of the abstract entered in Block 20, if different from Report)

18. SUPPLEMENTARY NOTES

19. KEY WORDS (Continue on reverse side if necessary and identify by block number)

Gas turbine engines, marine surface propulsion, Brayton cycle, axial flow turbines, axial flow compressors, heat resistant alloys, high temperature materials tests, heat exchangers, bearings, gas bearings.

20. ABSTRACT (Continue on reverse side if necessary and identify by block number)

This report presents the final results from a three year study which evaluated the feasibility of a closed Brayton cycle power conversion system for compact light weight naval propulsion plants. The results from the first year of this Compact Closed Cycle Brayton System (CCCBS) study were documented in detail in Report Number WAES-TNR-233 of July 1977.

This final report includes the detailed results from Years 2 and 3 of this study. It also includes sufficient Year 1 results to provide an understanding

DD FORM 1 JAN 73 1473 EDITION OF 1 NOV 65 IS OBSOLETE

"UNCLASSIFIED"

SECURITY CLASSIFICATION OF THIS PAGE (When Data Entered)

of the total results, but does not include restatements of all of the detailed results derived during Year 1. This approach has been followed in order to fully document the study results while maintaining the report at a size reasonable for the users.

The overall objective of the program was to conduct the analytical study and experimental research required to evaluate and to demonstrate feasibility of a closed Brayton cycle power conversion system for a low volume, light weight marine propulsion plant. Another objective was to insure relevance of power conversion system study results to all candidate applications, including recognition of the various energy sources which the Navy could desire to use in the future.

The scope of the power conversion system for this study excluded specific energy sources, specific loads, and specific heat rejection subsystems. However, consideration was given in the study to the reasonable ranges of conditions for each of these interfaces to insure that the study results meet or exceed the conditions which may be required.

The contracted tasks have been completed as planned and the objective of the study has been fulfilled. As a result of the analytical study and experimental research of this program, the feasibility of a closed Brayton cycle power conversion system for a low volume, light weight naval propulsion powerplant has been shown.

The Compact Closed Cycle Brayton System (CCCBS) program has included derivation of the most stringent representative requirements for the CCCBS power conversion system, consideration of the interfaces with the ship and with other powerplant components which were outside the scope of the system under study, investigation and evaluation of the components which are most critical to feasibility, iterative definition of a reference 52.2 M Pa (17,000 HP) CCCBS design concept; extensive creep-rupture tests of candidate turbine materials in helium and in air at 927°C (1700°F), and overall evaluations and assessments. The results have shown the feasibility and attractive characteristics of a CCCBS and have indicated that no high risk developments or technology breakthroughs are needed for the CCCBS power conversion system.

The results of this program provide a valuable baseline of data for use by the Navy in defining the advanced powerplants which will enhance the capabilities of many types of naval vessels. However, this CCCBS research program has been only one step in the process of actually providing the improved powerplant capabilities that will be needed. This program should be supplemented by vehicle installation and application design work, energy source evaluations and characterizations, additional materials tests, and overall powerplant evaluations and characterizations as next steps towards acquisition of the achievable powerplant gains.

CONTENTS

CONTENTS (CONTINUED)

CONTENTS (CONTINUED)

CONTENTS (CONTINUED)

CONTENTS (CONTINUED)

CONTENTS (CONTINUED)

FIGURES

FIGURES (CONTINUED)

FIGURES (CONTINUED)

FIGURES (CONTINUED)

FIGURES (CONTINUED)

FIGURES (CONTINUED)

FIGURES (CONTINUED)

FIGURES (CONTINUED)

FIGURES (CONTINUED)

TABLES

TABLES (CONTINUED)

APPENDICES

6.0 SYSTEM ANALYSES

6.1 CYCLE ANALYSES

The performance of the CCCBS was evaluated both during steady-state operating and in response to a select number of transients. For all analyses the base system configuration was used, with the flow diagram as shown in Figure 6-1.

During the preliminary cycle analyses a plant control scheme was developed that would result in an acceptable tradeoff between component life and plant efficiency. At present a sliding heat source outlet temperature control is used, which results in the turbine inlet temperature changing linearly from 927°C (1700°F) to 900°C (1650°F) between a 100% to 25% throttle position. Also, inventory control is used in this throttle range. Below 25% throttle, the system is controlled solely by varying heat source outlet temperature.

In the system analyses, the BAM computer model (Reference 1) was used. While the turbomachinery, heat exchangers, and nuclear heat source modeling in the BAM model were not changed, the control system was changed to be applicable to the particular case being investigated.

6.1.1 STEADY-STATE ANALYSES

The steady-state operation of the CCCBS was investigated at both full and part-power to determine the state points. In order to allow the results to be valid for a wide range of possible uses of the CCCBS, both variable and constant speed power turbine operating philosophies were considered. In addition, the full-power plant performance as a function of heat source outlet temperature and heat exchanger effectiveness was investigated, as well as the full and part power performance as a function of the sea water temperature.

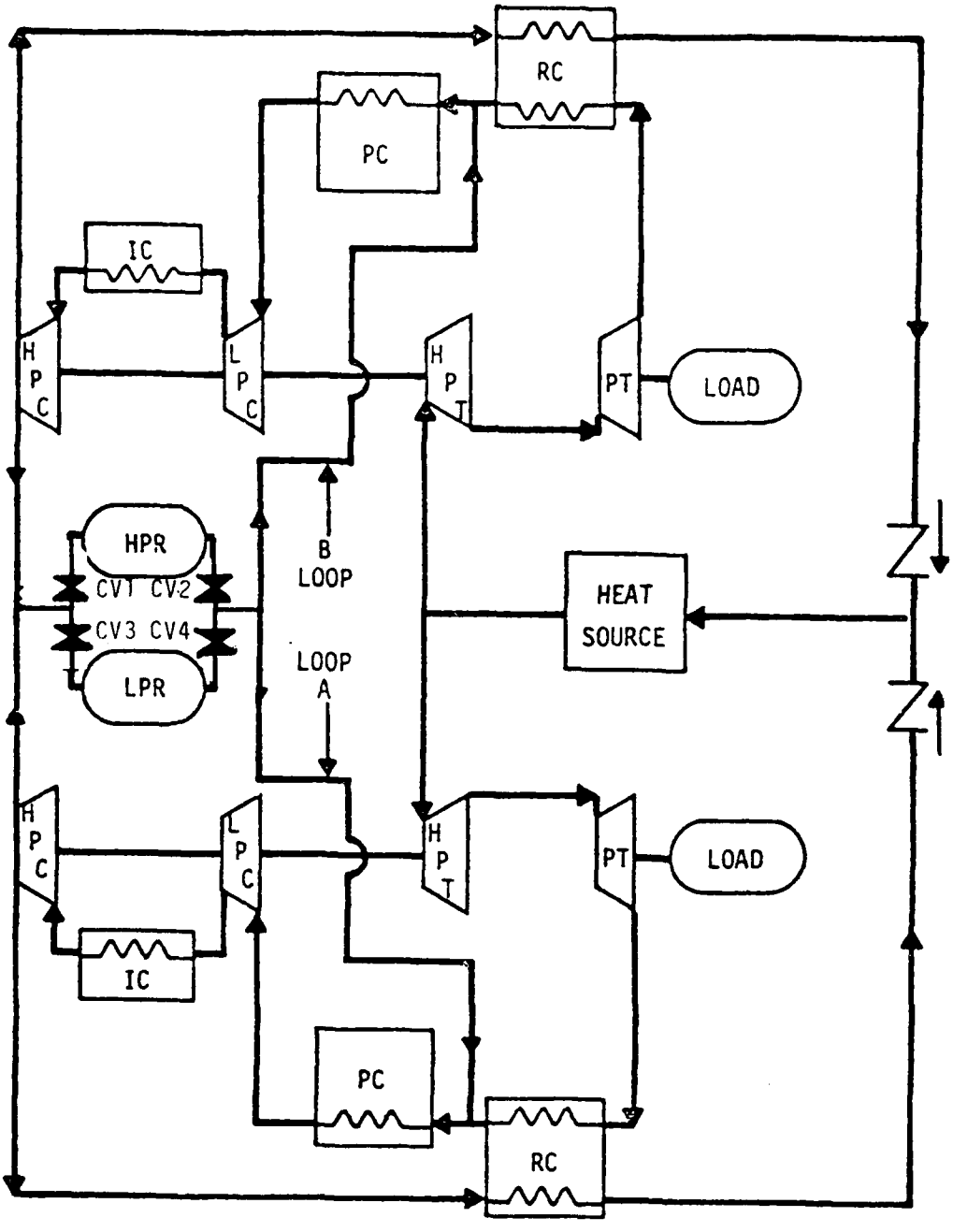

CV	Control Valve	SV	On-Off Valve
PT	Power Turbine	RC	Recuperator
HPT	High Pressure Turbine	PC	Precooler
LPC	Low Pressure Compressor	IC	Intercooler
HPC	High Pressure Compressor	HPR	High Pressure Reservoir
		LPR	Low Pressure Reservoir

Figure 6-1. Helium Inventory Control Schematic

6.1.1.1 REFERENCE SYSTEM STATEPOINTS

Tables 6-1 and 6-2 show the system state points for constant and variable speed turbine operation, respectively. The plant efficiency and the system temperatures and pressure, are shown in Figures 6-2 and 6-8.

The plant efficiency versus power can be seen in Figure 6 2. For constant speed turbine operation, there is actually an increase in the plant efficiency at part-power, due to the turbine efficiency staying approximately constant and the heat exchanger effectiveness increasing with the reduced load. This is an attempt of using inventory control rather than a bypass control or heat source outlet temperature control.

The station temperatures are shown in Figures 6-3 and 6-4 for constant speed turbine operation, and in Figures 6-5 and 6-6 for variable speed turbine operation. Again the advantages of using helium inventory control above 25% power can be seen, as the maximum change in station temperatures was 31°C (55°F), and occurred at the inlet to the high pressure turbine. Also, this change was not due to any component performance characteristics, but rather to the sliding temperature controller used between 100% and 25% power.

A parametric analysis was performed on the CCCBS to determine the impact of certain parameters on the plant performance. These were limited to variations in the sea water temperature, heat source outlet temperature, and the heat transfer effectivenesses of the precooler, intercoolers, and recuperators. For these analyses, the turbomachinery parameters (compressor map, turbine efficiency and flowrate characteristics) were held constant. Even though the plant was not optimized for every new value of each parameter, the general performance trends are still valid.

6.1.1.2 IMPACT OF SEA WATER TEMPERATURE

The influence of sea water temperature can be seen in Figures 6-2, 6-7 and 6-8, and also by comparing Figures 6-3 and 6-4 for constant speed turbine operation and Figures 6-5 and 6-6 for variable speed turbine operation. The major effect is a large improvement in plant efficiencies with the lower sea temperatures (Figure 6-2). The overall system pressure level also dropped with the lower sea

TABLE 6-1

CCCBS STATE POINTS CONSTANT SPEED TURBINE, 85°F SEA TEMPERATURE

Output Power (%)

COMPONENT		100	80	60	40	25	15	10
	P_{in}, KPa	1130	2572	1917	1317	848	945	945
	T_{in}, °C	38.1	35.1	33.7	32.0	30.9	30.5	30.3
L P Compressor	M, kg/sec	58.1	47.4	35.9	24.4	15.7	14.1	11.5
	P_{out}, KPa	6110	5019	3792	2579	1655	1689	1572
	T_{out}, °C	151.4	147.6	144.8	142.6	140.9	125.3	114.2
	M, kg/sec	58.1	47.4	35.9	24.4	15.7	14.1	11.5
Intercooler	P_{out}, KPa	6088	4970	3765	2558	1641	1675	1565
	T_{out}, °C	38.1	35.1	33.7	32.6	31.4	30.7	30.5
	M, kg/sec	57.0	46.4	35.2	23.9	15.4	11.8	11.1
H P Compressor	P_{out}, KPa	11,204	9108	6883	868	299.	2648	2186
	T_{out}, °C	138.7	135.1	132.6	130.1	128.1	104.2	85.9
	P_{in}, KPa	11,163	9074	6860	4654	2985	2641	2179
	T_{in}, °C	138.7	135.1	132.6	130.1	128.7	104.2	85.9
Recuperator	M, kg/sec	54.7	44.5	33.7	23.0	14.7	13.2	10.7
	P_{out}, KPa	11,121	9039	6832	4631	2972	2622	2122
	T_{out}, °C	484	469	448	469	489	433	454
	P_{in}, KPa	11,211	9111	6964	4737	2944	2599	2151
	T_{in}, °C	669	668	668	668	668	631	612
	P_{out}, KPa	10,825	8811	6605	4484	2785	2461	2041
	T_{out}, °C	944	936	929	921	916	805	760
	P_{in}, KPa	10,342	8412	6357	4309	2765	2441	2027
	T_{in}, °C	927	920	913	906	901	790	745
H P Turbine	M, kg/sec	56.4	45.9	34.8	23.7	15.2	13.6	11.0
	P_{out}, KPa	5874	4785	3620	2455	1579	1489	1374
	T_{out}, °C	708	704	698	692	688	619	604
	M, kg/sec	56.1	45.9	34.8	23.7	15.2	13.6	11.0
L P Turbine	P_{out}, KPa	5296	4303	3260	1386	889	972	965
	T_{out}, °C	528	511	508	503	500	484	507
	P_{in}, KPa	5354	4347	3311	1385	836	965	958
	T_{in}, °C	511	506	502	499	498	482	506
Recuperator	M, kg/sec	58.1	47.4	35.9	24.4	15.7	14.1	11.5
	P_{out}, KPa	5185	2611	1972	1344	862	951	951
	T_{out}, °C	216	210	205	201	196	171	160
	M, kg/sec	58.1	47.4	35.9	24.4	15.7	14.1	11.5
Precooler	P_{out}, KPa	1137	2572	1917	1317	848	947	945
	T_{out}, °C	38.1	35.1	33.7	32.0	30.9	30.5	30.3

TABLE 6-2

CCCBS STATE POINTS — VARIABLE SPEED TURBINE, 85°F SEA TEMPERATURE

COMPONENT		Output Power (%) 100	80	60	40	25	15	7.5
L. P. Compressor	P_{in}, KPa	3130	2599	2027	1448	1013	1103	1172
	T_{in}, °C	38.1	35.9	33.7	32.0	31.4	30.9	30.7
	W, Kg/sec	58.1	47.9	37.3	26.8	18.6	16.4	13.2
	P_{out}, KPa	6136	5081	3944	2827	1972	1972	1896
	T_{out}, °C	151.4	147.6	144.8	142.6	140.9	125.3	111.4
Intercooler	W, Kg/sec	58.1	47.9	37.3	26.8	18.6	16.4	13.2
	P_{out}, KPa	6088	5040	3916	2806	1958	1965	1889
	T_{out}, °C	38.1	35.3	33.7	32.6	31.4	30.7	30.5
H. P. Compressor	W, Kg/sec	57.0	47.0	36.5	26.2	18.2	16.0	13.0
	P_{out}, KPa	11,204	9218	7156	5116	3564	3082	2572
	T_{out}, °C	138.7	135.3	132.6	130.3	128.7	103.7	81.4
Recuperator	P_{in}, KPa	11,163	9183	7129	5106	3551	3075	2565
	T_{in}, °C	138.7	135.3	132.6	130.3	128.7	103.7	81.4
	W, Kg/sec	54.6	45.0	35.0	25.1	17.5	15.4	12.4
	P_{out}, KPa	11,121	9149	7101	5081	3537	3061	2558
	T_{out}, °C	453	450	451	459	471	447	461
Heat Source	P_{in}, KPa	11,011	9059	7032	5033	3502	3027	2530
	T_{in}, °C	499	488	450	458	470	446	461
	W, Kg/sec	55.2	45.5	35.5	25.4	17.7	15.5	12.5
	P_{out}, KPa	10,425	8576	6653	4757	3309	2868	2399
	T_{out}, °C	944	936	929	921	916	805	755
H. P. Turbine	P_{in}, KPA	10,342	8508	6605	4723	3282	2847	2385
	T_{in}, °C	927	920	913	905	900	790	740
	W, Kg/sec	56.4	46.5	36.2	25.9	18.0	15.9	12.8
	P_{out}, KPa	5874	4847	3764	2696	1875	1737	1586
	T_{out}, °C	708	704	698	693	689	620	605
L. P. Turbine	W, Kg/sec	56.4	46.5	36.2	25.9	18.0	15.9	12.8
	P_{out}, KPa	3296	2737	2123	1524	1069	1144	1193
	T_{out}, °C	526	515	514	519	528	501	519
Recuperator	T_{in}, °C	511	503	505	511	521	497	516
	W, Kg/sec	58.1	47.9	37.3	26.8	18.6	16.4	13.3
	P_{out}, KPa	3185	2647	2054	1475	1034	1117	1179
	T_{out}, °C	216	213	211	206	203	177	161
Precooler	W, Kg/sec	58.1	47.9	37.3	26.8	18.6	16.4	13.3
	P_{out}, KPa	3137	2606	2027	1448	1013	1103	1172
	T_{out}, °C	38.1	35.9	33.7	32.0	31.4	30.9	30.6

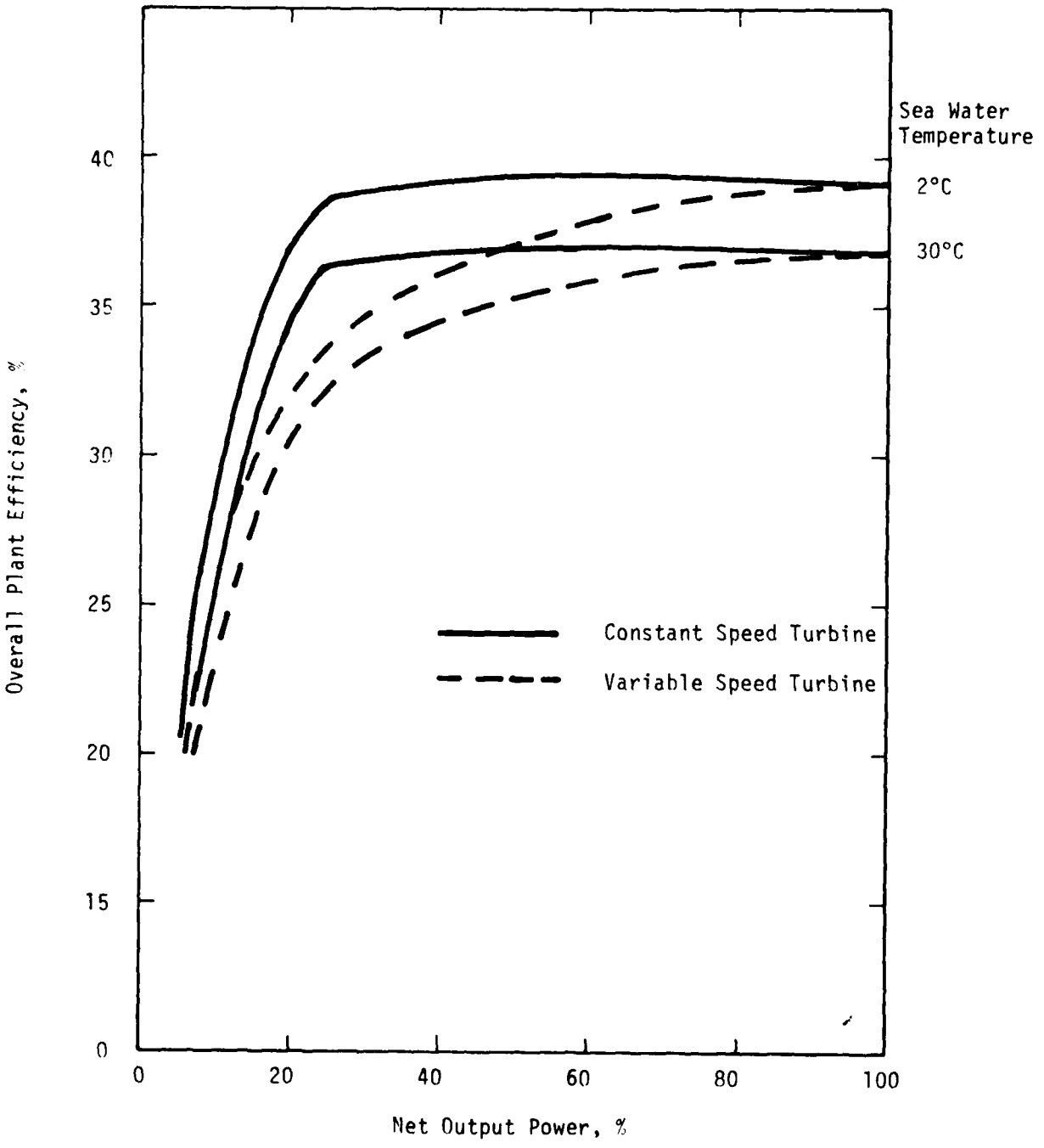

Figure 6-2. Plant Efficiency vs. Output Power

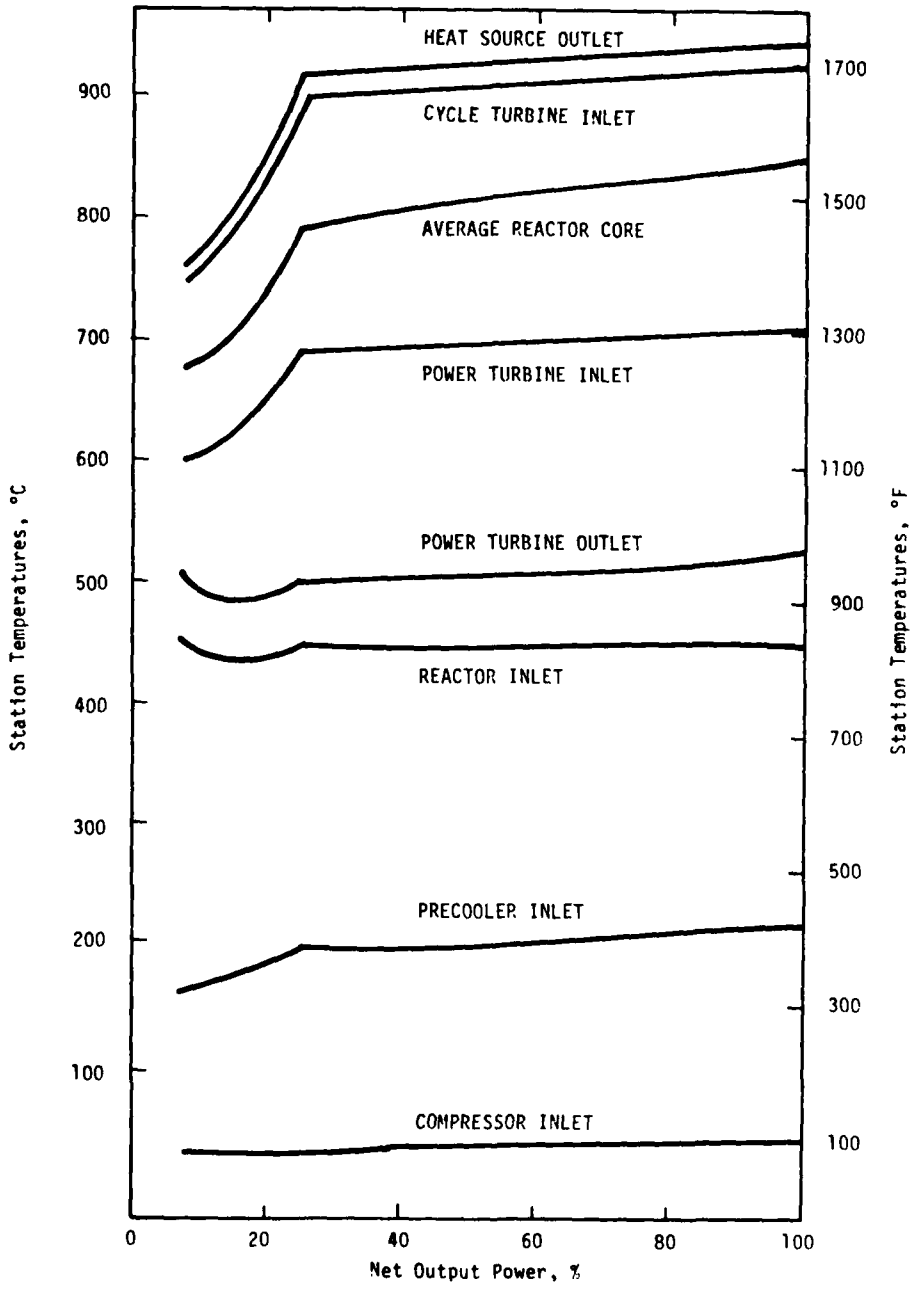

Figure 6-3. Station Temperature vs. Output Power — Constant Speed Turbine, 30°C Sea Temperature

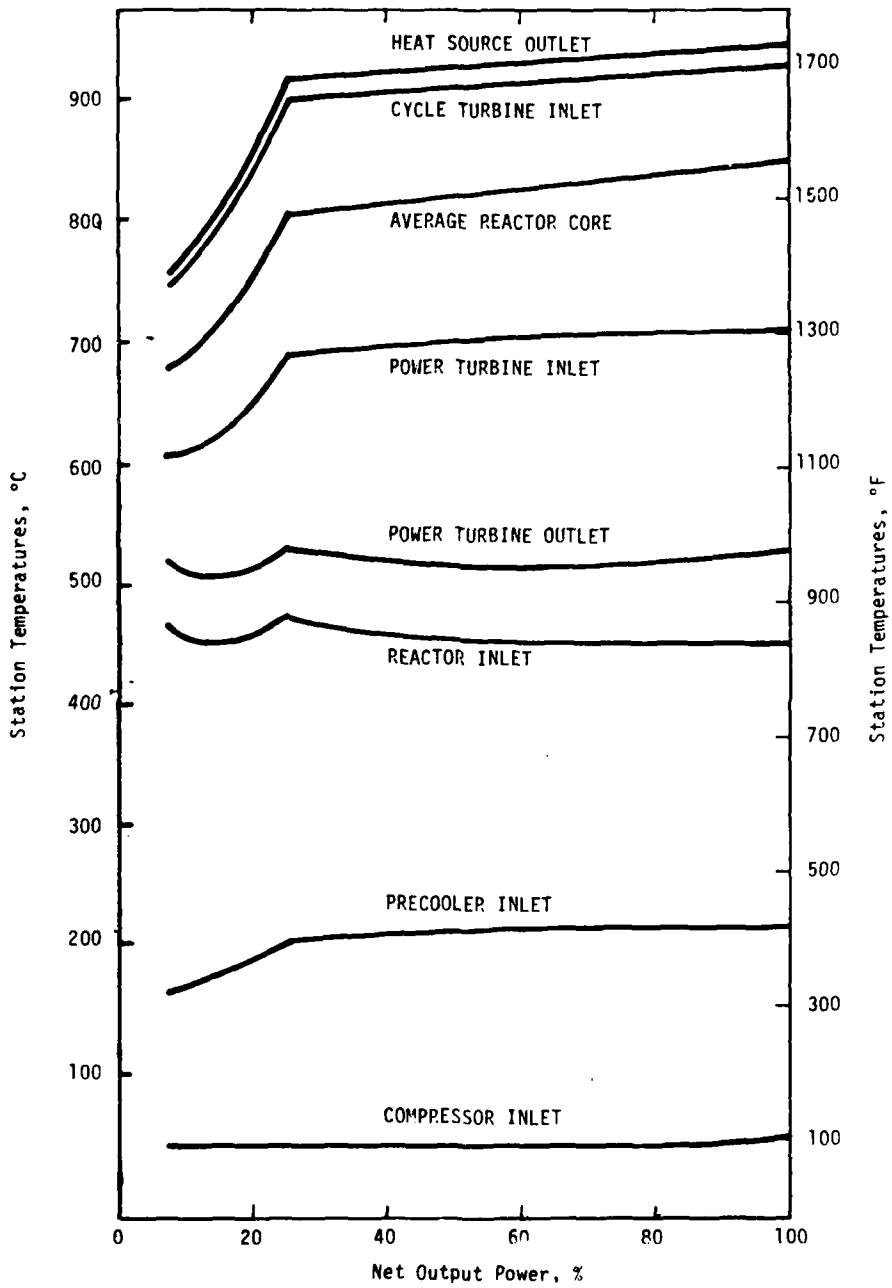

Figure 6-4. Station Temperature vs. Output Power — Variable Speed Turbine, 30°C Sea Temperature

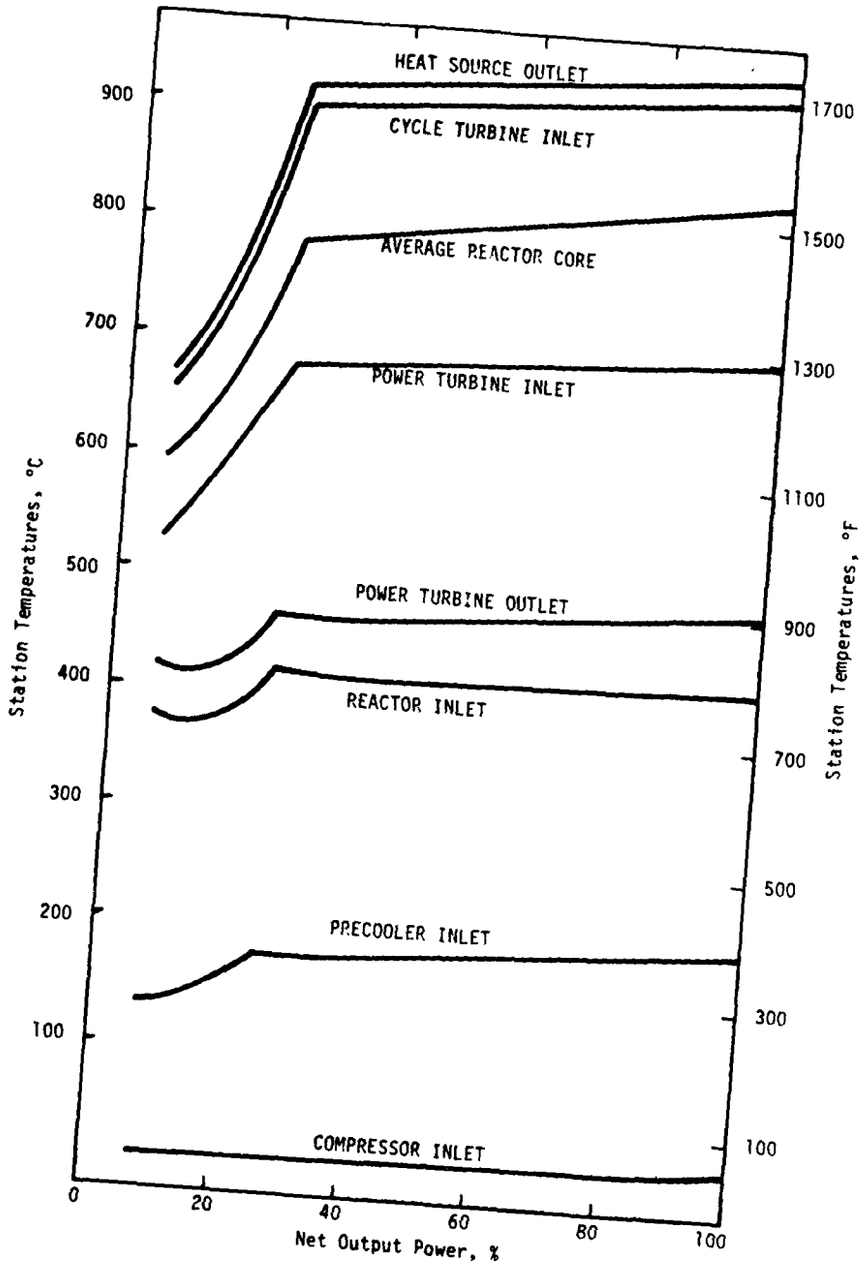

Figure 6-5. Station Temperature vs. Output Power — Constant Speed Turbine, 2°C Sea Temperature

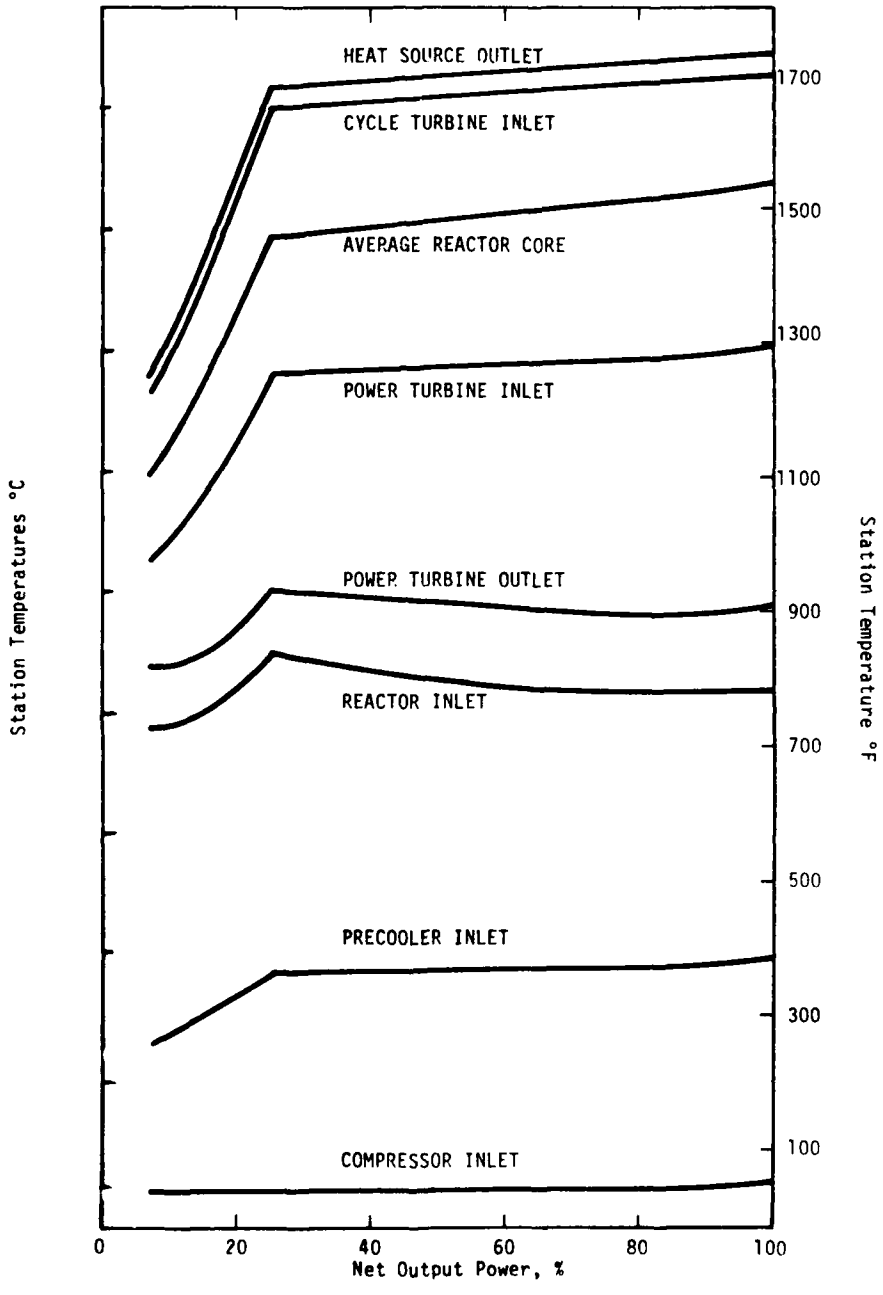

Figure 6-6. Station Temperature vs. Output Power – Variable Speed Power Turbine, 2°C Sea Temperature

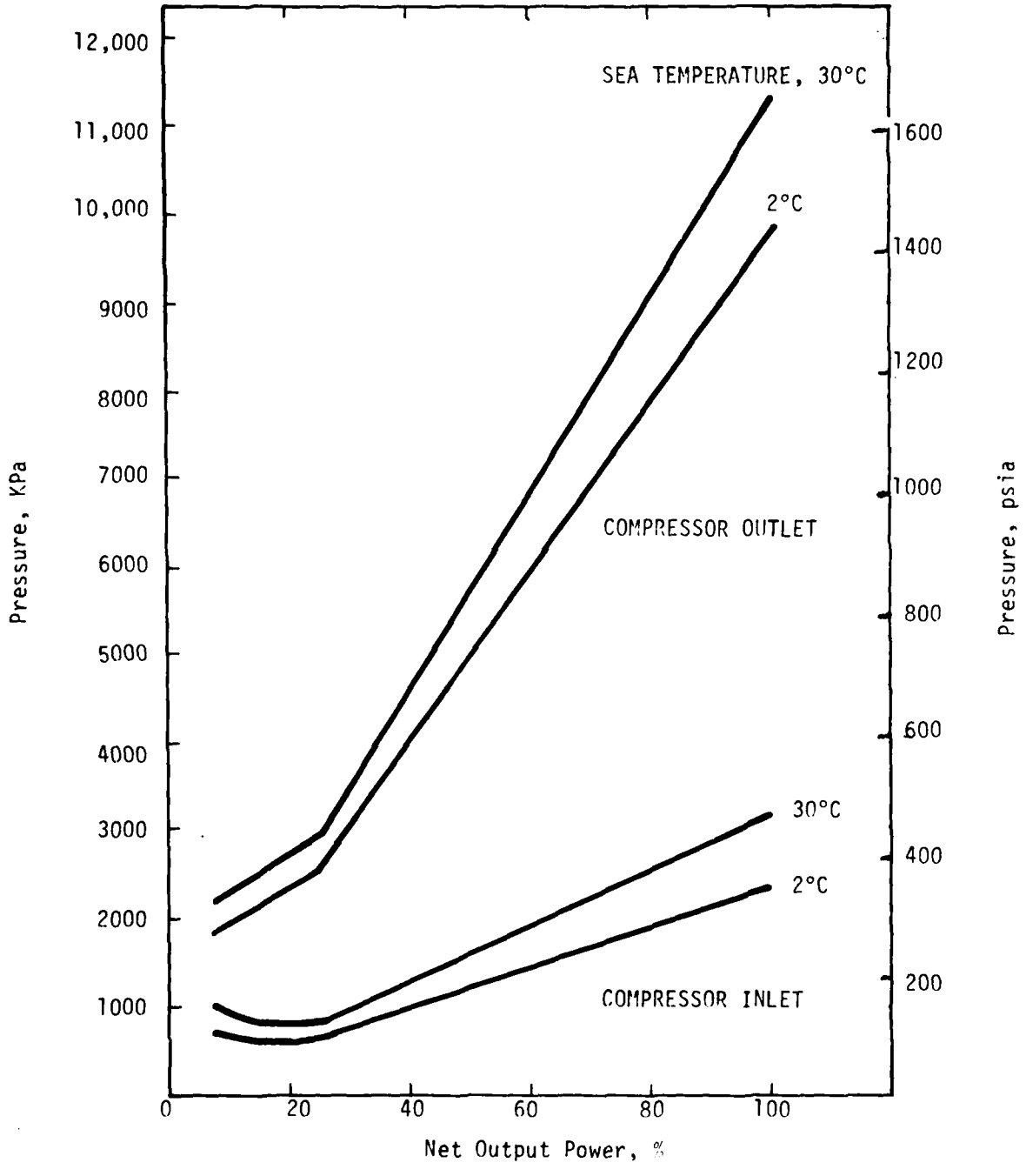

Figure 6-7. Compressor Inlet and Outlet Pressures vs. Output Power, Constant Speed Turbine

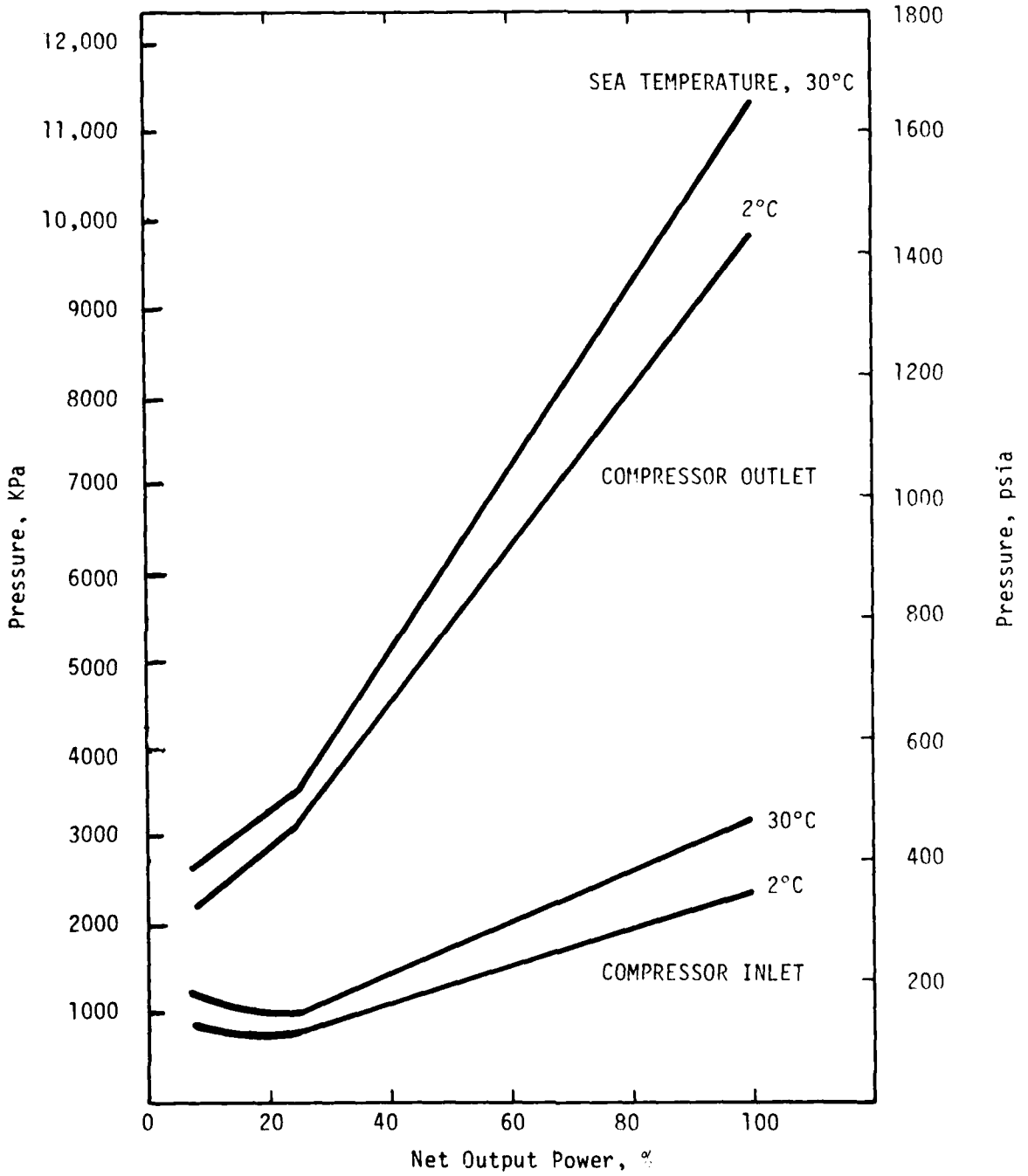

Figure 6-8. Compressor Inlet and Outlet Pressures vs. Output Power, Variable Speed Turbine

water temperature, due primarily to a reduction in the helium temperature (and hence the density and pressure) at the compressor inlet (Figure 6-7 and 6-8).

6.1.1.3 IMPACT OF HEAT SOURCE OUTLET TEMPERATURE

The influence of heat source outlet temperature can be seen in Figure 6-9 through 6-11, where the full-power plant efficiency, and the system temperatures and pressures are shown as a function of the heat source temperature.

The major benefit to be realized by increasing the heat source outlet temperature can be seen in Figures 6-9 and 6-11. The efficiency improvement to be felt with increasing heat source outlet temperatures varied from about 1.5%/20°C to about 0.3%/20°C (Figure 6-9), with the larger rates of improvement to be felt at the lower outlet temperatures. Also, the station temperatures tend to increase with the increased heat source outlet temperature (Figure 6-10). Downstream of the power turbine, however, there was at most a 22°C (40°F) rise for a heat source temperature rise of 105°C (350°F). The system pressures (Figure 6-11) tended to drop with the increase heat source outlet temperatures, with the greatest effect being felt at the lower outlet temperatures.

All of these results show the benefit of using the highest possible heat source outlet temperature. The increased efficiency allows for a smaller heat source heat exchanger (or, if nuclear powered, a smaller reactor), although changes of only a few percent would not have a very great effect on weight or volume. Greater benefit can be obtained in the turbomachinery, however, due to the reduced pressure levels. In addition, the turbine pressure ratio is increased, which results in reduced system flow rates. In general, an increase in the heat source outlet temperature of 28°C (50°F) results in a decrease in the system flow rates of from 5 to 7 percent.

6.1.1.4 IMPACT OF HEAT EXCHANGER EFFECTIVENESS

The precoolers and intercoolers used in the CCCBS are both finned-tube cross counterflow heat exchangers with high effectivenesses (defined as the ratio of the helium temperature drop to the difference in the helium and water inlet temperatures). The effectivenesses at full power are about 98 percent for both the

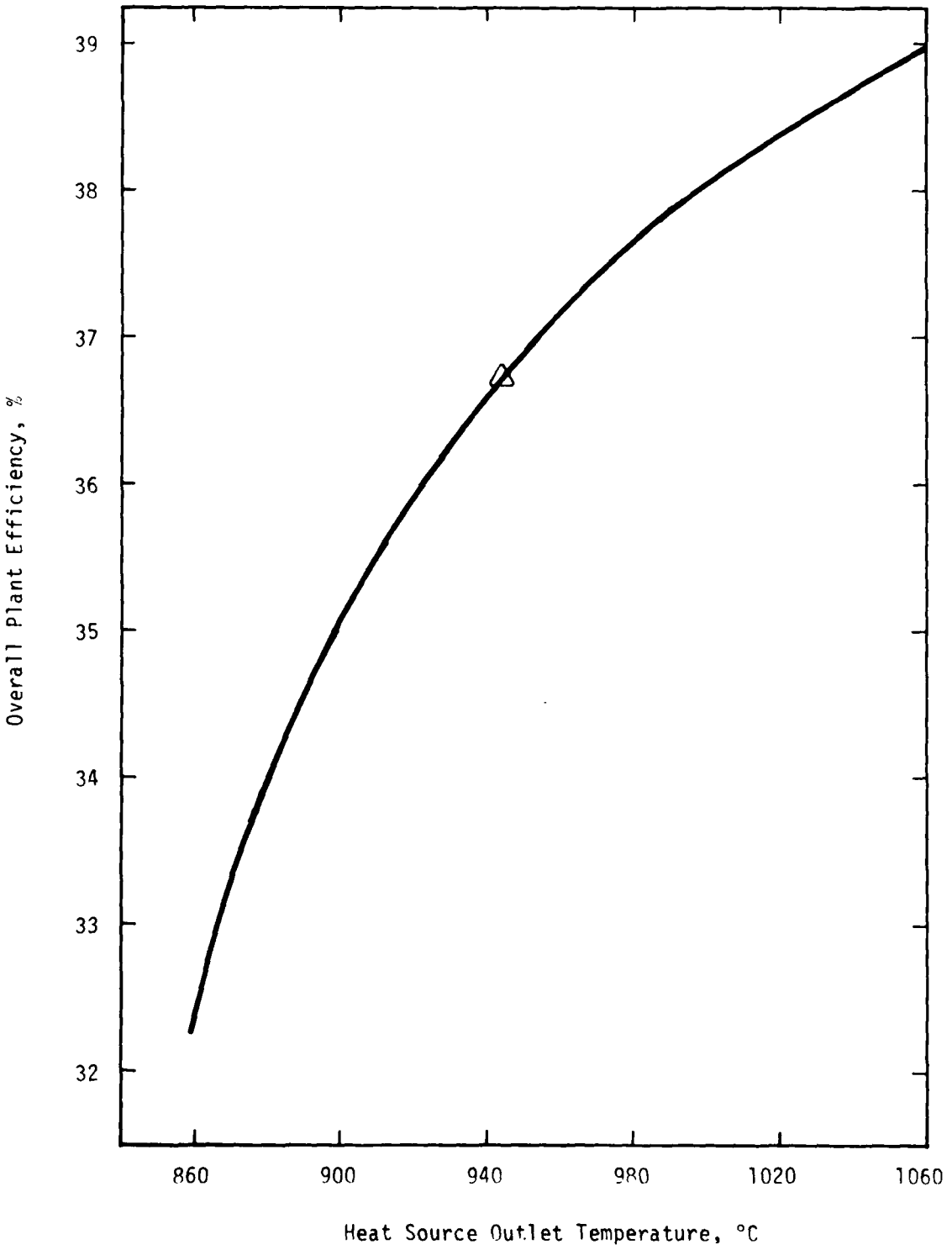

Figure 6-9. Plant Efficiency vs. Heat Source Outlet Temperature

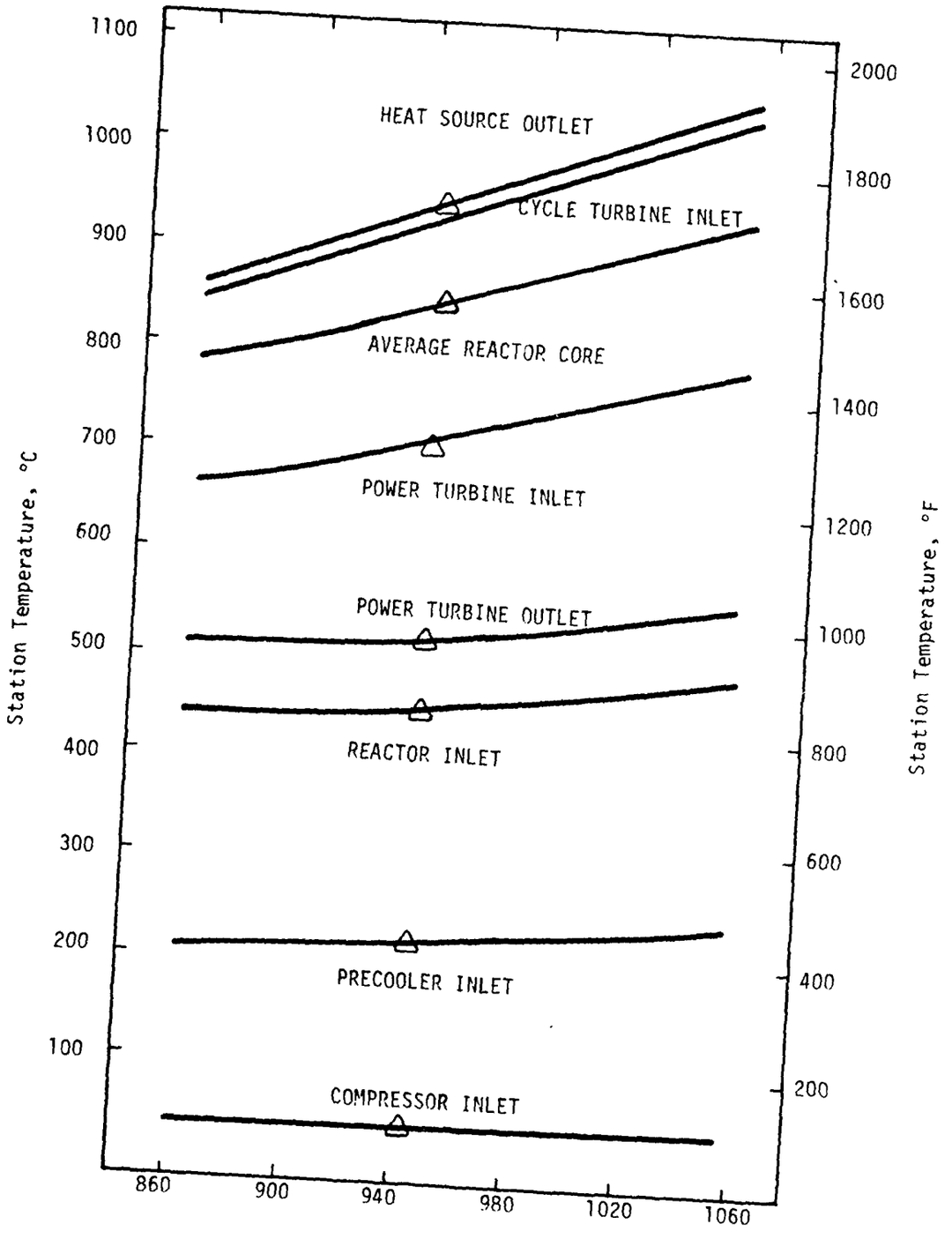

Figure 6-10. Station Temperature vs. Heat Source Outlet Temperature

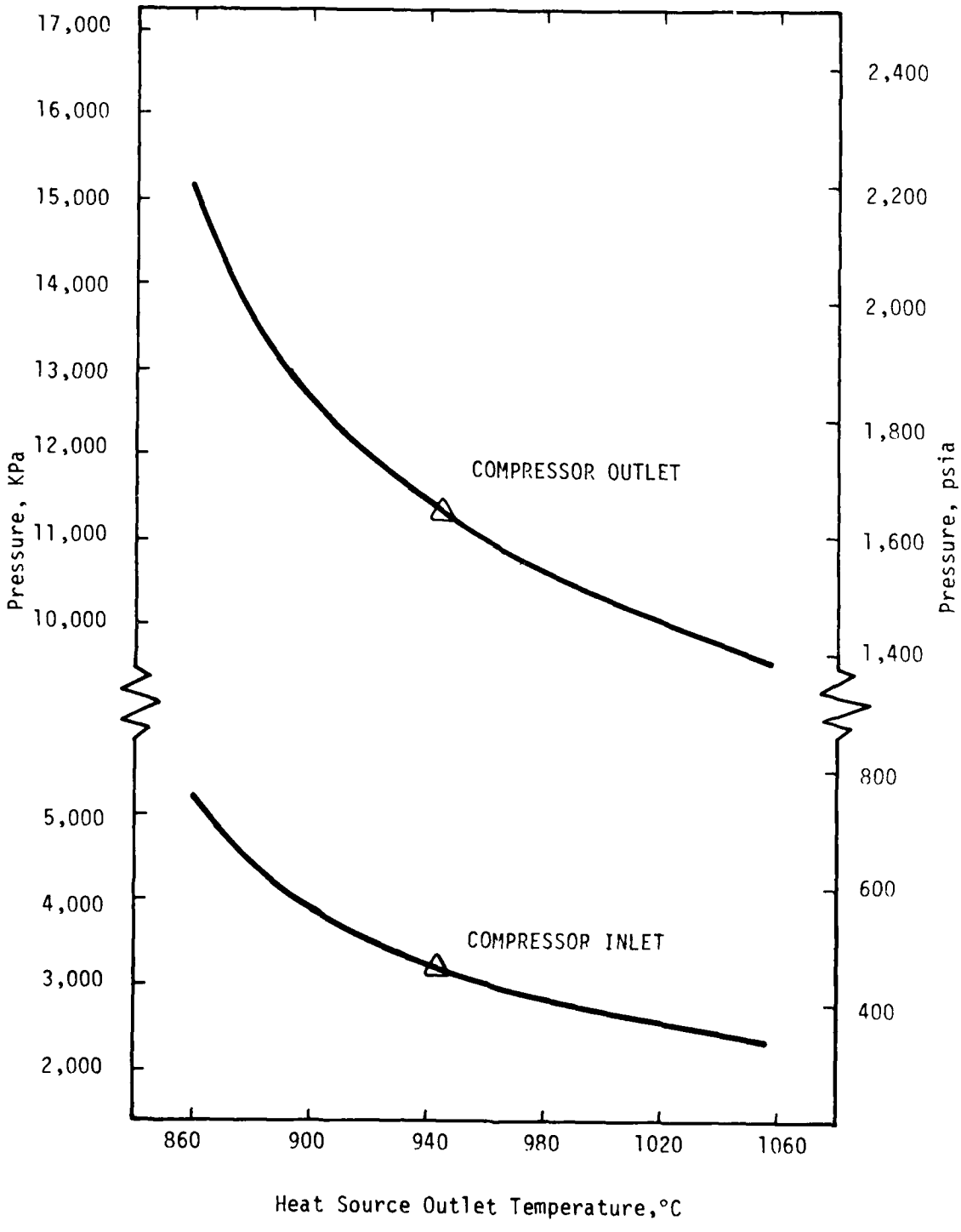

Figure 6-11. System Pressures vs. Heat Source Outlet Temperature

precoolers and the intercoolers, mainly due to the mass capacity rate ratio $\left[\frac{(w \cdot Cp)_{He}}{(w \cdot Cp)_{water}}\right]$ being less than 0.28, and the number of transfer units (NTU) being about 5. These high effectivenesses result in the helium being cooled to within 3°C (5°F) of the water inlet temperature.

Due to the high NTU values and low mass capacity rate ratios for the precoolers and intercoolers, there is little variation in their performance with large variations in the heat exchanger area. A reduction of 40% in the heat transfer area in either component reduces the effectiveness of that component from 98% to 95%. This translates to about a 10°C (17°F) rise felt in the helium outlet temperature, for the same flowrates and inlet conditions. In a CCCBS application, the reduced heat transfer area if felt as only about a 0.3% drop in the overall place efficiency, with a rise in the system flowrates (and in the total system helium inventory) of about 2% at full power.

The recuperator design is essentially a tube-shell heat exchanger, used to increase the overall plant efficiency. In constrast to the precoolers and intercoolers, heat transfer is helium to helium, which necessitates a larger heat exchanger than the helium to water heat exchanger designs described previously. The full-power effectivenss is approximately 82%, resulting in the compressor exit helium being heated to within 70°C (125°F) of the temperature at the exit of the low pressure turbine.

Due to the reduced effectiveness, and the capacity rates ($w \cdot C_p$) being approximately equal on the hot and cold sides of the recuperator, changes in the recuperator heat transfer area have a larger effect than similar magnitude of changes in the precoolers or intercoolers. A reduction of 40% in the heat transfer area causes the effectiveness to decrease from 82% to 77% at full power. This then impacts the whole cycle performance, most notably by reducing the overall plant efficiency from 36.73% to 35.35%. Also, the low pressure recuperator exit helium temperatures rises by about 20°C (35°F), while the high pressure exit temperature drops by an equal amount. Unlike the precooler and intercooler cases, however, there is no increase in the helium inventory or the flowrates. This is due to the precooler still lowering the compressor inlet temperature to about 38°C

(100°F), while the heat source outlet temperature is controlled to 944°C (1730°F). This results in no change being felt by the turbomachinery, and hence no change in the system flowrates. The efficiency reduction is simply due to the increased reactor temperature rise needed because of the reduced recuperator effectivenesses.

This data can also be used to analyze the effects of heat exchanger fouling or scale buildup. In the precoolers and intercoolers, in order to result in a reduction in heat exchanger effectiveness from 98% to 95%, the overall heat transfer coefficient would have to drop by about 30%. This would necessitate a fouling heat transfer coefficient of the same magnitude as either the helium or waterside heat transfer coefficient. If this total fouling resistance was assumed to occur on the helium side, the fouling resistance would be an order of magnitude greater than that expected. Due to the inertness and high purity of the cycle helium very little fouling or scaling is expected on the helium side.

If this total fouling resistance was assumed to occur on the water side, it would result in a fouling heat transfer coefficient of almost double what would be expected for an industrial heat exchanger using treated boiling feed water (Ref. 2). The CCCBS, however, uses treated distilled water of a high purity, coupled with the use of stainless steel tubes in the heat exchangers. As a result, tube fouling is not seen to be a problem. Even with fouling occurring of the magnitude as discussed above, it would result in only about 20°C increase in either precooler or intercooler helium outlet temperature, and only about a 0.3% drop in the overall plant efficiency.

The recuperator performance should degrade even less due to fouling. Since it is located downstream of the turbines in a relatively low temperature region of the cycle (600°C maximum temperature), very little fouling is expected. Due to its location, and the purity level and chemical inertness of the cycle helium, deposition and fouling during normal operation should be of a very small magnitude.

6.1.2 TRANSIENTS

Besides steady state operations, the CCCBS must be operated and controlled safely during a number of expected transients. Most common are simple throttle rampups and rampdowns. In addition, it is desirable for the system to be able to with-

stand certain malfunction accidents without severe damage occurring to the equipment. As a result a number of expected and malfunction transients were analyzed to determine their impact on the system design.

Before discussing the results of the analysis, a description of the CCCBS system flow path is in order. Figure 6-1 is a flow schematic of the reference CCCBS system. Helium picks up energy as it passes through the heat source (a high temperature gas cooled reactor for the cases analyzed), is expanded in the high pressure and power turbines, and gives up heat in the recuperator and precooler. It is then recompressed in the low and high pressure compressors, and passes through the recuperator and then back to the heat source. Ultimate heat rejection is from the precoolers and intercoolers, to an intermediate water loop, then via a water-to-water heat exchanger to the sea. A 30°C (85°F) sea temperature was used in the analyses.

Initially a constant 944°C (1730°F) reactor outlet temperature was chosen as the desired setpoint during inventory control. It was judged, however, that at 25% power the cycle turbine could not meet the operational requirement of 10,000 effective full power hours (40,000 hours of operation at 25% power). Reducing the turbine inlet temperature at part power allowed the operating life of the turbine to be extended to meet the desired operating life.

The 25% power switchover point (inventory control to pure temperature control) was selected to minimize the practical size of the two inventory bottles. Switching over at 25% power allows for a bottle size of approximately 85 m^3 (3000 ft^3). This is approximately twice as big as each turbine-compressor-heat exchanger package. Using helium inventory down to 10% power would require the bottles to be an order of magnitude larger, due to the low helium pressures and densities available at these low power levels.

The reference control scheme was defined as follows: between 100% and 25% net output power the system was controlled by varying both the reactor outlet temperature and the helium inventory. The reactor outlet temperature controller operates by sensing a temperature error (demand minus measured temperatures), and operating on the control drums through a proportional-integral controller:

$$\theta_{drum} = K_1 \left(T_e + K_2 \int T_e \, dt\right)$$

where T_e = demand - measured temperature

Between 25% and 100% power, the demanded temperature varies linearly with throttle position:

$$T_d \ (°C) = 906.6 + 37.0(F)$$

where F = throttle position (.25 to 1.0)

Below 25% power, the system uses solely reactor outlet temperature as a means of control. When operating in this region, a reactor outlet temperature setpoint was generated as a function of the demanded output power by using a correlation obtained from the steady-state analysis discussed in Section 6.1.1. This correlation can be seen in Figure 6.4, where the reactor outlet temperature is shown as a function of outpower power.

This modeled helium inventory controller used a power turbine speed error signal (N_e), operating through a proportional-integral-derivative controller to generate a demand flowrate:

$$W = K_1 \left(N_e + K_2 \int N_e \, dt + K_3 \dot{N}_e\right)$$

To simulate the valve dynamics, a 1/3 sec. lag was used on the demand flowrate.

The cases analyzed assumed a variable speed power turbine (i.e., direct mechanical drive to the load). Assuming that output power varies as speed cubed, the demand speed can be related to the throttle position (or power demand):

$$N_d = N_1 + N_2 \ (F)^{1/3}$$

where N_1 is the no-load idle speed. Differentiating with respect to time:

$$\dot{N}_d = 1/3 \ N_2 \ (F)^{-2/3} \cdot (\dot{F})$$

where $\dot{F}$ is the demanded throttle rate of change.

It was felt that the controllers described above would be sufficient to obtain the plant response to certain induced transients. In general, they were able to control the plant in an acceptable manner, and allowed the plant transient performance characteristics to be recognized. From these analyses and the proposed application of the CCCBS, the actual plant control scheme can be developed. Some improvements that could be made to improve the plant response and to be more representative of an actual control system are discussed in Section 8.4.3.

The following normal and malfunction cases were investigated:

(1) Rampdown from 100% power at 10% throttle change per second.

(2) Rampup from 10% power at 10% throttle change per second.

(3) Reactor scram at full power.

(4) Full loss of load at full power.

(5) Inventory valve between compressor discharge and high pressure reservoir (CV1) fails open at full power.

(6) Inventory valve between high pressure reservoir and precooler inlet (CV2) fails open at 25% power.

The scenario and results for each transient will be discussed separately.

6.1.2.1 THROTTLE RAMPDOWN FROM 100% OUTPUT POWER

The results for the throttle ramp case are shown in Figures 6-12 through 6-20. The demanded ramprate was a 10% per second rate of change between 100% and 25% throttle position, followed by a 3% per second rate of change after this time. The lower rate of change below 25% throttle position was used to avoid possibly running the reactor control drums fully in. Figures 6-12 and 6-13 show the various station temperatures during the transient. Inventory control was used up to about 7 seconds, when the low inventory valve differential pressure shut off the inventory flow. During this time the reactor exit temperature decreased steadily, but lagged behind the demand temperature. Due to this temperature

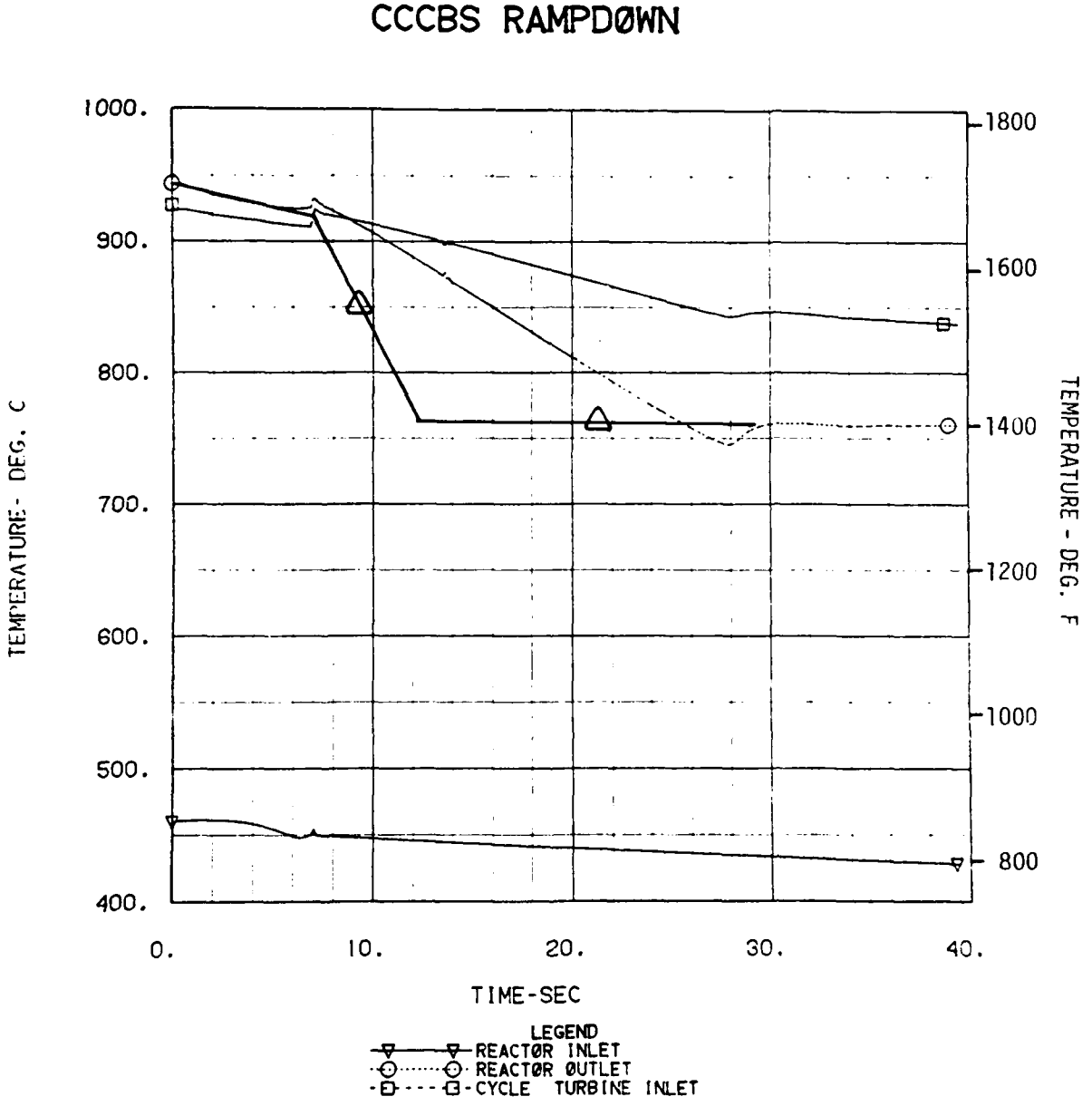

Figure 6-12. Heat Source Temperatures

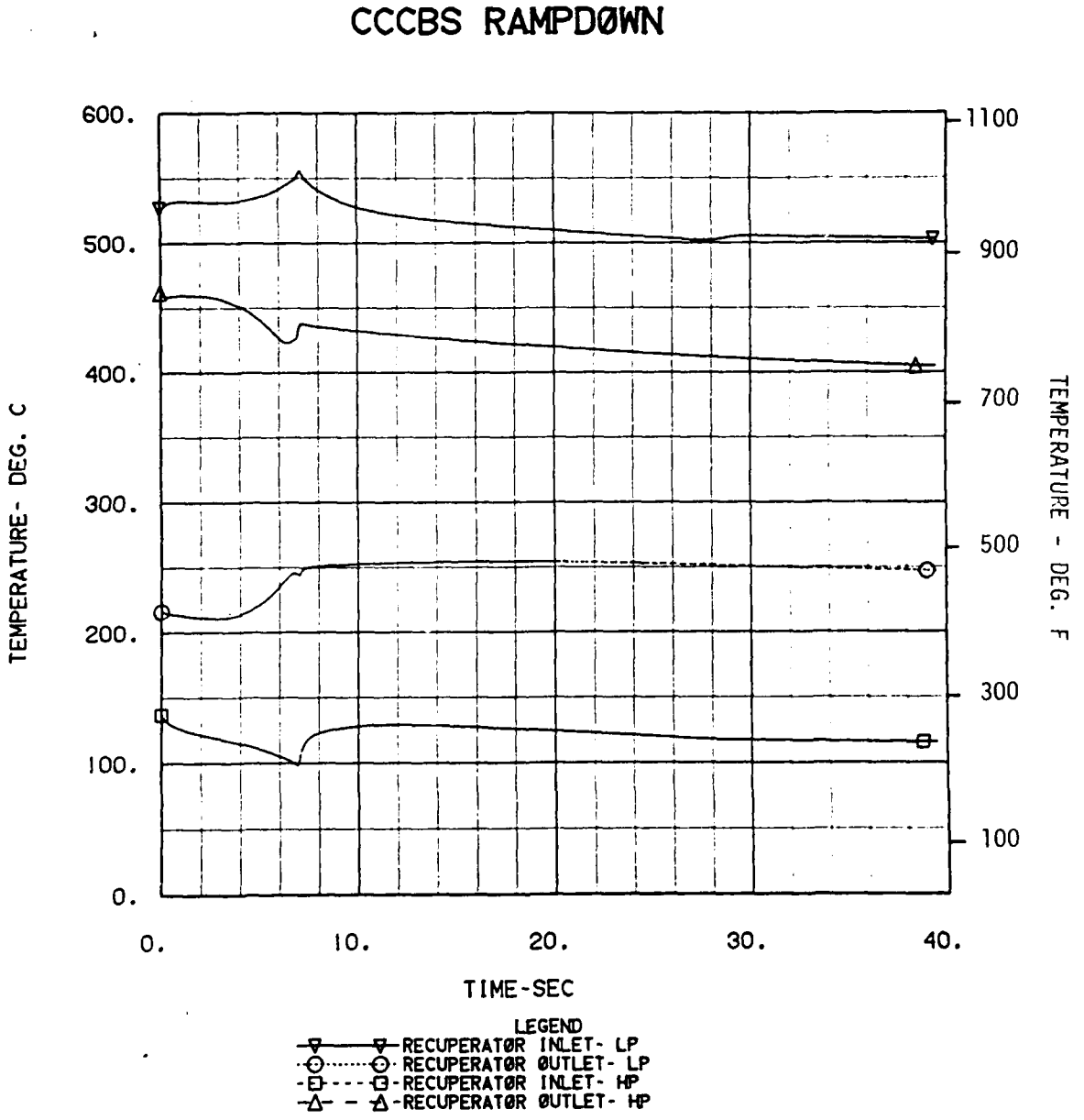

Figure 6-13. Recuperator Gas Temperatures

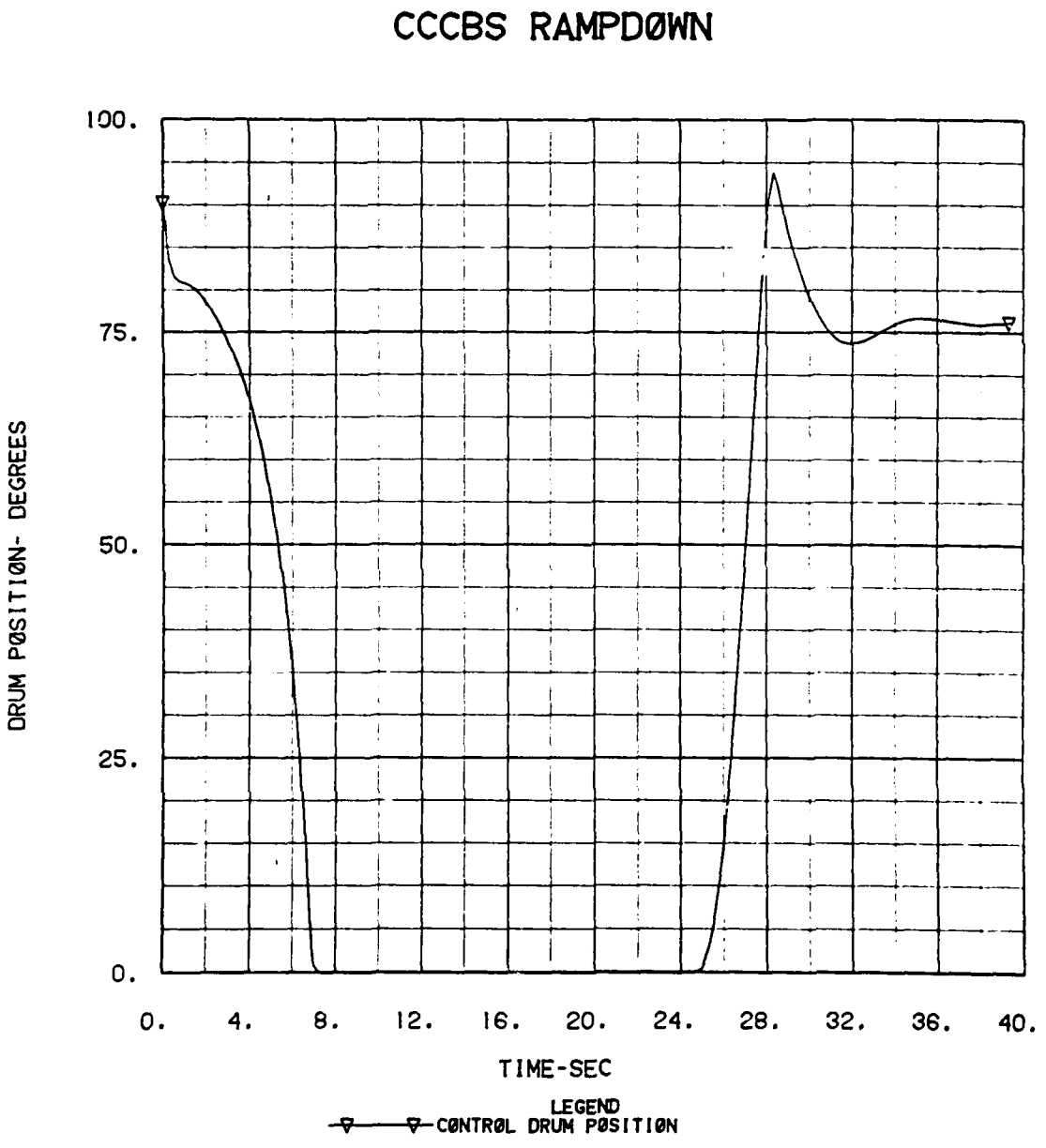

Figure 6-14. Control Drum Position

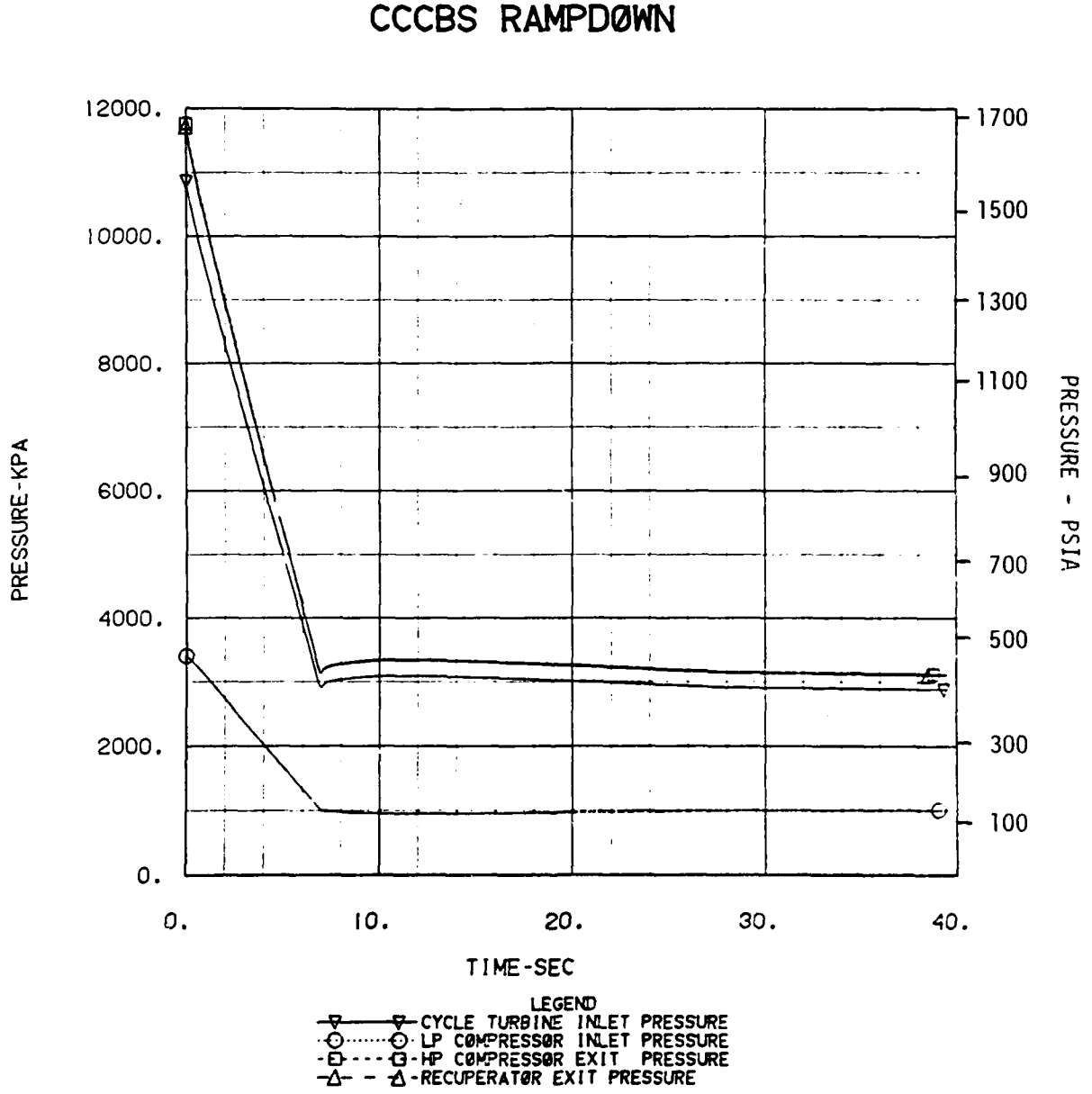

Figure 6-15. Turbomachinery Pressures

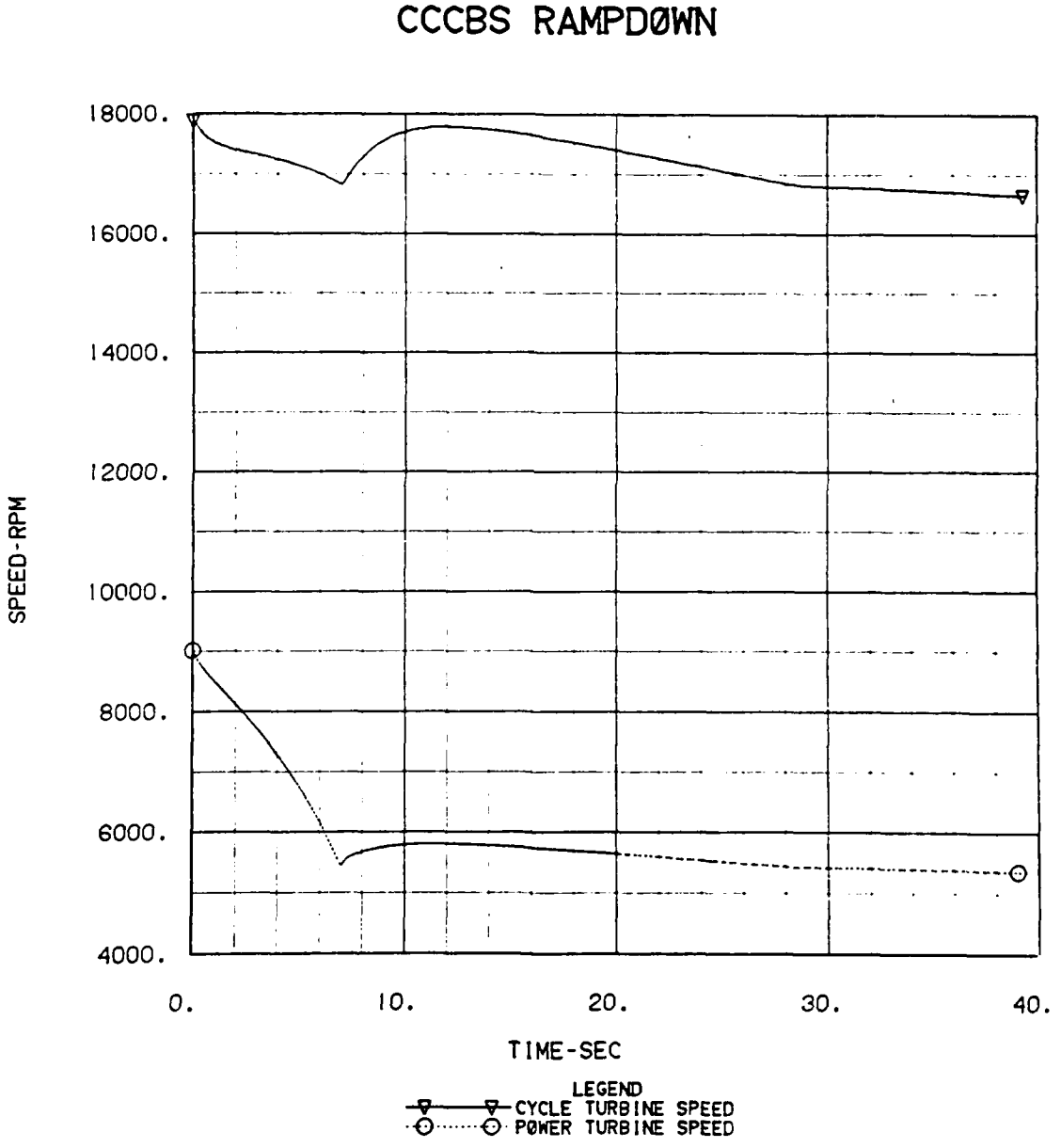

Figure 6-16. Turbomachinery Speeds

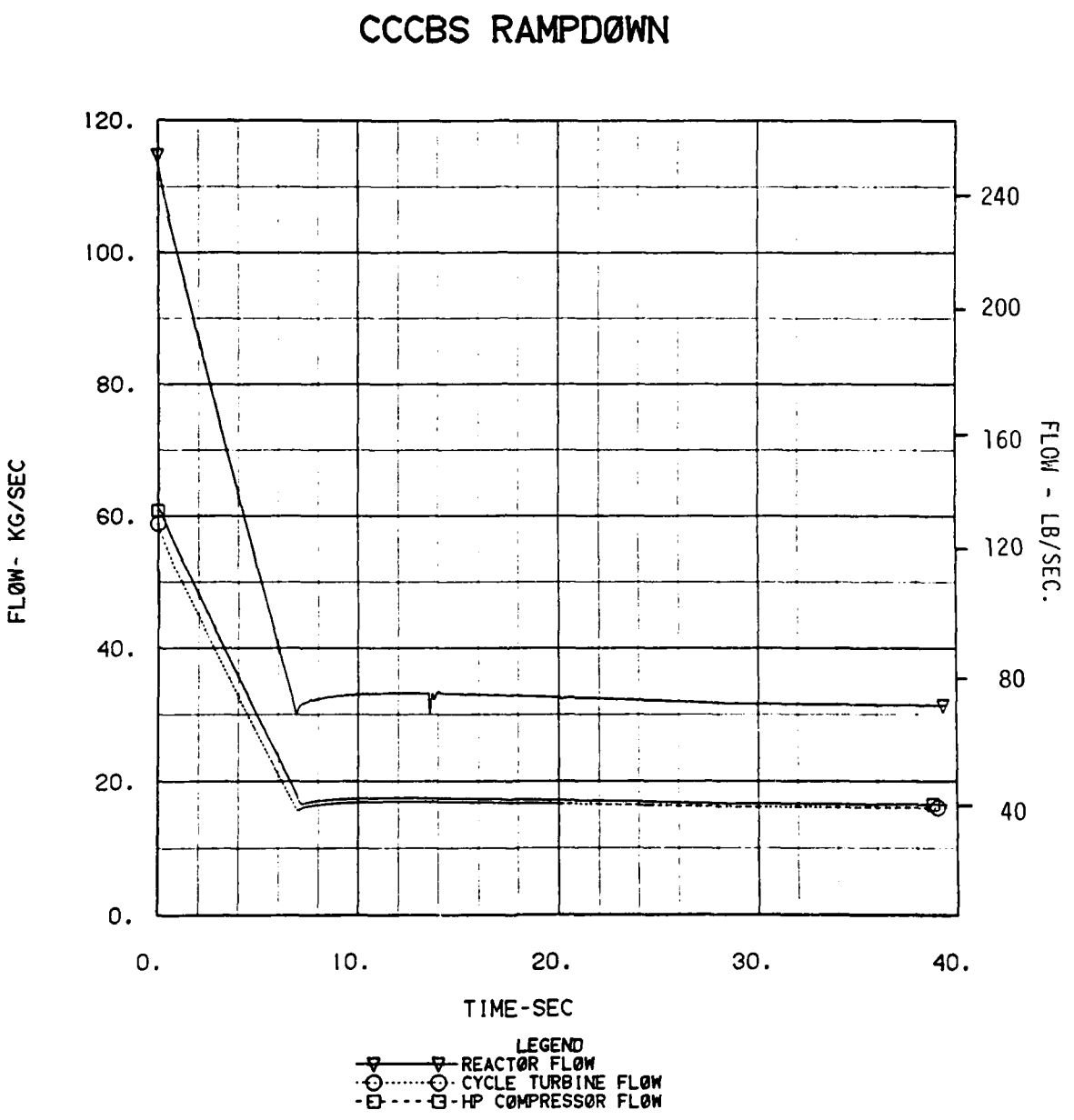

Figure 6-17. Turbomachinery Flow Rates

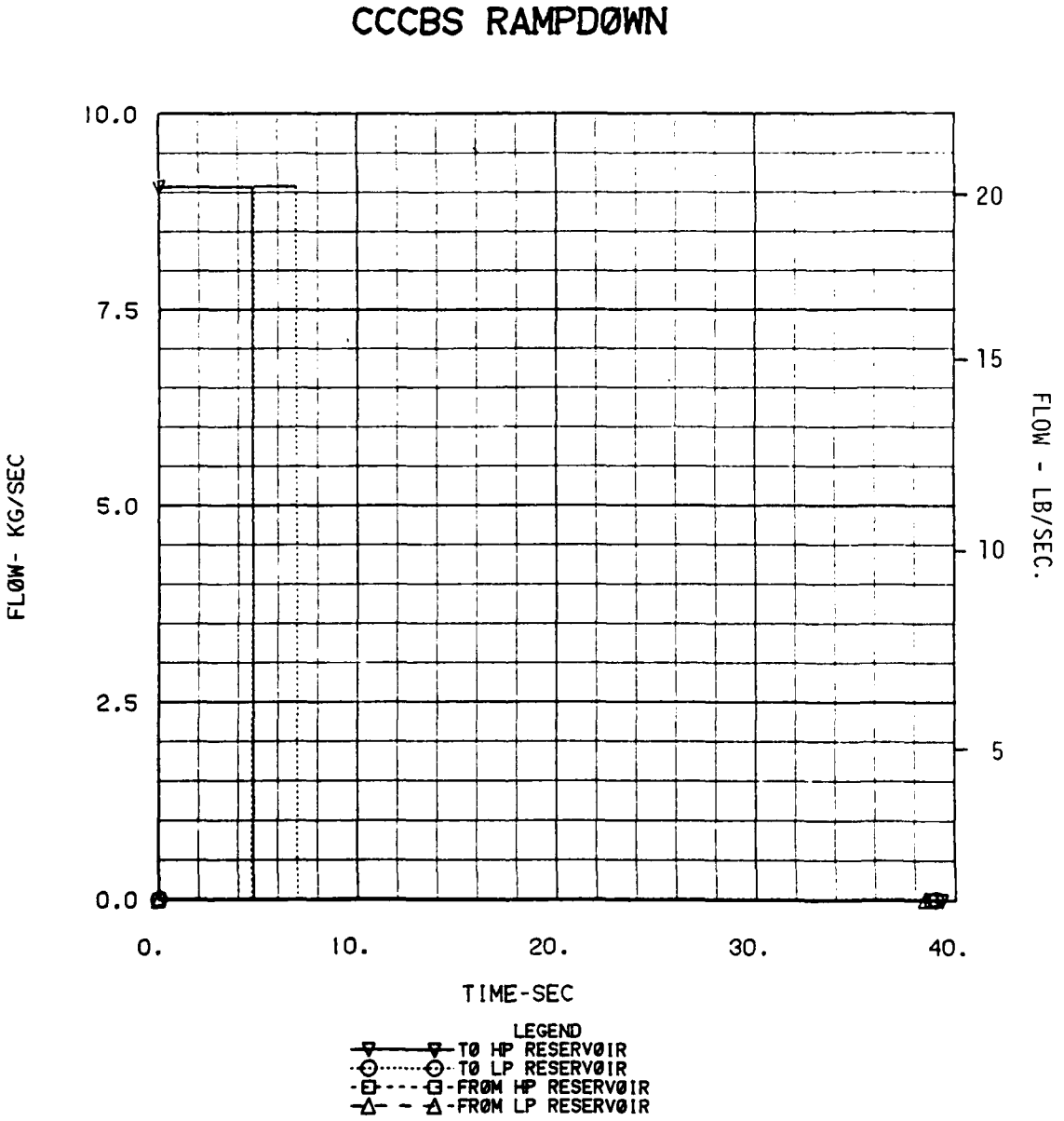

Figure 6-18. Inventory Flow Rates

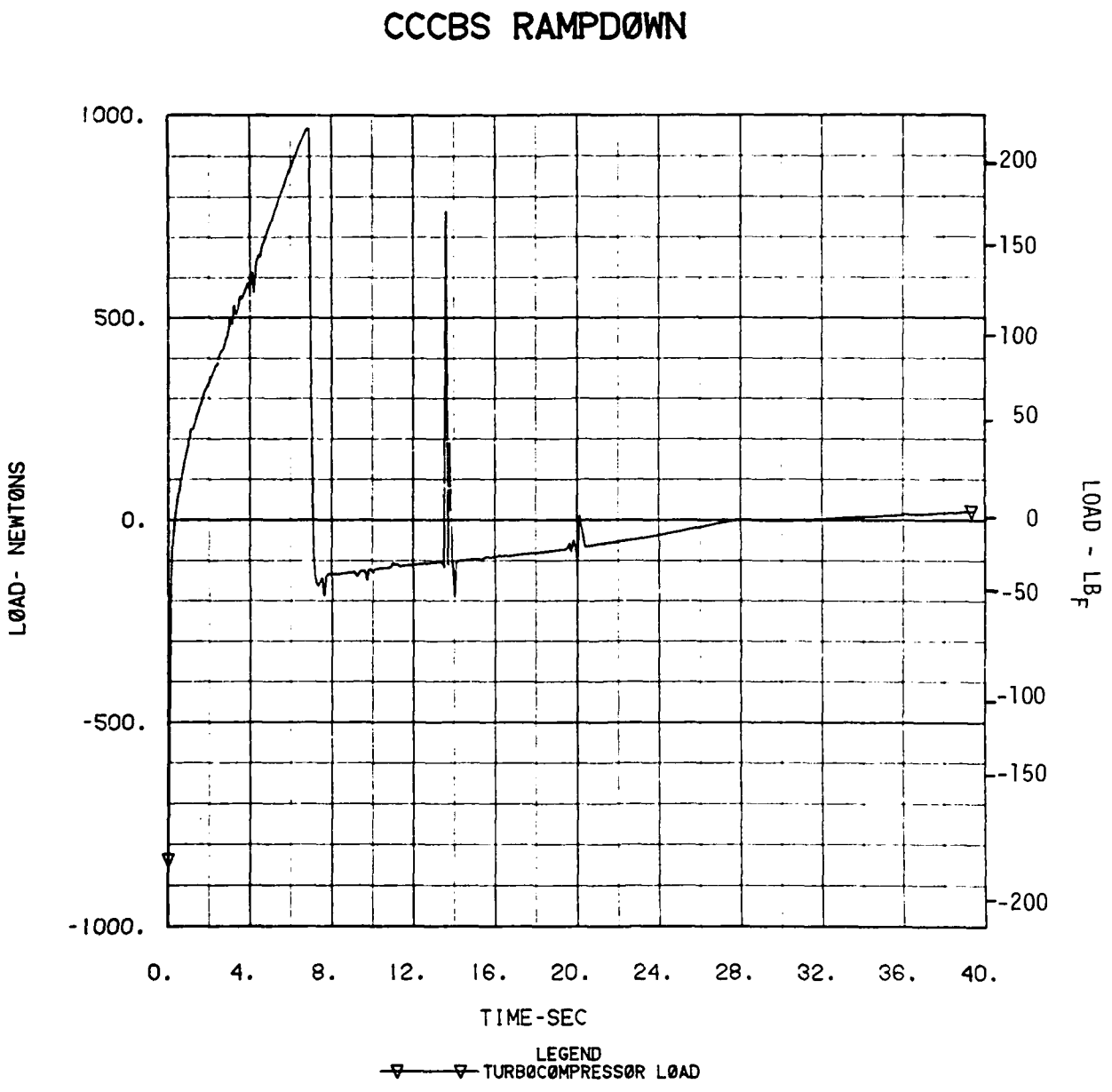

Figure 6-19. Turbocompressor Thrust Bearing Load

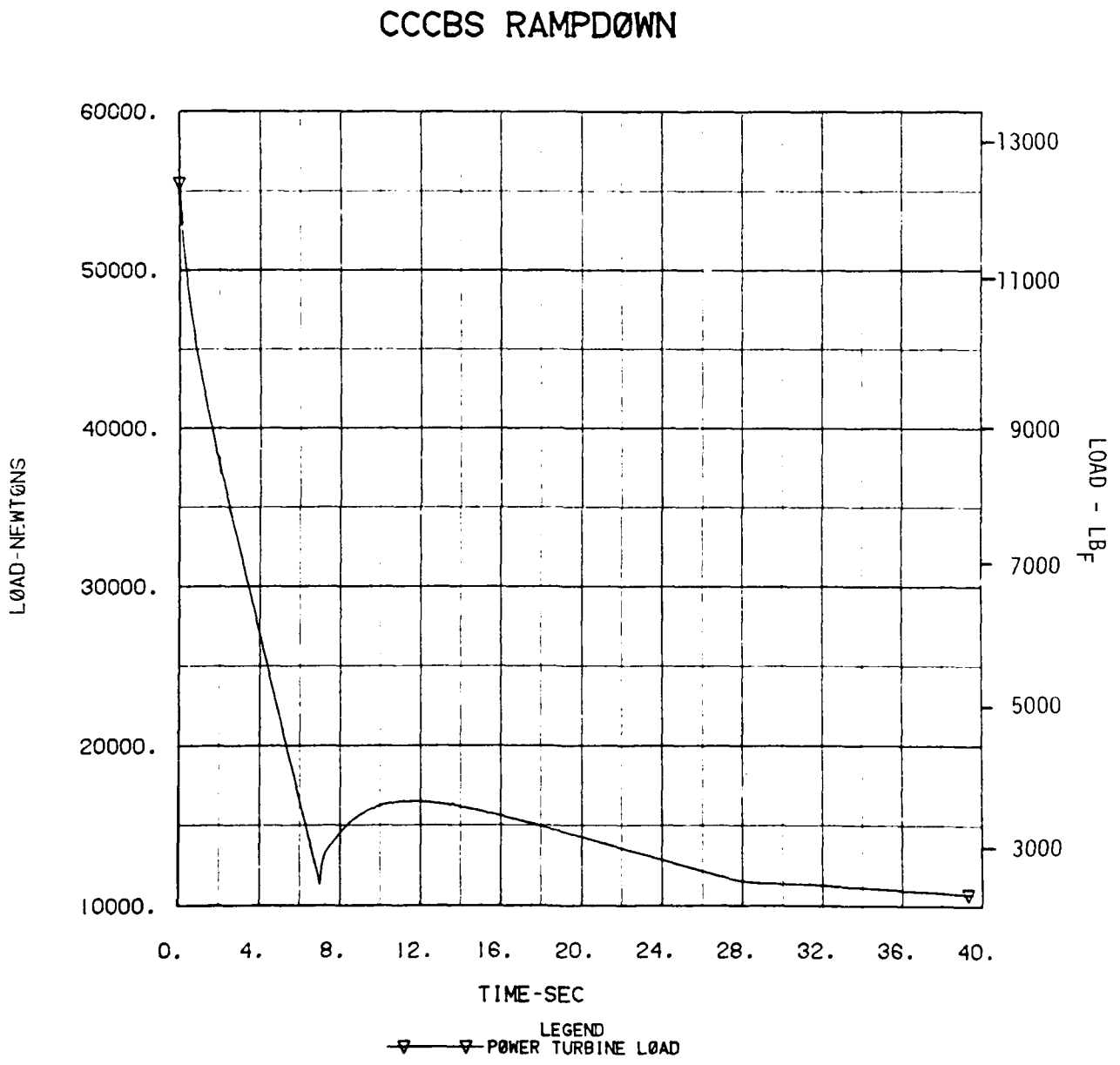

Figure 6-20. Power Turbine Thrust Bearing Load

error, the control drums were run in steadily until they bottomed out also at about 7 seconds (Figure 6-14). The small temperature spike past this point was due to a combination of the control drums being fully in, and the cessation of inventory flow causing a leveling off of the system pressures (Figure 6-15). This leveling of pressures also caused the spike in helium temperatures seen in Figure 6-13. These spikes, however, are on the order of about 20°C (35°F), and do not appear to place any constraints on the design of the CCCBS.

As described above, the control drums bottomed out at about 7 seconds into the transient. This was still while the plant was in inventory control, and appears to indicate that the nuclear heat source is unable to decrease power at the desired 10% per second when decreasing power from the 100% to the 25% throttle position. In addition, when decreasing power below a 25% throttle position, it appears as if even a 3% per second rate of change of power is too great. It would appear that for a controlled throttle rampdown from a 100% down to a 10% throttle position, the maximum rates of change of power would be about 5% per second above a 25% throttle position, and 1% per second below 25% throttle. However, for smaller power decreases (about 10% to 20%) from full power, the 10% per second desired rate of change can be maintained without problems with the reactor control drums.

The cycle and power turbine speeds are shown in Figure 6-16. During inventory control the power turbine speed drops at approximately the expected rate to match the 10% per second power rampdown rate. However, once the CCCBS switches to pure temperature control there is initially a slow rise in turbine speed, followed by a very gradual speed decrease past 12 seconds. The speed increase was caused by the rebalancing of the system pressure and flow rates following the sudden stopping of the inventory flow (Figure 6-19). This can be seen in Figure 6-14 and 6-16, where the system pressures and flows both increased between 7 and 12 seconds. The slow rate of decrease of the power turbine speed past 12 seconds was due to the generator turbine torque beong almost identical to the load torque.

The thrust bearing loads on the turbocompressor assembly and the power turbine are shown in Figure 6-19 and 6-20, respectively. Between 0 and 8 seconds the turbocompressor thrust load (Figure 6-19) varied dramatically with the inventory

flow. The essentially step changes in bearing loads at 0 and 7 seconds were due to the modeled step changes in the inventory flow, and show the strong interrelation between the inventory flow and turbocompressor load.

While in actuality the bearing loads would not change as rapidly as shown due to the dynamics of the inventory control valves, it should be noted that any rapidly acting inventory controller is going to cause correspondingly rapid changes in the turbocompressor thrust bearing loads. Also, the thrust bearing would have to be designed to accommodate thrusts of the same magnitude in either direction (i.e., towards the front or the back of the CCCBS).

The power turbine thrust bearing load (Figure 6-20) exhibited a much smoother behavior. Comparing Figures 6-20 with the power turbine speed shown in Figure 6-16 indicates an almost direct relationship between the bearing load and turbine speed, mainly due to both being strong functions of the turbine pressure ratio for variable speed turbine operation.

6.1.2.2 THROTTLE RAMPUP FROM 10% OUTPUT POWER

The results for the throttle rampup case are shown in Figures 6-21 and 6-22. The transient was essentially the inverse of the throttle rampdown case analyzed previously. The 10% output power start point was approximately the minimum steady-state operating point. The demanded ramprate was 3% per second below 25% power, followed by a 10% per second throttle ramp above 25% power. Figure 6-21 shows the controlled reactor outlet temperature as well as the reactor and cycle turbine inlet temperatures. Unlike the rampdown case, here the control drums were able to match the demand and actual reactor outlet temperatures to within 1°C for the major portion of the transient. The only significant deviation occurred at about 5.5 seconds, where the reactor temperature overshot the demand by about 8°C. This region was where the CCCBS switched to inventory control, which also necessitated a much smaller rate of increase in the reactor outlet demand temperature. The control drums were simply unable to match the demand and actual temperature in the neighborhood of this slope discontinuity. The overshoot is too small, however, to require any major changes to the drum controllers.

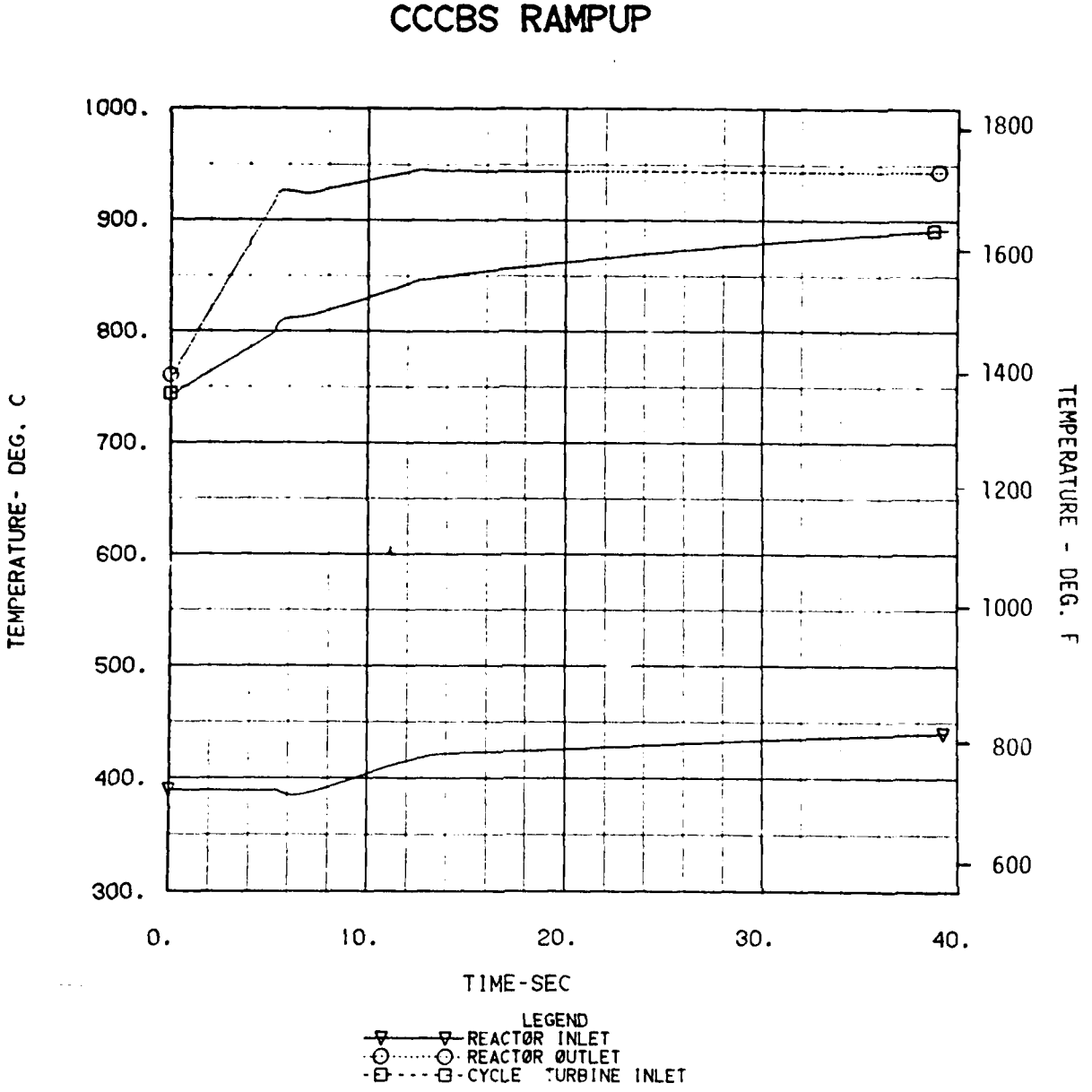

Figure 6-21. Heat Source Temperatures

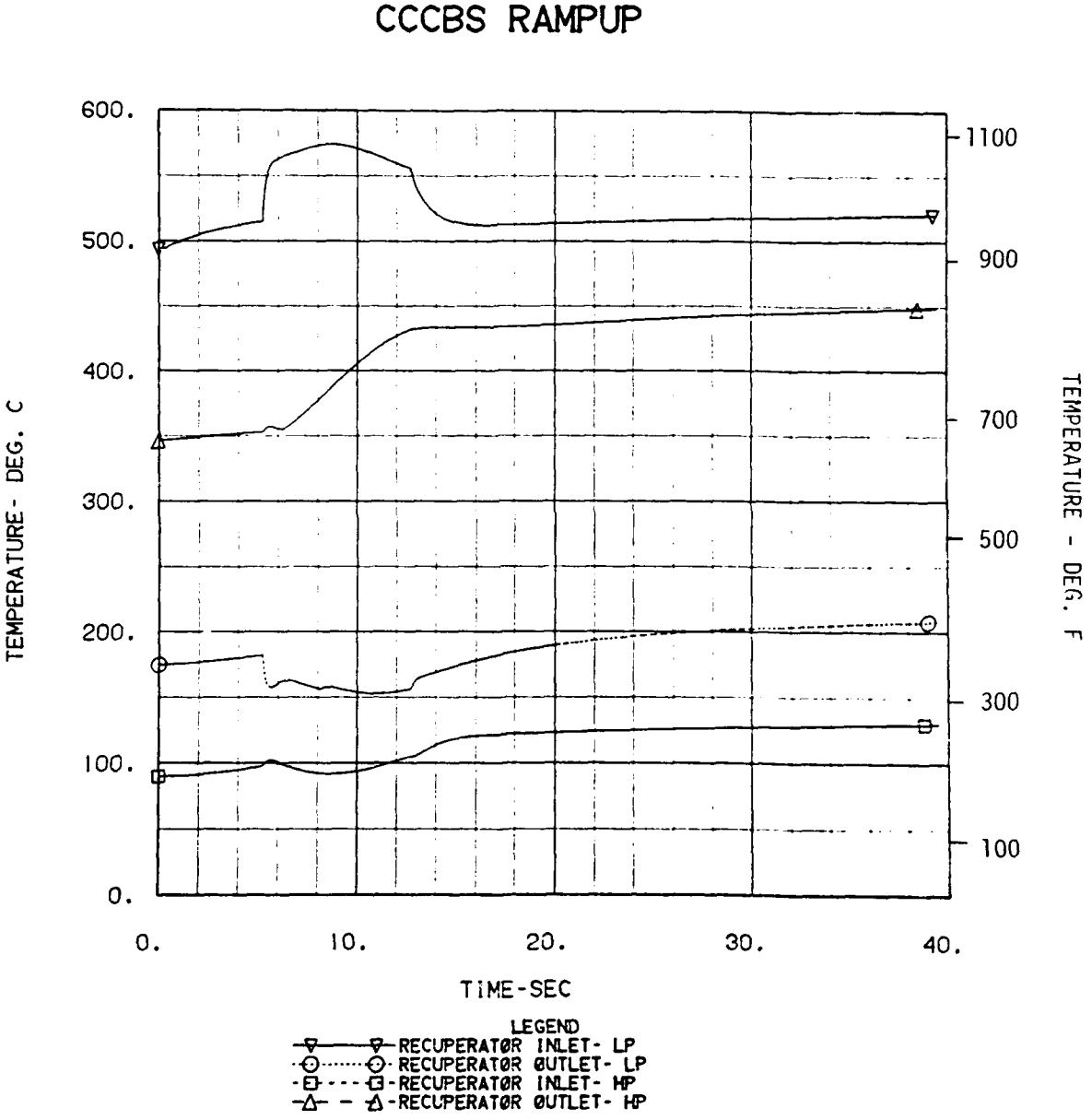

Figure 6-22. Recuperator Gas Temperatures

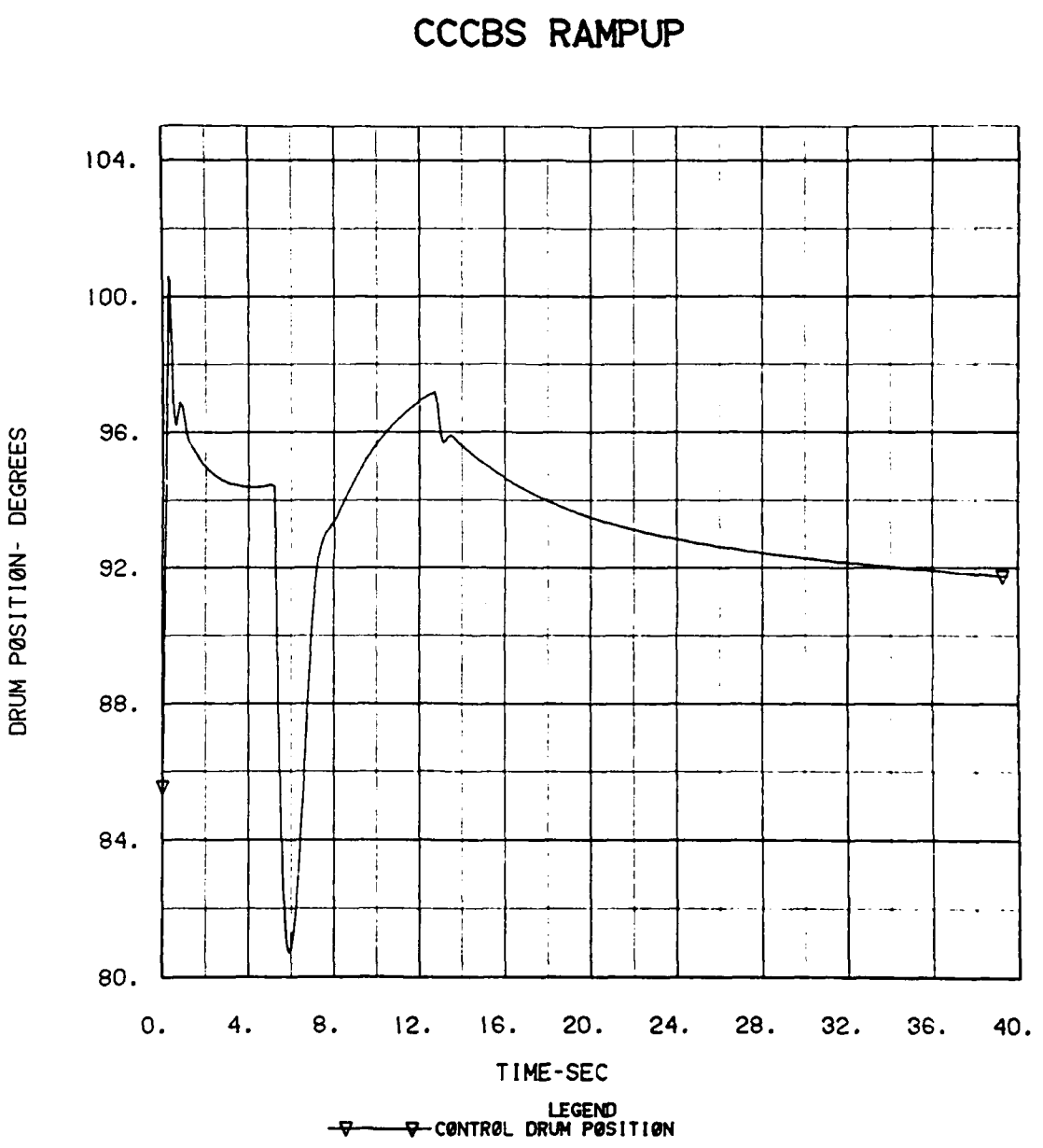

Figure 6-23. Control Drum Position

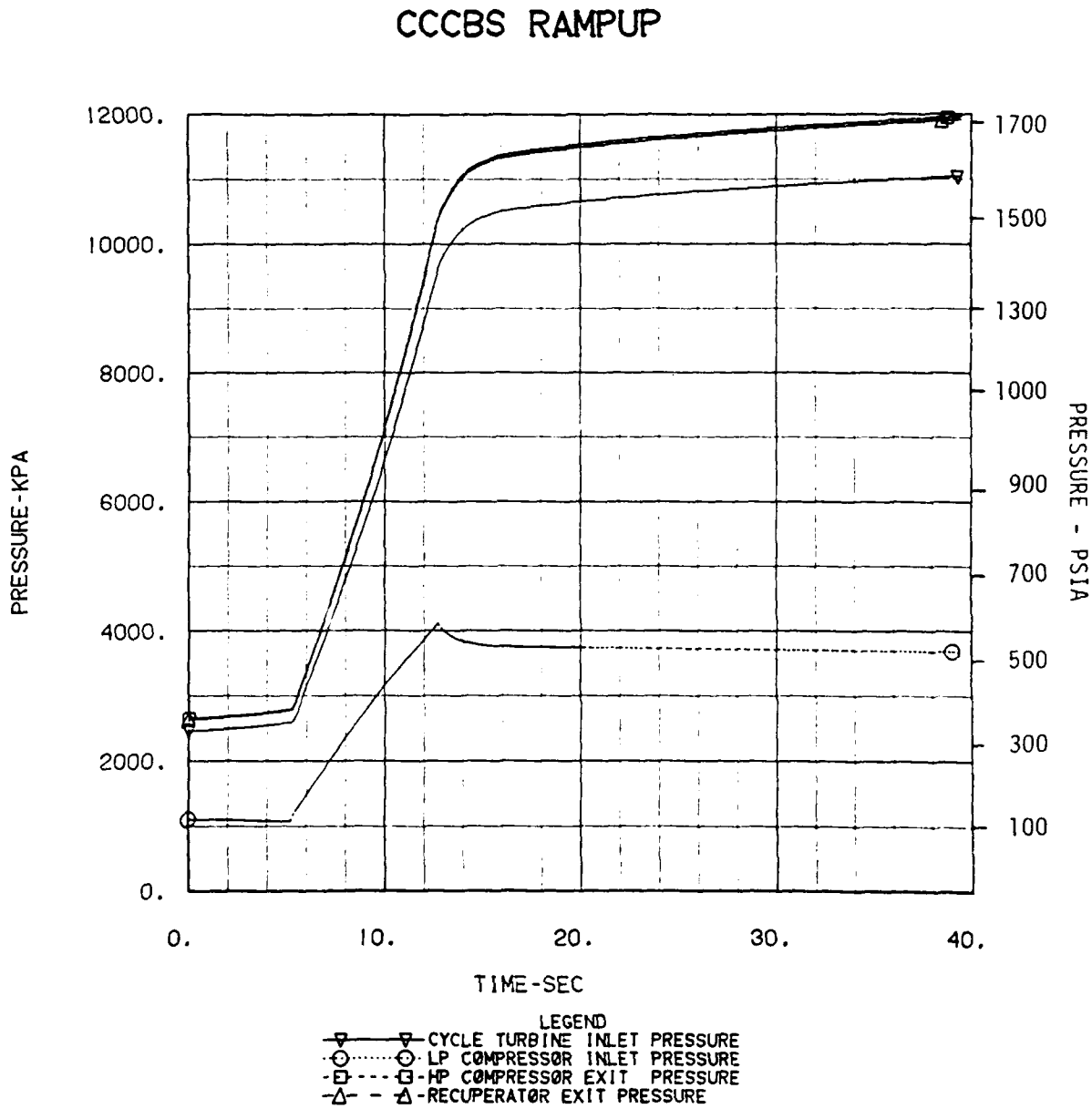

Figure 6-24. Turbomachinery Pressures

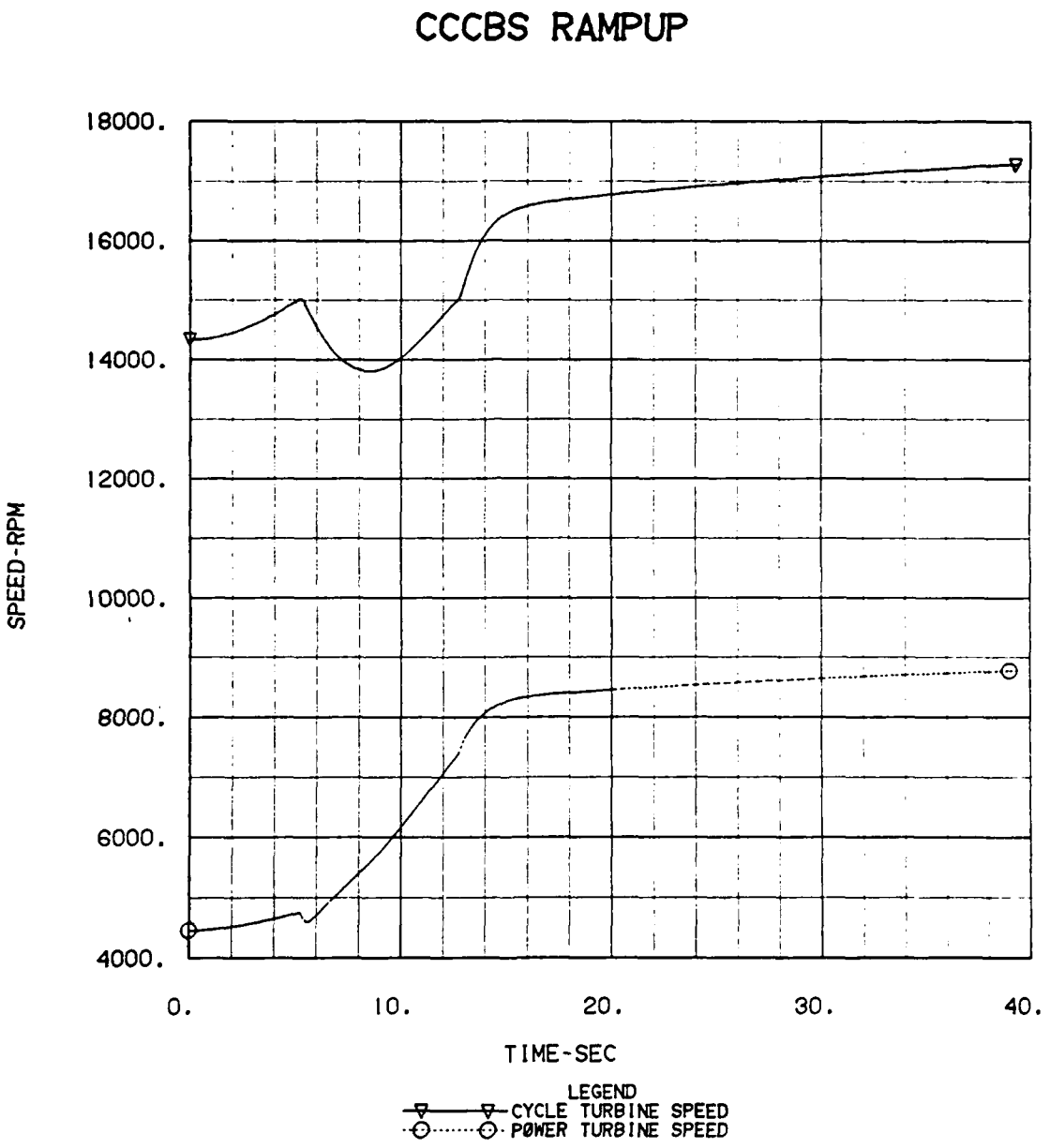

Figure 6-25. Turbomachinery Speeds

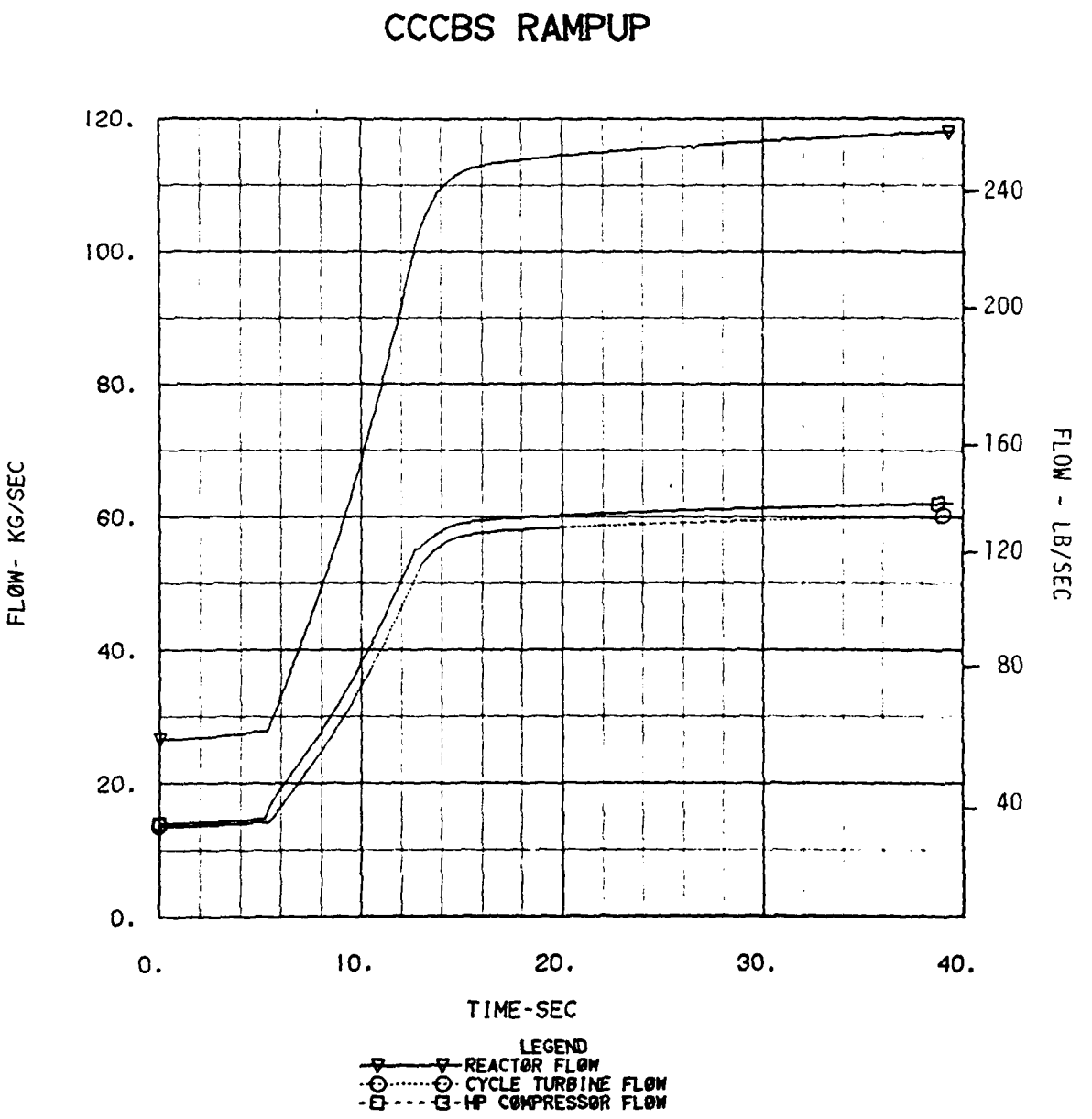

Figure 6-26. Turbomachinery Flow Rates

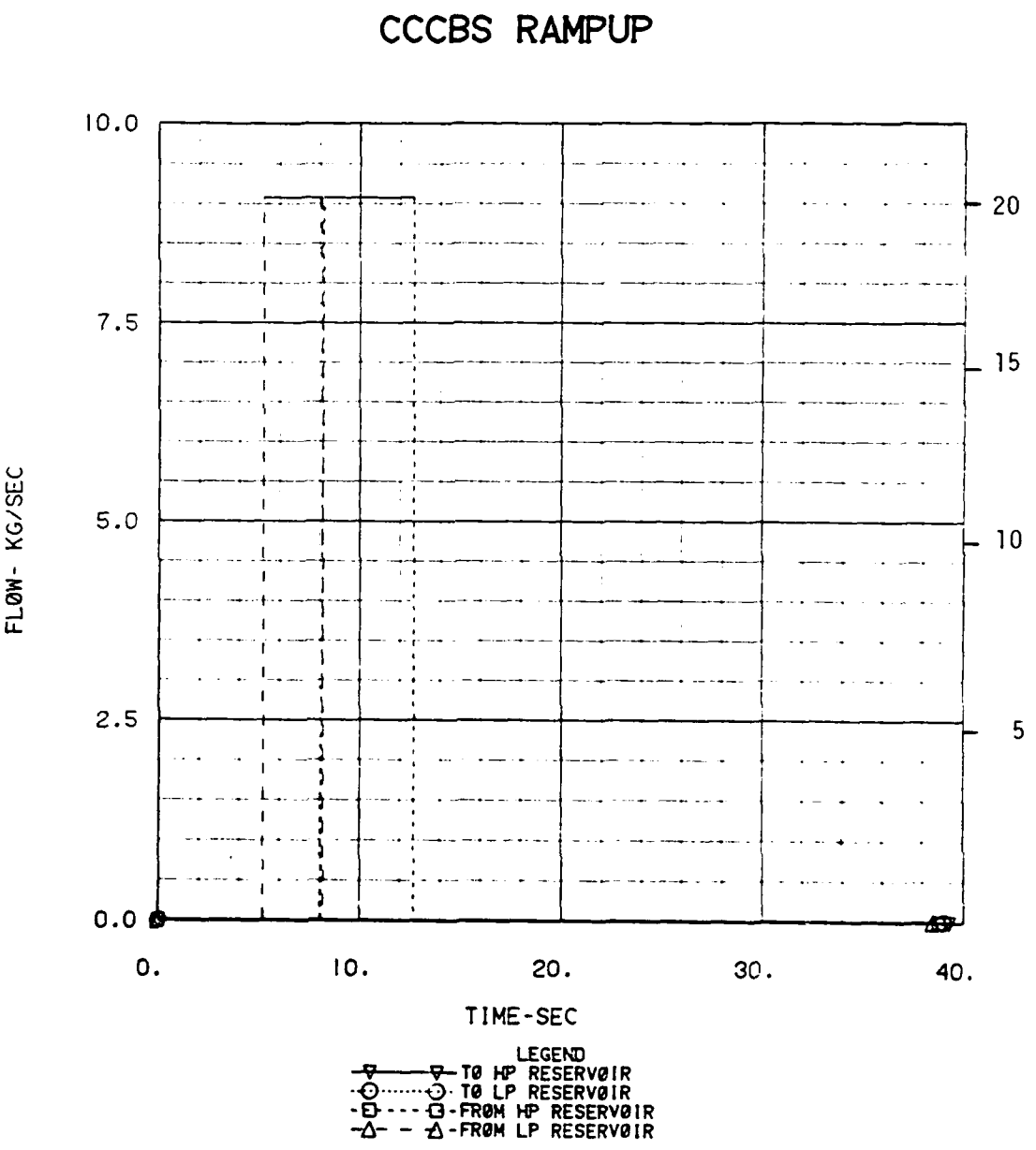

Figure 6-27. Inventory Flows

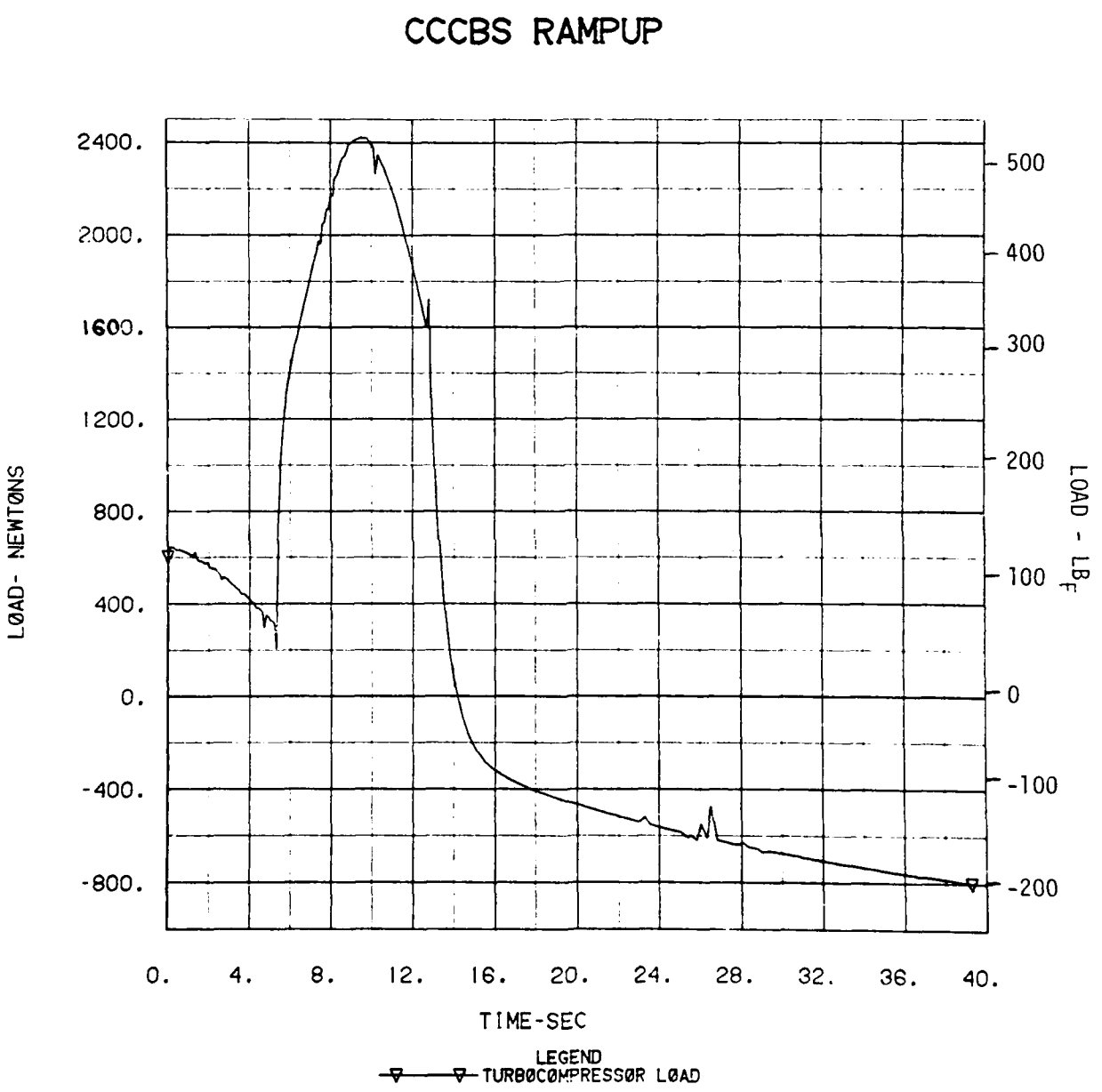

Figure 6-28. Turbocompressor Thrust Bearing Load

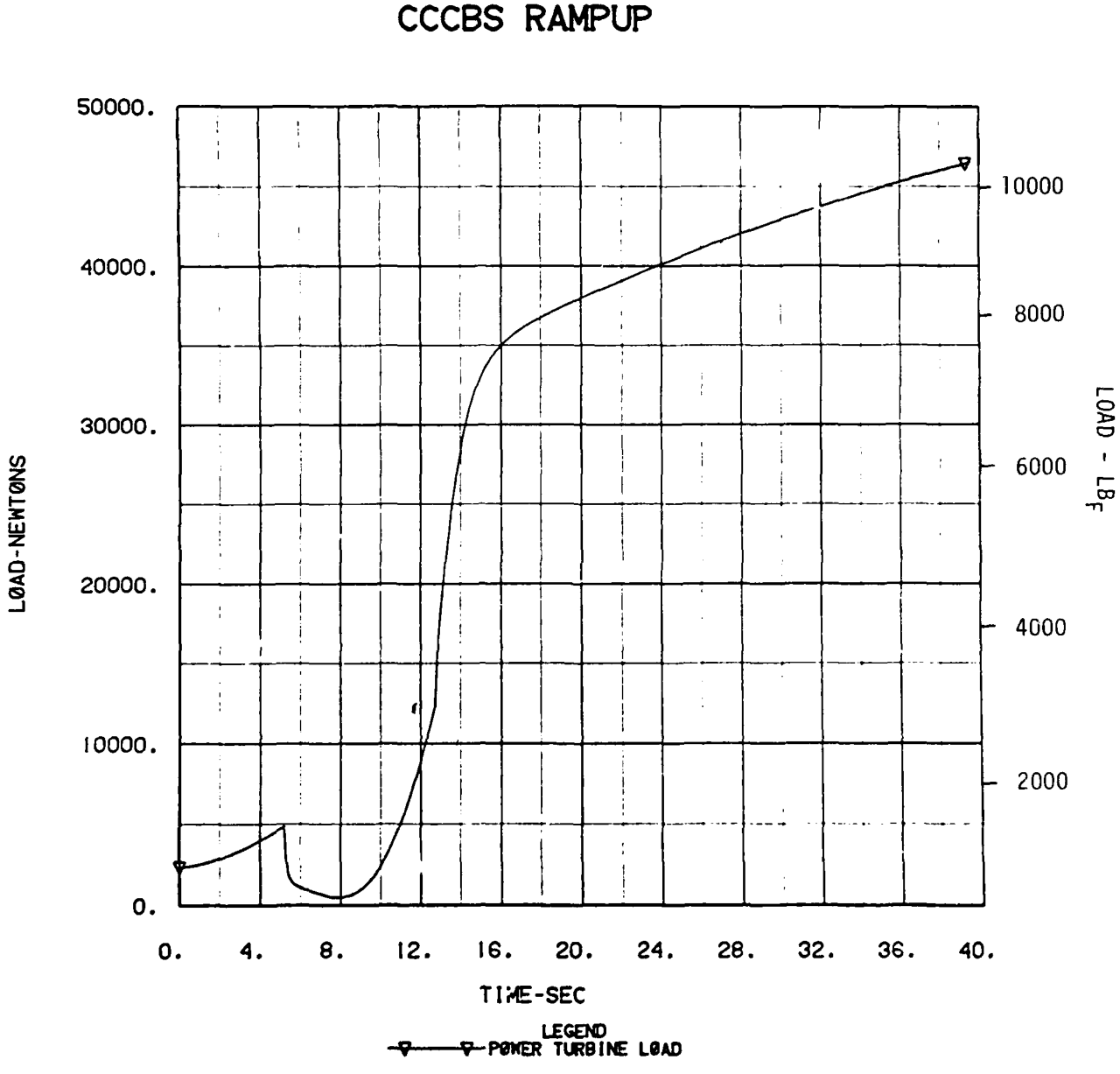

Figure 6-29. Power Turbine Thrust Bearing Load

Figure 6-22 shows the major turbomachinery temperatures. Before 5 seconds and after 13 seconds, the CCCBS was in pure temperature control, and the turbomachinery helium temperatures were all changing at approximately the same rate. This was due to the approximately equal flows in both the compressor and turbines (Figure 6-26). During inventory control, however, there is a 10% to 25% flow difference between the two, with the largest percentage variation being at the start of inventory control. This caused the dip in the temperature exiting the low pressure side of the recuperator.

The sudden addition of helium at the precooler inlet caused a sudden increase in the pressure in this region, with a corresponding increased in the back pressure in the power turbine.

This decreased the flowrate momentarily through the power turbine, and hence increased the power turbine outlet temperature (stated as "Recuperator Inlet - LP" on Figure 6-22). This was also reflected in a momentary reduction in shaft power produced and a corresponding reduction in the power turbine speed (Figure 6-25).

The turbomachinery flowrates (Figure 6-26) were relatively constant during temperature control, and increased at about a 10% per second rate during inventory control in response to the 9 Kg/sec (20 lb/sec) inventory flow (Figure 6-27). The inventory flow was stopped at 12.5 seconds, the time when the helium inventory reached its full-power value.

The turbocompressor and power turbine thrust bearing loads are shown in Figures 6-28 and 6-29, respectively. During temperature control the bearing thrust loads changed at a fairly constant rate. The most radical changes occurred during inventory control, especially for the turbocompressor load which changed by about 2000 Newtons (450 lb_f) at the start and end of the inventory flow. A larger percentage of this change was most likely due to the sudden step changes in the helium flow causing a rapid change in pressure at the power turbine exit. A more realistic modeling of the inventory flow would decrease the loads rate of changes as will be seen in the succeeding sets of transients.

6.1.2.3 REACTOR SCRAM FROM 100 PERCENT OUTPUT POWER

The results for this reactor scram case are shown in Figures 6-30 through 6-38. The reactor scram was simulated by running the control drums in at their maximum rate. The speed demand was set to zero, resulting in the inventory valves going full open and allowing the maximum flow possible into the inventory bottles. This was done to insure that the helium inventory was reduced to the 25% value desired for shutdown and low power operation.

The large inventory flow which occurred due to the valves going full open (Figure 6-36) did not cause any problems with controlling the reactor outlet temperature (Figure 6-30). Peak temperature reached was 950°C (1740°F), only about 6°C (10°F) above its normal full power value. Two temperature spikes were noted at 2 and 3.5 seconds. This was due to the switching from dumping into the high pressure inventory blottle to dumping into the low pressure bottle at 2 seconds, and due to the stoppage of the inventory flow at 3.5 seconds (Figure 6-36).

Figure 6-30 shows a large temperature lag between the reactor outlet temperature and the cycle turbine inlet temperature. This is due to the heat capacity of the reactor outlet plug shield. As presently defined, this shield is composed of a number of layers of plugs arranged in a manner to result in a labyrinth flow path for the cycle helium. These plugs are composed of a tungsten-beryllium oxide powder enclosed in a steel jacket. For the cases analyzed, the plug shield design was not optimized for the CCCBS application. By redesigning the outlet plug shield, a closer agreement between the reactor outlet and cycle turbine inlet helium temperatures can be obtained. This would allow the plant to respond more rapidly to a change in the reactor outlet temperature. While an assessment of the feasibiltiy of obtaining a large change in the heat capacity of the outlet plug shield is beyond the scope of this study, it is felt that measurable design improvements can readily be made.

The recuperator gas temperatures are shown in Figure 6-31. The temperature variations noted below about 3.5 seconds were due to the inventory flow causing a flow mismatch in the low and high pressure sides of the recuperator.

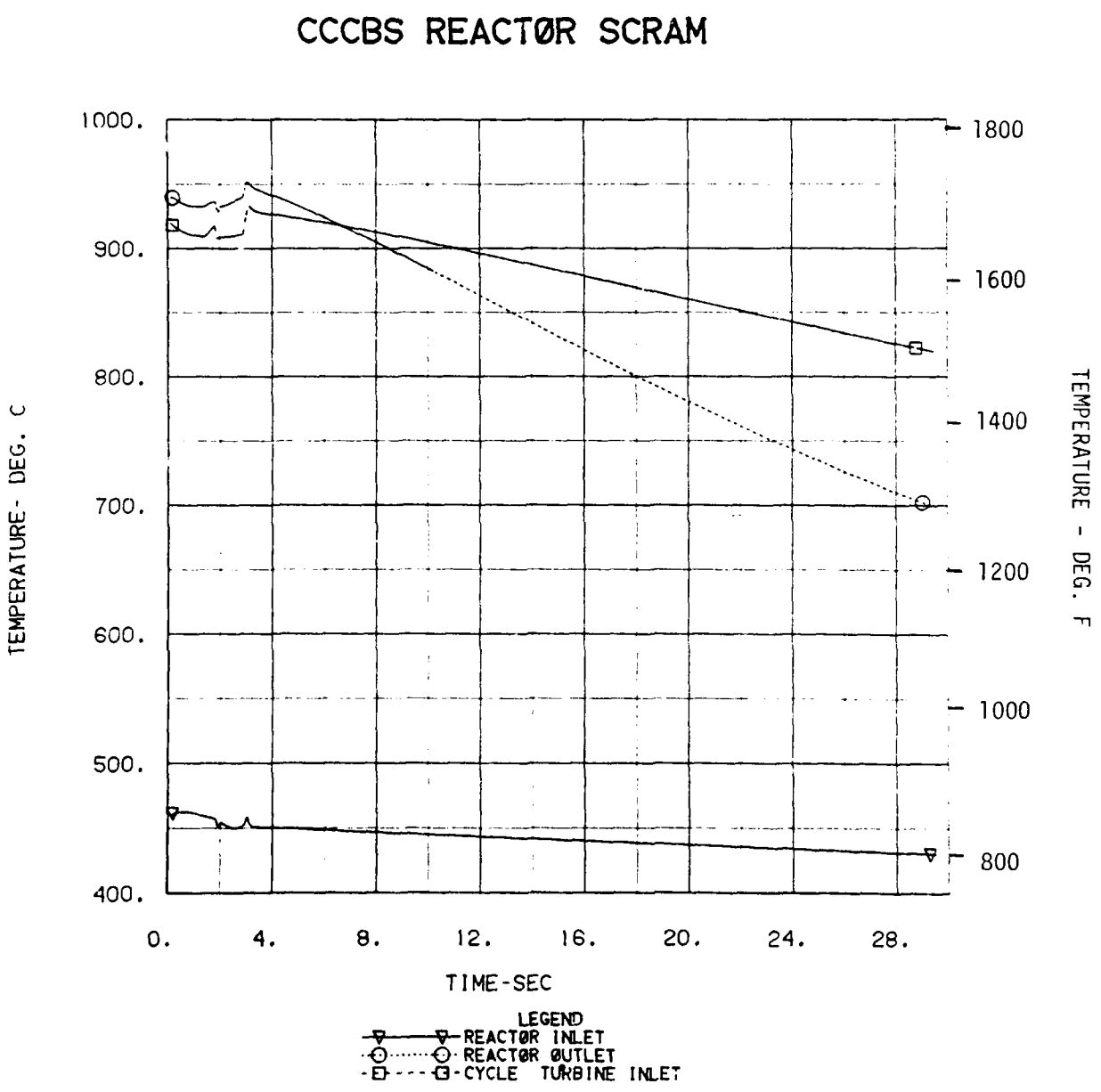

Figure 6-30. Heat Source Temperatures

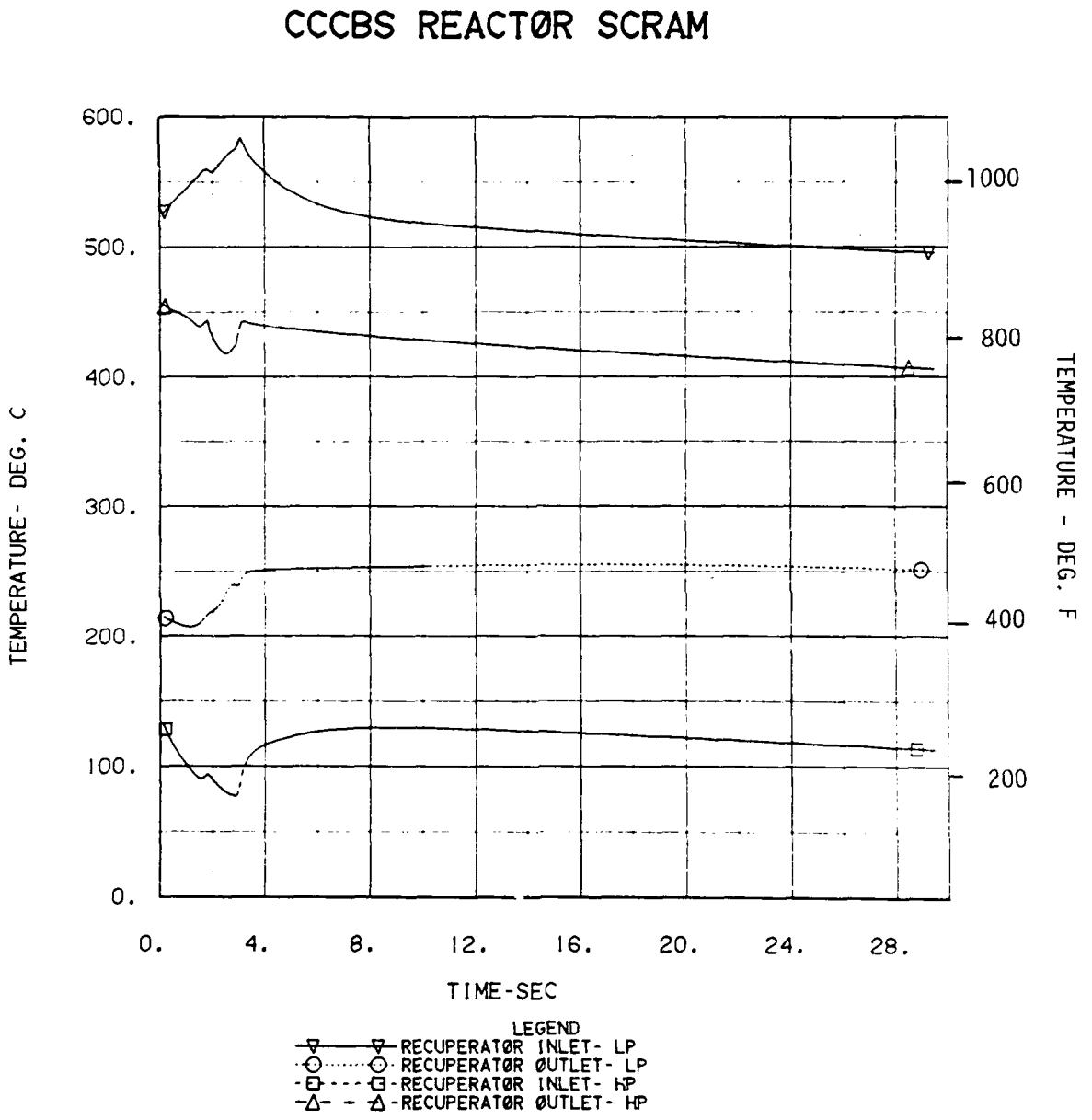

Figure 6-31. Recuperator Gas Temperatures

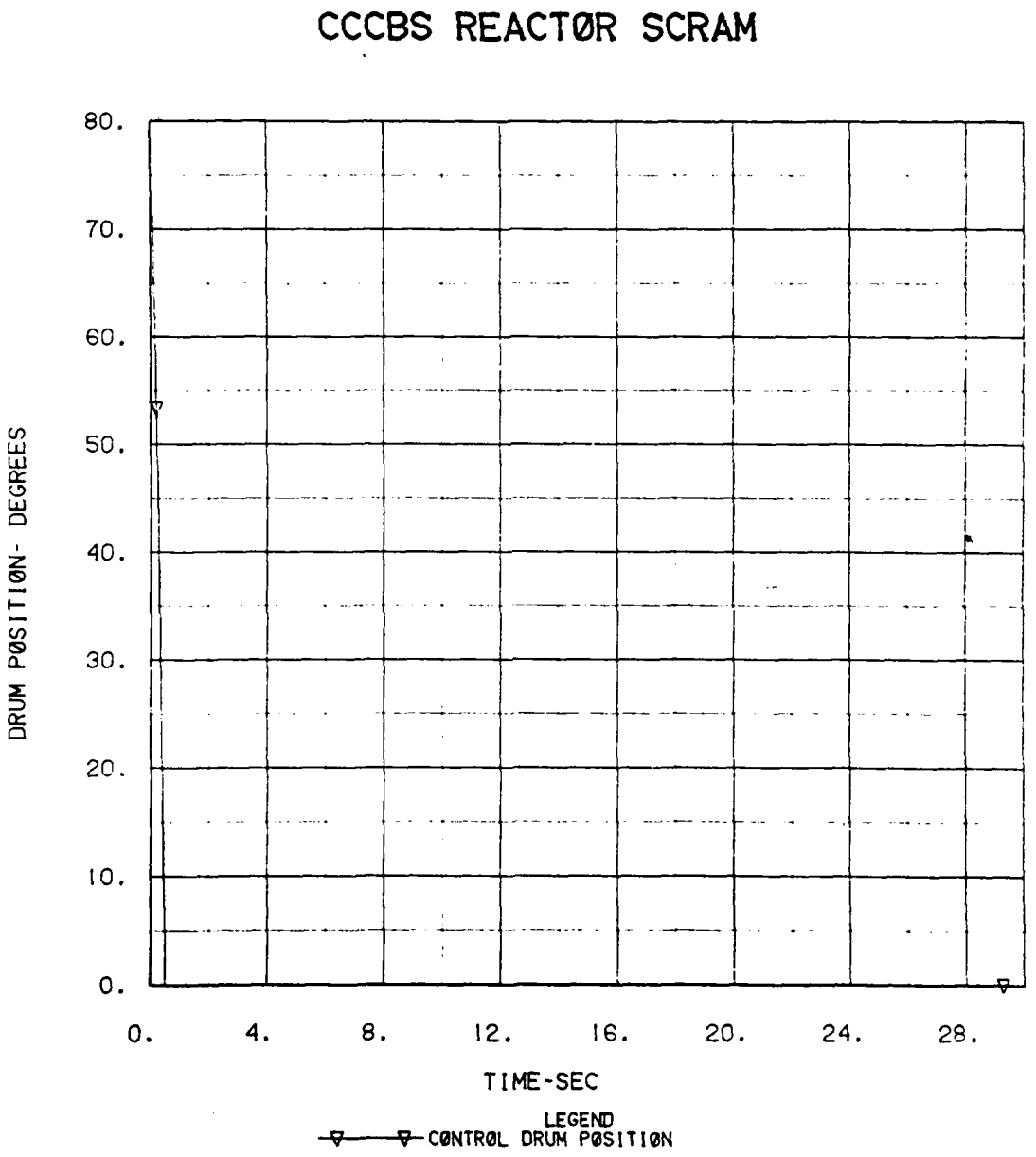

Figure 6-32. Control Drum Position

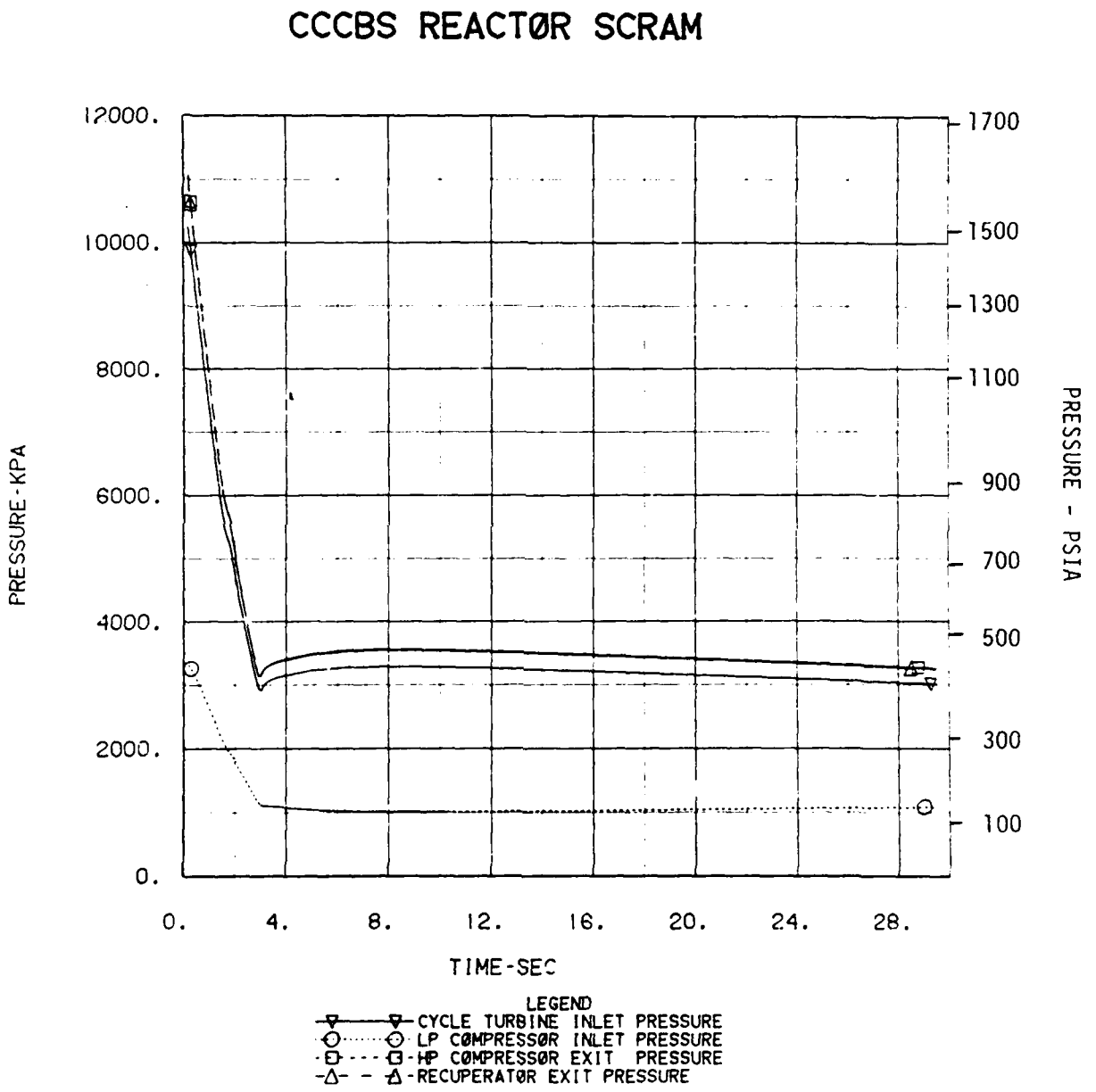

Figure 6-33. Turbomachinery Pressures

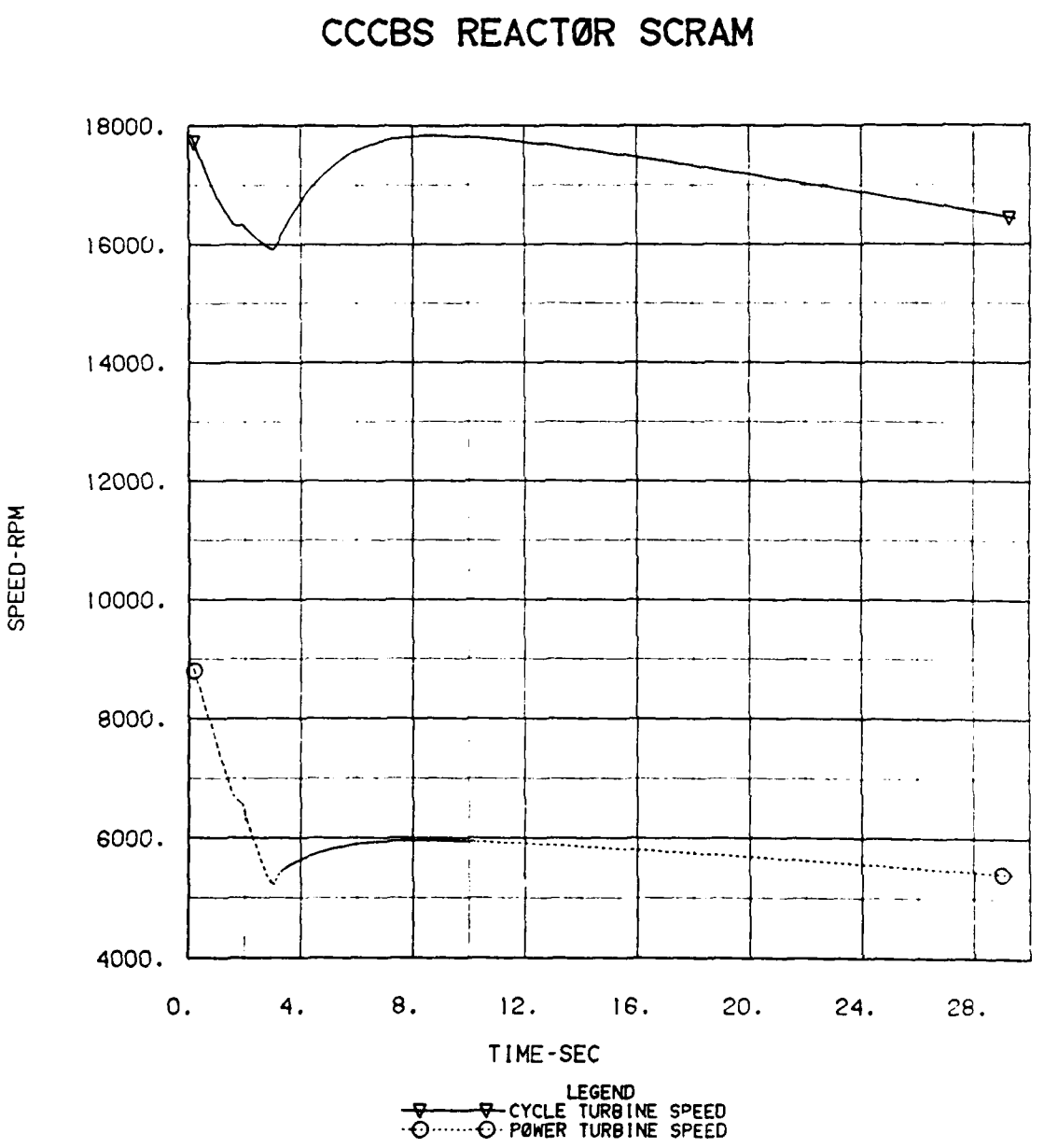

Figure 6-34. Turbomachinery Speeds

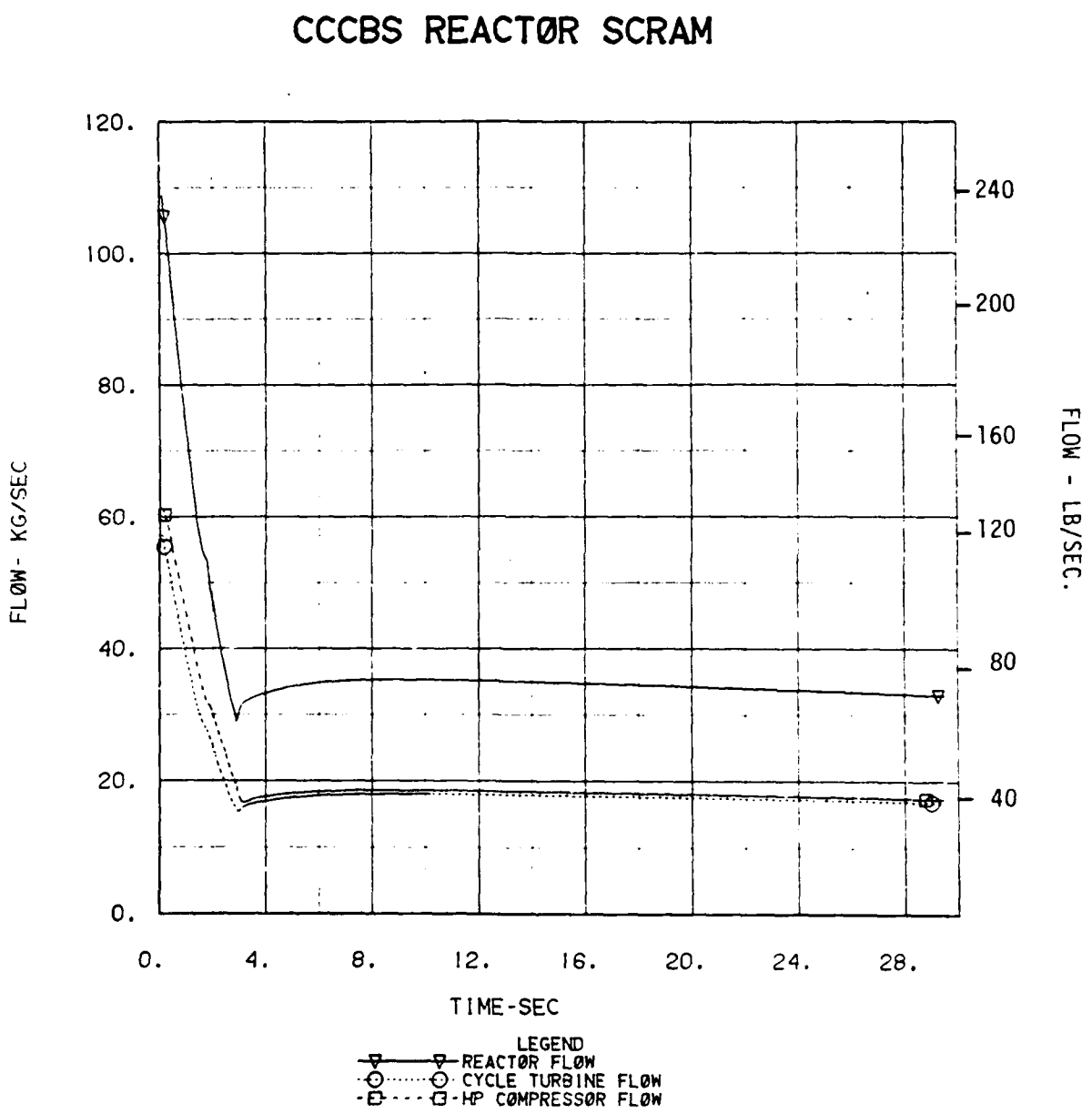

Figure 6-35. Turbomachinery Flow Rates

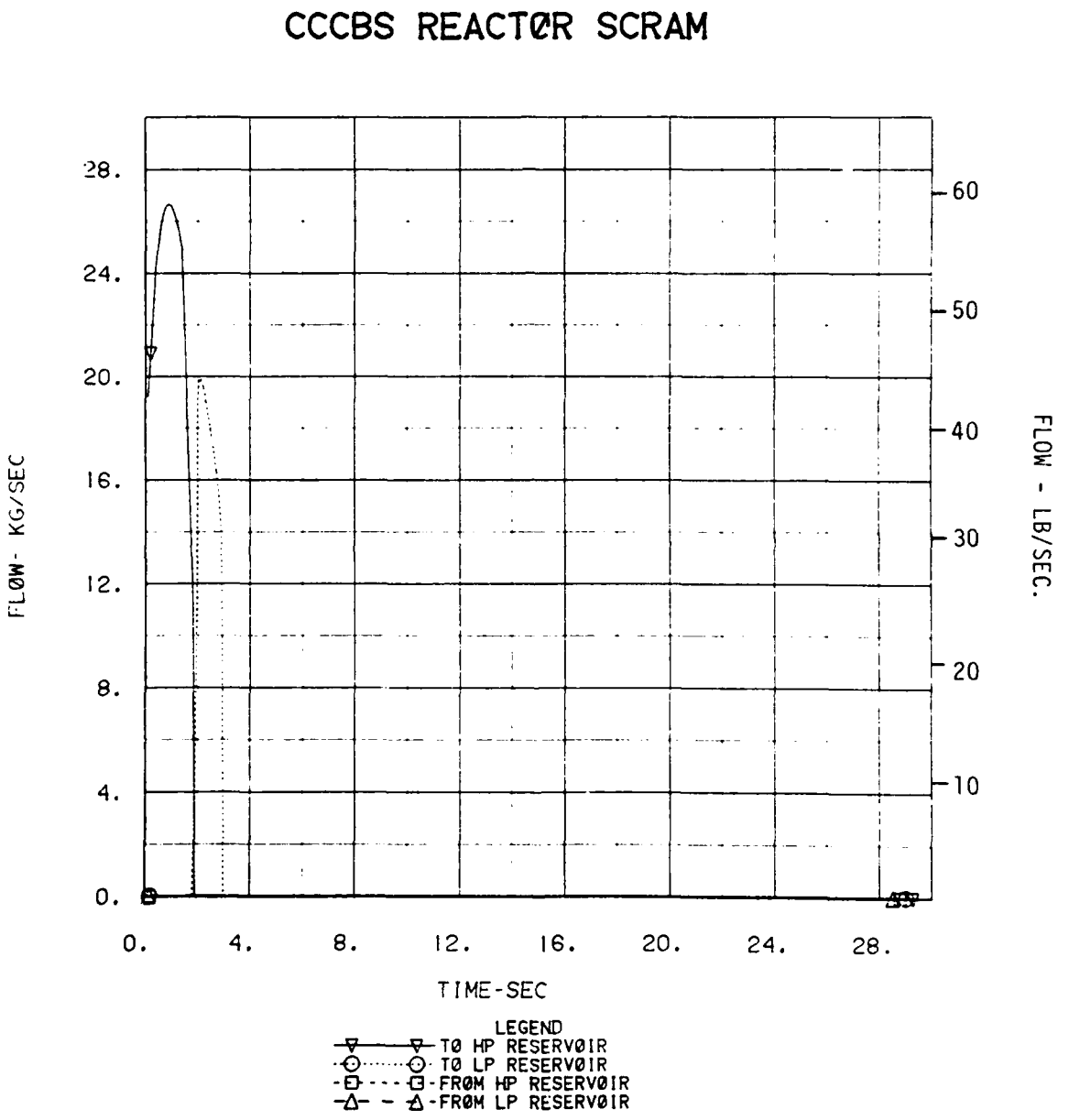

Figure 6-36. Inventory Flows

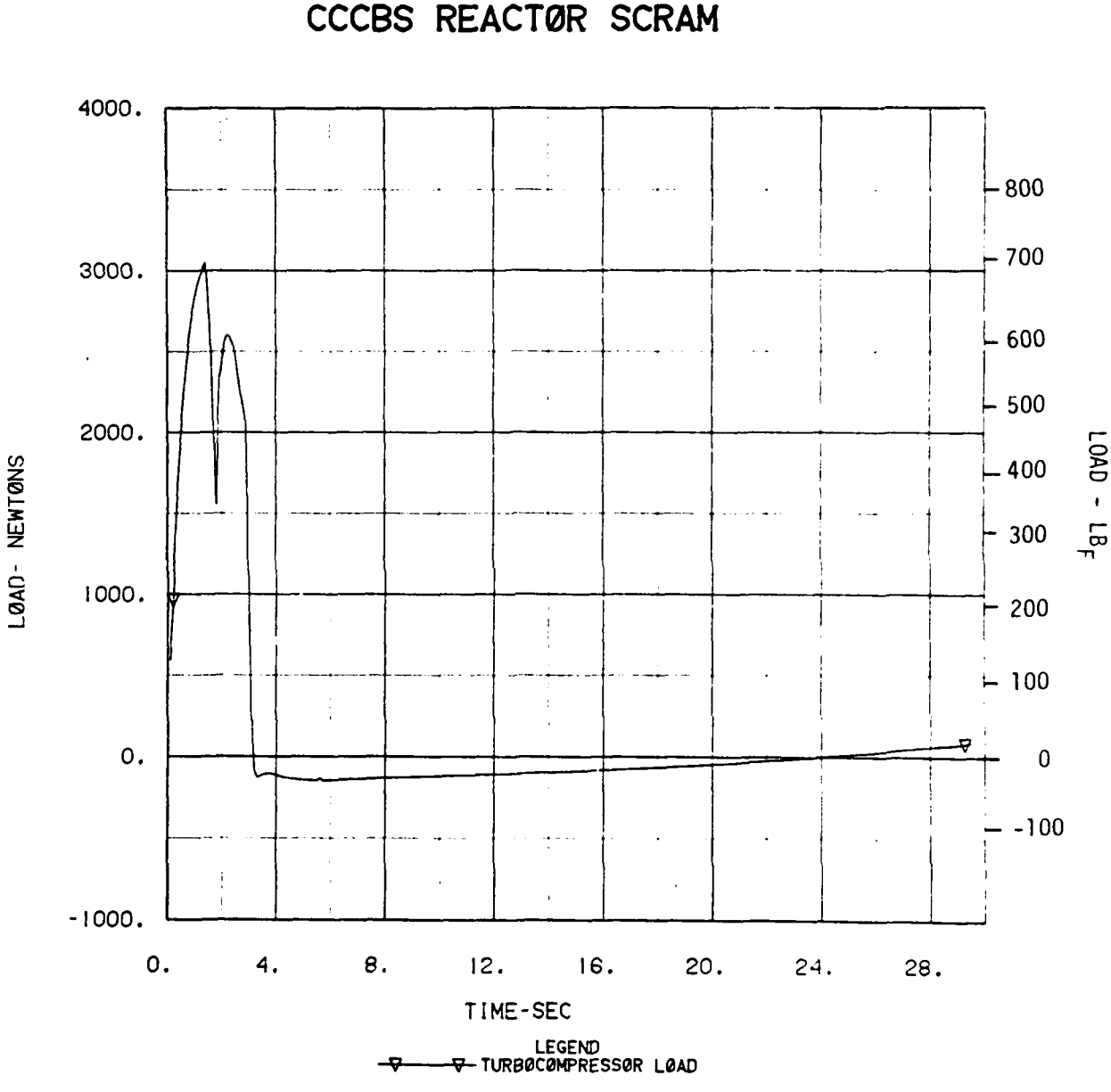

Figure 6-37. Turbocompressor Thrust Bearing Load

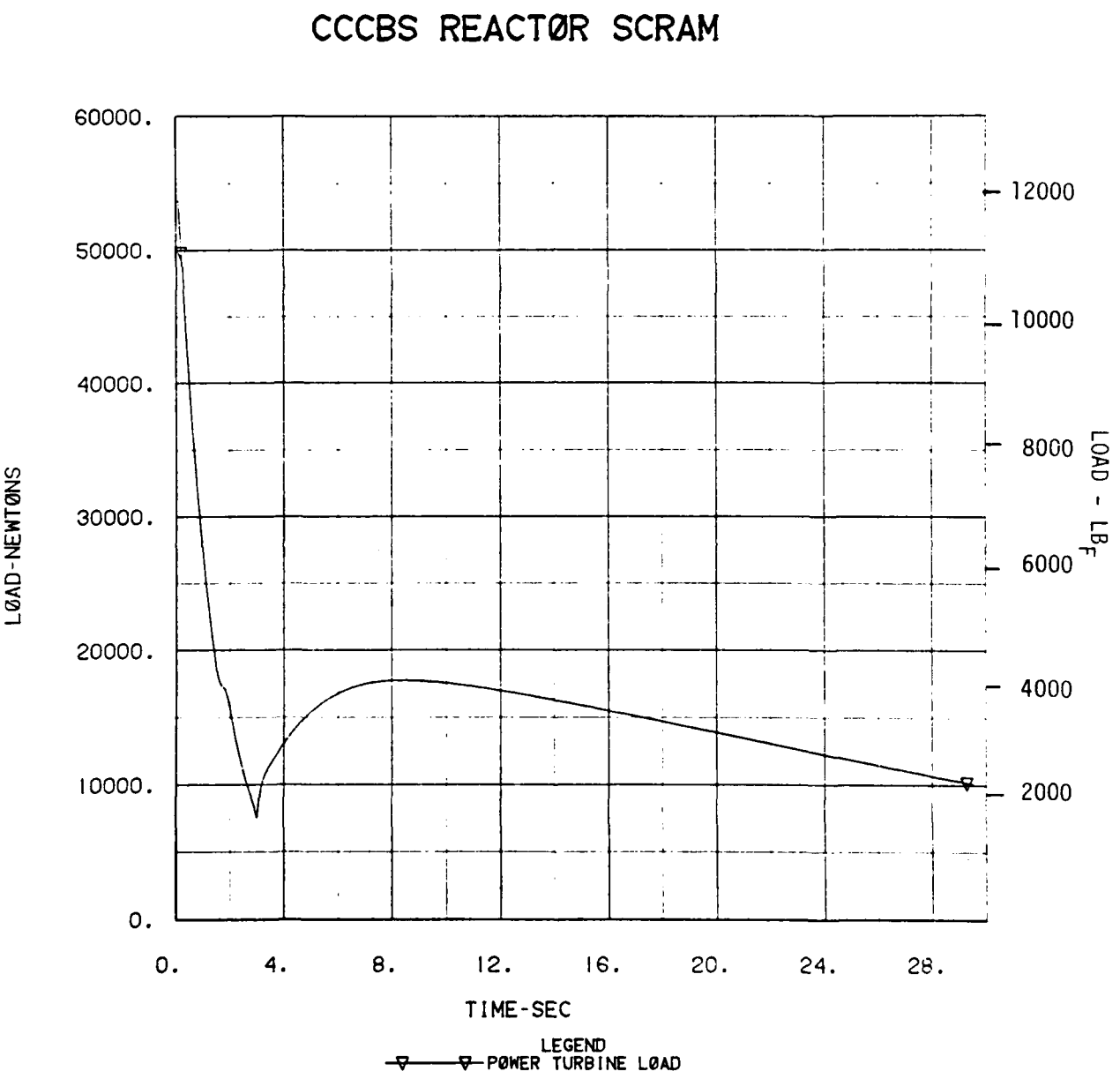

Figure 6-38. Power Turbine Thrust Bearing Load

As the inventory flow decreased the turbomachinery helium inventory, the system pressures, speeds, and flowrates also dropped sharply (Figures 6-33, 6-34 and 6-35). Following the stoppage of the inventory flow at 3.5 seconds, an increase was noted in all these parameters due to the restabilization of the flowrates through the system. The helium that would have been dumped to the inventory bottle during inventory control was now allowed to circulate back through the reactor and then through the turbomachinery again (Figure 6-35). This can also be seen in the drop in the reactor outlet temperature after 3.5 seconds, due to the increased reactor flow.

The turbocompressor thrust bearing load (Figure 6-37) exhibited a behavior similar to that noted in the previous transients. The bearing load changed dramatically when inventroy control was either initiated or stopped. After inventory control was halted, the bearing load started on a slow upramp from -125 Newtons (-25 lb). The power turbine thrust load (Figure 6-38) also behaved similarly to previous transients, roughly changing in the same manner as the power turbine speed.

6.1.2.4 FULL LOSS OF LOAD AT FULL POWER

The results for the complete loss of load at full power are shown in Figures 6-39 through 6-47. The transient is assumed to be a sudden and complete rupture of the power turbine output shafts. This scenario would be the most radical loss of load transient that would be experienced by the plant, and would bound the more likely cases of a loss of a propeller or fan blade with a direct mechanical drive, or a loss of electrical load for a motor-generator drive system. For both of these applications, the added inertia of the driven machinery would tend to reduce the rate of increase of the power turbine speed, and hence allow the control system to reduce the peak overspeed reached.

To simulate operation of a plant control system, a reactor scram signal was assumed to be generated upon the attainment of a 10% overspeed condition (110% of design speed) in the power turbine. A 1/4 second delay time was used to represent a typical delay between the signal initiation and the start of the control drum roll in. A maximum drum roll in rate of 180° per second was used, which is typical of a high temperature gas reactor and has been used in previous studies.

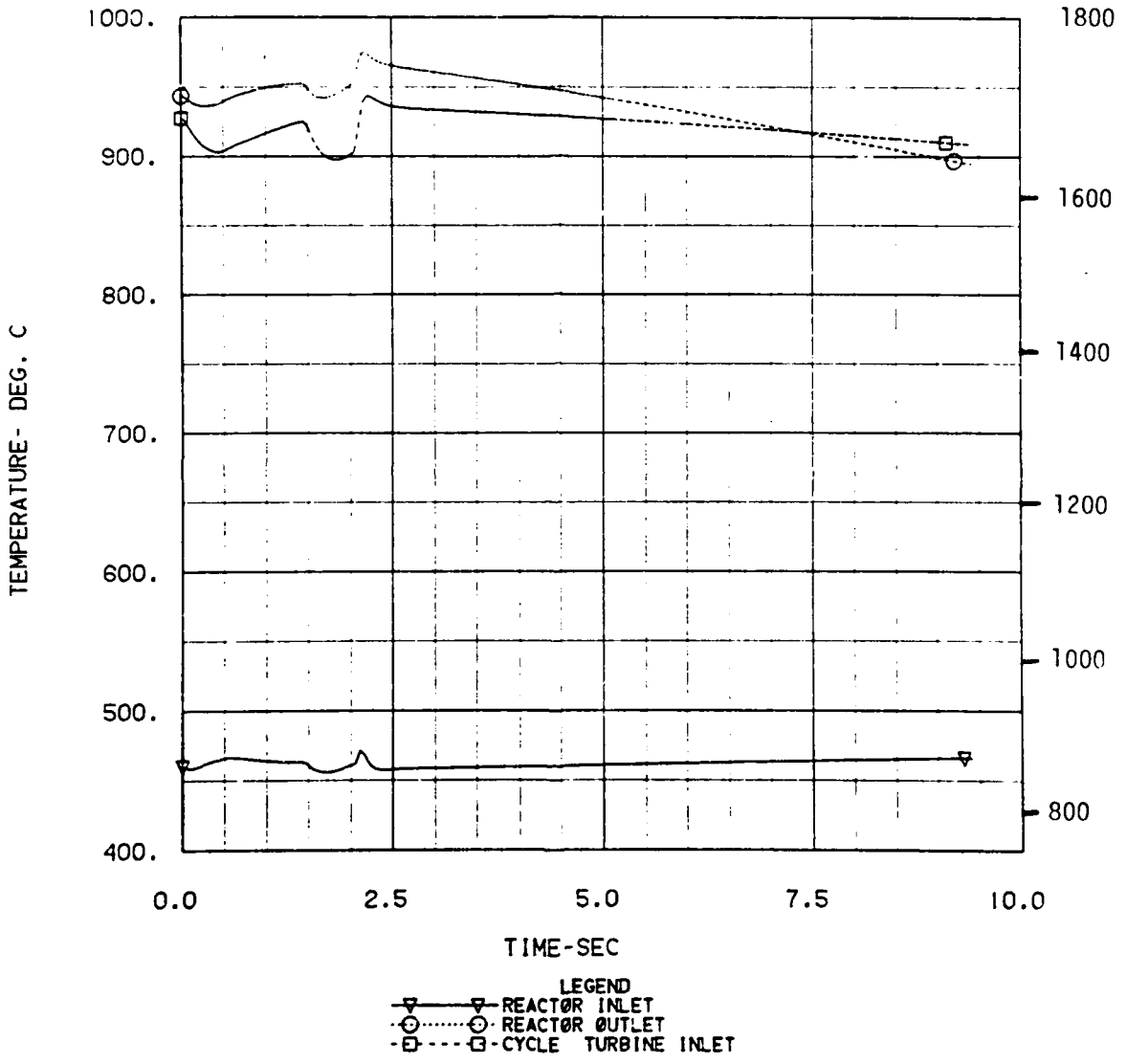

Figure 6-39. Reactor Helium Temperatures

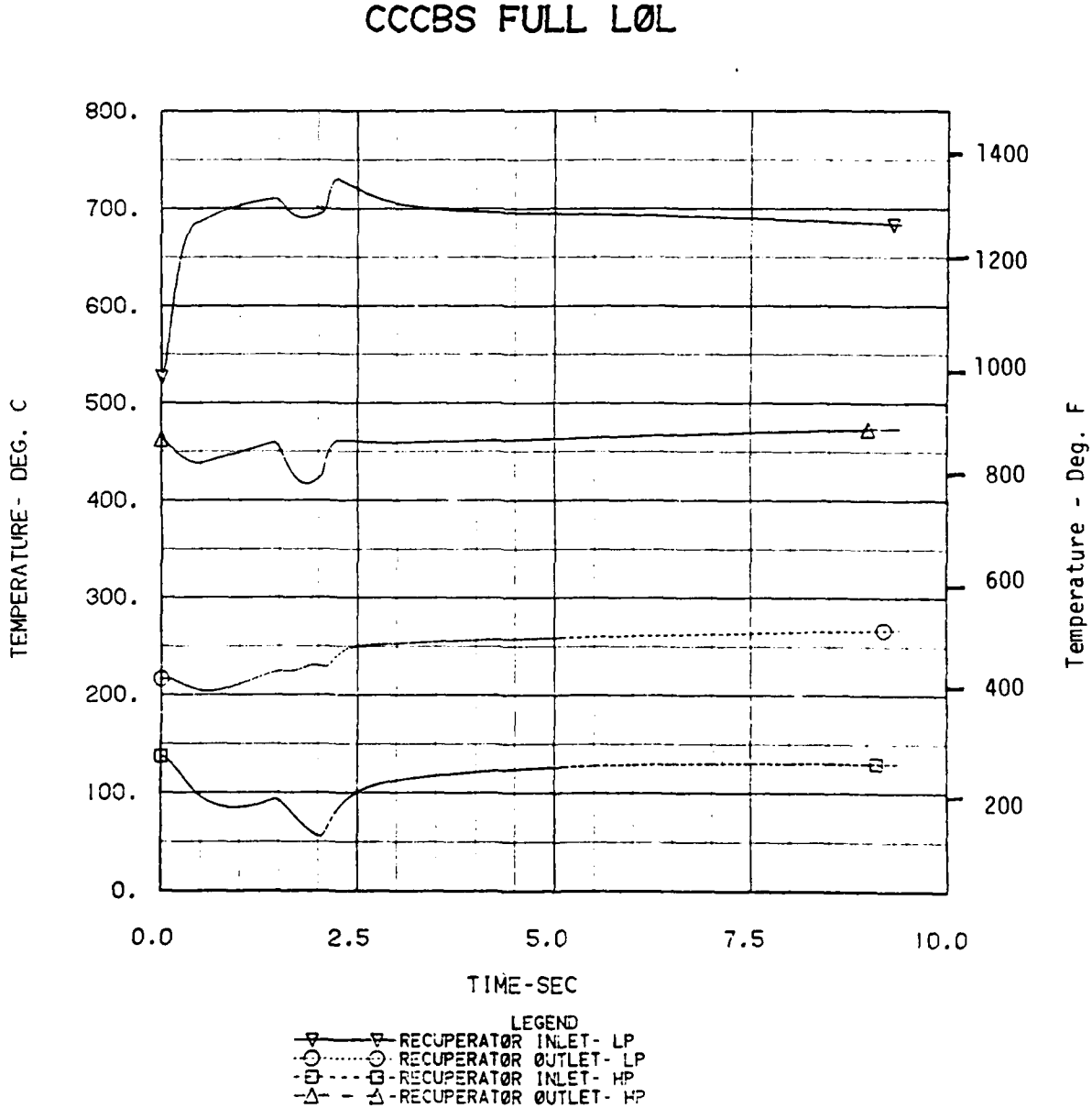

Figure 6-40. Recuperator Helium Temperatures

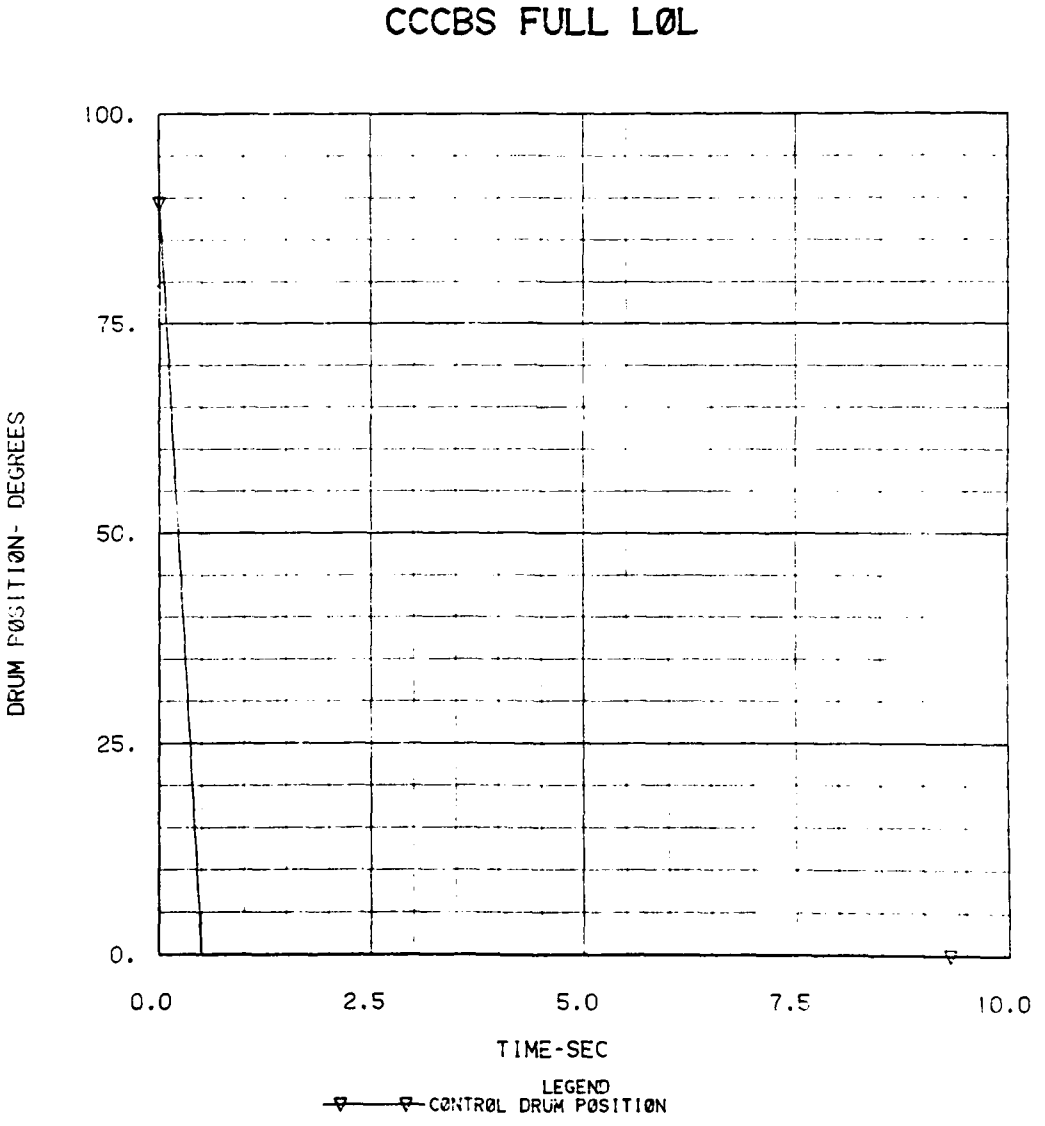

Figure 6-41. Control Drum Position

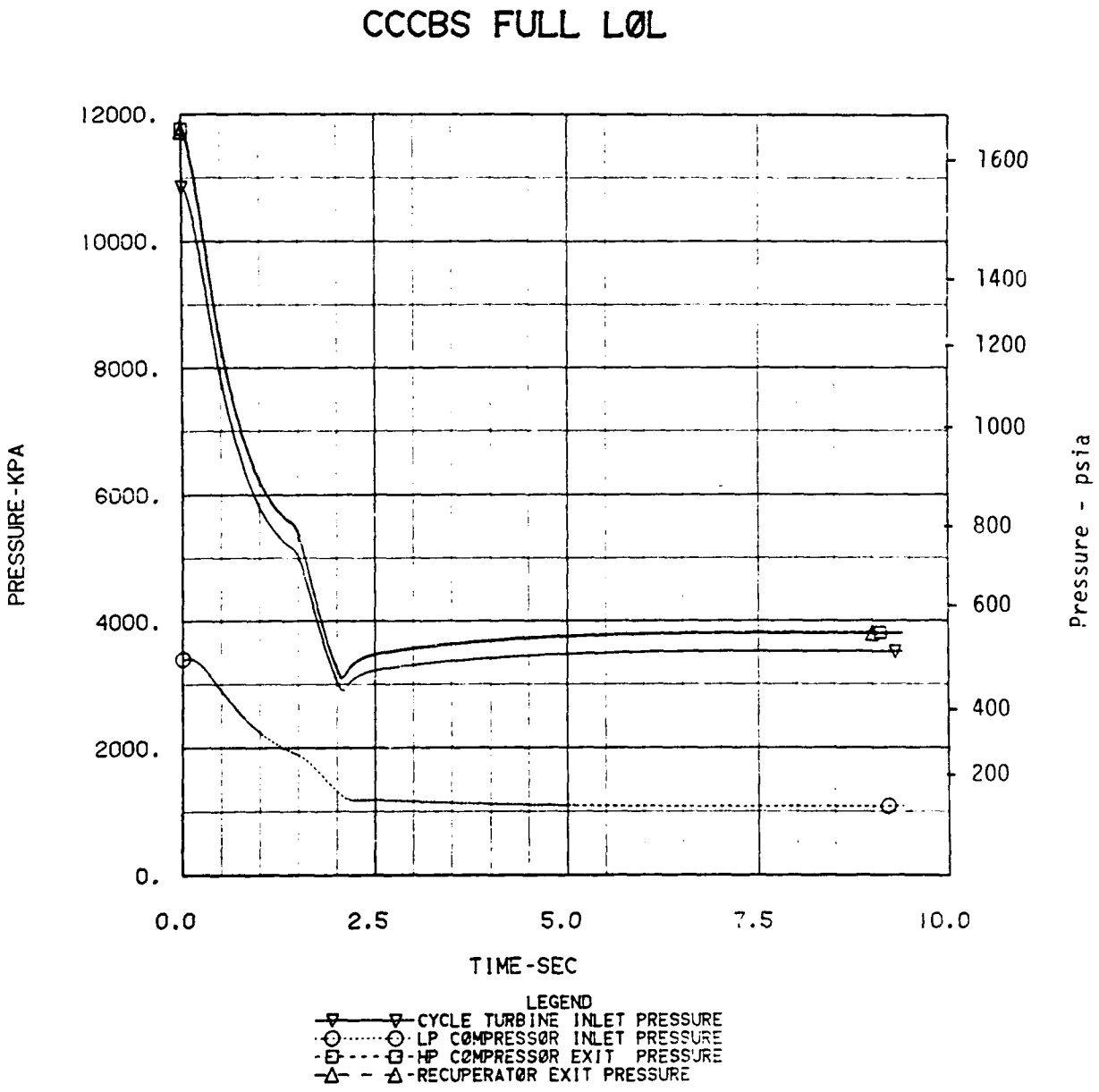

Figure 6-42. Turbomachinery Pressures

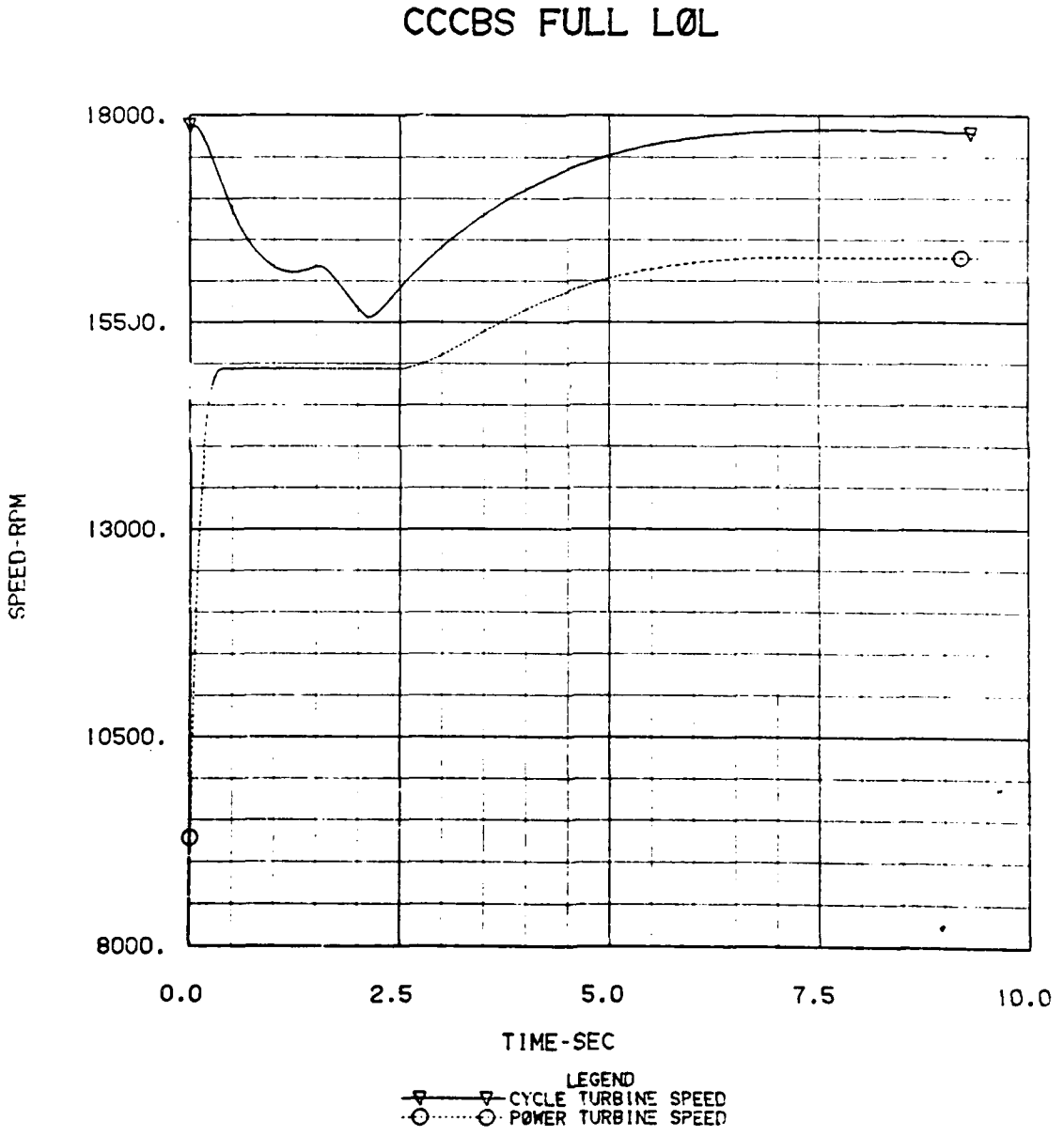

Figure 6-43. Turbomachinery Speeds

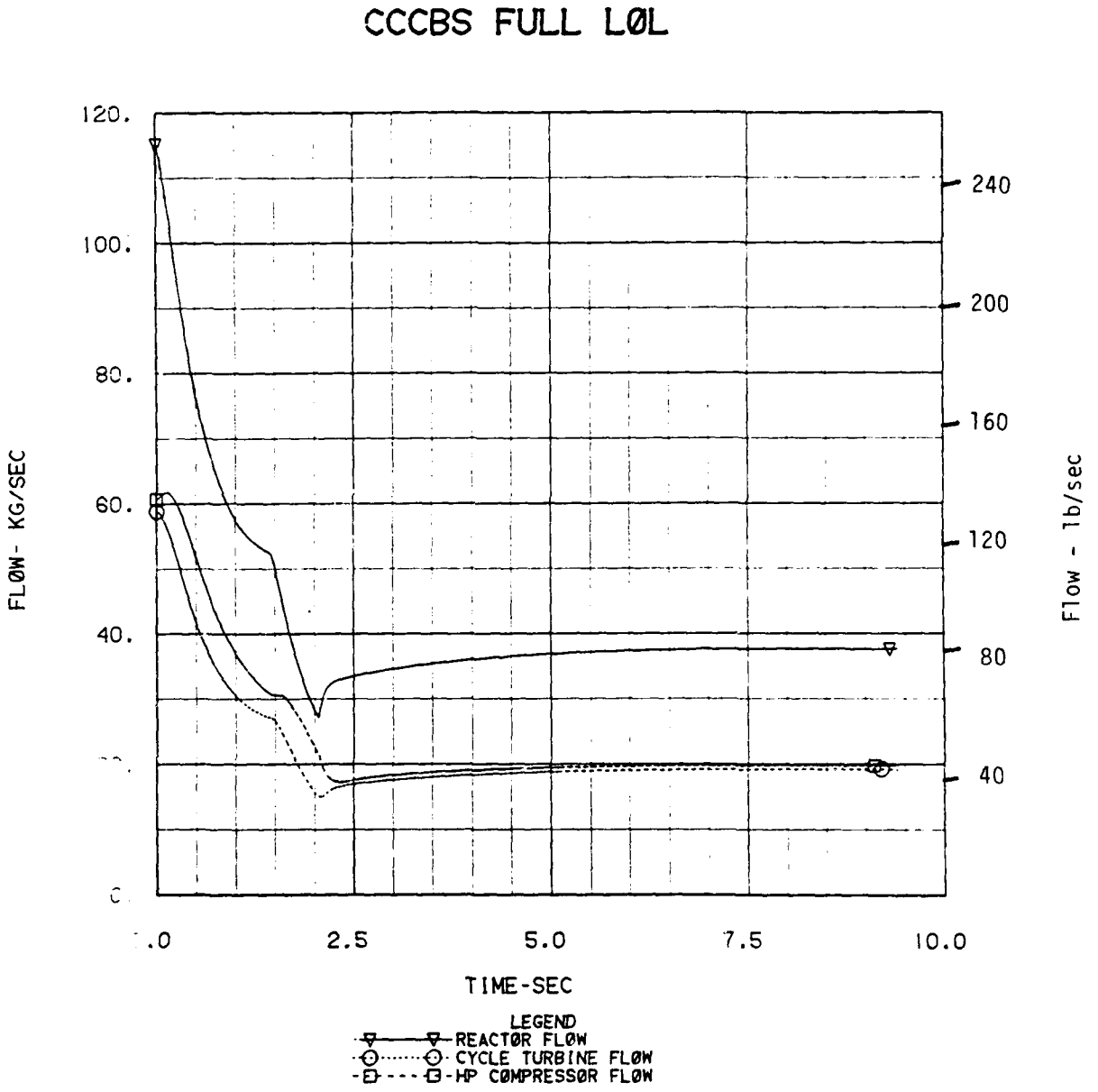

Figure 6-44. Turbomachinery Flows

CCCBS FULL LØL

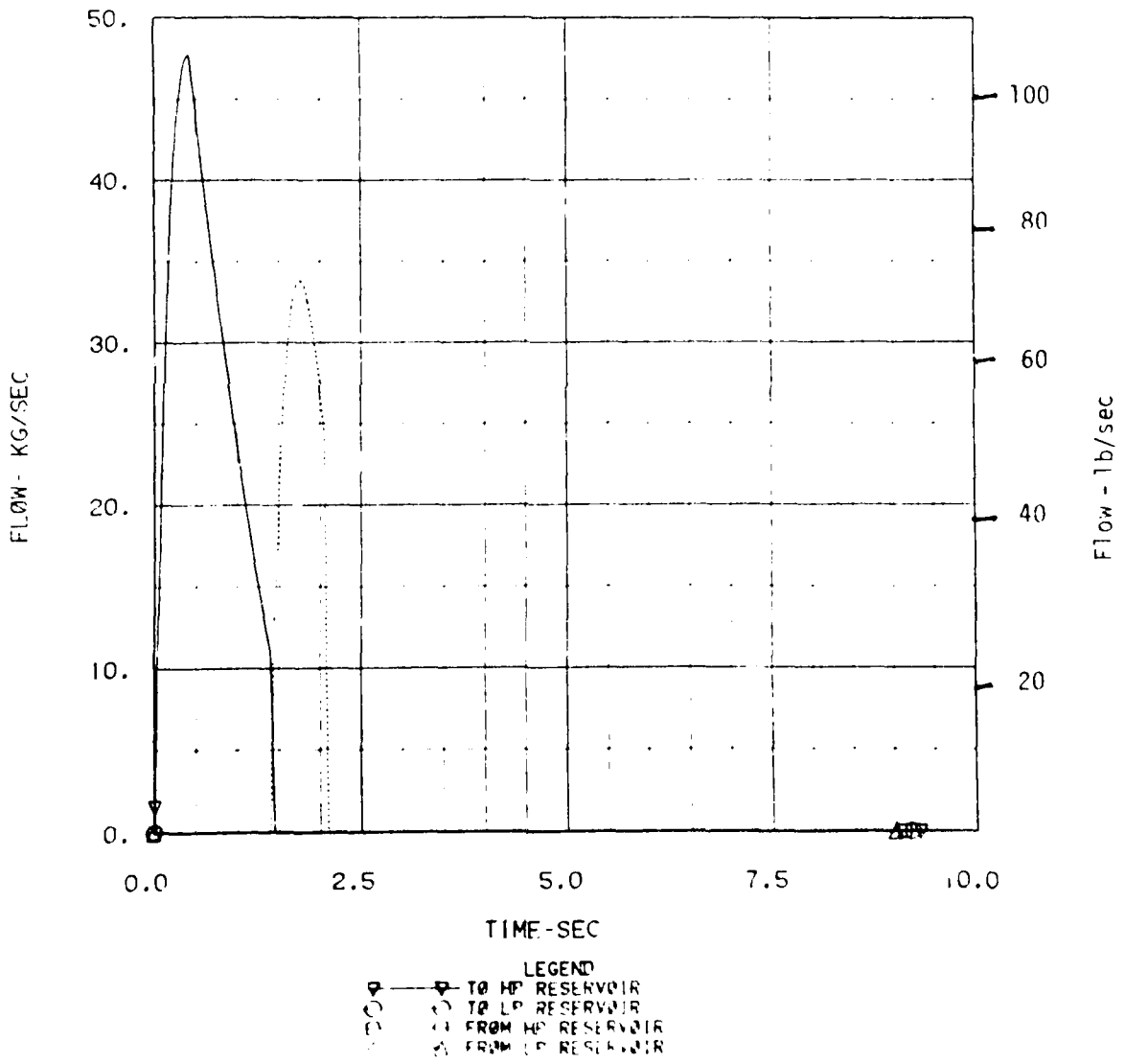

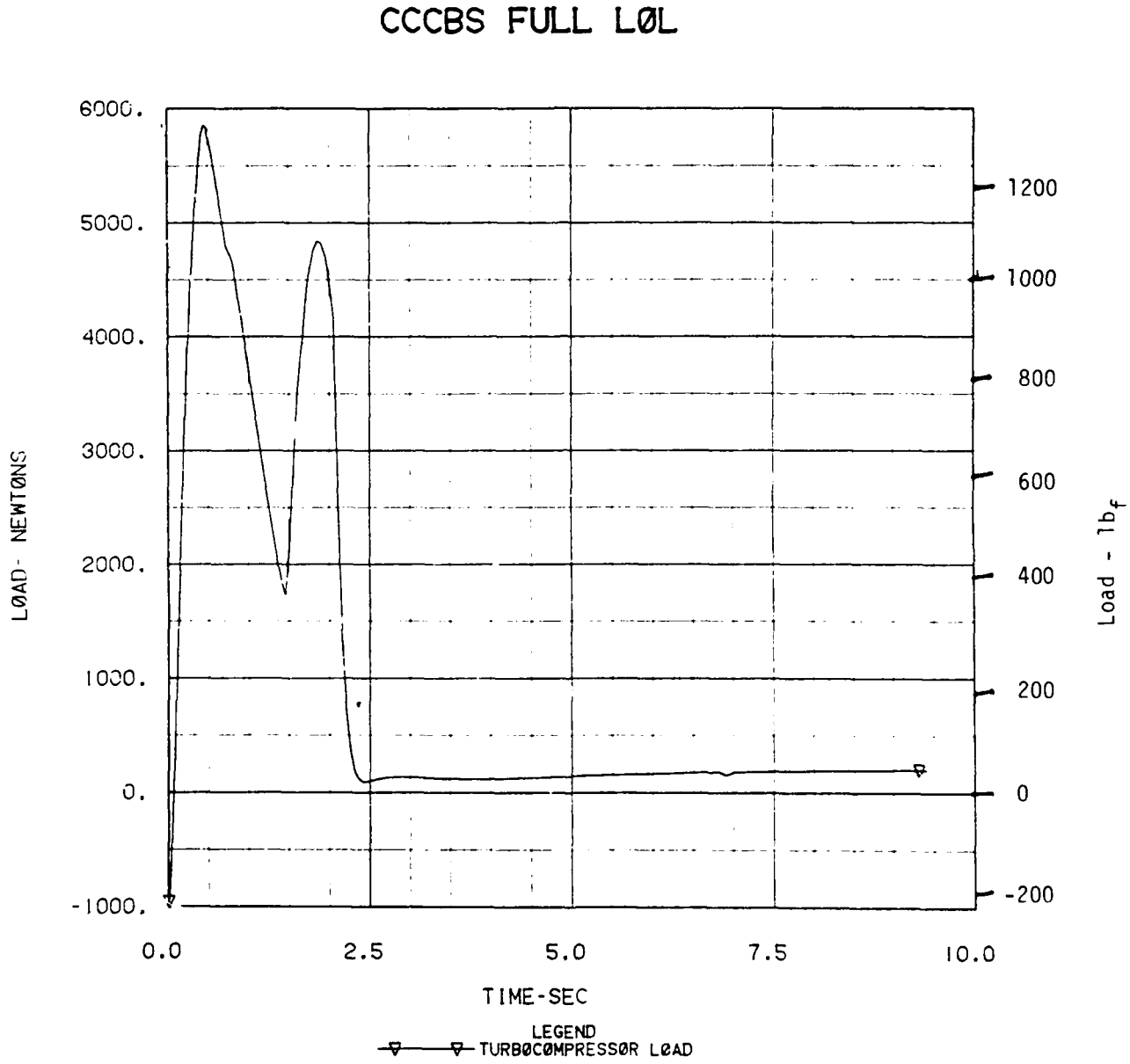

Figure 6-46. Turbocompressor Thrust Bearing Load

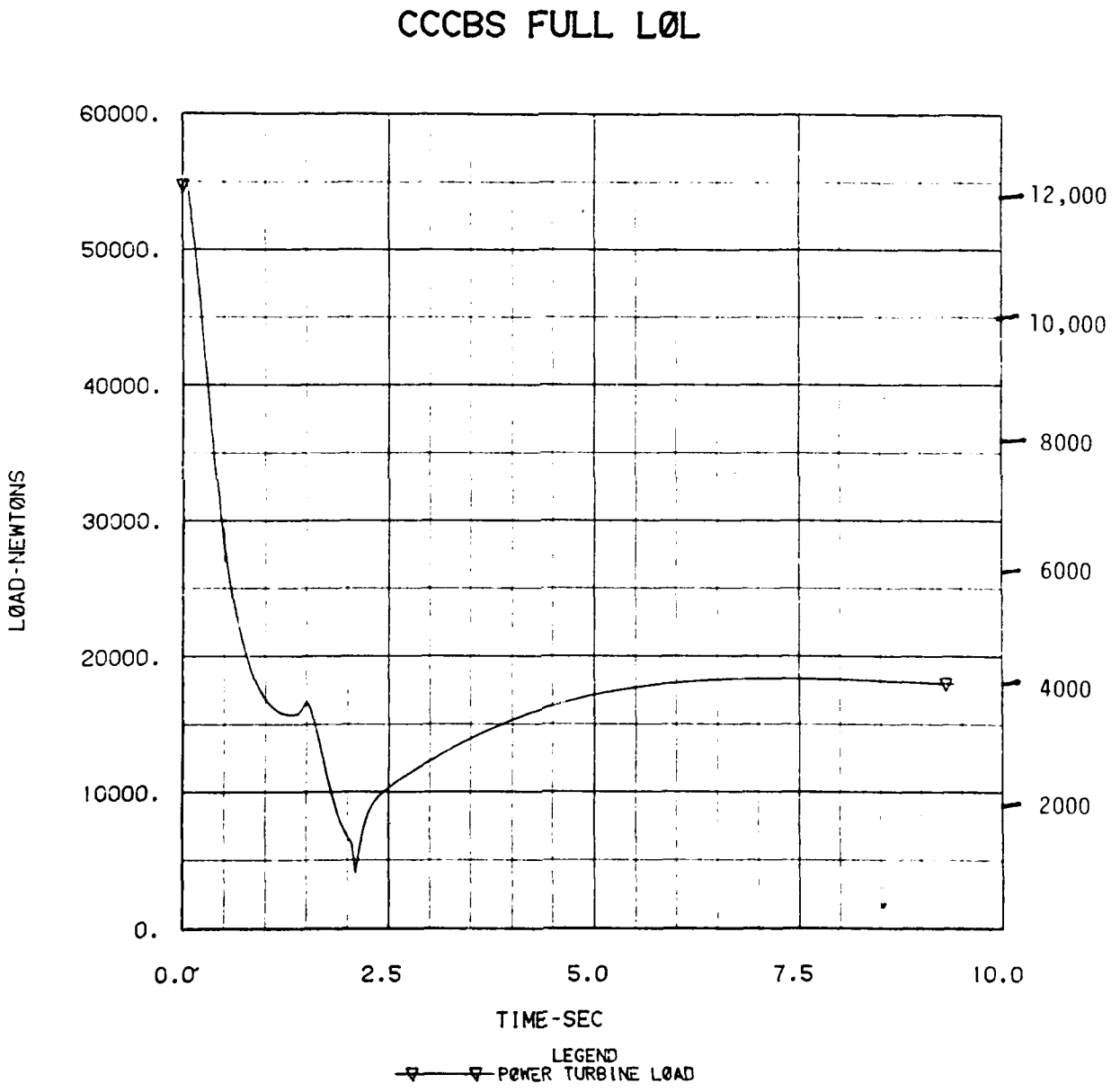

Figure 6-47. Power Turbine Thrust Bearing Load

The sudden loss of load caused a rapid increase in the power turbine speed (Figure 6-43). This caused the reactor scram signal to be generated almost immediately (Figure 6-41), and tended to initially reduce the reactor exit temperature (Figure 6-39). As the overspeed opened the inventory valves, the turbomachinery flows were reduced (Figure 6-44) as the flow was diverted to the inventory bottles (Figure 6-45). Due to the reactor decay heat and the heat capacity of the reactor and plug shields, the ramprate of the reactor exit helium temperatures (Figure 6-39) tended to alternately increase and decrease as the inventory flow changed the reactor power-to-flow ratio.

As the inventory flow increased, more of the compressor exit flow was diverted to the inventory bottles. This reduced the cycle and power turbine flowrates, and caused the system pressure levels to drop (Figure 6-42). In addition, the flowrate difference between the cycle turbine and the compressor (Figure 6-42) caused a reduction in the cycle turbine speed (Figure 6-43).

The turbine efficiency characteristic can be approximated by an equation like:

where

$$\eta_t = \eta_d \, (2X - X^2)$$

$$X = \frac{N}{N_d}\sqrt{\frac{\Delta T_d}{\Delta T}}$$

$$\Delta T = T_i \left(1 - \left(\frac{P_e}{P_i}\right)^{\frac{\gamma - 1}{\gamma}}\right)$$

The subscript (d) represents the design conditions, which is the full-power operating point for the reference case.

As the turbine speed increased, the variable X tended to increase to a value of about 2.0, at which point the efficiency dropped to zero. This initially occurred at about 0.5 seconds, where the power turbine speed had increased to about 14,900 RPM, about a 67% overspeed condition (Figure 6-43). Once the inventory flow was shut off at 2.5 seconds, the power turbine speed again started to increase due to the reestablishment of a flow equality in the turbines and compressor. This increased the peak overspeed to about 16,250 RPM, which is about an 80% overspeed condition.

The turbocompressor thrust bearing loads are shown in Figure 6-46. The general characteristics were as described previously, with large changes in the bearing load with inventory flow. The peak thrust load was about 5800 KPa (840 lb), and occurred about 0.5 seconds into the transient. In addition, the thrust load reversed direction, intially being -1000 KPa (minus being defined as toward the compressor and turbine outlets), then reversing direction and reaching a peak of +5800 KPa.

The power turbine thrust bearing load (Figure 6-47) tended to change in a similar manner to the system pressures (Figure 6-42). Up to 2.5 seconds, the thrust load tended to decrease sharply as the inventory flow reduced the system pressures. Past this point, the thrust load increased as the compressor and turbine flows rebalanced, increasing the cycle turbine work and the pressure level between the compressor exit and power turbine inlet.

The 80% overspeed condition appears as if it would possibly lead to design problems in the power turbine to safely accommodate this load. As a result, methods other than the one described were analyzed to determine the performance of alternate schemes of overspeed protection.

The first method tried was using a larger inventory control valve to evacuate the system faster. The peak RPM reached during inventory control was about 59% overspeed in comparison with the 67% overspeed stated previously. However, once the inventory bottles were full, the restabilization of the system once again brought the overspeed up to the 80% value reported previously. As a result, changing the inventory valve characteristic alone does not result in any reduction in the overspeed condition.

Another method available is to alter the design point of the power turbine so that the peak efficiency point does not occur at the full power point. This has the disadvantage of reducing the plant efficiency at full power, but this is offset by an efficiency increase felt when operating at the design point. For the case analyzed, the design point was taken to be at 95% of the full-power operating condition. This reduced the peak overspeed reached to about 60% over the full power speed of 9000 RPM. At the same time the full power plant efficiency was

reduced by about 1% of the reference value of 36.73%. In the actual plant, the design point would be determined by the application of the CCCBS and the expected operating times at each power level.

Both of the above designs needed no additional hardware to perform their functions; they are part of the basic design of the CCCBS. If it is deemed necessary, however, a bypass control system could be added to solely serve as an overspeed protection. The usual method is to bypass part of the compressor exit flow back to the power turbine exit, thus bypassing the reactor and the turbines. While this case has not been analyzed expressly, the results from the Inventory Control Valve 2 Failure Case (Section 6.1.2.6) closely simulated a bypass controller. For this case, the helium flow was essentially "short-circuited" from the compressor exit, through the inventory bottle, and back to the low pressure exit side of the recuperator. This flow starved the power turbine, and caused the speed to drop. In a loss of load case, this bypass condition would reduce the power turbine pressure ratio and flow and allow the zero efficiency point to be reached at a lower RPM. A conservative estimation would be that the overspeed could be limited to the 67% value obtained during inventory control. It would appear that a 67% overspeed condition could be accommodated by the present power turbine configuration with no major redesign being needed.

6.1.2.5 CONTROL VALVE 1 FAIL OPEN AT 100% POWER

The results for the control valve 1 fail open case are shown in Figures 6-48 through 6-56. The transient is an assumed malfunction in either the control valve or its associated logic, which causes the valve to stay in the full-open position. This would most likely occur during a reduction from full power operation, when the system helium inventory is being dumped to the high pressure bottle through control valve 1. (See Figure 6-1).

The large inventory flow through the failed full-open valve caused a sharp pressure reduction in the system (Figure 6-51), as well as a rapid reduction in the system flowrate (Figure 6-52). This flowrate reduction caused the reactor control drums to move fully in (Figure 6-50) in order to try to maintain the reactor outlet temperature at its 945°C (1730°F) setpoint (Figure 6-48).

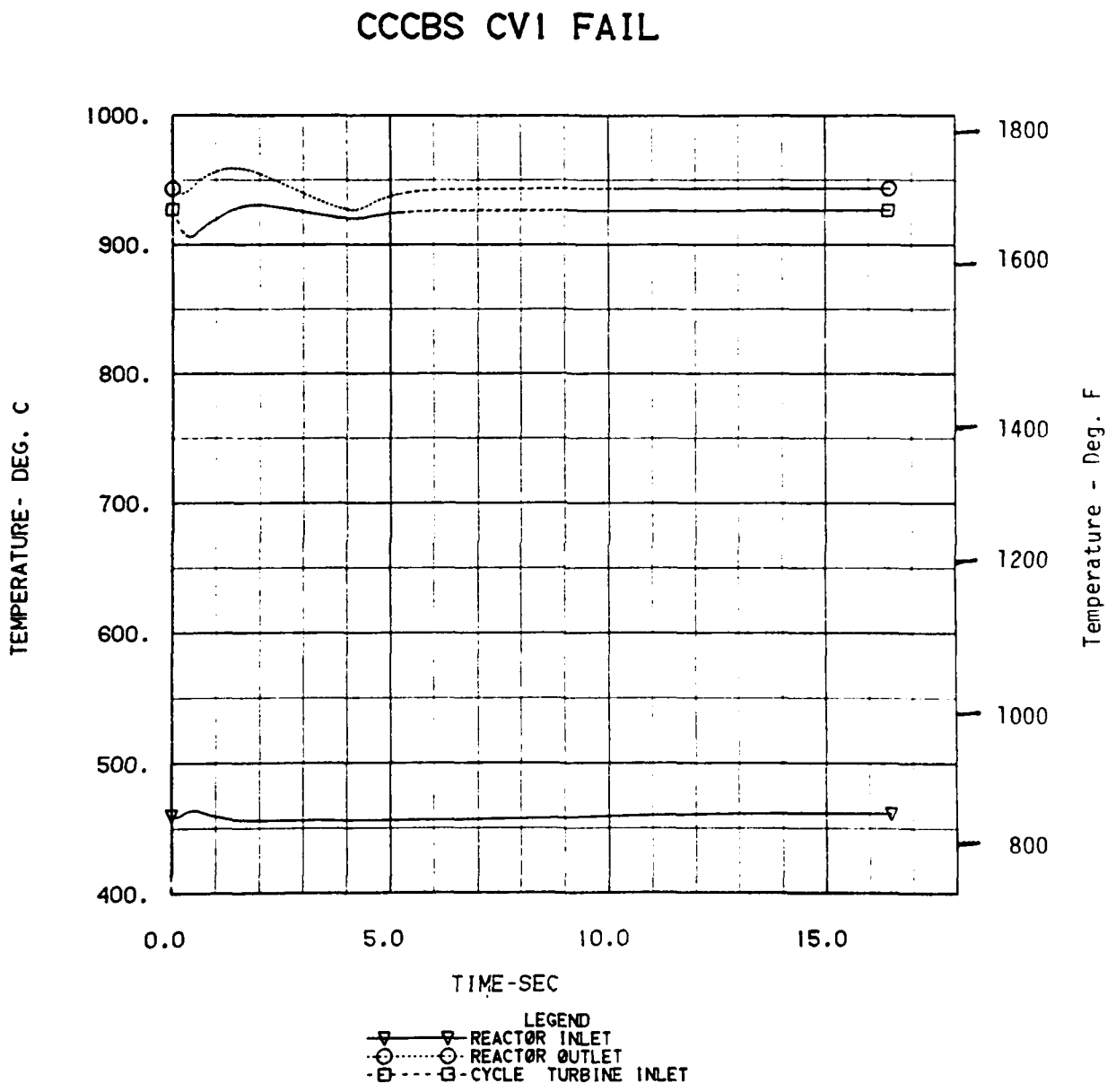

Figure 6-48. Heat Source Temperatures

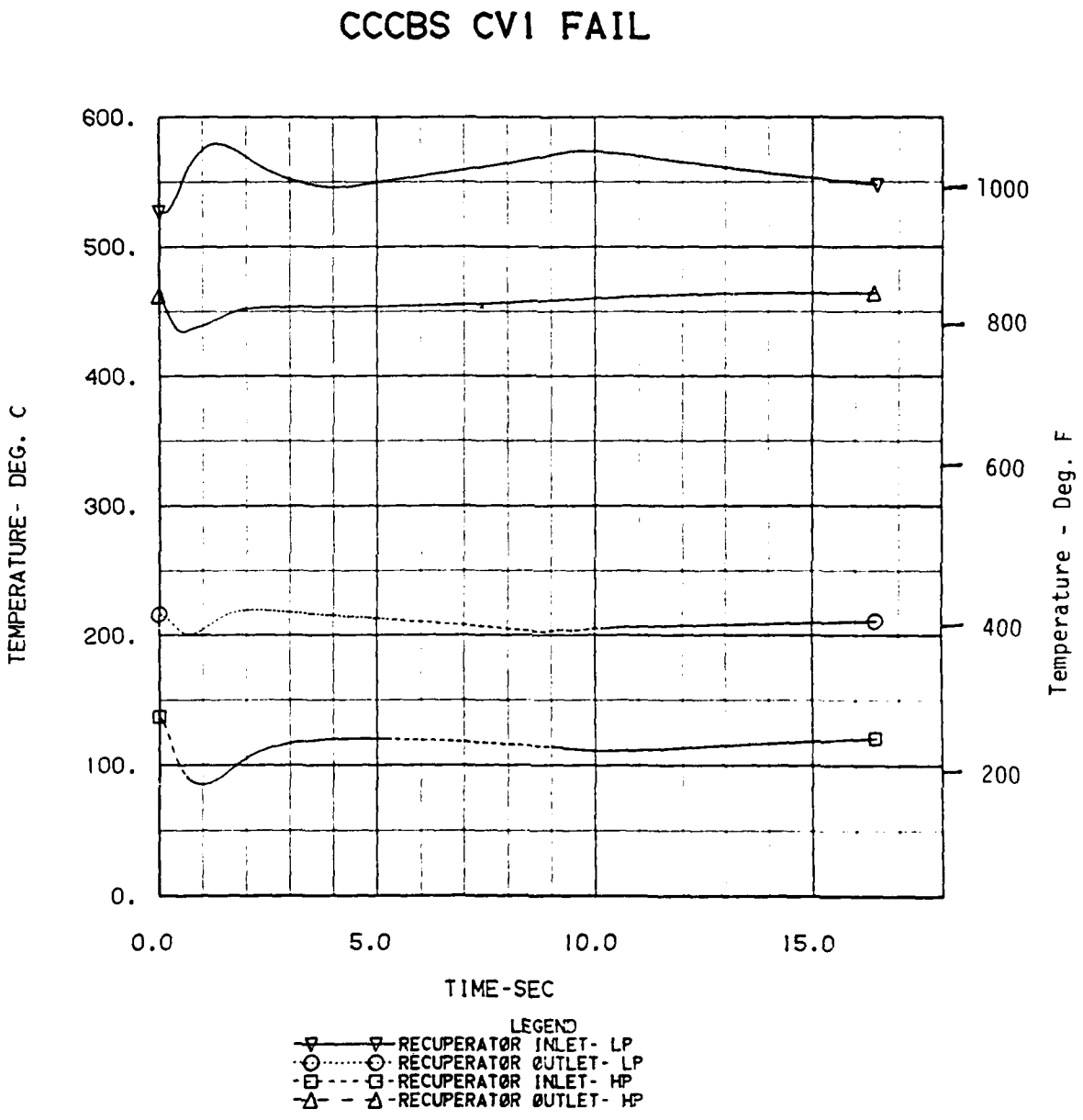

Figure 6-49. Recuperator Gas Temperatures

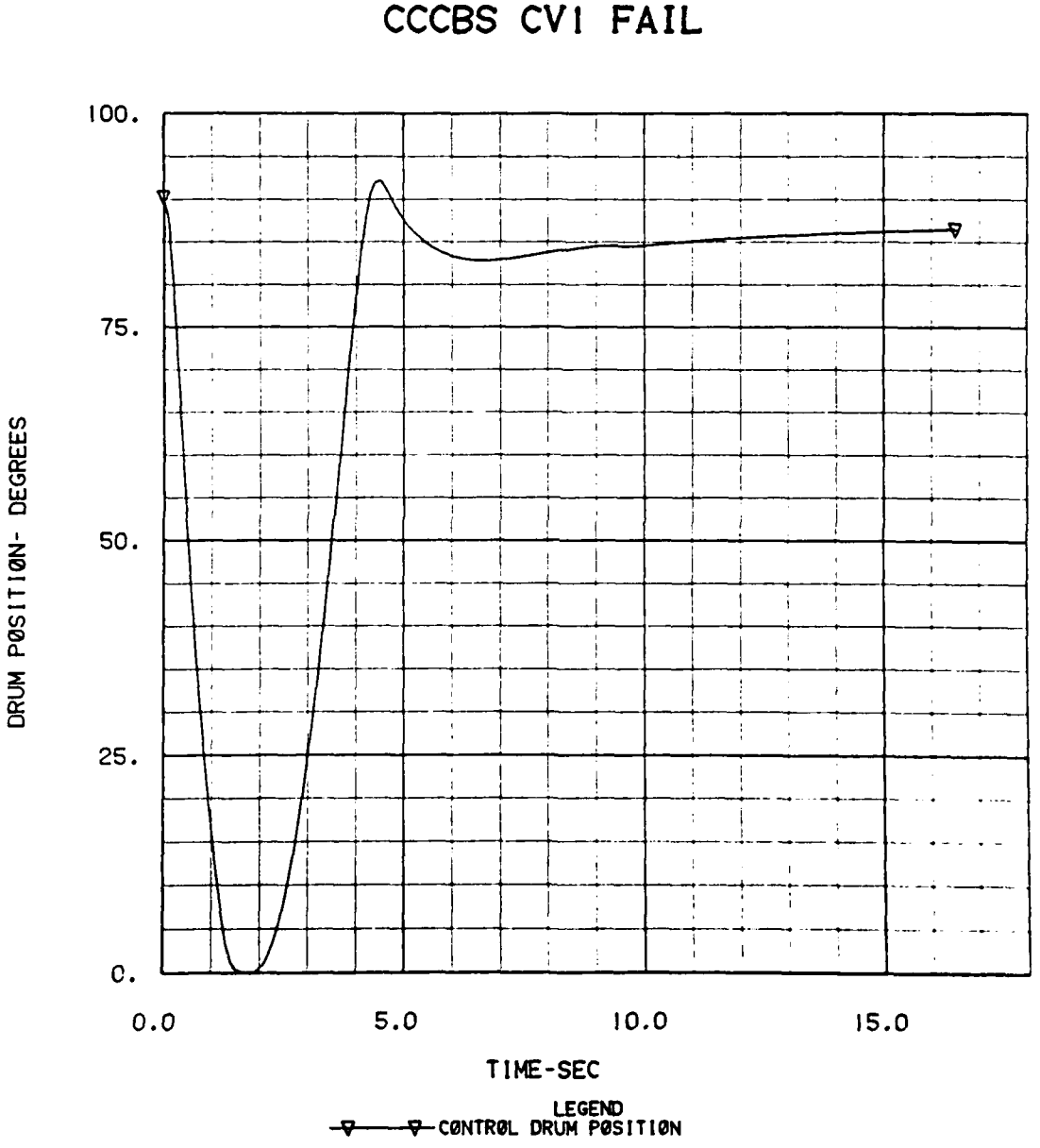

Figure 6-50. Control Drum Position

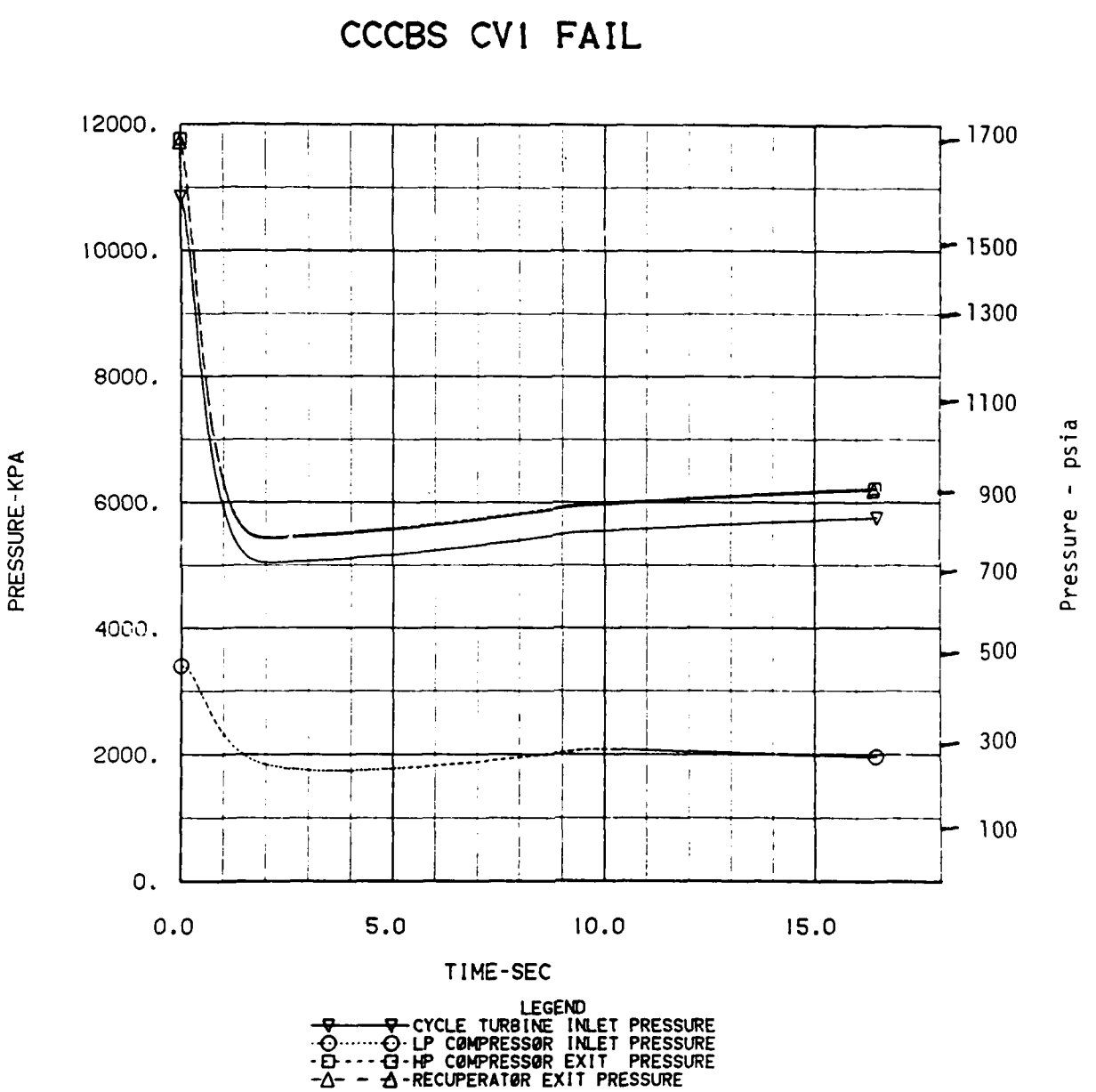

Figure 6-51. Turbomachinery Pressures

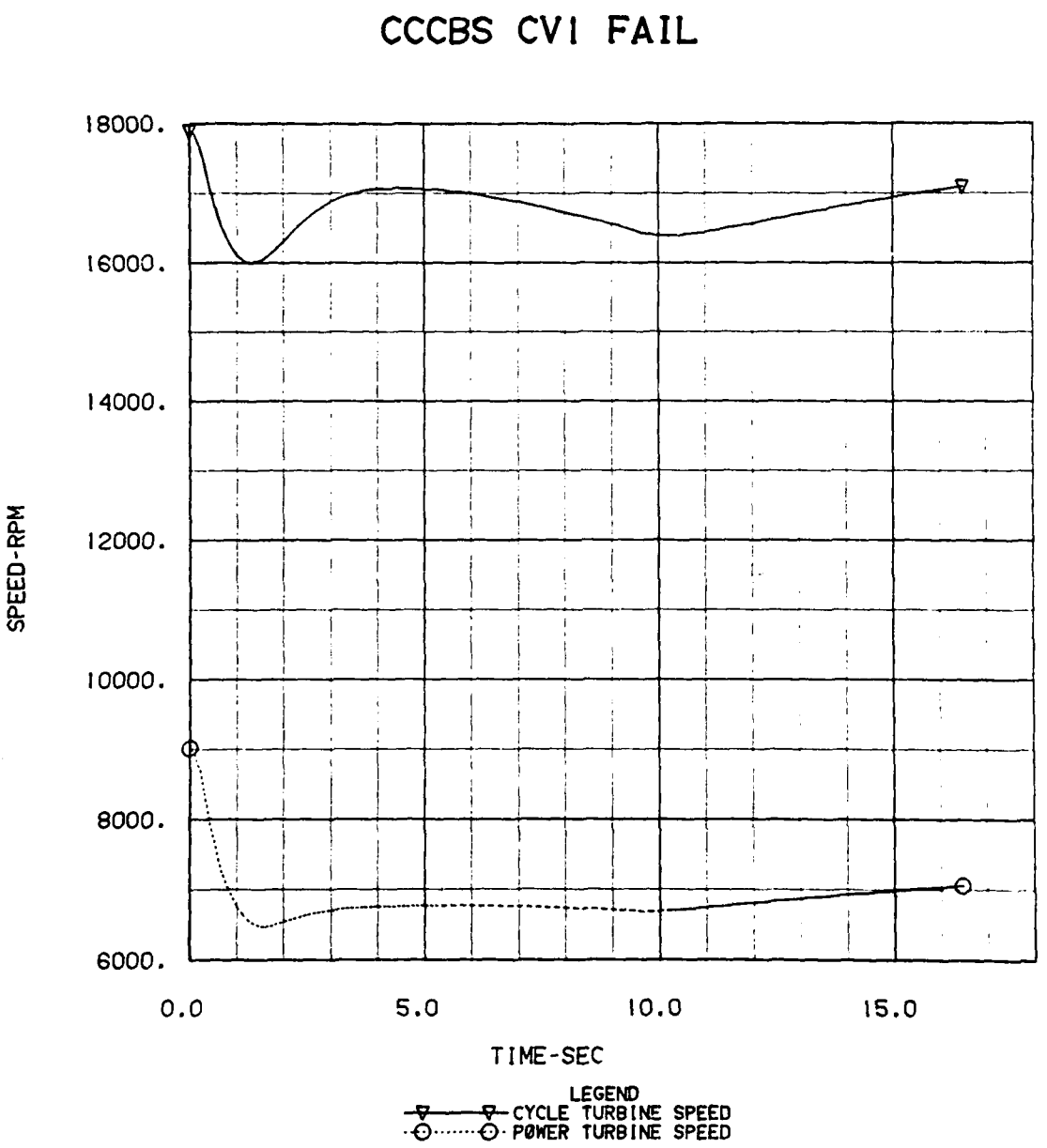

Figure 6-52. Turbomachinery Speeds

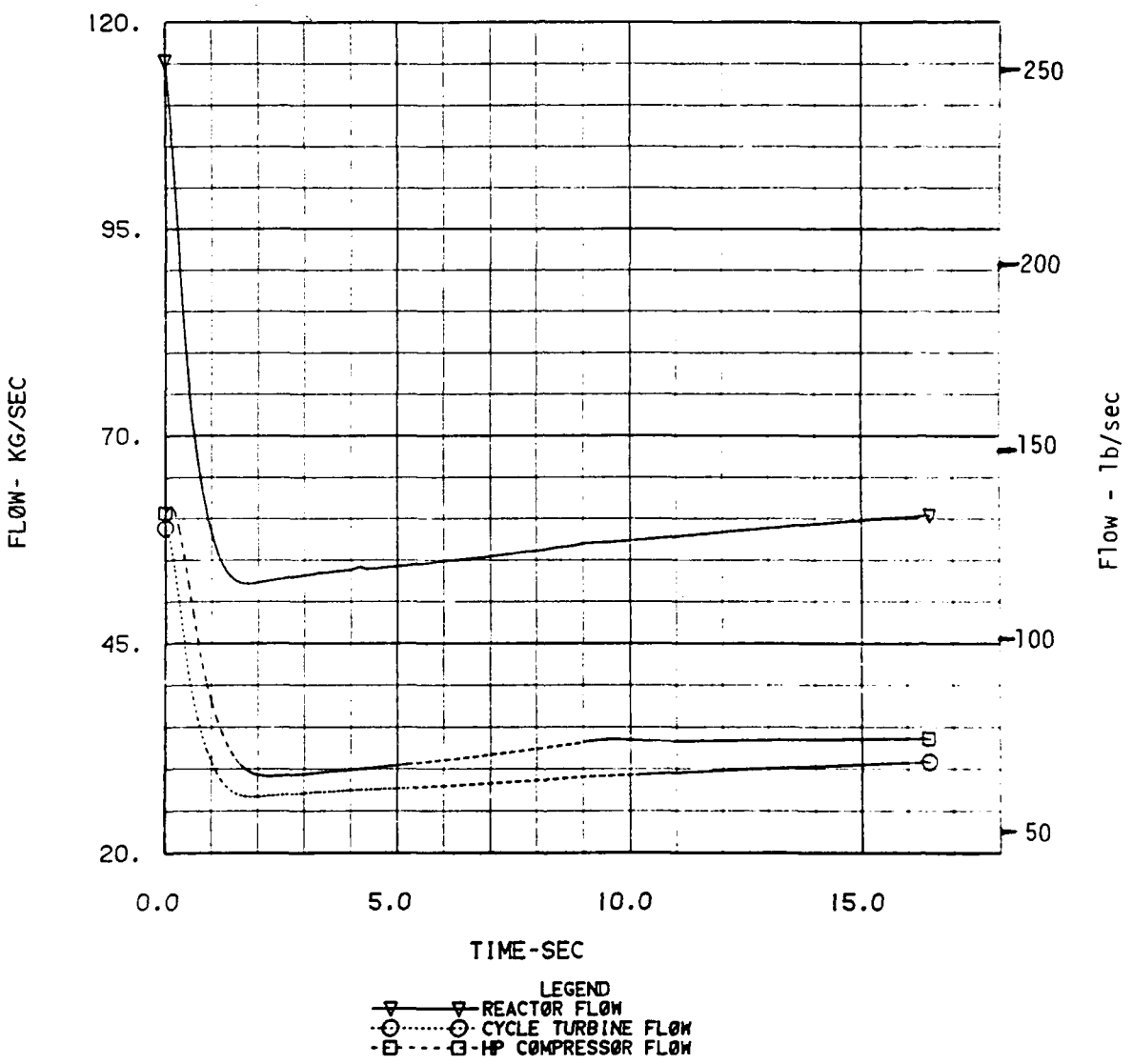

Figure 6-53. Turbomachinery Flow Rates

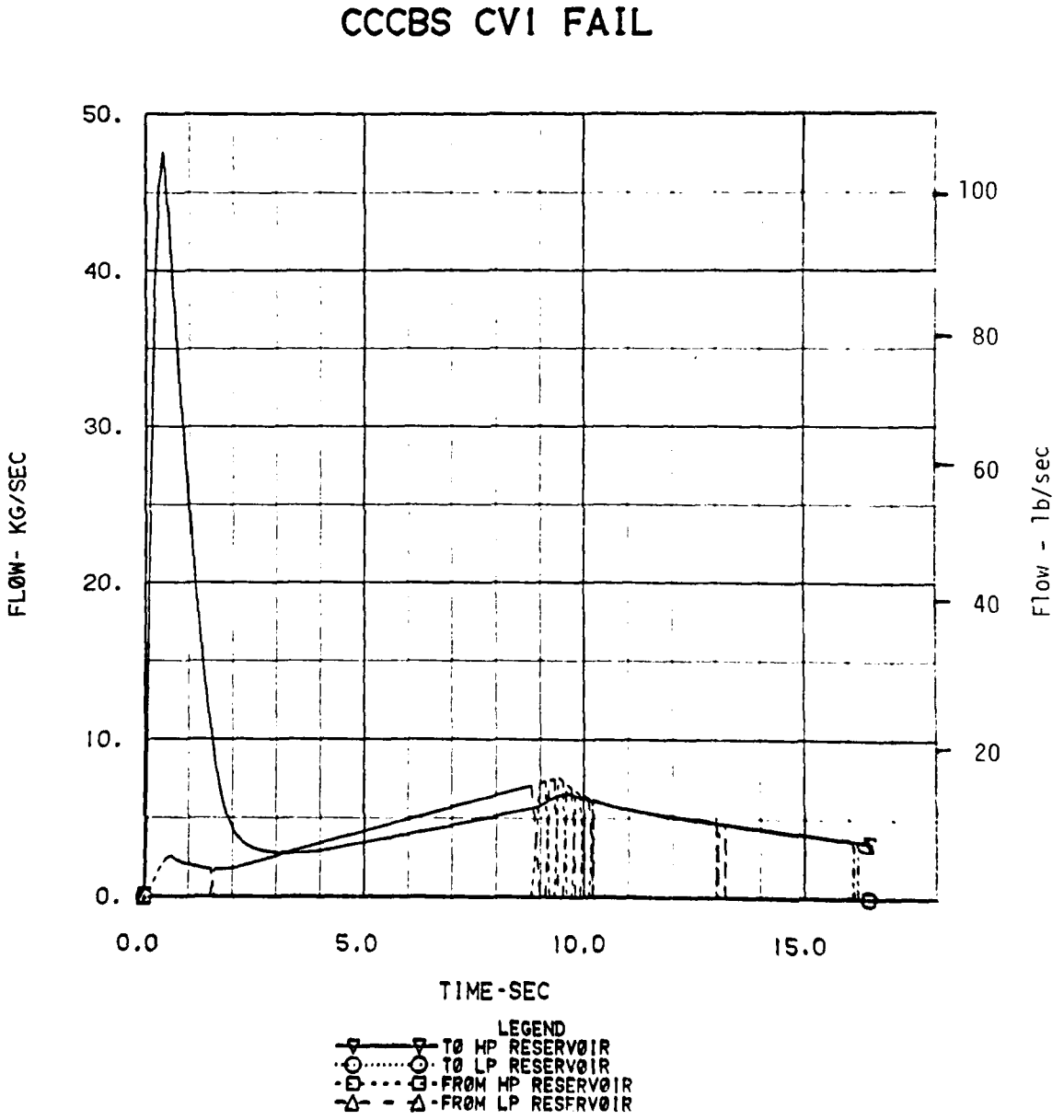

Figure 6-54. Inventory Flow Rates

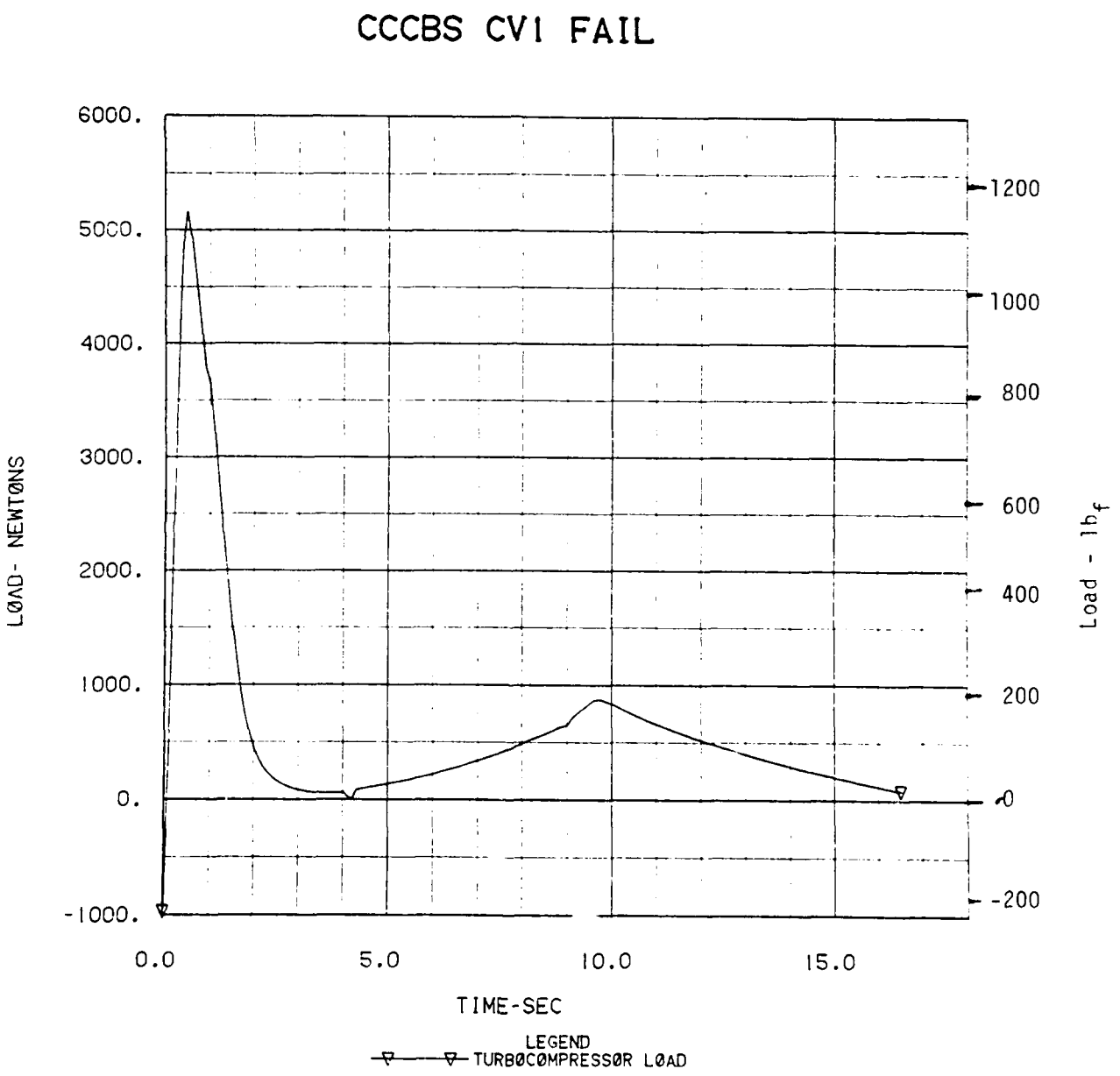

Figure 6-55. Turbocompressor Thrust Bearing Load

AD-A081 380 WESTINGHOUSE ELECTRIC CORP PITTSBURGH PA ADVANCED ENE--ETC F/G 20/13
COMPACT CLOSED CYCLE BRAYTON SYSTEM FEASIBILITY STUDY. VOLUME I--ETC(U)
AUG 79 R E THOMPSON, R L AMMON, R CALVO N00014-76-C-0706
UNCLASSIFIED WAES-TNR-237-VOL-2 NL

2 OF 6
AD A081380

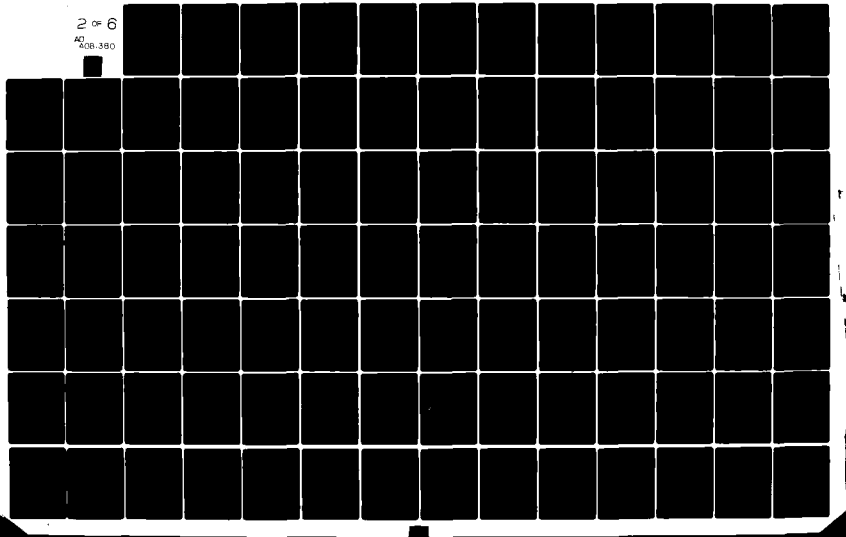

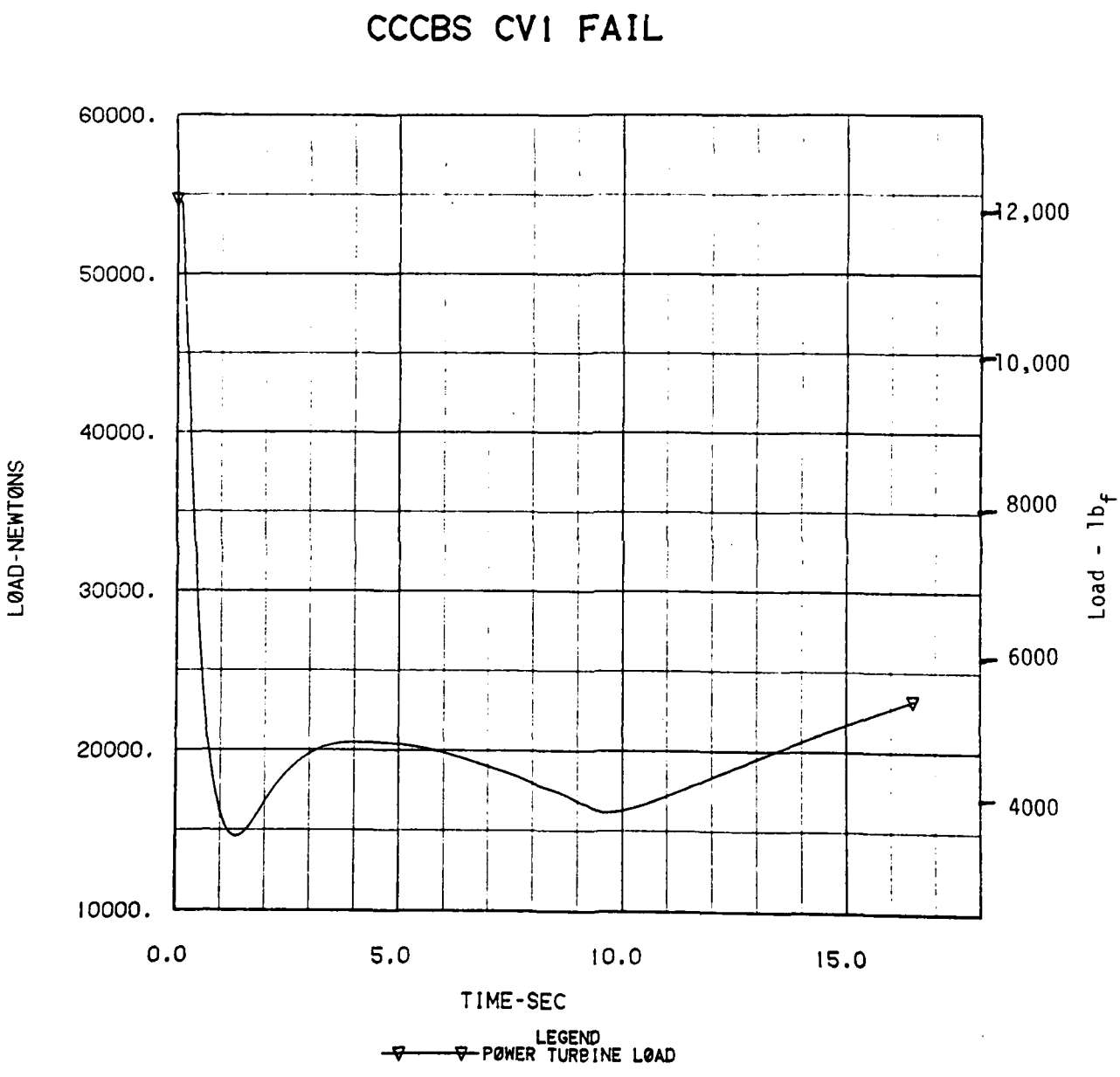

Figure 6-56. Power Turbine Thrust Bearing Load

This drastic a control drum movement would not be physically possible in the actual plant, and a reactor scram signal would be generated at about 1 second into the transient (due to the minimum operating drum position). This would result in the plant being shut down. However, the plant inventory would not be able to be reduced to the minimum 25% point due to some of the helium in the high pressure reservoir bleeding down to the low pressure reservoir through the failed control valve.

On the start of the transient, the inventory controller started bleeding helium back into the system from the high pressure tank. As the pressure differential between the compressor discharge and the high pressure inventory bottle decreased, the 170 KPa (25 psia) differential setpoint was reached at about 1.5 seconds. Flow was then bled into the system from the low pressure reservoir (Figure 6-54).

This was continued until about 9 seconds, when the 170 KPa setpoint was reached on the pressure differential between the low pressure inventory bottle and the precooler inlet. The source for the inventory flow being bled back into the system was then switched back to the high pressure bottle. This switching between the bottles continued for the rest of the transient.

In actuality this rapid switching would not occur. Only the high pressure bottle would be used as a source for the inventory bleed, and a steady-state would be reached with the flows being equal entering and leaving the bottle. The major difference in the results would be that the flowrates in and out of the high pressure bottle would both steady out at a value between 5 and 10 Kg/sec, (9 and 18 lb/sec). Since the net result of the transient would be a rapid throttle rampdown, the plant would stabilize at a power level slightly above the minimum possible with just the high pressure bottle (approximately 45% of the full power condition). This was the case for the analyzed transients.

The turbocompressor thrust bearing load (Figure 6-55) varied almost directly with the inventory flow through the failed control valve. The largest variations once again occurred during the periods of maximum inventory flow. The peak bearing load reached was almost 5 times the steady state full power value of -1000 Newtons. In addition, the bearing thrust reversed directions, resulting in a net change of 6000 Newtons (1300 lb_f) in less than a second.

The power turbine thrust bearing load (Figure 6-56) essentially varied directly with the power turbine speed (Figure 6-52). Since the peak bearing load occurred at full power, no special designing of the power turbine thrust bearing appears necessary to be able to withstand this transient.

Since the initial portion of the transient is essentially a rapid throttle rampdown, a comparison can be made between this case and the 10% per second throttle rampdown case analyzed previously. For the previous case, using a constant inventory flowrate of about 10% of the full-power helium inventory (about 9 Kg/sec) resulted in the power turbine output being reduced at about a 10% per second rate. Increasing the inventory flow to the maximum possible through the full-open control valve resulted in the turbine output being reduced initially at a 70% per second rate, then decreasing to zero at about 1.5 seconds as the net flow at the inventory bottles approaches zero. Therefore, rapid power reductions of upwards of 50% per second appear to be possible with a fossil fueled heat source, where there is no nuclear decay power which could cause problems in controlling the heat source outlet helium temperatures.

6.1.2.6 CONTROL VALVE 2 FAIL OPEN AT 25% POWER

The results for the control valve 2 fail open case are shown in Figures 6-57 through 6-65. The transient is caused by the assumed malfunction of the control valve logic or positioner, driving it open at a time when it is normally closed.

This would also bound the more likely case of the fail open of control valve 4, which would normally supply the inventory flow to the plant during a rampup from 25% power. (See Figure 6-1).

The sudden addition of helium to the system intially caused a rapid rise in the system pressures (Figure 6-60). The control system then tried to maintain the power level at a 25% level by dumping helium to the low pressure inventory bottle (Figure 6-63). The rapid pressure rise reduced the pressure differential between the low pressure inventory bottle and the compressor discharge to zero within 1 second of the start of the transient. Dumping was then switched to the high pressure reservoir.

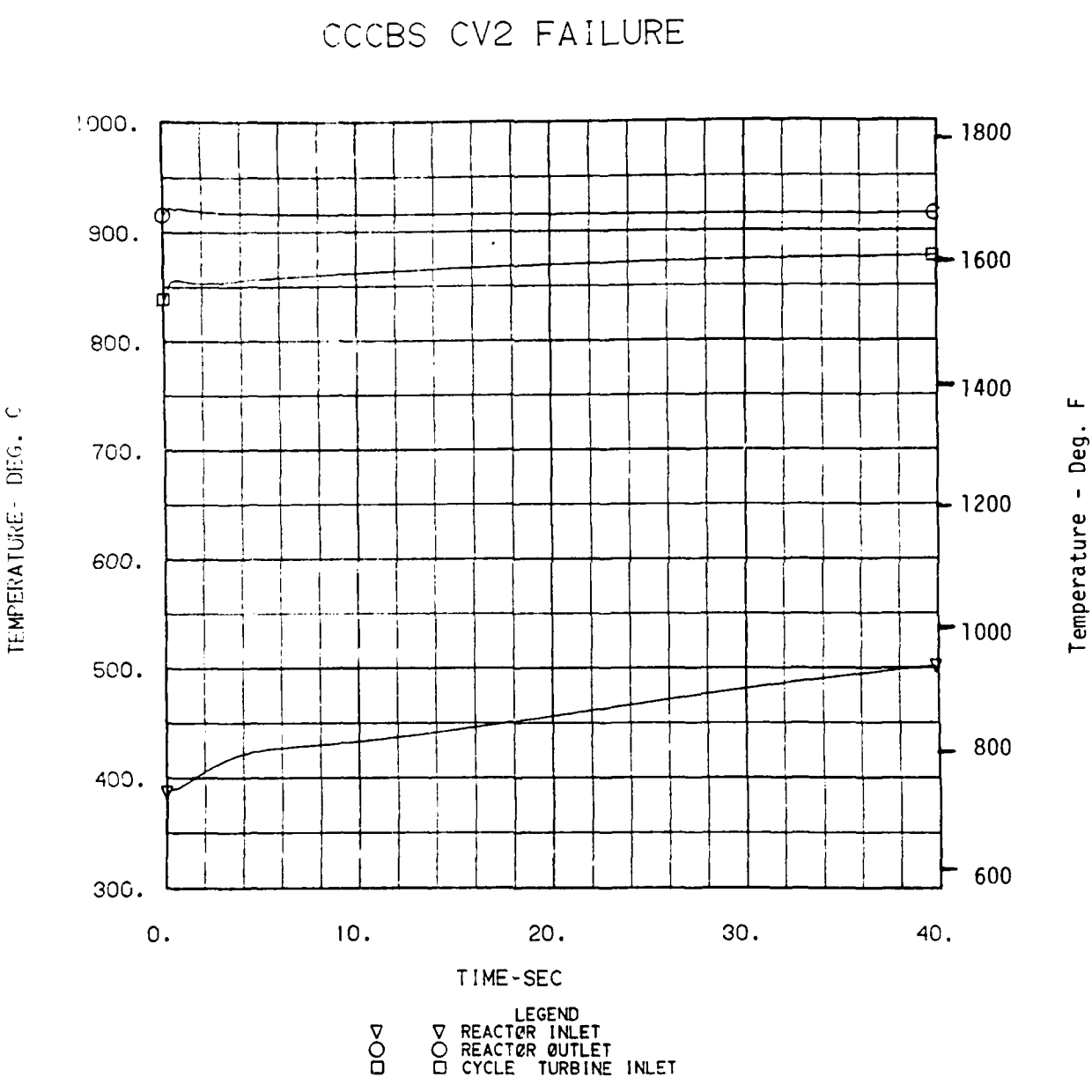

Figure 6-57. Heat Source Temperature

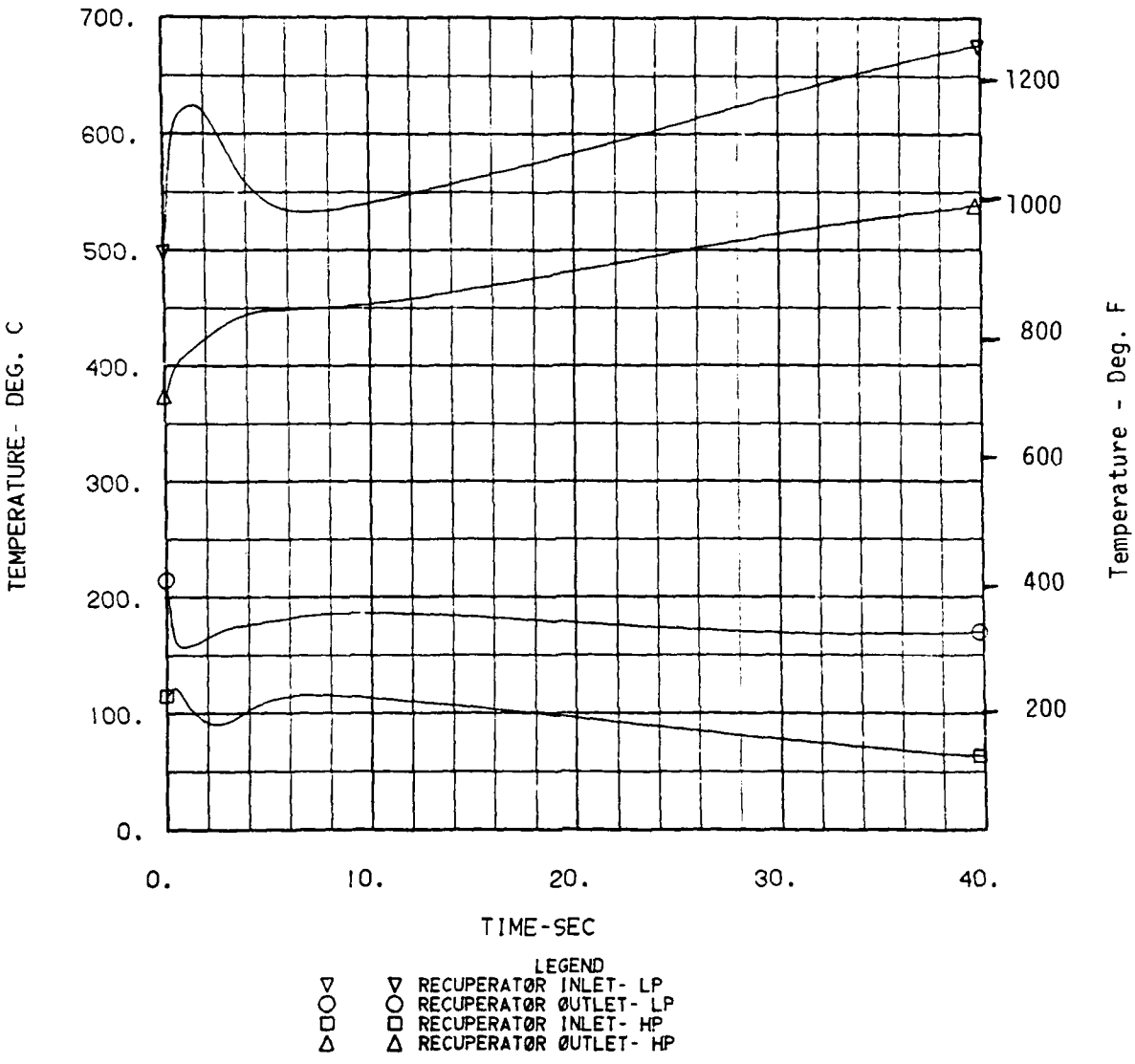

Figure 6-58. Recuperator Gas Temperatures

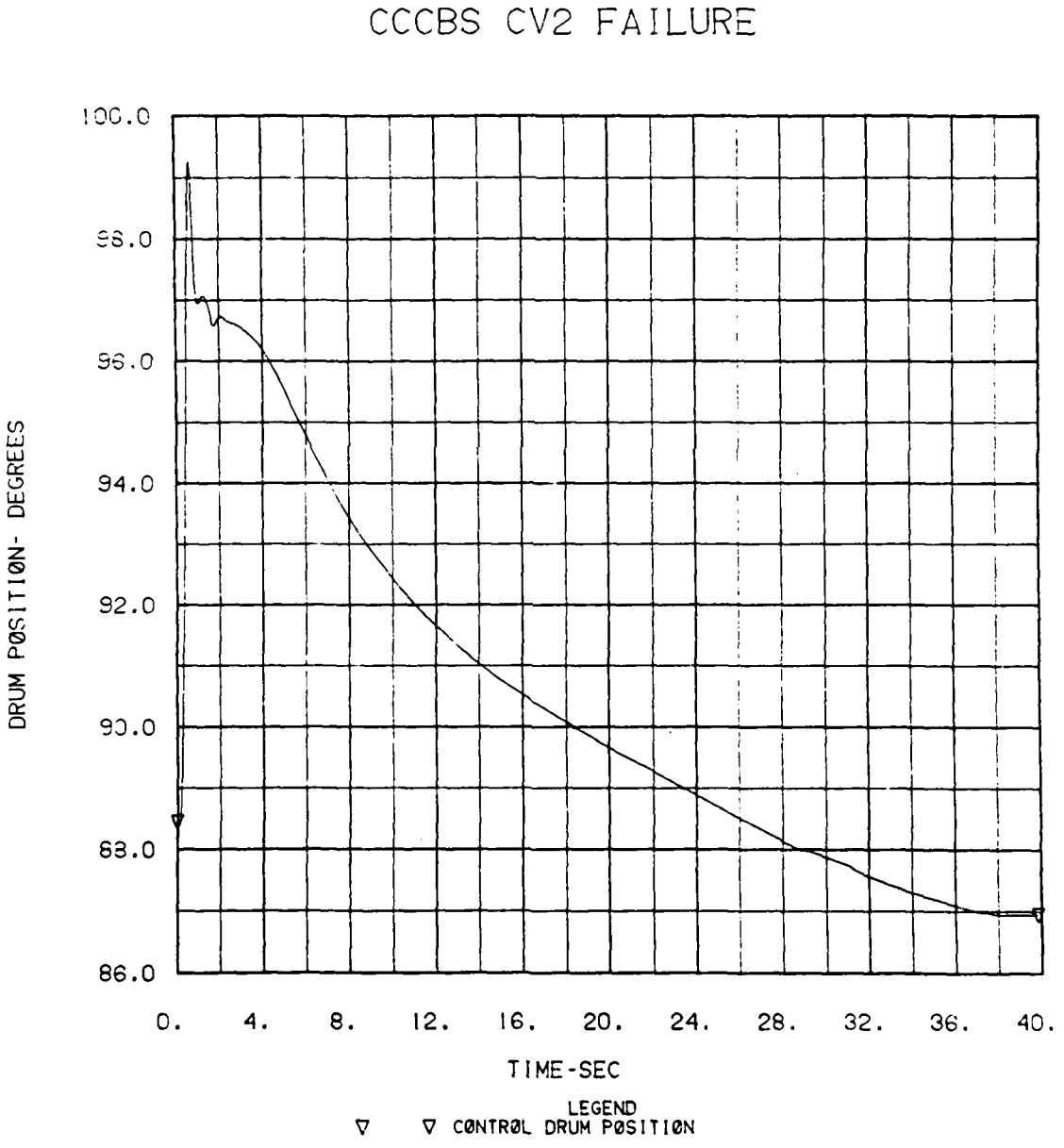

Figure 6-59. Control Drum Position

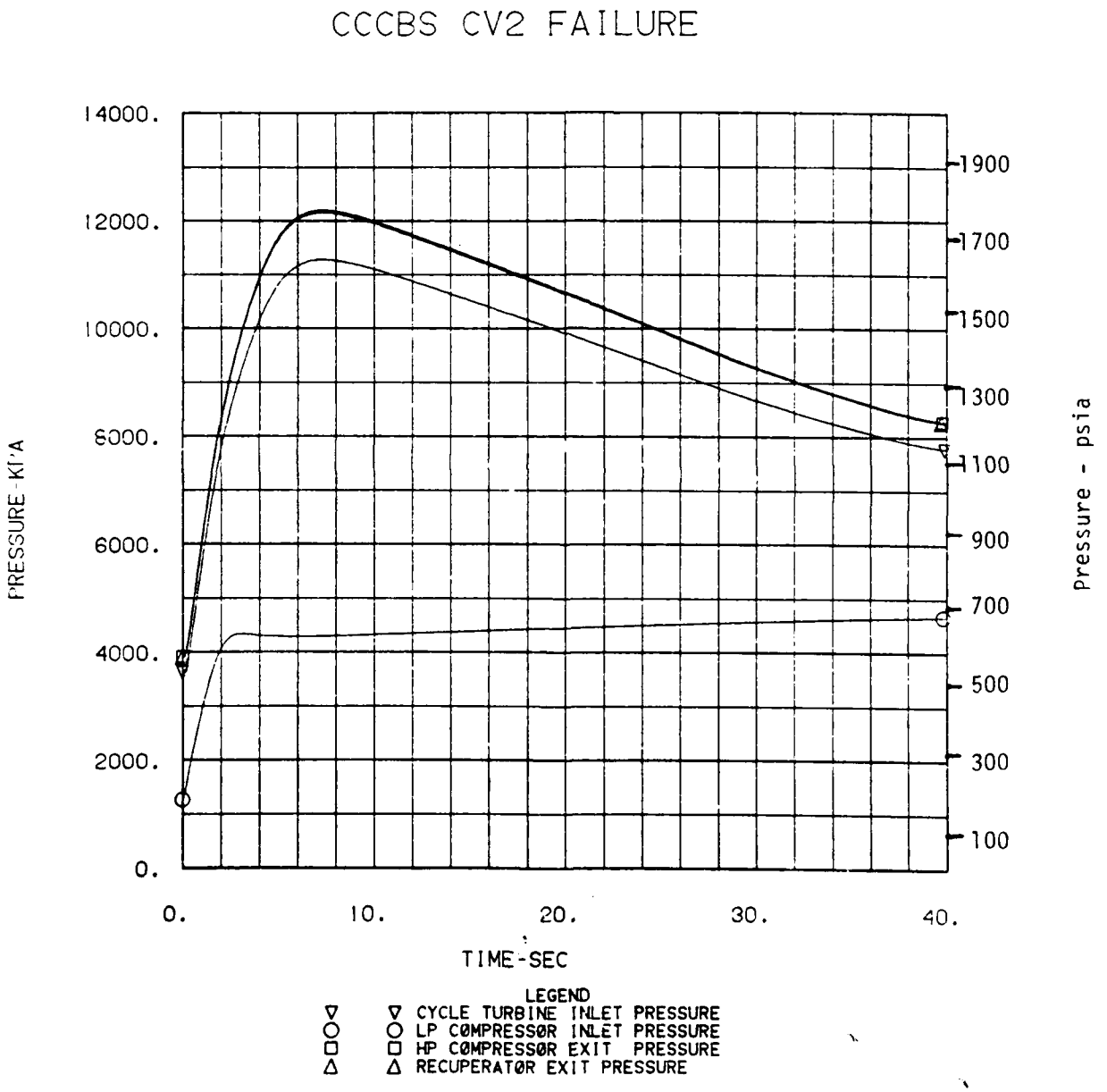

Figure 6-60. Turbomachinery Pressures

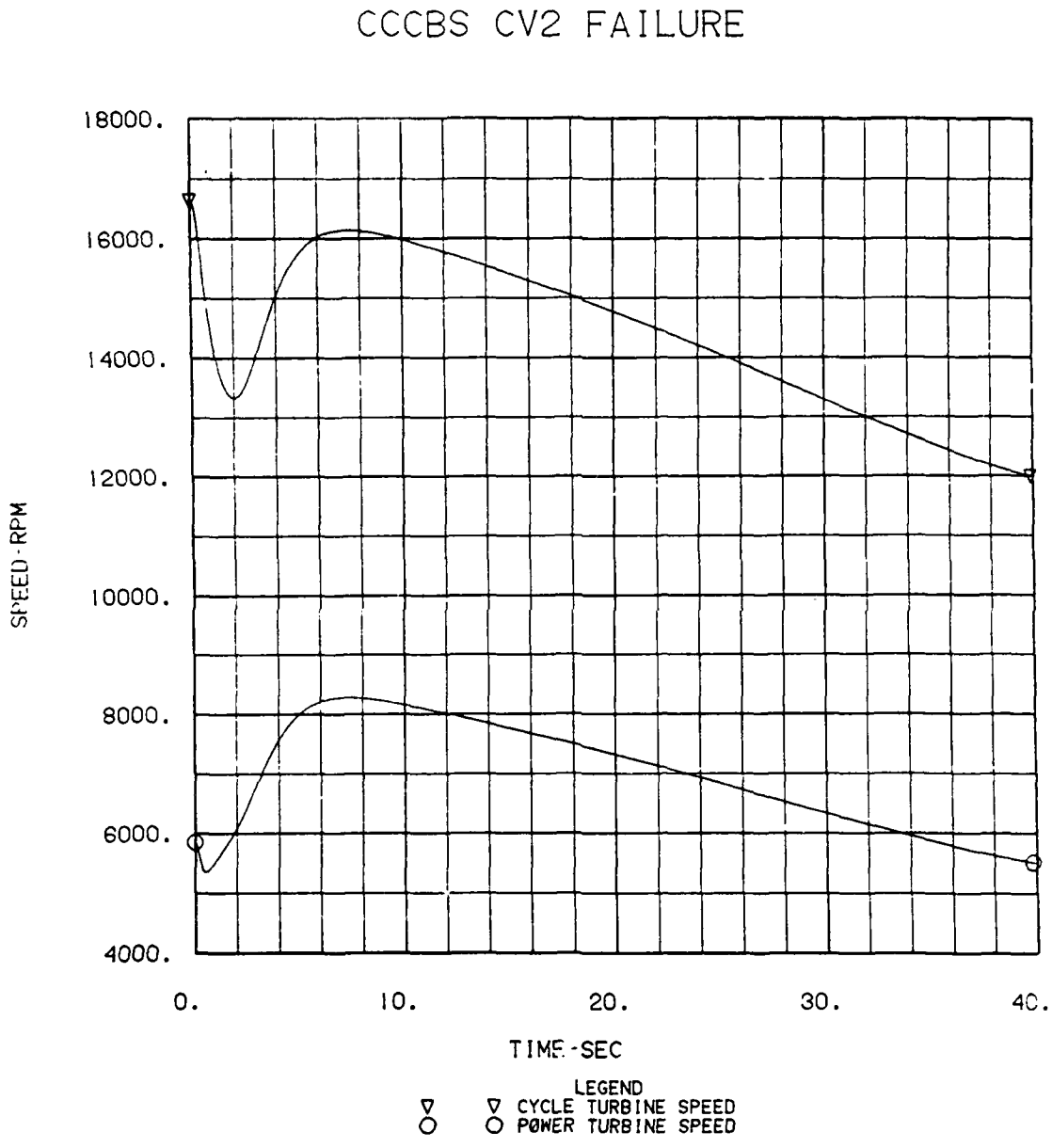

Figure 6-61. Turbomachinery Speeds

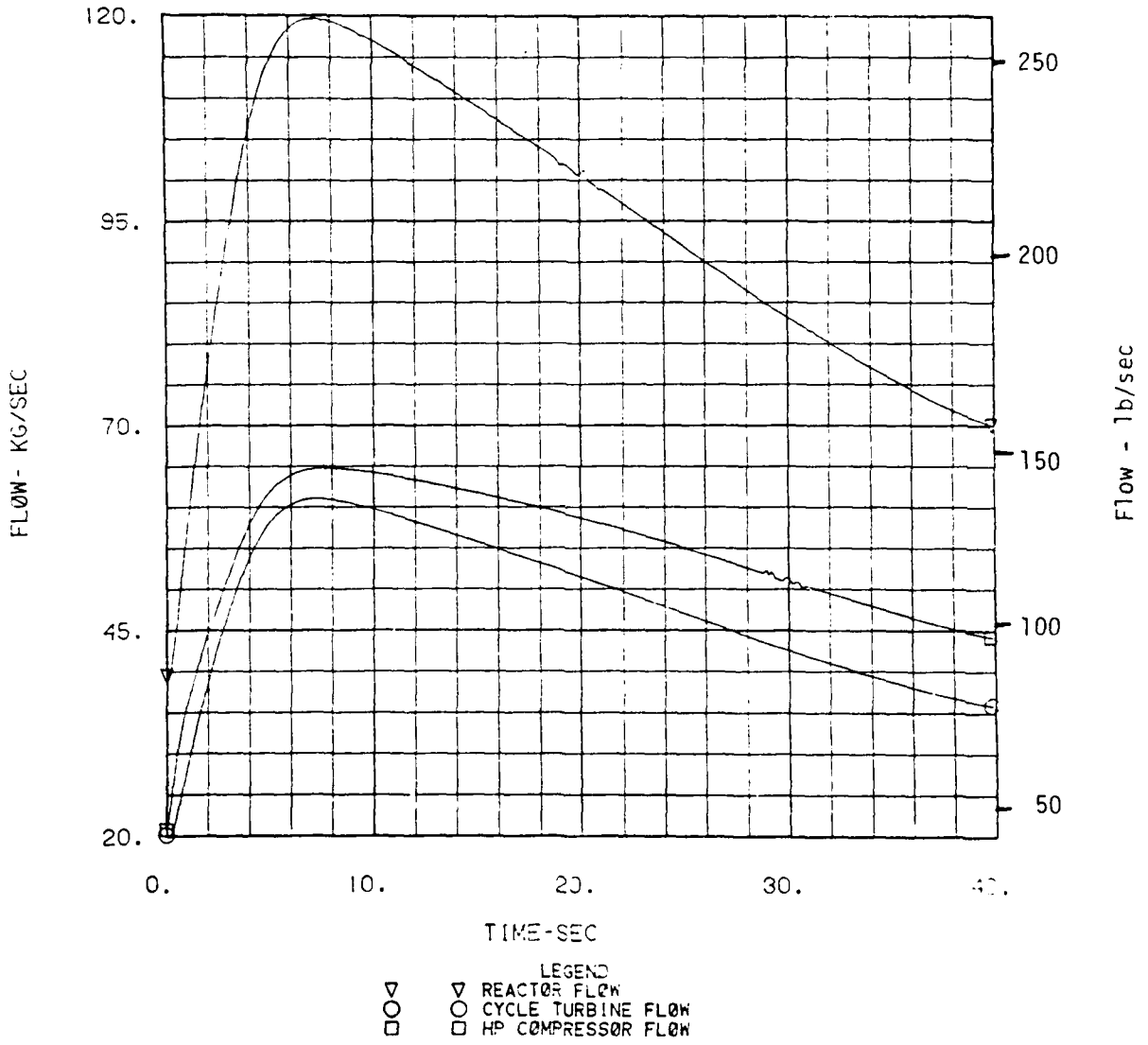

Figure 6-62. Turbomachinery Flow Rates

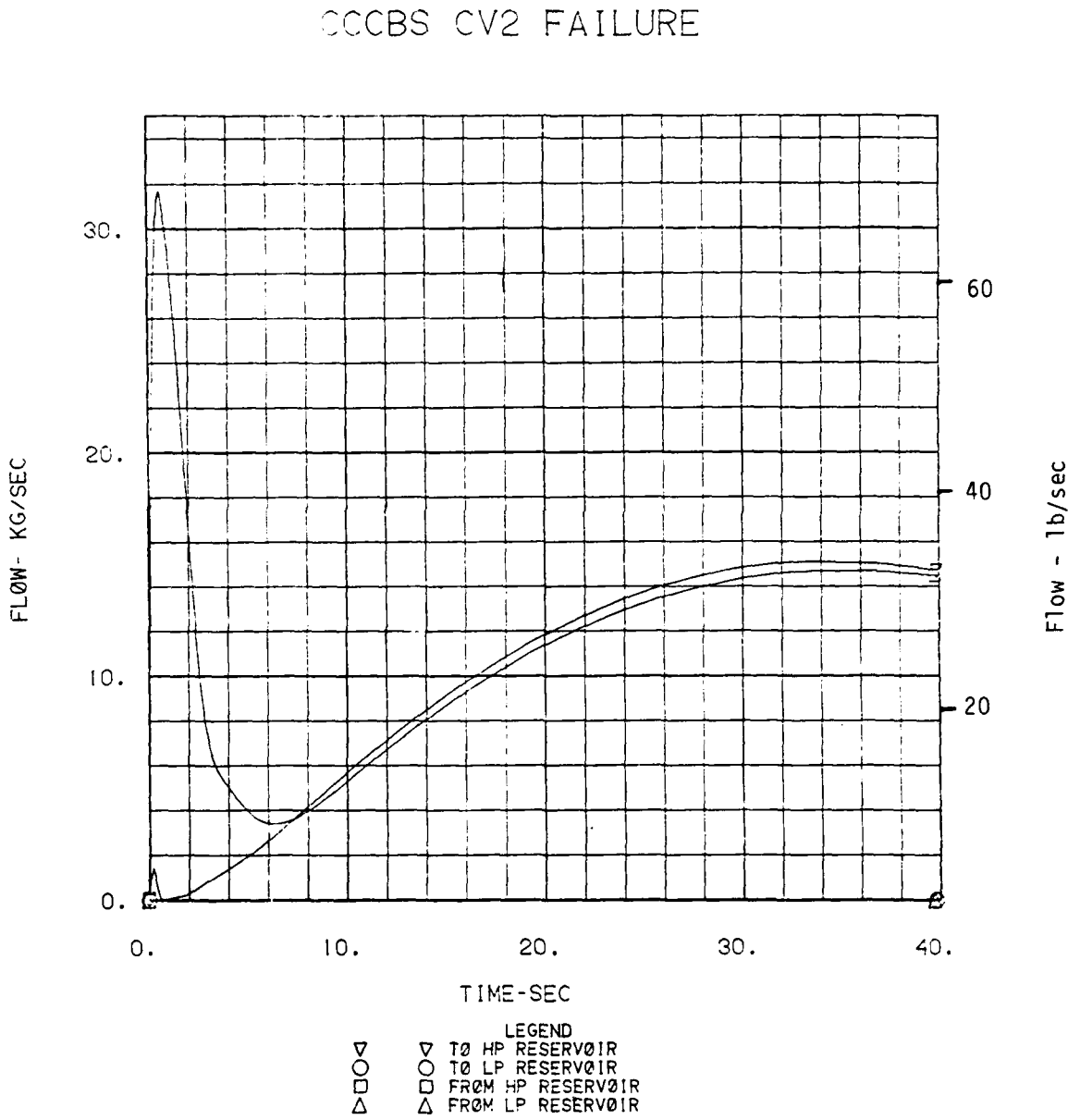

Figure 6-63. Inventory Flow Rates

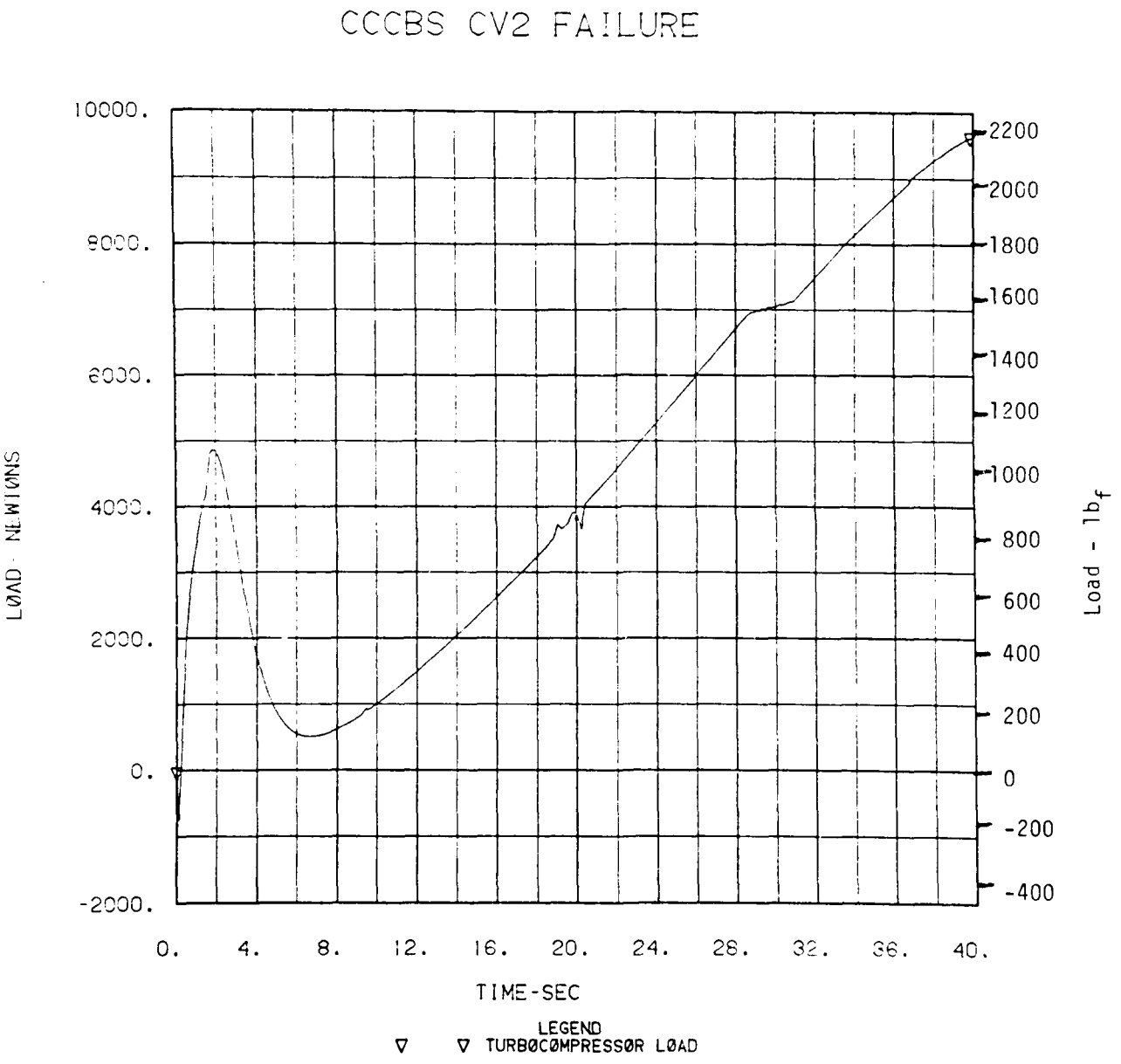

Figure 6-64. Turbocompressor Thrust Bearing Load

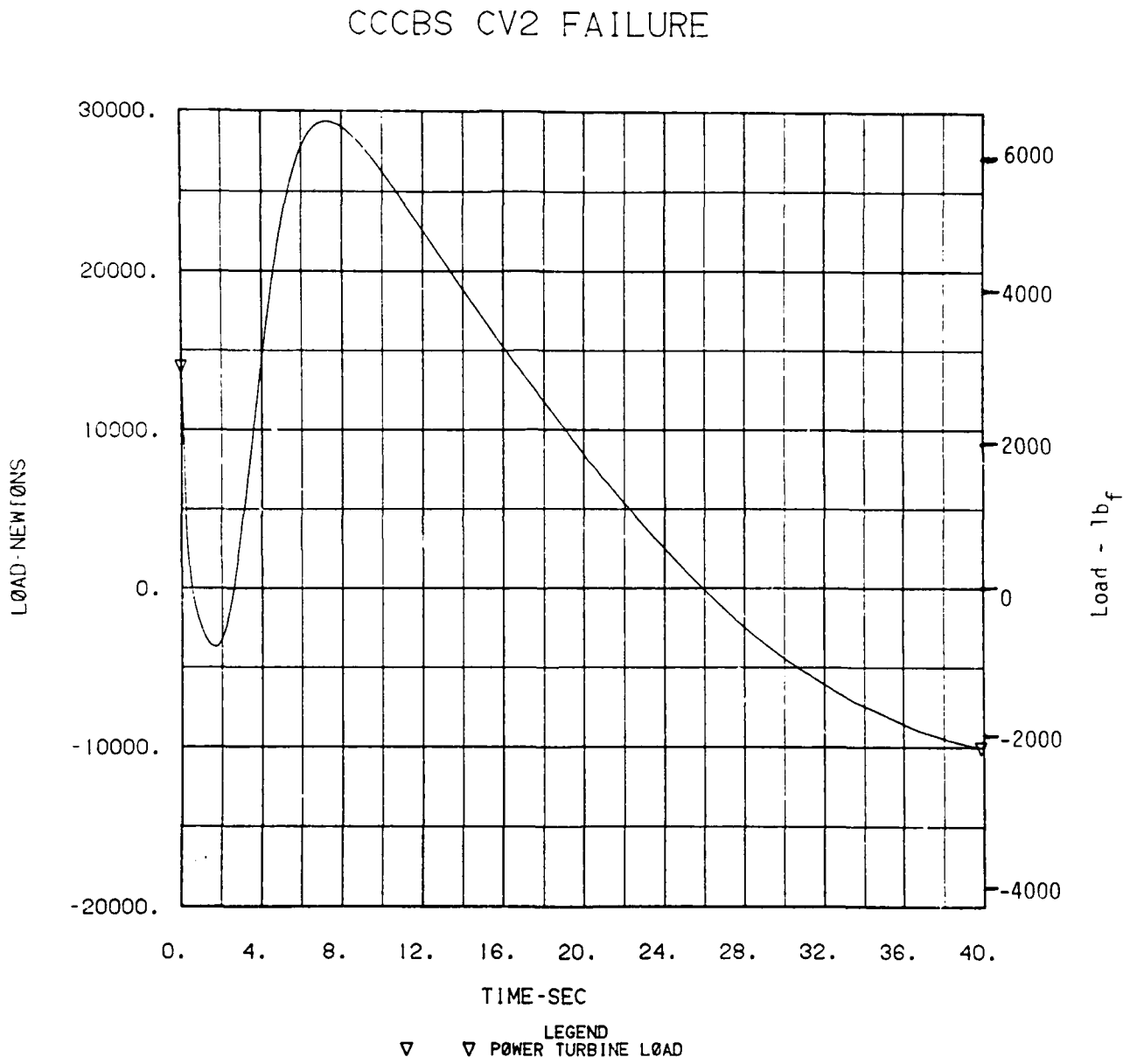

Figure 6-65. Power Turbine Thrust Bearing Load

Once the system switched over to using just the high pressure bottle at 1 second into the transient, the flows into and out of the system tended to stabilize. By about 10 seconds the two flows had equalized to within 5% of each other (Figure 6-63).

As the system pressures dropped after 8 seconds (Figure 6-60), the inventory flow entering the system through the failed control valve tended to increase (Figure 6-63). In response to this, the control system increased the inventory flow from the compressor to the inventory bottle. This reduced the CCCBS flowrates as more flow bypassed the high pressure side of the system (Figure 6-62), and reduced the turbine speeds as the shaft power decreased with the reduced flowrates and pressure drops (Figure 6-61).

The turbocompressor thrust bearing load (Figure 6-64) varied directly with the flowrate through the failed control valve (Figure 6-63). The steady rise in the bearing load after 7 seconds was due to the increasing difference between the flowrates in the compressor and cycle turbine (Figure 6-62) as a greater percentage of the compressor flow was bled off into the inventory bottle. The peak thrust load would appear to be about 10,000 Newtons (2250 lb_f).

The power turbine thrust bearing load (Figure 6-65) once again changed in a similar manner as the power turbine speed (Figure 6-61). However, for this case the power turbine bearing load reversed direction around 1 second and again after 26 seconds.

This case was the only one of the five cases reported which exhibited this behavior, and resulted in a peak bearing load of about -12,000 Newtons (-2700 lb_f).

6.1.3 OPERATION OF PARALLEL UNITS

One of the design requirements of the CCCBS was that it should be capable of operation in the configuration of having two power conversion assemblies coupled in parallel to a single energy source. Up to this point, the transient analyses have all assumed that both power conversion assemblies are identical units, and that any transient initiator affects both units equally. It was felt that an evaluation of the plant performance for conditions where non-identical power

conversion units were operating in parallel was in order. Typical cases of the two power conversion units not operating identically would be differing plant characteristics (such as compressor or turbine efficiencies, line pressure drop losses, heat exchanger effectivenesses, etc.) or transients that would affect primarily one unit only (loss of cooling water in one precooler or intercooler, loss of load, etc.).

Detailed analyses were performed on a number of cases where non-identical performance would result in one unit. These were primarily limited to step changes in the compressor and turbine efficiencies in one of two identical turbocompressor units. Based on these results, and the performance of the CCCBS during the normal and malfunction events described in Section 6.1.1 and 6.1.2, the system performance characteristics for a number of other one-unit malfunction conditions could be described.

A desirable feature of the CCCBS would be that each unit would be able to operate independent of the other as much as possible. This would require that a malfunction condition initiated in one power conversion unit would not be carried over into the other unit, and possibly require the complete shutdown of the whole CCCBS.

To determine the sensitivity of the system to an imbalance between the two power conversion loops, the system response to a step change of 5% in the turbomachinery efficiencies was investigated. A sudden change of this magnitude is unlikely, but it does bracket the more probable case of a slow change in the turbomachinery performance over the life of the plant. The cases analyzed consisted of step changes of 5% each in the compressor and cycle turbine efficiencies.

6.1.3.1 STEP CHANGE IN CYCLE TURBINE EFFICIENCY

The results for the cycle turbine efficiency case are shown in Figures 6-66 through 6-75. The step drop in efficiency caused the cycle turbine speed in the affected unit (referred to as "A" in the plots) to drop due to the reduction in the shaft power being produced (Figure 6-70). This initially caused the A-unit power turbine speed to drop (Figure 6-70), and generated a signal for additional helium to be added to the system.

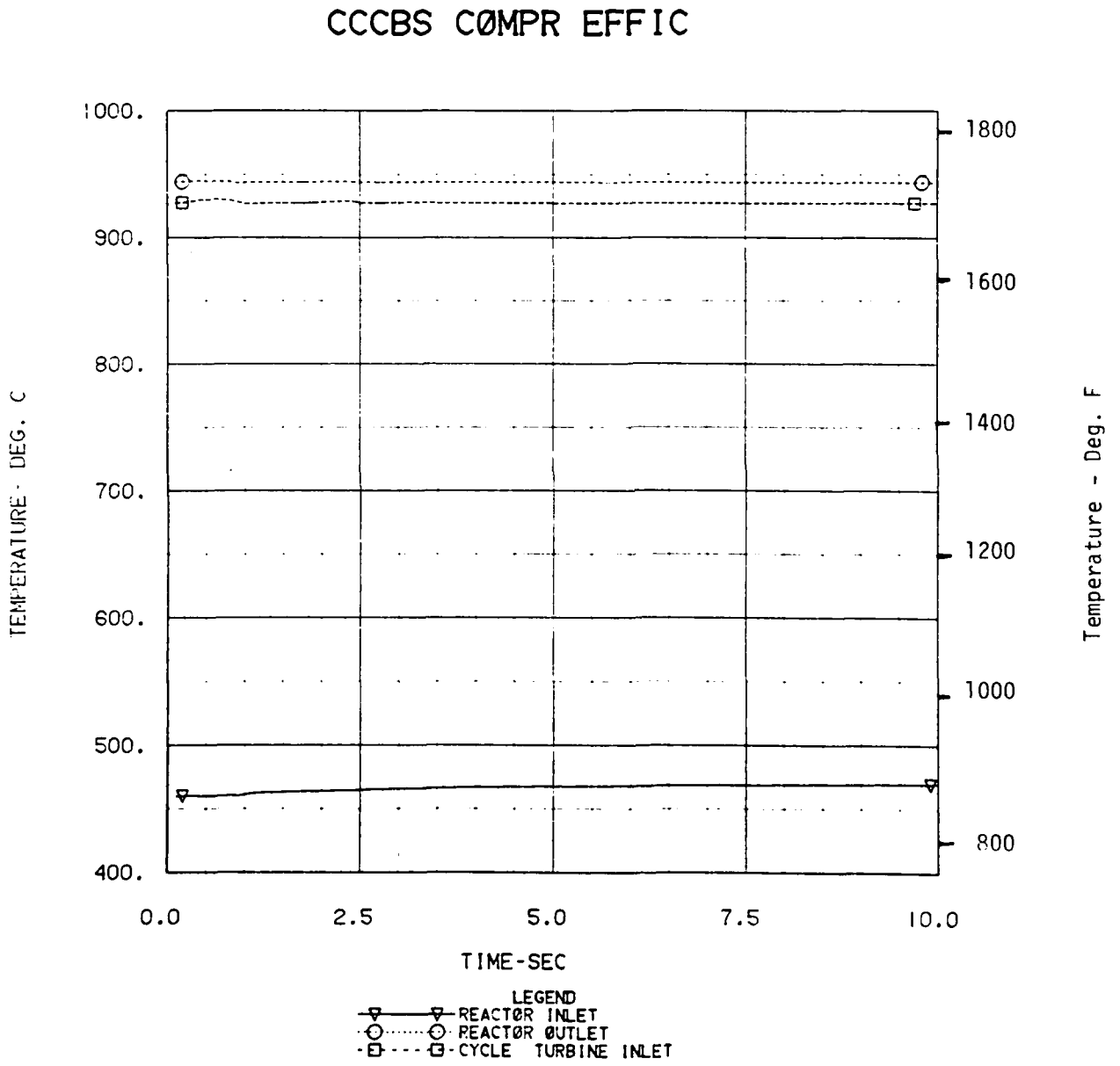

Figure 6-66. Reactor Helium Temperatures

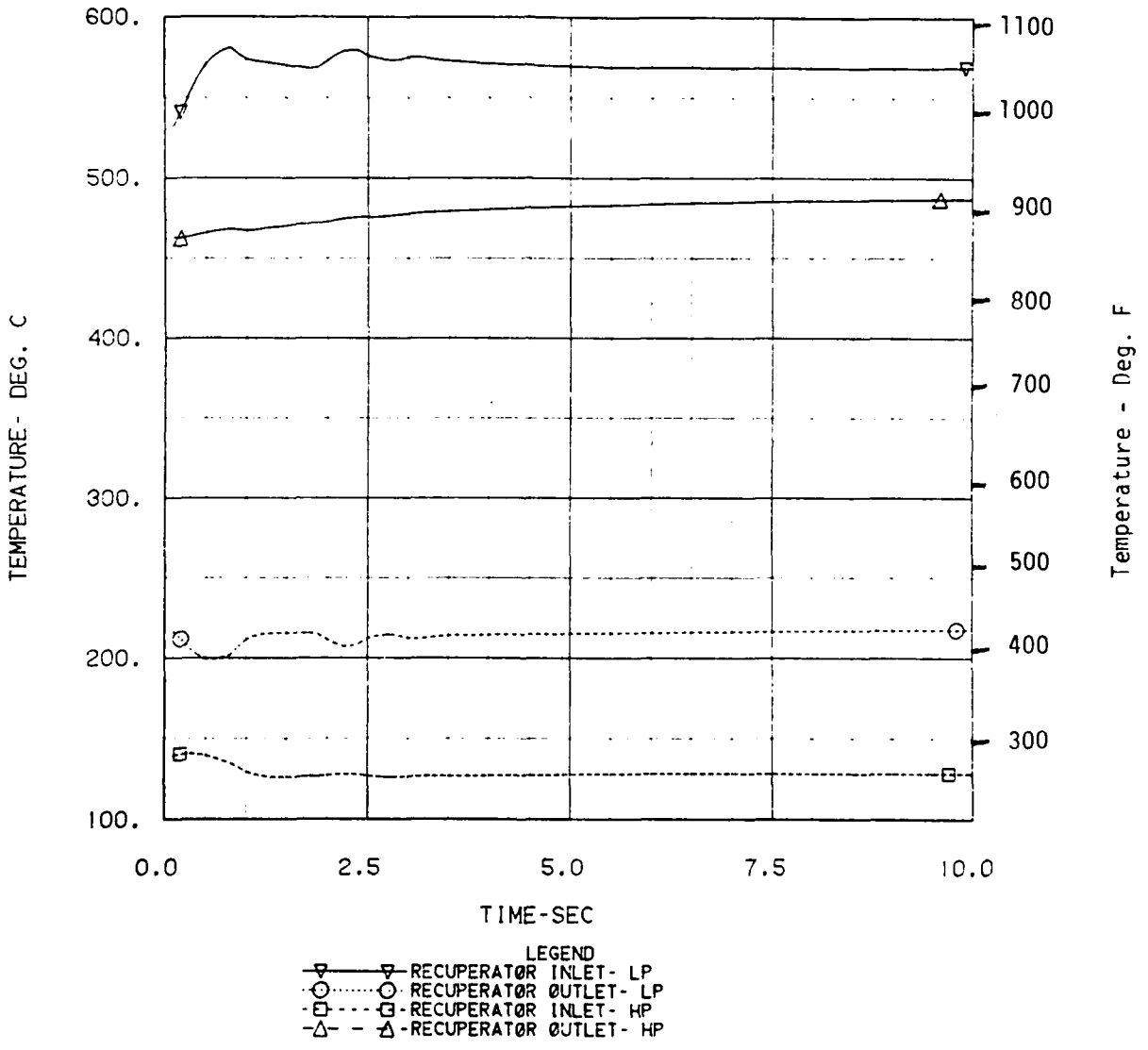

Figure 6-67. Recuperator Helium Temperatures in Faulted Unit

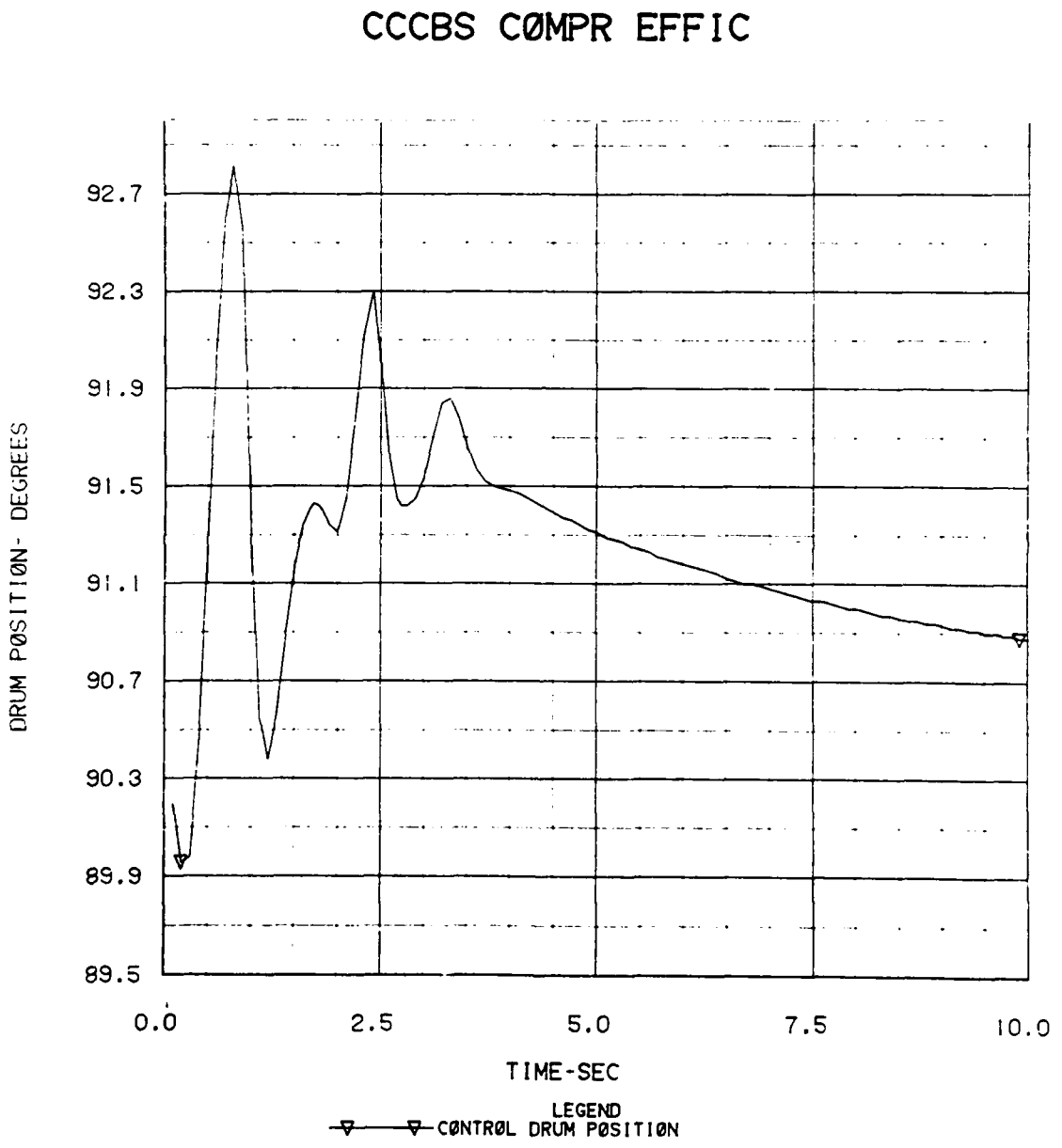

Figure 6-68. Control Drum Position

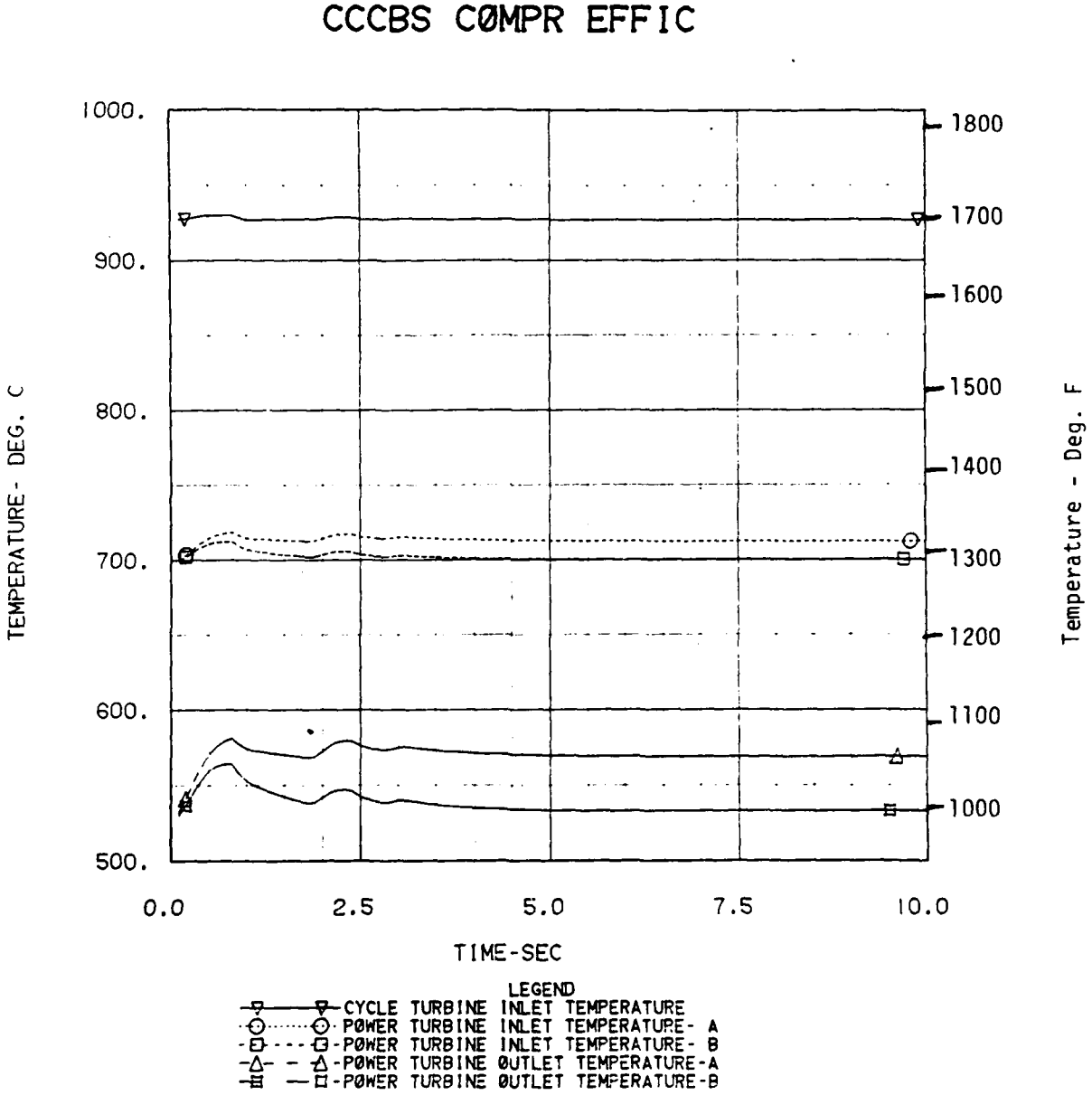

Figure 6-69, Turbine Helium Temperatures

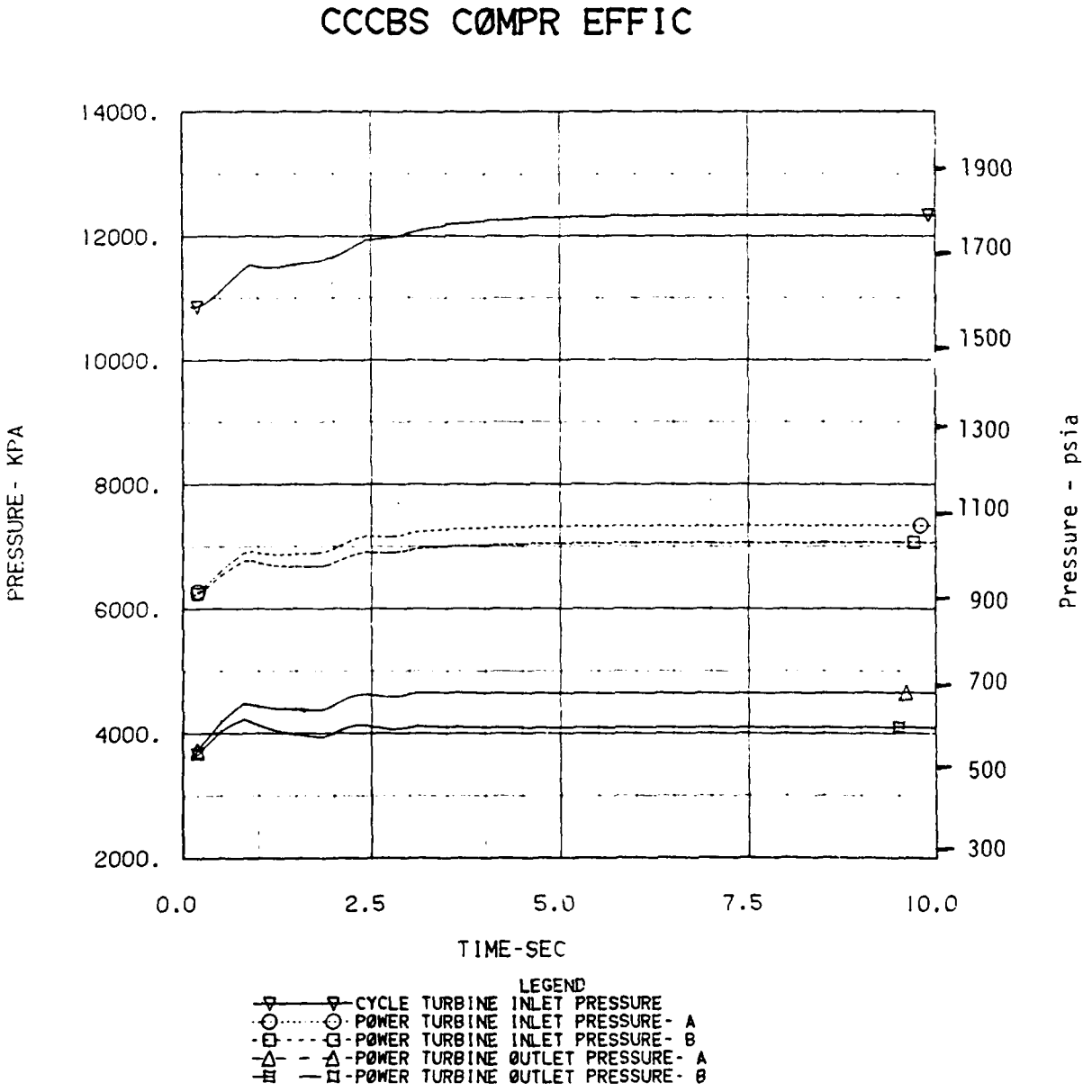

Figure 6-70. Turbine Helium Pressures

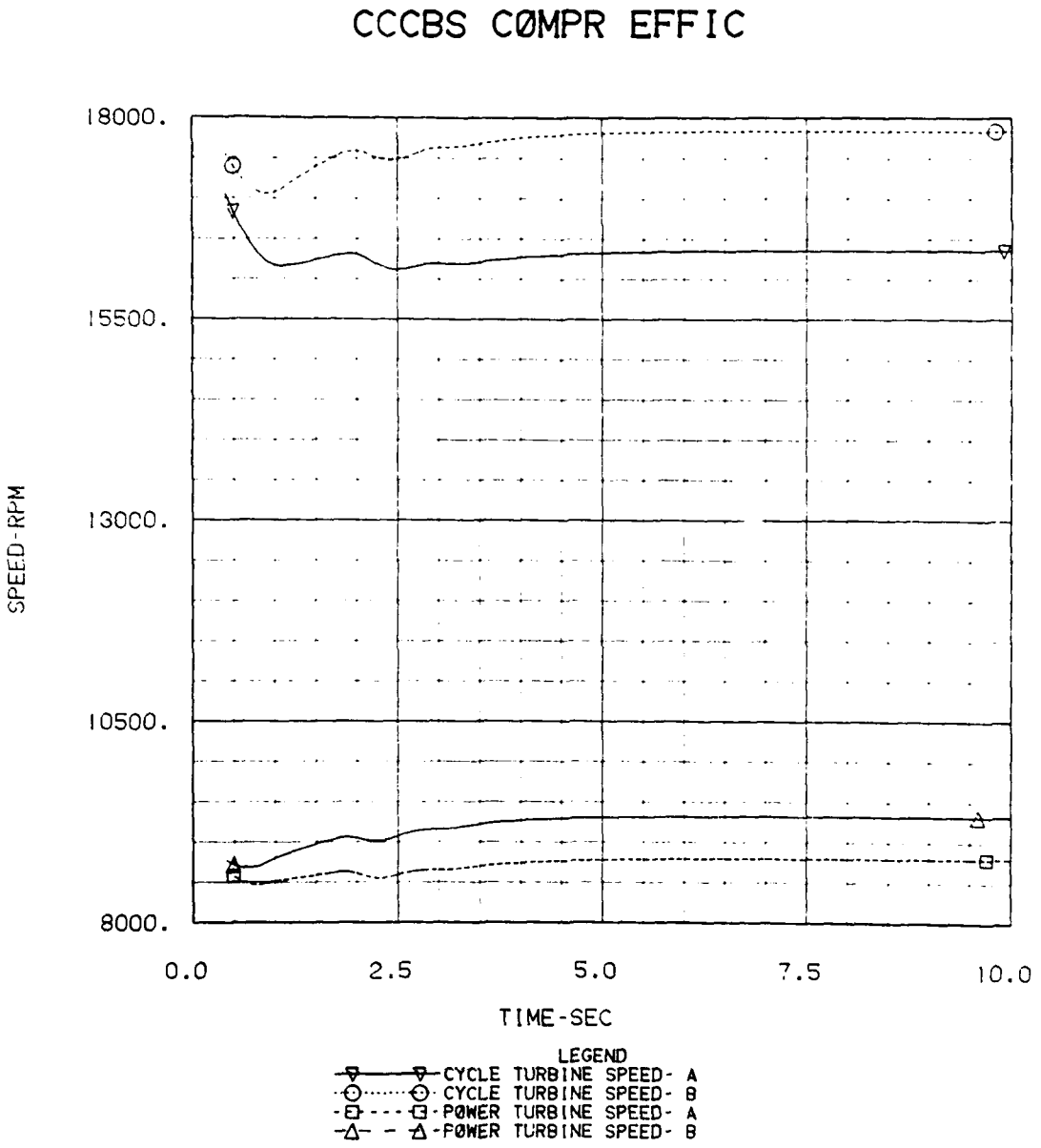

Figure 6-71. Turbine Speeds

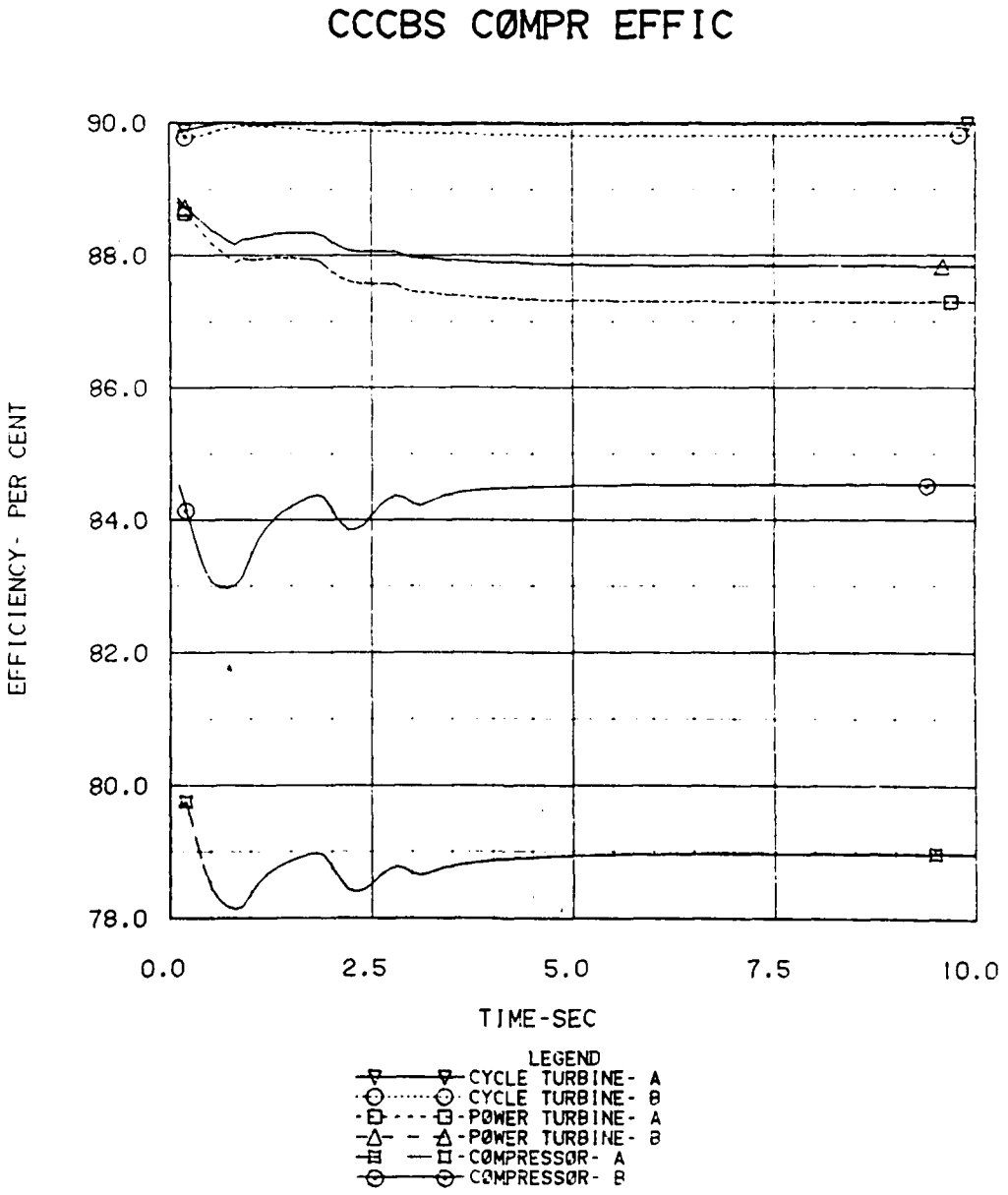

Figure 6-72. Turbomachinery Efficiencies

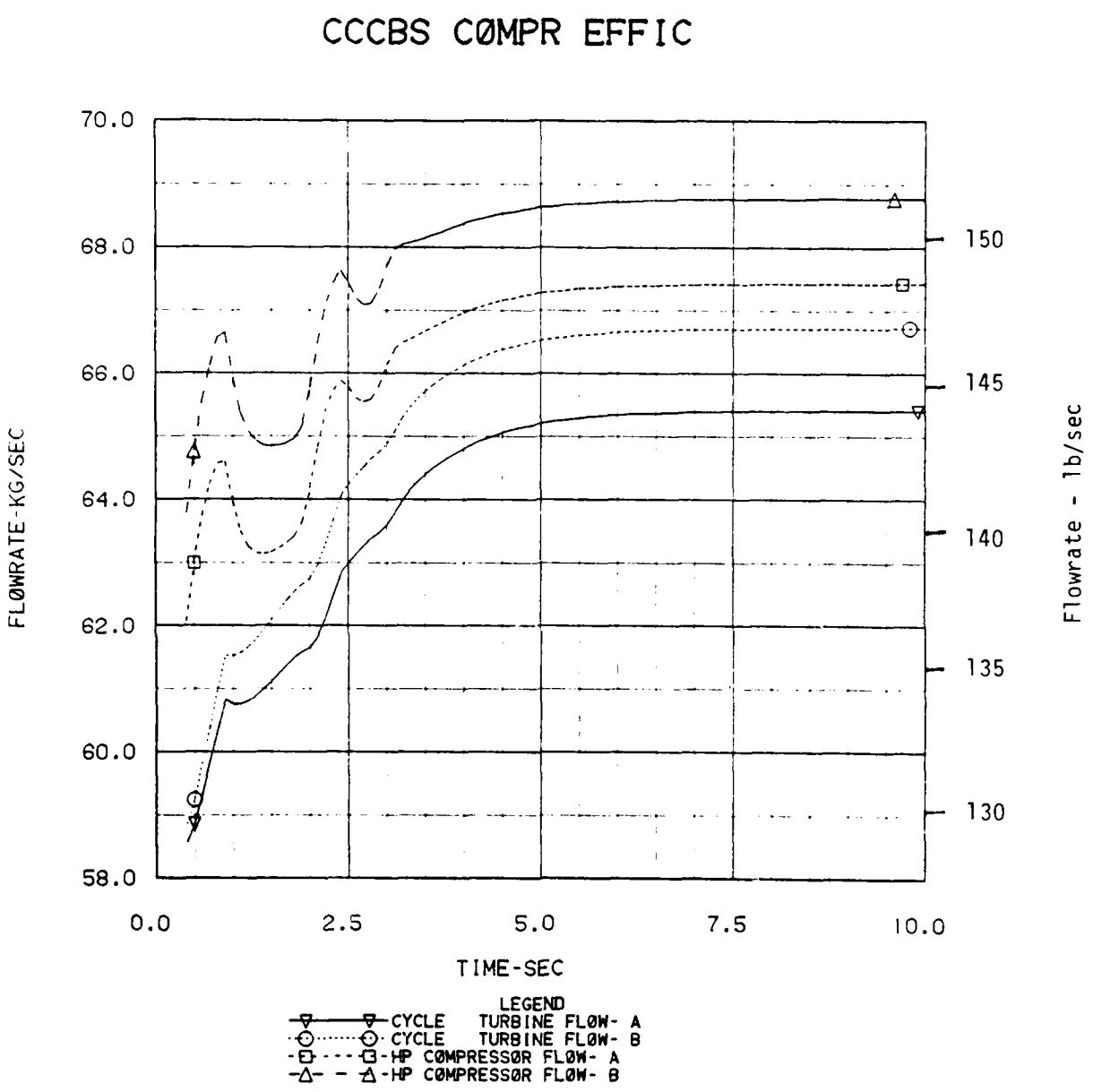

Figure 6-73. Turbomachinery Helium Flows

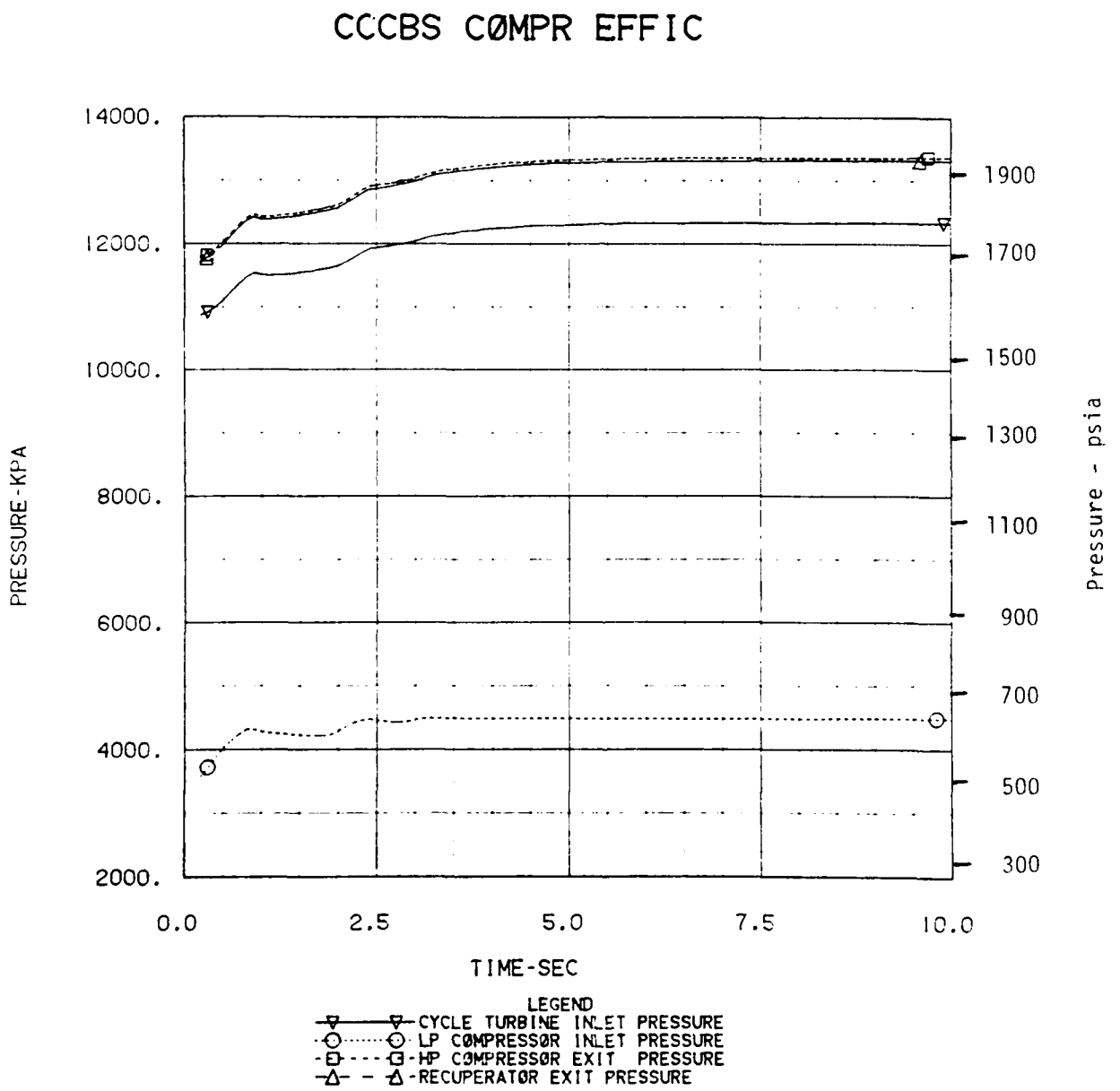

Figure 6-74. Turbomachinery Helium Pressures in Failed Unit

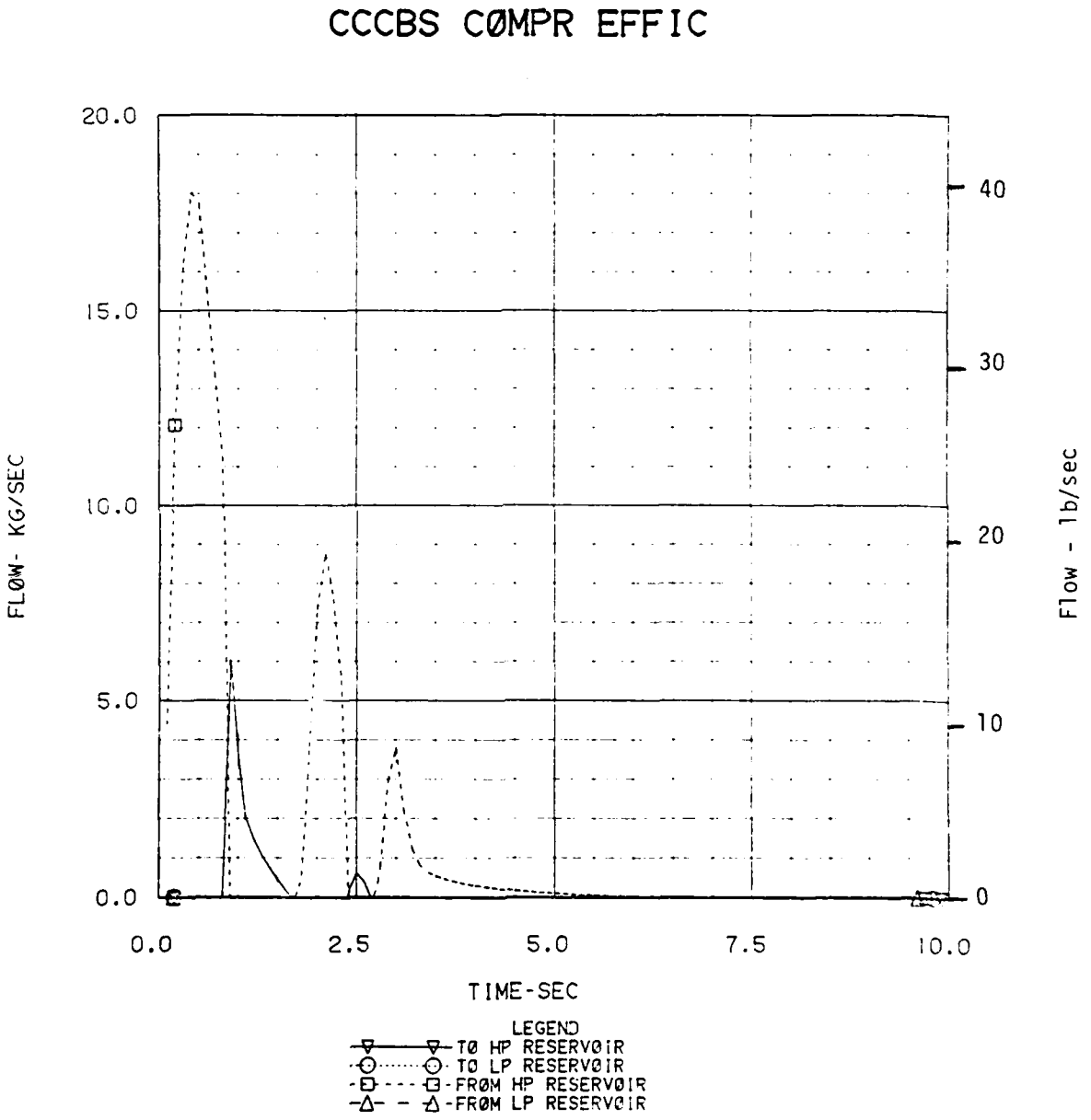

Figure 6-75. Helium Inventory Flows

As described in Section 6.2, the inventory control system generated an inventory flow rate demand. The power turbine speed used is an average of the speeds of both units. As a result a steady-state is reached with one unit being above the design point full-power condition, with the affected unit generating less than full power. For the case described here, the plant inventory is increased by about 12%, with the load split about 46%-54% between the units. Expressed in relation to the full-power design point, the power produced by the "A" and "B" units would be about 92% and 108% of the full power design values, respectively.

The additional helium inventory increased the pressure levels throughout the CCCBS by about 600 and 100 KPA (90 to 160 psi) in the low and high pressure regions, respectively (Figure 6-73). A rise in this magnitude would most likely require design changes to parts of the system to accommodate this condition. If no design changes were to be made, the plant would have to operate at a net power level below the full-power point. This operating point would be at about 92% of the full-power design point, with the power once again split about 46%-54% between the two units.

With the reduced power being produced by the affected ("A") unit, there is a rise of about 50°C in the power turbine outlet temperature. Together with the increased flowrates, there is a small rise in the recuperator exit temperature (Figure 6-67). This rise, however, is small in comparison with the rises seen during a number of the malfunction transients, and therefore should not force any design efforts to be initiated to allow the system to operate in this mode.

The recommended course would be to operate the system at a reduced power level for a malfunction condition such as that described. Any design changes that would have to be made to the system to allow for the additional pressure levels would not be justified by the weight and volume penalty that would result. The better solution would be to operate the plant at the reduced 90% output power point.

6.1.3.2 STEP CHANGE IN HIGH PRESSURE COMPRESSOR EFFICIENCY

The results for the step change in compressor efficiency are shown in Figures 6-76 through 6-85. The results were very similar to the change in turbine efficiency case shown previously. The cycle turbine speed dropped (Figure 6-80) as the

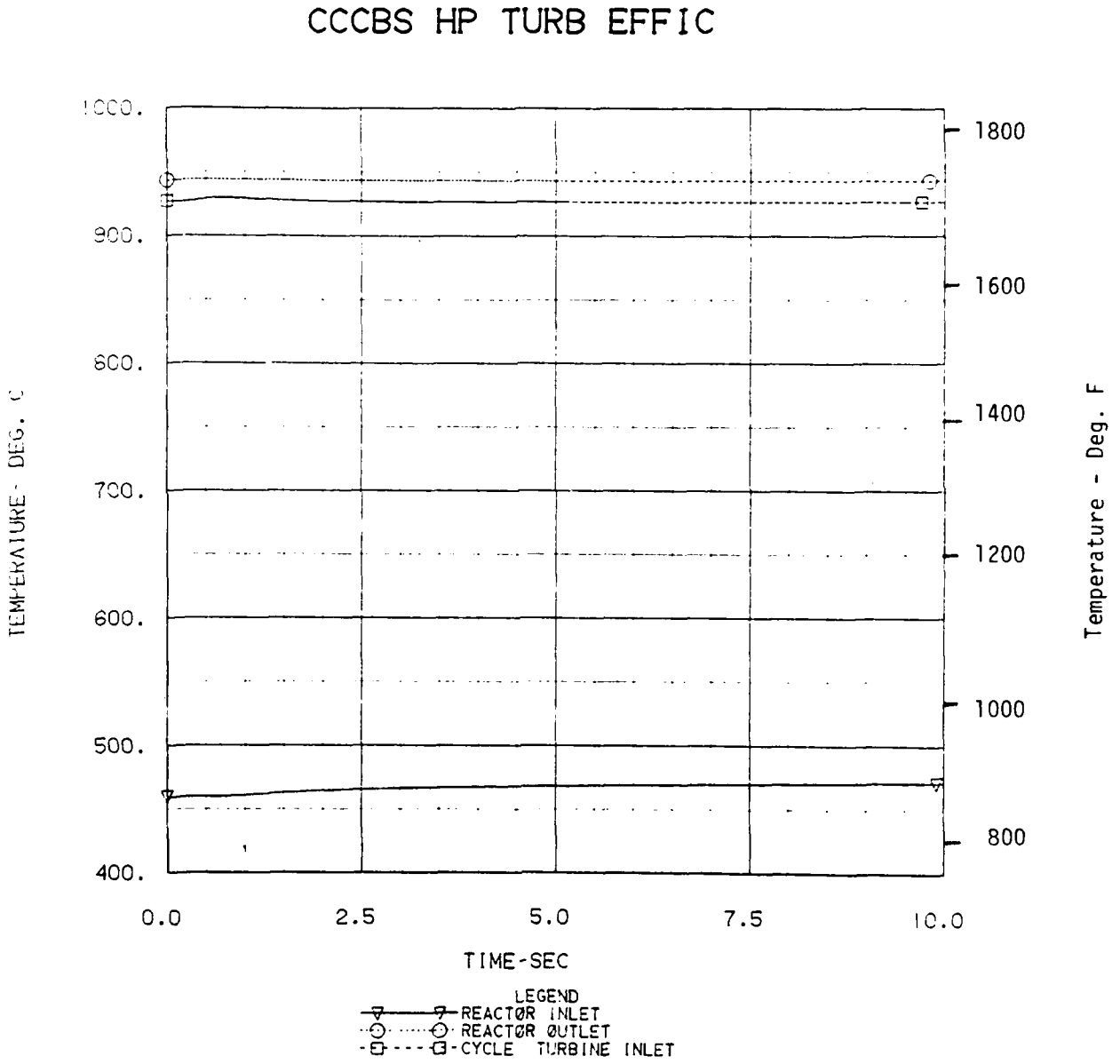

Figure 6-76. Reactor Helium Temperatures

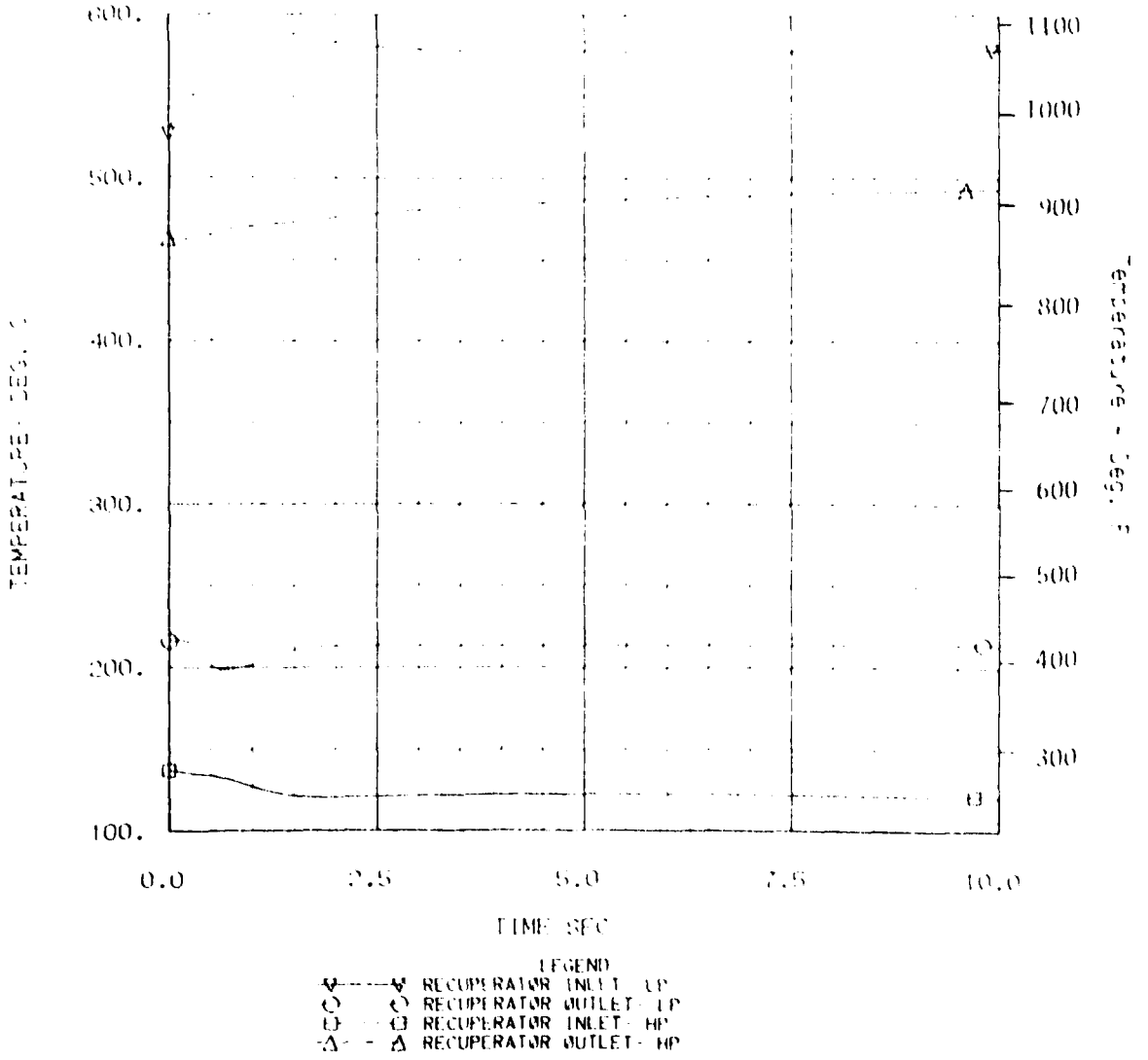

Figure 6-77. Recuperator Helium Temperatures in Failed Unit

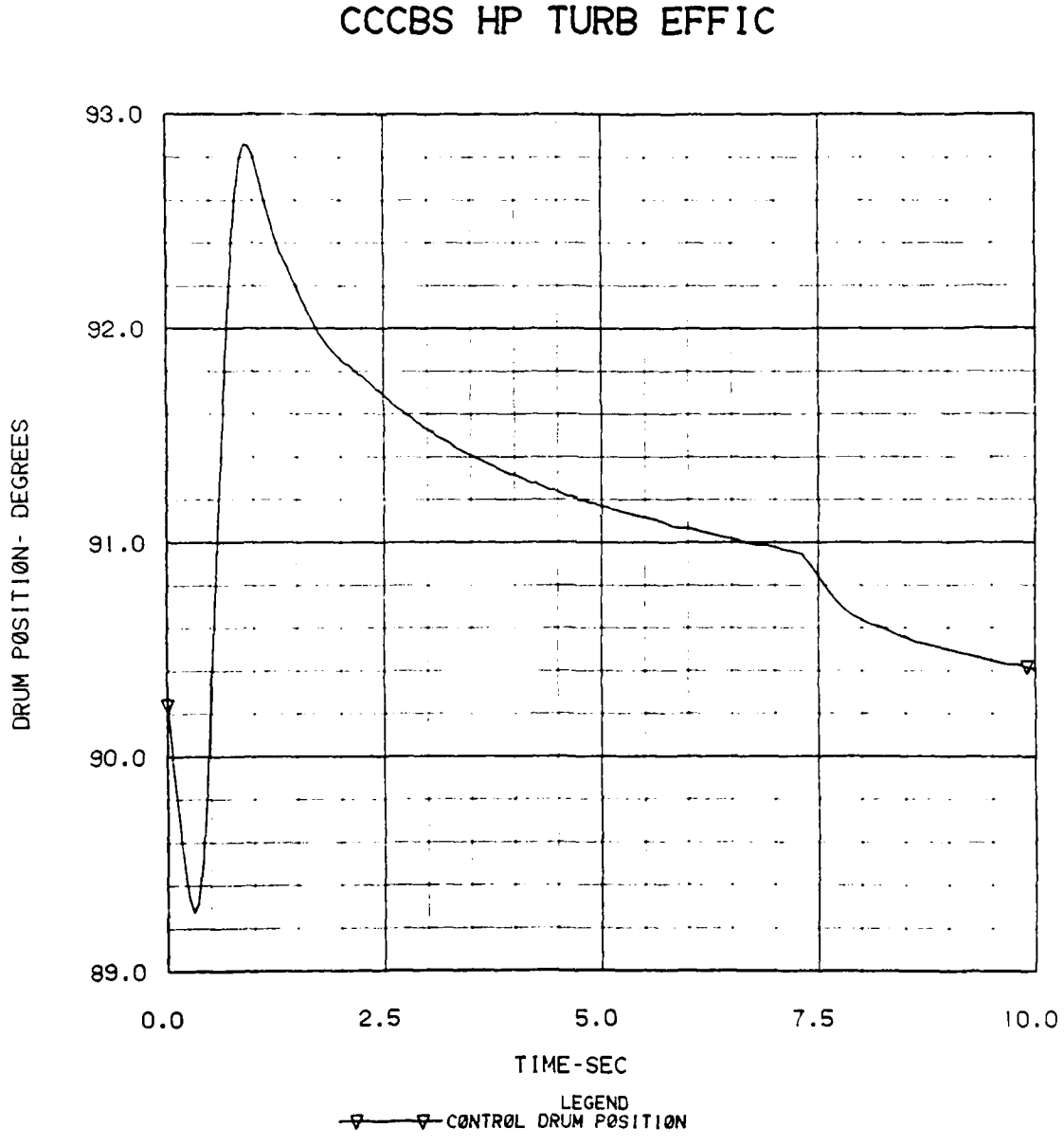

Figure 6-78. Control Drum Position

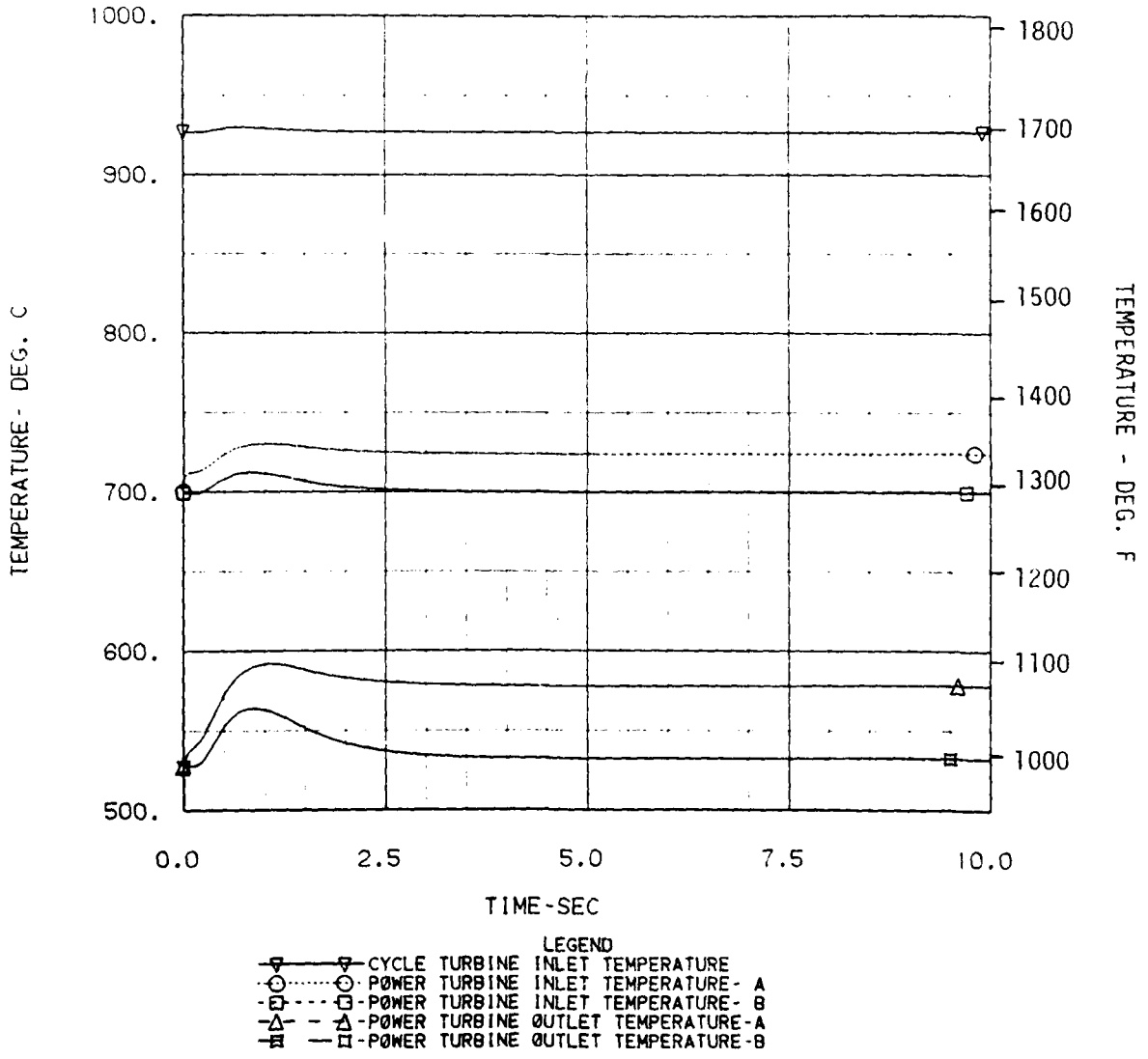

Figure 6-79. Turbine Helium Temperatures

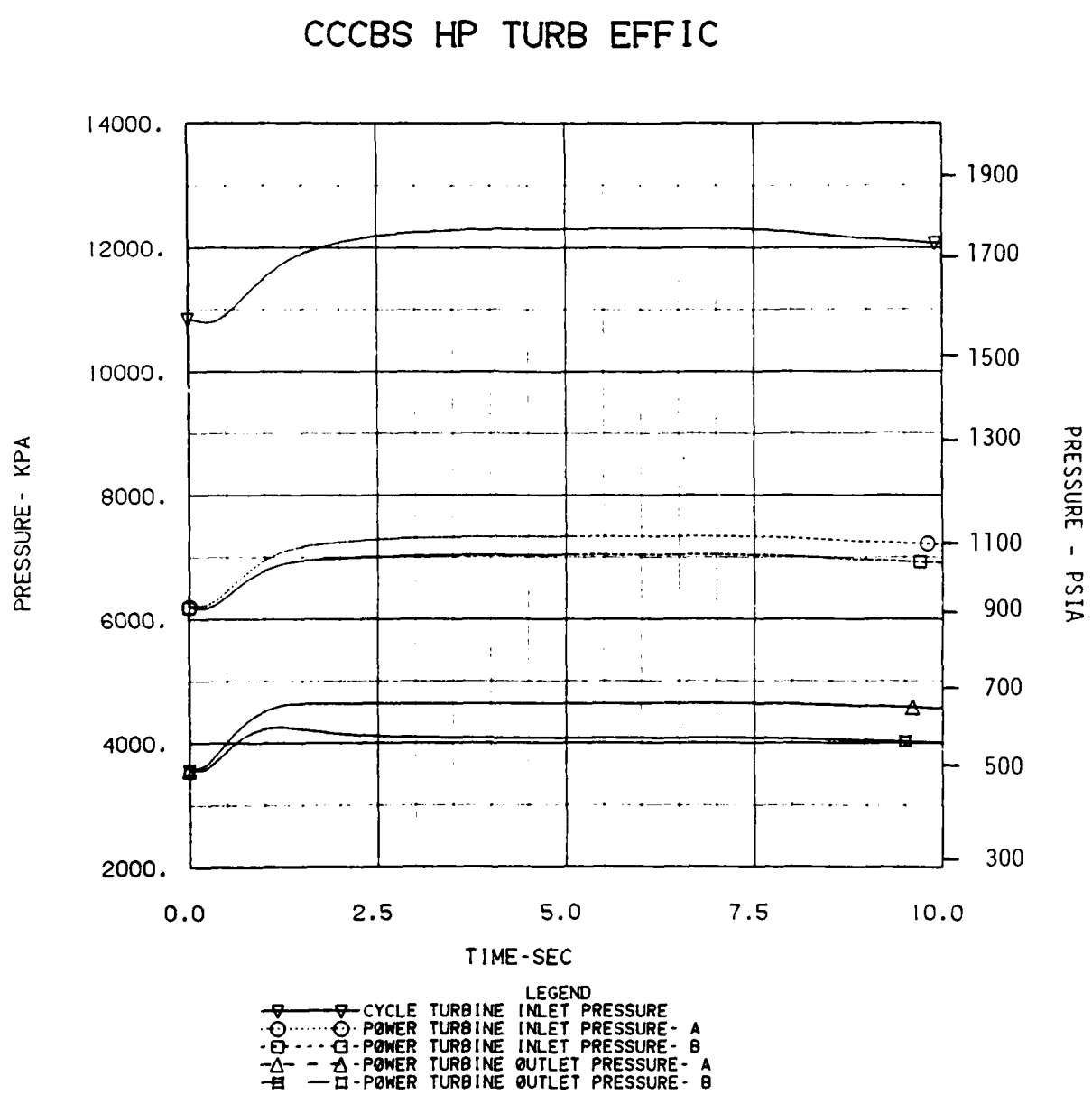

Figure 6-80. Turbine Helium Pressures

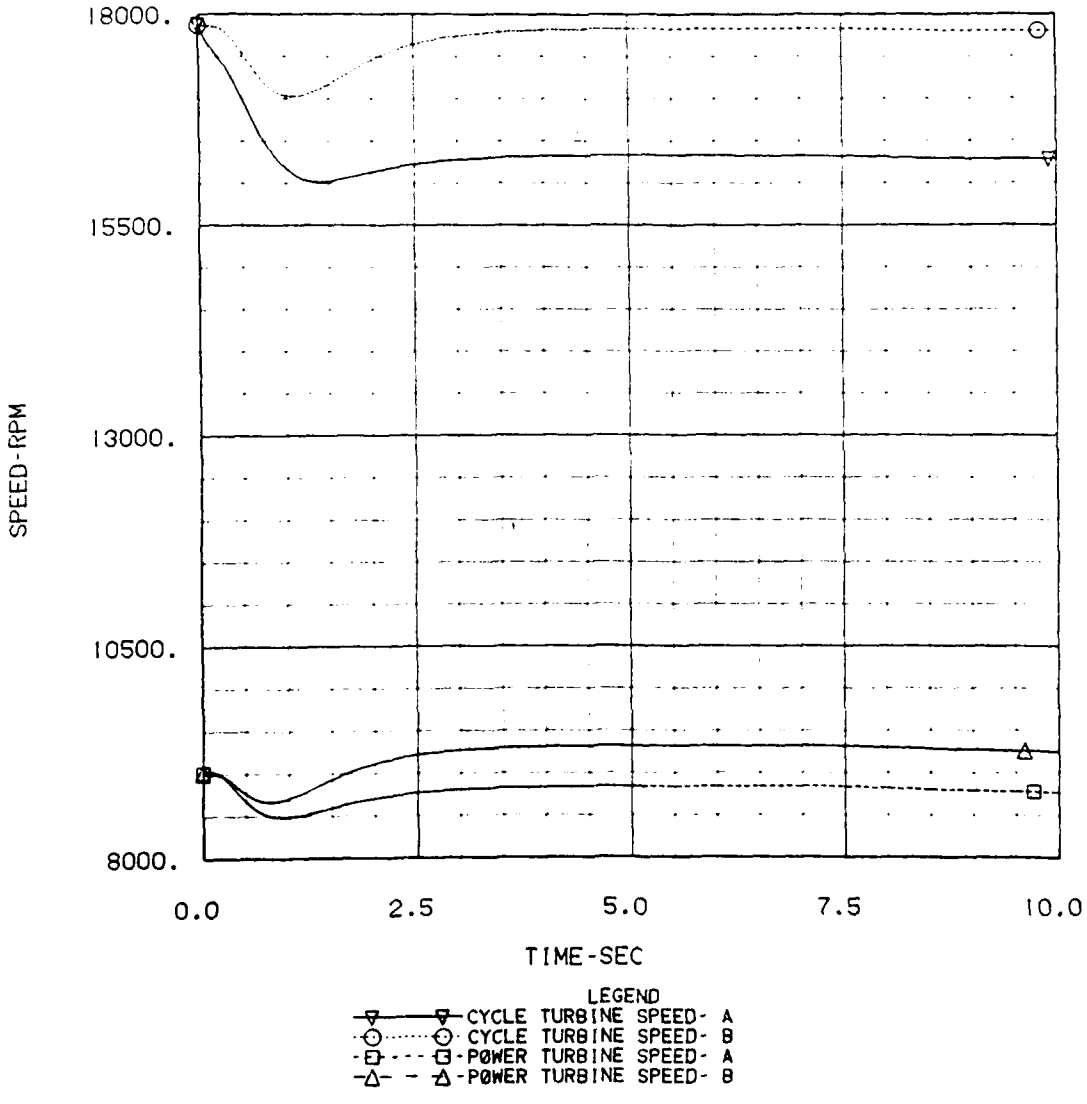

Figure 6-81. Turbine Speeds

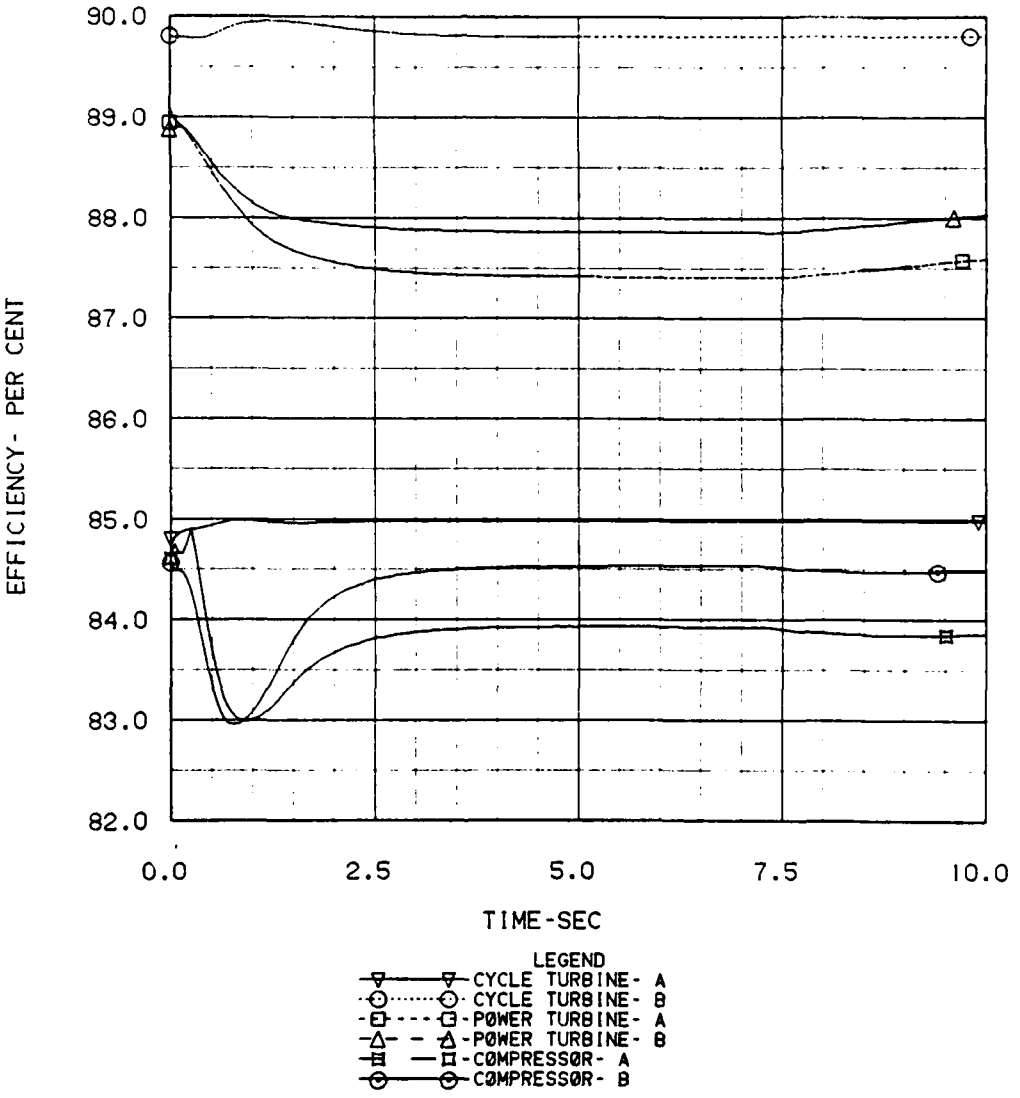

Figure 6-82. Turbomachinery Efficiencies

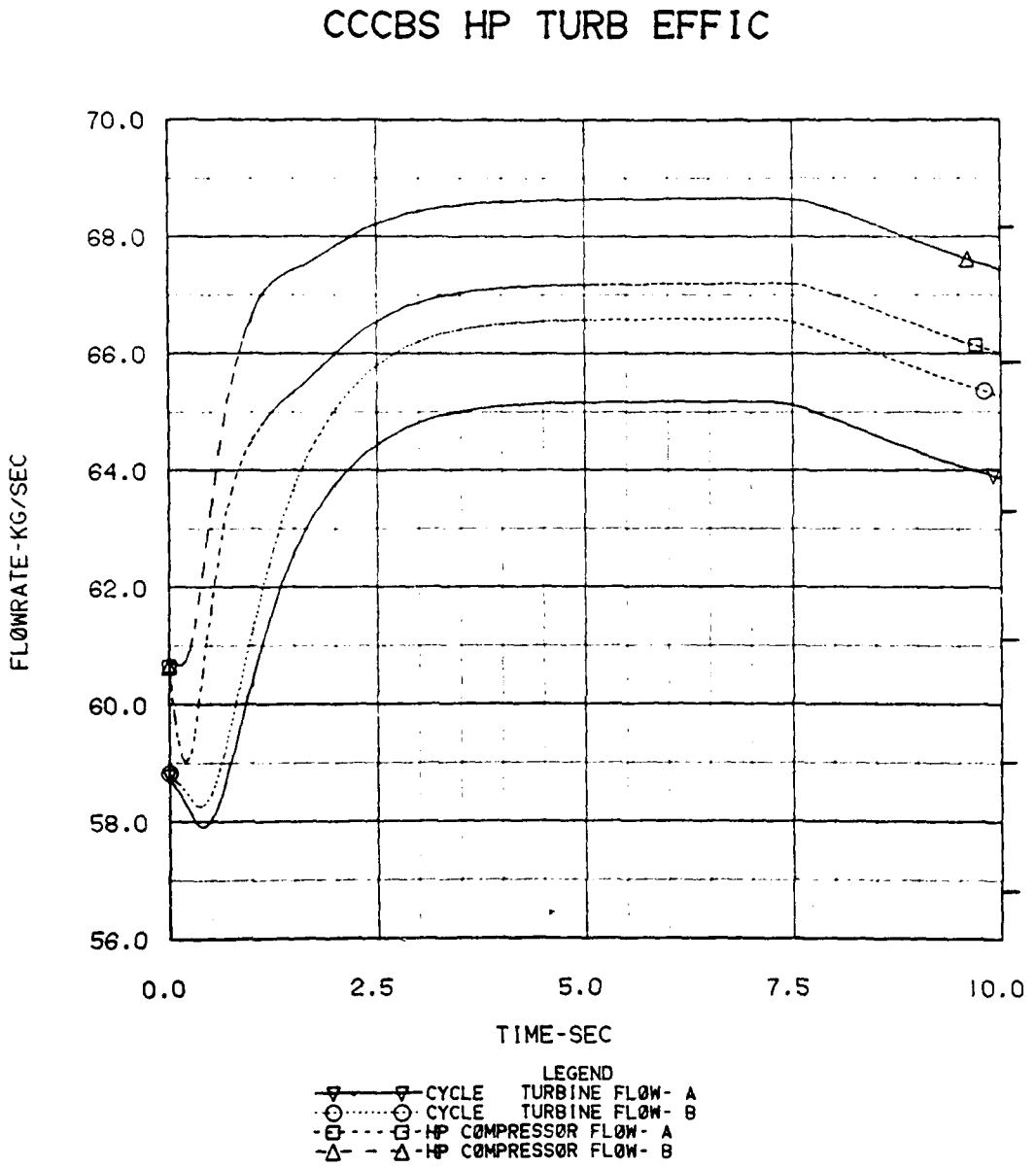

Figure 6-83. Turbomachinery Helium Flows

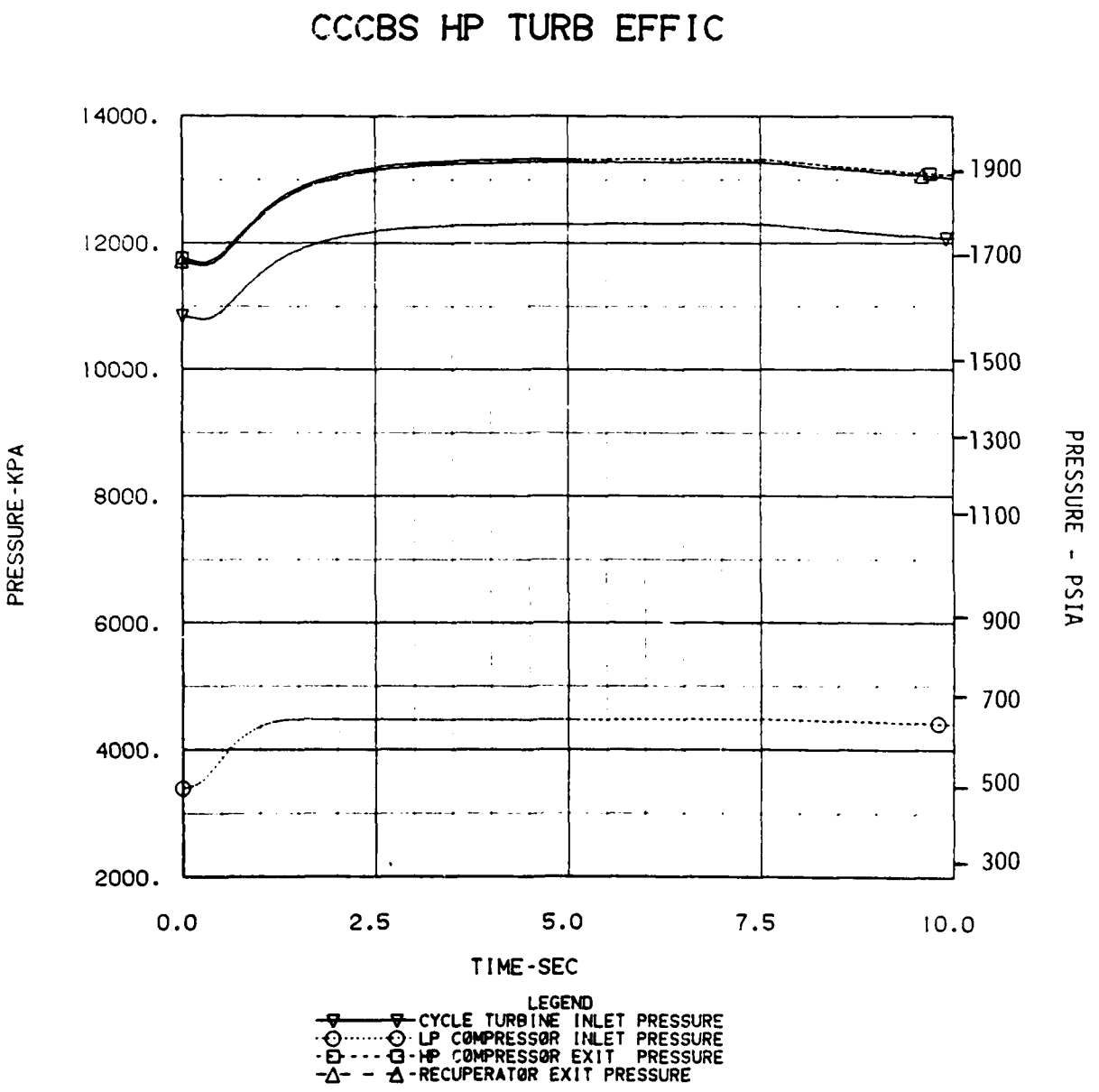

Figure 6-84. Turbomachinery Helium Pressures in Failed Unit

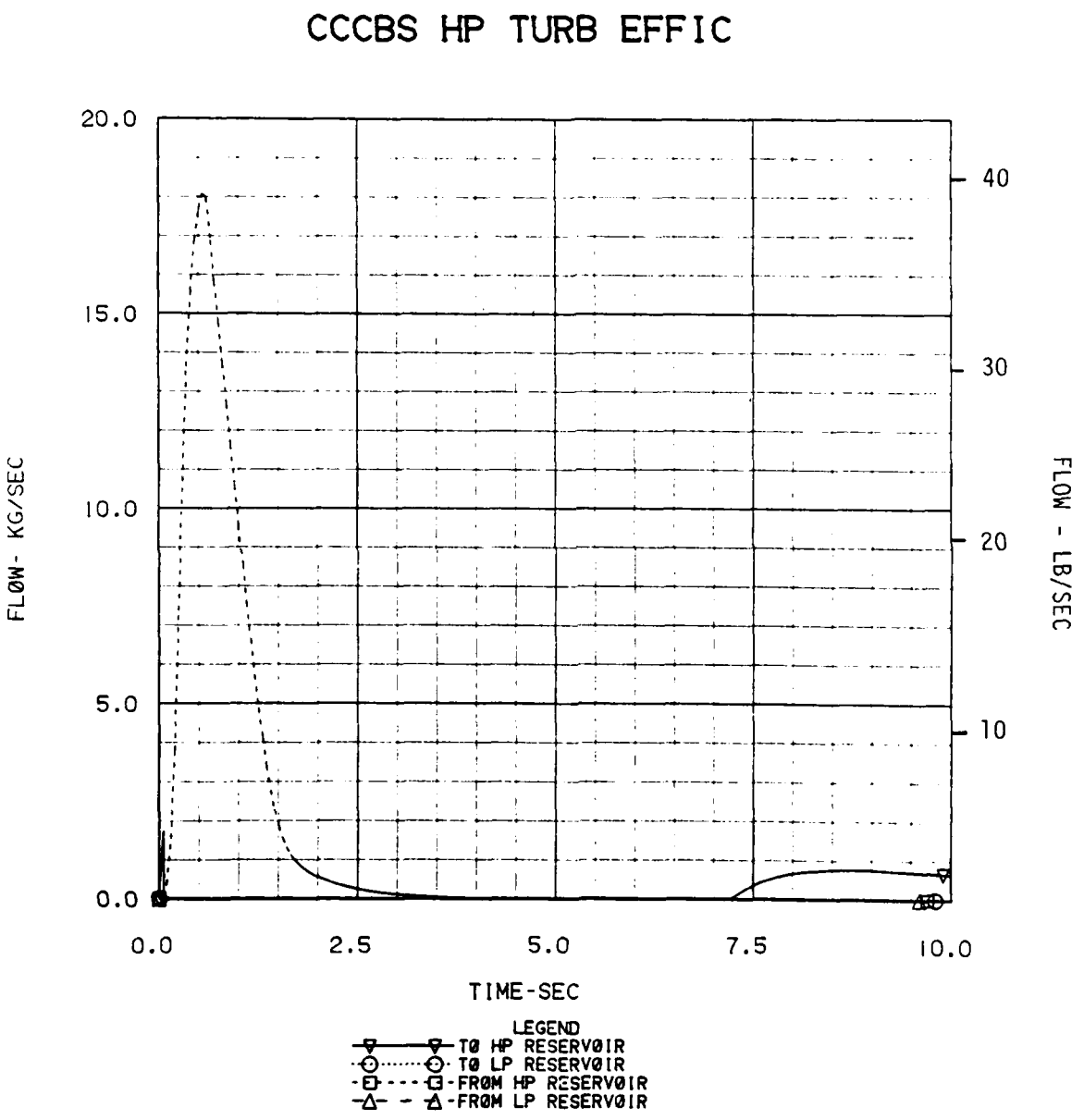

Figure 6-85. Helium Inventory Flows

compressor power increased due to the lower efficiency. This then caused the power turbine speed and output power to drop, resulting in the generation of a helium inventory demand signal.

Similar to the previous case, the plant stabilized with a higher helium inventory and with increased pressure levels. The inventory increased by about 15%, which resulted in about a 700 and 1300 KPA (100 and190 psi) increase in the pressure levels in the low and high pressure regions of the CCCBS (Figure 6-80). The total output power is split once again 46%-54% between the power conversion units, with the normally functioning unit ("B") operating at about 11% over the full-power design point.

The increased pressure levels could possibly require design changes in order to allow the plant to operate at full power. Due to the small likelihood of such a malfunction occurring together with a conservatively high sea water temperature of 30°C, the preferred method would be to operate the plant at a reduced power level. For this case, a total output power level of about 92% of the full-power design point would prevent the normally functioning power conversion unit to run close to the design point, and still permit about 85% of the design point power to be obtained from the malfunctioning unit.

6.1.3.3 STEP CHANGE IN POWER TURBINE EFFICIENCY

Based on the results of the previous analyses, there appears to be no reason why the system cannot be operated with small differences between the two power turbines.

The flow split between both power conversion units would require the plant to operate at a total output power level less than the design point if no redesign efforts are made. However, the shaft power difference between both units is not expected to be more than about 10%, and no major control problems are foreseen as long as the ship is able to operate with this power imbalance.

6.1.3.4 LOSS OF LOAD IN ONE UNIT

During a loss of load condition in only one unit, it would be desirable if the load could be maintained on the unaffected unit and the plant continue to operate Due to the rapid turbine speed increase, this would not be possible with the

reference configuration, which uses solely inventory control and reactor outlet temperature control. The way to control overspeed would be to rapidly reduce the pressure drop through the power turbine. This can be done with either a bypass valve, a helium inventory controller, or a combination of the two. Based on the results for the complete loss of load transient (Section 6.1.2.4), the method that allows for the lowest overspeed condition would be helium inventory control operating in conjunction with a bypass valve in the affected unit.

In Section 6.1.2.4 it was states that a bypass valve might be needed for a complete loss of load case. However, it was found that by shifting the turbine design point to a lower power level the power turbine overspeed could be reduced to a reasonable amount. If one unit operation is desirable, using this method alone would result in much higher turbine speeds. With one unit operating at full power, the helium inventory in the system would be closed to 100 percent of the full-power design point, in contrast to the complete loss of load case where the helium inventory would be reduced to around 25 percent. This results in higher flow rates, higher compressore discharge pressures, and a correspondingly higher turbine pressure drop for the case with one unit operating. All of these conditions would tend to amplify the overspeed condition in the power turbine.

To control the turbine overspeed and still allow for one unit operation, a bypass valve would appear to be called for. A possible valve configuration is shown in Figure 6-86. There could be up to seven of these valve systems in each unit, one for each recuperator. For each system, a pneumatically operated valve allows helium to bypass the turbine and be dumped directly into the recuperator inlet. To avoid overspeeding the turbocompressore shaft or overtemperaturing the recuperator inlet, flow is also bypassed from the compressor exit and mixed with the power turbine bypass flow. To ensure that all the flow is bypassed around the power turbine, a block valve is used at the turbine exit.

The scenario for the loss of load in one unit case would be as follows: the power turbine speed increase in the tripped unit would generate a signal to open the bypass valve and close the block valve. This would cut off the power turbine flow and eliminate the overspeed. As more of the compressor exit flow is bypassed to the power turbine exit, the turbocompressor shaft ramps down to a shutoff

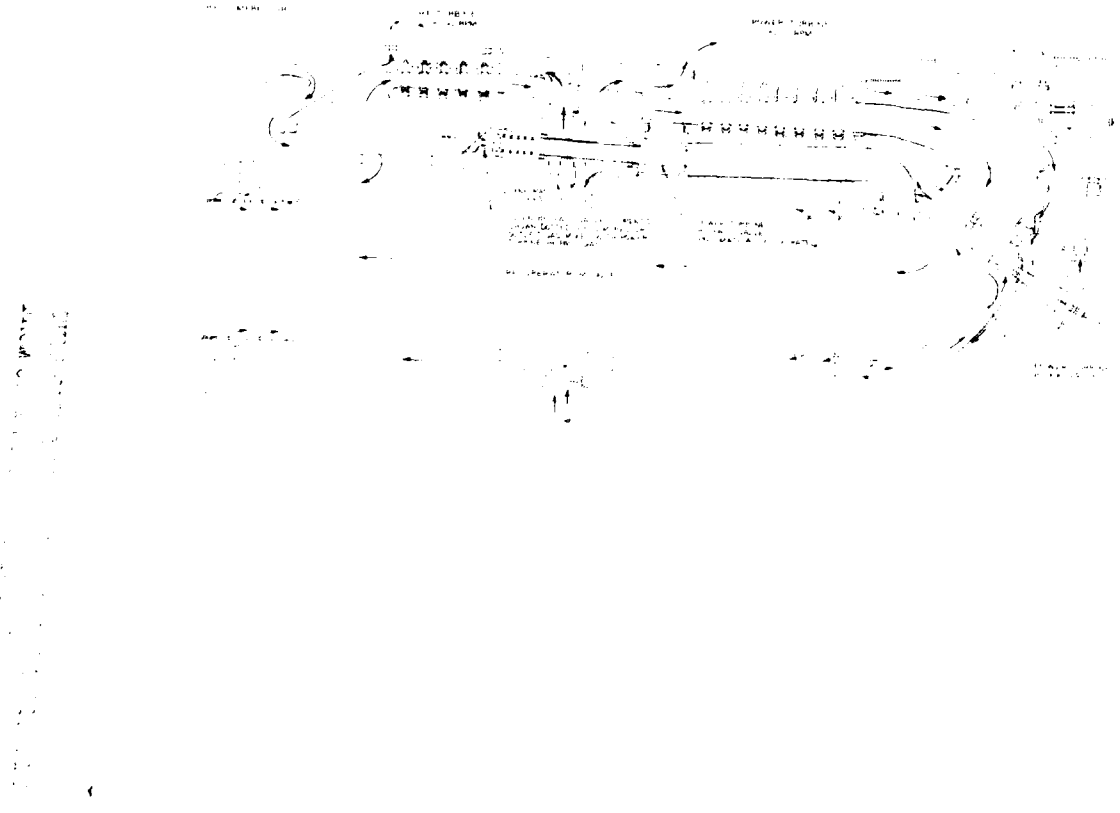

Figure 6-86. Bypass and Block Valve Layout Drawing 102E074

speed. Less and less of the compressor flow from the tripped unit enters the reactor, and the check valves would close to prevent flow from reversing and entering the compressor discharge. Once these valves are closed, the tripped power conversion unit would be isolated from the rest of the plant, and the second unit could continue on line to meet part of the demand load.

While the tripped unit is coasting down and the check valves are starting to close, the helium pressure in the low pressure region of the tripped unit will start to increase as the compressor, cycle turbine, and power turbine pressure differentials are reduced. Also, the temperature in this region will be maintained at about 30°C, which is the water temperature entering the precoolers and intercoolers. As a result, the helium inventory in the tripped unit will increase until it's helium pressure has stabilized at about the level at the exit of the reactor. Since the inventory bottles would be practically empty at the full power point, the helium entering the tripped unit will be drawn from the operating unit thus reducing its output power to between 70 and 80% of its full power value.

The one-unit loss of load transient should not result in any temperature transients in the components downstream of the recuperator that are worse than the cases previously analyzed. The CCCBS components are all designed to meet the high pressures expected during such a transient. In addition, the compressor bypass flow would tend to reduce the pressure difference that exists through the recuperator tubes, enabling the unit to withstand high thermal stresses. The recuperator tubes are made of stainless steel and are able to withstand temperatures in the region of 815°C (1500°F). Thus no redesign of the recuperator would appear to be necessary to meet this transient.

The power turbine could be subjected to higher temperatures than it is designed for as the cycle turbine speed ramps down. At present a detailed analysis has not been performed on the cycle response and hence the resulting temperatures during such a transient. However, there does not appear to be any major problem in designing the turbine to meet the expected high temperatures. If needed, the power turbine could be constructed of the same material as the cycle turbine, and thus allow it to withstand temperatures similar to those that are experienced by the cycle turbine (about 927°C).

6.2 POWERPLANT INTEGRATION

Feasibility of the CCCBS obviously must take into account the interfaces with other propulsion system components and ship installation/interface considerations. Other sections of this report document many of those considerations as they enter into specific concept feature definitions. In addition, this section presents the results of several specific evaluations that were accomplished to define the expected characteristics of interfacing systems and to evaluate the capabilities of the CCCBS to fulfill installation criteria.

6.2.1 DESIGN SHOCK ENVIRONMENT

The shipboard equipment and structures on Navy vessels are subjected to shock loads from underwater explosions. The response of this equipment to a shock load will depend to a large extent upon the structural stiffness of the equipment, the equipment masses and the natural frequencies and mode shapes of vibration of these masses. Other dependencies include the equipment orientation and its location of mounting on the ship. The objective of this work was to perform the necessary analysis upon the subject equipment to determine the component dynamic load response spectra according to the procedures originally developed by the Naval Research Laboratory, Washington, D.C., and these procedures are defined in Reference 3. The dynamic load response spectrum is the equivalent static G load that can be applied to the equipment masses over the range of frequencies of natural vibration for the structural system.

The purpose of this work was to derive the methods for defining shock loads on the CCCBS turbomachinery and to perform an analysis with the objective of establishing the underwater explosion shock loads that could be applied to the turbomachinery masses for rotor and bearing design considerations. The two basic configurations studied and compared here include: (a) the reference design where the reactor and turbomachinery are supported from a pedestal assumed to be hull mounted on a surface ship, and (b) the modified design where the turbomachinery is supported by its flow pipes to the reactor which is assumed to be rigidly attached to the hull of a surface ship at the reactor's pressure vessel lower head flange.

The loads imposed on the turbomachinery masses are computed and compared for the two designs to include only the low frequency contributions from the system which excludes the natural frequencies of the shafts themselves. The reason for this exclusion was that the assumed shafts were found to have natural frequencies in the range of 90 to 97 Hz, resulting in loads in excess of 100 Gs. Future studies may have to be performed to determine how stiff these shafts must be to reduce these high G levels by reducing the participation factors of these masses in the resultant natural mode shapes. Another reason for excluding these modes can be rationalized from their low modal weights being at most only about 5 percent of the total system weight. Usually only the mode shapes contributing about 10 percent or more of the system weight are included.

With the above stated conditions Table 6-3 summarizes the G loads on the turbomachinery masses, and based upon this comparison the modified design with no pedestal shows slightly more favorable loads than the reference design with the exceptions of perhaps the slight differences indicated for bearing thrust loads.

6.2.2 ELECTRIC POWER TRANSMISSION INTERFACES

The characteristics and limitations of a power transmission system have a significant impact upon the power turbine. The characteristics of mechanical power transmissions are well known and their requirements on the power turbine were readily apparent. Compact electric power transmission systems are recognized to be candidates for some of the Navy ships of the future. Although such systems are external to the power conversion system scope as defined for this feasibility study, the impact of the characteristics of this type of load as they effect the interfaces with the gas turbine is of importance. Application of electric power transmission systems to a compact closed cycle Brayton powerplant could introduce interface considerations which do not exist in other installations. Therefore, studies were conducted to identify and address those considerations which could possibly have an important impact upon gas turbine powerplant design characteristics or upon powerplant/ship interfaces that must be considered in the subsequent evaluations of the study. The results of these studies are fully discussed in Reference [ ] and are summarized in this section.

TABLE 6-3

SYSTEM SHOCK LOADS FROM UNDERWATER DETONATION IMPARTED TO THE CCCBS TURBOMACHINERY COMPONENTS WITH HULL MOUNTING ON SURFACE SHIPS

Component	Model	Thrust, G^S	Normal, G^S
Power Turbine	Ref.	5.50	17.76
Power Turbine	Mod.	7.00	16.37
High Pressure Turbine	Ref.	7.84	17.39
High Pressure Turbine	Mod.	7.30	12.86
High Pressure Components	Ref.	7.24	15.37
High Pressure Components	Mod.	7.23	12.41
Low Pressure Components	Ref.	6.46	15.56
Low Pressure Components	Mod.	7.13	13.83

Ref. = Reference Design with 63 DDOF

Mod. = Modified Design with 44 DDOF

Interest in electrical propulsion systems has resulted from its inherent ability to provide a satisfactory speed reduction between a high speed, efficient, lightweight prime mover and a slower, efficient propulsor. As well, certain flexibility of design regarding plant choice and arrangement yields rewards to the naval architect and owner. Rapid maneuvering control is advantageous to the ship operator. Briefly summarized, the advantages of electrical propulsion include:

- Flexibility of ship arrangements due to freedom of location of major components relative to prime movers.
- Economy of operation with multiple prime movers to reduce the high fuel rate at part load.
- Flexibility, availability, and interchangeability among multiple prime movers.
- Use of high efficiency unidirectional prime movers.
- Optimum maneuverability through relatively simple control systems.
- Capability to provide higher torques at reduced speeds.
- Ease of adaptation to automated plant control.
- Possible reduction in crew size through automated control of machinery.
- Low maintenance cost of electrical transmission system.
- Ease in providing pilot house and remote controls.
- Reliability of operation of overall system.
- Reduced vibration and structure-borne noise.

These manifold advantages of electric dirve are related to specific applications. Further, the advantages and merits of one system over another are in a complex relationship among the following variables:

- Horsepower level and rpm required in the ship concept under study.
- Desired maneuvering requirements and the minimum maneuvering requirements acceptable.
- Alternative uses of main propulsion power anticipated in the ship system.

- Proportion of weight fraction that can be allotted to the propulsion system.
- Geometrical constraints of the hull-propulsion system interface.

The excellent reliability of electrical propulsion systems and the flexibility provided by the ability to separate prime mover from propeller shafting have been significant in the history of marine propulsion. In particular, the advent of superconducting electrical machinery suitable for ship propulsion had indicated great reductions in weight and volume. This is particularly evident for high performance ships -- including hydrofoil and Surface Effect Ships, where the use of lightweight electrical propulsion apparatus will allow the unusually high horsepower required to be delivered from the prime mover to the thrusters usually located remote from the powerplants. This is an attractive alternative to right angle gearing which experiences low endurance and reliability in the marine environment. The hydrofoil motor can be contained within a propulsion pod due to its small diameter and the SES can be propelled by super-cavitating props or water jets. In summary, the application of superconduction electrical machinery to ship propulsion will result in an increase of flexibility, system efficiency, and a decrease of volume and weight relative to conventional systems.

The use of superconducting transmission bus, however, is not practical at this time for ship propulsion systems, thus generators and motors are the most feasible candidates for superconducting technology. Systems under consideration are presently all ac, all dc or hybrid combinations of ac and dc. Certain applications to high speed propeller ships such as hydrofoils and SES, which do not require reversal, appear naturally suited for ac synchronous installations. Other installations are not so easily defined as to the optimum propulsion plant. The traditional high maneuverability aspect of dc propulsion that has been in service in tugs, ferries and icebreakers may be difficult to achieve in certain installations of superconducting homopolar generators and motors, due to the extremely high magnetic energy stored in the fields and the requirements that they be varied in very short time intervals.

Many electrical propulsion installations have used generator field control coupled with control of governing of prime mover speed. The importance of prime mover and load scheduling will increase as the need is recognized for good fuel consumption.

In many propulsion applications utilizing electrical components, control of motor speed is achieved through variations of several parameters:

- Generator output voltage by speed control of prime mover, generator excitation, or combinations of both.
- Field of propulsion motor.
- Input voltage to the motor terminals through control circuitry.

The required power level is determined by the torque demanded at specific propulsor speeds as a function of ship speed. This torque is generally proportional to the current drawn by the propulsion motor, and the field strength which is related functionally to the speed of rotation.

Several cases of ship propulsion have been surveyed, with information gathered to determine feasibility of concept application over the power and rpm range involved. Some of these applications will require reversal and operation at various rpm in both forward and reverse directions. In some instances, the reversals are required quickly, possibly in rapid succession and in minimum time.

A number of ship propulsion applications involve high powers at revolutions much higher than those of conventional displacement ships. These include advanced marine vehicles such as hydrofoils, surface ships, and certain types of planning hull vessels. In these types of installation, reversal is not required for the high power shaft and these ship types are the most likely to use the compact CCCBS power source. For use in the nonreversing high rpm propulsion system, superconducting ac synchronous generators and motors, seem more attractive combinations. Indeed, the use of homopolars, superconducting or not, for SES thrust and lift would be difficult due to distribution problems of the low voltage, high current power to lift fans and propulsions thrusters through extraordinarily heavy copper bus bars. Higher voltage dc generators to alleviate this problem have to be considered by they lead to other design problems discussed later.

With regard to variation of field current and flux parameters, it will suffice here to note that typical dc electrical propulsion applications utilize variation of generator excitation to achieve voltage control over the range from zero

output to saturation voltage output at the minimum speed of the prime mover. The remaining system voltage is generated by increase of prime mover speed from the minimum to maximum speed. In a ship propulsion application, this variation of voltage will vary the motor speed in a reasonably linear fashion, with the increased torque loading drawing current as required by the characteristics of the load.

Typical ac electrical propulsion installations rely on simultaneous control of excitation, prime mover, and phase interconnections. In typical synchronous ac installations, switchgear or contactors are used to interconnect the phase order of power into the synchronous motor for directional control. The prime mover is brought from set power to a low value to permit the interchange of phases. Simultaneous control of excitation is required, decreasing to enter the asynchronous induction mode of operation. Over excitation of generators and run-up of prime movers will lock the motor into synchronism in the reverse direction.

The steady state and transient response of superconducting electrical machines must be completely defined prior to successful shipboard implementation. The naval ship propulsion system must be capable of reliable operation under a wide range of typical marine environment operating conditions that represent transient motion of the naval vessel, including:

- Conventional speed and course changing maneuvers
- High-speed turns
- High-speed reversals
- Ship twisting maneuvers
- Any combination of the above

These maneuvers introduce transient departure from steady state conditions into the electromechanical power transmission system, transients which must either be accepted or attenuated, as they manifest themselves in certain instances as ac rotor losses. The general thermal transients introduced into the cryogenic superconducting mode, the quench situation must be avoided. The transients under consideration could generate inception of quench (normalization) in the superconductor

if they are not understood and considered. This combination of transients, reflected from the thruster element of the ship propulsion transmission system, is manifest as electrical and mechanical phenomena in the system, and is ultimately transmitted to the prime mover through the electromechanical network.

These transients will reflect themselves into motions departing from the electromechanical steady state and manifest themselves as certain ac losses in the superconductor field winding. These losses must be compensated for in the design with sufficient helium flow for the field winding or eliminated by sufficient shielding by damper attenuating windings or by electromagnetic shielding coils. While these losses must be tolerated in some sense, they will essentially determine the refrigeration sizing in propulsion systems.

6.2.2.1 ELECTRICAL EQUIPMENT SYSTEM CONSIDERATIONS

This section considers the factor influencing the selection of various components and subsystems, and the resulting identifiable parameters and characteristics of the system.

The selection of systems requires the investigation of the alternative ac, dc, and hybrid combinations; the influence and significant consequence of candidate propulsor types; and the optimization of the liquid helium refrigeration system configuration for a given ship concept.

System composition may then be detailed into identification of such major components as motors, generators, and refrigeration, as well as essential subsystems of excitation, cables and current transmission, control, power conditioning, switchgear, and protection circuitry. The characteristics of available prime movers, and the requirements of significant auxiliaries will be discussed.

System parameters such as voltage, temperature, overload capacity, and ventilation must be considered, as well as an examination of the critical speed range in the propulsor-shaft-motor elastic mass system.

A large number of candidate systems for electric ship propulsion applications can be separated into three distinct families, each of which can be further divided into superconducting and non-superconducting:

- Alternating current (ac) systems
- Direct current (dc) systems
- Hybrid combinations of ac and dc components

The results of studies of these basic systems are discussed and further classified in Reference 4. The studies indicated that the characteristics and interface requirements of the ac superconducting system are representative of the electric power transmission conditions which should be considered in the CCCBS evaluations. Therefore, some of the results for the ac superconducting system are included below.

6.2.2.2 SIZE AND WEIGHT OF MACHINES

To determine approximate sizes of machines for this study, several computer codes (developed earlier by Westinghouse) were utilized. The aim was to ascertain the approximate diameters, lengths, weights and efficiencies of superconducting machines capable of generating power at an assumed level of 52.2 MW (70,000 HP) and powering assumed loads of 37.3 MW (50,000 HP) and 3.7 MW (50,000 HP). These power levels were assumed in order to take advantage of previous work performed on high performance class vehicles at these levels as both a reference and a base for extrapolation to higher or lower power levels. Since one of the goals of the Compact Closed Brayton Cycle System (CCCBS) Study was to utilize electrical machinery that was small and of low weight and yet capable of delivering the stated powers, it was anticipated that there would exist optimum machines to fulfill this goal. With the realization that these machines would be used for ship propulsion systems, and without a specification of either the type of ships on which they would be installed or the types of propulsors on these ships, some basic assumptions had to be made. It was therefore assumed that since small, lightweight machinery was desired, these electrical propulsion systems would be used on high performance ships such as hydrofoils or Surface Effect Ships where size and weight are primary concerns. It was considered that their application to conventional displacement type ships would be of secondary importance. It was further assumed that since the CCCBS would most likely be used on these high performance ships, high speed propulsors typified by supercavitating propellers or waterjet pumps would be utilized. Required power was assumed to vary as the cube of the speed for supercavitating propellers while duct control was assumed

to vary as the cube of the speed for supercavitating propellers while duct control was assumed for thrust control of the waterjet. Until a specific ship type and control method is specified, the electrical equipment arrangement assumed must be considered only in general terms. In addition the dimensions and weights given here must be considered approximate as complete designs were not made since the same general guidelines and include the essential electrical, magnetic and mechanical components and probably reflect the actual machine weights and dimensions within 10 percent. Such components as shaft extensions, pedestal, brush supports and mounting feet are not included, nor are any internal or external cooling devices.

In all systems, ship's service power was assumed to be obtained from an auxiliary generator and not from the main power source. This was done to allow higher speed main generators. Thus for the ac system, main power could be at a frequency higher than 60 Hz, allowing more compact generators and propulsion motors while ship's service power could be generated at 440 volt, 60 Hz to comply with the loads.

6.2.2.3 SUPERCONDUCTING GENERATOR

Investigating the effects of changing output voltage and speed of the main superconducting ac generators while varying the rotor diameter indicated that output voltage did not have a great impact on machine size. Figure 6-87 shows the trend in machine weight and efficiency as rotor diameter is varied. As the plot indicates, speed has a decided impact on weight of the generator of approximately 2122 kg (6000 pounds) between the 12,000 rpm and 6000 rpm designs. Efficiency is also improved by approximately one-tenth of 10 percent, although this slight improvement may not be significant. Thus if weight were the prevalent parameter, the optimum design would be the 12,000 rpm design. However if compactness is considered, all of the optimal weight designs tend towards small diameters and long lengths, being more pronounced at the 6000 rpm design than the 12,000 rpm deisgn. Figure 6-88 indicates the stator OD and the bearing-tobearing length variations plotted against rotor OD. By comparing Figures 6-87 and 6-88, it is seen that the lowest weight machines are in the range of rotor diameters of 19 to 20 cm (7-½ to 8 inches which are still on the steep part of the length to rotor diameter curve. Thus if compactness is desired, a rotor diameter of about

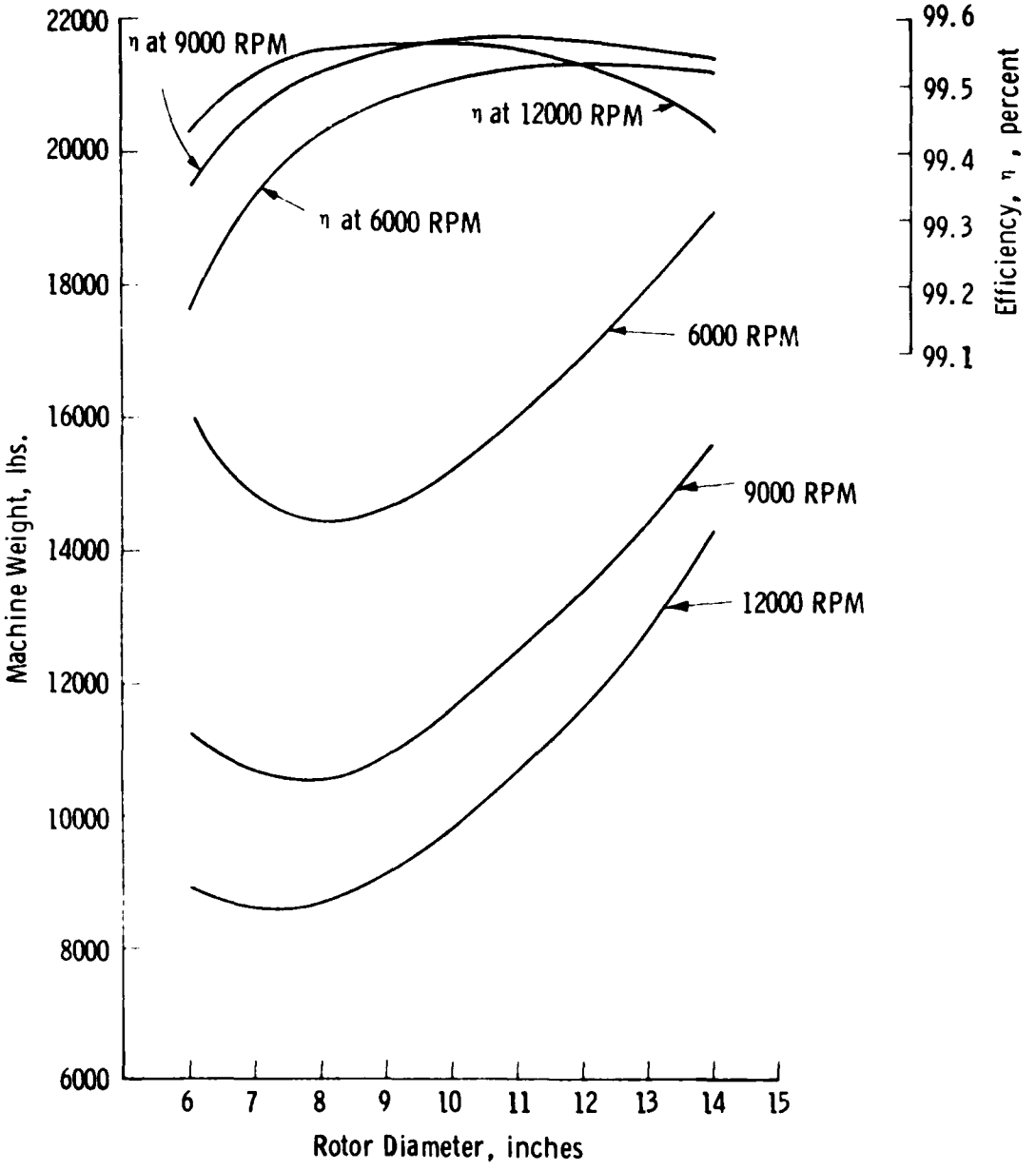

Figure 6-87. 52.5 MVA (70 KHP) Generator 13.8 KV

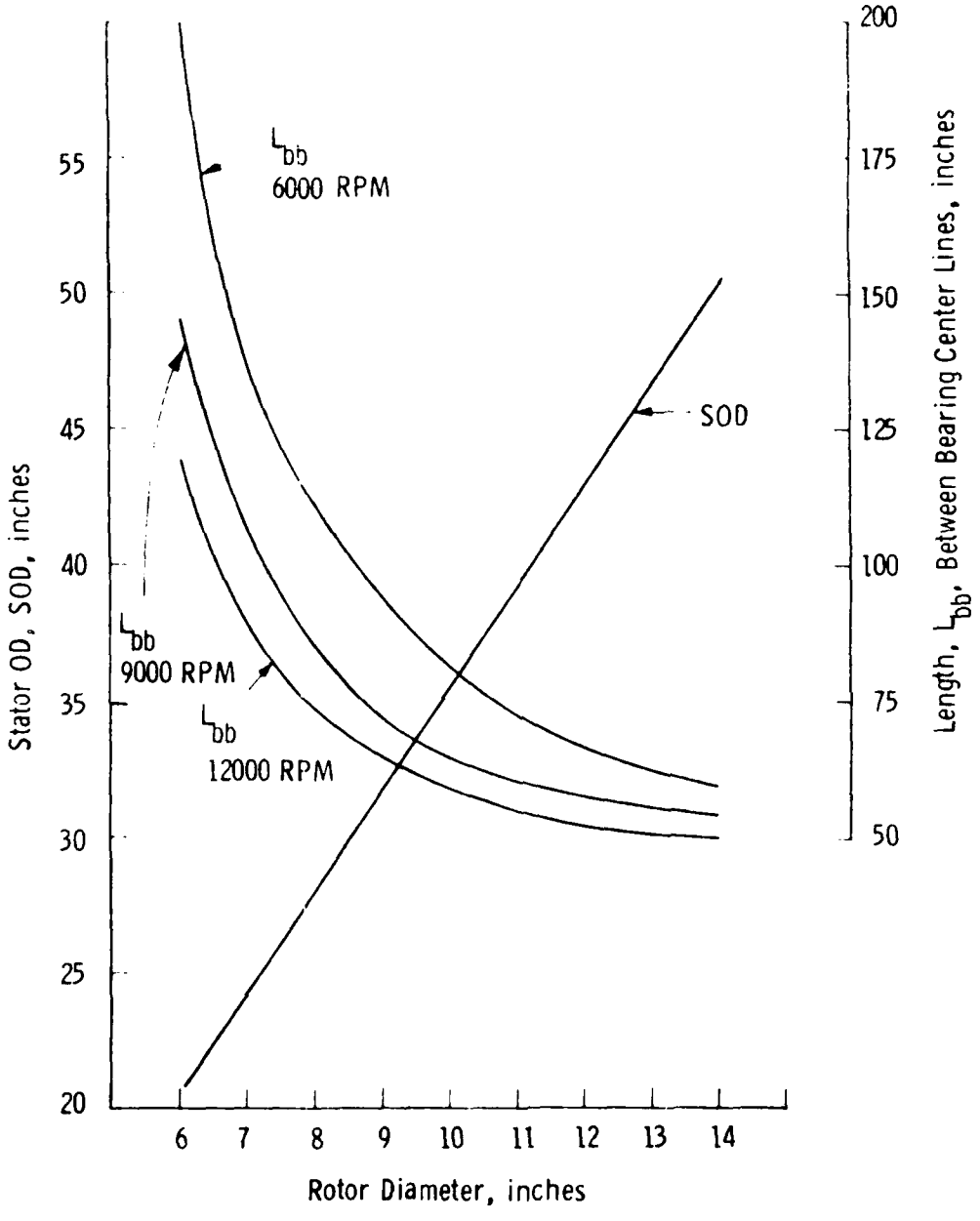

Figure 6-88. 52.5 MVA (70 KHP) Generator 13.8 KV

23 to 25 cm (9 to 10 inches), at a slight weight penalty might be a better choice. The stator outside diameter curve increases linearly with increased rotor diameter. If the optimum designed machine is defined as that machine with the highest efficiency, then machines in the range of 23 to 30.5 cm (9 to 12 inches) would be selected, again however, at a penalty in weight.

As stated previously, the optimum machine in terms of size, weight and efficiency is better at 12,000 rpm than at 6000 rpm. There are however some design problems associated with the higher speed machines, particularly in regard to the helium flow for rotor cooling, bearings and rotor deflection stresses that would require more development effort before they can be proven to be economically and technically feasible at the smaller rotor radii.

For a 52.2 MW (70,000 HP) dc generator of the SEGMAG II design, voltage is a much more critical parameter, particularly as it determines the current output. The highest voltage that was considered practical was a 2000 volt machine which gave an output current of 26,100 amps. This large current required large conductor cross-sectional areas and because of the limited circumferential length of the 40 cm (15-3/4 inch) rotor diameter led to deep bars which increased the magnetic gap of the machine and a larger number of ampere turns for excitation. Lowering the system voltage intensified this problem and raising it led to current collector bar voltages that were excessively high. Going to larger rotor diameters alleviated the excitation ampere turns; however, the tip velocities of the collector bar-brushes interface became excessively high. Even with the 40 cm (15-3/4 inch) rotor diameter, tip speeds at the brush interface are considerably higher than conventionally accepted values. The length of the machine between bearings ia approximately 610 cm (240 inches) which would present critical speed problems. With a stator outside diameter of 108 cm (42.5 inches) and a total machine weight of 28,100 kg (62,000 pounds). This dc generator could not be considred small, compact or lightweight and hence was dropped from further consideration. The only feasible machine design at this power rating would be at a much slower speed and therefore larger, heavier generators; however, since this slower speed reflects back to a slower, larger power turbine it was not further considered.

6.2.2.4 SUPERCONDUCTING MOTORS

Although the ac motor speed was assumed to be driving a 37.3 MW (50,000 HP), 1200 rpm load, the parametric variations of superconducting generator speed resulted in changing the number of poles of the motor to accommodate the different frequencies. At 6000 rpm and 12,000 rpm generator speed, the number of motor poles were 10 and 20 respectfully; however at the 9,000 rpm generator speed the number of motor poles was 16, resulting in a motor speed of 1125 rpm which is the closest speed match to 1200 rpm possible. In the optimization process, the higher number of poles results in lighter weight machines at slightly higher rotor diameters due to the improved pole-face to pole-pitch ratio. This is shown on Figure 6-89 which indicates minimum weight at rotor diameters of 96.5, 132, and 152.4 cm (38, 52 and 60 in.) respectfully for the 100, 150 and 200 Hz motors. As in the case of the generators, machines of minimum weight are not necessarily the most compact, as shown on Figure 6-90 where the length (between bearing centerlines) is plotted for each motor. The more compact machines in terms of length and stator outside diameter tend toward the higher rotor diameter at a slightly higher weight penalty. Peak efficiencies also tend to favor the higher rotor diameter designs.

For ac motors of lesser capacities, usually used for lift fans in SES vessles, 3.7 MW (5000 HP) was chosen as a typical horsepower rating at a speed of 1500 rpm. As in the other ac machines, varying the machine voltage had little effect on the motor size. Frequency variations, dependent on the generator speed, also produce only small variations in motor weight, as shown on Figure 6-91. As shown on this figure, the minimum weight for both the 100 Hz and 150 Hz motors is about 2000 kg (4400 pounds) while the 200 Hz motor is about 2130 kg (4700 pounds) which is within the 10 percent accuracy of the calculations. These minimums occur at rotor diameters of 50.8, 71.1 and 86.4 cm (20, 28 and 34 inches) for the 100, 150 and 200 Hz machines respectively. Machine lengths are plotted on Figure 6-92 which show that these minimum weight machines are near but not quite at the optimum lengths. For more compact motors, rotor diameters 10 cm (4 inches) greater would be more nearly optimum. Efficiencies would also be significantly improved at these slightly larger rotor diameters.

Investigating dc motors for delivering 37.3 MW (50,000 HP) at 1200 rpm, it quickly became apparent that the weights of the machines would not be comparable with the

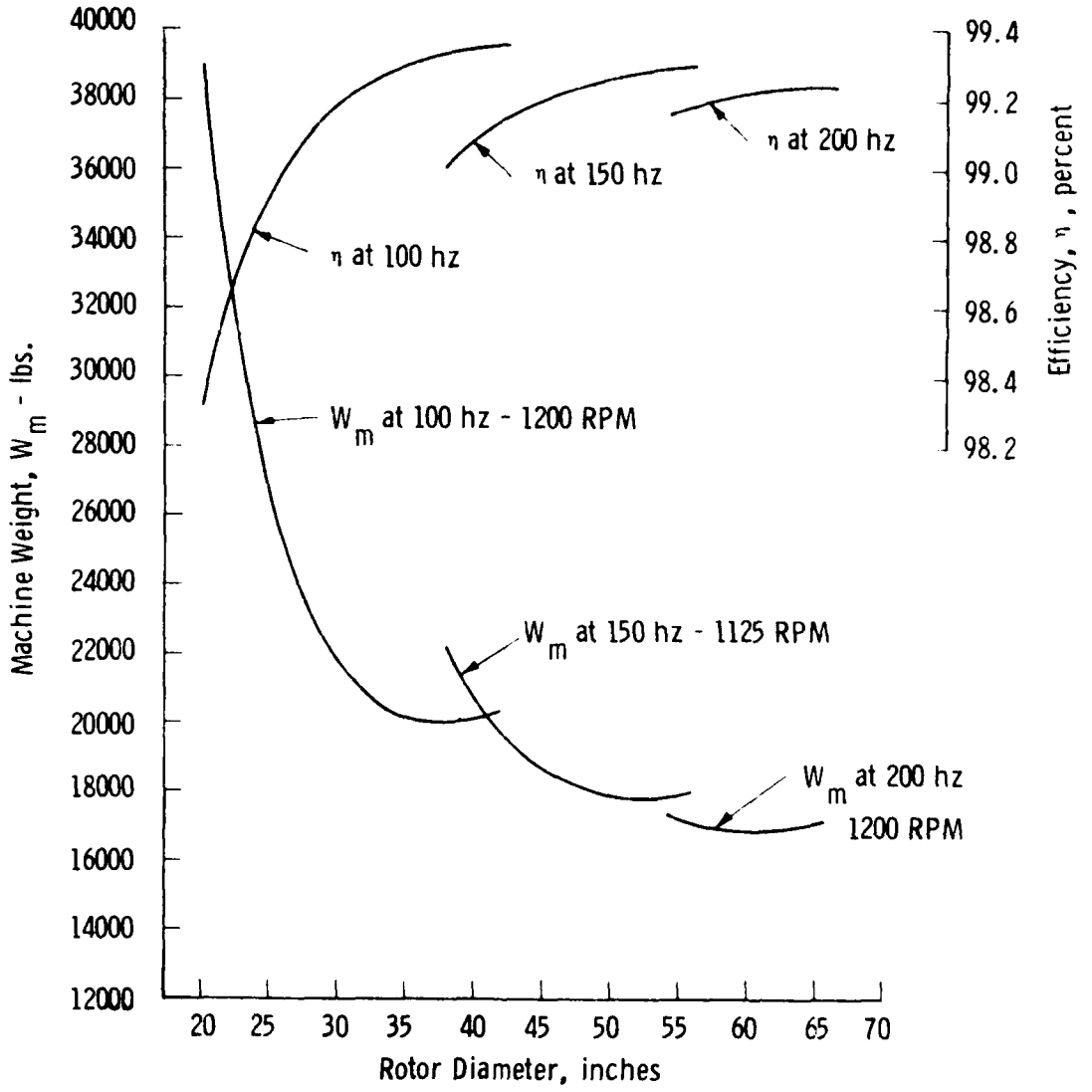

Figure 6-89. 37.3 MW (50,000 HP) Motor

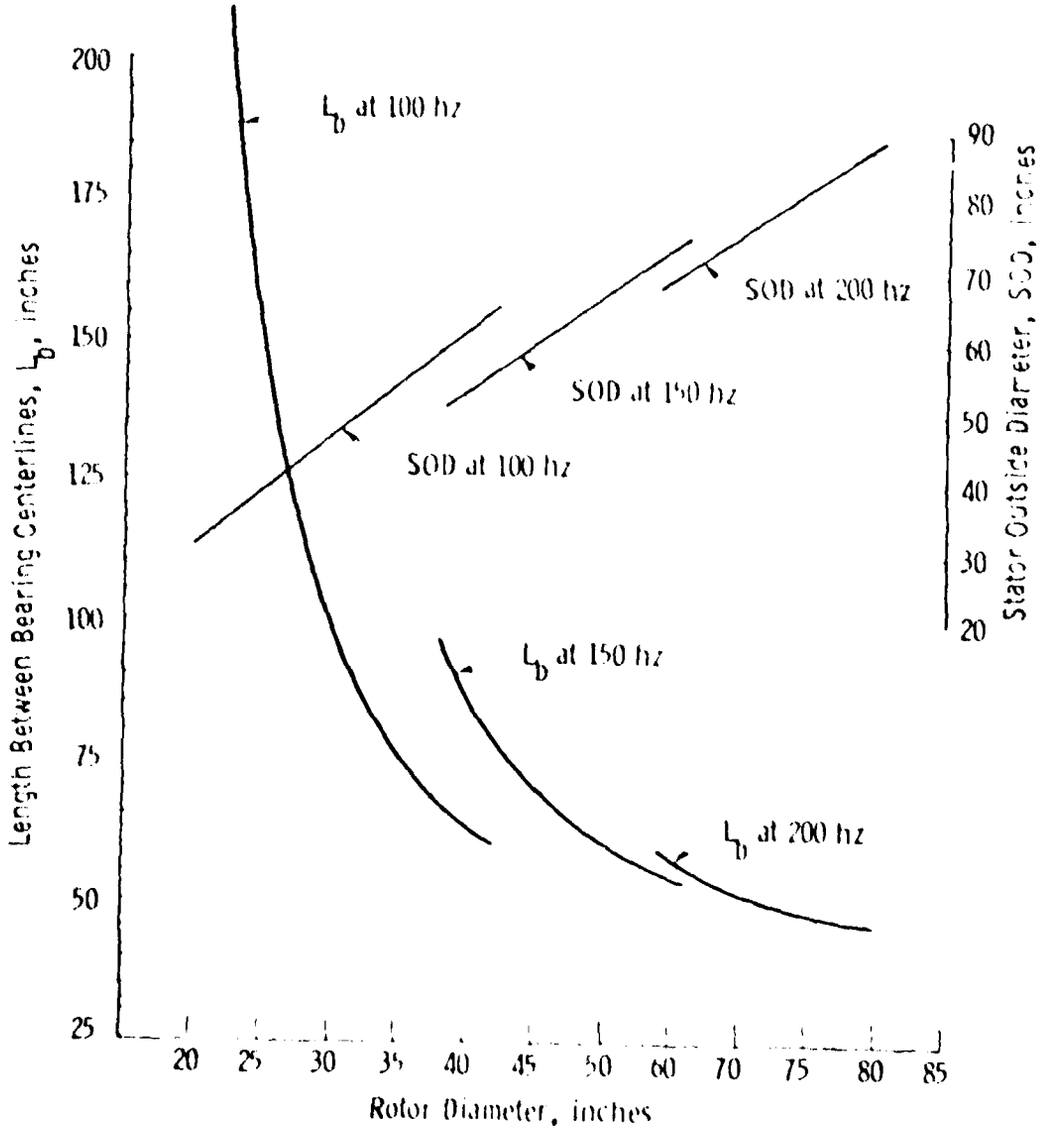

Figure 6-90. 37.3 MW (50,000 HP) Motor

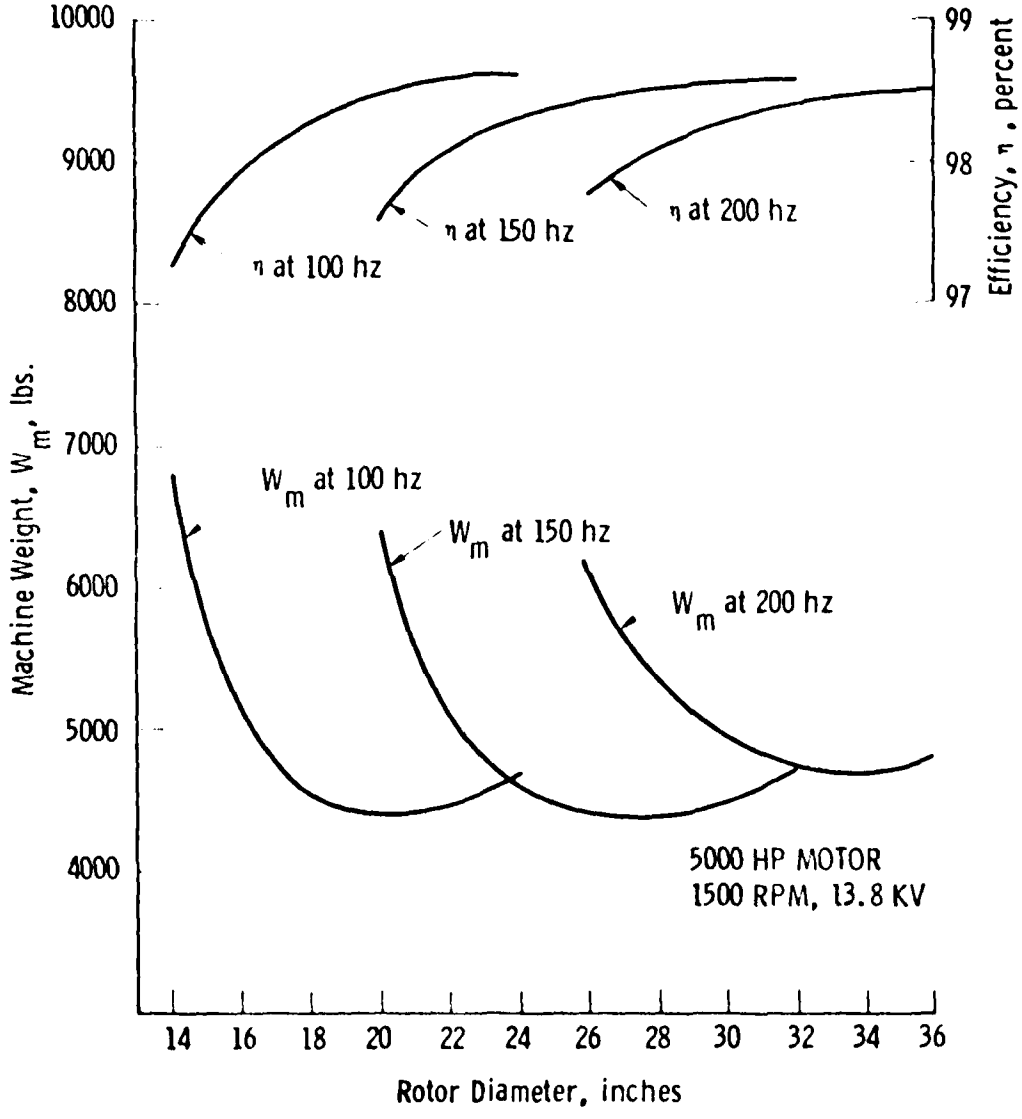

Figure 6-91. 3.7 MW (5000 HP) Motor 1500 rpm, 13.8 KV

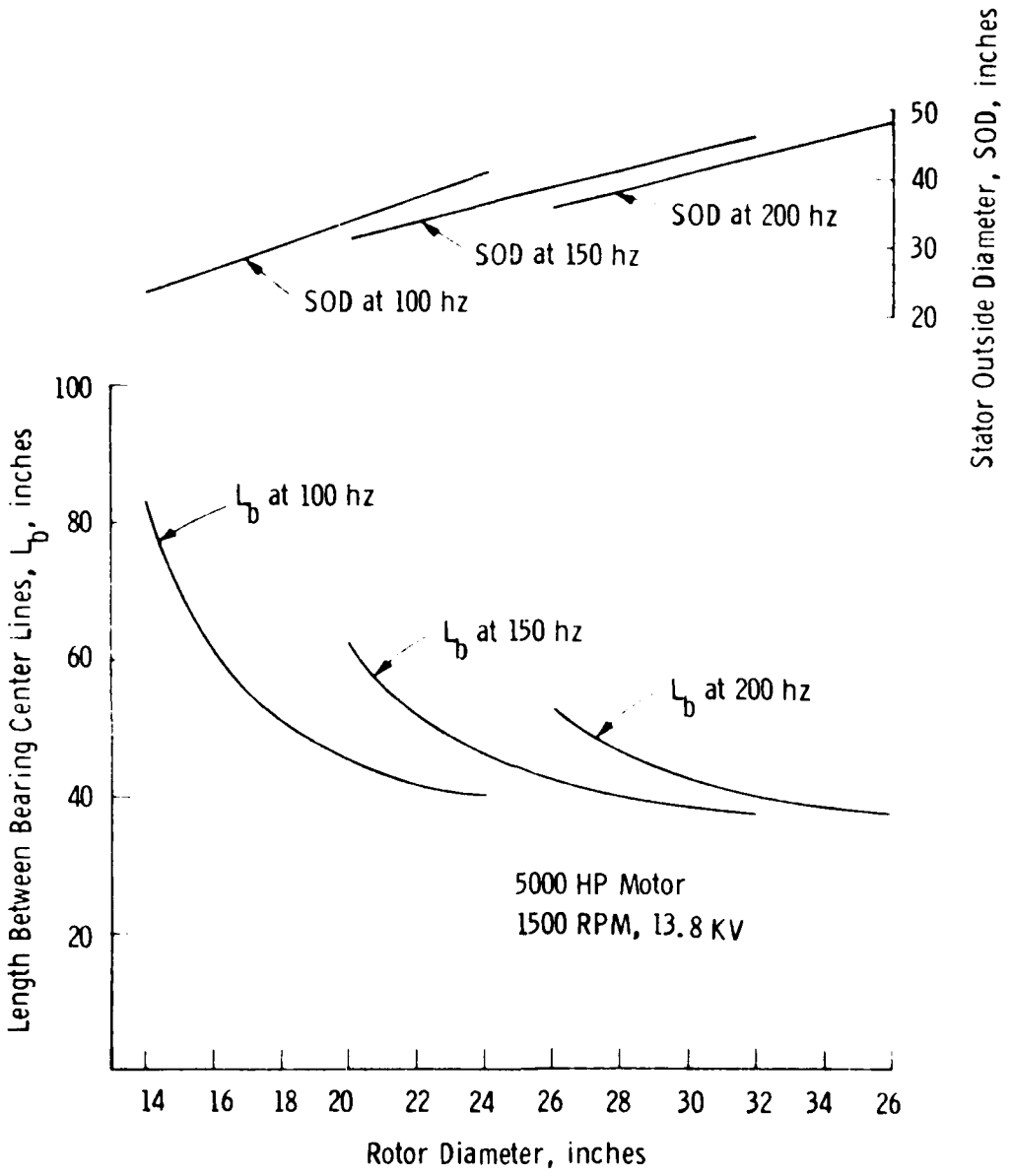

Figure 6-92. 3.7 MW (5000 HP) Motor 1500 rpm, 13.8 KV

superconducting ac machines. This is primarily due to the lower flux densities inherent in these machines and the amount of iron necessary to carry the required flux. The principle parameters of the most promising design developed are:

Rotor Diameter	114 cm (45 inches)
Stator Outside Diameter	170 cm (67 inches)
Length Between Brg. Centerlines	378 cm (149 inches)
Total Weight	47,620 kg (105,000 pounds)

Parametric variations of rotor diameter around 115 cm (45 inches) had no appreciable effect on the machine weight. Since this weight was five times greater than the ac motor and also since the corresponding dc generator was similary large and heavy, further investigative effort on dc motors seemed unwarranted.

By observing the plots of ac machines, one can pick designs which are the lightest weight, most compact or the most efficient depending on which criteria is used in defining the most optimum machine. It would appear however that machines with rotor diameter slightly greater than those with minimum weight would be more nearly optimum in terms of compactness and efficiencies with only slightly greater weight penalties. Systems incorporating these machines (assuming 13.8 KV machine voltages) would utilize exciters, switchgear and control equipment of approximately the same size and weight and therefore total system weight would be dependent on the generator speed-chosen. For example if it is assumed that a system consists of four propulsion generators, two propulsion motors and four lift-fan motors, total machine weights would be as shown in Table 6-4.

Selecting the 12,000 rpm generators over the 6000 rpm design would then result in a system machinery weight advantage of about 12,880 kg (28,400 pounds) if minimum weight machines were selected. If a weight penalty is accepted in order to achieve compactness and slightly higher efficiencies, this weight advantage would decrease to 11,340 kg (25,000 pounds). It must be reiterated here that this weight advantage may not be achievable due to problems of the 12,000 rpm generator. A much more detailed design of the generator would be required to determine its feasibility.

TABLE 6-4

MACHINE WEIGHTS

	Weight at 100 Hz		Weight at 200 Hz	
	Minimum	Penalty	Minimum	Penalty
Generators	26,300 kg (58,000 lbs.)	6,170 kg (2,800 lbs.)	15,600 kg (34,400 lbs.)	1,090 kg (2,400 lbs.)
Prop. Motors	18,140 kg (40,000 lbs.)	360 kg (800 lbs.)	15,420 kg (34,000 lbs.)	270 kg (600 lbs.)
Lift	7,980 kg (17,600 lbs.)	90 kg (200 lbs.)	8,530 kg (18,800 lbs.)	180 kg (400 lbs.)
	52,420 kg (115,600 lbs.)	1720 kg (3,800 lbs.)	39,500 kg (87,200 lbs.)	1,540 kg (3,400 lbs.)

Based upon these and other studies, it appears that a speed of 9,000 rpm for the ac superconducting generators should be acceptable and can be assumed for CCCBS interface conditions.

6.2.3 ENERGY SOURCE HEAT EXCHANGER INTERFACE CONSIDERATIONS

As discussed in Section 1.0, the results of the overall CCCBS study are to be as generally applicable as possible and the scope of the CCCBS power conversion system therefore does not include a specific energy source. The CCCBS power conversion system is considered to interface with, but not include, either a fossil fired heat exchanger or a gas cooled nuclear reactor wherein the energy is added to the closed Brayton cycle. This CCCBS system definition permits studies and evaluation of the system with consideration given to the various alternate heat sources which the Navy may desire to use without constraining the studies by the characteristics of a single fuel and heat exchanger assumption.

Evaluations of the power conversion system must, however, recognize and give proper consideration to the expected ranges of fossil fired energy source heat exchanger characteristics to insure that the results are appropriate for applications which may be selected. An early study was therefore required to provide the necessary consideration of power conversion system/energy source heat exchanger interfaces. In this study the state-of-the-art of heat exchangers was evaluated to identify and quantify the interfaces of importance and the requirements placed upon the power conversion system from energy source heat exchanger considerations. These results therefore provide input to the Design Concept definition and later evaluation of feasibility.

6.2.3.1 HEAT EXCHANGER DESIGN CONSIDERATIONS

The state-of-the-art survey to evaluate representative heat exchangers and their performance limits is constrained by several factors that must be considered in the design of a fossil fuel fired CCCBS. A principal requirement for high temperature heat exchangers is that they must operate for long periods at high temperatures with large pressure differentials between the gas streams. For compact lightweight propulsion systems, the energy source heat exchager must provide high effectiveness with a minimum impact on overall system volume and weight and must be capable of withstanding the high shock environment required for naval propulsion powerplants. To minimize potentially significant performance penalties, [illegible] between the gas streams [illegible] minimized. The

characteristics of the combustion gas stream also impose additional considerations such as oxidation resistance and susceptibility to flow stoppage.

Table 6-5 summarizes generalized candidate configurations and potential advantages and disadvantages. The tube and shell configuration is inherently more suited for this application compared to the plate/fin configuration because it is better suited to withstand high stress loadings and to minimize leakage and plugging of the combustion products.

For high temperature heat exchangers, material temperature limits provide a major constraining factor. Superalloys have been utilized in most high temperature metallic concepts and the design and fabrication of superalloy heat exchangers is a well developed technology. In addition, superalloys are oxidation resistant. A major drawback is their limited maximum temperature capability. Refractory metals have high temperature strength capability, but are difficult to fabricate and have little resistance to oxidation, thus precluding their use as the energy source heat exchanger. Graphite is an excellent high temperature structural material; however, its permeability to low molecular weight gases and the lack of high integrity joining process make its use unlikely. Ceramics also are excellent high temperature structural materials that are oxidation resistance and low in cost, but are brittle, Permeability and fabrication of ceramic heat exchangers are design problems. The considerable development efforts currently being applied to ceramic heat exchangers should lead to a solution to these problems for stationary powerplants. The material candidates that offer the best potential for near term and, eventually, long term consideration, therefore, are the superalloys and ceramics, respectively.

As a result of these considerations, the state-of-the-art survey was concentrated on tube and shell designs incorporating superalloys and ceramics.

6.2.3.2 RESULTS OF CONSIDERATIONS

The state-of-the-art survey consisted of evaluating heat source heat exchangers, intermediate heat exchangers and recuperators which have been designed for several technologies and have been carried to various states of development ranging from conceptual design to operational.

TABLE 6-5

BASIC DESIGN CONSIDERATIONS

	ADVANTAGES	DISADVANTAGES
CONFIGURATION:		
Tube and Shell	Leak Tight High Stress Loading	Headering
Plate Fin	Lower Material Cost for Equivalent Surface Area to Volume Ratio	Stress Load Capability Lack of Leak Tightness Susceptible to Plugging of Combustion Gases
MATERIALS:		
Superalloys	Low Cost Oxidation Resistance Fabrication Experience	Temperature Limited to 955°C (1750°F) for Long Life Limited Long Life Experience
Refractory Metals	High Temperature Strength Capability	High Cost, No Oxidation Resistance Difficult Fabrication Little Experience in Long Life
Ceramics	High Temperature Capability Oxidation Resistance Low Cost Material	Brittle Questionable Permeability Limited Fabrication Capability
Graphite	High Temperature Capability Low Material Cost Fabrication Experience	No Oxidation Resistance High Permeability Brittle

Applications considered included:

- Closed Cycle Gas Turbines Systems
- Process Industry Systems
- High Temperature Gas Cooled Reactor (HTGR) Systems
- Central Plant Topping Cycles
- Magnetohydrodynamics Systems
- Rankine Cycle Systems

The characteristics of several metallic heat exchangers at various stages of development are shown in Tables 6.6a and 6.6b. For heat exchangers presently in operation, peak wall temperature up to 860°C (1580°F) have been noted with process gas temperatures up to 1430°C (1450°F). The pressure level for these designs have ranged from 0.2MPa to approximately 3.4MPa (50 to 500 psia). Commonly used tube materials have included the superalloys Inconel 807, Incoloy 800, and Haynes 188. Tube diameters have ranged from 0.6 to 5.1 cm (0.25 inch to 2.0 inches).

The upper limits in temperature and pressure for the Inconels presently used today is a wall temperature of approximately 900°C (1650°F) with pressure differentials in the 3.4 to 6.9MPa (500 to 1000 psi) range. In a practical design, a process gas temperature of 815°C (1500°F) could be achieved within these material limits. Other Inconels such as Inconel 617 have been considered (References 5 and 6) in designs which can be operated at a peak wall temperature of 955°C (1750°F) with a pressure differential of 6.9MPa (1000 psia). This offers a potential of achieving a process gas exit temperature as high as 870°C (1600°F). However, the technology for Inconel 617 operating in an oxygen environment of these temperatures is not as firm as for the Incoloy 800 or Inconel 807 materials.

Current day tube technology indicates that tubes with diameters considerably smaller than 0.6 cm (0.25 inch) are readily available; however, at smaller diameters plugging of the combustion gas products may become significant.

TABLE 6-6a

METALLIC HEAT EXCHANGERS FROM VARIOUS TECHNOLOGIES

Type	Gas Fired Heater	Heat Exchanger	Air Heater for Fluidized Bed	IHX for VHTR Application
Function	Closed Cycle Helium Turbine Plant	ANP	Closed Cycle Gas Turbine	Process Heat
Development Status	Designed in 1972 for Test in 1974	Small Scale Testing in 1960	Detail Design	Conceptual Design
Fluids	Comb Gas/He	Salt/Nak	Comb Gas/Air	He/He
Configuration	Cross Parallel Tube in Shell	Counterflow Tube and Shell	Counterflow Tubular Arrangement	Counterflow Tube and Shell
Tube Material	Inconel 807	Inconel	Inconel 800	Inconel 617
Tube O.D.	2.0 Inches	0.23 Inch	0.5 Inch	0.6 Inch
Process Gas Exit Temperature	1382°F	-	1450°F	1600°F
Peak Wall Temperature	1472°F	1540°F	1580°F	1750°F
Pressure Level	409 psi	-	-	600 to 1000 psi
Pressure Differential	~400 psi	50 psi	130 psi	600 to 1000 psi
ΔP/P	4.2%	-	-	3%
Effectiveness	0.92	-	-	0.9
Q/V	-	-	-	0.3 MW/Ft³
Advantages	Proven Technology in Fabrication and Joint Design	Proven Technology in Fabrication and Joint Design	Based on Technology for Industrial Processes	Based on Proven Technology in Joint Design and Fabrication
Disadvantages	-	Experienced Failures During Cyclid Thermal Test	-	Needs Design Development

TABLE 6-6b

METALLIC HEAT EXCHANGERS FROM VARIOUS TECHNOLOGIES

Type	Gas or Oil Fired Potassium Boiler	HTGR Recuperator	Heat Source Heat Exchanger	Primary Heat	Helium Heater
Function	Central Plant Topping Cycles	Nuclear Powered Closed Cycle Gas	Mini Brayton Cycle	Liquid Metal MHD System	Helium Direct Cycle CTF
Development Status	Built and Tested in 1971	Design and Under Construction	Under Development	Conceptual Design	Detailed Design
Fluids	Gas/K	He/He	He/Xe	Argon/Liquid Metal	Combustion Gas/He
Configuration	Counterflow Tube and Shell	Counterflow Tube and Shell	Tubular	-	Dual Concentric Tube
Tube Material	SS-304	2-1/4 Cr-1 Mo/316 SS	Columbium Alloy	Haynes 188	Inconel 617/ Incoloy 800
Tube O.D.	1.0 Inch	0.44 Inch	-	2.0 Inches	1.5 Inches
Process Gas Exit Temperature	-	930°F	1600°F	1500°F	1500°F
Peak Wall Temperature	1580°F	970°F	1600°F +	~1500°F	1600°F
Pressure Level	-	960 psi	58 psia	1200 psia	1000 psia
Pressure Differential	120 psi	550 psia	~58 psia	-	950 psia
ΔP/P	-	1 to 2%	0.5%	9%	1.5%
Effectiveness	-	0.89	-	-	-
Q/V	-	-	-	-	-
Advantages	Fabrication Joint Design Established	Fabrication Joint Design and Stress Design Established	Demonstrates Design and Fabrication Facility	-	Demonstrates Design and Fabrication Feasibility
Disadvantages	-	Low Temperature Limit	-	Needs Design Development	Not

Table 6-7 summarizes the characteristics of several designs incorporating ceramic tubes. Reference 7 discusses an operating recuperator that uses ceramic tubing. This particular design utilizes spring loaded metallic headering. As a result, the peak gas temperature on the heat removal side (which would be equivalent to the working gas temperature in the energy source heat exchangers) is limited to 980°C (1800°F) although the silicon carbide tubing can withstand wall temperatures up to 1370°C (2500°F). Furthermore, this particular heat exchanger was designed for a low pressure differential. It is anticipated that with a significant pressure differential, considerable leakage between gas streams would occur in this design. Conceptual designs (References 8 and 9) indicate a potential for achieving wall temperatures as high as 1370°C (2500°F) and process gas temperatures of approximately 1230°C (2250°F). Pressure differentials of the order of 3.4M Pa (500 psi) appear achievable. Presently, the ceramic heat exchanger is a developing technology with major questions of the fabrication of leak tight headering and permeability characteristics. Developmental work is in progress, however, which indicates probability of successful development for stationary powerplants.

Representative characteristics of the heat source heat exchanger are summarized in Table 6-8. In this table, current technology represents heat exchangers now in operation or in detail design. The near term development category represents performance estimates which should be achievable with moderate technology development. The long range development category represents performance levels that require significant technology development.

6.2.3.3 CONCLUSIONS

For assessing feasibility of CCCBS with fossil heat sources, the most promising characteristics of the energy source heat exchanger are those that can be achieved with moderate technology development. Based on the results of the state-of-the-art survey and reasonable design practices, representative interface characteristics that can be expected using superalloy materials are:

- Maximum Wall Temperature ≈925°C (≈1700°F)
- Maximum Gas Temperature 815 - 845°C (1500 - 1500°F)
- Pressure Level 6.9M Pa (1000 psi)

TABLE 6-7

STATE-OF-THE-ART OF CERAMIC HEAT EXCHANGERS (CONTINUOUS FLOW TYPES)

Type	Coal Fired Heat Exchanger	Recuperator	Heat Source Heat Exchanger
Function	Process Heat	Slot Furnace	Closed Brayton Cycle
Development Status	Conceptual Design	Built and Tested	Under Development
Fluids	Comb Gas/Helium	Comb Gas/Argon	Comb Gas/He-Xe
Configuration	Counterflow Tube and Shell	Cross-Counterflow Tube and Shell	Cross-Counterflow Tube and Shell
Tube Material	Ceramic/Superalloy Doublewall	SiC	SiC
Tube O.D.	-	-	-
Process Gas Exit Temperature	2250°F	1800°F	2250°F
Peak Wall Temperature	2500°F	2500°F	2500°F
Pressure Level	500 psi	Low	500 psi
Pressure Differential	~500 psi	Low	~500 psi
ΔP/P	2 to 3 %	-	-
Effectiveness	~0.8	0.55	~0.5
Q/V	-	-	-
Advantages	Metal-Sealing Ceramic Stress	Simple Design Simple Fabrication	Simple Design
Disadvantages	• Complex Design • Unproven Fabrication • Permeability Unproven	• Ceramic Metal Spring Loaded Seals • Questionable Shock Resistance • Questionable Stress Capability • Low Effectiveness (55%)	• Fabrication Capability Not Fully Developed • Permeability Capability Not Fully Developed • Low Effectiveness

TABLE 6-8

HEAT SOURCE HEAT EXCHANGER STATE-OF-THE-ART

	CURRENT TECHNOLOGY	NEAR-TERM DEVELOPMENT	LONG RANGE DEVELOPMENT
Configuration	Counterflow Tube and Shell	Counterflow Tube and Shell	Cross Counterflow Tube and Shell
Tube Materials	Inconel, Stainless Steel, Hastelloy	Inconel	Silicon Carbide
Peak Wall Material	1600°F	1650 to 1700°F	2500°F
Process Gas Outlet Temperature	1500°F	1550 to 1600°F	~2250°F
Pressure Level	500 psi	600 to 1000 psi	~500 psi
Tube Outside Diameters	0.25 to 0.5 Inch	0.25 to 0.5 Inch	~0.5 Inch
$\frac{\Delta P}{P}$ (Working Fluid)	1 to 4%	1 to 3%	1 to 3%

- Effectiveness 0.8 - 0.9
- $\frac{\Delta P}{P}$ (Working Fluid) 1 - 3%

These interface conditions are consistent with the study guidelines and are judged to be sufficiently conservative to support conservative assessments of CCCBS feasibility. The constraints associated with the limitation to superalloys has been imposed because of the recognition of the high shock and vibration capabilities required for naval propulsion powerplants and because of the relative maturity of superalloy heat exchanger technology. It should be recognized, however, that on-going developments of very high temperature heat exchangers can, when successfully completed and adapted for naval powerplants, further enhance the performance of fossil fired closed Brayton cycle systems.

6.3 REFERENCES

1) Pierce, B.L., "Controls Considerations and Description of the Compact Closed Cycle Brayton System Analysis Model (BAM)," TME-902, February 1978.

2) McAdams, W.H., "Heat Transmission," McGraw-Hill Book Company, New York (1954).

3) "Shock Design Criteria for Surface Ships," NAVSEA 0908-LP-000-7010, May 1976.

4) "Compact Closed Cycle Brayton System Feasibility Study, Year 1-Final Report," Westinghouse AESD, WAES-TNR-233, July 1977.

5) "Very High Temperature Reactor Engineering Design Studies," Westinghouse AESD, WAES-TME-2800, September 1976.

6) Larson, V.R., et al., "Helium Heater Design for the Helium Direct Cycle Component Test Facility," AIAA Paper No. 75-1262, September 1975.

7) Bjerlic, J.W. and P.S. LaHayne, "A Practical Ceramic Recuperator System for High Temperature Furnaces," 11th IECEC, May 1976.

8) "Proposal to Electric Power Research Institute for a Coal-Fired Prototype High Temperature Continuous Flow Heat Exchanger," WANL-M-10-0513, Westinghouse AESD, May 1975.

9. Fayrweather, D.J., et al., "Advanced Marine Closed Brayton Engines," AiResearch Paper No. 76-312002, September 1976.

7.0 DESIGN CONCEPT DEFINITION

The CCCBS design concept as presently defined is a modification of the Second Definition Design concept as developed during year 1. The more detailed analyses of the plant components done following the development of the Second Definition Design concept has allowed for refinement of certain parts of the CCCBS and increased the feasibility of the design.

Design changes were made principally in the following components:

- Power Turbine
- Gas Journal Thrust Bearings
- Turbocompressor Shaft Coupling
- Precooler and Intercooler Matrix

The CCCBS turbomachinery, heat exchanger, and structural support and containment concepts are described in Section 7.1 and 7.2. The proposed gas journal and thrust bearings are described in Section 7.3. The proposed coupling between the high pressure compressor and the low pressure compressor/high pressure turbine shafts is discussed in Section 7.4.

7.1 General Description

The "third definition" of the CCCBS design concept is illustrated in Figure 4.2-1-1. The flowpath, throughout the integrated assembly of the major components, is almost identical to that of the second definition developed in the first years work program and described in the final report for year 1 (WAES-TNR-233).

Flow Path

Figure 7-2 illustrates the flow path in simplified form. High temperature gas from the heat source enters the module through the inner pipe of the concentric duct flows to the high pressure turbine. The high pressure turbine drives both the low and high pressure compressors. After leaving the high pressure turbine, the gas flows to the low pressure turbine (power turbine) which drives the load. A free power turbine is used to permit either constant or variable speed loads. The gas then enters the low pressure side of the recuperator and is subsequently cooled in the precooler. The gas is then recompressed in the low pressure compressor, cooled in the intercooler and further compressed in the high pressure compressor. The high pressure gas from the compressor then flows through the high pressure side of the recuperator, where it is heated by the energy extracted from the low pressure side gas. The heated gas then passes into a collector manifold from which it is piped through two check valves in series to the outer annulus of the concentric duct to the heat source.

State Points

The temperatures, pressures, helium flow rates and component efficiencies at the full power design conditions are specified in Table 7-1. More detailed state points at part power, under both constant and variable speed load conditions, have also been developed and are fully reported in Section 6.0.

Integrated Assembly

The integrated assembly, illustrated in Figure 7-1 was conceived as a means of achieving the compactness needed for low specific weight, while eliminating the need for interconnecting ducting between the various components of the

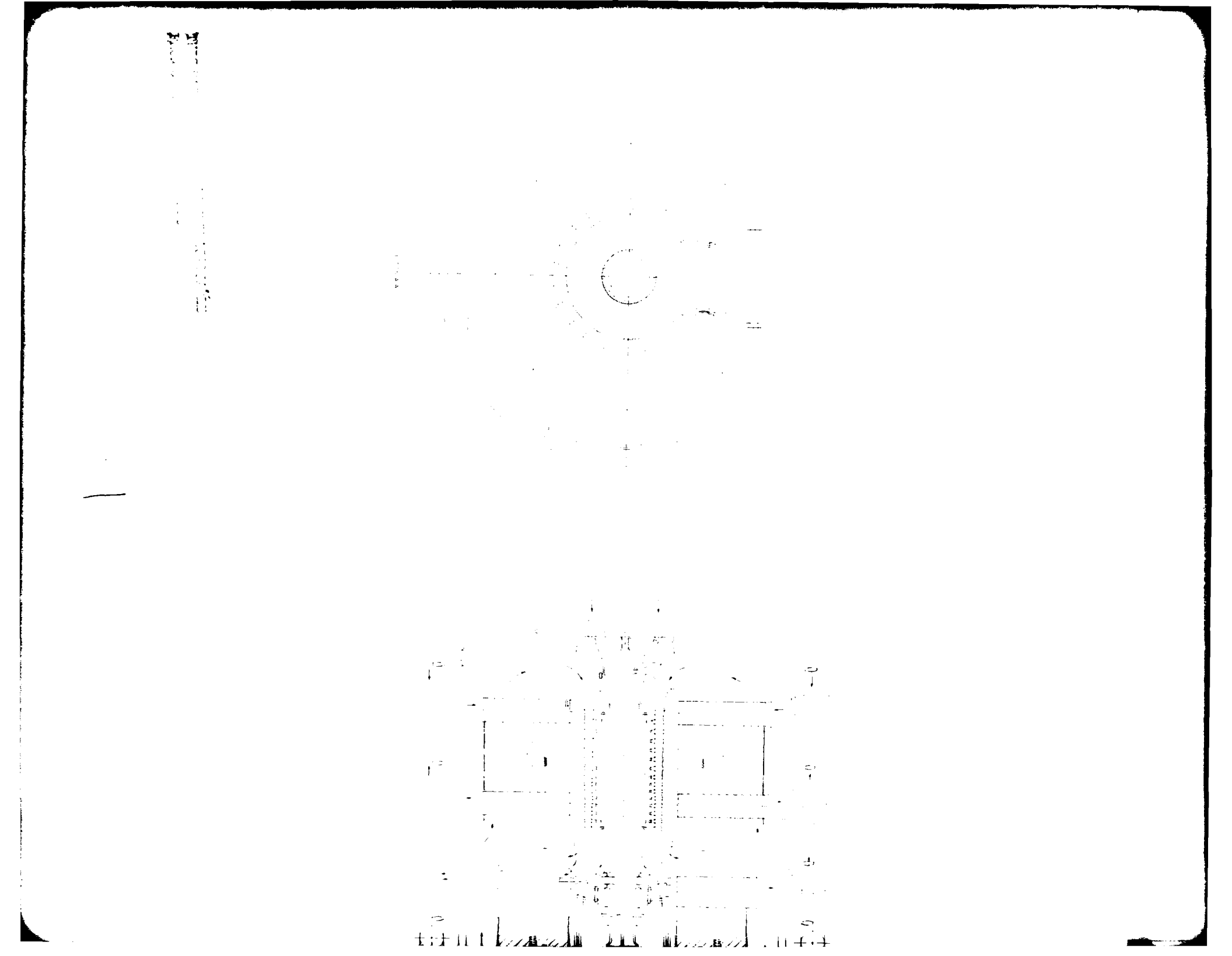

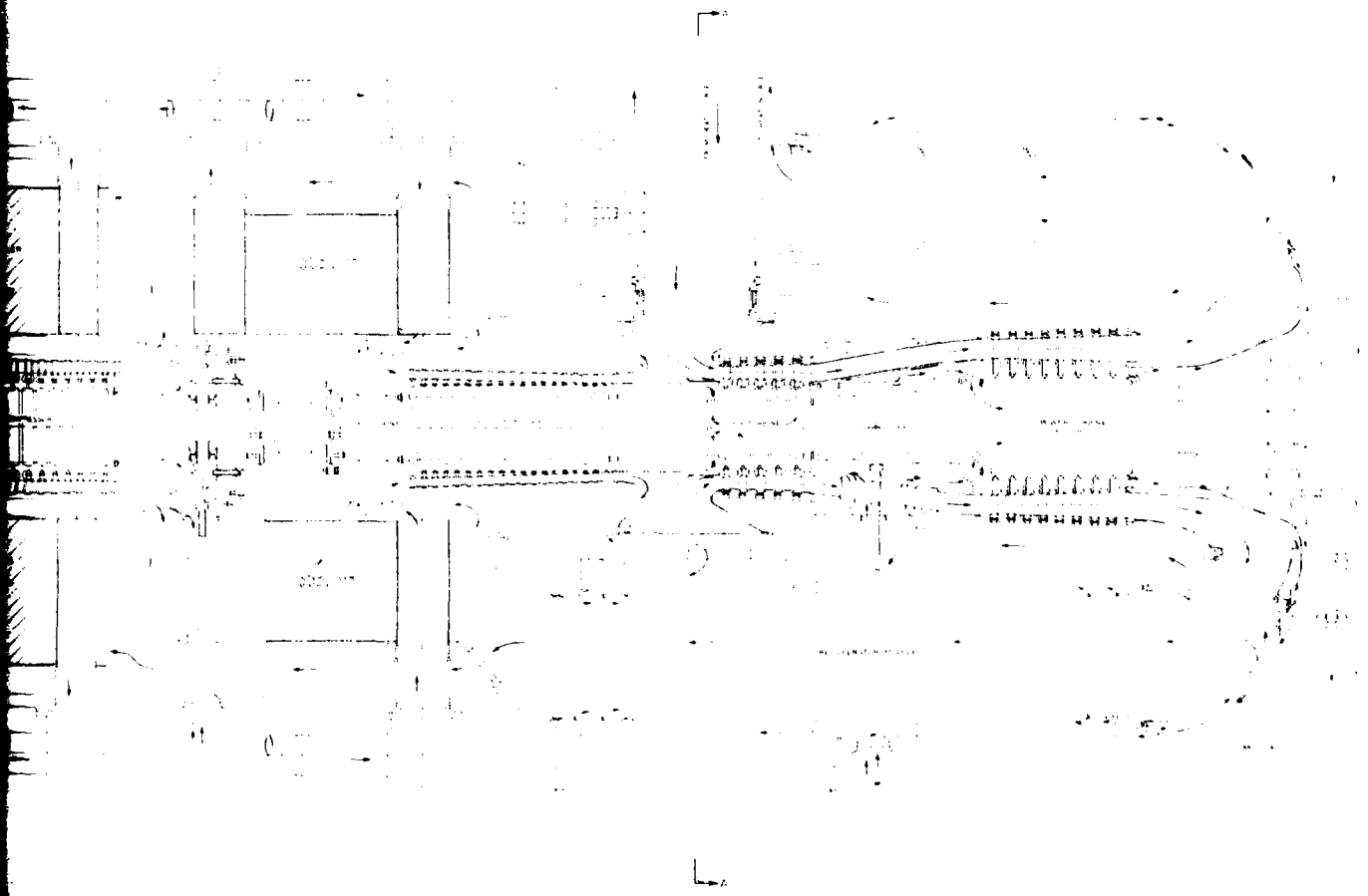

Figure 7-1. Reference CCCBS Design Concept

TABLE 7-1

CCCBS STATE POINTS

	Pressure psia	Temp °R	Rate lb/sec	Power MW	Efficiency
COMPRESSOR	454 890	560 764	127.9	34.1	.85
INTERCOOLER	890 883	764 560	127.9	34.1	.98
COMPRESSOR	883 1625	560 741	125.3	29.7	.85
RECUPERATOR	1619 1613	741 1307	120.2	88.9	.84
ENERGY SOURCE	1597 1512	1300 2190	121.5	141.2	-
TURBINE	1500 852	2160 1766	124.0	63.4	.90
POWER TURBINE	852 478	1766 1438	124.0	53.2	.90
RECUPERATOR	472 462	1411 880	127.9	88.9	.84
PRECOOLER	462 455	880 560	127.9	53.4	.982

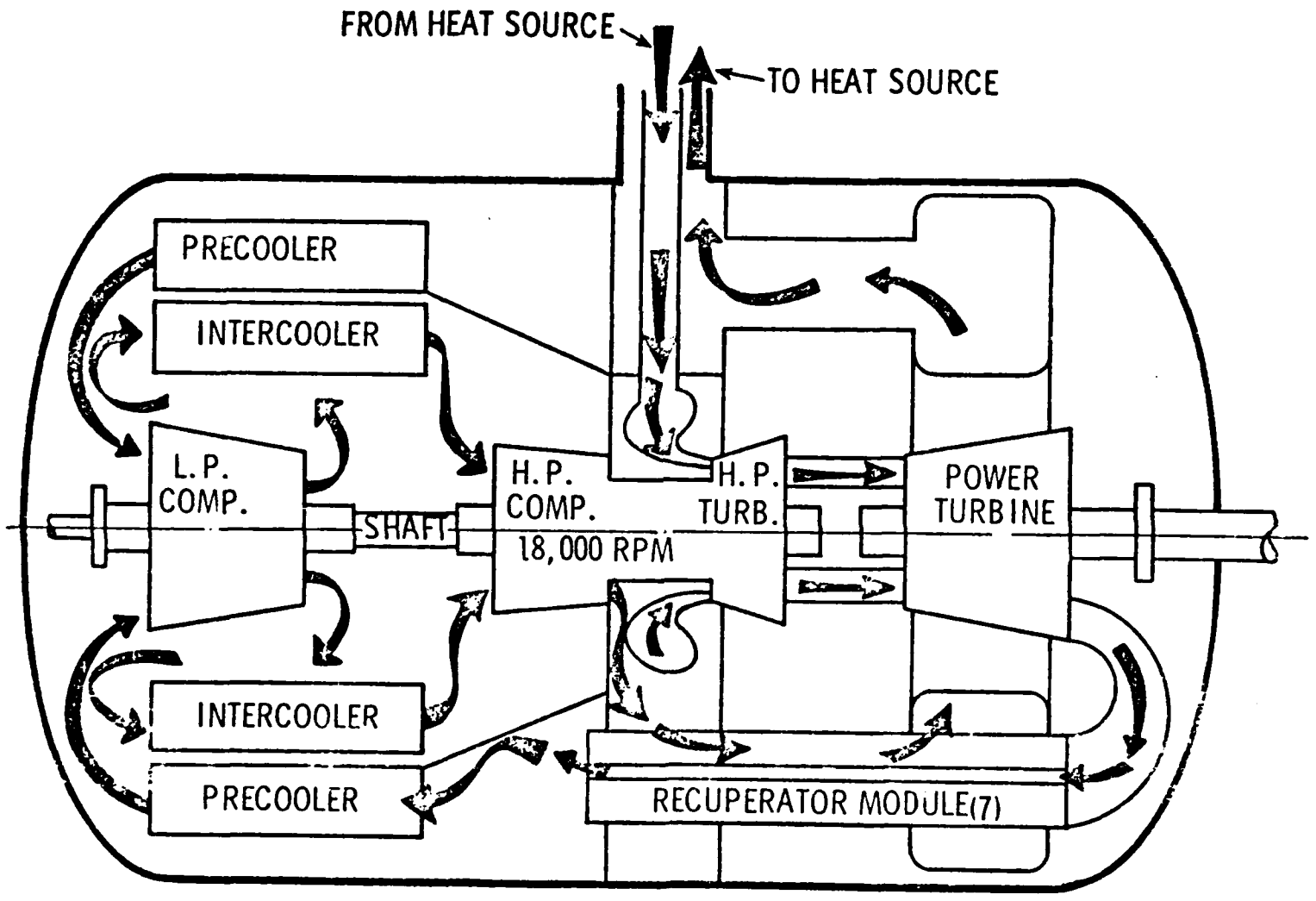

Figure 7-2. Helium Working Gas Flow Path

system and the associated problems of thermal expansion, pressure retention and headering. All of the major components of the power conversion assembly are contained within a cylindrical pressure vessel made of low alloy steel, capable of accommodating the maximum system pressure. The design of the pressure vessel is generally similar to that of the second definition concept described in the first year final report (WAES-TNR-233). Although local pressures throughout most of the power conversion assembly are below maximum system pressure under normal operating conditions, operation with one of two parallel units shut down dictates casing design conditions. Pressure throughout the inoperative unit tends to approach full system pressure as a result of leakage through the shut-off valves.

The pressure vessel is made in three sections; a center frame structure and forward and rear sections. The three sections are joined together by bolted flanges, sealed by elastomer or metal O-rings or, alternatively, seal welded. The maximum temperature of the pressure vessel is approximately 204^{o}C (400^{o}F).

The forward section of the pressure vessel accommodates the intercooler and precooler in an annular arrangement around the turbomachinery. Both units employ the crossflow configuration using finned water cooled tubing arranged in a helical fashion which was conceived by Airesearch during the first contract year.

The center frame structure consists of a short cylindrical section of casing having two diaphragm members, one at each end, extending radially inward towards the center. Central holes in the diaphragm members provide radial support for the turbomachinery casing. The two diaphragms are supported in the axial direction, one from the other, by eight essentially radial webs. Each diaphragm is pierced by seven holes, located midway between the webs. These holes locate the seven recuperator modules. The eighth inter-web location accommodates the ducting connecting the powerplant to the heat source and at this location one of the diaphragms remains unpierced. A penetration on the exterior cylindrical portion of the center frame structure provides a passageway for the concentric duct to the heat source.

During operation, the center frame structure is pressurized by high pressure compressor outlet gas and serves as the recuperator high pressure inlet plenum. Sealing of the turbomachinery to the center frame is effected by elastomer o-rings, carried in grooves machined into the turbomachinery casing, which engage with prepared surfaces at the inner diameter of the center frame diaphragm members. The gas temperature at this location is approximately 138°C (280°F).

Flanged tubular members are attached to the rear diaphragm of the center frame structure at each of the seven recuperator locations. The tubular members support a rectangular section toroidal vessel which functions as the recuperator high pressure outlet plenum. The recuperator modules are constructed in the form of long circular cylinders and are inserted into holes in the rear of the toroidal vessel, extending through the vessel into the support tubes and center frame structure. Relative thermal expansion between a recuperator module and its support members and between the tubing and shell of the recuperator module is accommodated by sliding joints sealed by o-rings at the cold $\simeq$ 149°C (300°F) end. The modules are axially located and sealed at their hot ends by means of bolted flanges.

The high pressure gas flows from the center frame structure through the shell side of the recuperators to the toroidal outlet plenum. The gas then flows around the toroidal vessel to the eighth pipe through which it passes into the outer annulus of the concentric duct to the heat source. Two check valves are located at the entrance to the eighth pipe to prevent backflow of gas from the operating unit in the event of the shutdown of one unit of a two unit system. A short inner pipe connects the check valves to the annular duct and is sealed to them by means of piston rings. A piston ring is also used to seal the annular duct to the center frame. The piston rings allow the pipes conveying the hot gas from the check valves to the heat source to expand and contract independently of the relatively cool center frame structure.

The rear section of the pressure vessel supports and axially locates the turbomachinery at the power turbine outlet end. The turbomachinery receives additional support in the radial direction from the center frame structure and

from the forward section of the pressure vessel. The rear section of the pressure vessel also supports an electric generator in one possible compact close coupled arrangement.

The turbomachinery is designed to be insertable into or removable from the power conversion assembly as a unit together with the generator and the rear section of the pressure vessel. During this operation the pressure vessel rear section serves as a lifting fixture and allows the complete turbomachinery assembly to be suspended at its center of gravity from a crane or transporter device while it is removed axially from the power conversion assembly. The transporter device can be furnished as an in-containment system in a nuclear plant, thus allowing transport of the turbomachinery inside the containment to a suitably located penetration. The protrusion of the rear pressure vessel casing through the containment penetration, while still supported from the transporter inside the containment, would then allow a special lifting fixture to be bolted to the rear pressure vessel from outside the containment. The lifting fixture would be designed such that an external crane hook would apply its lift force over the center of gravity of the assembly, by suitably shaping and counterbalancing the lift fixture. Transfer of the assembly weight from the in-containment transporter to the external crane could then be completed.

During removal of the turbomachinery from the powerplant, the internal flow path is separated by means of sliding joints at the low pressure recuperator inlets. A conical sheet metal vessel confines the relatively warm $\simeq 510^{o}C$ ($950^{o}F$) turbine outlet gas to the immediate vicinity of each recuperator inlet. Each conical vessel receives hot gas from the power turbine outlet diffuser through a radial pipe which passes through the turbomachinery rear support structure. The interior surface of the rear section of the pressure vessel, the exterior surfaces of the toroidal recuperator high pressure outlet plenum and the exterior of its rear support structure are exposed to cooler $\approx 204°C$ ($400°F$) gas originating from the power turbine balance piston labyrinth seal.

The removal of the turbomachinery from the powerplant requires that the coaxial duct connecting the turbomachinery to the heat source be retracted together

with the gas service lines to the turbomachinery. The provisions made in the third definition of the design for satisfying these prerequisites are generally similar to those of the second definition design described in the first year final report (WAES-TNR-233) and are illustrated in Figure 7-1

Changes Made in "Third Definition" Concept Design

Although the general arrangement of the power plant, as described in this section has undergone very little change from that of the earlier second definition, several of the major components of the system have been greatly refined as a result of the current year's design effort. The low pressure compressor has been subjected to more detailed engineering effort by the Westinghouse Combustion Turbines Division as has the last power turbine stage and the high pressure turbine first stage blade root/disc interface. The high speed rotor thrust bearing has been relocated to a more central location between the high pressure and low pressure compressors to reduce the maximum stack-up of tolerance and thermal expansion effects between rotor and stator. The thrust balance piston of the high speed rotor has been relocated at the low pressure compressor end of the rotor to facilitate the use of the full compressor pressure ratio in balancing. The power turbine balance piston has also been reduced in size to allow the use of full compressor pressure ratio balancing. These changes in the thrust balancing provisions were made as a result of a study of the thrust bearing load variations which occur at part power. The use of full compressor pressure ratio across the balance pistons was found to greatly reduce the variation of thrust bearing load in both the high speed and power turbine rotors.

As a result of the rotor critical speed analysis performed by Airesearch during this period, the rotor shaft thicknesses have been substantially increased. These changes together with the removal of material from inside the ends of the rotor have elevated the critical speeds of most immediate concern well above the maximum operating speeds. In addition to the critical speed investigation, Airesearch have also refined the design of the cycle coolers and the gas bearings. Changes to the design of the gas bearings have been made to accommodate shock loadings identified in the shock analysis performed by (W) AESD during this period.

In addition, changes have been made in the design of the H.P. turbine inlet ducting to reduce thermal stresses and improve sealing. Conceptual designs have also been developed for a 3600 RPM mechanical drive turbine and its driveshaft sealing arrangement.

These changes are described in more detail in the Sections which follow.

7.2 MAJOR COMPONENTS

Mechanical Design - General

The design of the powerplant is generally similar to that of the first and second definition concepts developed in the first contract year and described in WAES-TNR-233. However, as outlined in the previous section, several of the major components of the system have been subjected to critical design changes. These changes, although relatively minor in terms of their effect on the powerplant overall size, weight and general configuration, nevertheless have resulted in a substantial improvement in the design maturity or credibility of the concept. The evaluations have included the more detailed development of the design of certain components and, in some cases, an examination of the consequences of operation at other than design conditions. An examination of the latter type has indicated a deficiency in the thrust balancing arrangement employed in the second definition design which would not have been apparent had the work been limited to a "design point" study. This deficiency has been corrected in the third definition concept by the use of the overall compressor pressure ratio across the balance pistons, rather than a portion of the compressor pressure ratio, as was used in the earlier configurations. The resulting third definition concept thrust balancing arrangement greatly reduces the variations in thrust bearing loads which arise during power changes from rated to 7.5% power and thereby simplifies the problem of providing sufficient thrust bearing capability at the low power condition, where the maximum gas pressure available for use in a hydrostatic bearing is limited as a result of the general reduction in cycle pressure level under inventory control. It is expected that the change described will be similarly beneficial in limiting bearing thrust loads during rapid transient conditions. Additional analysis is underway to examine these effects.

High Pressure Rotor Mechanical Design

The high pressure rotor construction is similar to that of the earlier second definition concept and consists of high pressure turbine and compressor rotors joined together by a short length of large diameter hollow drive shaft. The resulting rotor is supported at each end in gas journal bearings. The

bearings are discussed in detail in Section 7.3. Axial location of the high pressure rotor is provided by the low pressure compressor rotor gas thrust bearing through the drive shaft which connects the two rotors.

The high pressure rotor employs multiple discs joined by through bolts and curvic couplings. The curvic couplings are machined onto cylindrical extensions at the front and rear of each disc and provide accurate radial alignment of the discs while transmitting the driving torque. As a result of the critical speed analysis, performed by Airesearch, the thicknesses of these cylindrical extensions, which form the shaft elements of the rotor, have been increased from an original value of approximately 6.35 mm (.25 in.) to 25.4 mm (1.0 in.). In addition, the bearing stubshafts at each end of the rotor have been made hollow to eliminate unncessary weight while retaining bending stiffness. These changes were successful in raising the first bending critical speed to a value 42% above the maximum operating speed from its original value within the operating speed range. The critical speed analysis, performed by Airesearch, is discussed in more detail in Section 8.3.4.

The high pressure turbine rotor design is similar to that of the second definition concept which was described in some detail in WAES-TNR-233. The first stage rotor blades are made of IN100 superalloy and are unshrouded since rotating shrouds would not confer an efficiency improvement and would increase centrifugal stresses and thus reduce the permissible inlet temperature. The blades have extended root fixings which provide a thermal barrier between the hot airfoil section and the firtree attachment at the disc. Cooling gas, at approximately 138^{o}C (280^{o}F) is directed over the extended root and disc regions to limit the temperature of the disc rim.

During this report period, detail design changes to the first stage blade configuration were defined to adapt the design to 927^{o}C (1700^{o}F) turbine inlet temperature from the 911^{o}C (1671^{o}F) value assumed in the first year work. The changes to the blade configuration were limited to a relatively minor redistribution of blade chord (and resulting cross section area) with radius. The revised distribution retains the hub and tip sections unchanged but reduces the blade section area below that of the earlier linearly tapered

blade. The reduced blade weight resulting from this modification reduces the centrifugal stress at the blade root permitting an increase in blade metal operating temperature. This work is discussed in more detail in Section 8.3.1.

In addition to adapting the first year blade study results to 927°C (1700°F) inlet temperature, the blade root and disc attachment design was defined in sufficient detail to permit a meaningful evaluation of the thermal conditions in this region. For this purpose a short extended blade root was defined in detail capable of transferring the blade loads into the firtree fixing and limiting heat conduction into the disc. Provision was made in the extended root design for sealing between the extended root shanks. (The earlier blade root design used in the Westinghouse Combustion Gas Turbines Division stress analysis model and reported in WAES-TNR-233 was not optimized in this respect and merely provided sufficient input to the stress analysis program). The resulting extended root and disc rim detail provides the initial design basis for estimating the local thermal conditions. This work is discussed in more detail in Section 8.3.1.

The high pressure compressor rotor design is similar to that of the second definition concept of Reference 1. The blades are attached to the discs using conventional dovetails and grooves. Blade widths vary from 15.24mm (0.6 in.) at inlet to 12.7mm (0.5m) at exit resulting in acceptable gas bending stresses, in the region of 103.4 MPa (15,000 psi) while achieving a reasonably short compressor assembly. Rotor/stator axial gaps are 3.2mm (.125 in.) at all locations. The relocation of the thrust bearing to a more central position between the two compressors, together with the relatively low temperature range to which the compressor parts are exposed, should make this clearance practicable. Blade centrifugal stresses range from approximately 110.3MPa (16000 psi) at inlet to 89.6 MPa (13,000 psi) at exit. The design of the root fixings and discs has not yet been optimized but no problems are anticipated since the mean blade speed ($\simeq$ 350 m/s) (1150 ft/sec) and temperature ($\simeq$138°C) (280°F) are reasonably low. AISI type 403 stainless steel material has been extensively used in similar combustion turbine applications and should be appropriate in the CCCBS.

The large diameter hollow driveshaft which joins together the high pressure turbine and compressor rotors incorporates a disc-like appendage at the turbine end. Radial passages in the disc portion of the shaft allow cooling gas from the high pressure compressor outlet to flow into the inter-disc regions of the high pressure turbine rotor. (This gas flows radially outward, through the curvic coupling slots, into the interstage diaphragm seal region where it provides "make-up" cooling gas to the leakage flow in the extended blade root and disc rim region). The radial passages prevent the inward flowing gas from forming a free vortex which would produce high tangential velocities in the disc bore region causing high frictional losses and reduced static pressure. Tapped holes are provided in each end of the driveshaft to accommodate the through bolts which clamp together the high pressure turbine and compressor discs.

High Pressure Stator Mechanical Design

The high pressure stator follows the practice described for the first and second definition concepts in Reference 1. The high pressure stator consists of the high pressure turbine stator, the high pressure compressor stator and their interconnecting structure. The interconnecting structure is a rigid assembly formed by the compressor outlet/turbine inlet plenum casing and the high pressure turbine outlet diffuser casing.

The high pressure turbine stator is attached, by means of a flange at its outlet end, to a mating flange on the inlet end of the high pressure turbine outlet diffuser casing which, in turn, is attached by means of a flange at its outlet end, to a flanage on the compressor outlet/turbine inlet plenum casing. A flange on the other end of the compressor inlet/turbine outlet plenum casing is attached to a mating flange on the high pressure compressor casing. The stator casings can be machined from ductile iron castings or low

alloy steel weldments. Circumferential grooves are machined in the periphery of the compressor outlet/turbine inlet plenum casing for o-rings which engage with machined surfaces at the inner diameter of the powerplant center frame structure and provide the sealing necessary to prevent leakage of high pressure compressor outlet gas from the center frame. In addition to the circumferential mating flanges, all of the high pressure stator casings are provided with axial split flanges to allow half of the stator structure to be removed for inspection of the blading or the hot gas duct and plenum carrying helium from the heat source to the turbine inlet.

The high pressure turbine inlet plenum and hot gas duct have been subjected to more detailed design refinement to improve sealing and minimize thermal stresses. The turbine inlet plenum is completely surrounded by relatively cool $\simeq 138^{o}C$ ($280^{o}F$) helium flowing from the compressor outlet diffuser to the recuperator modules in the powerplant center frame. The cool gas leaves the turbomachinery compressor outlet/turbine inlet plenum casing through several holes in the casing and passes into the center frame. The hot gas duct is surrounded by the intermediate temperature $\simeq 454^{o}C$ ($850^{o}F$) gas flowing from the recuperator outlet plenum to the heat source. Both of these gas streams are, however, substantially cooler than the $927^{o}C$ ($1700^{o}F$) high temperature turbine inlet gas inside the plenum and hot gas duct.

In the first and second definition concepts, the hot gas duct and turbine inlet plenum were conceived as single wall vessels which would have been exposed to $927^{o}C$ ($1700^{o}F$) on the inside and the much cooler $454^{o}C$ ($850^{o}F$) or $138^{o}C$ ($280^{o}F$) gas on the outside. As a result of these large gas temperature differences and the low film temperature drops expected at the walls in flowing ($M \simeq .06$) helium, concern was felt that the conductive temperature gradients induced in the single metal wall thickness might result in excessive short time fatigue stresses which would unduly limit the number of startup and shut down cycles to failure. In addition, the sealing of the high temperature turbine inlet gas from the cooler, higher pressure streams was effected by a simple clearance fit. This, and the other joints in the plenum needed for accessibility, could obviously benefit from a more detailed design effort to improve sealing and general structural integrity.

The resulting third definition hot gas duct and high pressure turbine inlet plenum employs double wall construction to create a stagnant layer of gas separating the hot turbine inlet gas from the cooler surrounding gases and thus function as an insulator to reduce the rate of heat transfer and resulting temperature gradients in the metal walls. The details of the design are illustrated in Figure 7-1. The inner wall, exposed to the hot gas, functions as a protective liner or fairing for the outer wall which serves as a pressure vessel and performs the sealing function. Thus the essentially unloaded inner liner operates close to turbine inlet temperature while the outer pressure vessel member is relatively cool.

The outer wall of the turbine inlet plenum is divided into three sections; forward and rear conical members and an outer cylindrical section. The three sections are all split diametrally at a plane normal to the hot gas duct centerline and employ bolted flanges at the split lines to achieve sealing and structural integrity. The inner wall is similarly divided into three sections, diametrally split, but employing joggled overlaps at the diametral split line. The turbine inlet plenum outer casing is supported from the high pressure turbine casing and first stage nozzle diaphragm by bolted flanges.

The inner liner of the hot gas duct is located from the outer by means of a conical transition piece which accommodates the temperature difference between the two members as an axial gradient. The length and thickness of the transition cone are such that the thermal stresses resulting from the temperature gradient in the cone are not excessive. The inner liner extends into a mating diameter on the turbine plenum liner which locates it radially. The diametral interface at this point is not required to function as a seal so that a fairly loose fit is acceptable. The sealing function is performed by a face seal on the outer hot gas duct which engages a machined face on the outer plenum vessel. The face seal is maintained in contact with the vessel face by means of a bellows which accommodates duct thermal expansion and ensures alignment of the seal face. It is envisaged that the face seal could employ either a metal or a graphite seal ring, in one piece or as an articulated assembly of appropriately shaped segments, suitably overlapping and interlocking to achieve the required sealing. The complication of the segmented

design may not be required if the distortion of the mating face seal members can be limited sufficiently. It is also conceivable that the face seal ring, either solid or articulated, may be unnecessary and that some suitable termination of the bellows member could provide adequate sealing and also accommodate local distortion of the plenum sealing face. In any event, the assignment of the sealing function and structural pressure vessel role to the cooler outer wall components, which are thermally isolated from the hot gas stream by the inner liner members and the stagnant gas layer. should greatly improve the potential sealing and structural integrity.

The inner liner of the plenum is axially and radially located in peripheral grooves provided at the forward and rear flanges of the outer plenum casing. Tangential location is defined by a pin which protrudes into the peripheral groove area from the rear outer casing flange and engages with a slot in the plenum inner liner periphery. The location slot is aligned with the centerline of the hot gas duct so that expansion of the inner liner in the tangential direction does not disturb the location of the duct. Thermal expansion of the plenum inner liner relative to the cooler plenum outer case results in tangential motion of the liner in its locating grooves. The accumulated motion of both halves of the inner liner is accommodated by sliding at the joggled overlap on the axial split line. Sufficient gap is provided at the in-groove portions of the liner to allow unrestricted motion. Relative expansion in the axial direction between the plenum inner liner and outer casing results in axial sliding of the liner in the locating grooves. Sufficient axial gap is provided to permit unrestricted axial expansion. The application of special coating materials in the areas of sliding may be necessary to ensure freedom from galling and bonding in the high temperature helium environment.

Materials used in the double wall turbine inlet plenum and pipe can be selected in accordance with the differing roles of the inner and outer members. Hastelloy X or Haynes 188 would be good candidates for the inner liner components since these materials are used in similar combustion gas turbine liner and combustion chamber applications and are highly resistant to

cracking and distortion. The high oxidation resistance of these materials would not, however, be required in the helium environment and it is possible that other materials, less suitable in an oxidizing environment, would be viable in helium. Earlier, Inconel 617 was thought to be a good candidate for helium hot liner applications but was later found to be vulnerable to corrosion in helium.

The outer pressure casing members of the turbine inlet plenum and pipe need not be made from such high temperature materials as Hastelloy X and Haynes 188. Such intermediate temperature materials as Inconel 718, type 347 stainless steel or possibly 2-1/4 Cr - 1 Mo low alloy steel would be suitable for operating temperatures ranging from 704°C (1300°F) down to 482° (900°F). While the operating temperature of the outer casing members has not been established, judgment indicates that it will probably be well below 704°C (1300°F) due to the protection from the 927°C (1700°F) turbine inlet gas provided by the inner liner and stagnant gas space, combined with the cooling resulting from exposure to the surrounding lower temperature gas.

The high pressure turbine stator design is essentially unchanged from that of the first and second definitions described in Reference 1.

The stator vane assemblies are of the diaphragm type having outer and inner ring and vane assemblies split diametrally. The half diaphragm assemblies are radially keyed to the turbine casing halves to locate them concentrically in the casing while accommodating relative thermal growth in the radial direction. The outer ring halves are saw cut at appropriate intervals to relieve the relative thermal expansion between the inner and outer rings. The radial keys which locate the diaphragm halves in the casing are formed in the heads of bolts which attach several machined segmented rings to the casing. The segmented rings, in turn support the segmented stationary turbine shrouds. The shroud segments have axial extensions at their outermost radii which engage with machined grooves in the segmented rings. Abradable material such as metal honeycomb, "feltmetal" or some other sintered or sprayed material is applied to the inner surfaces of the shroud segments to accommodate potential blade tip rubs.

The resulting stator assembly accurately defines the turbine shroud and diaphragm seal radii, minimizing leakage at the blade tips and interstage seals, while providing freedom for the individual components to expand and contract. The segmented shroud region insulates the turbine casing from the hot gas passage and minimizes the temperature gradient to which each component part is exposed. The turbine casing is cooled by compressor outlet gas at approximately 280^{o}F which is circulated around it. Some of this gas can be bled into the segmented shroud region through small holes in the casing, if additional cooling should be required. A complete half casing and half stator assembly can be removed without disassembling the rotor to facilitate inspection of the blading.

Candidate stator materials are MAR 509 vanes, Type 321 stainless steel ring segments and diaphragm halves and low expansion Ni-resist cast turbine casing. Alternatively the turbine casing could be fabricated from 2-1/4 Cr-1 Mo. plate. Stator assemblies can be fabricated by welding or brazing. The high pressure turbine design illustrated in Figure 7-1 lends itself to the use of a low expansion cast Ni-resist casing because the casing is maintained in a state of circumferential compression by the high pressure compressor outlet gas which surrounds it. This arrangement eliminates any possibility of catastrophic tensile failure in the cast material and minimizes the stresses in the bolted flange at the axial split line. The use of low expansion material in the high pressure turbine casing, minimizes thermal distortion due to local temperature gradients in addition to minimizing total casing growth. Both of these effects help to minimize the tip clearance required.

The diaphragm type of construction described achieves good interstage sealing by permitting the use of a multistage labyrinth seal and minimizing the relative thermal expansion of the rotor and stator components of the seal. The advantages of diaphragm construction are particularly significant when the turbine shaft diameter can be kept small in relation to the blade root diameter. In this respect the power turbine provides a somewhat more suitable application for this type of construction than the high pressure turbine. In the high pressure turbine a large diameter shaft is employed to maximize the rotor bending stiffness. The resulting geometry restricts the radial space available at the hub to accommodate the diaphragm type of structure. As a result, alternatives

to diaphragm construction will receive more consideration in the high pressure turbine than in the power turbine. One such alternative would support the stator vanes from the casing as a series of individually cantilevered vanes or as a series of multi-vane segments. This arrangement eliminates the structural problems of the diaphragm but tends to result in poorer interstage sealing. Relative thermal expansion of the rotor and stator components of the seal may be increased due to the inward motion of the stationary seal which can result from the vane growth. However this effect is less important in a machine having an essentially constant operating temperature such as the CCCBS turbine. The quantitative evaluation of the magnitude of the various expansion effects and the structural capability of the various design candidates must await the more detailed design phases. The selection of the preferred design approach can then be made from the results of trade studies supported by more extensive and analytical work.

The high pressure turbine outlet diffuser consists of a sheet metal assembly, in the form of an annular passageway penetrated by eight airfoil section struts and a cooled structural casting or fabrication protected from the hot gas leaving the high pressure turbine by the sheet metal assembly. The structural assembly consists of an outer pressure casing and an inner ring member supported from it by eight hollow radial struts. The housing for the high pressure turbine outlet journal bearing and the power turbine inlet journal bearing is supported from the inner ring member. The structural casings, the sheet metal fairing assembly and the bearing housing are all designed to split diametrally for access to bearings and blading. Candidate materials are Hastelloy X for the sheet metal assembly and cast ductile iron or fabricated 2 1/4 Cr - 1 Mo for the structural assembly.

The high pressure compressor stator is similar in design to that of the first and second definition concepts described in Reference 1. The stator vanes are of the shouded type brazed or welded into half ring members at the inner and outer diameters. The stator vane assembly inner half rings carry honeycomb or some other abradable material machined to provide a close clearance with labyrinth seal fins machined onto the rotor disc curvic coupling extensions. The stator casings are machined from ductile iron castings or low alloy steel weldments.

Low Pressure Compressor and Drive Shaft Mechanical Design

The low pressure compressor has undergone dimensional changes during this period as a result of a more detailed evaluation of the first stage design by Westinghouse Combustion Turbines Division. The most obvious change is a reduction in the mean blade diameter at inlet from 442 mm (17.419 in.) to 409 mm (16.116 in.) together with an increase in blade height from 44 mm (1.742 in.) to 45.5 mm (1.791 in.). This work is described in detail in Section 6.3. However the dimensional changes have not affected the basic construction of the compressor.

The low pressure compressor rotor is of multiple disc construction, using curvic couplings and through bolts and is generally similar to the high pressure rotor. The curvic coupling cylindrical extensions, which form the shaft elements of the rotor, have been increased in thickness from the original value of approximately 6.35 mm (0.25 in.) to 19 mm (0.75 in.) as a result of the critical speed analysis performed by Airesearch. In addition, material was removed from the inside of the shaft ends and added to the stubshaft flanged areas of the original design to reduce the local flexibility. These changes had the effect of raising the first bending critical speed to a value 48% above the maximum operating speed from its original value only 5% above operating speed. The critical speed analysis is discussed in more detail in Section 8.

Several more recent changes, have been made to the low pressure compressor rotor, resulting in substantially reduced bearing center distance, which should further increase the critical speed. The stubshafts have been integrated with the first and last stage discs to reduce rotor length and provide space for the drive shaft and flexible couplings. Also, the balance piston has been relocated to the extreme forward end of the rotor.

The rotor is supported in gas journal bearings. Axial location is provided by a gas thrust bearing at the outlet end of the low pressure compressor rotor. The journal and thrust bearings are discussed in Section 7.3.

The thrust bearing has been relocated from its earlier position at the inlet end of the low pressure rotor to reduce the maximum stackup of tolerance and thermal expansion effects between the high pressure rotor and stator. This change has the effect of minimizing the permissible rotor to stator gaps and, as a result, the overall length of the rotor.

The thrust balance piston which was originally located at the outlet end of the low pressure compressor rotor has been relocated at the inlet end. This was done to facilitate the use of the overall compressor pressure ratio (H.P. compressor outlet to L.P. compressor inlet) for balancing and thus minimize the variation of thrust bearing load which occurs with variation in output power. Studies made, during this report period, of the thrust bearing load variation from full power to 7.5% power indicated that the use of high pressure compressor pressure ratio only (H.P. compressor outlet to H.P. compressor inlet) across the balance piston resulted in large swings in thrust bearing load from 44480N (10,000 lb_f) towards outlet at rated power to 16902N (3800 lb_f) towards inlet at 7.5% power) which adversely affected the thrust bearing design problems. Obviously, by increasing the size of the balance piston, the load at 7.5% power could be reduced but only at the expense of a much larger increase in the load at rated power. Similarly, by reducing the size of the balance piston, the thrust bearing load at rated power could be reduced, but with an accompanying increase in the load at 7.5% power. The use of the overall compressor pressure ratio in the revised arrangement greatly reduces the thrust bearing load swing (from 3291 N (740 lb_f) towards outlet at rated power to 8.9 N (2 lb_f) towards inlet at 7.5% power).

The new balance piston is smaller in size than that of the earlier design and is bolted to the inlet end of the low pressure compressor rotor shaft. The balance piston carries the starter motor drive stubshaft at its inner diameter. High pressure compressor outlet gas is piped to the upstream side of the balance piston and leaks to precooler inlet pressure through two multi-stage labyrinth seals, one at the balance piston periphery and another smaller one at the inner diameter stubshaft. The low pressure balance piston leakage gas is channelled through passages provided in the compressor inlet bearing support struts to the inlet of the precooler, thus minimizing the amount of

balance piston leakage gas which enters the low pressure compressor inlet directly.

The low pressure compressor rotor is driven from the high pressure rotor through a short driveshaft. The driveshaft is designed to transmit axial load and to have self-aligning capability in addition to the ability to transmit torque. The self-aligning capability is provided to accommodate the eccentricity and angular misalignment which can arise between the low pressure and high pressure rotors due to manufacturing tolerances. The axial load capability allows the shaft to transmit the net axial thrust, produced in the high pressure rotor, into the low pressure compressor outlet end. The driveshaft is designed to be easily disconnected to allow the removal of either the L.P. or H.P. compressor rotor.

The driveshaft self-aligning capability is achieved by the use of flexible metal diaphragms at each end which transmit torque but allow a small amount of angular misalignment. The axial load carrying capability is provided by a small diameter bar member on the shaft centerline which is capable of transmitting axial load in tension or compression but which is sufficiently flexible in bending to accommodate some angular misalignment. This driveshaft design avoids the use of sliding surfaces and therefore does not require lubrication. The design is therefore more compatible with the gas bearings which replaced the oil lubricated bearings used in the earlier first definition concept. The driveshaft used in the earlier machine employed gear tooth couplings and spherical sliding joints, both of which required lubrication. The design of the new unlubricated coupling was developed during this report period by Airesearch and is discussed in Section 7.4.

The low pressure compressor rotor blade axial widths at the root are 26 mm (1.025 in.) at inlet reducing to 19 mm (.75 in.) at outlet. The stator vane axial widths are 21 mm (.825 in.) at inlet and reduce to 15.2 mm (.6 in.) at outlet. Axial rotor to stator gaps are 3.2 mm (.125 in.) at all locations, a value judged to be achievable with the thrust bearing location shown but reduced from the over-conservative value of 6.4 mm (.250 in.) assumed previously. The outlet blade and vane widths were reduced from the inlet dimensions developed by Westinghouse Combustion Turbines Division in their

evaluation of the first compressor stage to maintain a fixed aspect ratio. The blade geometry finally selected has a tapered chord, increasing 8% at the root and decreasing 8% at the tip from the value at mean blade diameter. The thickness/chord ratio is 3% at the tip, 9.5% at mean blade and 16% at the root. The resulting centrifugal and bending stresses in the rotor blade are less than 138 MPa (20,000 psi) and 82.7 MPa (12000 psi) respectively. There are 49 rotor blades. The critical evaluation of the low pressure compressor first stage, conducted by Westinghouse Combustion Turbines Division is discussed in more detail in Section 8.3.3.

The low pressure compressor stator is similar in construction to the high pressure compressor stator. The stator vanes are of the shrouded type, brazed or welded into half ring members at the inner and outer diameters. The stator vane assemblies are assembled into grooves machined into the compressor stator casing. The stator vane assembly inner half rings carry honeycomb or some other abradable material machined to a close clearance diameter with labyrinth seal fins machined onto the rotor disc curvic coupling extensions. Type 347 stainless steel is a candidate stator assembly material. Ductile iron castings or low alloy steel fabrications are candidates for the compressor stator casing.

The low pressure compressor stator casing is attached by a bolted flange at its inlet end to the inlet bearing support structure which transfers the bearing journal and balance piston thrust loads to the compressor casing through several airfoil section struts traversing the compressor inlet annulus. Passages are provided in the struts for balance piston leakage gas. A flange at the outlet end of the compressor casing attaches the structure to the compressor outlet diffuser casing which, in turn, carries the outlet journal bearing and the thrust bearing. The thrust bearing housing is attached to the driveshaft housing which carries the high pressure compressor inlet and bearing support structure. All the structural casings are split diametrically for access to bearings, shafting and blading. Bearing pressurizing gas is supplied to the journal and thrust bearings through drilled passages in the driveshaft housing and bearing housings. The drilled passages are supplied from supply tubes, sealed by o-rings, which traverse the intercooler region to the power plant pressure casing. The supply tubes are designed to be easily withdrawn to facilitate the removal of the turbomachinery from the power plant assembly.

The compressor stator casings are sealed to the power plant assembly by means of large diameter O-rings engaging machined diameters on the coolers and the power plant pressure casing. The details of the sealing arrangements are illustrated on Figure 7-1 and are generally similar to those of the second definition concept described in Reference 1.

Starter Motor

The starter motor drives the high speed rotor through a short quillshaft and accelerates the rotor to self-sustaining speed during the initial phase of startup. The type of starter motor has not been selected but either pneumatic or electric options are conceivable. A pneumatic starter motor could make use of the large volume of stored high pressure helium in the inventory control system used to regulate the power output of the plant.

Low Pressure Turbine Mechanical Design

Two of the potential applications for the CCCBS plant place widely differing requirements on the low pressure turbine design. In the first of these applications, the power turbine drives a superconducting generator to provide power for an electrical transmission system. The optimum rotational speed in this case is approximately 9000 RPM. In the second application, the power turbine drives a mechanical power transmission system such as a ships propeller reduction gear for which a speed of 3600 RPM is more suitable. The power turbine in the first and second definition concepts was designed for a speed of 6000 RPM which represented a compromise between these conflicting requirements but was not a completely effective solution for either application. Therefore, during the current report period, two new power turbine designs were defined, one for 9000 RPM and the other for the 3600 RPM application.

The 9000 RPM design was conceived as a close-coupled assembly with the superconducting generator. In this case the generator is completely enclosed and operated at turbine outlet pressure simplifying the driveshaft sealing requirements. The liquid helium transfer system, located at the generator

AD-A081 380 WESTINGHOUSE ELECTRIC CORP PITTSBURGH PA ADVANCED ENE--ETC F/G 20/13
COMPACT CLOSED CYCLE BRAYTON SYSTEM FEASIBILITY STUDY, VOLUME I--ETC(U)
AUG 79 R E THOMPSON, R L AMMON, R CALVO N00014-76-C-0706
UNCLASSIFIED WAES-TNR-237-VOL-2 NL

3 OF 6
AD A081380

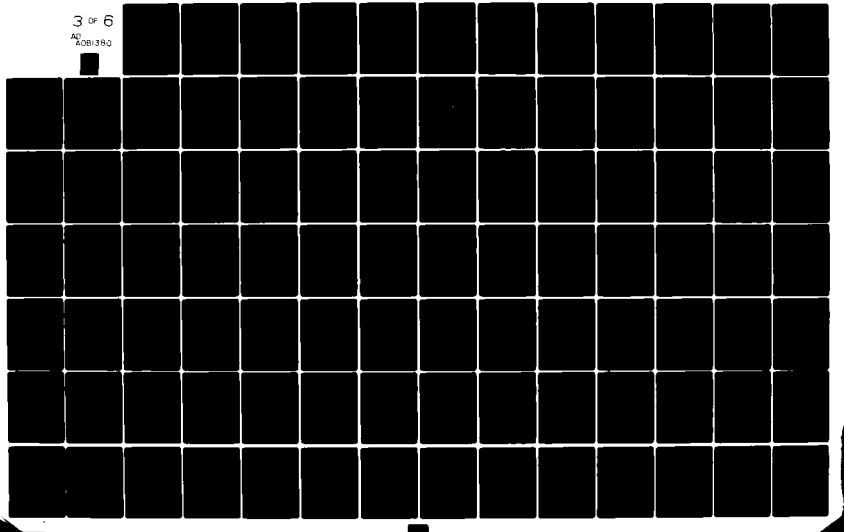

bearing remote from the turbine, which conveys the low pressure generator coolant to and from the rotor, requires rotating seals compatible with the high pressure generator environment. These considerations have been reviewed with Westinghouse superconducting generator design personnel and neither the generator pressurization nor the associated helium transfer sealing appear to present significant problems.

The 3600 RPM turbine was designed to be completely independent of its driven load components from the sealing standpoint. In this case the turbine output drive shaft penetrates the power plant pressure boundary and sealing is effected by a double face seal using a liquid (water) barrier between the seals.

In addition to the two potential applications described, a study was made of the possibility of using the 9000 RPM turbine together with a reduction gear to provide the 3600 RPM shaft speed. As a part of this study, the application of the double face seal liquid barrier to the 9000 RPM turbine driveshaft was examined and found to be feasible. The application of a magnetic seal was also studied and judged to be a potentially attractive device. However, engineering development would be required to thoroughly assess its potential. The resulting gear drive arrangement was judged to be less desirable from the standpoint of overall length and reliability than the 3600 RPM direct drive turbine. The feasibility of the 9000 RPM turbine driveshaft sealing also makes possible the use of the 9000 RPM turbine driving a superconducting generator at ambient pressure conditions. This could be used to enhance generator maintainability in a nuclear installation, where the generator could be mounted outside the containment. However, the overall length in the case would exceed that of the close coupled arrangement.

9000 RPM Low Pressure Turbine Mechanical Design

The 9000 RPM turbine has eight stages having a mean blade diameter of 0.539 m (21.23 in.) with blade heights of 59.7 mm (2.35 in.) at inlet and 86.1 mm (3.39 in.) at exit. These dimensions were obtained by scaling the 6000 RPM design of the first and second definitions, maintaining the same load and flow coefficients. This is discussed more fully in the aerodynamic design section. An evaluation

of the last power turbine stage has been performed by (W) Combustion Turbine Division. This work is discussed in Section 8.3.2.

The construction of the turbine is similar to that of the 6000 RPM first and second definition turbine described in Reference 1. Figure 7-1 illustrates the design of the 9000 RPM power turbine. The rotor employs stacked disc construction using curvic couplings and through-bolts. Unshrouded blading is shown in Figure 7-1 but rotating shrouds could be employed to provide support in bending for the blading. The journal bearing stubshafts are attached to the inlet and outlet ends of its rotor by means of through-bolts and curvic couplings. The outlet end stubshaft also carries the thrust bearing runner and the balance piston used to limit the thrust bearing maximum load.

Thrust balancing has been improved in the third definition concept by the use of high pressure compressor outlet gas at the balance piston. This has been found to greatly reduce the variation in thrust bearing load resulting during power reduction from rated to 7.5% power, compared with the arrangment used in the first and second definition concepts which employed low pressure compressor outlet gas in the balance piston. Studies made during this report period indicated that the use of low pressure compressor outlet gas in the balance piston resulted in large swings in thrust bearing load from 65,354 (14,693 lb_f) towards outlet at rated power to 27,315N (6141 lb_f) towards inlet at 7.5 percent power which adversely affected the thrust bearing design problems, especially at the low power condition. By reducing the size of the balance piston and increasing the thrust bearing load at rated power to 97,856N (22,000 lb) a reduction of the 7.5 percent power thrust bearing load to 18,673N (4198 lb) could be achieved. The use of the overall compressor pressure ratio in the revised arrangement greatly reduces the thrust bearing load swing (from 60,004N (13,490 lb) at rated power to zero at 7.5 percent power). High pressure compressor outlet gas is piped from the center frame structural plenum and supplied to the balance piston chamber via drilled passages in the turbine outlet bearing housing and power plant pressure vessel. The gas which leaks from the balance piston labyrinth seals subsequently cools the turbine outlet bearing housing, the power plant pressure vessel and the power turbine casing before rejoining the main flow path gas at entry to the precooler.

The stator construction employs diaphragms extending radially inward from the stationary blading to small diameter labyrinth seals on the rotor curvic coupling diameters. The stationary blade diaphragm assemblies are made in halves and radially keyed to the half turbine casing. Other details of the stator assemblies are similar to those of the high pressure turbine. A half casing can be removed together with its stator diaphragms to permit inspection of blading without interfering with the structural integrity of the assembly. Split casing construction is also employed at the outlet end casing which supports the turbine casing from the power plant pressure vessel and at the high pressure stator casings to which the power turbine casing is attached at its inlet end. Thus the whole of the turbomachinery rotating assembly can be exposed for inspection and maintenance in this design. The bearing housings are also split to permit access to the bearings or to allow a rotor to be removed from its stator assembly.

The turbine outlet diffuser is a sheet metal assembly made of Hastelloy X or Type 347 stainless steel mounted inside the turbine casing and conical structural member thus protecting the casings and power plant pressure vessel from the hot turbine exhaust gas. The outlet diffuser and the conical structural member are penetrated at seven circumferential locations by radial pipes which convey the turbine exhaust gas to the recuperator inlet plena. The recuperator inlet plena are simple conical vessels, supported from the conical structural member via short flanged pipes, which engage with the recuperator bolted flange region. A simple floating ring retained in each recuperator inlet plenum provides sealing while accommodating misalignment. These details are illustrated in Figure 7-1.

Some consideration has been given to the prevention of power turbine overspeed under loss of load conditions. Figure 7-3 illustrates a system of 7 bypass valves and 7 block valves which could be employed to divert 100 percent of the power turbine mass flow around the power turbine. The bypass valves are designed to mix the bypassed gas with high pressure compressor outlet gas bled from the compressor outlet plenum. The compressor bleed reduces the tendency of the high speed rotor to overspeed as the power turbine is bypassed and also reduces the temperature of the bypass gas at the recuperator inlet, helping to reduce thermal transient stresses.

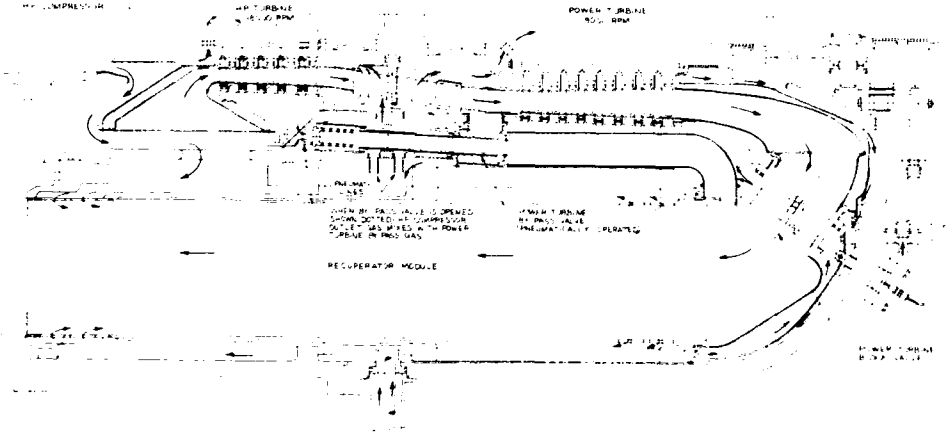

Figure 7-3. Closed Brayton Cycle Power Plant Power Turbine By-Pass and Block Valve Concept

When the initial design for the system of bypass valves and block valves was being developed, it was not clear whether or not they would be needed for overspeed protection. A preliminary analysis showed the power turbine to be capable of withstanding 60 percent overspeed without permanent deformation, and transient analyses performed to date have indicated that overspeed for complete loss of load on both power conversion units to be approximately 60 percent. However, as described in Section 6.1.3, for a loss of load on one unit with the other unit remaining on line, there is the possibility of the turbine overspeeding beyond a 60 percent condition and self-destructing. To reduce the overspeed to a manageable amount requires the use of the bypass and block valve arrangement in the unit suffering a loss of load. This would eliminate the overspeed in this unit and allow the remaining unit to stay on line.

3600 RPM Low Pressure Turbine Mechanical Design

The 3600 RPM turbine has 15 stages having a mean blade diameter of 0.985 mm (38.76 in.) with blade heights of 50.8 mm (2 in.) at inlet and 71.1 mm (2.8 in.) at exit. These dimensions were obtained by scaling the 6000 RPM first and second definition design to maintain similar load and flow coefficients. This is discussed more fully in the aerodynamic design section.

Figure 4.2.2.2 illustrates the design of the 3600 RPM power turbine. The construction is similar to that of the 9000 RPM design in its use of a stacked disc rotor with curvic couplings and through-bolts. However, the increased turbine casing diameter has made it impossible to accommodate within the inside diameter of the recuperator high pressure outlet plenum casing in the manner of the 9000 RPM turbine. Consequently, the 3600 RPM turbine is removed axially from the recuperator plenum casing in the downstream direction. The increased distance between the power turbine inlet and the high pressure turbine outlet has necessitated an annular diffuser duct of increased length connecting the two turbines. Lengthened power turbine inlet shafting and transition casings have also been required. The resulting increased length of the turbomachinery has necessitated a corresponding increase in the length of the powerplant pressure casing.

In the course of the 3600 RPM design work, a study was made of an alternative arrangement which minimized the turbomachinery length by increasing the diameter of the recuperator assembly sufficiently to allow the power turbine casing to be

accommodated within the recuperator high pressure outlet plenum. However, the increased powerplant pressure vessel diameter required in this arrangement resulted in greater overall plant and containment weight. This approach was therefore rejected in favor of the smaller diameter plant made possible by displacing the power turbine axially.

In order to minimize the overall length of the power plant assembly as much as possible, a recessed bearing arrangement has been adopted at the outlet end of the 3600 RPM power turbine. In this design, the turbine disc assembly is overhung from the shaft assembly allowing the outlet journal bearing housing to extend inside the bores of the discs. The balance piston is provided as a cylindrical extension on the conical portion of the turbine driveshaft. The use of high pressure compressor outlet gas in the balance piston chamber results in a relatively small balance piston diameter of 5.6 m (22 in.) which can be accommodated inside the turbine disc bores. As was the case in the 9000 RPM power turbine, the use of high pressure compressor outlet gas for thrust balancing greatly reduces the variation in thrust bearing load between rated and 7.5 percent power. Using L.P. compressor outlet gas for thrust balancing and sizing the balance piston to achieve zero thrust bearing load at 7.5 percent power, the resulting load at rated conditions was 616,468N (138,635 lb) which is completely unacceptable. Using H.P. compressor outlet gas and sizing the balance piston for zero load at 7.5 percent power, the resulting load at rated conditions is 115,128N (25,883 lb) which, although higher than desirable, is a great improvement and within the thrust bearing capability. By slightly increasing the balance piston diameter to reduce the rated power load to 57,824N (13,000 lb) a better tradeoff between rated and 7.5 percent power thrust bearing loads can be achieved resulting in a load at 7.5 percent power of 9977N (2243 lb). The provision made for supplying the high pressure gas to the balance piston and its use in cooling the turbine components are similar to those of the 9000 RPM turbine. The recessed bearing arrangement requires that the turbine rotor be assembled axially into the outlet end journal and thrust bearing assembly and, consistent with this requirement, the thrust bearing runner is designed to be demountable from the turbine drive shaft.

Sealing of the 3600 RPM turbine driveshaft at the pressure boundary penetration is effected by a double face seal using water between the seals. The seal illustrated on Figure 7-4 is a proprietary design by Crane Packing Company and is described by them as a "double-8B1 type - 8 HARP 170 mm shaft seal." Water at a pressure of 0.345 MPa (50 psi) higher than the turbine outlet pressure is fed into the space between the two seals. Inboard leakage, estimated to be 2.8 cc/hr., is drained, together with labyrinth seal leakage helium from a labyrinth seal immediately inboard of the inboard face seal, to a molecular sieve, where the entrained water is removed, after which the dried helium gas is returned to the powerplant. Outboard leakage, estimated to be 4 cc/min., is drained by gravity to a tank under ambient conditions from which it is pumped to the interseal space via a filter and a cooler. A water flow rate of 22,700 cc/min. (6 GPM) is circulated through the interseal space, cooler and filter by the pump in order to remove heat resulting from 13 kW (17.5 HP) seal power loss and 2.2 kW (3 HP) pump power loss. During periods of powerplant shutdown, a positive seal adjacent to the shaft coupling can be energized pneumatically, allowing the liquid seal pumping system to be shut down.

The use of the liquid seal results in essentially zero helium loss from the system during operation. An earlier study investigated the use of noncontacting face seals under 3.45 MPa (500 psi) helium pressure differential for turbine shaft pressure boundary sealing. However, the gas leakage in the absence of the liquid barrier, was found to be on the order of 0.907 kg/hr. (2 lb_m/hr.) which represented, for a two unit plant, approximately 20 times the 454 kg (1000 lb.) plant inventory per year. (Fort St.Vrain permits leakage of purified helium equal to 100% inventory or contaminated helium equal to 1% inventory per year.) This amount of leakage was judged to be excessive and all efforts to apply purely gas seals to the turbine shaft sealing problem were terminated.

The 3600 RPM power turbine stator construction is generally similar to that of the 9000 RPM turbine in its use of half diaphragm assemblies radially keyed into half turbine casings. The split casing construction permits easy access to the blading without interfering with the structural integrity of the assembly.

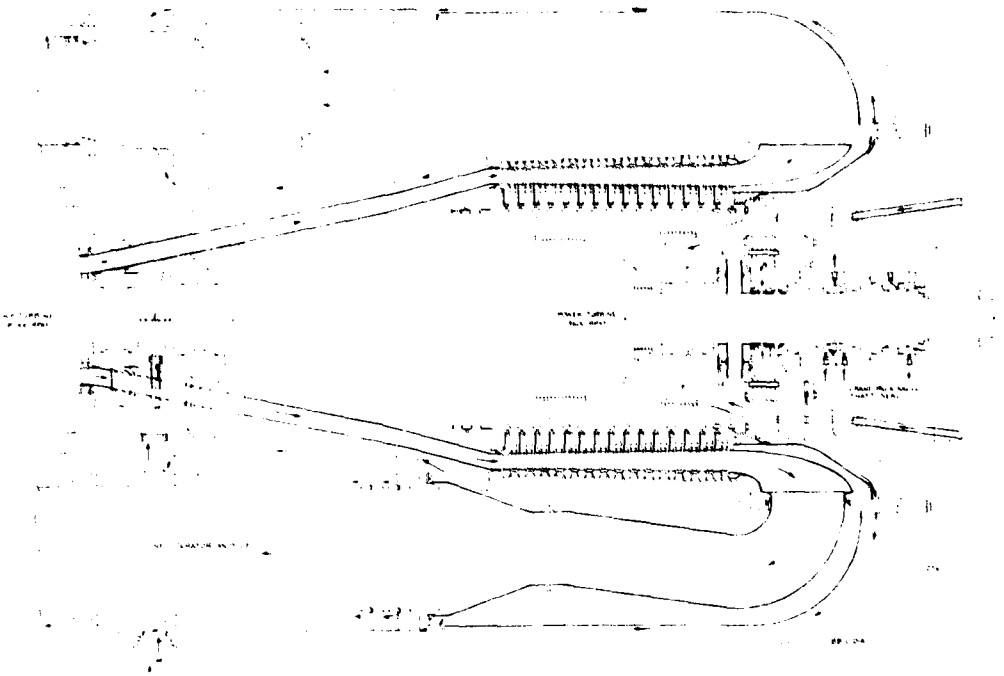

Figure 7-4. 3600 RPM Power Turbine

Access to the turbine outlet bearing is not obtainable in this design, however, without completely removing the rotor from the bearing assembly. This is effected by releasing the coupling nut at the outlet end of the shaft and then withdrawing the shaft from the thrust bearing runner and sleeve. After removal of the rotor, the journal and thrust bearing housings can be split to obtain access to the bearing pads.

The turbine outlet diffuser and ducting to the recuperators are similar in concept to those of the 9000 RPM design. However, the seven pipes which carry the turbine exhaust gas to the recuperator inlet plena are longer than in the 9000 RPM design to accommodate the axially displaced 3600 turbine location. The provision of turbine bypass and block valves has not been studied in detail in the 3600 RPM design, but it is judged that sufficient space is available to incorporate a suitable system if this should prove to be necessary.

Gear Drive Alternatives

During the development of the 3600 RPM mechanical drive power turbine, a study was made to assess the feasibility and relative merits of a 2·5/1 ratio reduction gear driven by the 9000 RPM turbine. Three reduction gear alternatives were examined: a five "planet" star gear; a single mesh gear (both designed by Westinghouse Sunnyvale Division); and a four layshaft multiple path gear designed by Cincinnati Gear Company. The three gearbox/powerplant combinations are shown compared with the 3600 RPM turbine powerplant in Figures 7-5 and 7-6.

The single mesh gear had high scoring factors. The star gear was much better in this respect but still "on the high side" in the judgment of the Sunnyvale gear engineer. Both gearboxes were designed for K factors of 350 and assumed the use of hardened and ground teeth. The Cincinnati Gear Company judged the star gear approach to be inappropriate at the 3600 RPM output speed and recommended a four layshaft multiple path drive. In this arrangement, the four layshafts are equally spaced around coaxial input and output sun gears. A large gear on each layshaft is driven by the small sun gear. Each large layshaft gear drives a small gear

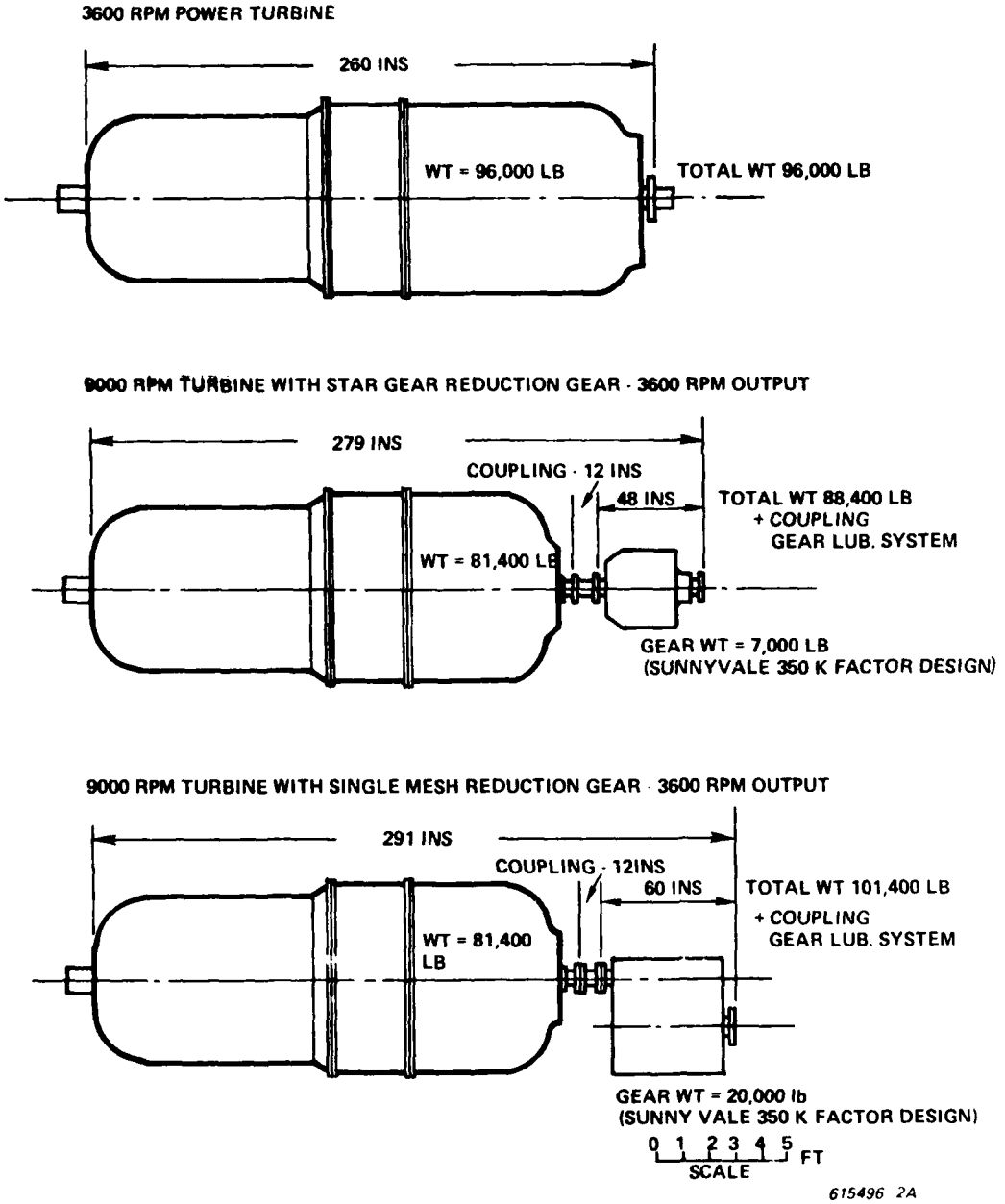

Figure 7-5. CCCBS Length Comparison

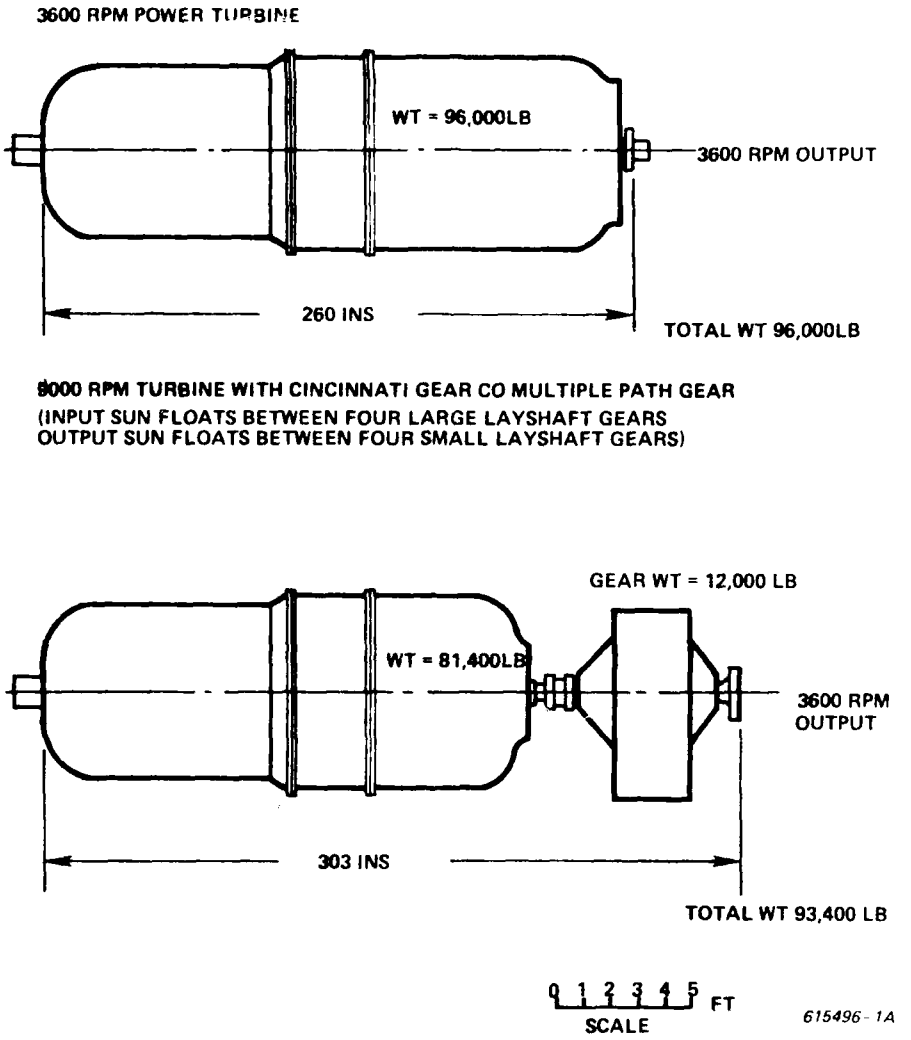

Figure 7-6 CCCBS Length Comparison

directly connected to it. The four small layshaft gears, in turn, drive the large output sun gear. Both input and output sun gears float between the layshaft gears to effect load sharing. Cincinnati personnel considered the design suitable for up to 100,000 hrs. life and did not expect any significant development problems.

As shown in Figures 7-5 and 7-6 the gearbox drive alternatives were all longer than the 3600 RPM turbine powerplant. Two of the gearbox alternatives were lighter in weight than the 3600 RPM turbine powerplant, but the weight savings of 3,455 KG (7600 lb_m) for the Sunnyvale stargear and 1182 KG (2600 lb_m) for the Cincinnati Gear Company multiple path gear were judged to be insufficient to justify the disadvantages, such as a reduced reliability and increased noise, associated with the gearing.

Bearings, Housing, and Seals Mechanical Design

The bearings are rigid geometry hydrostatic gas bearings which use helium as the lubricant. The bearings are illustrated in Figures 7-1 and 7-3. The journal bearings employ four pads supported from the housing through compliant diaphragm members and supplied with helium from drilled holes in the housing through metering orifices at the pads. The orifices discharge the helium lubricant into a recessed area machined into the pads. The thrust bearings are similar in their use of the rigid geometry hydrostatic design but employ eight sector shaped pads. The thrust bearing stator assembly is supported from a gimbal mechanism to achieve uniform circumferential load distribution. The bearing design is discussed in more detail in Section 7.3.

The rigid geometry hydrostatic concept has been adopted quite recently to limit rotor motion under shock load conditions. The gas bearings originally selected to replace the oil lubricated bearings of the first definition design employed a compliant foil arrangement capable of operating hydrodynamically at rated speed but employing hydrostatic augmentation at the lower speeds via a gas supply fed to the rotor members. The foil design, although very forgiving of thermal and mechanical distortion, was inherently flexible and would have exhibited excessive deflection under shock load conditions resulting in blade tip rubbing.

Bearing housings are split diametrally to facilitate manufacture and simplify access to the pads. The gimbal support for the thrust bearings is not split but is arranged in such a way that the accessibility to the machinery facilitated by the split casing construction is not impaired. In the case of the high speed rotor thrust bearing, the completely assembled thrust bearing is designed to be removable with the low pressure compressor rotor. To this end the thrust bearing stator mounting bolts are easily accessible over the full 360° by reaching around the inter-compressor driveshaft. In the case of the power turbine thrust bearing the unsplit gimbal components are mounted at the extreme outlet end adjacent to the powerplant pressure vessel. In this location, the split bearing housing components can be withdrawn clear of the completely circular members.

The seals associated with the gas bearings and their housings have been essentially eliminated. The oil lubricated bearings of the first definition concept required extensive sealing provisions to prevent the leakage of lubricating oil into the helium working fluid. These generally took the form of labyrinth and windback (screw thread) seals and required careful pressure balance provisions at the bearing housings to ensure leak free operation. The need for such provisions has been eliminated with the adoption of gas bearings.

The hydrostatic augmentation applied to the foil bearings of the second definition concept involved the use of a rotor to stator sealing system to introduce the bearing pressurizing gas into the rotor. This sealing system, with its leakage losses, is no longer required with the rigid geometry hydrostatic bearings, which are all supplied from the stationary members.

Sealing provisions at the bearings to limit gas leakage are confined to O-rings at the various casing joints and supply pipes. The bearing pressurizing gas, after performing its function in the bearings, leaks directly into the primary helium flow circuits with no contamination effects.

Heat Exchanger Mechanical Design

Figure 7-1 illustrates the precooler, intercooler, and recuperator general arrangement and location with respect to the turbomachinery and power plant pressure casing.

The precooler and intercooler are similar in design and employ finned tubing arranged in a helical matrix around the turbomachinery. The tubing is headered in four equally spaced radial pipes at each end of the matrix. A "four-start" arrangement of the tubing provides compatibility with the header pipes. Cooling water is piped into the radial header pipes through "bobbin" and O-ring connectors, flows through the helical tubing and leaves through the radial header pipes and connectors at the other end. The helium cycle gas flows axially across the finned tubing.

The intercooler matrix is accommodated within a cylindrical pressure shell which is terminated at each end in pressurized headers. The headers convey the helium gas from the low pressure compressor outlet into the intercooler and from the intercooler into the high pressure compressor inlet. The intercooler/header/vessel assembly is supported from a flange on the powerplant pressure vessel through a conical support member and is sealed to the turbomachinery by means of elastomer O-rings. Complete separation of the higher pressure gas in the intercooler from the lower pressure gas entering the precooler is thus achieved while permitting the turbomachinery to be freely withdrawn from the assembly through the O-ring seal interfaces. The conical support member is penetrated by a number of large diameter holes which allow the passage of the low pressure gas from the recuperator to the precooler inlet.

The precooler and its headers are integrated into a similar assembly and supported from a flange on the powerplant pressure vessel.

The coolers have been carefully located in the axial direction to avoid interference with the radial pipes supplying the pressurizing gas to the bearings. Pressurizing gas is fed to the bearings through small diameter pipes which are accommodated inside the larger turbine cooling supply pipes.

The design of the coolers has been considerably refined since the second definition design described in Reference 1. This design work was performed by Airesearch and is reported in Section 8.2.1. As a result the diameters of the precooler and intercooler have been significantly reduced.

The recuperator modules are similar to those of the first definition concept described in Reference 1 and are constructed as simple thin walled cylinders containing bundles of heat transfer tubing. The flow configuration is that of a counterflow heat exchanger with the turbine exhaust helium flowing in the tubes and with the compressor exit helium flowing on the shell side. The recuperator is composed of seven modules which are approximately 415.5 mm (16.36 inches) in diameter. Each module contains about 10700 tubes with an outer diameter of 3 mm (0.120 inch) and a thickness of 0.25 mm (0.010 inches).

The tubes are formed at their ends into a hexagonal section. The tube ends are furnace brazed together. The tube bundle is also brazed at the ends to an external cylinder and a cold end ring. Filler pieces are used to fill the gaps at the tube and cylinder interface. No tube sheet is required in this arrangement since each tube carries the local axial tension force.

The tube module is free to expand and contract due to the floating end ring. O-rings are used to seal the floating cold end ring. The modules are located and sealed at the hot end by bolted flanges. This arrangement eliminates the need for tube sheets with their numerous drilled holes. However, the hex-end forming is an additional operation. The conventional tube sheet approach can be substituted if manufacturing studies show this to be desirable.

The common duct structure located around the power turbine section is supported axially from the center frame by eight SA 533 pressure tubes, seven containing the recuperator modules and one containing the check valves and delivery pipe. The eight pressure tubes contain helium at compressor outlet pressure.

The recuperator modules are located axially from the common duct structure by bolted flanges which separate the high and low pressure sides of the system. Differential thermal growth, in the axial direction, between the recuperator modules and the pressure tubes is accommodated by the sliding O-ring seals at the cold ends of the modules. The O-rings separate the high and low pressure gases and are made of silicon rubber capable of operating at temperatures in excess of 204°C (400°F).

Differential thermal growth between the delivery pipe and the eighth pressure tube is accommodated by piston rings. The piston ring leakage is acceptable in this location since it will be very low because the leakage pressure difference is small (recuperator module plus check valve ΔP).

The radial pipe located in the center frame structure, which receives the heated gas from the delivery pipe, is also sealed from the compressor outlet gas in the center frame by piston rings which can slide to accommodate the thermal growth between the radial pipe and the center frame. The radial pipe carries the heated gas radially outward to a penetration on the pressure casing whence it flows to the energy source. A double-walled Hastelloy X (or similar) inner pipe passing through the radial pipe, delivers hot gas from the energy source to the high pressure turbine inlet scroll. This area of the design has been subjected to detailed refinement to reduce leakage and thermal stresses and was fully described in the High Pressure Stator Mechanical Design Section.

The hot gas from the heat source passes through the high pressure turbine, which drives the compressors, and into the low pressure turbine via an intermediate bearing support casing. After passing through the low pressure power turbine, the

gas is ducted into the low pressure side of the recuperator module. A stainless steel liner system separates the hot turbine outlet gas from the pressure casing and turbine bearing and support assembly. The turbine outlet gas then flows axially forward through the recuperator modules, transferring heat to the tube bundle containing the high pressure compressor outlet gas. The cooled low pressure turbine outlet gas leaves the forward ends of the recuperator modules and enters the precooler annulus.

Aerodynamic Design - General

During this report period, aerodynamic refinements have been made in the low pressure compressor and the low pressure turbine. The high pressure turbine and compressor are essentially unchanged aerodynamically from the designs described in Reference 1 for the first and second definition concepts. However, the high pressure turbine first stage rotor blade chord distribution has been somewhat modified to adapt the design to 927°C (1700°F) inlet temperature from the 911°C (1671°F) value used in the first year. In addition, the blade root/disc fixing region of the first stage blade has been refined to provide a basis for more detailed thermal and mechanical analysis.

Low Pressure Compressor Aerodynamic Design

The aerodynamic design of the low pressure compressor first stage has been evaluated in more detail by Westinghouse Combustion Gas Turbine Division, resulting in some changes to the geometry of the earlier concept design.

The inlet blade mean diameter has been reduced to 409 mm (16.116 in.) from the 442 mm (17.419 in.) value of the earlier design. Also, the inlet blade height has been increased to 45.5 mm (1.791 in.) from the earlier value of 44 mm (1.742 in.). The first stage rotor has 49 blades having tapered chords increasing 8% at the root and decreasing 8% at the top from the mean blade value.

The chords are 28.0 mm (1.134 in.), 26.7 mm (1.05 in.) and 24.7 mm (0.972 in.) at root, mean and tip, respectively. The root chord of 28.8 mm results in an axial width at the root of 26 mm (1.025 in.). Rotor blade thickness/chord ratio is 0.160, 0.095, and 0.030 at root, mean, and tip, respectively.

The first stage stator vanes have constant chord of 27.8 mm (1.094 in.) and thickness/chord ratio of 10%. The resulting axial width at the root is 21 mm (0.825 in.). There are 48 first stage stator vanes.

The number of stages (14) is unchanged from the earlier design. In defining the later stages, the ratio of outlet to inlet blade height of the second definition design has been retained and blade and vane chords have been reduced to maintain constant aspect ratio. The resulting outlet (14th stage) blades have an axial width at the root of 19 mm (0.75 in.). The stator vanes at outlet have an axial width of 15.2 mm (0.6 in.).

Helium temperature and pressure conditions are 38°C (100°F) and 3.13 MPa (454 psia) respectively at inlet and 151°C (304°F) and 6.14 MPa (890 psia) at outlet. Mass flow is 58 kg/sec. (127.9 lb_m/sec.).

The compressor design employs symmetric 50% reaction blading at the mean blade diameter with free vortex distribution and constant axial velocity (≃212 m/s) (≃697 ft/sec.) from hub to tip. Mean blade speed is 386 m/sec. (1266 ft/sec.).

The aerodynamic design of the low pressure compressor first stage is discussed in more detail in Section 8.3.1.

Low Pressure Turbine Aerodynamic Design

The 9000 RPM free power turbine has eight stages having a mean diameter of 0.539 m (21.23 in.) with blade heights of 59.7 mm (2.35 in.) at inlet and 86.1 mm (3.39 in.) at exit. These dimensions were obtained by suitably scaling the corresponding dimensions of the 6000 RPM second definition design to maintain the same load coefficient (3.56) and flow coefficient (0.8). Load coefficient is defined as stage enthalpy drop divided by the enthalpy equivalent of the blade velocity or:

$$\psi = \frac{\Delta h/\text{stage}}{U^2/2gJ} \qquad (1)$$

Flow coefficient is defined as the axial component of velocity divided by blade velocity:

$$\phi = \frac{V\alpha}{U} \qquad (2)$$

The turbine efficiency to be expected may be estimated by relating the above design parameters to published performance curves. Reference 2 has correlated turbine efficiency with stage load coefficient and flow coefficient. Figure 7-7 is a copy of Smith's correlation taken from page 127 of J. H. Horlock's book, "Axial Flow Turbines - Fluid Mechanics and Thermodynamics," 1966, Butterworth and depicts the design point of the 9000 RPM low pressure turbine. (The high pressure turbine design point is also shown for comparison. Note that Horlock's definition of stage load coefficient has one half the value defined in equation (1) above. The load and flow coefficient values were deliberately selected to be higher than optimum from the efficiency standpoint in order to reduce the size of the machine. The power turbine design point falls approximately at 92.3% efficiency. This efficiency must be adjusted for leaving loss and tip leakage.

The axial leaving velocity from the 9000 RPM power turbine is 198 m/s (650 ft/sec.) corresponding to 1% leaving loss (η_{LL} = 0.99), assuming 50% diffusion recovery. If a clearance/diameter ratio of 0.0015 is assumed, the tip clearance is 0.8 mm (0.032 in.) and the average clearance/blade area ratio is 0.022 (η_{leak} = 0.978). The resulting net turbine efficiency is 0.923 x 0.99 x 0.978 = 0.894, which is sufficiently close to the assumed value of 0.9.

The scaling process used to derive the eight stage 9000 RPM turbine dimensions from the earlier 6000 RPM twelve stage design while maintaining the load and flow coefficients unchanged is as follows:

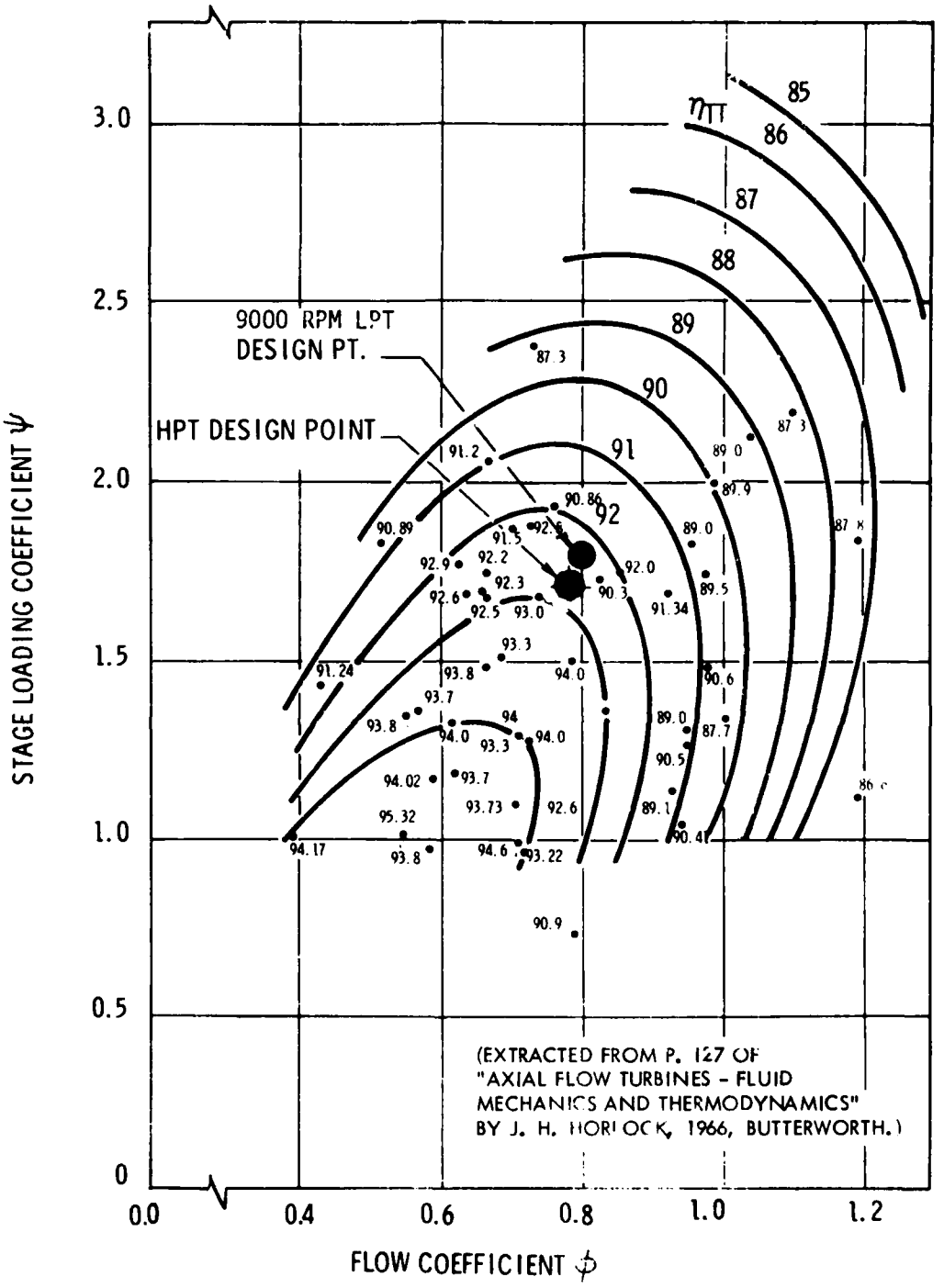

Figure 7-7. Correlation of Measured Turbine Stage Efficiencies (Corrected for Zero Tip Leakage)

Δh/stage is increased by a factor of 1.5 due to the reduced number of stages. Therefore, U^2 must increase by the same factor if ψ is to remain constant or U must increase in the ratio of $\sqrt{1.5}$.

If the mean diameter of the 6000 RPM turbine were to be retained unchanged in the 9000 RPM design the blade velocity U would increase in the ratio of 1.5 which is greater than the required $\sqrt{1.5}$ increase. Therefore, the mean blade diameter of the 9000 RPM turbine must be reduced in the ratio of $\frac{1.5}{\sqrt{1.5}} = \sqrt{1.5}$ to achieve the required blade speed and load coefficient.

Having increased the blade speed U in the ratio of $\sqrt{1.5}$, the axial velocity must also increase in the same ratio if the flow coefficient is to remain unchanged. By retaining the inlet and outlet blade heights of the 6000 RPM turbine unchanged, the axial velocity is increased in the ratio of $\sqrt{1.5}$ as a result of the reduction in the mean diameter.

The resulting turbine is considerably more compact than the earlier 6000 RPM turbine and, in retaining the same load and flow coefficients, is believed to represent an effective compromise between the conflicting requirements of efficiency and compactness. The 9000 RPM turbine design was used as the basis of the critical evaluation of the last stage by Westinghouse Combustion Gas Turbine Division described in Section 8.3.2.

The 3600 RPM free power turbine has fifteen stages having a mean diameter of 0.095mm (38.76 in.) with blade heights of 51 mm (2 in.) at inlet and 71 mm (2.8 in.) at outlet. The design was derived from the earlier 6000 RPM turbine by a scaling process similar to that described in the immediately preceeding pages for the 9000 RPM turbine. In the case of the 3600 RPM design, however, a somewhat lower flow coefficient (0.7 at inlet) was used to achieve longer blades and limit hub/tip ratio to a maximum value of 0.9 at inlet. The same load coefficient (3.56) as that employed in the 6000 RPM turbine was retained in the 3600 RPM design. The resulting design point is shown in Figure 7-8 located on Smith's efficiency correlation map. The 9000 RPM turbine design point is also shown for comparison. The 3600 RPM turbine design point falls approximately at 92.5% efficiency. This efficiency must be adjusted for leaving loss and tip leakage.

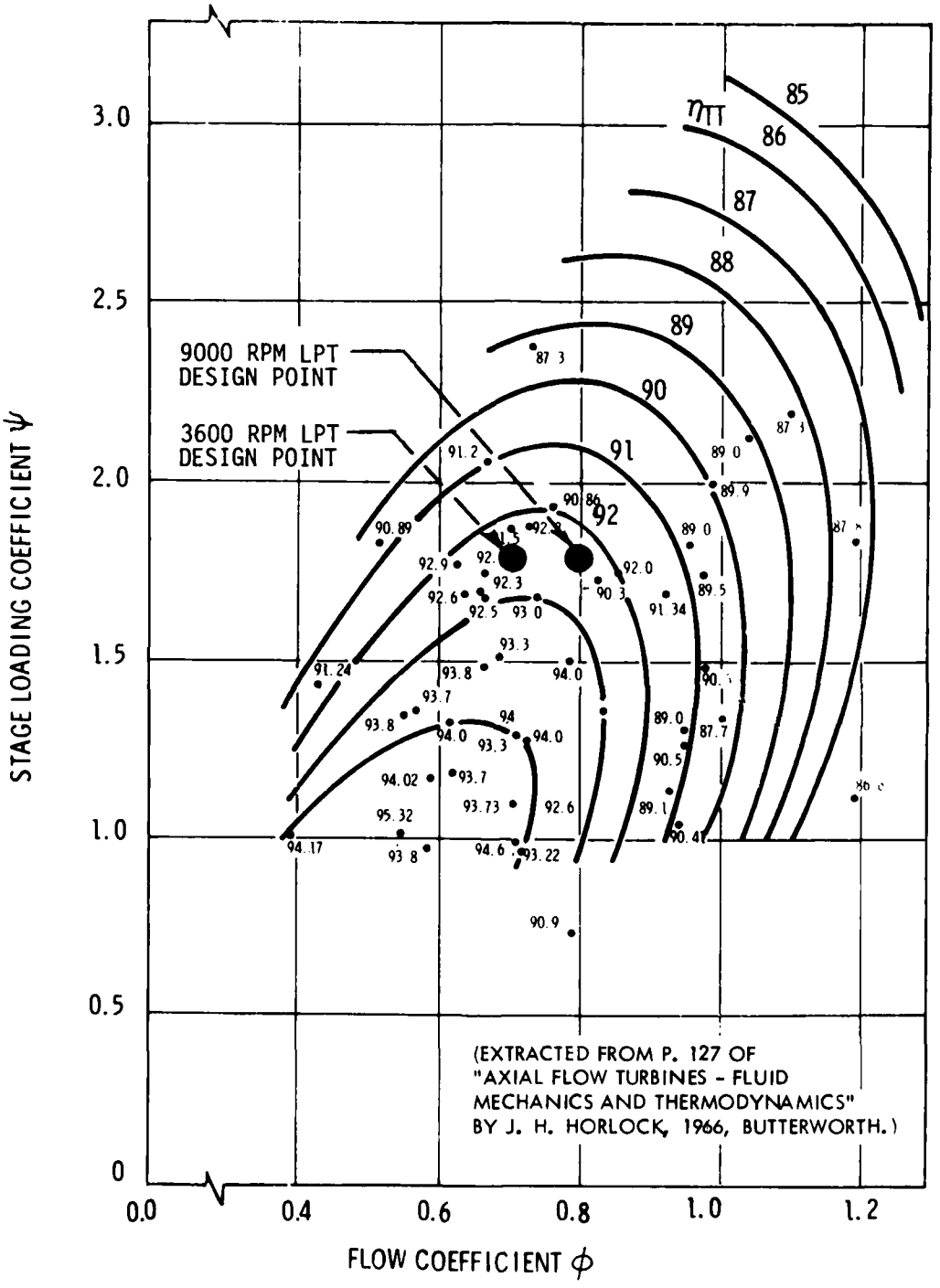

Figure 7-8. Correlation of Measured Turbine Stage Efficiencies (Corrected for Zero Tip Leakage)

The axial leaving velocity from the 3600 RPM turbine is 131 m/s (430 ft./sec.) corresponding to 0.4% leaving loss (η_{LL} = 0.996) assuming 50% diffusion recovery. If a clearance/diameter ratio of 0.0015 is assumed, the tip clearance is 1.5 mm (0.058 in.) and the average clearance/blade area ratio is 0.048 (η_{leak} = 0.952). The resulting net turbine efficiency is 0.925 x 0.996 x 0.952 = 0.877 which is more than two points lower than the assumed value of 0.9. However, the tip clearance allowance of 0.058 may be unduly pessimistic in such a high hub/tip ratio machine where a relatively large percentage of the radius would consist of well cooled disc material. The reduced thermal growth associated with the discs, combined with the use of low expansion casing material could conceivably permit a much lower operating tip clearance. Another possibility is the use of rotating blade tip shrouds. Although MGCR test experience showed no efficiency advantage for rotating shrouds if tip clearances were held to less than 0.0017 diameter, the test turbine had a much lower hub/tip ratio ($\simeq$ 0.7) so that tip leakage effects would have been substantially less than those of the high hub/tip ratio 3600 RPM power turbine. With the use of rotating shrouds and multiple seals the leakage loss could perhaps be reduced to half of the unshrouded value which would raise the resulting turbine efficiency to 0.899.

The 3600 RPM turbine dimensions were derived by scaling from the earlier 6000 RPM design to maintain the same load coefficient (3.56) but somewhat reduced flow coefficient (0.7).

Δh/stage was reduced by a factor of 0.8 due to the increased number of stages. Therefore, U^2 decreased in the same ratio and U decreased by a factor $\sqrt{0.8} = 0.894$.

To maintain the required U with the new reduced 3600 RPM necessitated an increase in mean diameter in the ratio $\frac{6000}{3600} \times 0.894 = 1.491$ to achieve the required blade speed and load coefficient.

Having reduced the blade speed U by a factor of 0.894, the axial velocity would have had to reduce in the same ratio to maintain the original 0.8 flow coefficient but, in order to reduce the flow coefficient to 0.7 at inlet and so maintain a minimum hub/tip ratio of 0.9, the axial velocity was reduced still further in the ratio $0.894 \times \frac{0.7}{0.8} = 0.782$ at inlet.

The resulting turbine is quite bulky and, as discussed in the mechanical design section, could not be accommodated inside the recuperator high pressure outlet plenum. As a result, the mechanical design of the 3600 RPM turbine had to be arranged quite differently than that of the 9000 RPM design, resulting in the configuration illustrated in Figure 7-4.

7.3 GAS BEARING DEFINITION

Based upon the work done during Year 1, gas bearings were chosen for incorporation in the CCCBS definition. This section details the critical design features of the gas bearings designed for the plant, taking into account critical speed analysis, normal and off-design loads, and shock loads.

7.3.1 BEARING DESIGN CONSIDERATIONS

7.3.1.1 ORIGINAL BEARING LOADS AND SELECTION

Study of the Year 1 Trial Design of the CCCBS engine resulted in defining the static bearing loads shown in Figure 7-9. The design featured an 18,000-rpm gas generator and a 6,000-rpm power turbine. An evaluation of possible bearing designs further resulted in the tentative recommendation of hybrid hydrostatic/hydrodynamic compliant foil-type gas bearings for the engine journal bearings. Hydrostatic solid geometry pad-type gas bearings were recommended for the gas generator and power turbine thrust bearings. The various bearing sizes are shown in Table 7-2. During the Year 1 Study, it was assumed that a differential pressure of 2.758 MPa (400 psi) would be available continuously for thrust-bearing hydrostatic gas supply and 1.379 MPa (200 psi) differential for the journal bearings during startup and shutdown of the engine.

7.3.1.2 YEAR 2 GAS BEARING RECOMMENDATIONS

Refinement of the CCCBS engine design and the establishement of new criteria during the second year of study have resulted in changes to the recommended bearing support system. Shock requirements as well as definition of off-design cycle state points have combined to change the baseline gas bearing recommendation from hydrostatic/hydrodynamic compliant foil type to solid geometry hydrostatic pad type for all journal and thrust bearings.

This current recommendation does not preclude the eventual use of foil-type gas bearings. It does consider, however, that the better definition of the bearing requirements during Year 2 has placed the foil-type gas bearing design into a technology area where it cannot be confidently scaled or extended without further full-scale research.

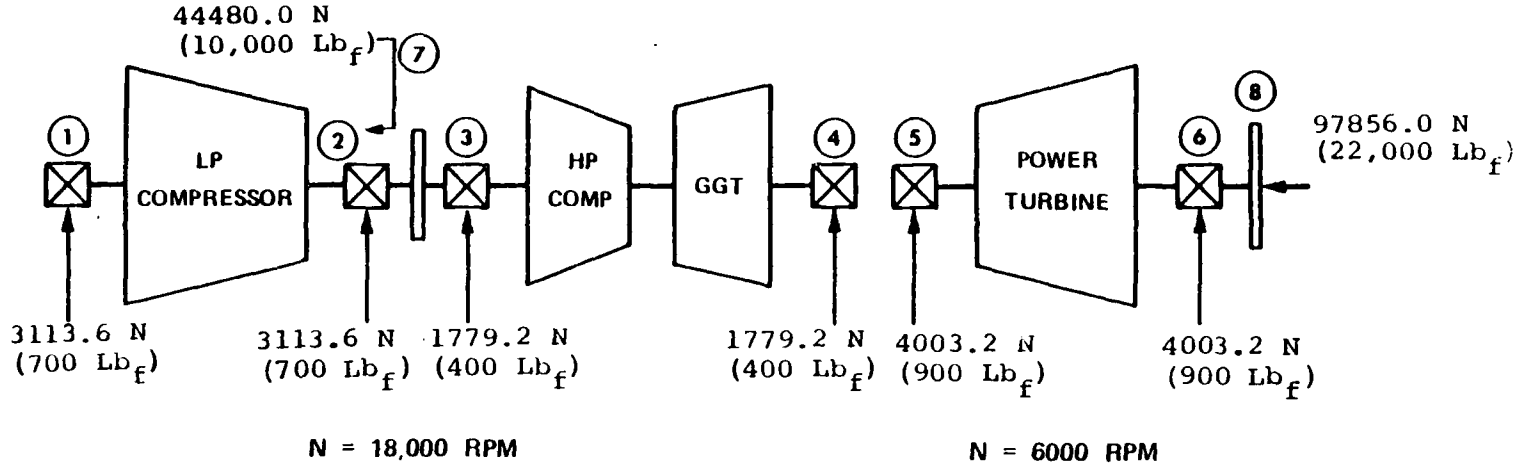

Figure 7-9. 70,000 HP CCCBS Engine Bearing Support Schematic

TABLE 7-2

HYDROSTATIC/HYDRODYNAMIC
FOIL JOURNAL BEARING AND
HYDROSTATIC THRUST BEARING DESIGNS

Bearing Number	Bearing Load		Bearing Size	
	kN	(lb)	M x 10^{-2}	(in.)
1	3.113	(700)	15.85 x 15.85	(6.24 dia x 6.24 long)
2	3.113	(700)	15.85 x 15.85	(6.24 dia x 6.24 long)
3	1.779	(400)	11.96 x 11.96	(4.71 dia x 4.71 long)
4	1.779	(400)	11.96 x 11.96	(4.71 dia x 4.71 long)
5	4.003	(900)	17.91 x 17.91	(7.05 dia x 7.05 long)
6	4.003	(900)	17.91 x 17.91	(7.05 dia x 7.05 long)
*7	44.48	(10,000)	25.53 OD x 8.84 ID	(10.05 OD x 3.5 ID)
*8	97.85	(22,000)	38.10 OD x 13.97 ID	(15.0 OD x 5.5 ID)

*Hydrostatic pad type thrust bearings.

7.3.1.3 CURRENT GAS BEARING REQUIREMENTS

The Year 2 Study has resulted in a number of changes and additions to the application of the basic CCCBS engine concept. Each new application has required changes to the power turbine speeds, thrust loads, geometry, and steady-state and transient operation which, in turn, have influenced the gas-bearing designs for the gas-generator section. The power-turbine variations are summarized in Table 7-3.

Definition of shock loads for the rotating groups of the CCCBS was established during the second year; they are summarized in Table 7-3.

These loads combine to apply approximately ±18 g loads to the engine journal and thrust bearings and are the primary cause for changing the recommended bearing designs from foil type to solid pad type hydrostatic.

7.3.1.4 BEARING LOADS

As a result of the critical speed analysis, rotor properties for the various CCCBS engine configurations were established. A summary of the rotor properties for the 9,000-rpm small power turbine configuration is given in Table 7-4 and reflects the original design and that of the LP and HP spools as modified to exhibit acceptable critical speeds. The rotor properties for the large power turbine using the 66.04 cm (26.0 in.) mean diameter blading are also included in Table 7-4.

The rotor properties were used to derive the bearing loads, as shown in Figures 7-10 and 7-11, for small- and large-diameter power turbine configurations, respectively. The thrust loads reflect only the full-rated power values and are subject to considerable change as a function of engine power level and whether the power turbine is a constant speed as variable speed design.

7.3.2 DESCRIPTION OF BEARING CRITICAL FEATURES

The introduction of off-design cycle state points, variable-speed turbines, and shock loads during the second year of the study necessitated a

TABLE 7-3

POWER TURBINE DESIGN VARIATIONS

Power Turbine Variation	Speed rpm	Max Thrust Load kN	(Lbs)
1	6000 (Constant)	97.856	(22,000)
*2	9000 (Constant)	97.856	(22,000)
**3	9000 (Constant)	65.163	(14,650)
4	9000 (Variable)	65.163	(14,650)
5	3600 (Constant)	Undetermined	

*66.04 cm mean dia turbine (26.00 in.)
**53.92 cm mean dia turbine (21.23 in.)

SHOCK LOADS

Shock Loads	Period
±16 g vertical	Approximately 0.055 sec
±8 g horizontal	Approximately 0.055 sec
±7.5 g axial	Approximately 0.055 sec

TABLE 7-4

SUMMARY OF ROTOR PROPERTIES CCCBS ENGINE

Standard Configuration	C.G. Location (From Front End of Shaft) cm	(in.)	Weight N	(Lb_f)	Polar Inertia cm-N-sec^2	(in.-lb_f-sec^2)	Diametrical Inertia cm-N-sec^2	(in.-lb_f-sec^2)
LP Compressor	94.2	(37.1)	4764.0	(1071)	772.3	(68.9)	7750.2	(691.4)
HP Spool	89.7	(35.3)	3603.0	(810)	535.8	(47.8)	10895.6	(972.0)
Small Power Turbine	76.2	(30.0)	5088.8	(1144)	1298.1	(115.8)	9012.4	(804.0)
Modified Configuration								
LP Compressor	92.0	(36.2)	4595.0	(1033)	830.6	(74.1)	5871.5	(523.8)
HP Spool	91.4	(36.0)	4408.2	(991)	723.0	(64.5)	10024.7	(894.3)
Small Power Turbine	76.2	(30.0)	5088.8	(1144)	1298.0	(115.8)	9012.4	(804.0)
Large Power Turbine	74.0	(29.1)	5903.0	(1327)	2174.6	(194.0)	9864.4	(880.0)

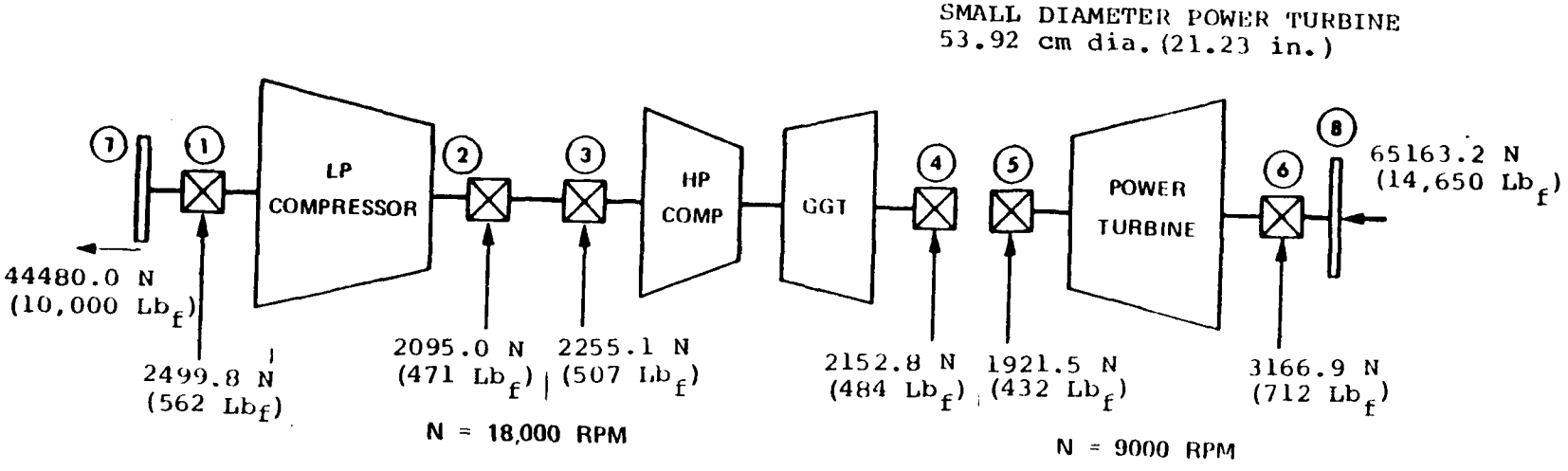

Figure 7-10. Second Year 70,000 HP CCCBS Engine Bearing Support Schematic-Modified

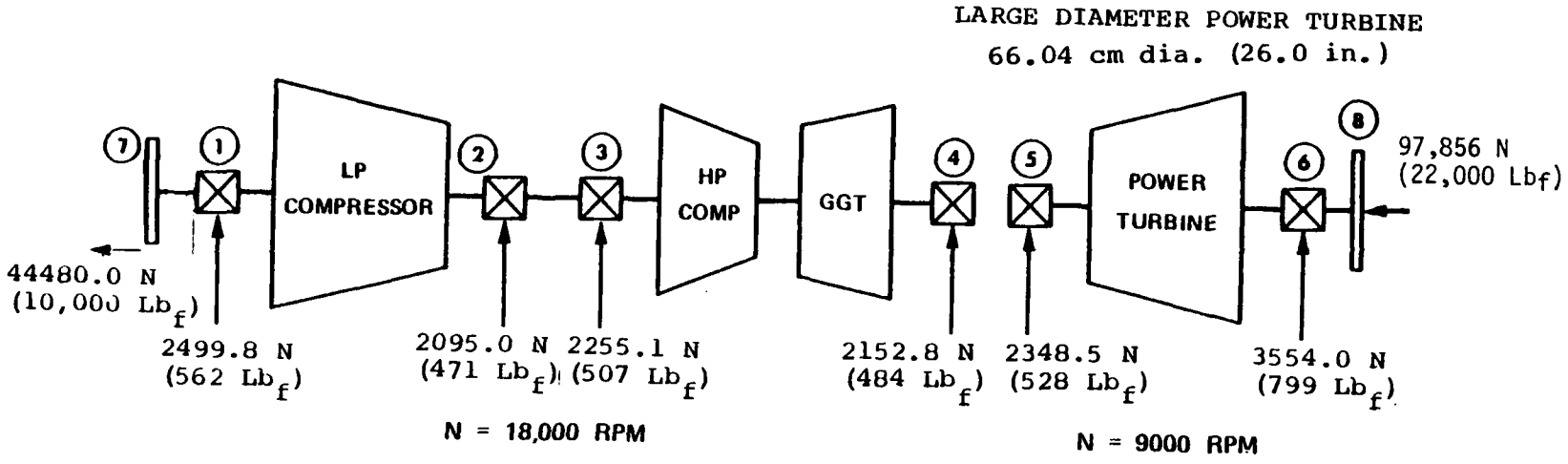

Figure 7-11. Second Year 70,000 HP CCCBS Engine Bearing Support Schematic - Modified

reassessment of the type of gas bearings used to support the rotating spools. As previously stated, hydrostatic/hydrodynamic foil-type gas bearings were recommended at the conclusion of the first year of study. The advent of 18-g shock loads, off-design conditions, and variable-speed power turbines immediately caused the use of the hydrodynamic gas bearings to be questionable. The load capacity of such bearings is a strong function of bearing speed and ambient pressures. The combination of off-design requirements and the variable-speed turbines under study created conditions where hydrodynamic bearing designs could not long survive. Secondly, the radial deflection of foil-type gas bearings designed and tested to date is relatively large under heavy shock loads, and such radial deflection might cause the blading of the aerodynamic components and thrust balancing piston seals to rub. The damage to the blading probably would be minor, but even minor damage to the thrust balancing piston seals could cause a gross thrust imbalance with subsequent overload and failure of the affected thrust bearing.

Another consideration related to foil radial stiffness also caused the use of foils to be suspect. The successful performance of foil-type gas bearings depends on their compliancy of surface to accommodate thermal growth, gradients and pressure variations, and geometric variations such as misalignment, taper, crowning, etc. The very compliancy permitting ideal bearing operation also causes larger radial movement under shock loads as compared to solid-geometry type bearings. The radial stiffness of foil bearings can be controlled over a wide range and bearings with the necessary stiffness to meet the various requirements of the CCCBS engines can be designed; however, the necessary compliancy cannot be reliably scaled at this time to the size and load capacity required. This decision does not preclude the eventual use of foil-type gas bearings in similar applications following suitable research and development.

Based on these reasons and the performance and characteristics of a 10.16 cm dia (4.00 in.) hydrodynamic foil bearing tested at AiResearch, the Year 1 Study recommendation for hydrodynamic foil-type gas bearings is changed to solid geometry pad-type hydrostatic gas bearings for all journal and thrust bearings required in the CCCBS engines.

7.3.2.1 HYDROSTATIC GAS BEARINGS

Analysis of the off-design conditions for the 9,000-rpm small power turbine configurations with constant- and variable-speed power turbine applications indicated that the most severe bearing designs occurred at the condition when the least differential pressure for hydrostatic operation was available. This condition was identified as the 7.5 percent power condition where the LP and HP compressor spool journal bearings and one journal bearing of the power turbine would have only 620.5 kN/m^2 (90 psi) differential pressure available for bearing support. This maximum differential pressure was obtained by using the HP compressor discharge pressure as the hydrostatic supply and venting the various bearing cavities to engine station pressures shown in Figure 7-12. As a result of refined aerodynamic thrust analysis and the use of the HP compressor discharge pressure for hydrostatic bearing supply and thrust balancing, the thrust balance piston was moved from the inlet end to a position between the LP and HP spools (as is shown in Figure 7-12). This interchange of thrust bearing and balance piston locations resulted in improved thrust balance and more accurate axial positioning and control of both the LP and HP compressors.

The hydrostatic gas bearings were designed on the basis of cycle gas pressures available for full-rated power and the 7.5 percent power condition. The most critical condition as determined by the minimum differential pressure available occurred for the 7.5 percent power rating with the constant-speed turbine. At this condition, only 1,206 kN/m^2 (175 psi) differential pressure was available for the power turbine thrust bearing support, and 620.5 kN/m^2 (90 psi) was available for the journal bearing and LP compressor thrust bearing support.

The available pressures for bearing support with the variable- and constant-speed power turbine engine configurations are shown in Table 7-5. Supply pressure (P_s) and bearing ambient pressures (P_a) are given for rated power, 100 percent speed, and the 7.5 percent power and 74.5 percent speed conditions.

The bearings at the HP turbine outlet and power turbine inlet locations are exposed to the inter-turbine pressure environment of 5.87 MPa (852 psi) and 1.32 MPa (192 psi) respectively at rated and 7.5% power for the constant speed

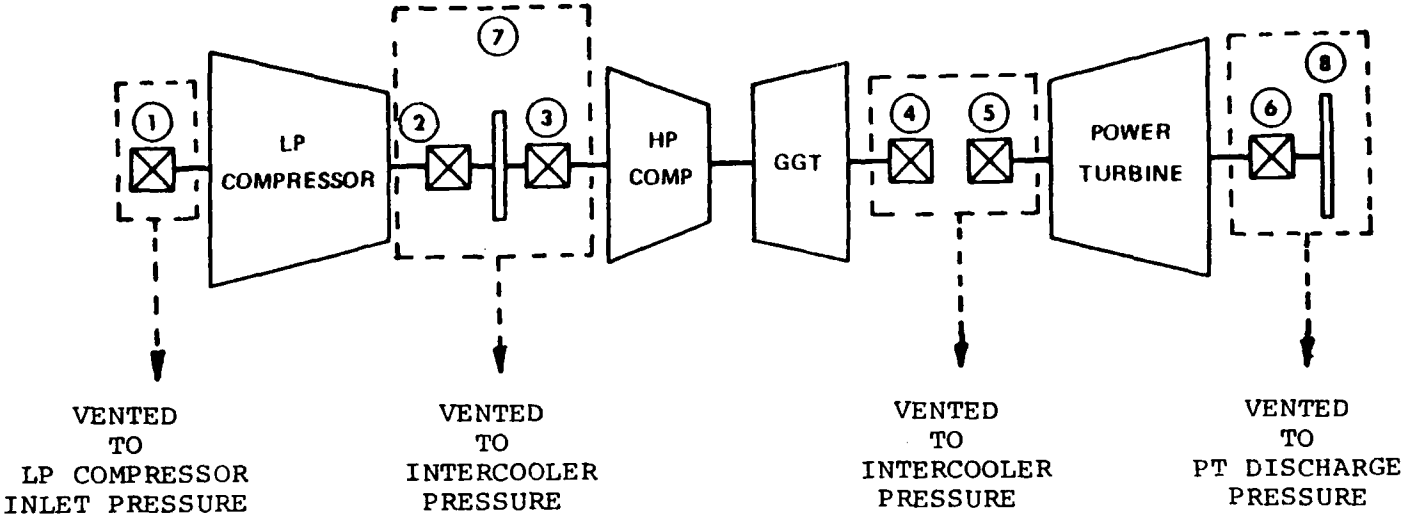

Figure 7-12. Vented Bearing Cavities

TABLE 7-5

AVAILABLE HELIUM GAS PRESSURES FOR BEARINGS

Variable Speed P.T. Condition								
Maximum Power - 100% Speed					7.5% Power - 74.5% Speed			
	Supply Pressure		Ambient Pressure		Supply Pressure		Ambient Pressure	
	MP_a	(PSI)	MP_a	(PSI)	MP_a	(PSI)	MP_a	(PSI)
LP_I	11.20	(1625)	3.13	(454)	2.57	(373)	1.17	(170)
LPC_P	↓	↓	6.09	(883)	↓	↓	1.89	(274)
HPC_I			↓	↓			↓	↓
HPT_D								
PT_I								
PT_D			3.30	(478)			1.19	(173)

Constant Speed P.T. Condition								
Maximum Power - 100% Speed					7.5% Power - 74.5% Speed			
	Supply Pressure		Ambient Pressure		Supply Pressure		Ambient Pressure	
	MP_a	(PSI)	MP_a	(PSI)	MP_a	(PSI)	MP_a	(PSI)
LPC_I	11.20	(1625)	3.13	(454)	2.57	(317)	0.045	(137)
LPC_D	↓	↓	6.09	(883)	↓	↓	1.57	(227)
HPC_I			↓	↓			↓	↓
HPT_D								
PT_I								
PT_D			3.30	(478)			.96	(140)

turbine case. These pressures are somewhat lower than the intercooler values of 6.09 MPa (833 psi) and 1.57 MPa (227 psi) quite properly assumed by AiResearch in their bearing design work. The AiResearch procedure is conservative since it bases the turbine bearing design on the assumption of a lower differential pressure available to support the bearing load than will actually be available using high pressure compressor outlet gas for bearing pressurization. The high pressure compressor outlet gas pressures is 11.2 MPa (1625 psi) at rated and 2.18 MPa (317 psi) at 7.5% power for the constant speed turbine case, which is the critical condition from the bearing design standpoint. The resulting differential pressures actually available to support the bearing load are therefore 5.33 MPa (773 psi) and 0.86 MPa (125 psi) at rated and 7.5% power respectively whereas the AiResearch bearing design assumptions produce differential pressures of (5.12 MPa) 742 psi and (0.62 MPa) 90 psi respectively. The degree of conservatism is smaller at rated power (≈4%) than at the 7.5% power condition (≈39%), implying a relatively larger margin of reserve capacity at the critical low power operating pressure conditions than indicated by the AiResearch analysis.

The conditions conservatively assumed by AiResearch can be considered to be the limiting values which could pertain if the gas bled from the intercooler for inter-turbine cooling were to be metered where it rejoins the flowpath at the inter-turbine diffuser, rather than at a flow restrictor in the line from the intercooler. The former condition is unlikely to be encountered in practice since the very modes cooling requirements and the need to limit cooling gas flow to preserve thermal efficiency will normally require a flow restrictor in the line from the intercooler causing the ambient pressure at the bearings to be depressed and approach the inter-turbine pressure level.

7.3.2.2 DESIGN PARAMETERS

The externally pressurized (hydrostatic) orifice compensated pad-type gas bearings for the second year CCCBS engine were designed on the basis of the following parameters and assumptions:

Lubricant	Helium Gas at 533 K Max (500°F)
Gas Constant	$R = 2.078$ J/°K mol (4,632 in/°R)
Viscosity	$\mu = (2.41)(10)^{-5} \frac{N \cdot sec}{m^2}$ ($3.5 \times 10^{-9} \frac{lb_f \, sec}{m^2}$)
Specific Heat Ratio	$C_p/C_v = 1.667$
Recess Area to Pad Area Ratio	1/9
Journal Pad Span Angle	84°
Thrust Pad Span Angle	40°
Number of Journal Pads	4
Number of Thrust Pads	8

The bearing loads determined by the critical speed analysis are summarized below:

Bearing Location	Load kN	(lb_f)
LP Spool Inlet	2.50	(562)
LP Spool Disch	2.10	(471)
HP Spool Inlet	2.25	(507)
HP Spool Disch	2.15	(484)
Small PT Inlet	1.92	(432)
Small PT Disch	3.17	(712)
Large PT Inlet	2.35	(528)
Large PT Disch	3.55	(799)
LP Compressor Thrust (Variable)*	15.6-44.5	(3,500-10,000 lbs)
Small PT Thrust (Variable)*	22.2-65.2	(3,000-14,650 lbs)
Large PT Thrust	29.35-97.9	(6,600-22,000 lbs)

*Loads are functions of power level and thrust balancing. Thrust reversals also occur on PT thrust bearings when engine is operated at reduced power levels.

7.3.2.3 BEARING GEOMETRY JOURNAL BEARINGS

The journal bearings for the CCCBS engine were designed on the basis of the pad geometry shown in Figure 7-13. Hydrostatic gas is supplied to the bearing recess area through 4 orifices. Each bearing consists of four pads arranged as shown schematically in Figure 7-14. The pads are rigidly attached to a diaphragm-type resilient mount that would be dimensionally controlled to give the required resilience for each bearing load and desired radial displacement. This design provides a flexible mount free of sliding joints that could fret and gall. In the final design of a bearing system, consideration would also be given to the affect of bearing resilience upon first and second rigid body criticals for the variable-speed power turbines. Mechanical stops would be included in the resilient mount design to limit the radial travel of the bearing to approximatley 0.127 mm (0.005 in.) to protect the aerodynamic and thrust piston seal under shock loads. The stops would be provided with sufficient clearance so as not to limit the desired resilience under normal bearing operation.

Based on the established 1-g loads, the dimensions for the journal bearings of the LP and HP spools were established. It was determined that one bearing design could be used for all four of the LP and HP spool journal bearings. The bearing dimensions were established as follows:

Diameter	15.88 cm Dia x 15.88 cm long (6.25 in. Dia x 6.25 long)
Pocket Area Ratio	1/9
Pocket Depth	0.508 mm (0.020 in.)
Orifice Size (4)	1.09 mm Dia (0.043 in. Dia)
Pad Arc Length	84°

The bearing loads, gas film stiffness, and frictional power loss for each bearing are given in Table 7-6.

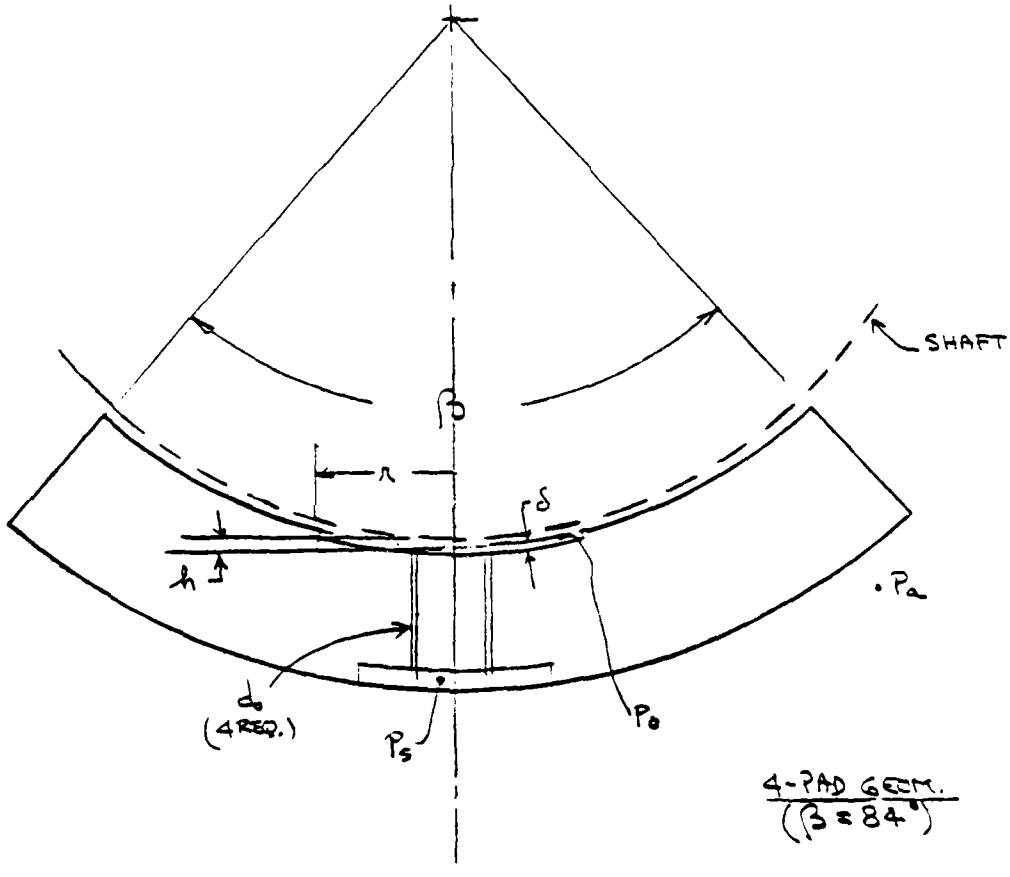

Figure 7-13. Hydrostatic Journal Bearing (Basic Pad Geometry)

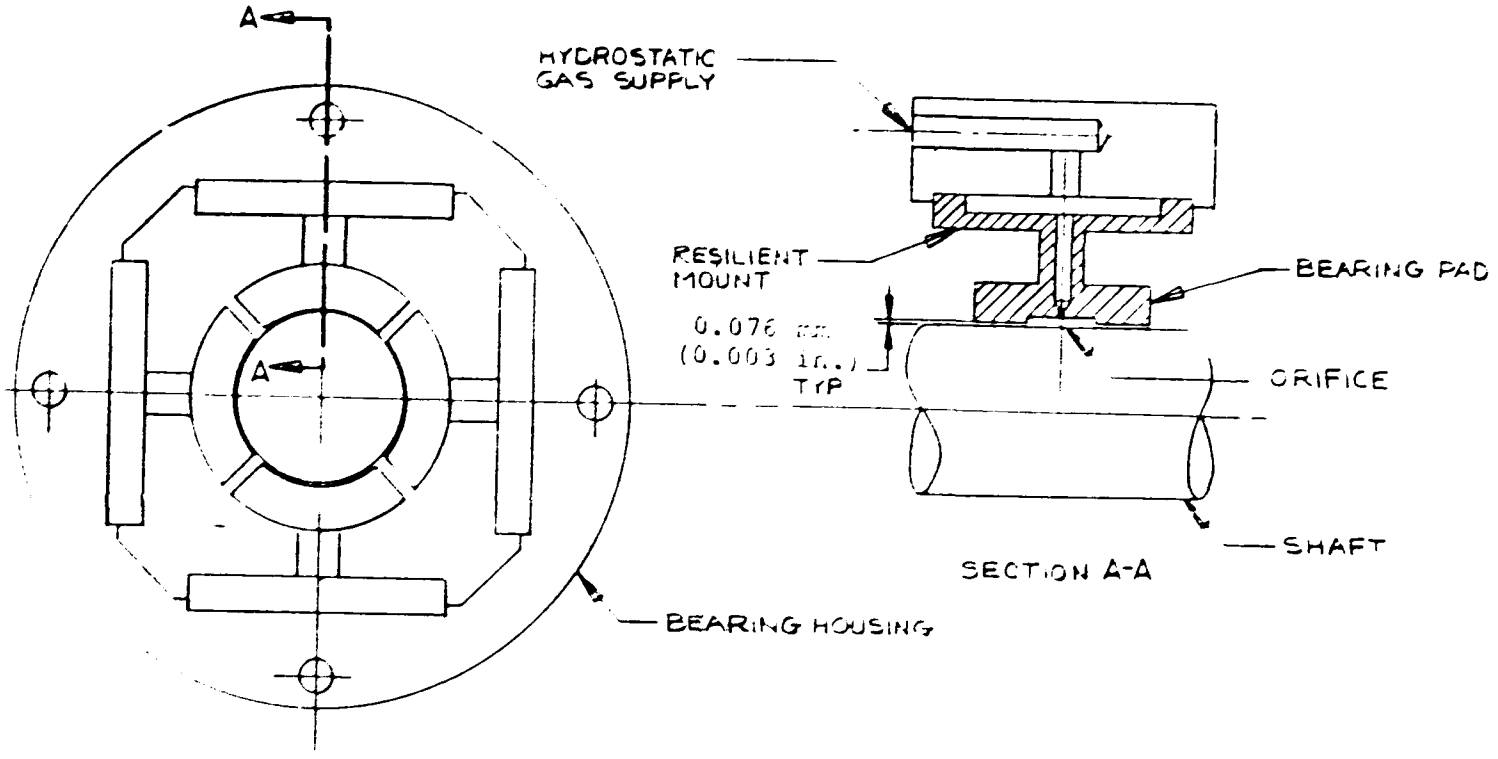

Figure [illegible]. Typical hydrostatic gas journal bearing

TABLE 7-6

BEARING PERFORMANCE

No.	Bearing Location	Load		Stiffness		Power Loss
		kN	(Lb_f)	kN/cm	(Lb_f/in.)	Watts (HP)
*1	LP Comp. Inlet	2.50	(562)	1085.8	(620,000)	589 (0.79)
2	LP Comp. Disch	0.95	(471)	844.1	(482,000)	507 (0.68)
3	HP Comp. Inlet	1.02	(507)	898.4	(513,000)	537 (0.72)
4	HP Turbine Disch	0.98	(484)	875.6	(500,000)	522 (0.70)

* Based upon orifice size(s) being reduced to compensate for larger available differential pressures on this bearing.

The various bearing gas film thicknesses and hydrostatic gas flows for the critical 7.5 percent power condition may be determined from Figure 7-15. It should be noted that the gas film thicknesses for bearings No. 2, 3, and 4 range between 0.069 mm and 0.076 mm (0.0027 and 0.003 in.) and are developed with 620.5 kN/m^2 (90 psi) differential pressure. The No. 1 bearing which is vented to the LP compressor inlet pressure operates at a differential pressure of 1241.0 kN/m^2 (180 psi) and, therefore, develops a larger load capacity and approximately 40 percent higher hydrostatic flow. The No. 1 bearing would be made to operate with the same film clearances, load capacity, and hydrostatic gas flow as the Nos. 2, 3, and 4 bearings by reducing the orifice size(s).

Operation of the CCCBS engine at full-rated power, with the correspondingly higher differential pressures available, would increase the load capacities of the bearings approximately 825 percent and the hydrostatic gas flows by approximately 290 percent for the same film thicknesses. This condition would provide additional margin for operation under severe shock loads, but it also suggests that a differential pressure regulator to maintain an adequate and relatively constant hydrostatic gas flow for all power conditions would increase overall engine efficiency by limiting the amount of hydrostatic gas bled from the cycle.

The dimensions for the journal bearings of the large and small 9,000-rpm power turbines were established as follows:

Diameter	17.78 cm Dia x 17.78 cm Long (7.00 in. Dia x 7.00 in. Long)
Pocket Area Ratio	1/9
Pocket Depth	0.508 mm (0.020 in.)
Orifice Size (4)	1.09 mm (0.043 in.)
Pad Arc Length	84°

The bearing loads, gas film stiffness, and frictional power loss for each bearing are given in Table 7-7 and are based on the assumption that the

NOTES:

1. Operating Conditions: Helium gas supplied at 260°C (500°F) and 2.186 MPa (317 PSIA), cavity pressure 0.945 MPa (137 PSIA) for bearing No. 1 and 1.565 MPa (227 PSIA) for bearings No. 2, 3, and 4.
2. Journal bearing diameter D = 15.88 cm (6.25 in.), length L = 15.88 cm (6.25 in.), four pad geometry, pad arc β = 84°.
3. Each pad has four orifices with each orifice diameter d_o' = 1.09 mm (0.043 in.)
4. Pocket area ratio 1/9, pocket depth δ = 0.051 cm (0.020 in.)
5. Diametral clearance = 0.025 cm (0.010 in.)

At Design Point:

Bearing No.	1	2	3	4
Load, kN, (lb_f)	2.50 (562)	2.10 (471)	2.26 (507)	2.15 (484)
Film thickness, mm, (in.)	0.086 (0.0034)	0.074 (0.0029)	0.069 (0.0027)	0.074 (0.0029)
Stiffness, MN/cm (lb_f/in.)	1.086 (620,000)	0.844 (482,000)	0.898 (513,000)	0.876 (500,000)
FHP loss, watts, (hp) at 18,000 rpm	589 (0.79)	507 (0.68)	537 (0.72)	522 (0.70)
Flow, g/sec, (lb_m/sec)	16.3 (0.036)	14.1 (0.031)	14.1 (0.031)	14.1 (0.031)

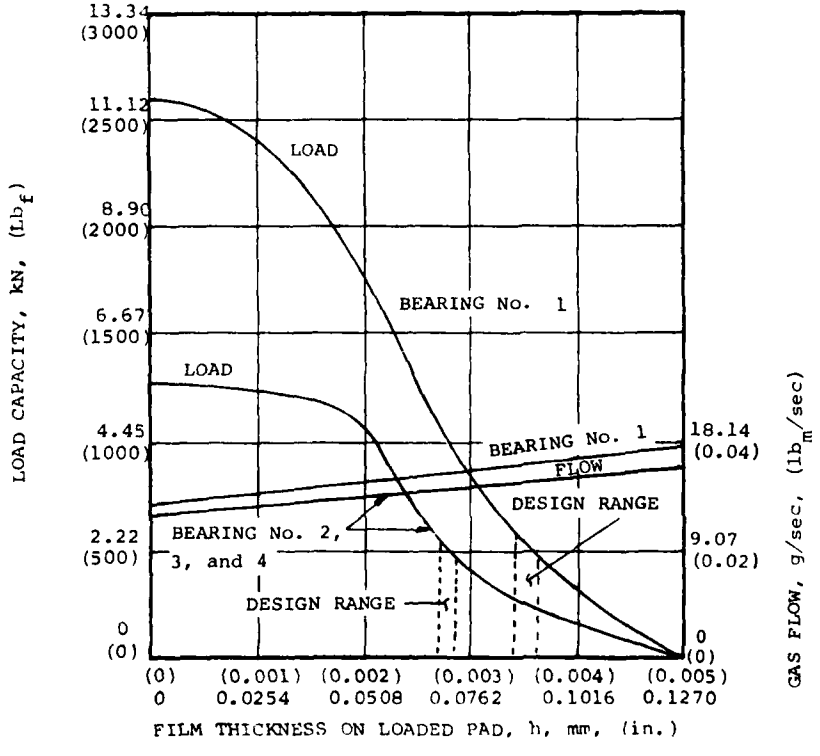

Figure 7-15. Load Capacity, Flow, Stiffness and Friction, Externally Pressurized Compressor Journal Bearing

TABLE 7-7

BEARING PERFORMANCE

No.	Bearing Location	Load		Stiffness		Power Loss	
		kN	(Lb_f)	kN/cm	(Lb_f/in.)	Watts	(HP)
5	P.T. Inlet (Small)	1.92	(432)	583.2	(333,000)	410	0.55
6	P.T. Disch (Small)	3.17	(712)	1500.8	(857,000)	432	0.58
5	P.T. Inlet (Large)	2.35	(528)	980.7	(560,000)	418	0.56
6	P.T. Disch (Large)	3.55	(799)	1514.8	(865,000)	440	0.59

orifice(s) in No. 6 bearing would be reduced in size to compensate for a larger available differential pressure.

The various bearing gas film thickness and hydrostatic gas flows for the critical 7.5 percent power condition may be determined from Figure 7-16.

The power turbine bearings operate with a gas film thickness between 0.065 mm and 0.084 mm (0.00255 and 0.0033 in.) which is slightly less than the minimum for the LP and HP spool bearings. The 0.065 mm (0.00255 in.) film thickness should be adequate for the large power turbine discharge bearing with the 3.553 kN (799 lb) load; however, if more margin is required, the bearing orifice size(s) could be increased from 1.09 mm dia. (0.043 in. dia.) to 1.196 mm dia. (0.047 in. dia.) and, thereby increase the film thickness to 0.0762 mm (0.003 in.) at the expense of a 20 percent increase in hydrostatic gas flow.

NOTES:

1. Operating conditions: Helium gas supplied at 260°C (500°F) and 2.186 MPa (317 PSIA), cavity pressure 1.565 MPa (227 PSIA).
2. Journal bearing diameter D = 17.78 cm (7.00 in.); length L = 17.78 cm (7.00 in.), four pad geometry, pad arc β = 84°.
3. Each pad has four orifices with each orifice diameter d_o' = 1.09 mm (0.043 in.)
4. Pocket area ratio 1/9, pocket depth δ = 0.508 mm (0.020 in.)
5. Diametral clearance = 0.305 mm (0.012 in.)

At Design Point:

Bearing No.	5	6
Load, kN, (lb_f)	1.92 (432)	3.17 (712
Film thickness, mm, (in.)	0.0813 (0.0032)	0.0686 (0.0027)
Stiffness, MN/cm, (lb_f/in.)	0.58 (333,000)	1.50 (857,000)
FHP loss, watts, (hp) at 9000 rpm	410.0 (0.55)	433.0 (0.58)
Flow, g/sec, (lb_m/sec)	14.1 (0.031)	13.6 (0.030)

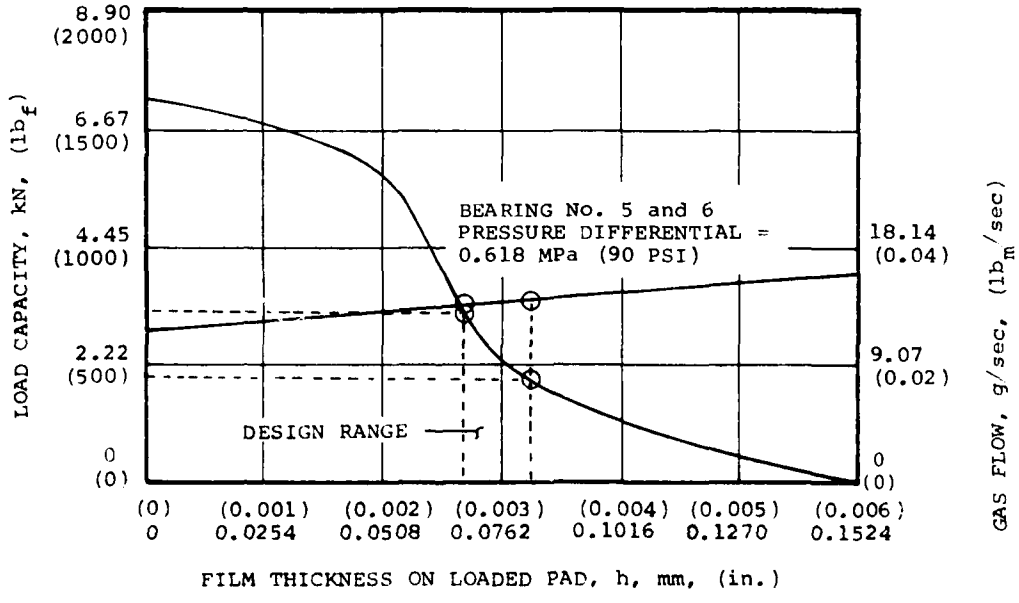

Figure 7-16. Load Capacity, Flow, Stiffness and Friction, Externally Pressurized Power Turbine Journal Bearing

7.3.2.4 BEARING GEOMETRY THRUST BEARINGS

The thrust bearings for the CCCBS engine were designed on the basis of the pad geometry shown in Figure 7-17. The geometry is very similar to that of the journal bearings except that the pads are flat instead of curved. Each unidirectional thrust bearing consists of eight pads that are attached to a resilient gimballed mount as shown in Figure 7-18. Two thrust bearings arranged on either side of a thrust rotor constitute the complete bidirectional thrust bearing assembly. The stiffness and mount of gimballing of the mount are controlled by varying the thickness of the mount flanges and flexture posts. This design provides an integral mount without sliding or frictional components that might fret or gall under prolonged unlubricated operation.

The loads applied to the two thrust bearings of the CCCBS engine vary as a function of the power level of the engine, the thrust balancing piston areas and differential pressures available, and whether the power turbine is a constant-speed or variable-speed design. Due to the unlimited combinations of thrust loads possible, it was decided to design the bearings on the conservative basis of the thrust loads established during the first year of study. The various maximum thrust loads calculated during the second year of the study were all less than originally established. It was, therefore, concluded that by using the original rated power thrust loads with suitable control of balance piston areas and pressures, adequate load capacity margin could be provided for the critical 7.5 percent power operation. In addition, any load capacity reserve could be used to offset the effects of shock loads.

The bearings were designed for the loads shown in Table 7-8.

TABLE 7-8

THRUST LOADS

Thrust Bearing Location	Maximum Load
LP Compressor Spool	44.5 kN (+10,000 lb_f)
PT Spool	97.9 kN (+22,000 lb_f)

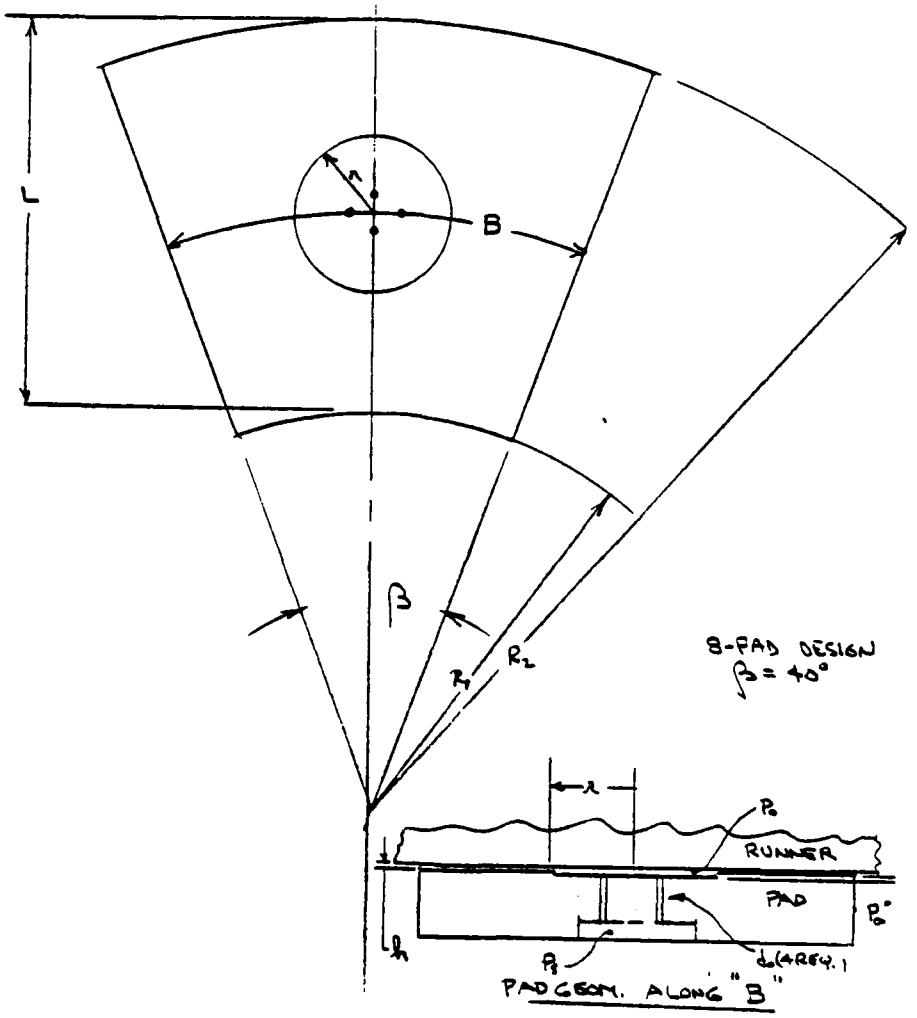

Figure 7-17. Hydrostatic Thrust Bearing Basic Pad Geometry

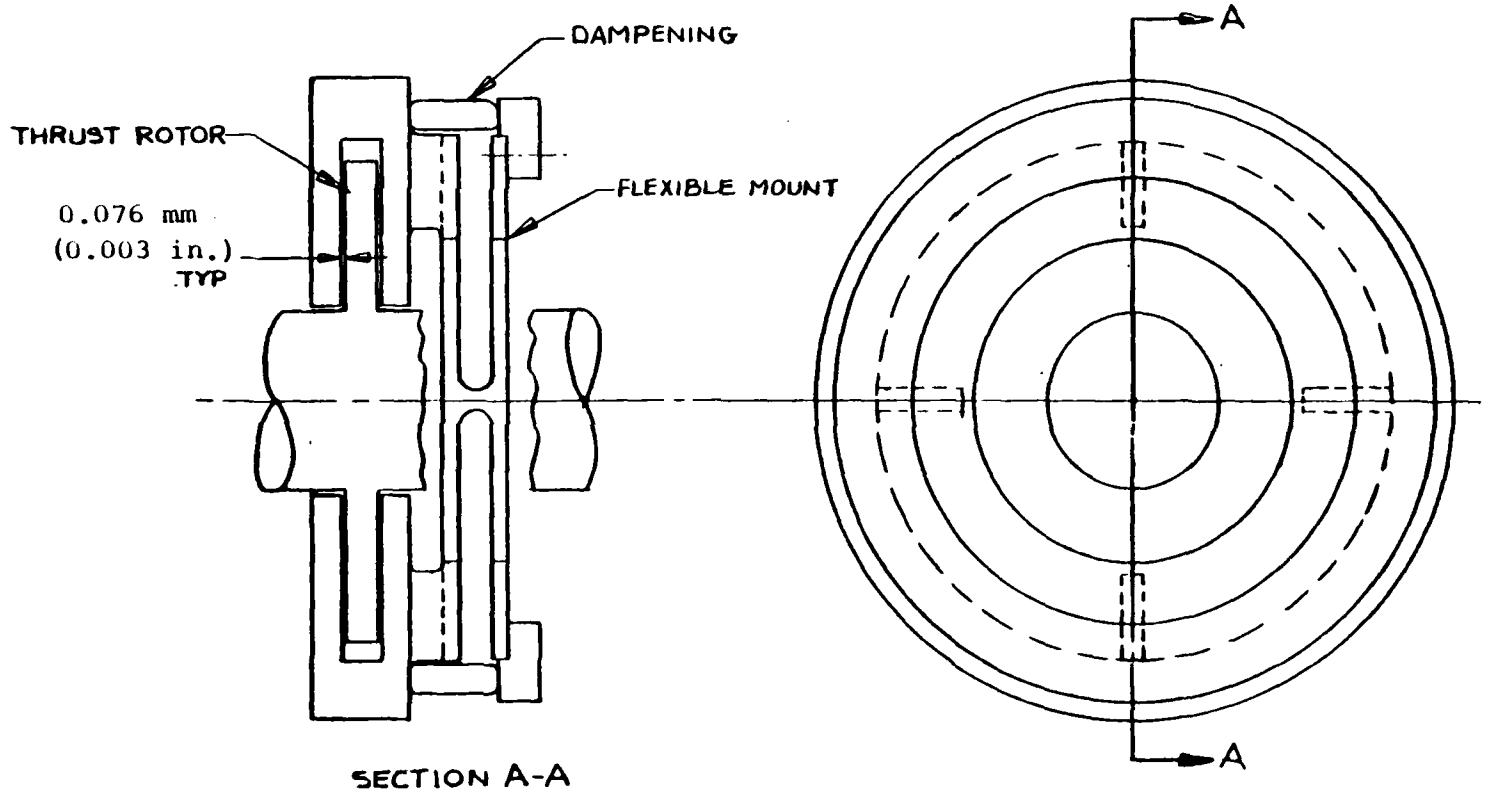

Figure 7-18. Typical Hydrostatic Gas Thrust Bearing

The bearings were designed to carry the maximum thrust in either direction in order to provide for thrust reversals during transient operation and low power operation. It is anticipated that the bearings can be decreased in size in at least one if not both directions when a detailed transient analysis becomes available.

7.3.2.4.1 THRUST BEARING DIMENSIONS

The dimensions established for the LP compressor and power turbine bearings are given in Table 7-9.

The bearing loads, gas film stiffness, and frictional power less at full load and speed for each thrust bearing are given in Table 7-10.

The gas film thicknesses and hydrostatic gas flows for the LP compressor and power turbine thrust bearings with two different orifice sizes are shown in Figures 7-19 and 7-20. For example, in Figure 7-19 the LP compressor thrust bearing would be operating with a film thickness of 0.0406 mm (0.0016 in.) under the full load of 44.48 kN (10,000 lbs) with the small orifice bearing design. Correspondingly, the power turbine thrust bearing, as shown on Figure 7-20, would be operating at a film thickness of 0.0355 mm (0.0014 in.) under a load of 97.86 kN (22,000 lbs). These film thicknesses may be too small to accommodate the surface distortions of such large bearings; therefore, increased load capacity with larger film thicknesses is highly desired. The dashed curves on Figures 7-19 and 7-20 show larger film thicknesses for the two thrust bearings as provided by larger orifices. Alternatively, smaller thrust loads would permit correspondingly larger gas films and add to the margin which must be allowed for meachnical and thermal distortions of the bearing surfaces.

The bearing performances, shown in Table 7-10 and Figures 7-19 and 7-20, are based on the use of a nominal low-pressure compressor discharge as supply pressure 5.888 MN/m^2 (854 psia) for the hydrostatic bearings. This was done to provide a recommended regulated pressure for the maximum power condition rather than operate the bearings at full available hydrostatic pressure of 11.20 MN/m^2 (1625 psi) and lose engine performance by excessive hydrostatic

TABLE 7-9

THRUST BEARING DIMENSIONS

	Low Pressure Compressor		Power Turbine	
Outside Diameter	30.48 cm	(12.0 in.)	41.91 cm	(16.50 in.)
Inside Diameter	15.24 cm	(6.0 in.)	15.24 cm	(6.0 in.)
Number of Pads/Arc Length	8/40°	--	8/40°	--
Pocket Area Ratio	1/9	--	1/9	--
*"A" Pocket Depth,	0.508 mm	(0.020 in.)	0.508 mm	(0.020 in.)
*"B" Pocket Depth,	1.016 mm	(0.040 in.)	1.016 mm	(0.040 in.)
Pocket Radius, r	14.73 mm	(0.508 in.)	21.84 mm	(0.86 in.)
*"A" Orifice Diameter, d_o (4/pad required)	1.067 mm	(0.042 in.)	1.067 mm	(0.042 in.)
*"B" Orifice Diameter, d_o (4/pad required)	2.156 mm	(0.0849 in.)	2.156 mm	(0.0849 in.)

*A and B pockets and orifices reflect versions of the bearings with different film thicknesses under the same load.

TABLE 7-10

BEARING PERFORMANCE

No.	Bearing Location	Loads		Stiffness		Power Loss	
		kg	(lbs_f)	MN/cm	(lb_f/in)	watts	(hp)
7	LP Compressor	44.4	(10,000)				
		Small Orifice		15.94	(9.1×10^6)	1276	(1.71)
		Large Orifice		7.88	(4.5×10^6)	828	(1.11)
8	Power Turbine	97.9	(22,000)				
		Small Orifice		21.0	(1.2×10^7)	1037	(1.39)
		Large Orifice		33.3	(1.9×10^7)	768	(1.03)

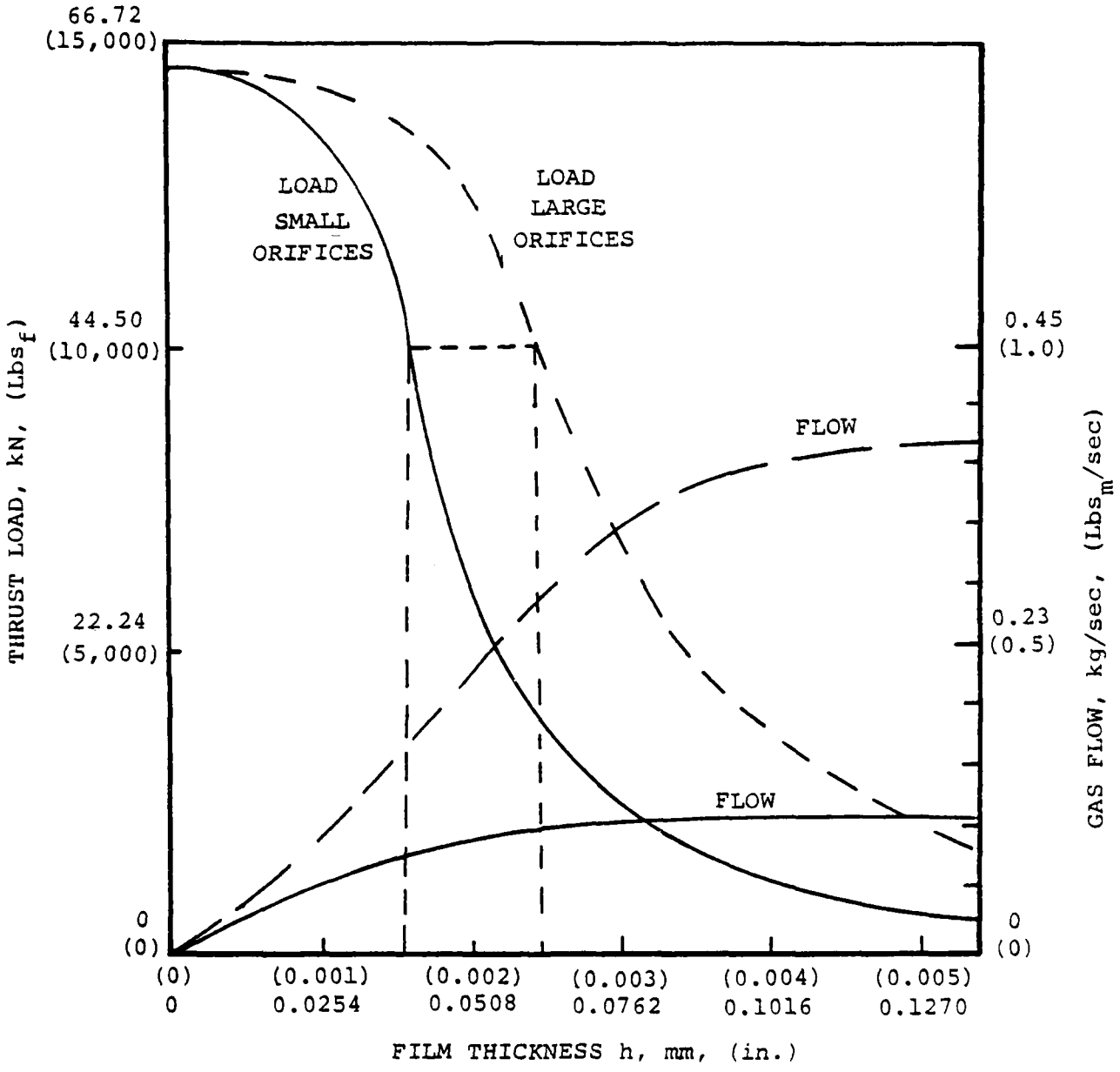

Figure 7-19. Load Capacity, Flow, Stiffness, and Friction 30.48 cm (12.0 in.) Diameter Hydrostatic Thrust Bearing (Full Power Condition)

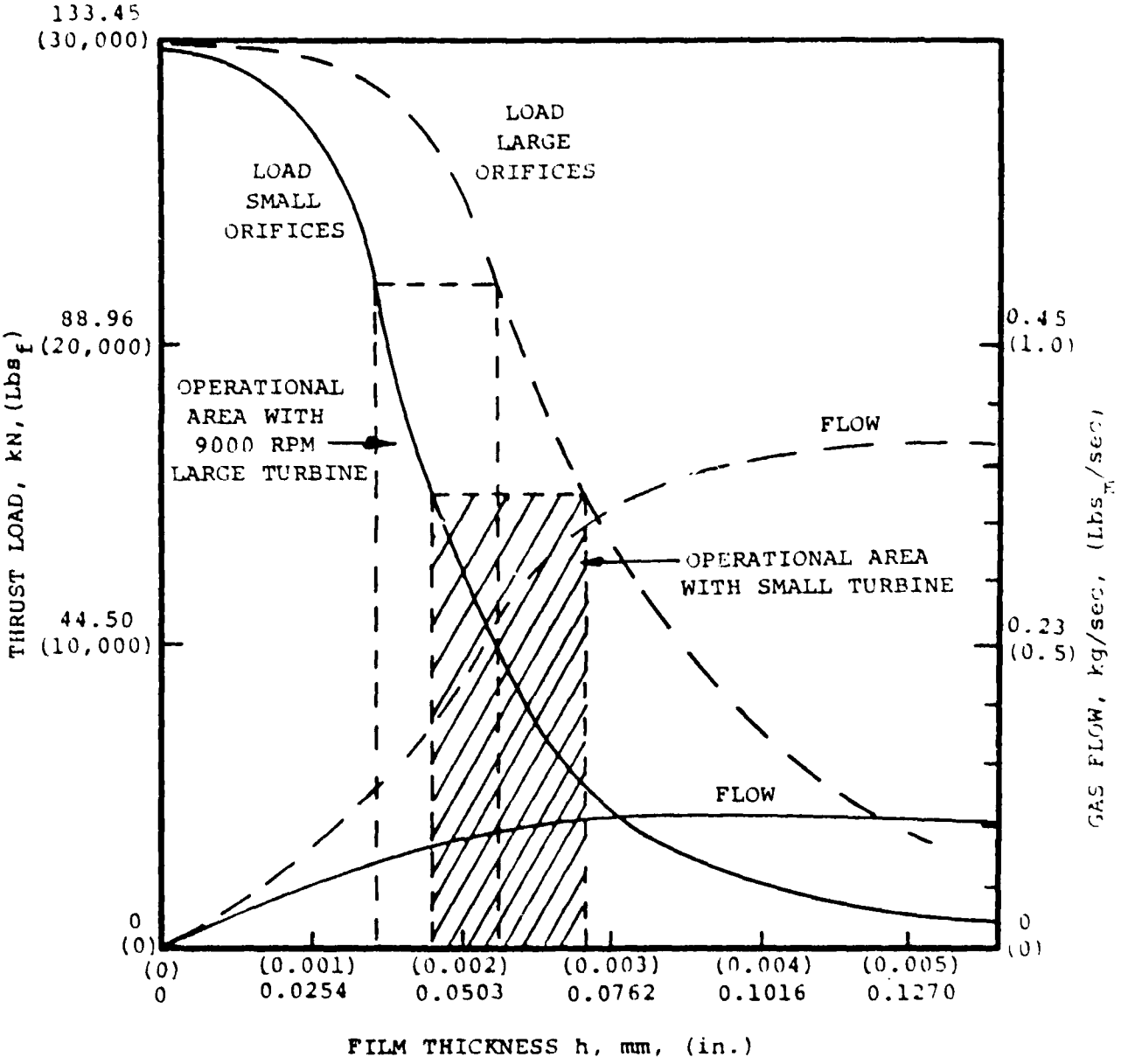

Figure 7-20. Load Capacity, Flow, Stiffness, and Friction 41.66 cm (16.4 in.) Diameter Hydrostatic Thrust Bearing (Full Power Condition)

flow. For the critical off-design 7.5 percent power condition, the load capacities of the thrust bearings would be a function of the differential pressures available. These relationships are shown in Figure 7-21. For example, if the HP compressor pressure of 11.2 MN/m^2 (1625 psia) were used as the hydrostatic supply, then a differential pressure of up to 5.1 MN/m^2 (742 psi) would be available for bearing support. In the case of the LP compressor thrust bearing, the load capacity would be increased from 44.5 kN (10,000 lbs) to 130.2 kN (29,275 lbs) with a significant increase in film thickness. Since the increase in load capacity is not necessary, the bearings could be reduced in size and still maintain an adequate film thickness of approximately 0.076 mm (0.003 in.). Operation at the reduced power level of 7.5 percent with an available differential pressure of 0.62 MN/m^2 (90 psi) results in a load capacity of approximately 9,341 N (2,100 lb_f) with design film thickness. Ultimately, the thrust bearings will be sized by the differential pressures available and an optimized thrust balance design.

7.3.2.5 3600-RPM POWER TURBINE GAS BEARINGS

Near the conclusion of the second year of study, the 3600-rpm power turbine configuration was added to the investigation. Analysis of this power turbine extended into the third year and as a consequence, the 3600-rpm power turbine bearing sizing and performance is reported under these separate paragraphs. The analysis was conducted in the same manner as previously described for the other power turbines, using the same basic four pad journal and eight pad thrust bearing designs modified for the static loads established during the dynamic analysis. The design bearing loads were:

DESIGN BEARING LOADS

Power Turbine Bearing	Load N	Load lb_f
Inlet End - Journal	3,247	730
Discharge End - Journal	14,612	3,285
Thrust Full Power	57,800	13,000
Thrust Low Power	9,977	2,243

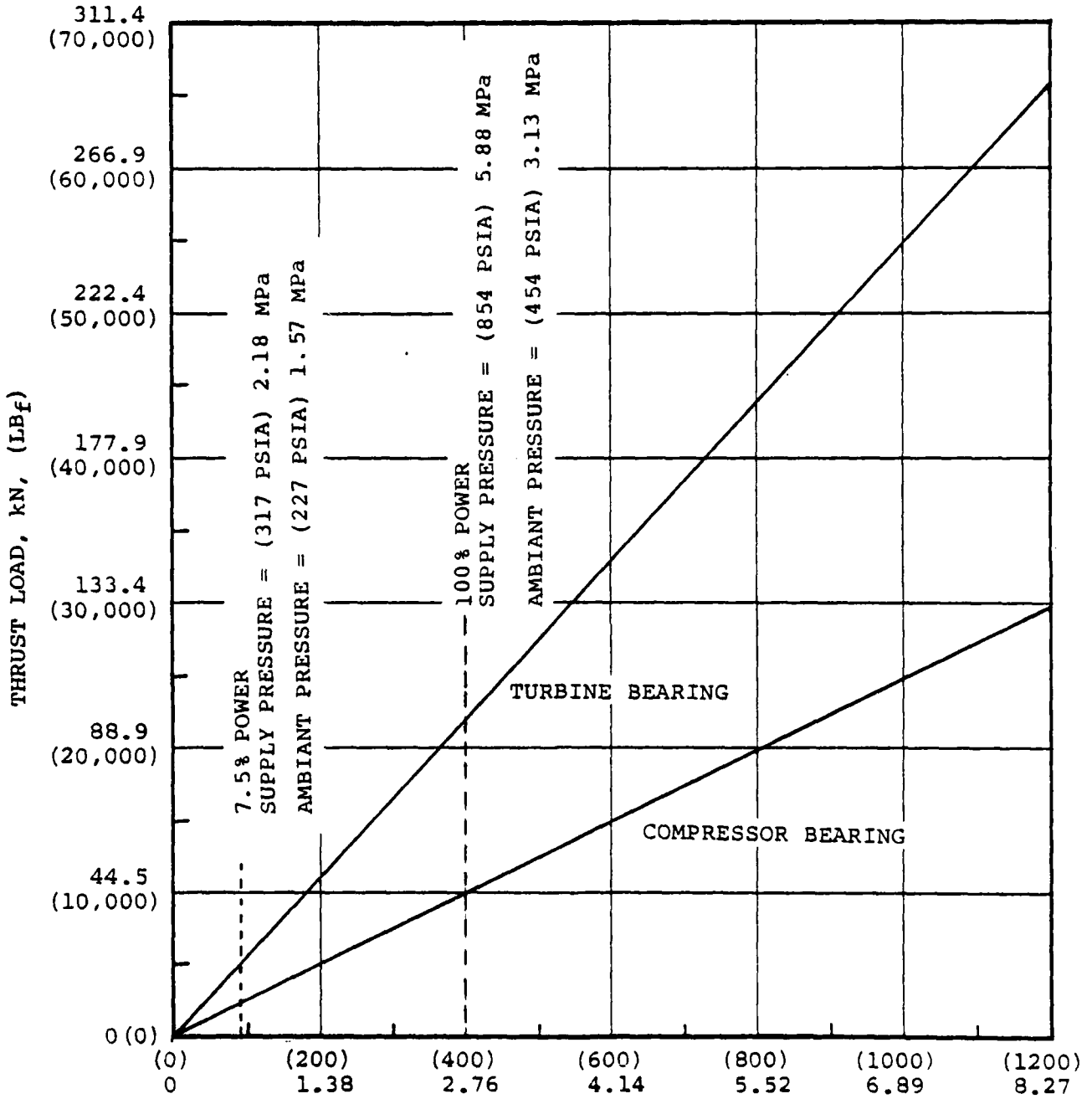

Figure 7-21. Effect of Power Level on Thrust Load Capacity Helium Lubricated Externally Pressurized Thrust Bearings

As with the other power turbines, the journal bearings were designed to support the rotor at the low power condition where the minimum differential pressure was available to the hydrostatic gas bearing system. The pressure was available to the hydrostatic gas bearing system. The pressures used in this analysis were:

Power Turbine Journal Location	P_{supply}, KPa	$P_{ambient}$, KPa	P_{supply}, psia	$P_{ambient}$, psia
Inlet End	2,186	1,565	317	227
Discharge End	2,186	958	317	139

The thrust bearing was sized for maximum thrust of 57,800 N (13,000 lbs) at full rated power decreasing and reversing direction to, -9977 N (-2243 lbs) at lower power. The pressure used in the analysis of the thrust bearing were:

Power Condition	P_{supply}, KPa	$P_{ambient}$, KPa	P_{supply}, psia	$P_{ambient}$, psia
Full	6,012	3,254	872	472
Low (thrust reversal)	2,186	958	317	139

7.3.2.5.1 JOURNAL BEARINGS

The 3600-rpm power turbine inlet end journal bearing was designed to support a static load of 3247 N (730 lb_f) and dynamic load of 1712 N (385 lb_f). The bearing selected was a 17.78 cm dia. (7.00 in.) x 17.78 cm long (7.00 in.) 4-pad configuration. Bearing load capacity as a function of gas film thickness as well as hydrostatic gas flow as a function of gas film thickness is shown in Figure 7-22. The design static bearing load of 3247 N (730 lb_f) results in a static gas film thickness of 0.0686 mm (0.0027 in.). Dynamic operation at the critical low power condition could add as much as an additional 1712 N (385 lb_f) if the power turbine is operated at full design speed of 3600 rpm. Lower power turbine speeds would greatly reduce the dynamic loading. In the worst case, the bearing would be required to support a 3247 N (730 lb_f) static load and a 1712 N (385 lb_f) dynamic load for a total load of 4959 N (1115 lb_f). The bearing would operate with a minimum gas film of 0.0596 mm (0.00235 in.).

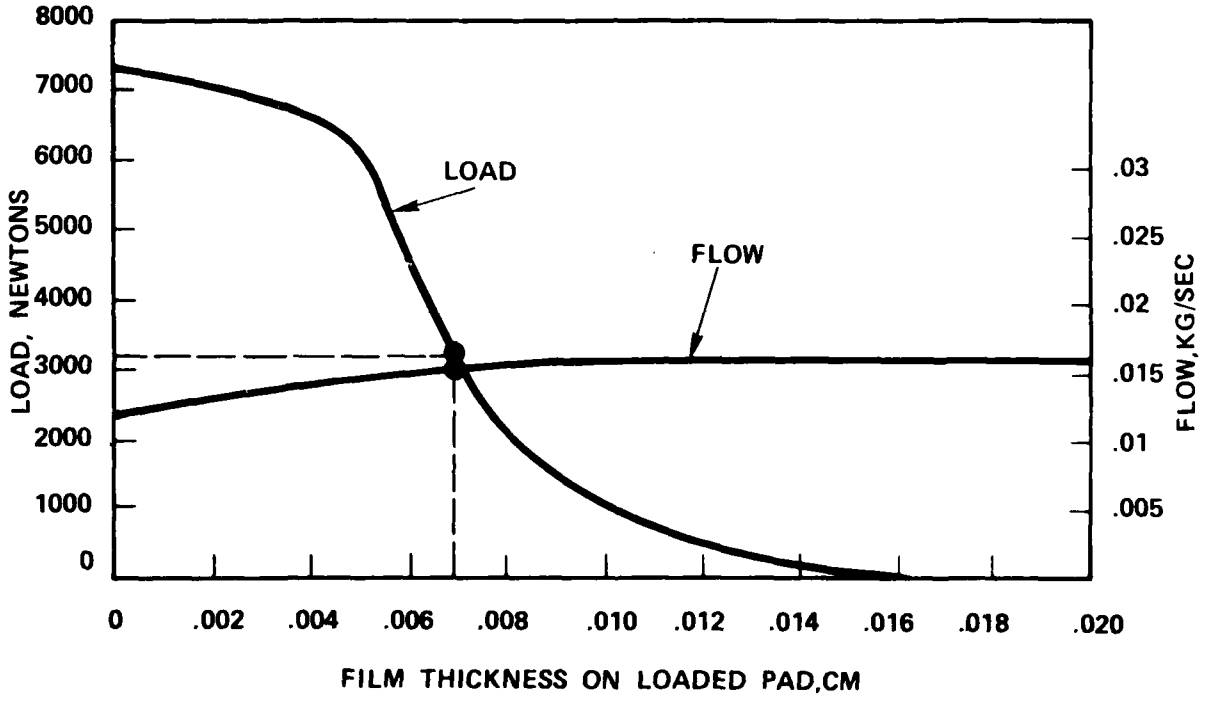

Figure 7-22. 70,000 HP Closed Cycle Brayton System Inlet End Journal Bearing Power Turbine

The rear journal bearing at the discharge end of the power turbine is overhung by the bulk of the turbine blading and output shaft and must support a static load of 14,612 N (3285 lb_f). As explained in the section on critical speed analysis, the shaft section in region of the rear journal bearing was increased to 254.0 cm dia. (10.0 in.) in order to raise the first bending critical speed at least 40 percent above the turbine operating speed. Initial sizing of this bearing was based upon using the 254.0 cm dia. (10.0 in.) and varying the bearing length. The first bearing length was selected at 203.2 (8.00 in.) to permit ready incorporation into the existing turbine design without any axial relocation of other components. The predicted bearing performance is shown in Figure 7-23. As can be seen, the static bearing load of 14,612 N (3285 lb_f) would result in a gas film thickness of 0.0609 mm (0.0024 in.). This gas film is considered to be a minimum safe value. Consequently, the bearing orifice sizes and number supplying the hydrostatic gas to the bearing were increased from six 1.041 mm dia. (0.041 in.) to thirteen 1.067 mm dia. (0.042 in.). The resulting bearing performance is shown in Figure 7-24. In this case, the static load is supported by a 1.219 mm (0.0048 in.) thick film, but hydrostatic gas flow to provide the increased film thickness increased 234 percent to .051 Kg/sec (0.113 lb_m/sec).

The ultimate load capacity of the 25.4 cm dia. (10.0 in.) x 20.32 cm (8.00 in.) long bearing is approximately 20,460 N (4600 lb_f) and is considered to be marginal for this application. In order to provide increased bearing load capacity without making major changes to the 3600-rpm power turbine design, the bearing length was increased from 20.32 cm (8.00 in.0 to 25.4 cm (10.0 in.) as shown in Figure 7-25. Only minor changes to the labyrinth seal adjacent to the 25.4 cm dia. (10.0 in.) journal bearing are required to accommodate the increased length. The bearing performance of the increased area bearing is shown in Figure 7-26. Hydrostatic gas flow has been reduced and bearing load capacity has been increased to provide approximately 75 percent margin.

7.3.2.5.2 THRUST BEARING - 3600-RPM POWER TURBINE

The thrust bearing for the 3600-rpm power turbine is designed as a bidirectional bearing with one side larger in area than the other to carry the full load thrust of 57,800 N (13,000 lb_f). The other side of the thrust bearing is adjacent to

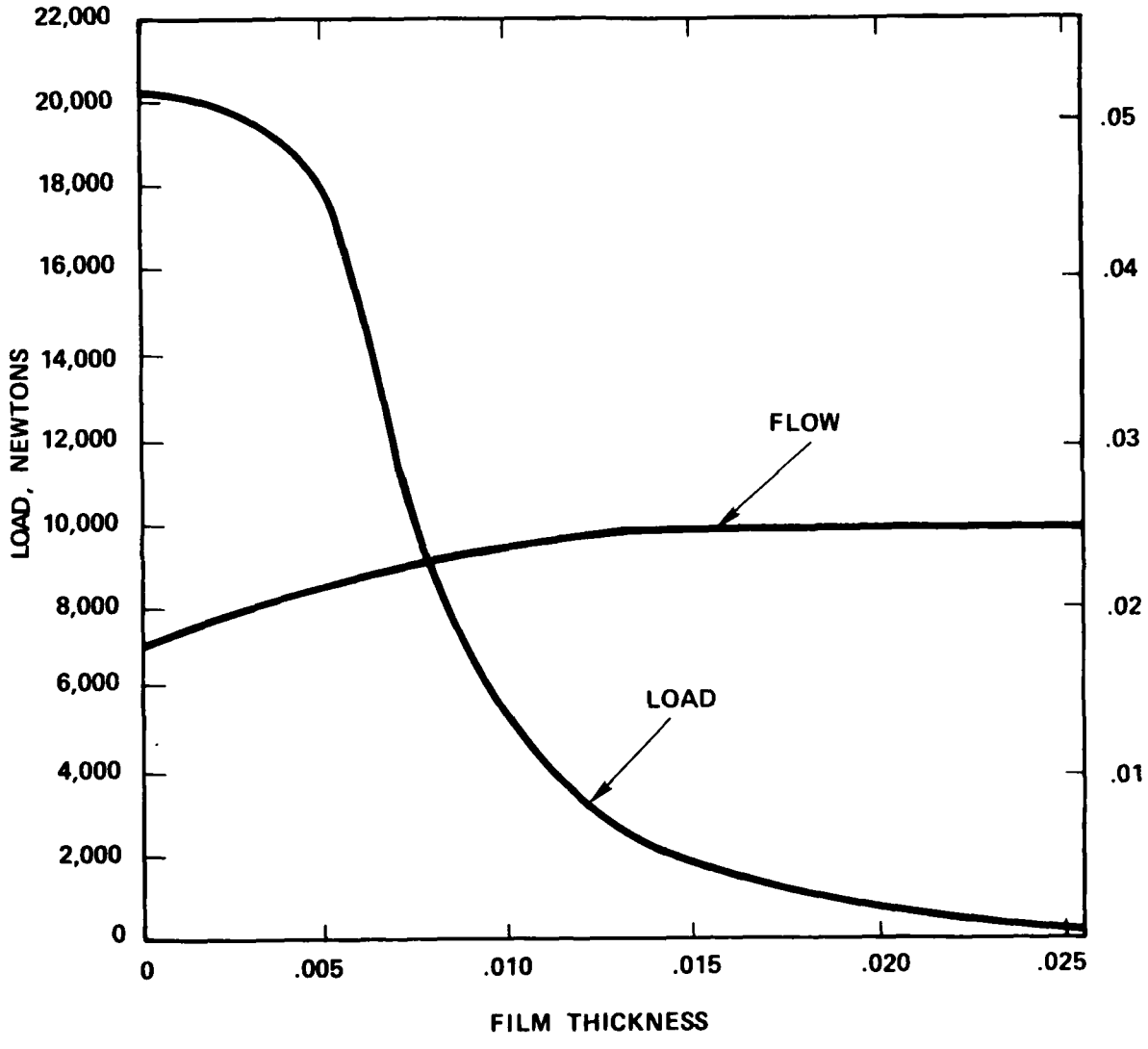

Figure 7-23. 70,000 HP Closed Cycle Brayton System Journal Bearing, Discharge End, Low Flow, d_o = 10 in. nominal

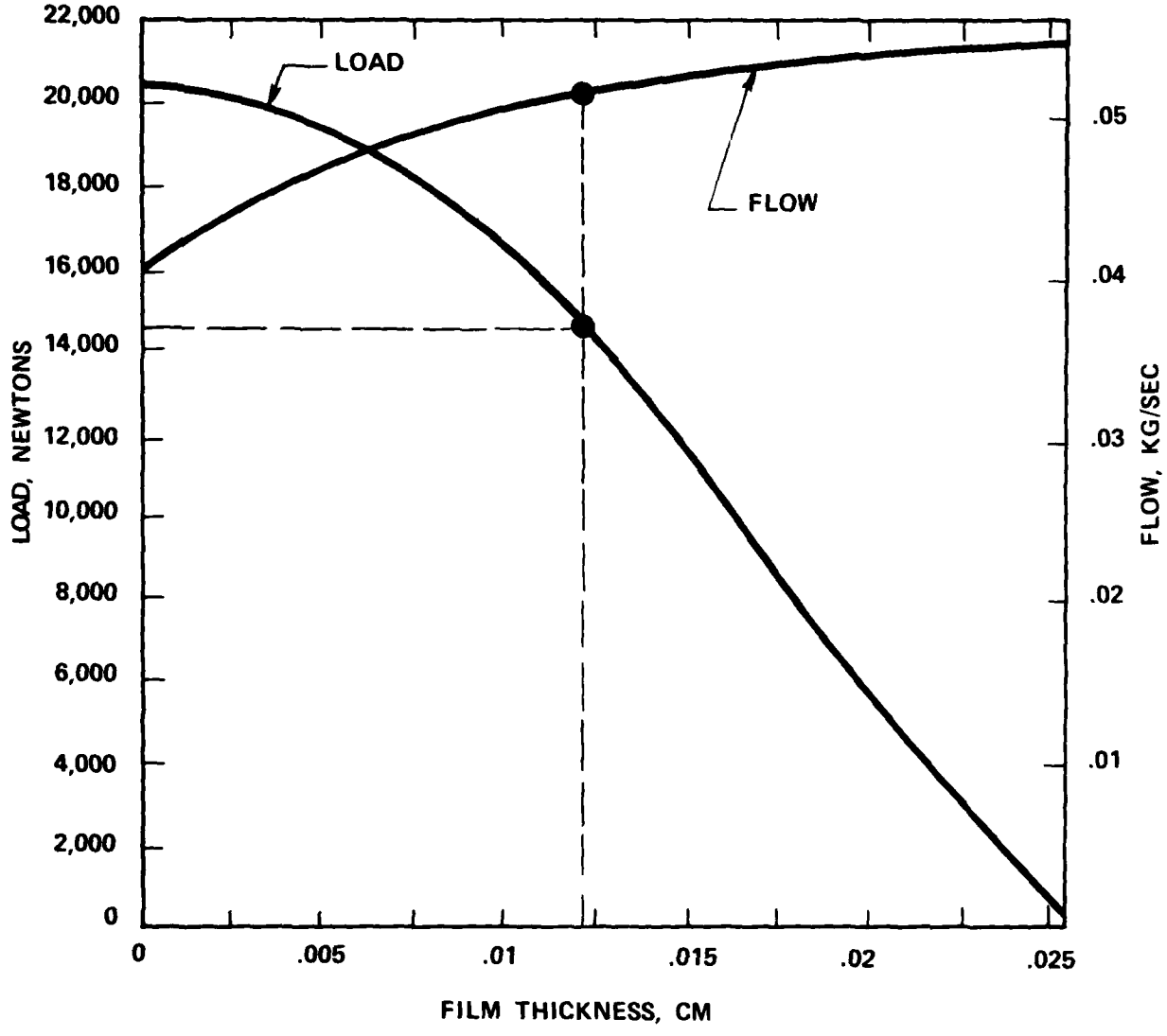

Figure 7-24. 70,000 HP Closed Cycle Brayton System Journal Bearing, Discharge End High Flow, d_o = 16 in. nominal

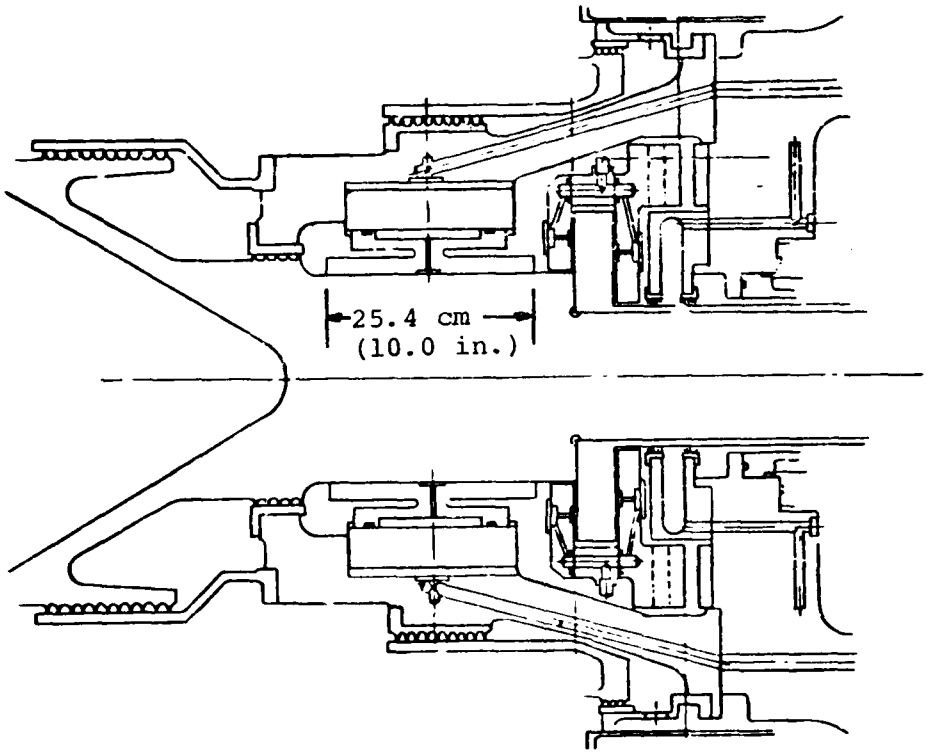

Figure 7-25. 3600 RPM Power Turbine Rear Journal and Thrust Bearing

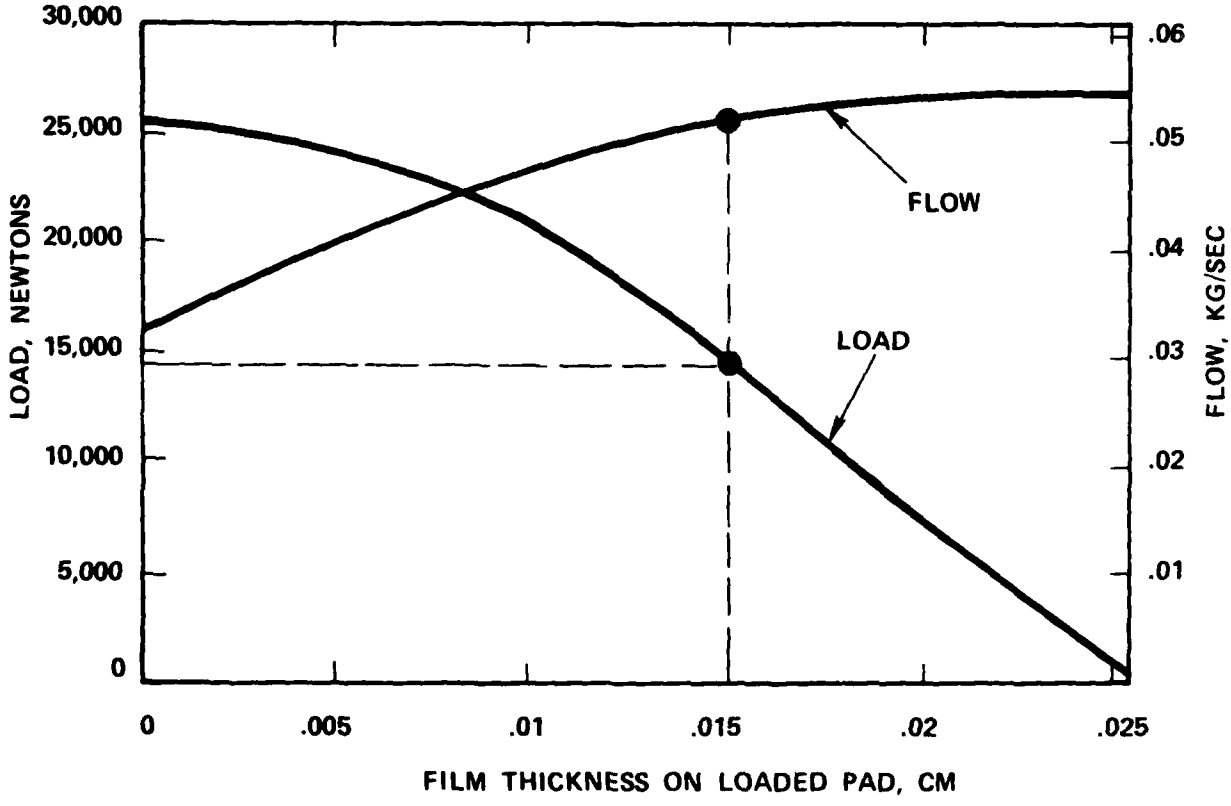

Figure 7-26. 7000 HP Closed Cycle Brayton System Journal Bearing Discharge End High Flow, d_o = 0.15 inch nominal

the 25.4 cm dia (10.0 in.) journal and is designed to carry the reverse thrust of 9977 N (2243 lb_f) associated with low power conditions. The thrust bearing arrangement is shown in the previously mentioned Figure 7-25. The thrust rotor is 38.10 cm (15.0 in.) in diameter with an internal diameter of 20.32 cm (8.00 in.) on the maximum thrust side of the bearing. The minimum thrust side of the rotor has a 27.94 cm (11.00 in.) internal diameter. The performance of the maximum thrust side of the bearing is shown in Figure 7-27. Rated design thrust is supported on a 0.0737 mm (0.0029 in.) thick gas film and hydrostatic gas flow is .393 Kg/sec (0.865 lb_m/sec). The performance of the smaller reverse thrust bearing is shown in Figure 7-28. The reverse thrust occurs during reduced power operation and only 1227 KPa (178 psi) differential pressure is available to the bearing. It is noted that in the detail design of a bidirectional thrust bearing that the thrust generated by one side of the bearing must be balanced by the other. The clearance between the various sides of the thrust bearing stators and rotor, therefore, becomes important not only from the standpoint of axial alignment and positioning of the turbine blading, but also determines the net thrust on each side of the bearing.

7.3.3 GAS BEARING LAYOUTS

Typical layouts of the journal and thrust bearings with envelope dimensions are shown in Figures 7-29 through 7-32. These layouts show the bearings may be installed within the CCCBS engine bearing cavities. The designs are such that the bearings may be installed by halves with horizontal split lines or as complete integral assemblies. Flexible hoses for the hydrostatic gas supply must be connected to the thrust bearings so that the resilience of the bearings is not affected.

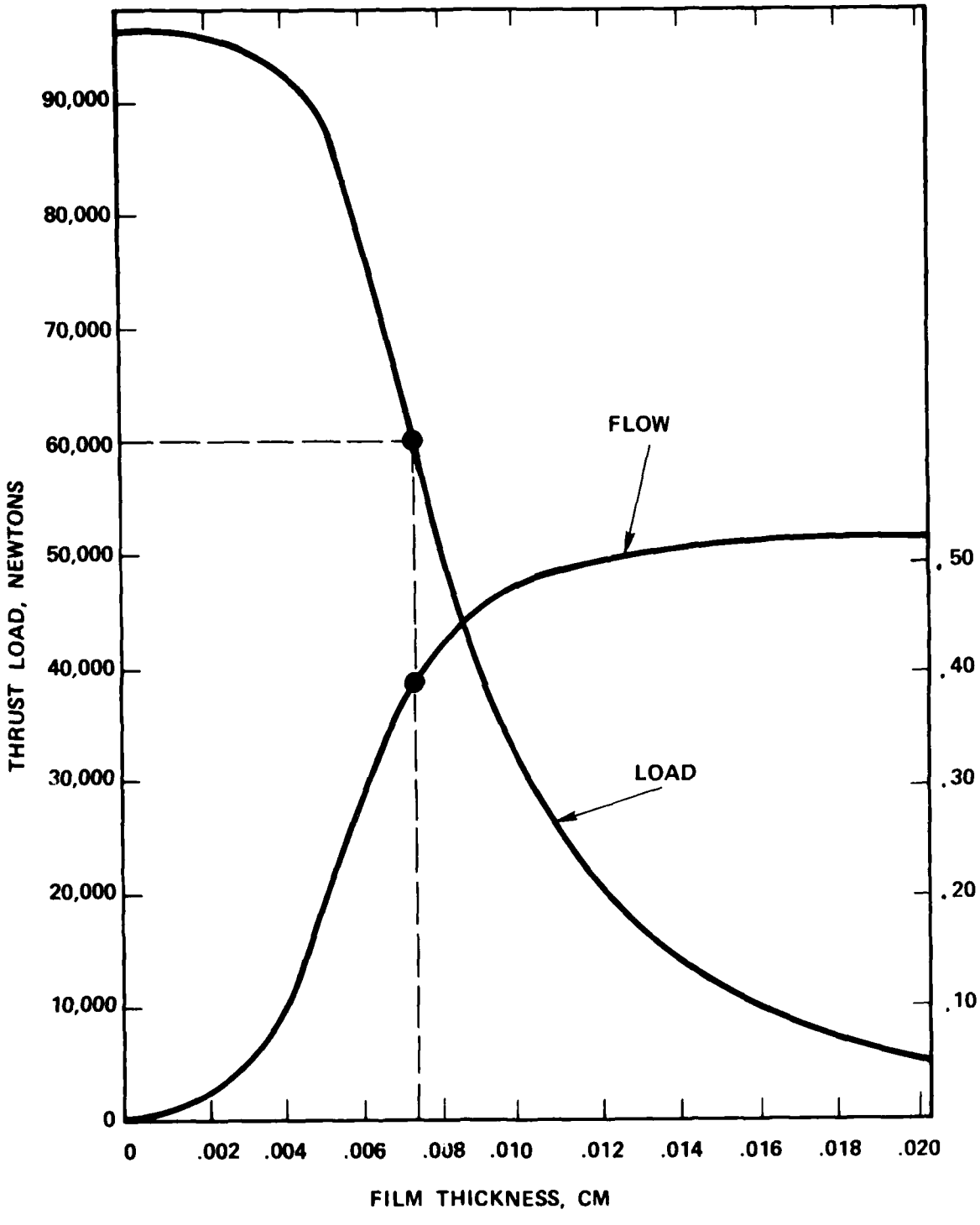

Figure 7-27. 70,000 HP Closed Cycle Brayton System Power Turbine Thrust Bearing

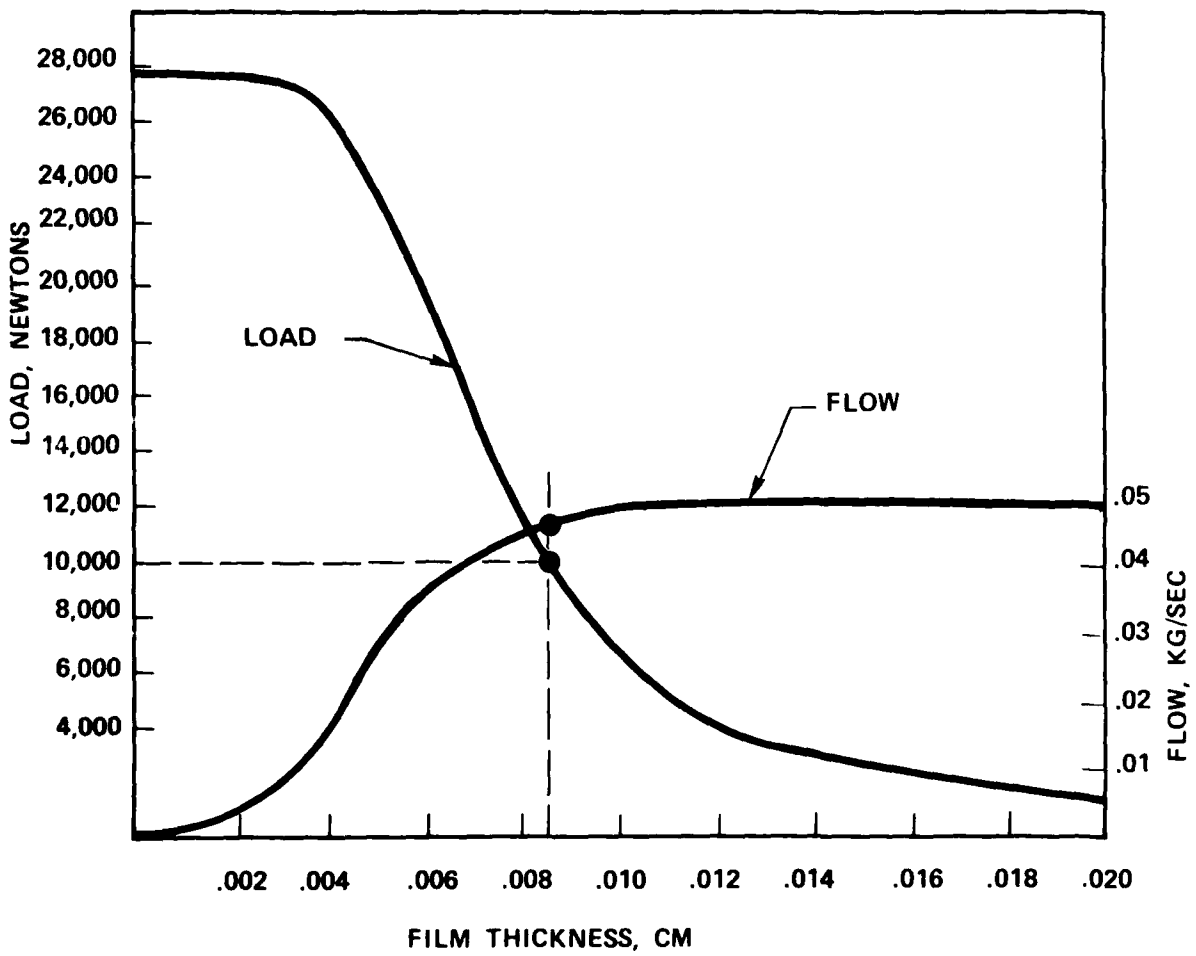

Figure 7-28. 70,000 HP Closed Brayton System Reverse Thrust Bearings, Power Turbine Low Power Thrust Load

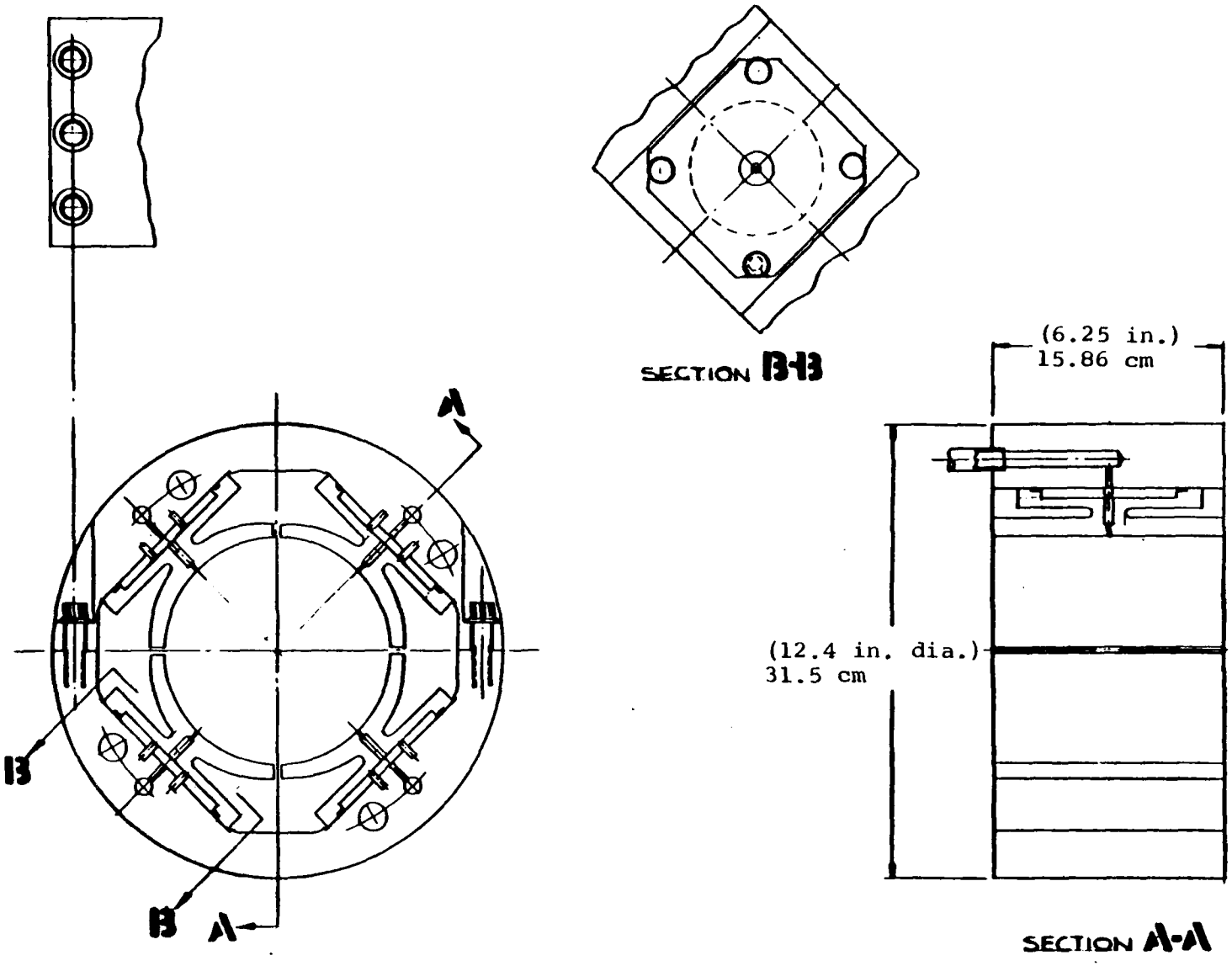

Figure 7-29. Hydrostatic Gas Journal Bearing Assembly for 15.88 cm dia. (6.25 in.) Shaft

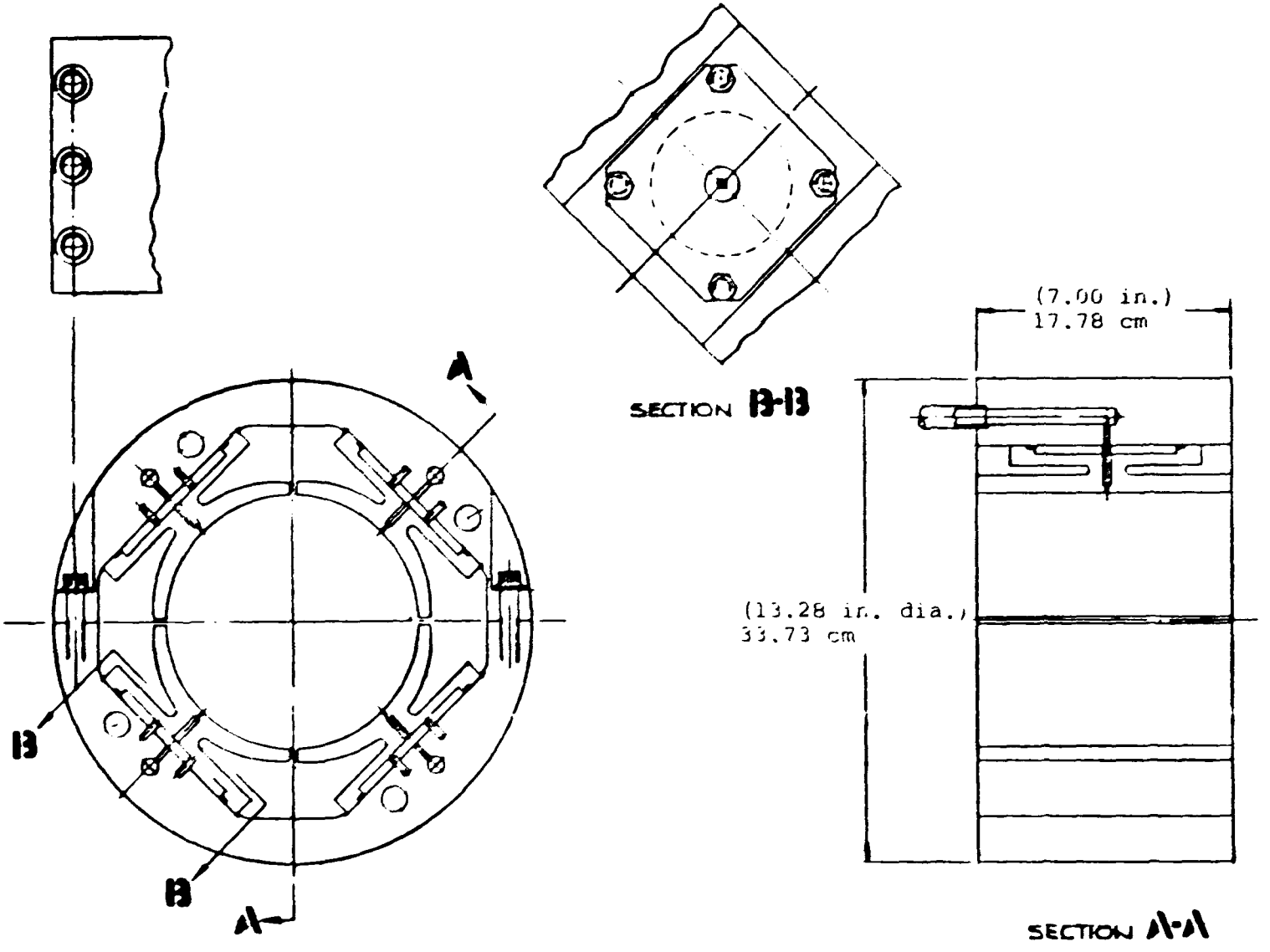

Figure 7-31. Hydrostatic Gas Journal Bearing Assembly for 17.78 cm dia. (7.00 in.) Shaft

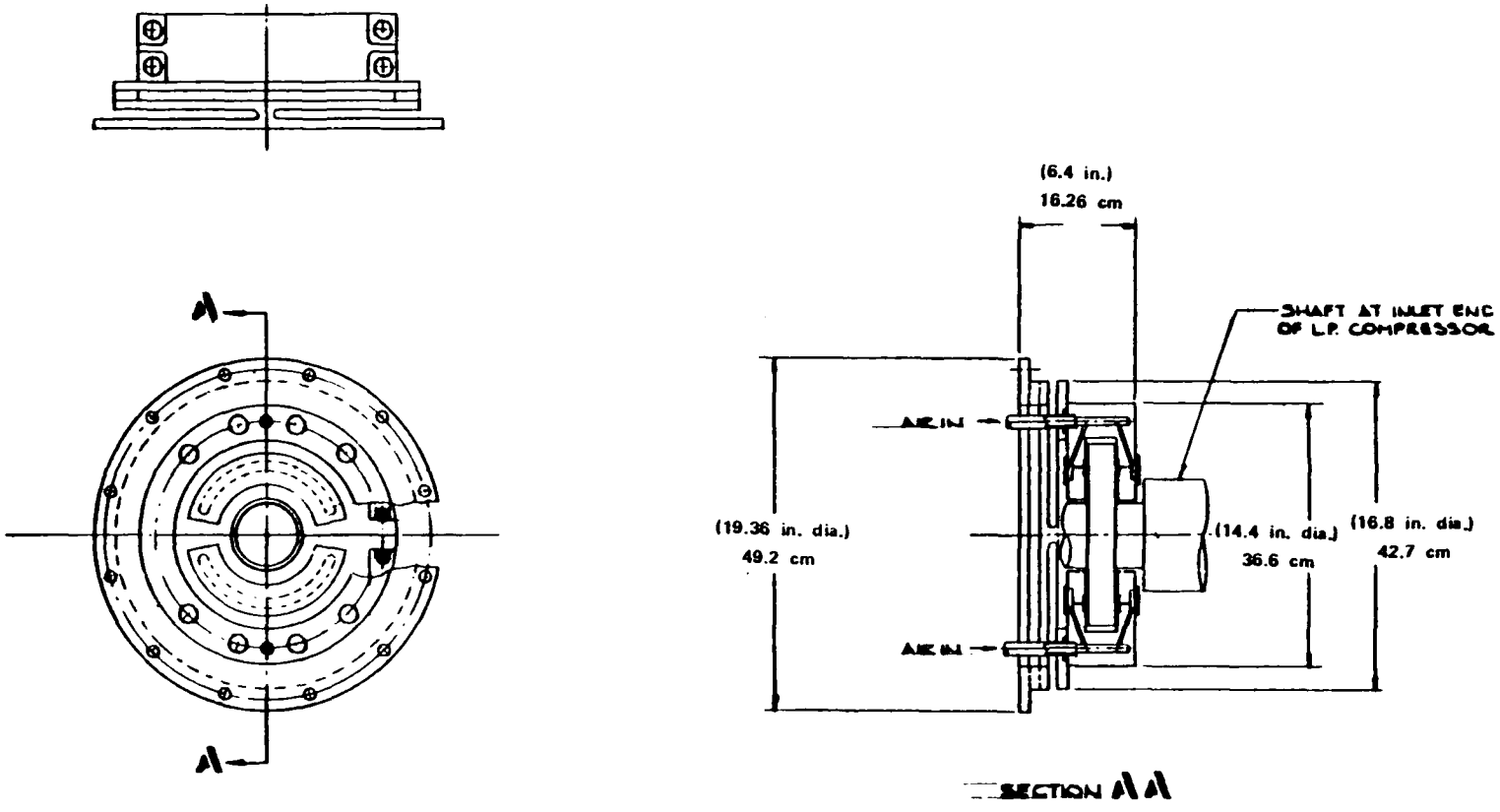

Figure 7-31. Hydrostatic Gas Thrust Bearing for Low-Pressure Spool

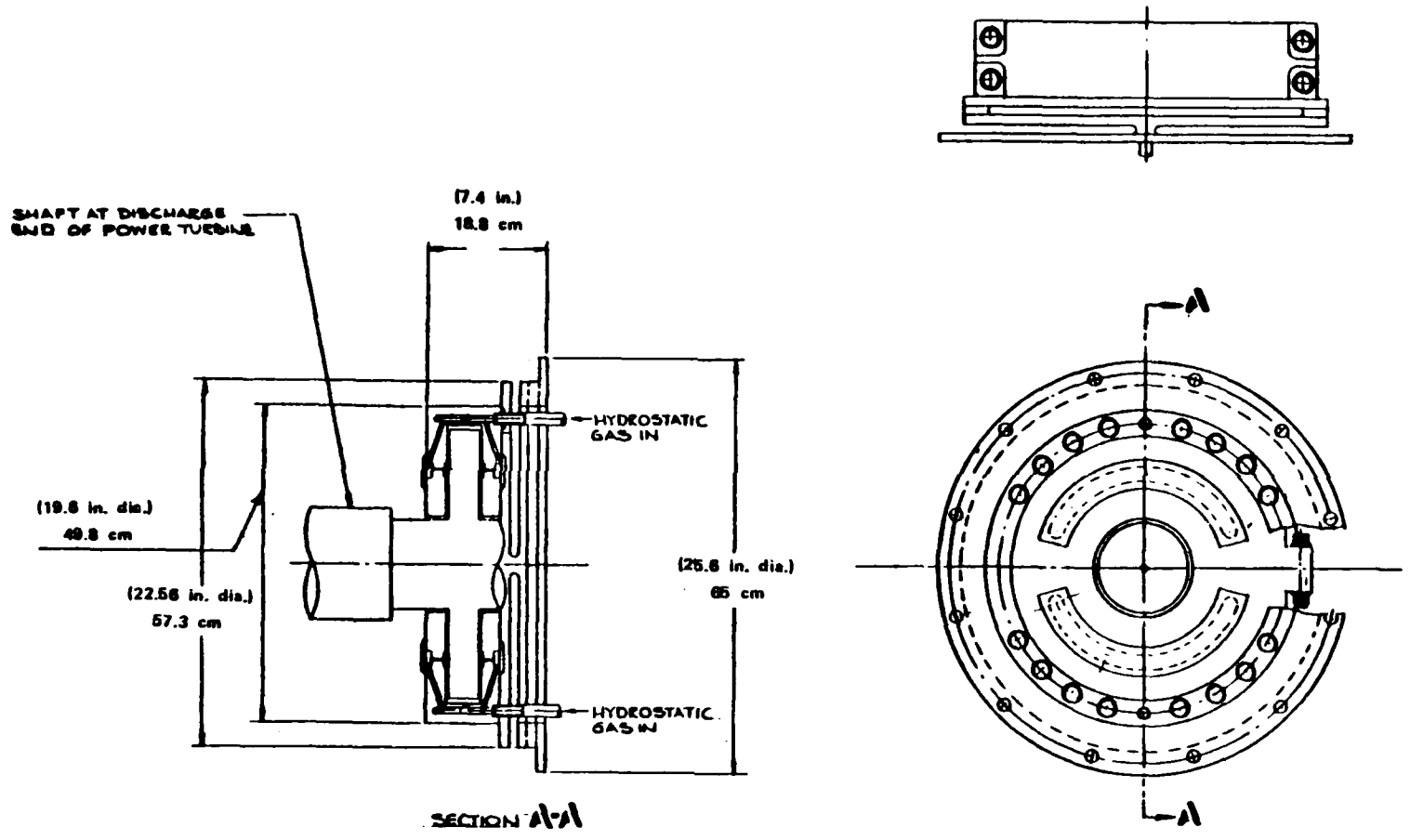

Figure 7-32. Hydrostatic Gas Thrust Bearing for Power Turbine

7.4 COUPLING

A suggested design for the flexible coupling between the LP and HP compressor spools is shown in Figure 7-33. The design makes use of a thin flexible center shaft to carry the nominal 44.48 kN (10,000 lb_f) thrust load. The shaft was sized for a ±88.98 kN (±20,000 lb_f) load to allow for transient conditions not yet fully identified.

The torque between the LP- and HP-spools is carried through two Bendix No. 67E312 AISI4340 alloy steel diaphragms welded to a spool. The spool has access holes to allow attachment of the center thrust shaft to the ends of the LP- and HP-spool shafts. The flexible diaphragms do not carry any thrust loads, but do permit radial misalignment and offset of the LP- and HP-spools.

The coupling was designed to meet the following requirements:

Thrust	±44.48 kN (±10,000 lbs) nominal ±88.96 kN (±20,000 lbs) transient
Torque	19094 N.m (169,000 in.-lb) nominal 22950 N.m (203,120 in.-lb) transient
Speed	1884.96 rad/sec (18,000 rpm)
Shaft Offset	±0.127 mm (±0.005 in.)
Shaft Angular Misalignment	3.665×10^{-3} rad (0.21°)

Stress levels for the center shaft and diaphragm were established for two axial lengths of the coupling. The recommended design shown in Figure 7-33 incorporates a 17.78 mm diameter (0.70 in.) center shaft that is 25.4 cm (10 in.) long. An alternate design uses a 16.51 mm (0.65 in.) diameter shaft that is 20.32 cm (8.0 in.) long and results in a coupling 5.08 cm (2.0 in.) shorter than shown in Figure 7-33. The stress levels and other relevant characteristics of the two coupling designs are given in Tables 7-11 and 7-12.

The shorter of the two couplings would operate at higher stress levels, lower safety factors, and higher imposed lateral loads on the LP- and HP-spool bearings while reducing the overall length of the CCCBS engine by 5.08 cm (2.0 in.).

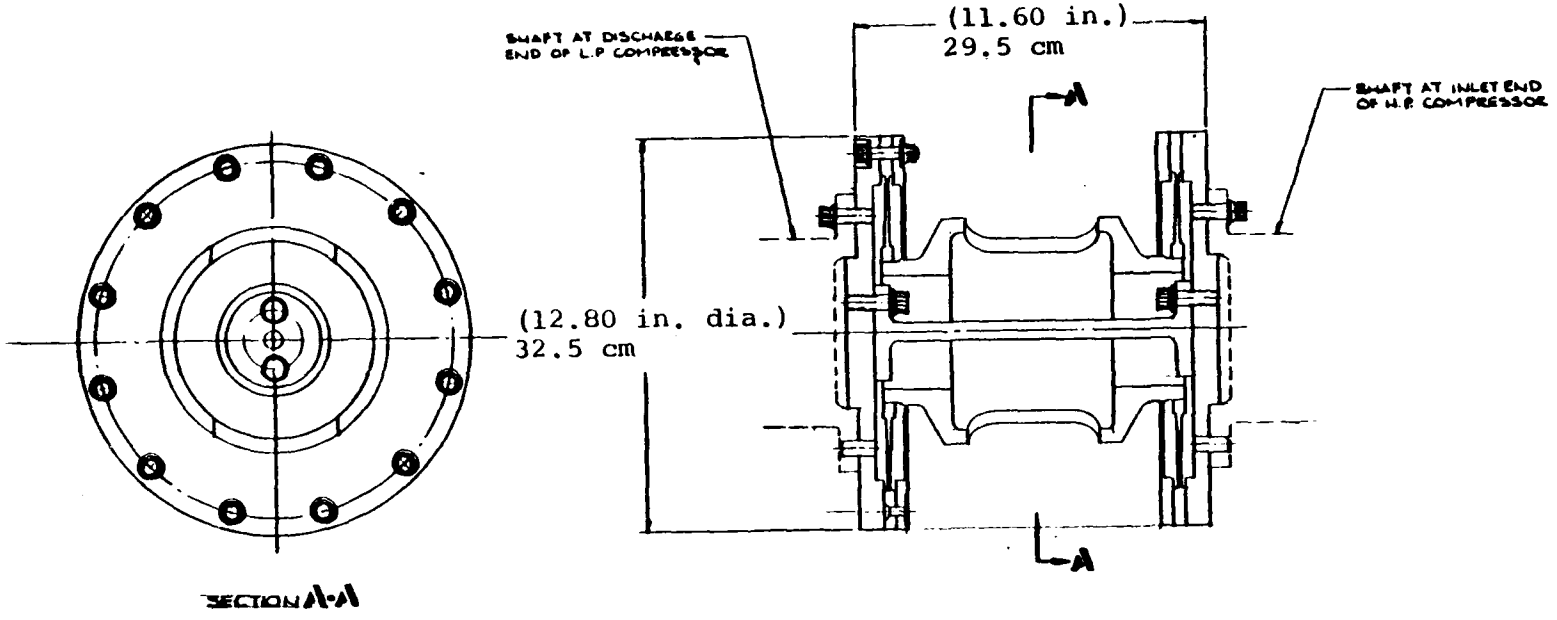

Figure 7-33. Low Pressure and High Pressure Spool Coupling

TABLE 7-11

RECOMMENDED COUPLING DESIGN
25.4 cm (10.0 in.) Shaft Length

	Shaft	Diaphragm*
Mean Stress	537 MN/m^2 (78,000 psi)	634.3 MN/m^2 (92,000 psi)
Alternating Stress	89 MN/m^2 (13,000 psi)	36.5 MN/m^2 (5,300 psi)
Factor of Safety	1.6	1.5

*Diaphragms apply 489.3N (110 lbs) lateral load to engine bearings.

TABLE 7-12

ALTERNATE COUPLING DESIGN
20.32 cm (8.0 in.) Shaft Length

	Shaft	Diaphragm*
Mean Stress	620.5 MN/m^2 (90,000 psi)	634.3 MN/m^2 (92,000 psi)
Alternating Stress	124.1 MN/m^2 (18,000 psi)	43.4 MN/m^2 (6,300 psi)
Reactor of Safety	1.35	1.5

*Diaphragms apply 667.2N (150 lb_f) lateral load to engine bearings.

The increased bearing loads resulting from the maximum offset and misalignment of either coupling design would not require redesign of the No. 2 and No. 3 gas bearings of the CCCBS engine (Refer to Figure 7-10 for bearing Nos.). The increased loads would reduce the gas film thickness of these two bearings– but not to dangerous levels. If additional gas film margin were desired, that margin could be provided through use of slightly larger hydrostatic gas orifices in those two bearings.

7.5 REFERENCES

1. "Compact Closed Cycle Brayton System Feasibility Study, Final Report Year 1": Westinghouse Advanced Energy Systems Division; WAES-TNR-233; July 1977.

2. "A Simple Correlation of Turbine Efficiency," S. F. Smith; Journ. R. Aero. Soc., 69 (1965) 468.

8.0 CRITICAL COMPONENT EVALUATIONS

During the course of the Year 1 analyses, the basic plant configuration of the CCCBS was developed. The Year 2 studies have refined the design and allowed for the detailed layouts of the components to be developed. This has necessitated an evaluation of these components to identify possible technology areas that would detract from the successful development of the CCCBS. These are discussed in Sections 8.1 through 8.3 for the various components comprising the CCCBS.

Besides the basic turbomachinery/heat exchanger package, there are a number of auxiliary systems needed for operation of the plant. These are identified and discussed in Section 8.4.

8.1 BEARINGS

During the course of the CCCBS study, oil and gas lubricated bearings have been investigated. At the end of the first year of study, foil type gas bearings were selected as the primary bearing concept with oil lubricated bearings occupying a back-up position. During the second year of study, rotor dynamics and shock loads were defined with the resulting recommendation that hydrostatic solid geometry pad-type gas bearings be used in place of foil gas bearings. As the study developed, further justification for the use of hydrostatic gas bearings was established. Static and dynamic load deflections of the bearings were minimized with the hydrostatic bearings. The advent of variable speed power turbine designs dictated the use of hydrostatic bearings so that the bearings could be fully supported over the entire operating range. Critical thrust balance piston seals also necessitated the use of less compliant hydrostatic gas bearings to control the seal clearances over the specified operating range.

The final study covered the design and analysis of the various CCCBS bearings given in Tables 8-1 and 8-2.

TABLE 8-1

JOURNAL BEARINGS

Bearing Locations	Diameter		Length		Static Load	
	cm	(in.)	cm	(in.)	N	(lb_f)
LP Compressor Inlet	15.88	(6.25)	15.88	(6.25)	2405	(562)
LP Compressor Out	15.88	(6.25)	15.88	(6.25)	2016	(471)
HP Compressor Inlet	15.88	(6.25)	15.88	(6.25)	2170	(507)
HP Turbine Out	15.88	(6.25)	15.88	(6.25)	2072	(484)
9000 RPM PT In	17.78	(7.00)	17.78	(7.00)	1849	(432)
9000 RPM PT Out	17.78	(7.00)	17.78	(7.00)	3047	(712)
3600 RPM PT In	17.78	(7.00)	17.78	(7.00)	3124	(730)
3600 RPM PT Out	25.40	(10.00)	25.40	(10.00)	14060	(3285)

TABLE 8-2

THRUST BEARINGS

Bearing Location	Outside Dia. cm	Outside Dia. (in.)	Inside Dia. cm	Inside Dia. (in.)	Thrust Load KN	Thrust Load (lb_f)
Gas Generator	30.48	(12.00)	15.24	(6.00)	42.8	(10,000)
9000 RPM PT	41.66	(16.40)	14.22	(5.60)	62.7	(14,650)
3600 RPM PT Reverse Thrust Side	38.10	(15.00)	27.94	(11.00)	9.6	(2243)
3600 RPM PT Full Power Thrust Side	38.10	(15.00)	20.32	(8.00)	55.64	(13,000)

An evaluation of the bearing analysis is made in the following paragraphs.

Journal Bearings

The journal bearing load performance characteristics presented in Section 7.0 were predicted based upon the following assumptions:

- The bearing and journal surfaces are represented by two parallel planes.
- Minimum film thickness of the journal bearing is modeled as average film thickness between two parallel plates.
- The gas lubricant is isothermal throughout the bearing system.
- The bearing surfaces are static (translation and normal motions of the two surfaces are ignored).
- Bearing film stiffness is inferred from static load versus film thickness; dynamic effects are ignored.
- Rotor dynamic behavior is based upon linearized gas film stiffness. Cross coupled stiffness and damping are ignored.

The above assumptions are motivated by realistic considerations within the study constraints so that bearing performance can be readily and relatively characterized.

The parallel surface assumption is first considered. For the journal bearing pivoted pad, film thickness in the circumferential direction is:

$$h = c\ (1 + \varepsilon \cos \theta)$$

where:

h = the film thickness at angle

ε = the journal eccentricity ratio

c = the pad clearance; the difference between the journal and pad curvature radii

θ = the angle measured from the line of centers to an arbitrarily specified point on the pad surface.

For the 15.88 cm (6.25 in.) diameter bearing, c = 0.152 mm (0.006 in.). For a minimum film thickness h = 0.076 mm (0.003 in.) at the pad orifice, the

maximum film thickness at the pad leading and trailing edges, θ = 42 degrees, is about 0.0965 mm (0.0038 in.).

The effect of the diverging film thickness is to reduce flow resistance, which reduces bearing film pressure rise above ambient. Hence, the qualitative effect is that the pad load capacity will be less than that predicted by the parallel plate assumption.

The initially predicted performance parameters for the journal bearings indicate that a substantial margin will exist in terms of gas film thickness adequacy. While these predictions are recognized to be optimistic, the compromise in film thickness for a given load is expected to be no more than the order 20 to 30 percent for the actual hardware. The initially sized values, when compromised by this order, should still result in film thickness values with sufficient operating margin beyond threshold limiting values of significant risk. The film thickness compromise can be reduced by special contouring of selected bearing pads.

The isothermal gas assumption implies that the local gas temperature will be constituted by the bearing and journal metal temperature and that both bearing and journal temperatures will be the same. This assumption is valid to at least second order in terms of load prediction results.

The assumption that the bearing surfaces are static ignores self acting pressure effects associated with journal rotation. This assumption deserves further quantification, but it is reasonable in establishing first order effects. However, the assumption that there is no normal relative motion of the bearing surfaces does have significant implications. The journal orbit trajectory will cause appreciable film thickness oscillations just due to the rotor imbalance. This squeeze film effect does add to the bearing load and stiffness, and these additions can be significant. Moreover, such squeeze film motions do constitute a source of pneumatic instability, sometimes called "air hammer," which can cause system failure. The bearing feed system is designed with multiple orifices feeding each pad recess, which is intended to reduce susceptibility to this pneumatic instability, but further quantitative studies in this regard are required.

The assessment of rotor dynamic behavior was limited to synchronous critical speed response due to the linearlized gas film stiffness representation and the absence of damping and cross coupled stiffness and damping effects. The susceptability of the bearing rotor system to sub-synchronous whirl instability must be recognized as a potential catastrophic failure mode, and further studies are required. The selected bearing design implicitly addresses the sub-synchronous whirl problem by using four pads per bearing. Interruption of the bearing film through the use of discrete pads does enhance system stability, and the concept does provide the necessary degrees of design freedom to finalize the bearing design parameters in a manner to preclude system instability.

Thrust Bearings

The thrust bearing designs presented in Section 7.0 comprise 8 pads per bearing surface, each externally fed through four or more orifices. The parallel surface assumption is valid in this case in the absence of slider nutation. Comments previously made in regard to the journal bearing isothermal film assumption, squeeze film effects, and pneumatic instability apply to the thrust bearing designs. The likelihood of the thrust bearing contributing to rotor whirl instability is remote.

System Integration

The performance characteristics of the externally pressurized gas film bearings, presented in Section 7.0, are based on the assumption that the flow within the bearing film is laminar and fiscous; fluid inertia effects are ignored. Then, for a prescribed film thickness distribution, the pressure and flow rate within the film are directly determined for a prescribed orifice discharge pressure. The orifice discharge pressure is determined based on the orifice supply pressure for prescribed orifice sizes and discharge coefficients. Flow rate through the orifices is equated to that leaving the boundaries of the pad to completely constitute the problem. The governing equations can be normalized in such a manner that generalized performance can be prediced independent of bearing size. The normalized performance characteristics can then be applied to a bearing of arbitrarily large or small size.

The limitations to accurate preformance predictions are essentially in the flow characterization through the orifices (orifice discharge coefficient), representation of local inertia effects as the flow enters the gas film, and the validity of the film thickness distribution representation. Each of these must be assessed quantitatively. For large bearings, the effects of elastic deflections due to pressure, thermal, and centrifugal effects become increasingly important, as do manufacturing considerations such as surface finish and dimensional control.

The elastic deflections must be predicted from rigorous thermal and structural analyses and iteratively incorporated into the bearing gas film performance predictions.

3600-RPM Power Turbine

The configuration selected for the 3600-rpm power turbine is feasible from the standpoint of supporting the rotor on gas bearings; however, the design necessitates a number of compromises in the gas bearing configurations and rotor dynamics. The overhung turbine blading design places a static load on the rear bearing that is 4.50 times larger than the load on the front bearing. This condition results in a much larger bearing with the attendant requirement for a very stiff bearing mount to keep the radial deflection within acceptable limits. Unfortunately, the rotor dynamics of the selected configuration are such that bearing stiffnesses above a very soft 175,126 N/cm (100,000 lb_f/in.) imposed severe dynamic loads in addition to the large static load. Reference Section 8.3.4.2.

The front journal bearing of the 3600-rpm power turbine also has relatively large dynamic loads even with bearing stiffnesses below 175,126 N/cm (100,000 lb_f/in.). The dynamic loads are 53 percent of the static loads and result in shaft orbits of approximately 0.196 mm (0.0077 in.).

The current design of the 3600-rpm power turbine places very difficult requirements on any hydrostatic gas bearing system. From the standpoint of gas bearing design considerations alone, it is desirable that the power turbine configuration be modified to equalize more nearly the static loads on each journal bearing and to shift the rotor dynamic pattern to permit use of much stiffer bearing mounts.

8.1.1 GAS BEARING SHOCK CAPABILITY

The definition of the CCCBS engine shock requirements during the second year of study had a pronounced influence on the type of gas bearing recommended at the end of the study period. During the first year of study, when no specific shock requirements for the bearings were available, the compliant foil-type gas bearings were recommended. However, as the shock loads as specified in Table 8-3 were developed and the rotor concentricities compatible with balance piston and aerodynamic seals were established, it became evident that the foil-type gas bearing designs, as originally sized and configured, could not provide the required rotor radial control. Foil-type gas bearings are known for their ability to accept very high shock loads and remain functional, but their shock capability is a result of the very compliancy that permits large radial movement under high loads. Radial stops can be incorporated to limit rotor travel under severe shock loads, but these stops must act as unlubricated bearings and would be large relative to the foil gas bearing itself. Foil gas bearings with less radial compliance (higher spring rate) are under research and development and may eventually provide a bearing design with high shock capability with limited radial displacement under shock loads. These designs are not current state of the art technology, however. For these reasons and the off-design bearing requirements, the gas bearing design recommendations were changed from hydrodynamic foil to hydrostatic pad-type gas bearings.

Hydrostatic solid geometry pad-type gas bearings shock capability is a function of the following factors:

- Hydrostatic differential pressure available for bearing support
- Gas film thickness (initial)
- Physical size
- Misalignment capability
- Material compatibility
- Duration of shock load

The hydrostatic gas bearing geometries established in 8.3.2.3 and 8.3.2.4 were designed to provide:

- Adequate bearing load capability under normal design and off-design conditions
- Relatively large initial gas film thicknesses
- Size compatible with the engine envelope
- Misalignment capability via resilient mount
- Limited radial displacement under shock by means of physical stops

The later design feature assures that the bearing ultimate load capacity will be exceeded under some shock loads and metal-to-metal contact will occur between the bearing surfaces. The material compability of the bearing surfaces, therefore, becomes the single most important factor in the ability of a gas bearing to sustain shock loads and remain functional. If the surfaces gall or thermally distort excessively, the bearing will ultimately fail.

A wide variety of materials and coatings have been evaluated for use on gas bearings. The best combinations of materials for shock applications have been found to be a very hard rotating member and a soft stationary member, although good experience has been gained using very hard materials in both members. Various coatings and platings such as tungsten carbide, chromium carbides, chromium oxides, aluminum oxides, and thin dense chrome have been tested with success, but are subject to crazing or damage if suitable thermal design and management of the bearing is not maintained during the shock application. Soft coatings, such as Teflon S, may ultimately be the best materials for the static portions of the CCCBS engine bearings. Teflon provides lubricity without galling and reasonable temperature capabilities up to 533.15°K (500°F) and may be applied to the bearing surfaces in adequate thicknesses to prevent metal-to-metal contact in the event of momentary rubs during shock loads.

It is thought that this rigorous thermal analysis and proper mechanical and material design that the hydrostatic pad-type gas bearings recommended during

the second year of study can be made to accept the $\pm$18 g shock loads without serious degradation of performance or failure. The number of such shock applications would probably be limited by the duration of shock which as yet has not been well defined. Based on tests of much smaller gas bearing supported turbomachinery, shock applications of short duration (0.02 mil sec) and several hundred g's can be accepted without failure for at least 100 cycles. The relevance of these tests to large high inertia rotors is unknown at this time.

8.2 COMPACT HEAT EXCHANGERS

8.2.1 PRECOOLER AND INTERCOOLER EVALUATION

Several heat exchangers were studied during the Year 1 - Compact Closed Cycle Brayton System Feasibility Study. Based on the results of this study, it was concluded that the finned tube cross-counterflow concept had the greatest promise. Therefore, further evaluation on a modular design concept and a helical design concept was performed. Both concepts were modeled with the core geometry listed in Table 8-3. The evaluation of these concepts is discussed in the following paragraphs.

8.2.1.1 DESIGN CONSIDERATIONS

The modular heat exchanger concept was modeled as four individual cross counterflow modules with four liquid passes each. These modules were wrapped annularly around the engine core. An unwrapped view of the modular design concept is shown in Figure 8-1.

Since each module has four liquid passes, a 15-percent packing factor was incorportated in the design to allow room for headering and manifolding. An overall heat transfer (UA) margin of 0.20 was assigned to the liquid side to allow for the liquid flow maldistribution due to the inability to pressure balance the tube flows. The thermal and flow characteristics of the modular heat exchanger are shown in Table 8-4.

The helical heat exchanger concept was modeled as one cross-counterflow annular module with four liquid passes. Each liquid pass begins 90° from the other and makes one complete revolution around the engine core in a helical configuration. As isometric view and a cross sectional view of this concept are shown in Figures 8-2 and 8-3.

The problems of balancing the flow through the tubes can be alleviated by orificing the inlet tubes or within the four tapered inlet manifolds. Therefore, an overall heat transfer (UA) margin of 0.05 was assigned to the liquid side. Since the helical design has no manifolds, no packing factor is necessary. The thermal and flow characteristics of the helical heat exchanger are listed in Table 8-5.

TABLE 8-3

HELICAL AND MODULAR COOLER AND INTERCOOLER INPUT GEOMETRY

	Coolant Cross Flow		Helium Flow	
Flow Area Ratio (Free Flow/Frontal)	0.33076		0.37956	
	cm^{-1}	$(in.^{-1})$	cm^{-1}	$(in.^{-1})$
Surface Area/Volume	2.621	(6.657)	8.4256	(21.401)
Fin Area/Volume	-	(-)	5.801	(14.734
Plate Area/Volume	2.621	(6.657)	2.625	(6.667)
Hydraulic Diameter	0.50483 cm	(0.19875 in.)	0.18020 cm	(0.07094 in.)
Entry loss	0.5 velocity head		-	
Turning Loss (Modular only)	1.5 velocity head		-	
Exit Loss	1.0 velocity head		-	

Tube

ID = 0.50483 cm (0.19875 in.)
Wall = 0.0254 cm (0.010 in.)
Density = 8.026 g/cm^3 (0.290 $lb_m/in.^3$) (stainless steel)
Conductivity = 6.84 Joule/m·sec·k° (12.8 Btu/hr·ft·R°)

Fin

$\frac{11.81}{cm}$ (30/in.) - nickel chrome clad copper

Length = 0.762 mm (0.03 in.) (Dia_f/OD = 1.27)
Thickness = 0.0762 mm (0.003 in.)
Density = 8.553 g/cm^3 (0.309 $lb_m/in.^3$)
Conductivity = 53.46 Joule/m·sec·k° (100.0 Btu/hr · ft · R°)

Spacing

Transverse = 1.1 cm (0.433 in.) δ_T/OD = 1.98
Longitudinal = 5.5 cm (0.0217 in.) δ_T/OD = 0.99

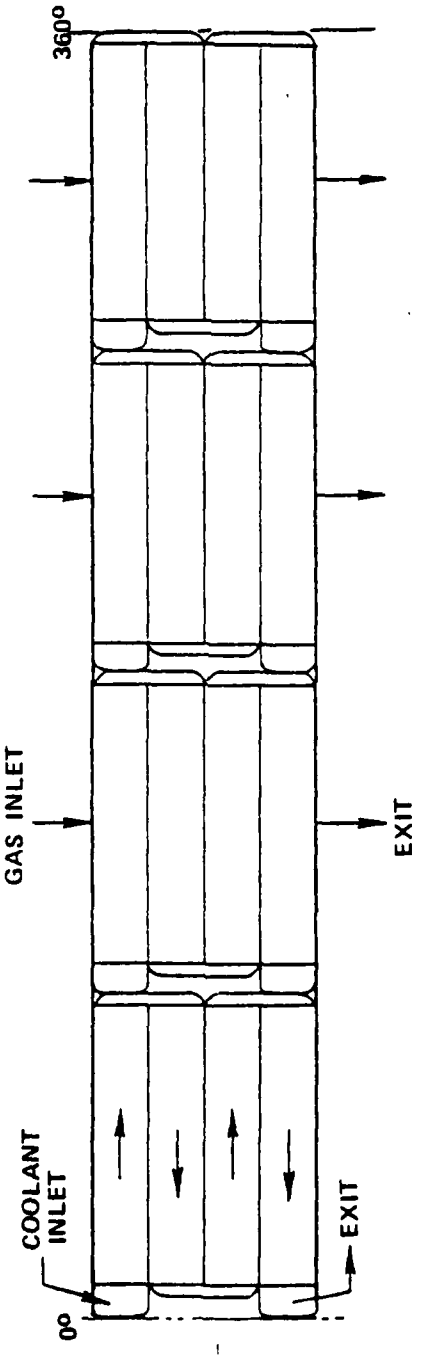

Figure 8-1. Unwrapped View of the Coolers

TABLE 8-4

MODULAR HEAT EXCHANGER PERFORMANCE SUMMARY

	Cooler			Intercooler		
	Cross Flow		Through Flow	Cross Flow		Through Flow
Fluid	Water		He	Water		He
Inlet Temperature	308.3°K (555°R)		488.9°K (880°R)	308°K (555°R)		424.4°K (764°R)
Outlet Temperature	347.7°K (626°R)		311.1°K (560°R)	340°K (612°R)		311.1°K (560°R)
Flow Rate	341.4 kg/sec. (752.6 lb_m/sec.)		58.01 kg/sec. (127.9 lb_m/sec)	271.3 kg/sec. (598.2 lb_m/sec.)		58.01 kg/sec. (127.9 lb_m/sec.)
Pressure Drop	137.4 kPa (19.93 psi)		--	100.8 kPa (14.62 psi)		--
Percent Pressure Drop ($\Delta P/P$)	--		0.01515	--		0.00787
Heat Exchanger Effectiveness		0.985			.976	
Fin Effectiveness			0.902			0.888
Reynolds Number	31,191		6,013	24,977		8,354
Flow Frontal Area		1.916 m^2 (2971 $in.^2$)			1.455 m^2 (2256 $in.^2$)	
Packaging Frontal Area		2.255 m^2 (3495 $in.^2$)			1.712 m^2 (2654 $in.^2$)	
Active Flow Length	387.56 cm (152.70* in.)		63.8 cm (25.12 in.)	353.3 cm (139.09 in.)		79.2 cm (31.18 in.)
Tube Mass		670.4 kg (1478 lb_m)			623.2 kg (1374 lb_m)	
Fin Mass		225.9 kg (498 lb_m)			210.01 kg (463 lb_m)	
Total Mass		1286.0 kg (2835 lb_m)			1198.0 kg (2641 lb_m)	
Volume		1.44 m^3 (50.81 ft^3)			1.36 m^3 (47.89 ft^3)	
Number of Passes	4			--		

*Flow length at the mean diameter.

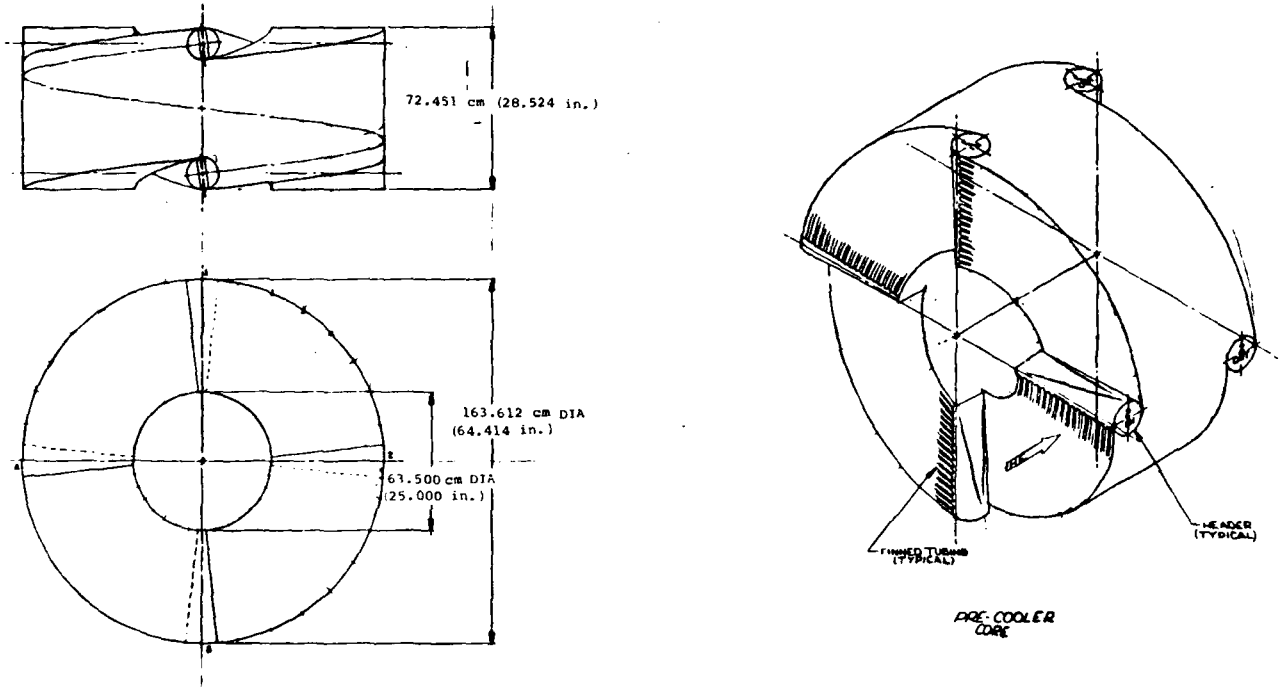

Figure 8-2. Helical Heat Exchanger Design Concept

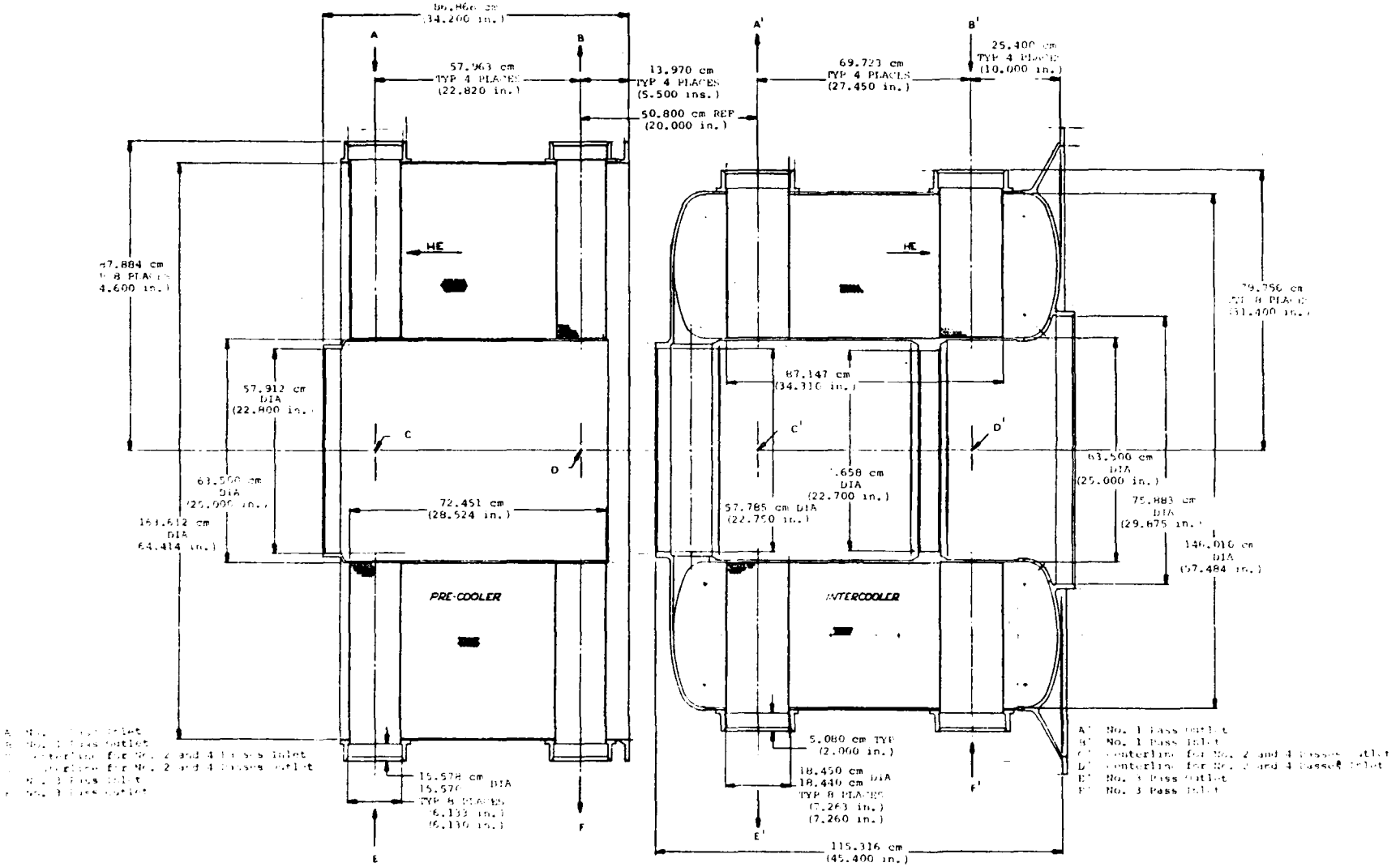

Figure 8-3. Helical Heat Exchanger Outline

TABLE 8-5

HELICAL HEAT EXCHANGER PERFORMANCE SUMMARY

	Cooler			Intercooler		
	Cross Flow		Through Flow	Cross Flow		Through Flow
Fluid	Water		He	Water		He
Inlet Temperature	308.3°K (555°R)		488.9°K (880°R)	308.3°K (555°R)		424.4°K (764°R)
Outlet Temperature	347.8°K (626°R)		311.1°K (560°R)	340°K (612°R)		311.1°K (560°R)
Flow Rate	341.4 kg/sec (752.6 lb_m/sec.)		58.01 kg/sec (127.9 lb_m/sec.)	271.3 kg/sec. (598.2 lb_m/sec.)		58.01 kg/sec (127.9 lb_m/sec.)
Pressure Drop	146.5 KPa (21.25 psi)		--	110.3 kPa (15.99 psi)		--
Percent Pressure Drop ($\Delta P/P$)	--		0.01515 velocity head	--		0.00787 velocity head
Heat Exchange Effectiveness		0.985			0.976	
Fin Effectiveness			0.90			0.883
Reynolds Number	37,006		6,475	29,996		9,032
Frontal Area		1.78 m^2 (2,760 $in.^2$)			1.35m^2 (2,086 $in.^2$)	
Active Flow Length	*356.7 cm (140.45 in.)		57.2 cm (22.52 in.)	329.1 cm (129.57 in.)		68.2 cm (26.85 in.)
Tube Weight		544.3 kg (1200 lb_m)			499.4 kg (1101 lb_m)	
Fin Weight		183.2 kg (404 lb_m)			168.3 kg (371 lb_m)	
Total Weight		1044.6 kg (2303 lb_m)			960.2 kg (2117 lb_m)	
Volume		0.821 m^3 (35.97 ft^3)			0.740 m^3 (32.41 lb_f)	
Number of Passes	4			4		

*Mean diameter length

A comparison of the modular and helical design concepts is shown on Table 8-6. The helical design concept was selected over the modular design concept due to the following attributes:

- More reliable due to the large reduction in the number of tubes, therefore, tube joints
- More compact and easier to package due to the smaller frontal area
- Better flow distribution due to the elimination of inner pass manifolding
- Reduction in mass

Thermal transients should pose no problems since the helical heat exchanger would grow uniformly.

The helical design concept has the disadvantages that complete module replacement is necessary if a major failure occurred, and the cross flow side pressure drop is slightly higher than the pressure drop on the module design concept. This increase in pressure drop would cause the pump power of the helical design to be slightly more than that required for the modular design.

8.2.1.2 CRITICAL DESIGN FEATURES

The helical heat exchanger design concept introduces several non-conventional fabrication and assembly features. The tubes must be precoiled and individually threaded into the assembly and then brazed to the headers. Because of the geometric method of tube penetration into the headers, the headers must be split, and the tube holes drilled from the inside. This split header arrangement does facilitate baffling and porting of the tubes to achieve equal flow distribution. There are no other critical design features associated with the helical heat exchanger design concept. However, a method of supporting the finned tubes (primarily at the larger radii) to meet the shock load requirements would require some design and development effort.

TABLE 8-6

CROSS COUNTERFLOW HEAT EXCHANGER COMPARISON

	Modular		Helical	
	Cooler	Intercooler	Cooler	Intercooler
Total number of tubes	24,192	24,640	4,500	4,440
OD, [ID = 63.5 cm (25 in.)]	183.4 cm (72.21 in.)	161.14 cm (63.55 in.)	163.6 cm (64.41 in.)	146.0 cm (57.43 in.)
Active flow length, (Gas)	63.8 cm (25.12 in.)	79.20 cm (31.18 in.)	72.4 cm (28.52 in.)	87.15 cm (34.31 in.)
Volume	1.44 m^3 (50.81 $ft.^3$)	1.36 m^3 (47.89 $ft.^3$)	1.02 m^3 (35.97 $in.^3$)	0.92 m^3 (32.41 $in.^3$)
Mass	1286.0 kg (2,835 lb_m)	1198.0 kg (2,641 lb_m)	1044.6 kg (2,303 lb_m)	960.3 kg (2,117 lb_m)
Overall heat transfer margin (UA)	0.20	0.20	0.05	0.05
Gas side pressure drop	0.0152	0.00787	0.0152	0.00787

AD-A081 380 WESTINGHOUSE ELECTRIC CORP PITTSBURGH PA ADVANCED ENE--ETC F/G 20/13
COMPACT CLOSED CYCLE BRAYTON SYSTEM FEASIBILITY STUDY, VOLUME I--ETC(U)
AUG 79 R E THOMPSON, R L AMMON, R CALVO N00014-76-C-0706
UNCLASSIFIED WAES-TNR-237-VOL-2 NL

4 OF 6
AD A081380

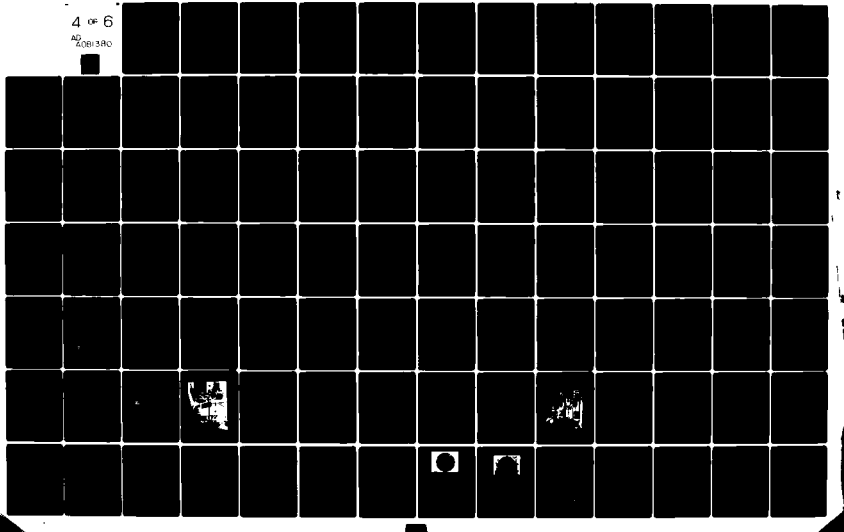

8.2.2 RECUPERATOR EVALUATION

In the year 1 Compact Closed Cycle Brayton System Feasibility Study both tubular and plate-fin recuperator constructions were investigated. Both types of construction have high ratings for this application and are very close in their overall rating. The shell and tube type was selected, for inclusion in the CCCBS Design Concept for further evaluations, based upon its slightly higher rankings in the areas of malfunction suitability and technology base.

The recuperator initially found acceptance in the large European industrial open and closed cycle gas turbines, introduced about thirty years ago. The recuperator was essentially a supplement to the cycle to provide reasonable specific fuel consumptions with the low component efficiencies of that era. These recuperators, of mainly tubular construction, were conservatively designed and have demonstrated a high degree of reliability and in many cases, have run virtually maintenance free for over 100,000 hours of operation (References 1 and 2).

8.2.2.1 DESIGN CONSIDERATIONS

The requirement for close-couple integration of the heat exchangers and turbomachinery into one compact package results from system requirements to minimize containment dimensions, and therefore total system weight and volume, and also from the desire to minimize connecting piping in order to provide high reliability. Compactness is required regardless of the energy source. In addition, an important design consideration of the CCCBS powerplant is the containment vessel which for safety reasons must completely surround a nuclear system. This vessel is heavy, surrounds the turbomachinery, heat exchangers and other components, and thus constrains the sizing of the power conversion assembly. For the CCCBS, the turbomachinery and the primary loop heat exchangers (precooler, intercooler and recuperator) have been integrated into a single compact assembly. Two parallel redundant assemblies are required in some applications. The recuperator is placed in an annular region around the free power turbine and the recuperator frontal area then determines the diameter of the turbomachinery/heat exchanger module. This module diameter then determines the containment vessel diameter. The recuperator frontal area has a significant effect on powerplant weight and volume. If the recuperator outer annular diameter is increased one inch, the

containment volume increases by 160 cubic feet and the weight increases by about 5900 pounds. As long as the recuperator overall length is less than 96 inches the containment vessel and turbomachinery/heat exchanger vessel weight and dimensions are not affected, since the vessel length is then determined by the turbomachinery length.

A plot of the range of surface compactness (area density per unit of volume) for tubular surface geometries is shown in Figure 8-4. Plain tubular surfaces used in recuperators for large industrial and marine gas turbines had compactness values in the range of 30 to 80 ft^2/ft^3 (Reference 3). The current large plain tubular recuperators built for closed cycle helium gas turbine plants have compactness values in the order of 100 ft^2/ft^3 (Reference 4). Compact tubular geometries used for lightweight recuperative gas turbines for helicopter application have surface compactness values of about 400 ft^2/ft^3 (Reference 2). Reference 5 describes a very compact tubular recuperator surface with a compactness value of almost 700 ft^2/ft^3. The expected range of compactness for this CCCBS application is from 150 to 250 ft^2/ft^3 (tube diameter 0.15 to 0.10 inch). Stainless steel (AISI 304L) tubular recuperator specimens, in the range of interest (outer diameter 0.3 cm (0.118 in) and a 0.01 cm (0.004 in) thickness), have been assembled, brazed and tested (Reference 6). The brazing alloy used in that work has a composition of 13% chromium, 10% phosphorus, balance nickel (AWS A 5.8, BNi-7). This brazing alloy has been successfully used for service temperatures as high as 700 C (1292°F) and has relative low cost. These recuperator specimens were thermal fatigue tested. The test consisted of 1000 thermal cycles where each cycle consisted of increasing the temperature from 200 (392) to 500 C (932°F) in two minutes and then soaking at this temperature for 10 minutes then cooling back to 200 C in two minutes. During these tests the recuperator was pressurized to 506 kPa (73.5 psi). No leakage in the pressure tests and no failures of the brazed joints in the thermal fatigue tests were observed.

Usually tubular designs are assembled into drilled header plates, however, the tubes can be designed to integrally form the header at the tube ends. The joining process can be done either using welding or brazing techniques. Typical end seals for tubular heat exchangers are shown in Figure 8-5. In the lightweight

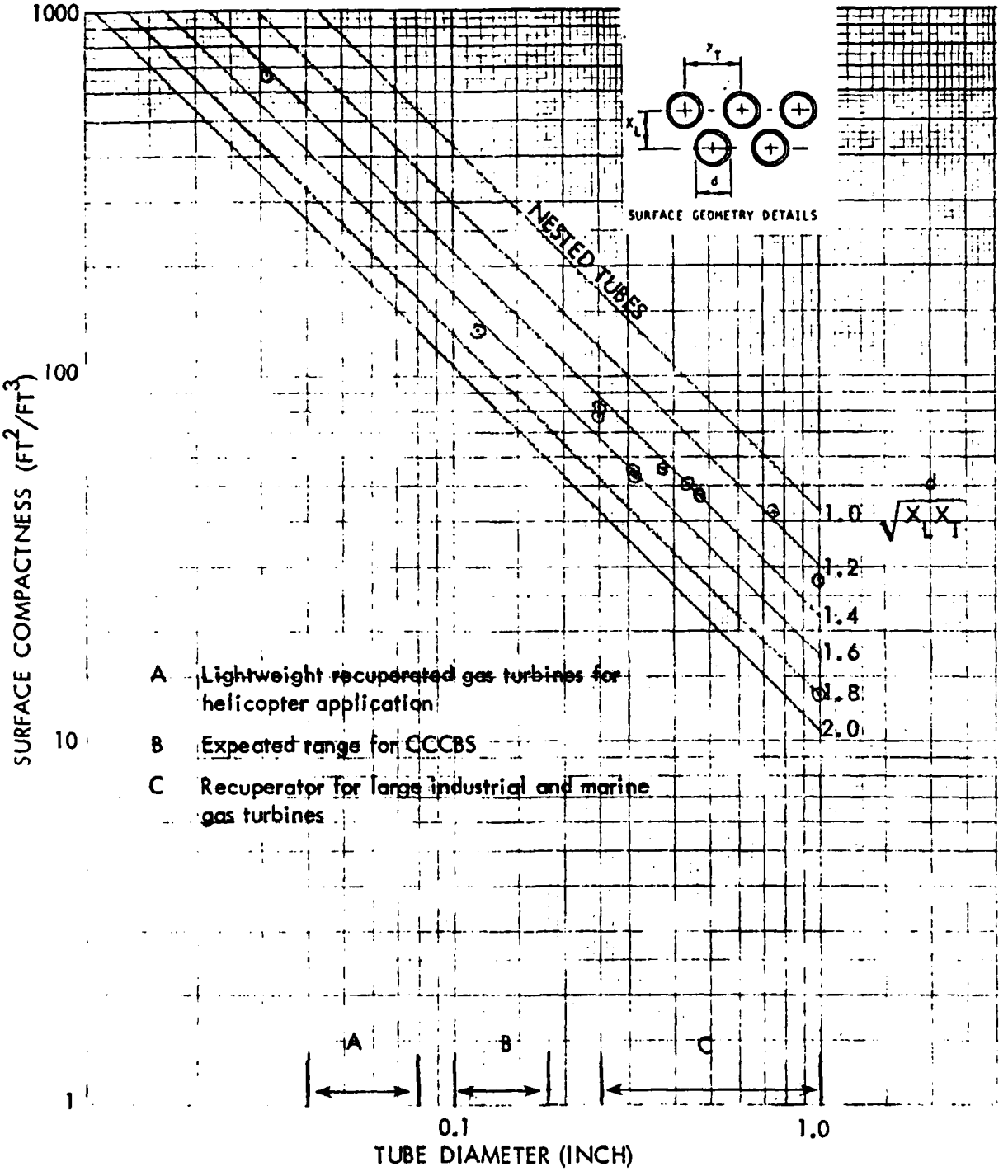

Figure 8-4. Surface Compactness Versus Tube Diameter

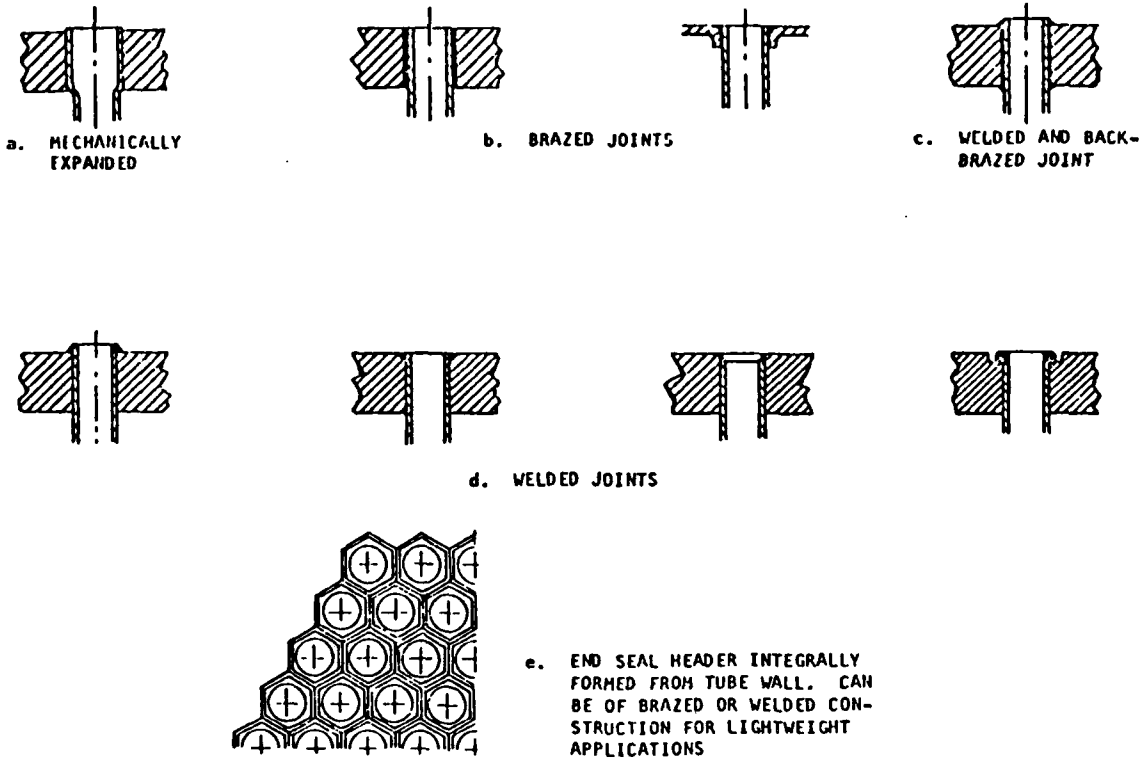

Figure 8-5. Typical Types of Tube to Header Joints (Reference 2)

tubular recuperators developed for aircraft gas turbines, compact geometries and small tube diameters are utilized, and this virtually necessitates brazing the assembly together. Extremely lightweight designs can be achieved by utilizing very compact geometries, in which the tube ends are expanded into the form of hexagons and brazed together to form the header (Reference 2).

Since the recuperator cross sectional (frontal) area has a significant effect on powerplant weight and volume, the approach of the tube and shell concept was to minimize the frontal area. For a given helium flow rate, effectiveness and pressure loss, it was shown (Year 1 Report Appendix B) that the frontal area is proportional to the square root of the ratio of the friction factor to Colburn modulus. This characteristic is shown in Figure 8-6. With a small relative roughness the frontal area minimizes at about a Reynolds Number of 15,000. Utilizing the Colburn factor evaluated at a Reynolds Number of 15,000 the tube diameter is a function of tube length and heat exchanger effectiveness. With an effective tube length of 70 inches and an effectiveness range of 0.8 to 0.9 the required tube diameter ranges from 0.080 to 0.180 inch. Based on the above, a tube ID of 0.100 inch and OD of 0.120 inch was selected for the design shell and tube recuperator concept. Using the above tube diameters, the tube and shell recuperator geometry was determined and is shown in Table 8-7 for a heat exchanger effectiveness of 0.84 with an overall heat transfer margin of 20% to allow for flow maldistribution.

Figure 8-7 shows a schematic drawing of the shell and tube design approach. The flow configuration is that of a counterflow heat exchanger with the turbine exhaust helium flowing in the tubes and with the compressor exit helium flowing on the shell side. The recuperator is composed of 7 modules which are each approximately 16.36 inches in diameter. Each module contains about 10,700 tubes with an outer diameter of 0.120 inch and 0.010 inch thickness.

The tubes are formed at their ends into a hexagonal section. The tube ends are furnace brazed together. The tube bundle is also brazed at the ends to an external cylinder and a cold end ring. Filler pieces are used to fill the gaps at the tube and cylinder interface. No tube sheet is required in this arrangement since each tube carries the local axial tension force.

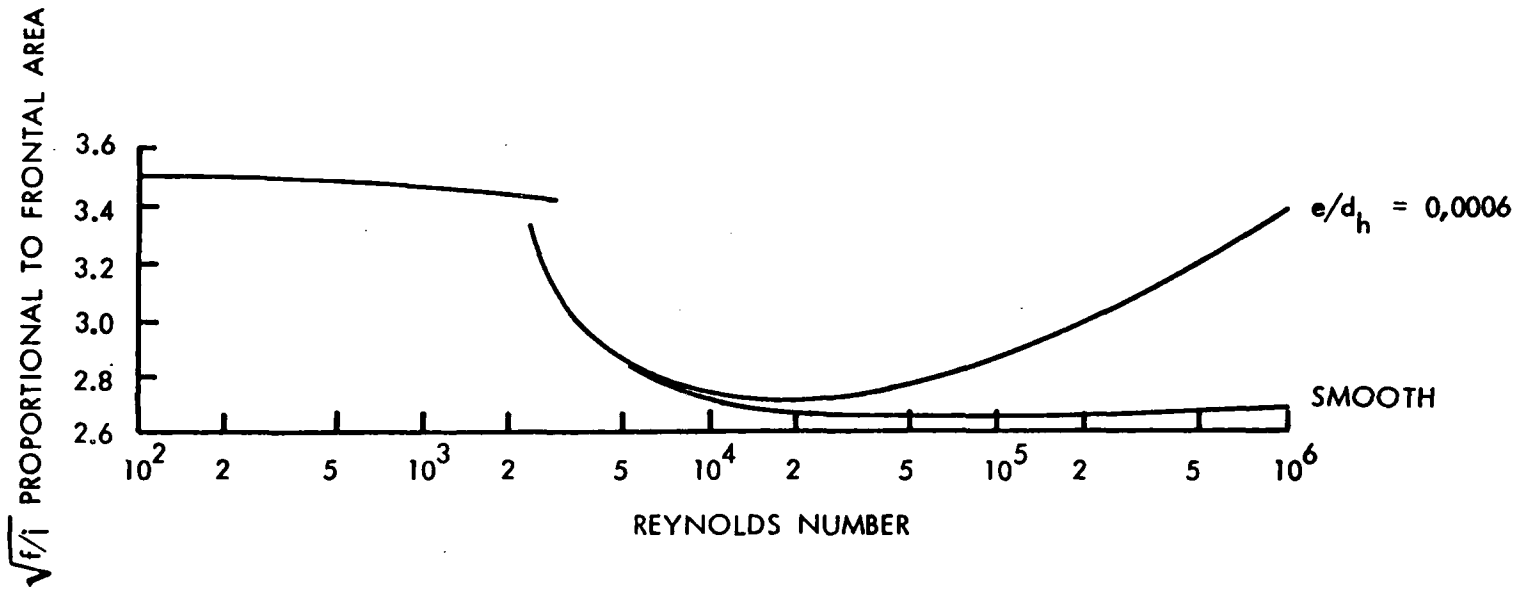

Figure 8-6. Proportional Frontal Area Versus Reynolds Number for Axial Flow in Tubes

TABLE 8-7

SHELL AND TUBE RECUPERATOR GEOMETRY
(One 70,000 HP Turbo-Unit)

Tube ID-inch	0.100
Tube OD-inch	0.120
Pitch to OD ratio	1.20
Effective Length-inches	70.0
Number of tubes/module	10700
Number of Modules	7

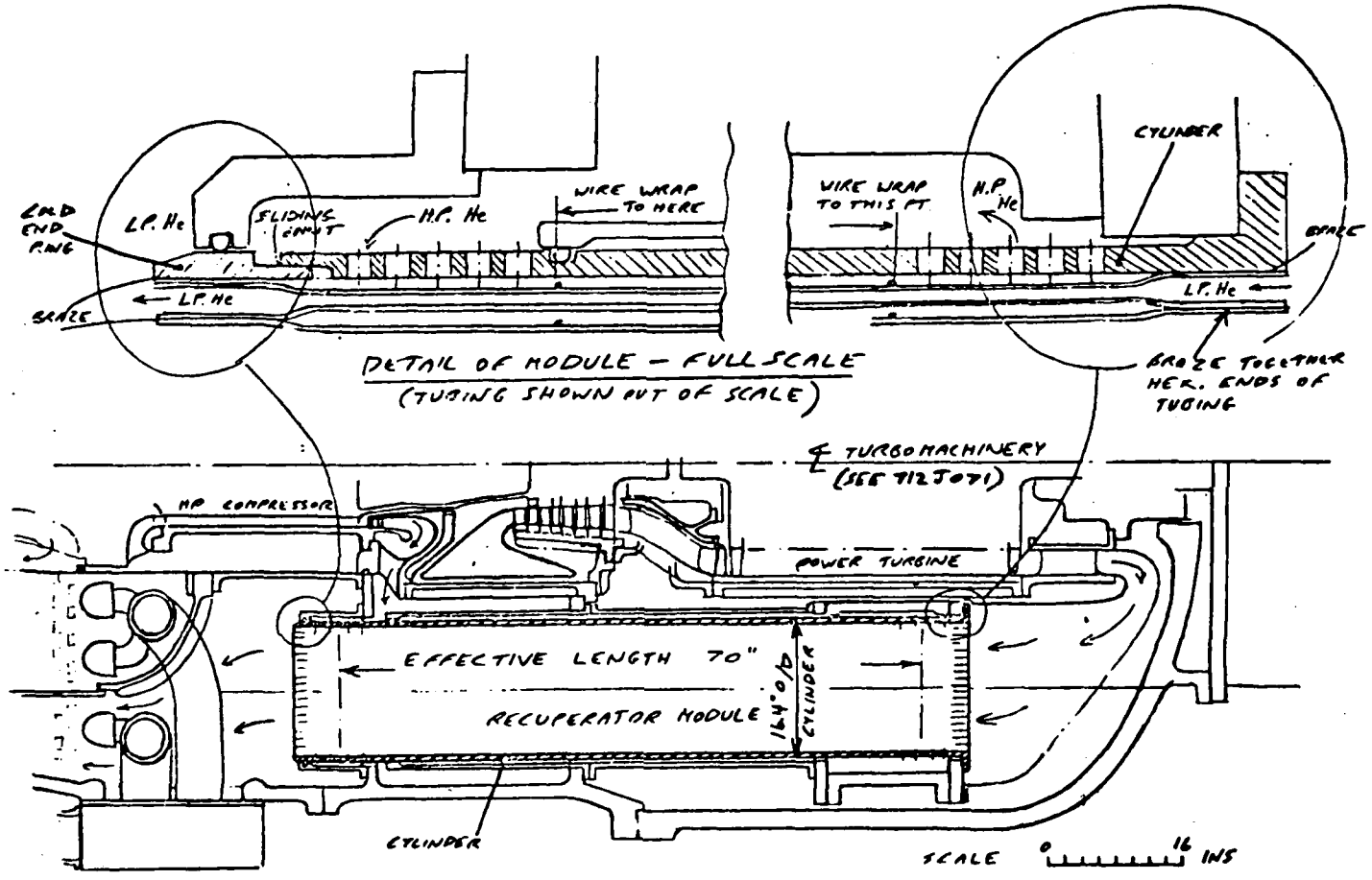

Figure 8-7. Recuperator Module Concept Using Hex Ended Tubing

The tube module is free to expand and contract due to the floating end ring. O-rings are used to seal the floating cold end ring. The modules are located and sealed on the hot end by bolted flanges. This arrangement eliminates the need for tube sheets with their numerous drilled holes.

The tubes are wire wrapped along the central portion of the tube (Figure 8-7) to maintain the proper tube spacing and to give tube support. A wire lead to tube outer diameter ratio of 40 produces a stable condition such that fluidelastic vibration will not occur while producing an acceptable increase in shell side pressure drop of 8.4 percent.

8.2.2.2 CRITICAL DESIGN FEATURES

The shell and tube recuperator design concept could be considered non-conventional by an industrial heat exchanger designer only in respect to the tube size, however an aerospace heat exchanger designer would consider the design conventional. The conceptual design would require some design and development effort to confirm that the heat exchangers meet the Navy's shock load requirements.

8.3 TURBOMACHINERY

8.3.1 FIRST STAGE TURBINE

During the first year effort, a first stage high pressure turbine inlet temperature of 1671°F had been used in the CCCBS program in order to build upon the results of earlier Westinghouse studies performed for similar design conditions and configuration. During the second year the first stage rotor blade airfoil area distribution has been refined to reduce centrifugal stresses at the blade root and allow the turbine inlet temperature to be increased to 927°C (1700°F) while maintaining 10,000 hour life capability at full power. Since some Navy applications can have a duty cycle approximating 25%, the CCCBS evaluations must also recognize that the total operating time to meet the top level requirement of 10,000 effective full power hours (EFPH) may be as high as 40,000 hours. The turbine inlet temperature is therefore scheduled to reduce linearly to 899°C (1650°F) at 25% power to achieve the required life. The plant overall thermal efficiency remains essentially constant over this power range. In addition, the extended root portion of the blade, between the airfoil root section and the disc rim, has been defined in greater detail to provide an initial design basis for further thermal and stress evaluation.

Blade Airfoil Refinement

The blade airfoil sections developed by Westinghouse Combustion Turbine Systems Division and contained in Appendix C of reference 7 are illustrated in Figures 1 to 11 of Appendix B. Two lines have been added to each figure to show the width for a Zweifel coefficient of .8 calculated from the inlet and outlet angles given at the top of each figure. Table 1 of Appendix B contains the calculation of the section widths (b).

As discussed on pages 4-76 through 4-80 of reference 7, the blade design employed airfoil section widths at the tip less than (and at the root greater than) those given by Zweifel's criterion. The section widths approached those for a Zweifel coefficient of .8 at a blade radius of about 1/3 blade height inward from the tip. This was done in order to reduce centrifugal stress at the root while maintaining section widths reasonably close to ideal over most of the blade height. Figure 12 of Appendix B

illustrates the blade width distribution from root to tip. The solid lines define the blade design of reference 1 and reveal a linear variation in width from root to tip. The chain - dotted lines show the "ideal" width distribution corresponding to a Zweifel coefficient of .8.

Also shown on Figure 12 is a modified profile (dotted line) which employs a non-linear variation of section width with blade height. The departure of this modified profile from the Zweifel = .8 profile was limited to an amount judged to result in an efficiency compromise no more severe than that of the linear profile employed in the reference 1 design. In the modified profile, the section widths approached those for a Zweifel coefficient of .8 at mid blade height.

Centrifugal stresses were calculated for the modified blade profile and these are given in Table 2 Appendix B . A material density value of 8.4 g/cc (.305 lb/in.^{3}) was assumed in the basic calculation to be consistent with the value used in the reference 7 Appendix C analysis. Also given in Table 2 are the somewhat lower values corresponding to the less dense IN 100 material which has a density of 7.75 g/cc (.28 lb/in.^{3}). As can be seen by reference to Table 2, the assumption was made that the section areas reduced in proportion to the squares of their widths.

The centrifugal stress, for a density of 8.4 g/cc (.305 lb/in.^{3}), resulting at the root of the modified blade is reduced to 122 MPa (17,694 psi) from the value of 137 MPa (19,874 psi) calculated for the reference 1 blade. The corresponding centrifugal stress at the root of the modified blade using the IN 100 density of 7.75 g/cc (.28 lb/in.) is 112 MPa (16,243 psi).

Judging from the materials data given in Figure 4.23 (Page 4-50) of reference 7 the modified blade should have a life potential of 10,000 hours at 927^{o}C (1700^{o}F) turbine inlet temperature.

This judgment tends to be confirmed by the testing performed to date at AESD on blade materials in ultra pure helium. An IN 100 sample, tested at 110 MPa

(16,000 psi) and 927°C (1700°F) survived for 9452 hours. The equivalent temperature for 10,000 hour life at this stress, using a Larson-Miller (T(20 + log t) relation between temperature in °R (T) and life in hours (t) is 925°C (1698°F). The 1.2°C (2°F) difference between this value and the 927°C (1700°F) turbine inlet temperature is less than the temperature drop through the first stage nozzle vanes 22°C (39°F). Thus, the IN 100 test sample performance to date represents a margin of approximately 21°C (37° F) of excess capability at 927°C (1700°F) turbine inlet temperature for 10,000 hours.

Obviously, such predictions, based on a single test, cannot be made with any precision. However, the ultra high purity testing currently underway at AESD is the most pertinent test data available at the present time. It is possible that future testing, to be performed in contaminated helium environments may result in performance degradation but it is suspected that any degradation experienced will not be severe.

It is therefore concluded that some minor refinement of the blade width distribution profile such as that described can reduce the centrifugal stress at the root sufficiently to provide 10,000 hour life capability at 927°C (1700°F) turbine inlet temperature judging from the limited long term in-helium test data available to date.

Blade Root Definition

The blade root design used in the Westinghouse Power Generation System stress analysis model is illustrated in Figure 4.31 (Page 4-81) of reference 7. As mentioned in reference 7, the geometry was not optimized in any way and merely provided sufficient input to the stress analysis program. No provision was made in the model for achieving adequate sealing between the extended root shanks. Also, the firtree fixing shown in Figure 4.31 of reference 7 was a schematic representation only and is probably somewhat marginal in its small radial dimensions.

In order to provide a basis for a critical evaluation of the blade root and disc attachment, the blade root design illustrated in Figures 13, 14 and 15 of Appendix B was devined.

Figure 13 shows the blade platform at 17.36 cm (6.8355 in.) radius superimposed on the root section profile. The dotted lines on the drawing show the extended root section.

Figure 14 shows the blade root design as viewed along the axis of the turbine. The proposed design has been superimposed on the reference 1 assumed model for convenience and ease of comparison.

Figure 15 shows the blade root design viewed normal to the blade stacking line in the tangential direction.

Referring to Figure 13, the extended root section, shown dotted, provides full width sealing between blade roots fore and aft of the narrow web member. The resulting I-beam shape confers increased section modulus to the extended root section and effects efficient transfer of stress from blade to extended root. The cross-sectional area of the extended root shank (.826 cm^2) (0.128 $in.^2$) is roughly comparable to that of the reference 1 assumed model (.774 cm^2) (0.120 $in.^2$).

The blade root design illustrated in Figures 13, 14 and 15 of Appendix B provides the initial design basis for estimating the thermal conditions of the blade root and disc. The scale used in the figures is approximately 7.5 times full size.

A preliminary scoping stress analysis of the disc and blade attachment has been performed and the pertinent stresses are given in Table 2 of Appendix B. These stresses will be subjected to further examination when the thermal conditions at the disc and blade root have been developed. Although the centrifugal stresses in the extended root (195.4 MPa) (28,337 psi) and firtree (208.4 MPa) (30,215 psi) are higher than the value at the blade root section (112 MPa) (16,243 psi) it is expected that they will be found to be acceptable at the lower metal temperatures expected in the root region.

8.3.2 POWER TURBINE

As discussed in Section 7.0 two new power turbines, an eight stage 9,000 rpm machine for generator drive application and a 15 stage 3600 rpm direct mechanical drive turbine have been defined to replace the 12 stage 6000 rpm first and second definition design. The new designs were derived by a simple scaling process from the earlier 6000 rpm design, maintaining similar values of load and flow coefficient.

Load and flow coefficients had been deliberately chosen to be higher than optimum from an efficiency standpoint to achieve compactness. However, the compromise in efficiency ($<2\%$) was judged to be acceptable.

The 6000 rpm power turbine was hitherto not developed to the same degree as the high pressure turbine, the first stage rotor blading of which was defined and evaluated in some detail in the first year program. During the second year, however, the last stage of the power turbine has been evaluated in further detail by Westinghouse Combustion Turbine Systems Division. This evaluation was based on the earlier 6000 rpm 12 stage design and the results extrapolated to the new 9000 rpm and 3600 rpm designs.

From the aerodynamic standpoint, the distinguishing features of the low pressure turbine are the high stage load coefficients $\psi = \frac{\Delta h/\text{stage}}{U^2/2g\ J}$ in the order of 3.5 to 4.5 at the mean diameter, and the small axial blade widths, approximately 3/4 inch. These are due on the one hand to the large number of stages associated with the use of helium and, on the other, to the need for compactness in axial length.

Thus it was necessary to trade with respect to the front and back end, to arrive at a reasonable choice of hub reaction and exit swirl in the last stage. A variation in load coefficient, at the mean diameter, of from 3.91 in the 1st stage to 3.32 in the last stage was selected. This in in line with load coefficients at the hub section of 4.69 in the 1st stage and 4.38 in the last. The exit swirl is 12.0 and 9.3 degrees and, in this stage, the reaction is .072 and .389 at the hub and tip.

The flow path, velocity triangles and boundary conditions for the last stage are defined by the tables and sketches contained in Appendix 3-1. Note that the velocity triangle calculation is in line with free vortex SRE. This is approximate, but is adequate for the preliminary draft of the stator and rotor blade.

As previously noted, the very short axial widths have a notable effect on the blade designs. The blade number is inversely related to pitching and axial width as -

$no \sim (S/W)^{-1} \times W^{-1}$

where S/W is specified, for preliminary purposes, by the Zweifel coefficient and the velocity triangles. Thus for given conditions, and an acceptable Zweifel coefficient, the number is inversely related to the width. As shown by the tables for the 12 stator vane and rotor blade, there are 116 stator vanes corresponding to approximately 2 cm (0.8 inch) axial width and 140 rotor blades corresponding to approximately 2.3 cm (0.9 inch) axial width. This very large number of blades tends to increase the blockage associated with the thickness of the trailing edge. The 0.4 mm (0.015 in.) trailing edge thickness corresponds to approximately 5% blockage in the rotor and stator blade row. Though 0.4 mm (.015 in.) thicknesses may appear very small, with such very small blade widths they are probably required.

Blade section data for the stator vane and for the rotor blade are contained in Appendix C. In each case, these include a tabulation of blading data, the computer printout of the blade coordinates together with geometric and mechanical data for a number of radius positions, blade section sketches, surface velocity plots, and streamline plots.

Referring to the velocity diagrams for the stator vanes, the suction surface diffusion is somewhat higher than desirable at the 37.8 cm (14.9 inch), tip radius position. This is due to the low solidity, corresponding to a Zweifel coefficient of 0.89 versus 0.76 at hub, and to the lower acceleration at the tip. Here the ratio of exit to inlet velocity is 1.96 compared to 2.34 at the hub. (See velocity triangles). Also note that the surface

diffusion would be much less severe in the trailing edge region (.6 M/WIDTH 1.) if the machine number were higher, due to the beneficial effect of the compressibility in this region. (The flow is essentially incompressible, approximately 1676 m/s (5500 fps) acoustic velocity. These comments also apply to the velocity diagrams for the rotor blade. The solidity corresponds to Zweifel coefficients of 0.90 and 0.86 at the hub and tip respectively. The exit to inlet velocity ratios are 1.10 and 1.88 respectively at the hub and tip.

The high suction surface diffusion is associated with the severity of the design and could be reduced to a limited extent by increasing the solidity (W/S) but as -
W/S $\sim$ (number of blades) * W

this would call for an increase in the number of blades and/or the widths of the blades. However, increasing the number of blades would tend to increase the blockage. Improvement could also be made by modifying the velocity triangles to increase the acceleration, particularly at the stator tip and rotor hub, by reducing the load coefficient. This would probably give greater improvement than the foregoing change in solidity, but would call for an increase in the number of stages. While some improvement could also be made by modifying the blade sections, the gain would be small.

In a more detailed design using controlled vortex (instead of the free vortex RE assumed) it would be possible to improve the velocity triangles, particularly in the region of the rotor hub. This would reduce the diffusion at the hub of the rotor blade.

It is probable that the total efficiency of the 12 stage turbine would be on the order of 88-90 percent, depending on the extent of optimization and manufacturing refinement. Generally this is in line with radial clearances on the order of 0.002 mm/mm tip dia., 0.38 mm (0.015) trailing edge thickness and 750-1000 nm (30-40 μ in) surface finish.

A comparison of the stress parameters with those for the last stage of W251X reveals that the disc and blade stresses are low. (See tabulation of mechanical data at the end of Appendix C.) The blade centrifugal stress is proportional to N^2 A which is 70.5 x 10^6 compared to 562.0 x 10^6 in the W251X. The disc stress depends in large part on the rim speed and is 183 m/s 602(ps) versus 271 m/s (890 fps) in the W251X. On the other hand, due to the short axial widths it appears that the bending stress is generally higher than in Westinghouse Combustion Turbine Systems Division designs. The maximum bending stress is approximately 69 MPa (10,000 psi) in the rotor blade and probably less than 138 MPa (20,000 psi) in the stator vanes depending on how they are secured by the shrouds.

Eight Stage 9000 RPM Turbine

An examination was made of the last stage of the eight stage, 9000 rpm turbine. This was to determine the change in the blading design with respect to the 12 stage, 6000 rpm turbine.

As shown by the flow path sketch contained in Appendix O, the mean radius was set at 27 cm (10.62 in.) to give the same mean radius load coefficients as in the 12 stage design. As the blade heights are the same, 5.8 cm (2.3 in.) in the 1st and last stage, the flow coefficient is also roughly the same. The only notable change is in the hub to tip radius ratio. In the last stage the ratio is .724 compared to .772 in the 12 stage. Due to this change the load coefficient at the hub position is slightly higher, 4.77 versus 4.38 in the case of the last stage.

Referring to the velocity triangles (Appendix 3-2) the angles are roughly the same, in fact the only notable difference is in the increase in exhaust swirl (about 2 degrees more swirl) and the slightly lower reaction at the hub (0.4 versus .07). Also the exhaust velocity is about 25% higher.

Thus, if the blade widths are the same, the rotor and stator blades will be almost exactly the same as in the 12 stage. Note however that the blade centrifugal stress will be higher in ratio of N^2A = 127.7 x 10^6 to N^2A = 70.5 x10^6 (but still less than a quarter of the 562 x 10^6 W251X value),

the bending stress will be somewhat higher, and it will be more difficult to mount the blades in the smaller radius disc.

15 Stage - 3600 RPM Turbine

Similarly a design for 3600 rpm, with 15 stages, would have nearly the same stator and stator blades assuming equal blade widths. The mechanical stresses would be lower and it would be easier to mount the rotor blades in larger radius discs. Due to the higher radius ratio, the aerodynamic loading would be less severe at the rotor hub. Also the exhaust velocity would be lower.

8.3.3 FIRST COMPRESSOR STAGE

The compressor designs defined for the first and second definition CCCBS concepts generated in the first year program were derived from earlier designs developed by Westinghouse Combustion Turbines Division in the MGCR program. (Reference 8. The MGCR (Marine Gas Cooled Reactor) program was funded by the Maritime Administration during the early 1960's and employed a direct cycle gas cooled reactor/gas turbine cycle using helium as the working fluid. The MGCR compressor data were adapted to the CCCBS requirements by assuming $\Delta P/P$ per stage to be proportional to the square of the mean blade speed and inversely proportional to the average gas temperature through the compressor. Flow coefficient was assumed to be 0.5, similar to the MGCR designs. While this scaling process was considered appropriate for the initial design concept development and was believed to provide a sound initial basis for component sizing, some greater assurance of the compressor design basis was sought in the second year program. To this end a design study of the low pressure compressor first stage has been performed by Westinghouse Combustion Turbine Systems Division compressor design personnel. The resulting first stage design is slightly smaller in diameter and greater in length than the earlier design but is easily accommodated in the CCCBS plant arrangement without requiring any overall length increase. The required number of L.P. compressor stages (14) is unchanged, confirming the general validity of the earlier design. The details of the redesigned first stage are discussed in the following paragraphs:

Stage Aerodynamic Selections

The stage aerodynamics are based on a symmetric velocity diagram at the mean blade height and free vortex tangential velocity distribution radially. These assumptions are consistent with the results used to optimize the "MGCR" high pressure compressor.

The selection of hub to tip diameter ratio, and the maximum "wall loading factor", which places a limit on the blade and vane aerodynamic loading, is a compromise between stage efficiency, stage work, and blade and disc stresses. The following design selections were made:

Flow Coefficient at Mean	0.55
Maximum Diffusion Factor	0.40
Inlet Hub to Tip Diameter Ratio	0.80
Inlet Blockage Factor	0.98

The basic assumptions used to complete the stage study were as follows:

Shaft RPM	18000
Fluid State Points at Inlet	
Flow	58.1 kg/s (127.9 lbs/sec)
Temperature	311^{o}K (560 ^{o}R)
Pressure	3.13 MPa (454 psia)

Stage Design

The design selections above result in a stage with 50 percent reaction at the mean blade height and constant axial velocity radially. To identify the stage work, blade and vane diffusion factor was chosen at the maximum of 0.4. The solidity of both blade and vane was initially chosen as 1.00, based on NACA 2-D cascade test data.

Iteration between the above aerodynamic design and sufficient mechanical design was done for a satisfactory overall stage configuration. To achieve this, the blade "load build-up" criteria and blade material selections were made to determine blade chords and preliminary disc shape.

Blade "Load Build-Up"	1.00
Blade Material (12% Chrom Steel)	AISI 403

Load build-up is defined as the ratio of actual magnification factor to allowable magnification factor. Minimum allowable magnification factor is derived from a Westinghouse design curve versus blade harmonic. Actual magnification factor is defined as the ratio of material fatigue strength to blade vibratory stress times a factor of safety of 1.75. High cycle fatigue strength as a function of mean stress, in this case centrifugal plus gas bending stress, was taken from Westinghouse materials property data.

The blade which evolves from this process has a chord which is tapered 14 percent from hub to tip, and a thickness/chord which is also tapered from hub to tip. The blade and vane design section geometries are tabulated on Table 8-8. Section profiles and section coordinates were developed from a circular arc mean line with W65 thickness distribution and are included in Appendix E.

Blade gas bending and centrifugal stress result in a total steady stress of 215 MPa (31,200 psi) at the blade base section of which 134 MPa (19,400 psi) is due to centrifugal force.

Tabulated on Table 8-9 is a summary of the important stress levels and overall stage design characteristics. The hub and tip radii tabulated in Table 8-8 for both blade and vane are equal. In fact, there would be some wall taper. If a constant hub diameter were chosen, blade grouping could be employed. If a constant mean diameter were chosen, the number of stages could be minimized. In either case the axial velocity would be held constant thru the compressor.

The overall compressor efficiency will be a function of both the individual stage efficiency and the compressor leaving loss. The performance for the first stage predicts an efficiency of 0.920. Based on a compressor polytropic efficiency of 0.920 and a leaving loss of 4 percent an 0.870 compressor efficiency results.

TABLE 8-8

BLADE AND VANE SECTION GEOMETRIES

NUMBER OF BLADES/ROW	49
NUMBER OF VANES/ROW	48
STAGE WIDTH	2.300 Inches
AXIAL CLEARANCES	0.125 Inches
BLADE HUB CF STRESS	19400 psi
BLADE HUB GAS BENDING STRESS	11800 psi
BLADE FREQUENCY (0.025 Root Extension)	2429 cps

TABLE 8-9

BLADE STRESSES

BLADE DESIGN SECTION GEOMETRY

RADIUS	CHORD	CAMBER	STAGGER	SOLIDITY	T/C
7.163	1.134	32.63	25.35	1.235	.160
8.058	1.050	23.28	37.89	1.016	.095
8.954	0.972	17.09	46.67	0.847	.030

VANE DESIGN SECTION GEOMETRY

RADIUS	CHORD	CAMBER	STAGGER	SOLIDITY	T/C
7.163	1.094	23.50	41.09	1.167	.100
8.058	1.094	23.50	37.78	1.037	.100
8.954	1.094	23.50	34.91	0.933	.100

8.3.4 CRITICAL SPEED ANALYSIS

The critical speed analysis of the 70,000 hp CCCBS for the second year was based on the Year 1 Second Definition, with variations of the power turbine staging and operating speeds to reflect the thinking and changing criteria of the second year of study.

Initially the critical speed analysis was conducted for the engine as defined at the end of Year 1 excpet that the power turbine was changed from the first year design of 12 stages, 66.04 cm (26 in.) mean diameter and 6000 rpm to 8 stages, 53.92 cm (21.23 in.) mean diameter and 9000 rpm. In lieu of inertia properties of the individual rotor disks, which were not available, the swept volume of the blades was considered to be 30 percent dense as compared to the shaft materials. The original blade width (axial) was used, and the interstage (axial) spacing was increased such that the reduced number of stages occupied the same shaft length.

Subsequently, analysis was conducted on two other versions of the power turbine. One analysis was made of a 9000 rpm, 8-stage turbine with the same mean diameter 66.04 cm (26.0 in.) as the original 6000-rpm turbine and blade heights reduced to 0.80 of the original 6000-rpm turbine. The second analysis was made of a 15 stage, 3600-rpm turbine.

The initial analysis of the CCCBS engine with the 8-stage, 9000-rpm power turbine was based upon the assumption that hydrodynamic foil type gas bearings would be used to support the various rotor spools of the engine. AiResearch experience has shown a tendency of foil type gas bearings to exhibit negative whirl ratio characteristics and, consequently, the analysis included negative as well as positive whirl consideration. As the study progressed and shock loads were defined and a relatively heavy 3600-rpm power turbine was added to the analysis, the decision was made to recommend the use of resiliently mounted hydrostatic solid geometry pad type gas bearings. The analysis performed is general in structure and applies equally to foil and pad type gas bearings, although, one type tends to exhibit negative whirl tendencies and the other, positive whirl tendencies. The only significant consideration is that given to the relative bearing stiffness of each type of bearing.

Generally, the pad type gas bearing would have a higher stiffness and would require more accurate control of that stiffness to avoid conflict between first and second critical speeds and the rotor operating speed.

The analyses were performed using an established and reliable computer program developed over many years of turbomachinery design. The mass and stiffness models for the CCCBS engine as originally conceived for the 9000-rpm power turbine variations are shown in Figures 8-8 through 8-11.

8.3.4.1 LOW AND HIGH PRESSURE SPOOLS

The initial analysis of the engine with the 9000-rpm reduced mean diameter power turbine indicated that the low-pressure (LP) compressor spool and the high-pressure (HP) compressor/turbine spool would operate too near the first bending mode. For reference purposes, a bearing spring rate of 350,252 N/cm (200,000 lb_f/in) was selected as being representative of foil-type gas bearings in this class of turbomachinery. It has been found to be good practice to operate turbomachinery with at least a 40 percent margin below the first bending critical speed. Using this reference, it can be seen from Figures 8-12 through 8-15 that the LP and HP spools as originally designed operate between 6 and 21 percent away from the first bending criticals. Of particular significance is the HP spool which operates 12 percent above the first bending critical when a negative whirl ratio is considered. It should be noted that negative whirl ratios result in lower bending critical speeds and this whirl phenomena is occasionally observed with the use of foil-type gas bearings but not with pad-type gas bearings.

The LP and HP spools were modified by stiffening the shafts and lightening their ends. It was also discovered that the disk-like portions of the shafts connecting the bearing journals and the larger center blading sections were more flexible than their flexural rigidities (EI) would indicate. The effect of this disk bending on the critical speeds was significant and was accounted for by including rotational springs of the proper stiffness in shaft models at the various disk locations. The modifications to the LP-spool included increasing the shaft wall thickness to 1.91 cm (0.75 in.), removing material

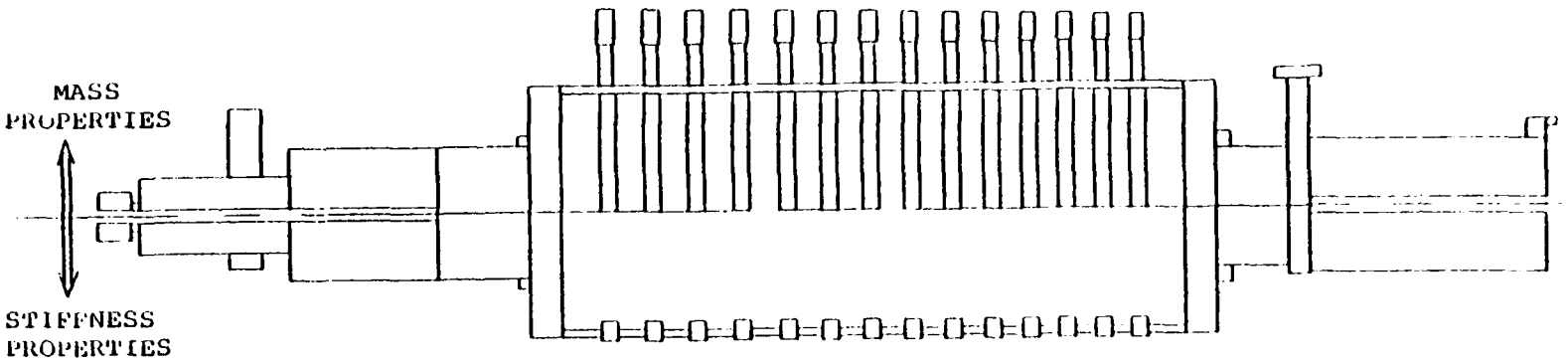

WESTINGHOUSE DWG. #7123430
18,000 RPM

Figure 8-8. CCCBS Engine Rotor Dynamics Model Low-Pressure Compressor, Standard Shaft

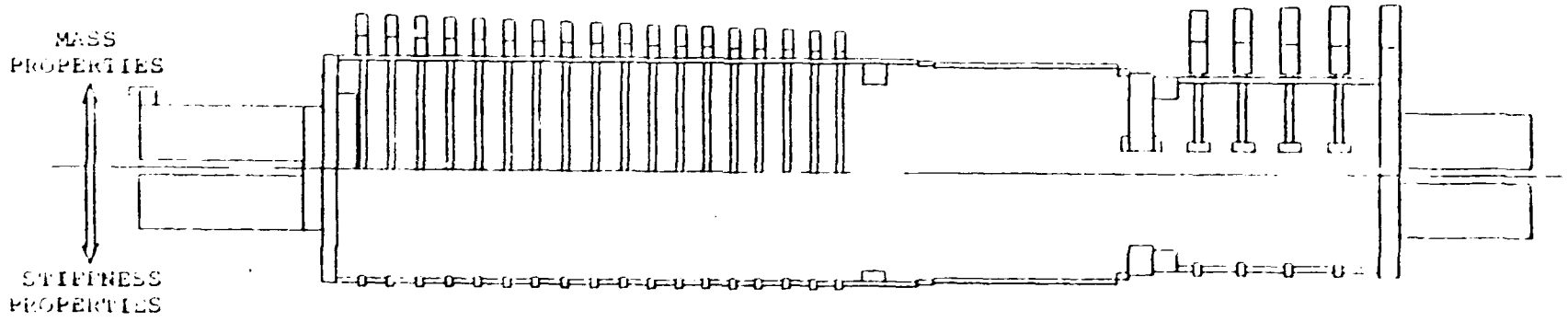

WESTINGHOUSE DWG. #712J430
18,000 RPM

Figure 3-8. CCBS Engine Rotor Dynamics Model High-Pressure Spool, Standard Shaft

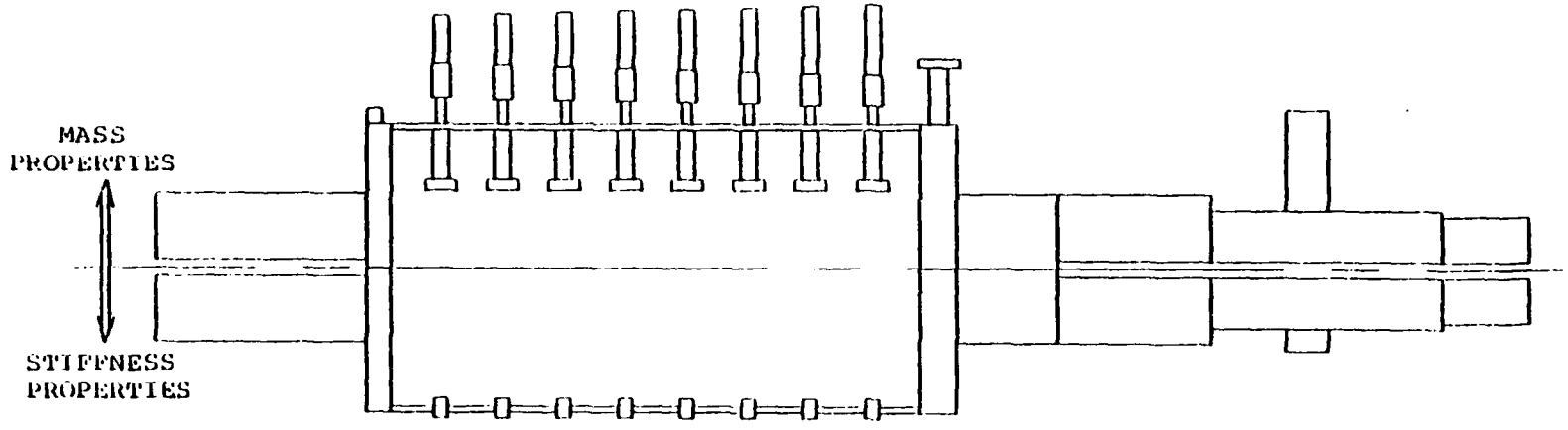

WESTINGHOUSE DWG. #712J430
CHANGED TO 8 STAGES AND
9000 RPM

Figure 8-10. CCCBS Engine Rotor Dynamics Model Power Turbine

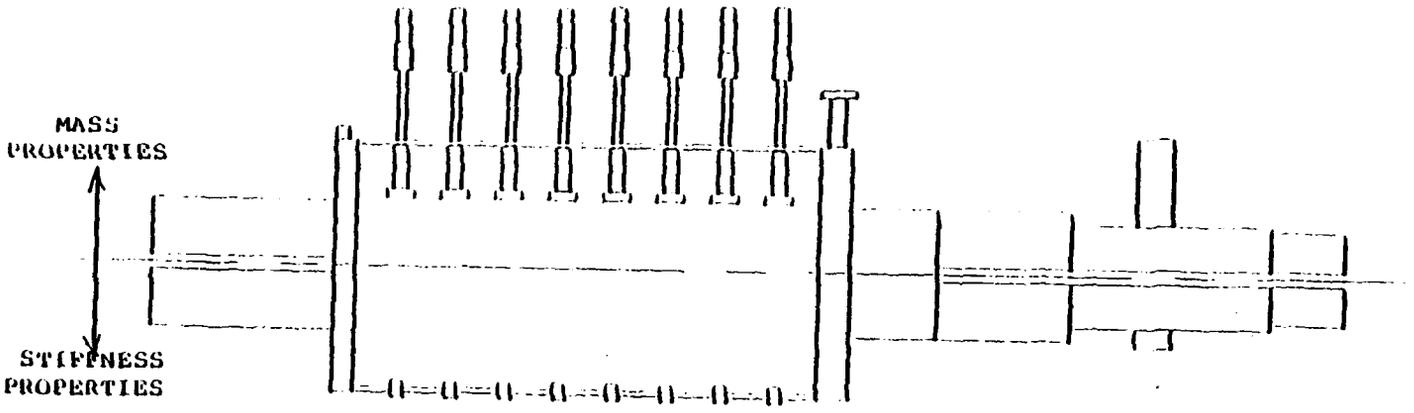

Figure 8-11. CCCBS Engine Power Turbine Model

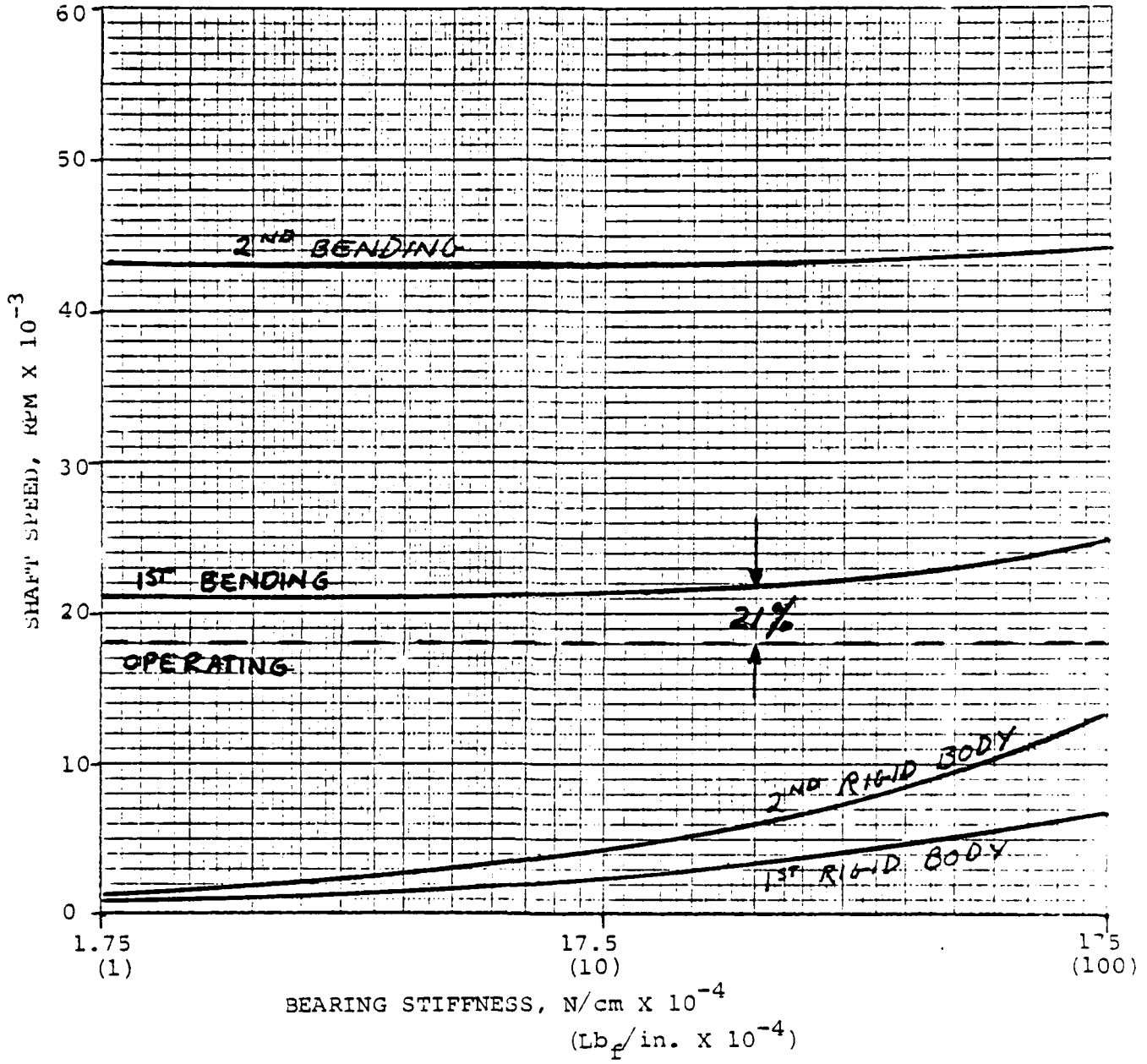

Figure 8-12. CCCBS Engine Critical Speeds Low-Pressure Compressor, Whirl Ratio = 1

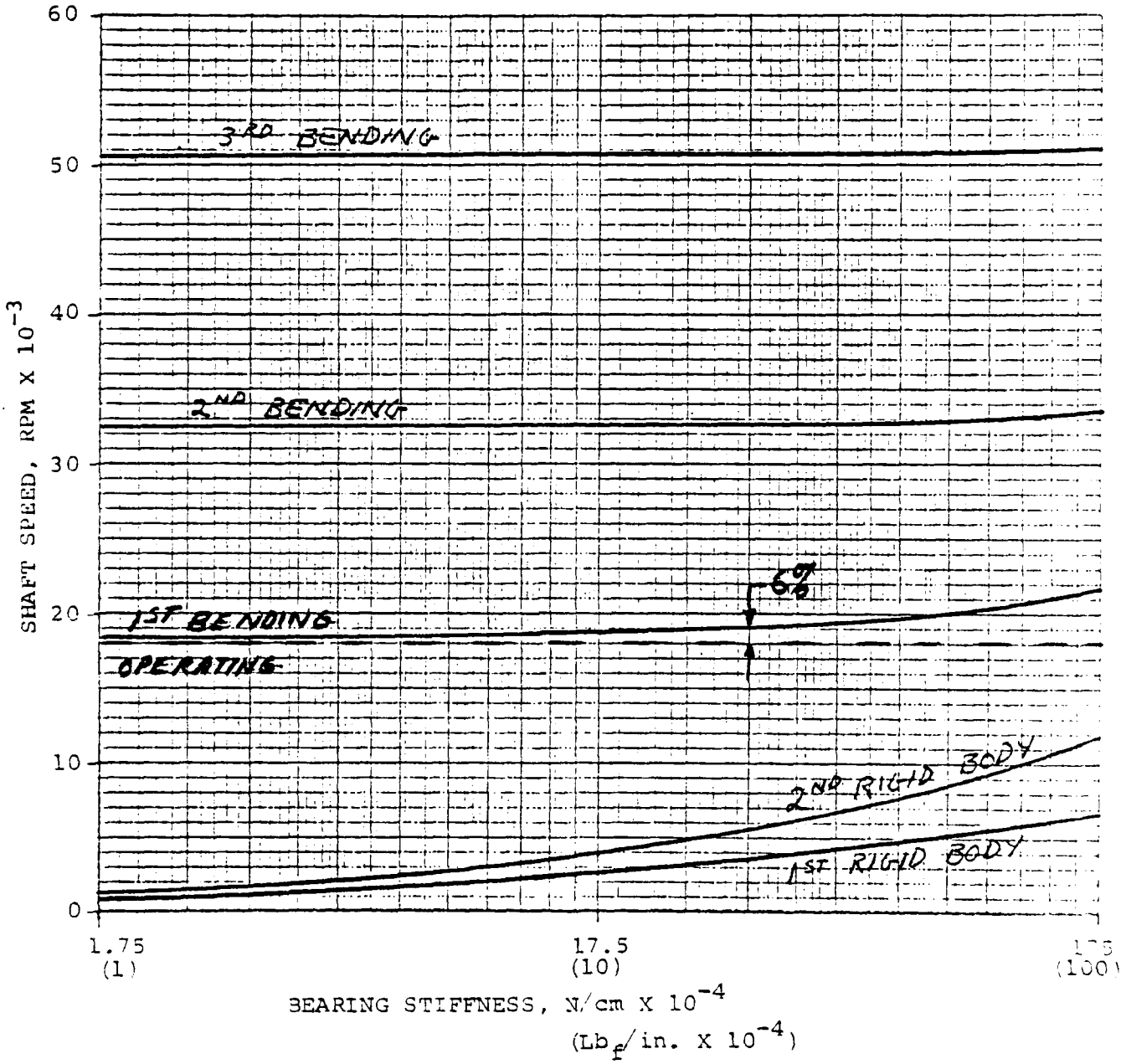

Figure 8-13. CCCBS Engine Critical Speeds Low-Pressure Compressor, Whirl Ratio = -1

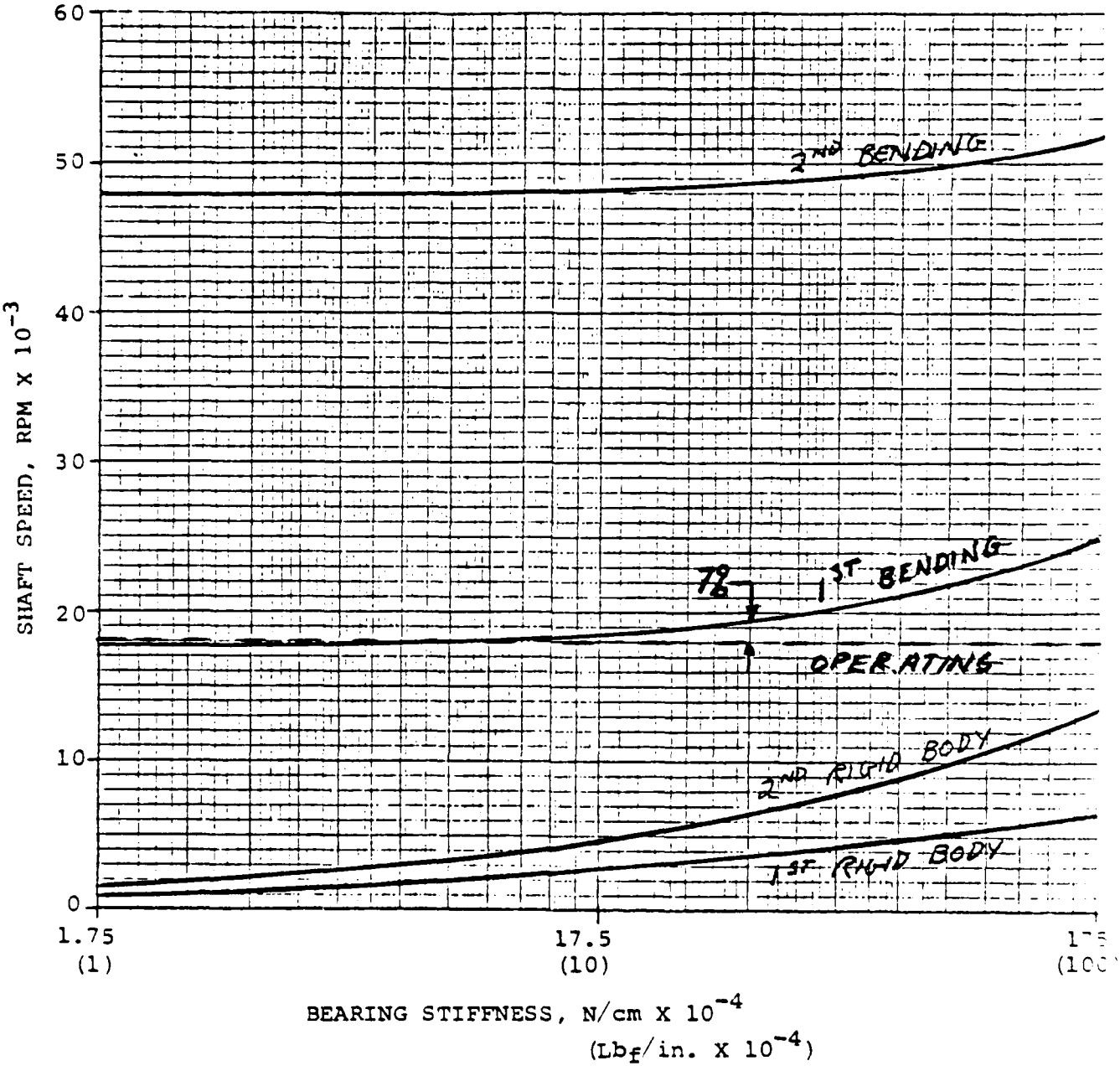

Figure 8-14. CCCBS Engine Critical Speeds High-Pressure Spool, Whirl Ratio = 1

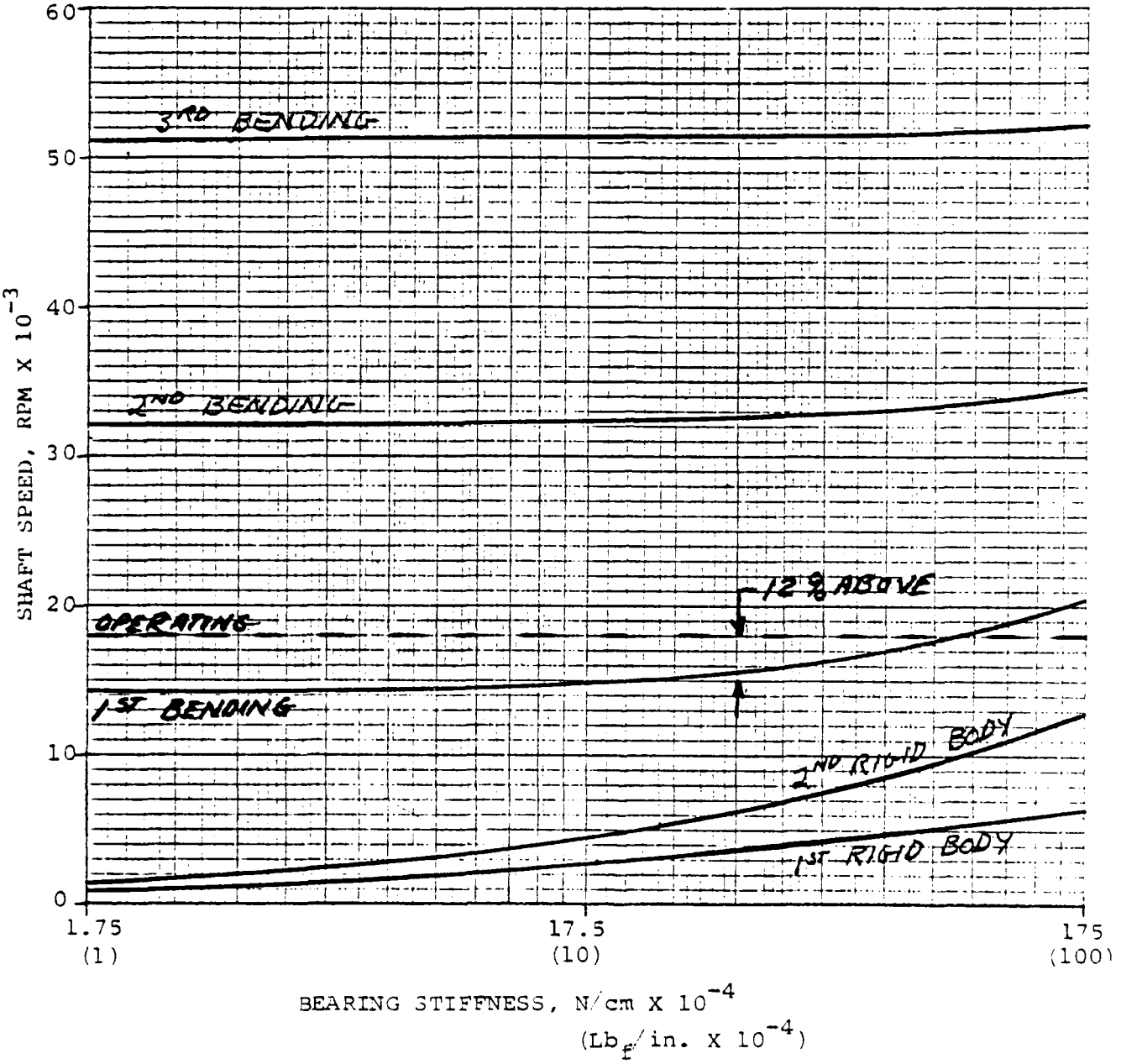

Figure 8-15. CCCBS Engine Critical Speeds High-Pressure Spool, Whirl Ratio = 1

from the inside of the bearing journals, and increasing material at the junctions of the center and end sections of the shaft to reduce the disk flexibility at these points. The HP-spool was modified by removing material from the inside of the bearing journals and thickening the wall of the center section to 2.54 cm (1.0 in.). The mass models of the modified spools are shown in Figures 8-16 and 8-17. The effect of these modifications is shown in Figures 8-18 through 8-21. For negative whirl ratios, the LP-spool has an operational speed margin 48 percent below the first bending critical, while the HP-spool has a margin of 42 percent. Positive whirl ratios provide margins of 81 and 93 percent for the LP and HP spools, respectively.

8.3.4.2 POWER TURBINES

The critical speed analysis of the 53.9 cm (21.23 in.) mean diameter 9000-rpm power turbine and the 66.04 (26.0 in.) mean diameter 9000-rpm power turbines indicated good margin between the operating and the first bending critical speeds. The least margin was 75 percent for the smaller power turbine and 62 percent for the larger power turbine operating with a negative whirl ratio. Positive whirl ratios provided 137 and 134 percent margin for the two turbines. The critical speed margins for the two turbines over a range of bearing stiffnesses of 17,512.6 N/cm to 1,751,268.0 N/cm (10,000 to 1,000,000 lb_f/in.) are shown in Figures 8-22 through 8-25.

Some applications of the CCCBS engine require a variable-speed power turbine. In those applications, it is desirable to have a low bearing spring rate so that the operating range of the turbine can be as broad as possible without encountering sustained operation at one or both of the rigid body critical speeds. For example, in Figure 8-22 a bearing stiffness of 350,252 N/cm (200,000 lb_f/in.) would produce first and second rigid body criticals of 3,200 and 5,000 rpm.

It would be good practice to avoid prolonged power turbine operation at or near these speeds so as to minimize bearing loads and rotor runout. If the bearing spring rate were to be reduced to 175,126 N/cm (100,000 lb_f/in.), the first and rigid body criticals would also be reduced to 2,100 and 3,500 rpm, thereby

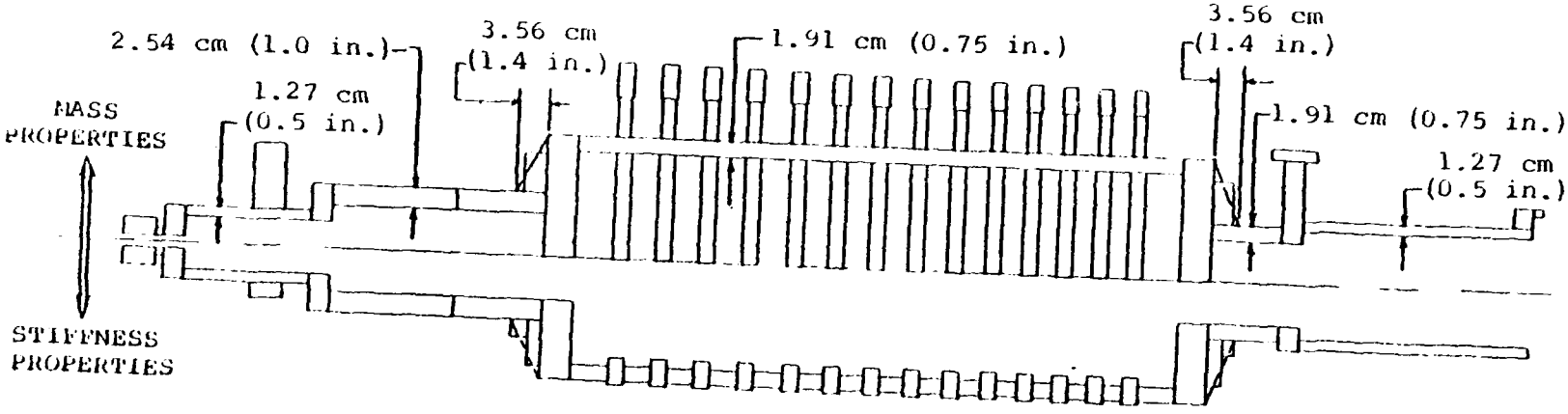

Figure 8-16. CCCBS Engine Rotor Dynamics Model Low-Pressure Compressor, Modified Shaft

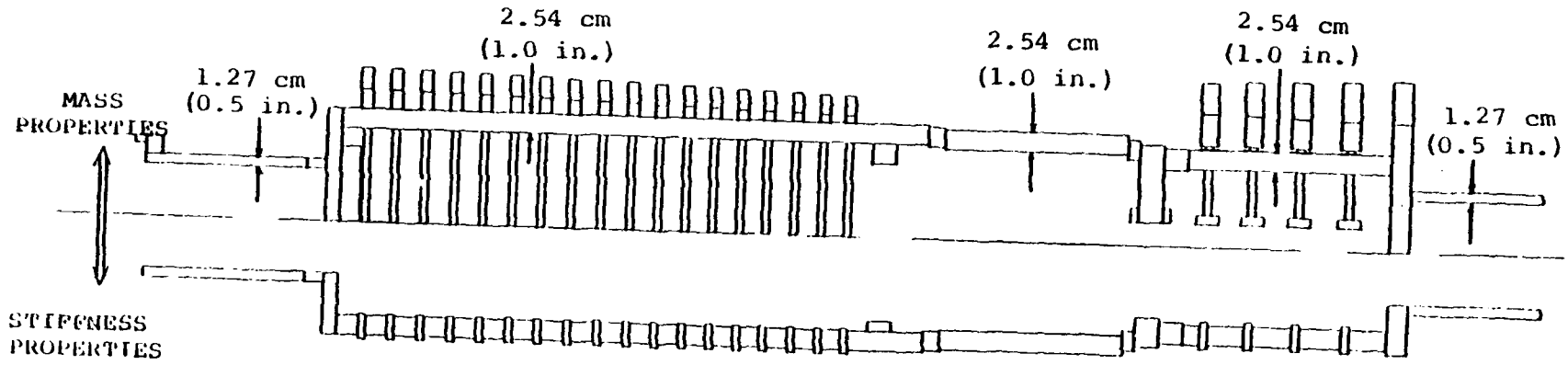

Figure 8-17. CCCBS Engine Rotor Dynamics Model High-Pressure Spool, Modified Shaft

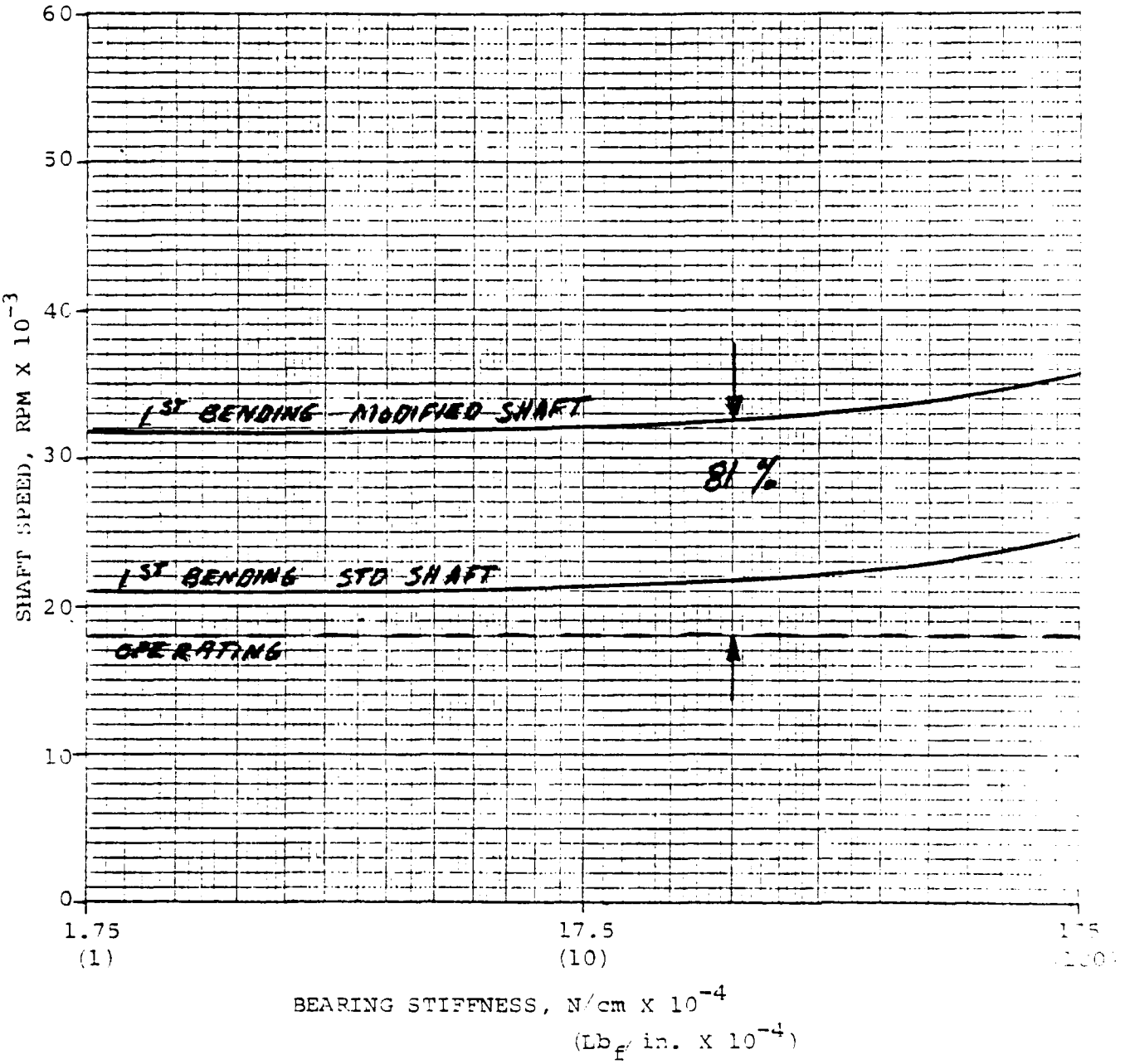

Figure 8-18. CCCBS Engine Effect of Shaft Modifications on First Bending Critical Low-Pressure Compressor, Whirl Ratio = 1

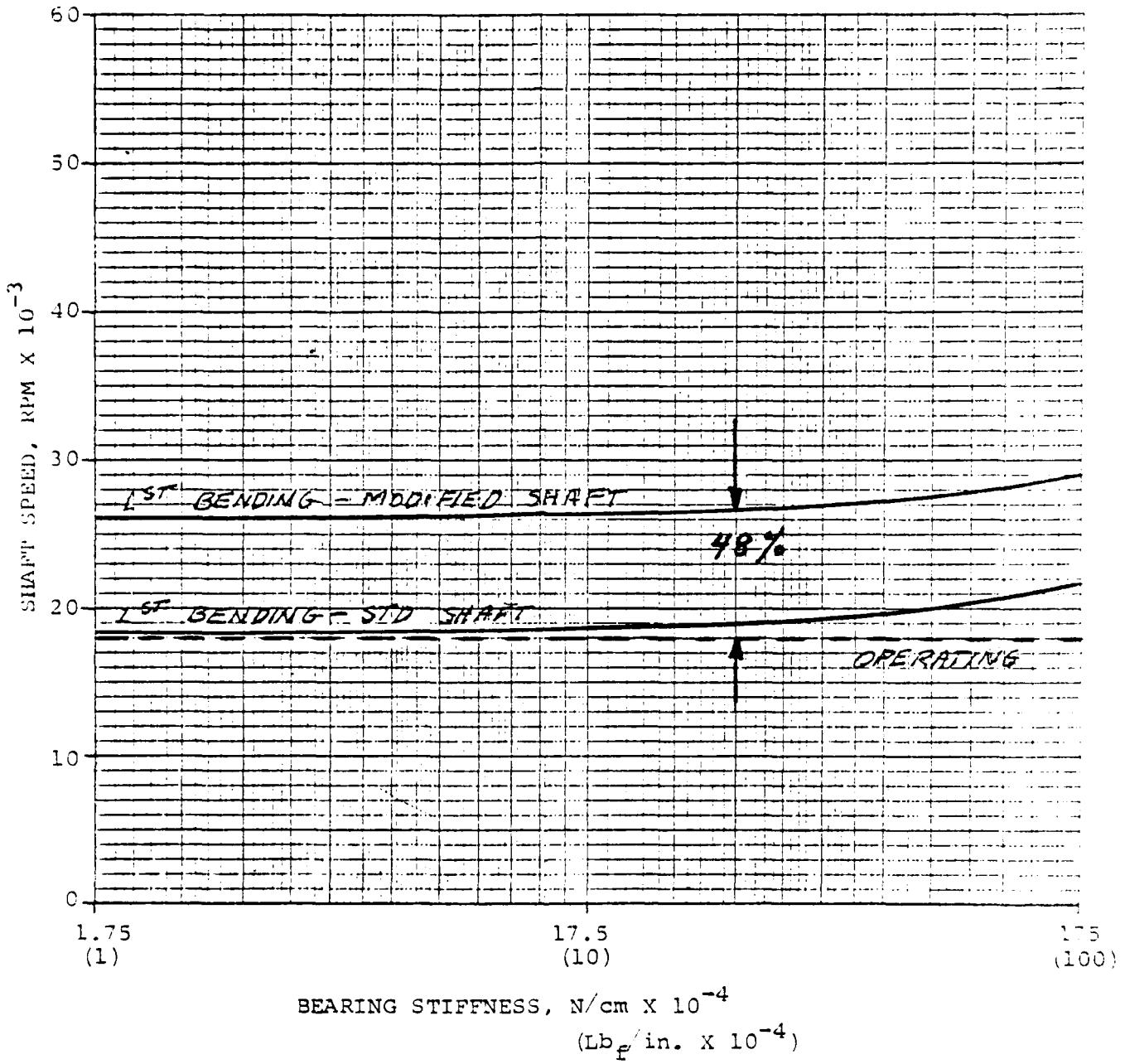

Figure 8-19. CCCBS Engine Effect of Shaft Modifications on First Bending Critical Low-Pressure Compressor, Whirl Ratio = -1

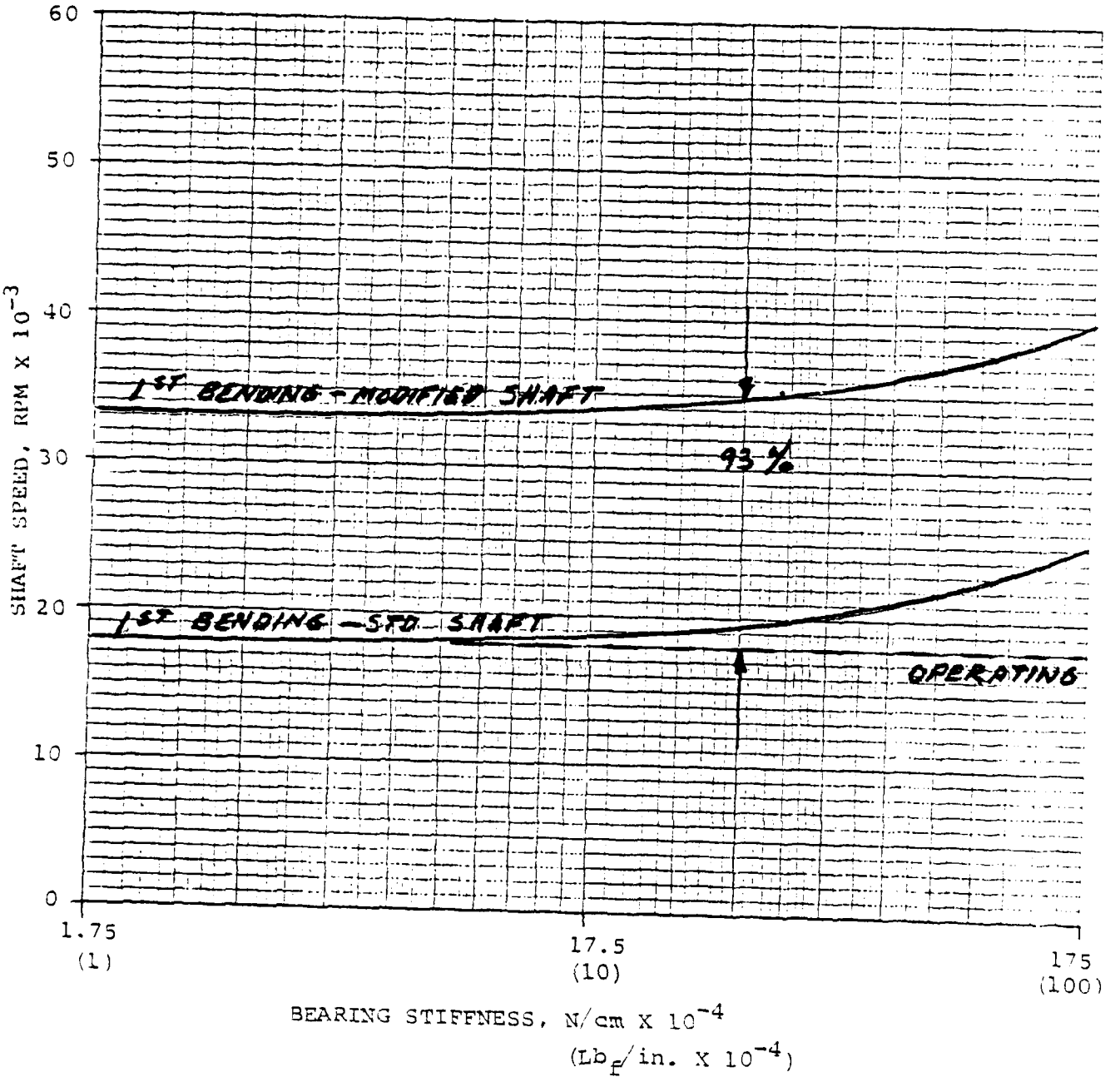

Figure 8-20. CCCBS Engine Effect of Shaft Modifications on first Bending Critical High-Pressure Spool, Whirl Ratio = 1

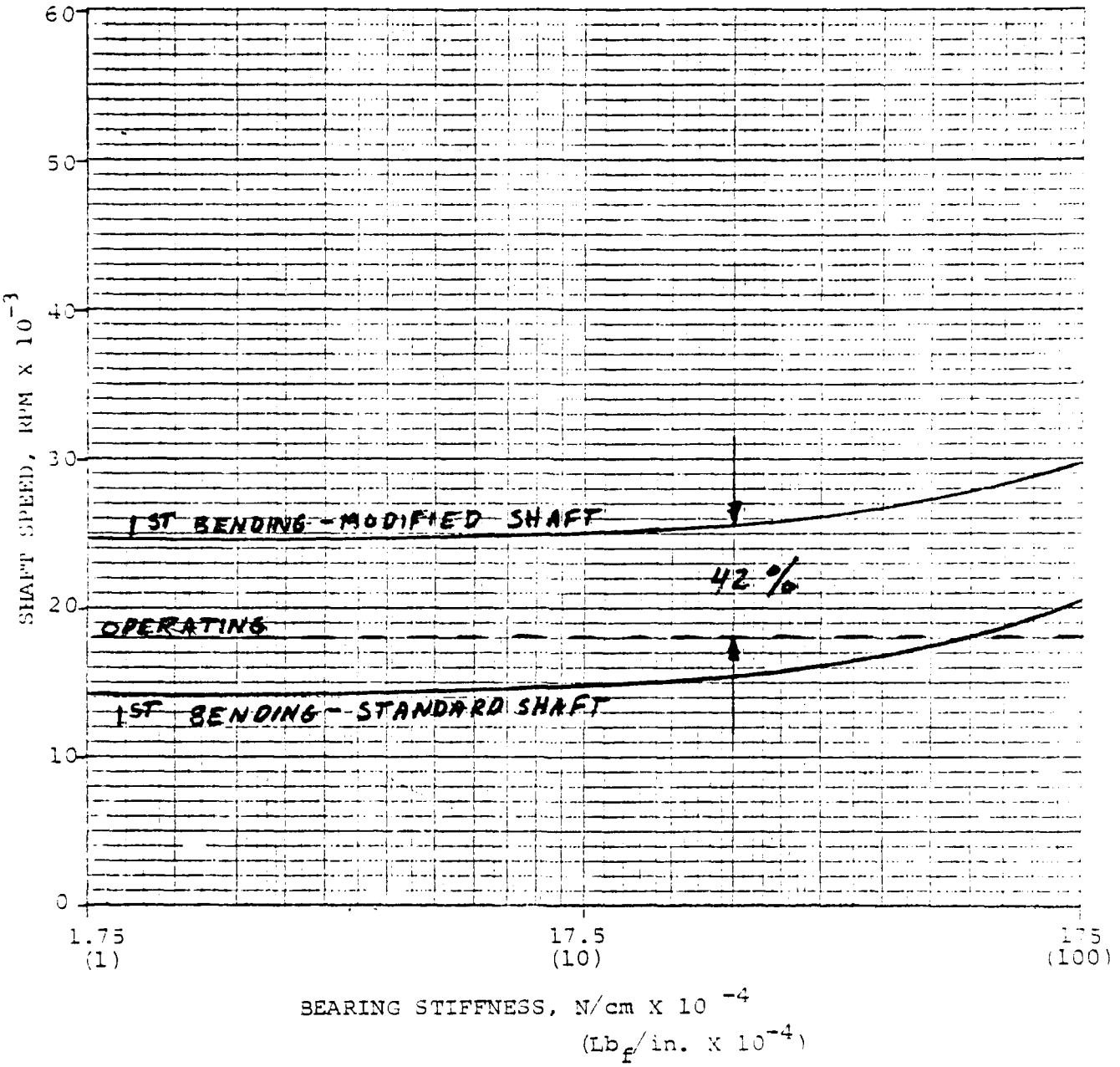

Figure 8-21. CCCBS Engine Effect of Shaft Modifications on First Bending Critical High-Pressure Spool, Whirl Ratio = -1

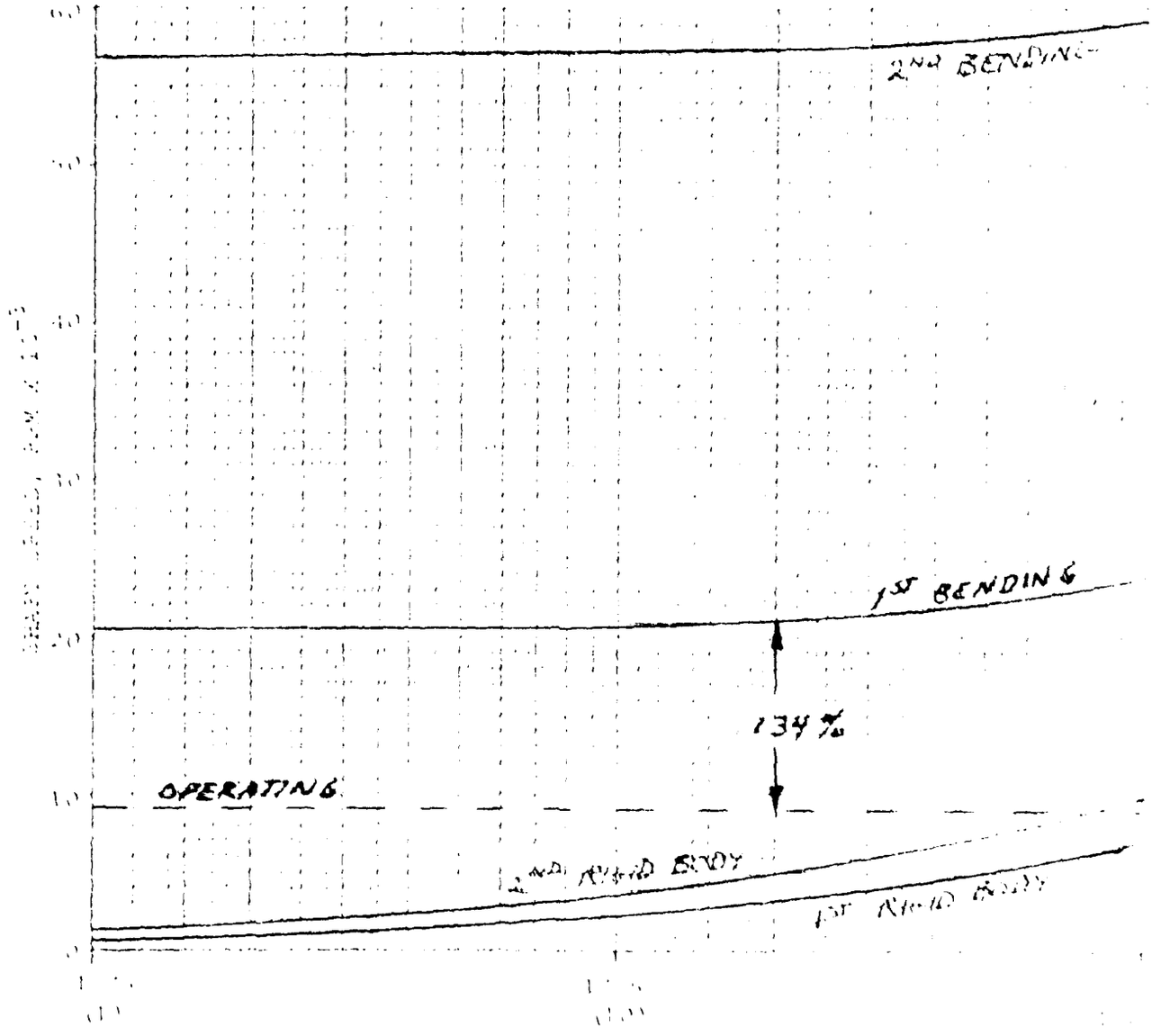
2ND BENDING
1ST BENDING
134%
OPERATING
2ND RIGID BODY
1ST RIGID BODY

Figure 3.2-2 [illegible]

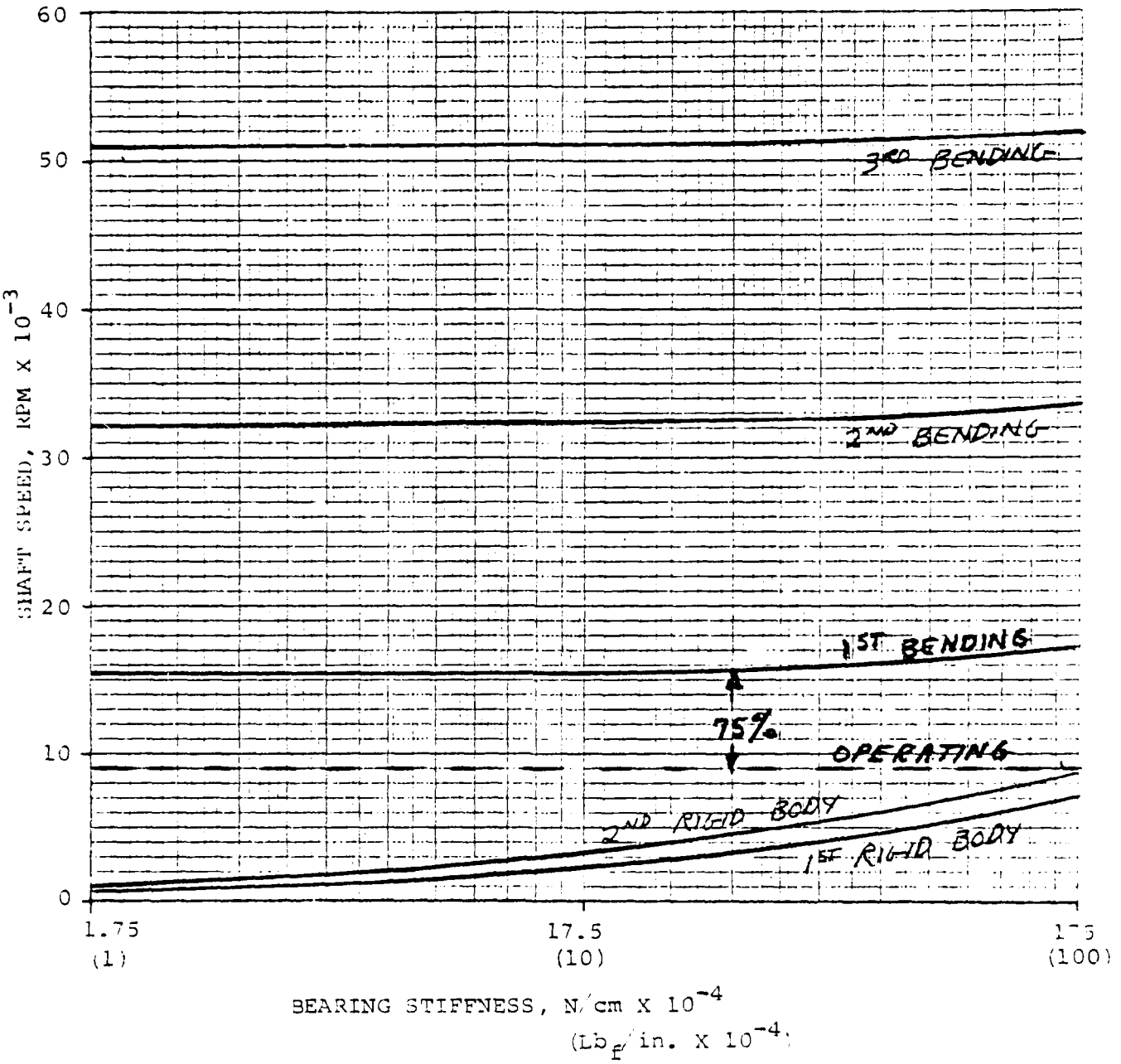

Figure 8-23. CCCBS Engine Critical Speeds Power Turbine, Whirl Ratio = -1 (9000 RPM, Diameter 53.9 cm)

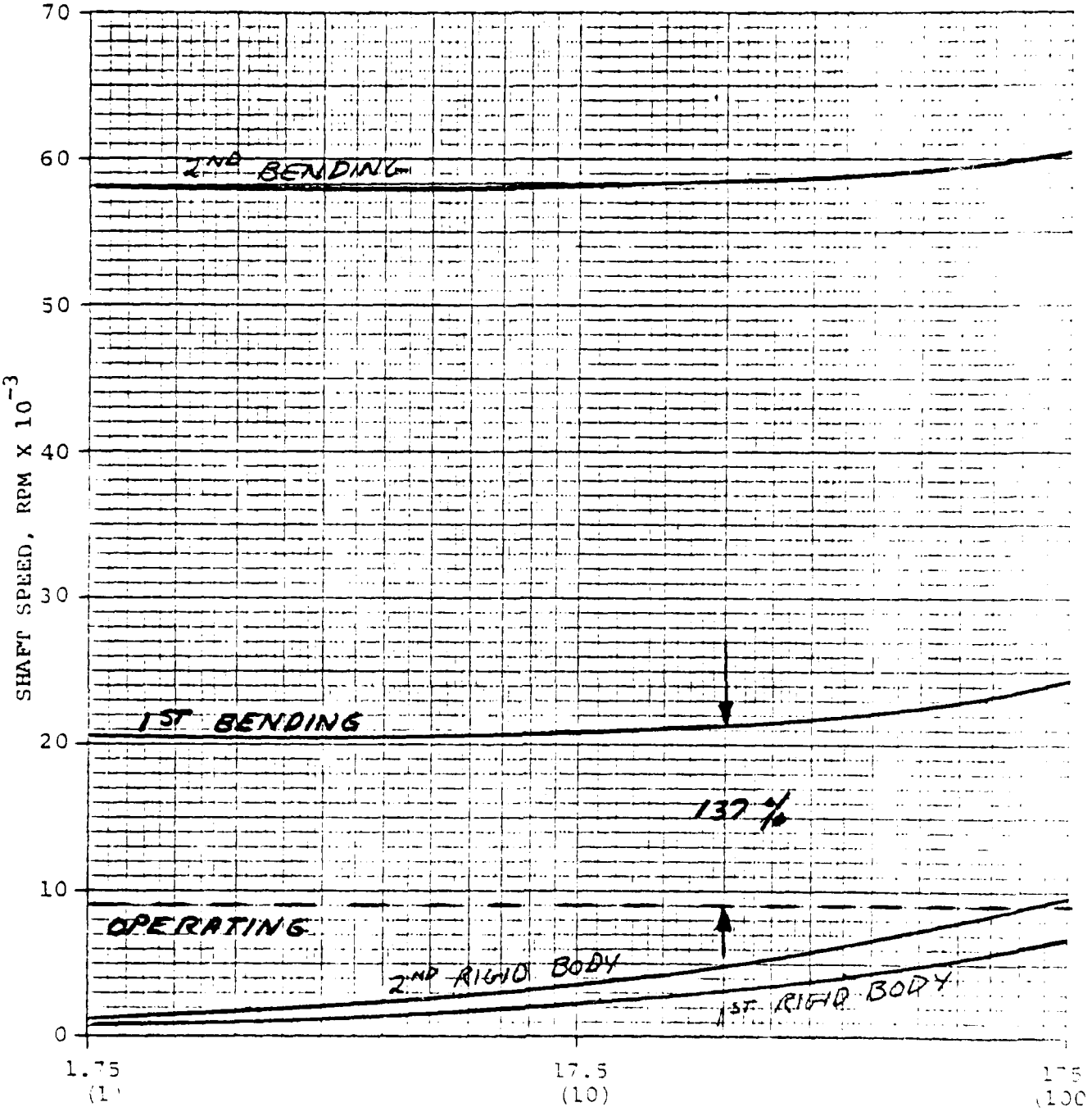

Figure 8-24. CCCPS Engine Critical Speeds Power Turbine, Whirl Ratio = 1 (9000 RPM, Diameter 66.04 cm)

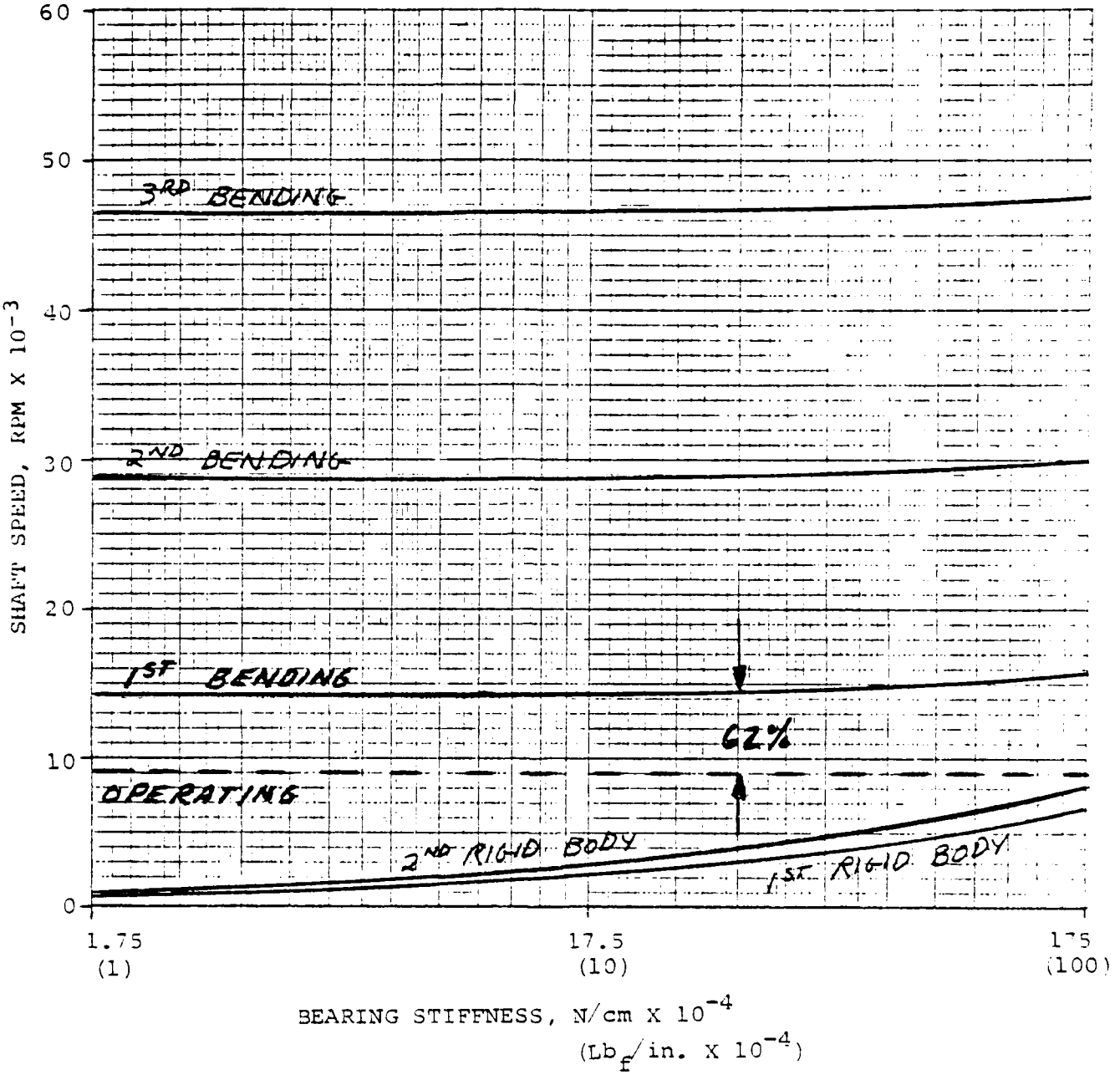

Figure 8-25. CCCBS Engine Critical Speeds Power Turbine, Whirl Ratio = -1 (9000 RPM, Diameter 66.04 cm)

permitting a larger operating range above 3,500 rpm where the turbine could be operated without high bearing loads and shaft runout. The disadvantages of the softer spring rates would be increased static and dynamic off-center operation of the power turbine shaft, seals, and aerodynamic components. The static off-center condition could be compensated by deliberate eccentricity designed into the bearing mounts.

A critical speed analysis of the 98.55 cm mean diameter (38.80-in.) 15-stage 3600-rpm power turbine as shown in Figure 7.4 was performed. The mass and stiffness model for the original configuration is shown in Figure 8-26. The critical speeds were established for both positive and negative whirl over a bearing stiffness range of 1.7513 N/cm (10,000 lb_f/in.). Since a margin of 40 percent above operating and 25 percent below operating is desired for successful shaft operation, the 17 percent margin is considered unacceptable. It is noted that the critical speeds determined for the positive whirl condition, as shown in Figure 8-27, are acceptable for first bending critical margin above the operating speed, but unacceptable for margin between the second rigid body critical and operating speed.

A preliminary determination of the static journal bearing loads for the original configuration indicated that the rear overhung 17.78 cm dia. (7.00 in.) journal bearing would be grossly overloaded and that a larger diameter bearing would be required. An increase in bearing diameter at the rear journal was also desirable from the standpoint of increasing the stiffness of the power turbine rotating group and increasing the margin between the first bending critical and operating speed for both positive and negative whirl modes.

In order to improve the critical speed margins and provide adequate bearing load capacity, the shaft geometry was changed by making its ends hollow, and enlarging its diameter in the region of the rear bearing. The modified mass and stiffness model is shown in Figure 8-29 and the resulting critical speed relationships are shown in Figures 8-30 and 8-31.

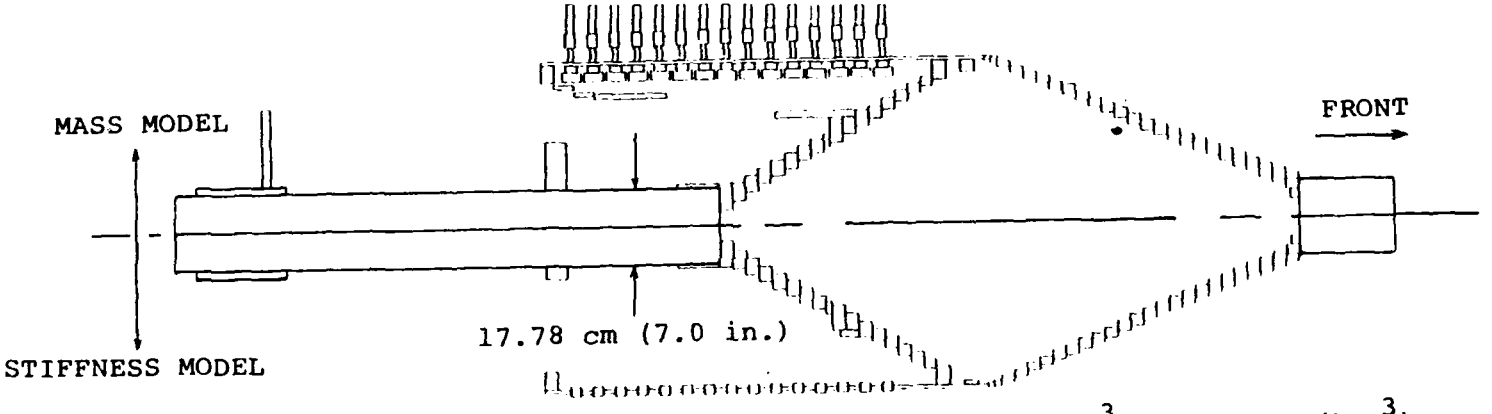

DENSITY = 7.8 g/cm^3 (0.283 lb$_m$/in.^{3})

MODULUS = 1.7926 x 10^{11} Pa (26 x 10^6 PSI)

SHAFT SPEED = 3600 rpm

Figure 8-26. CCCBS Engine 98.55 cm (38.8 in.) Power Turbine Rotor Dynamics Model

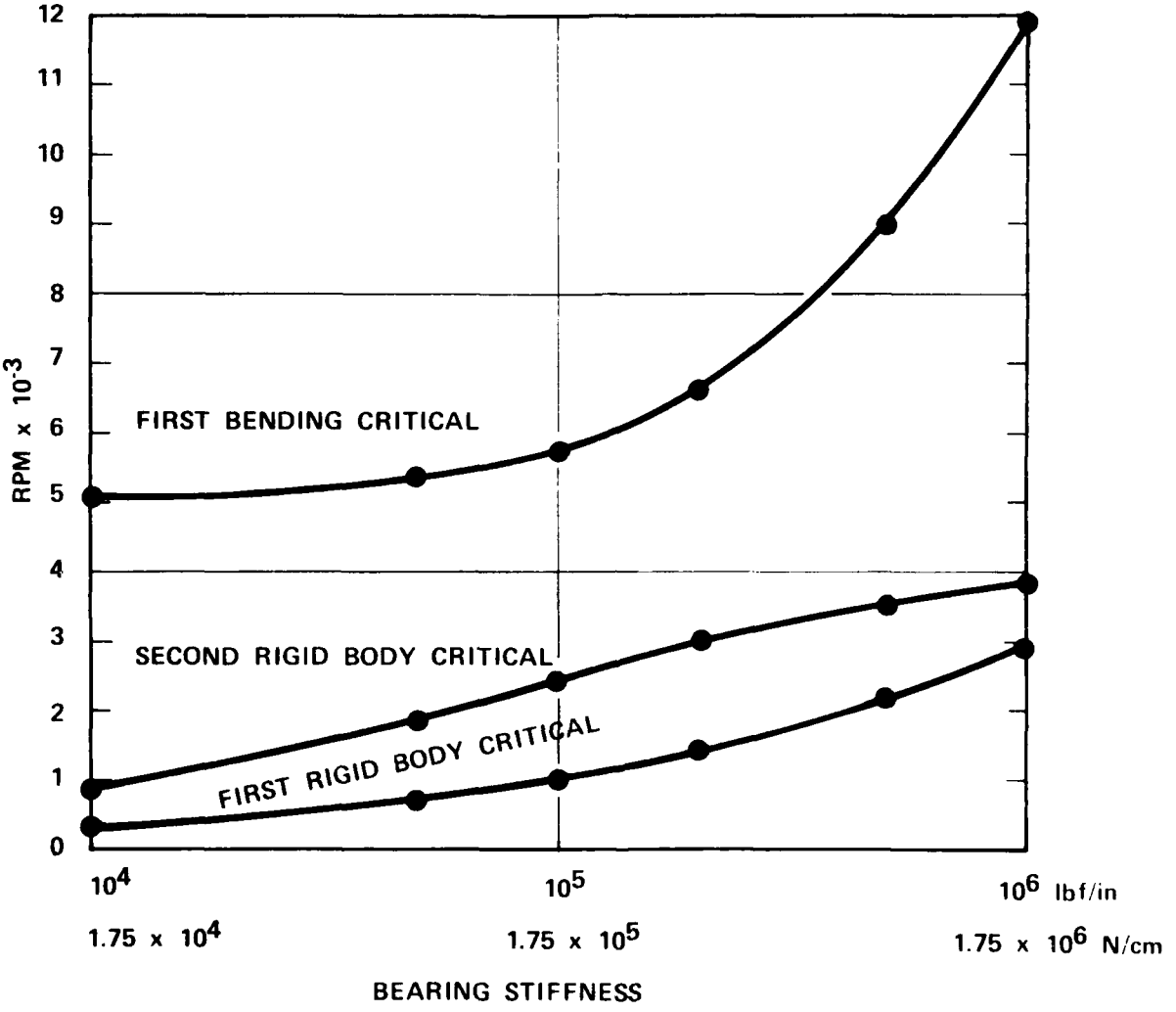

Figure 8-27. CCCBS Engine (38.8 in.) Power Turbine Critical Speeds, Whirl Ratio = 1

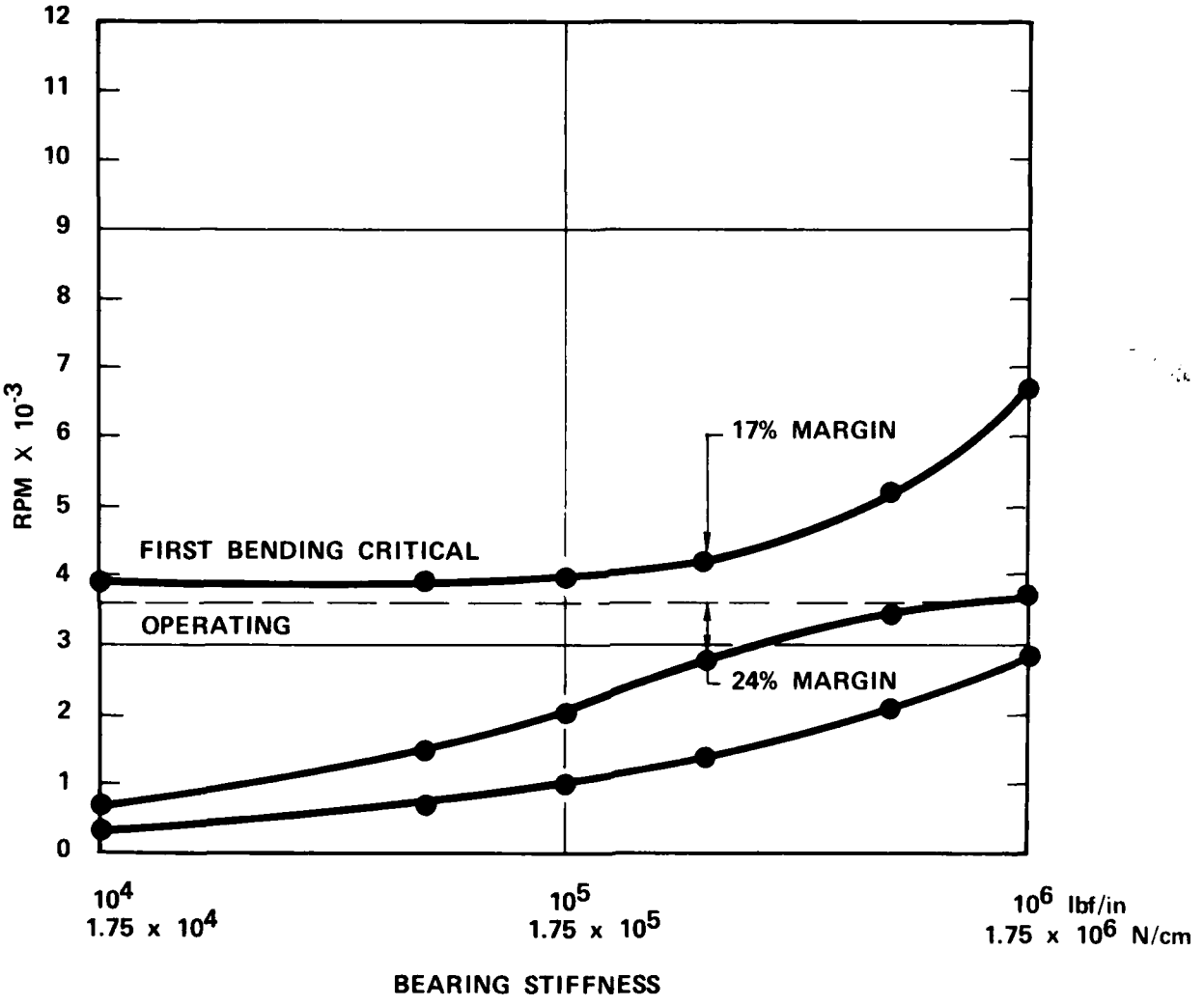

Figure 8-28. CCCBS Engine (38.8 in.) Power Turbine Critical Speeds, Whirl Ratio = -1

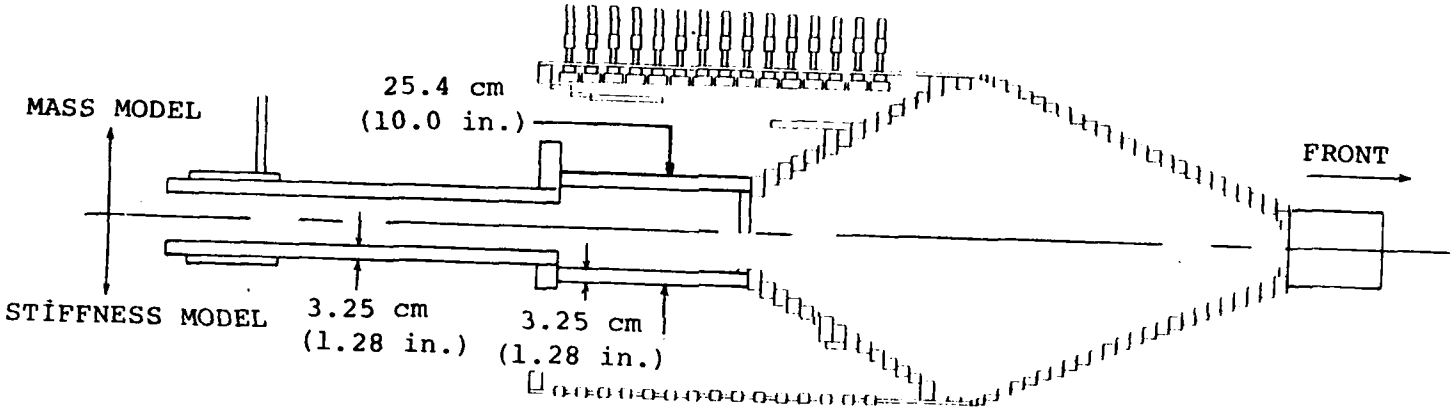

DENSITY = 7.8 g/cm^3 (0.283 lb$_m$/in.^{3})

MODULUS = 1.7926 x 10^{11} Pa (26 x 10^6 PSI)

SHAFT SPEED = 3600 rpm

Figure 8-29. Westinghouse CCCBS Engine 98.55 cm (38.8 in.) Power Turbine-Modified Rotor Dynamics Model

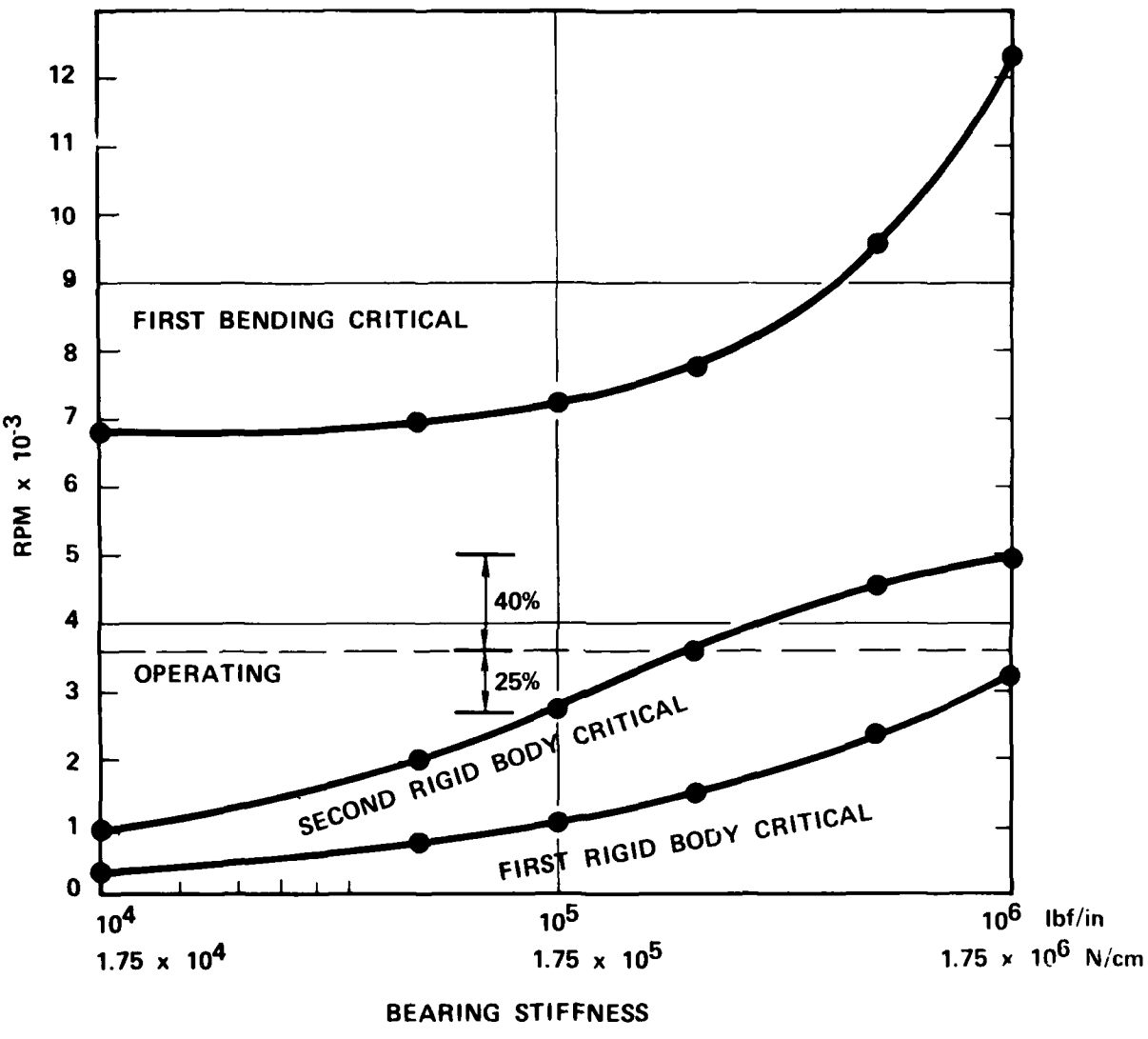

Figure 8-30. CCCBS Engine (38.8 in.) Power Turbine-Modified Shaft Critical Speeds, Whirl Ratio = 1

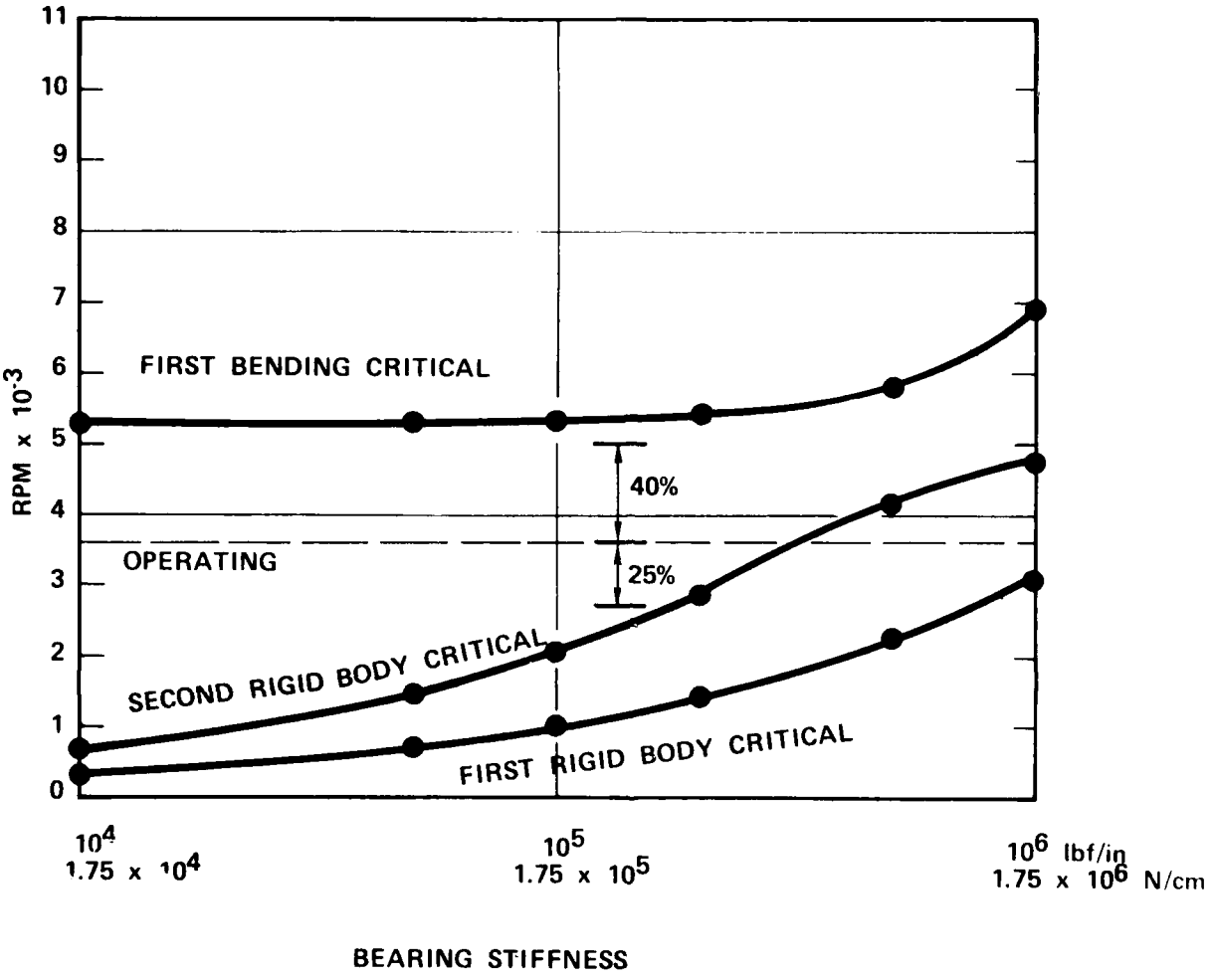

Figure 8-31. CCCBS Engine (38.8 in.) Power Turbine-Modified Shaft Critical Speeds, Whirl Ratio = -1

Sufficient margin between the first bending critical and operating speed is provided by the modified design for both positive and negative whirl modes; however, the first and second rigid body critical speeds have been correspondingly raised so that only bearing spring stiffnesses of 175,126 N/cm (100,000 lb_f/in.) and below would provide adequate margin if the rotor were to operate above both rigid body criticals. A relatively low spring rate of 175,126 N/cm (100,000 lb_f/in.) is not desirable on the 3600 rpm power turbine due to excessive rotor sag of 8.34 mm (0.033 in.) resulting from the static load of 14,612 N (3285 lb_f) on the overhung bearing. Any attempt to operate the rotor system with bearing stiffnesses above 175,126 N/cm (100,000 lb_f/in.) introduces other problems related to rotor unbalance. As an example, bearing loads due to rotor unbalance of an assumed 0.0254 mm c.g. eccentricity (0.001 in.) are shown in Figure 8-32. The loads are plotted as a function of bearing stiffness, and it is apparent that dynamic loads rapidly exceed acceptable levels above 175,126 N/cm (100,000 lb_f/in.) bearing stiffness. Although it would be desirable to operate the rotor system with bearing stiffnesses of 1.75 MN/cm (1 x 10^6 lb_f/in.) and a correspondingly small rotor sag of 0.08 mm (0.003 in.), it would be impossible to drive the rotor through the first rigid body critical without causing a failure of the bearings due to overlaod.

The seemingly impossible task of successfully mounting the current 3600 rpm power turbine design on gas bearings is not as negative as it first appears. The trade-offs of critical speeds, bearing load capacity, rotor sag, and rotor unbalance can be resolved by design change and an extensive analysis coupled with innovation. For example, the rotor sag can be greatly reduced by using a stiff mechanical bearing mount and designing the gas bearing with a thick gas film with a relatively soft initial stiffness that increases nonlinearly to limit the overall rotor displacement during passage through criticals. This option would, of course, increase the use of hydrostatic gas and would be one of the system trade-offs that would be investigated during detail design.

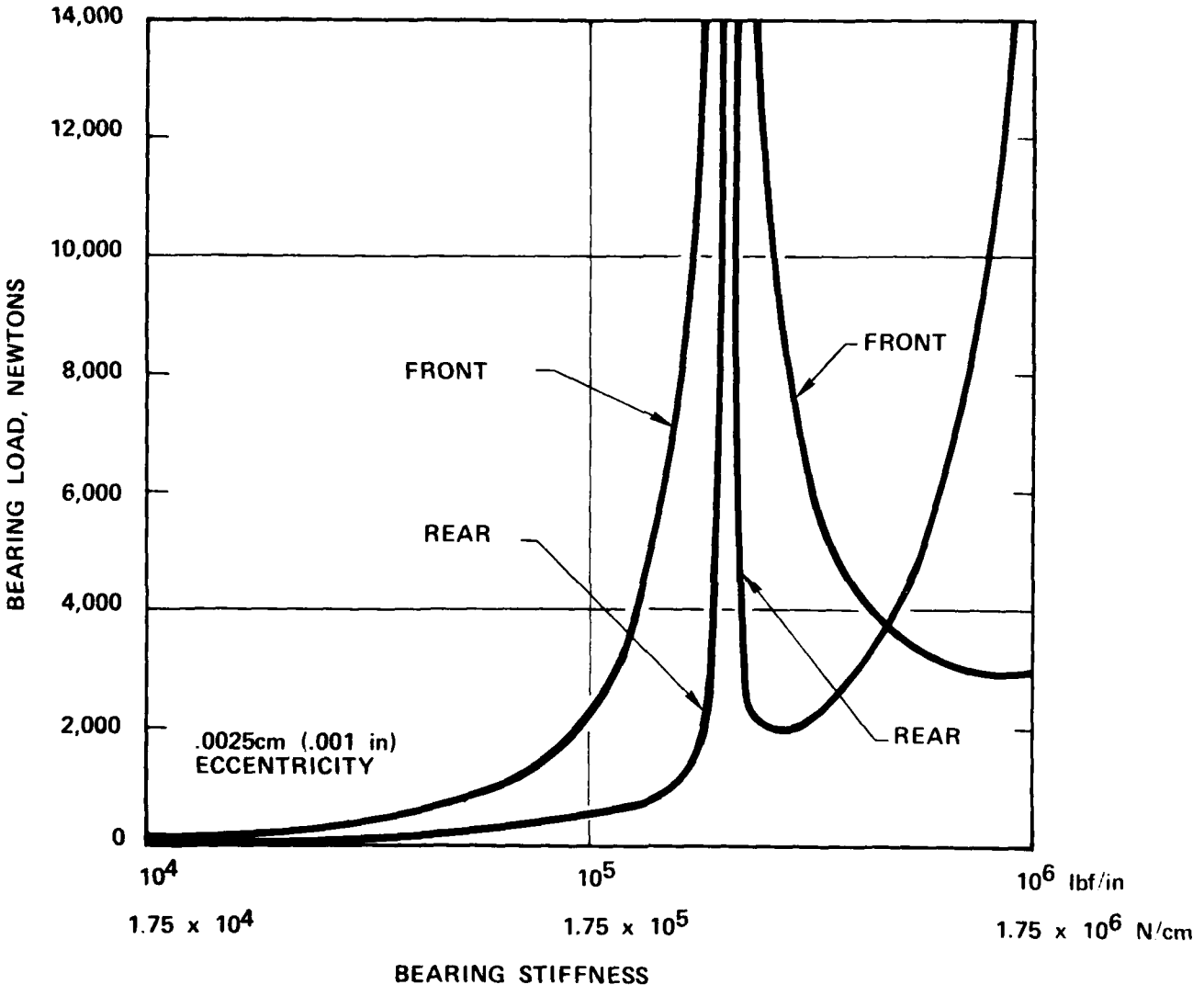

Figure 8-32. CCCBS Engine (38.8 in.) Power Turbine Unbalance Bearing Loads

The physical characteristics of the 3600-rpm power turbine as modified to provide first bending critical speed margin and adequate load capacity are listed below:

Rotor weight	1825 Kg (4015 lb_f)
Polar moment of inertia	21,127 cm-N-sec (1870 in.-lb_f-sec)
C.G. location	143.66 cm (56.36 in. from front end of shaft)
Static bearing loads	
Front	332.27 kg (731 lb_f)
Rear	1492.73 kg (3285 lb_f)
*Dynamic bearing loads	
Front	175.0 kg (385 lb_f)
Rear	52.27 kg (115 lb_f)

*Based upon 3600 rpm, 0.25 mm (0.001 in.) eccentricity and 175,126 N/cm (100,000 lb_f/in.) stiffness.

8.4 AUXILIARY SYSTEM IDENTIFICATION

8.4.1 GAS BEARING AUXILIARIES

The hydrostatic gas bearings selected for the CCCBS engine require a source of pressurized gas for startup, operation, and shutdown of three spools or rotating groups. The bearings have been designed to operate over the normal steady state power range and rotor speeds by supplying helium gas from the discharge of the CCCBS engine high pressure compressor. Under these conditions, the bearings require only a helium pressure control and no external source of pressurized helium. However, startup and shutdown modes of the engine require an external source of pressurized helium that is independent of the speed of pressure level of the closed loop CCCBS engine. Suitable controls that provide for automatic changeover between the start/stop helium hydrostatic supply and the pressurized gas from the engine high pressure compressor constitute a major development of the system.

In addition to the normal start/stop helium supply, an emergency system should be considered to provide hydrostatic gas in the event that the start-stop system should fail or an engine condition should develop that would require a rapid stop of the engine. A small high pressure helium tank in conjunction with a mechanical or helium braking system for the CCCBS engine rotors could provide the required emergency features.

A suggested external hydrostatic gas system suitable for the CCCBS engine is shown in Figure 8-33.

The schematic shows the CCCBS engine rotor arrangement and gas bearings. Each bearing is individually supplied with hydrostatic helium gas from either of two sources. During normal operation of the CCCBS engine, the hydrostatic gas supply is furnished by bleed from the high pressure engine compressor through a control valve and regulator to the respective bearings. During normal start/stop operation, the hydrostatic gas is supplied and controlled from a high pressure storage tank through separate pneumatically actuated valves and regulators that are functional in the event of malfunction or loss of electrical power to the normal controls. Actuation of an engine rotor brake would be made during emergency stops so as to ensure a complete stop of the rotors before the high pressure hydrostatic gas storage tank bled to unusable low pressures.

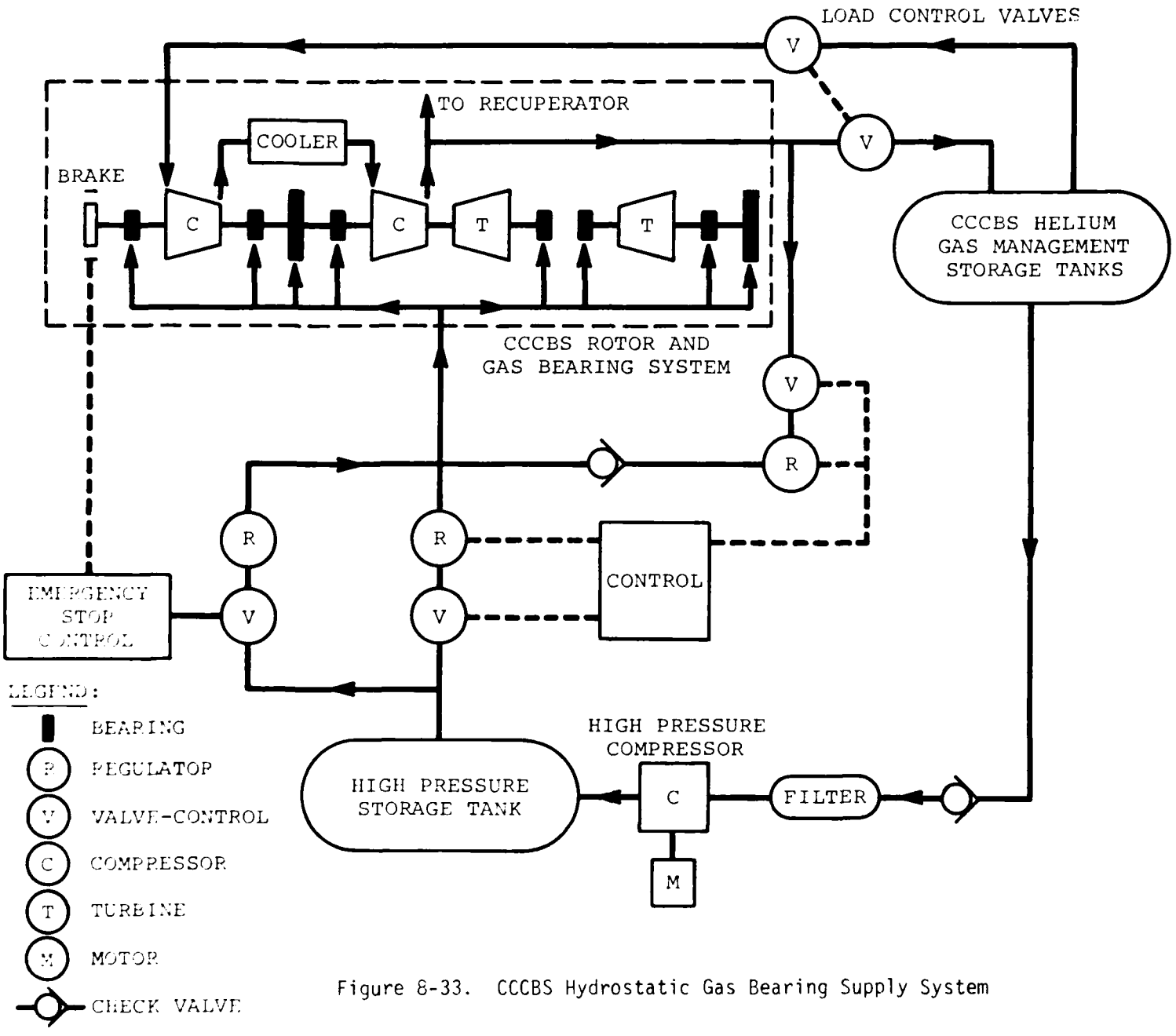

Figure 8-33. CCCBS Hydrostatic Gas Bearing Supply System

All hydrostatic gas supply controls would be integrated with the CCCBS control system.

A tentative sizing of the high pressure hydrostatic gas compressor was made on the basis of the calculated maximum flows to the bearings with the engine at rated speed. The compressor would be required to deliver approximately 1 Kg/sec (2.20 lb/sec) at a differential pressure of at least 2068 KPa (300 psi) in order to maintain steady state operation without depleting the hydrostatic gas storage tank. This compressor could be reduced significantly in size if the externally supplied hydrostatic gas were to be supplied only at engine speeds below 70% where the aerodynamic thrust loads are minimum and thrust bearings could be operated at reduced differential pressures.

8.4.2 HEAT REJECTION SYSTEM

The CCCBS uses sea water as an ultimate heat sink. A representative flow diagram is shown in Figure 8-34. The system shown is for a nuclear heat source, where some means of shield cooling are needed, and an emergency cooling capacity is needed to remove the plant decay heat when the power conversion units are shut down. Basically, an intermediate water cooling loop is used to connect the precooler and intercooler in each power conversion unit to a sea water heat exchanger. Each separate power conversion unit uses its' own intermediate cooling water loop, and the valving is arranged in such a manner to allow either sea water heat exchanger to act as the ultimate heat sink for both power conversion loops. This allows the CCCBS to continue operating up to about a 50% power level, as described in Section 3.4.1 on the operating characteristics of the precooler and intercooler, with a failure of one intermediate cooling water loop.

For the performance evaluation of the CCCBS, a counterflow heat exchanger arrangement was used. For a sea water inlet temperature of 30°C (85°F), the sea water exit temperature was about 47°C (110°F), and the intermediate water loop temperatures were 70°C (158°F) at the inlet and 35°C (95°F) at the exit. This resulted in a heat exchanger effectiveness of 87%, which is practically achieveable with standard water heat exchanger design practice. A sea water fouling factor of 11,500 watts/m^2-°K (2000 BTU/hr-ft^2-°F) was used (References 1 and 2), a value widely used in industry.

Constant speed pumps are used in both the sea water and intermediate cooling water loops. This results in essentially constant water flows on both sides of the sea water heat exchanger.

A water treatment system is shown in Figure 8-34. At the initial design phase, it was felt that some special water treatment facility would be needed to remove any impurities that might form in the coolant loop. However, at present it would appear that a large development effort would not need to be undertaken. Present commerical pressurized water reactors use demineralized water treated with sodium dichromate in the main coolant loops. This coolant is left in the loops for the life of the plant, and only treated makeup water is added to compensate for any leakage. In addition, many parts of the PWR coolant loops are constructed of carbon steel, unlike the stainless steel used in the precoolers and intercoolers

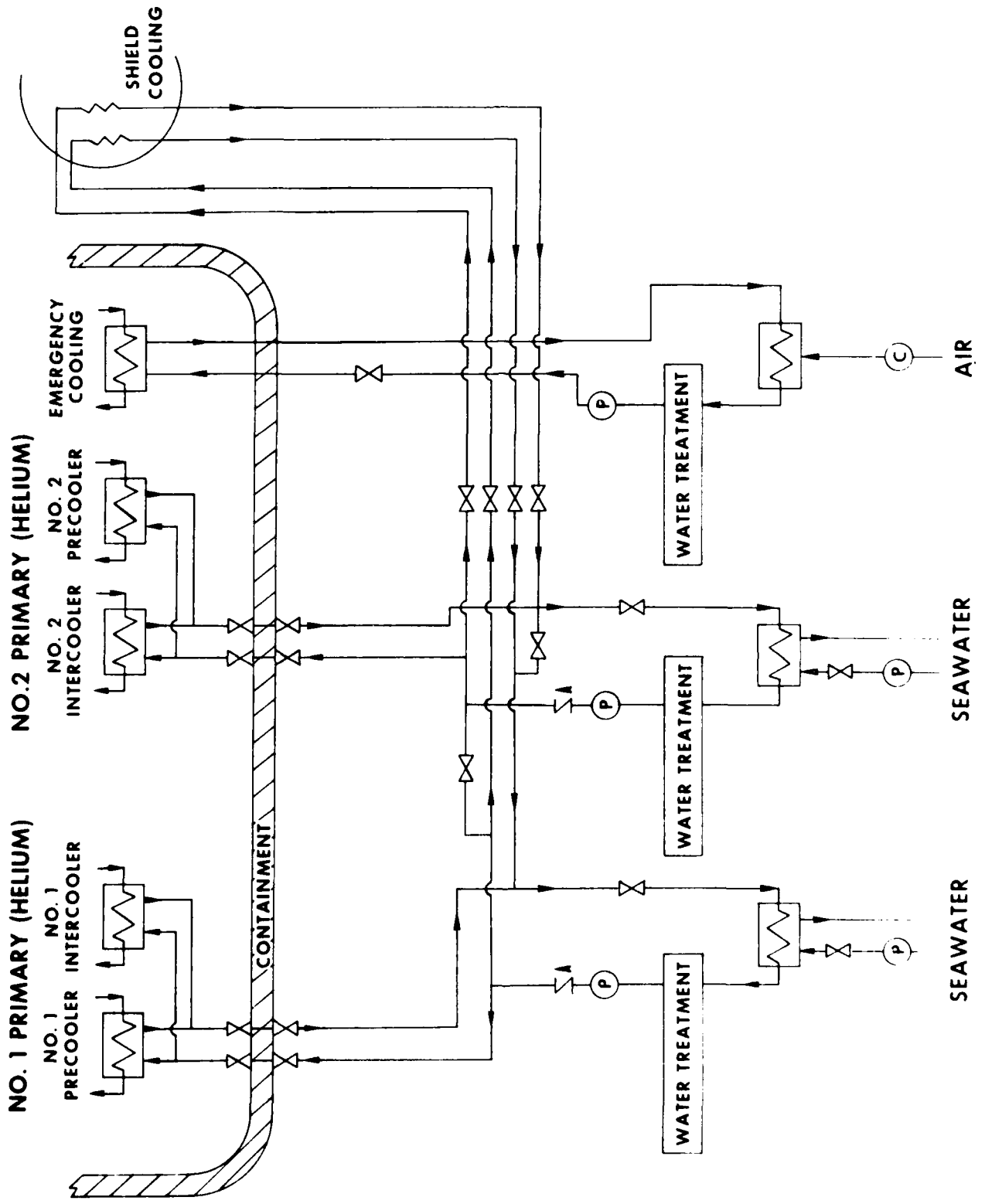

Figure 8-34. Intermediate Cooling Water Pump

and the copper-nickel-alloy (Reference 1) used in the sea water heat exchanger. Based on these facts, it would appear that the water treatment can largely draw upon the data base developed in the PWR program, and a great deal of additional effort would not be needed.

8.4.3 CONTROLS

One of the primary requirements is to provide fully automatic and stable control over the range from 25 to 100 percent of full power. Throttle ramprates up to 10 percent per second were set as a desired goal. In addition, automatic control of the plant startup and shutdown is to be provided. Both automatic and manual control capability is to be provided at local control stations to allow for plant manageability under all forseeable circumstances. Wherever feasible, the control and protection system shall make maximum practical use of diverse redundancy of sensors to maximize the system reliability.

For the CCCBS, the method of control decided upon was the use of a combination of helium inventory control and heat source outlet temperature control. The inventory control schematic is shown in Figure 6.1. The variations in power demand are adjusted by means of a two pressure level storage system in order to handle the required normal operating power range. This system allows the pressure level to be varied without using auxiliary compressors. If the power is to be reduced, the level is reduced by tapping helium from the HP compressor into the storage reservoirs which are filled one after the other until the required pressure level is attained. To raise the power (pressure) level, helium flows from the reservoirs into the loops upstream of the precoolers. The control of the heat source outlet temperature would be dependent on the type of heat source used. For a nuclear power plant, the outlet temperature is controlled by using reactivity control drums. For a fossil fired heat source, the temperature is controlled by means of adjusting the fuel firing rate.

A block diagram of the control concept for the CCCBS is shown in Figure 8-35. The specific of the inputs would be dependent on the application of the CCCBS. However, the controller blocks shown would be the basic ones that would be needed regardless of the application of the CCCBS.

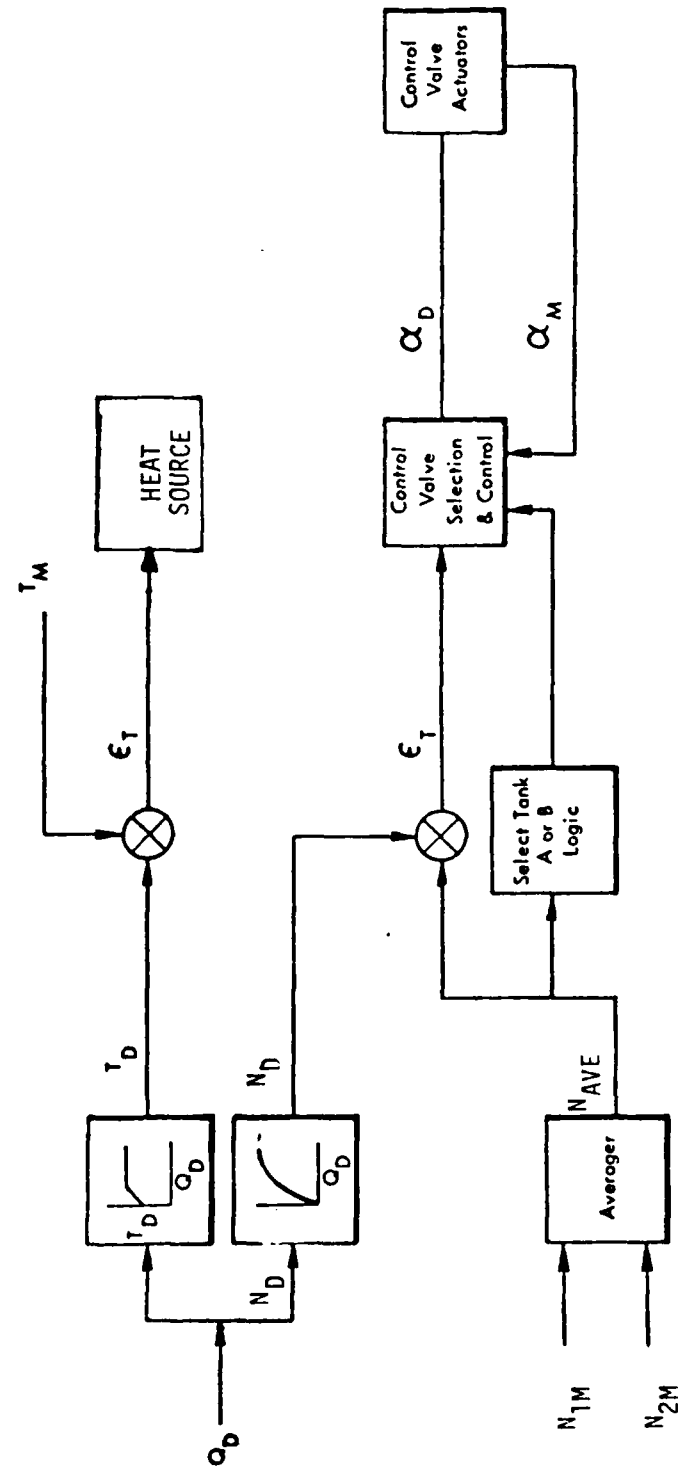

Figure 8-35. Proposed CCCBS Control Concept

The control method would be as follows: from an input throttle position demand (Q_D), the associated heat source outlet temperature demand (T_D) and power turbine speed demand (N_D) can be obtained. These temperature and speed relationships would be obtained from the operating range state points for the plant. For the present CCCBS configuration, the heat source outlet temperature demand would vary linearly from 944°C (1730°F) at full power down to 916°C (1680°F) at a 25% of full power throttle position. The power speed demand would depend on the operating mode of the power turbine. For constant speed turbine operation, the speed demand would be constant over the load range. For variable speed turbine operation, the speed demand would vary roughly as the cube root of the throttle position (or net output power):

$$N_D = C_1 + C_2 \, (Q_D)^{1/3}$$

where C_1 = idle speed of the power turbine

The heat source outlet temperature demand is then compared against the measured outlet temperature (T_M). The resulting error signal is used as an input to the controller on the heat source outlet temperature. The temperature controller used would depend on the heat source selected for the CCCBS.

The speed of the two power turbines (N_{1M} and N_{2M}) would be measured and averaged. This average turbine speed (N_{AVE}) would then be compared against the demand speed, generating a speed error (N_e):

$$N_e = N_D - N_{AVE}$$

A proportional-integral controller has been initially defined to obtain the demand inventory control valve position. This could require some means of controller compensation to improve the response of the plant:

$$\theta_D = K_1 \, (N_e + K_2 \int N_e \, dt)$$

This valve demand can then be used as the position signal for the helium inventory valve actuators. The rate of change of the valve stem position of the inventory valves could then be based on the difference between the actual (θ_c) and the demand (θ_D) positions.

$$\frac{d\,\theta_c}{dt} = K_c\,(\theta_D - \theta_C)$$

The two-level inventory storage system requires some means of switching from using one reservoir to another. At present, the selection logic uses a measurement of the pressure differential between the turbomachinery and the helium reservoirs in conjunction with a signal based on the control valve position demand. For example, when increasing power from a 25% throttle position, the demand control valve position would be positive. This would mean that helium flow must be added to the turbomachinery, thus limiting the choice of the control valves to either CV2 or CV4 shown on Figure 6.1. Based on the pressure differential between both reservoirs and the helium inlet side of the precooler, CV4 would have the lower value, and would be therefore begin opening and allow helium flow from the low pressure reservoir to the precooler inlet. Eventually, a point will be reached when the pressure differential decreases to some set value. At this time, the selector logic will begin opening CV2, and the high pressure reservoir will be used for the helium inventory supply. At the same time, the selector logic will ramp CV2 closed at the maximum slew rate to avoid bypassing helium from the high pressure reservoir directly to the low pressure reservoir.

Besides the normal control system mention avove, additional plant protection systems would be needed to protect the plant integrity during certain malfunctions. For example, a loss of cooling water flow would require an immediate plant shutdown. Also, temperature sensors would be needed at certain locations through the plant to avoid over temperaturing of any components and to alert the operators of a possible plant off-normal condition. If the need dictates, these temperature sensors could be tied into the plant protection system to allow for the automatic shutdown of the plant.

There is one type of malfunction that would appear to require an additional control system besides the ones mentioned. On a loss of load on only one power turbine, it would be desirable that the plant could continue operating on the remaining

unit. This would prevent the initiation of the overspeed protection method that would function for a complete loss of load on both power turbines (heat source shutdown coupled to a rapid dump of the turbomachinery helium to the reservoir bottles). To allow for one unit operation, the addition of a bypass system is necessary. A possible valve arrangement is shown in Figure 8-13. Upon receipt of an overspeed signal, the bypass valves in the affected power conversion unit would open. For example, a loss of load in Loop A shown in Figure 8-36 would cause the opening of valves CV1 and CV3. For the proposed CCCBS configuration, as shown in Figure 3-1, these two valves are actually a single assembly acted upon by a common controller. When the power turbine bypass (CV1 for the assumed affected Loop A) is opened, the pressure difference across the power turbine is decreased causing the helium temperature into the recuperators to increase. By adding relatively cool helium from the high pressure compressor (CV3) to the hot gas from the power turbine and power turbine bypass, thermal shocking of the recuperators can be avoided. Opening the power turbine bypass also increases the pressure difference across the high pressure turbine (increases power to the compressors) so that the opening of the compressor bypass valves also increases flow through the compressors to absorb the increased power available from the high pressure turbines, thereby preventing overspeed of the turbo-compressor shafts. Both the power turbine and turbo-compressor shafts will begin to ramp down in speed and a steady-state will be reached with the one power conversion unit stopped and isolated from the rest of the plant (due to the check valve in that loop), and the plant continuing to operate on just the other power conversion unit.

Based upon previous experience with the startup of a number of nuclear rocket engines, the CCCBS startup should not present any major technical difficulties. For a nuclear heat source, control of startup is assumed to be automated to provide maximum protection for the system against undesirable transients and to reduce requirements to the operator. The controls developed in the NERVA program provide direct input to design philosophy of the CCCBS controls. During the NERVA XE-Prime engine tests, the engine was repeatedly started with startup automatically controlled. Twenty temperature controlled autostarts were made, successfully demonstrating that nuclear instrumentation is not required in the engine control system (Ref. 3) (it is required, however, in the diagnostic and safety systems). For the CCCBS, one candidate sequence of operations using temperature autostart is as follows:

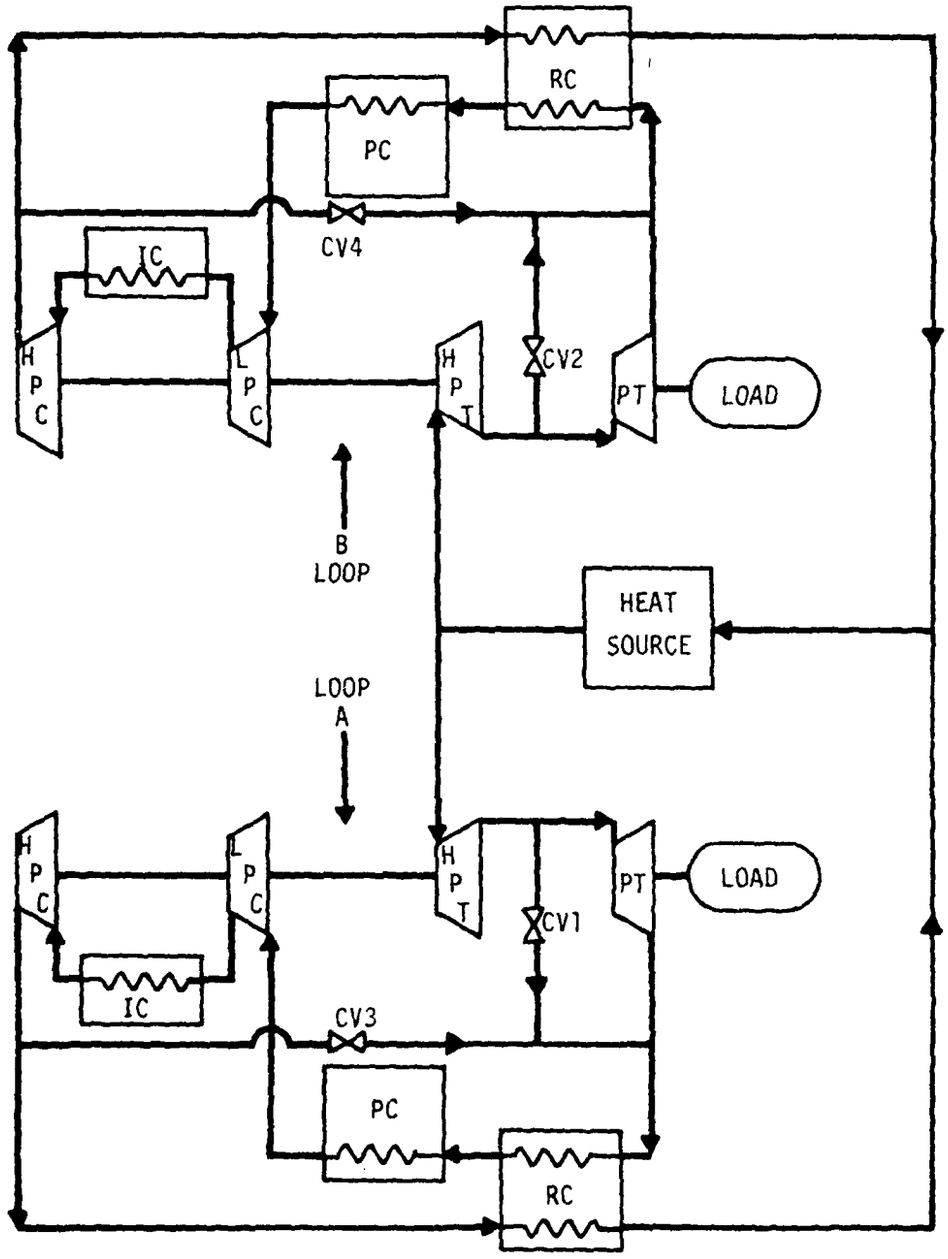

PT	Power Turbine	RC	Recuperator
HPT	High Pressure Turbine	PC	Precooler
LPC	Low Pressure Compressor	IC	Intercooler
HPC	High Pressure Compressor	CV	Control Valve

Figure 8-36. Proposed CCCBS Bypass Valve Arrangement for Overspeed Protection

1. Nuclear startup begins when the plant operator initiates a control drum rotation on a programmed time-based, position-control program. The rotation rates as a function of position are chosen by the operator on the basis of core and reflector temperature measurements and previous operating characteristics.

2. When the power has increased to a level sufficient to provide significant sensible reactor heat output, as verified by an increase in reactor material temperature, the drum control is transferred to in-core material temperature control.

3. In-core material temperature raised according to schedule to a level where the turbomachinery can self-sustain.

4. Turbomachinery started with electric or pneumatic starters followed by transfer of reactor control to reactor exit temperature control mode.

5. The control system would have output demand circuitry and would provide a reactor exit temperature demand signal (between 0 and 20% power).

Depending upon startup requirements and system design, alternate control sequences may be selected using other system parameters including nuclear power and/or computed period.

While the above scheme is primarily for a nuclear powered system, there does not appear to any reason why a similar startup strategy could not be used for a fossil fired heat source.

8.5 REFERENCES

1. K. Bammert, et. al., "Highlights and Future Development of Closed-Cycle Gas Turbines," ASME Paper No. 74-GT-7.

2. C.F. McDonald, "Gas Turbine Recuperator Technology Advancements," ASME Paper No. 72-GT-32.

3. H.R. Cox, Gas Turbine Principles and Practice, D. Van Nostrand Company, Inc. 1955.

4. K. Bammert, et. al., "Layout and Present Status of the Closed Cycle Helium Turbine Plant Oberhausen," ASME Paper No. 74-GT-123.

5. A.J. Wheeler, et. al., "Small Gas Turbine Engine Component Technology Regenerator Research," USAAV LABS Technical Report 66-90, January 1967.

6. I. Amato, et. al., "Brazing of Stainless Steel Heat Exchangers for Gas Turbine Applications," Paper presented at sixth AWS-WRC Brazing Conference Cleveland, Ohio, April 1975.

7. WAES-TNR-233, "Compact Closed Cycle Brayton System Feasibility Study, Year 1," July 1977.

8. MIL-C-15730K (Ships), "Military Specification; Cooler, Fluid, Naval Shipboard, Lubricating Oil, Hydraulic Oil and Fresh Water," 12 November, 1973.

9. Tubular Heat Exchanger Manufacturers Association, Inc., "Standards of Tubular Exchanger Manufacturers Association," Fourth Edition, 1959.

10. W.E. Durkee and F.B. Demerval, "Nuclear Rocket Experimental Engine Test Results," Journal of Spacecraft, Volume 7, No. 12, December, 1970.

9.0 MATERIALS TESTING AND EVALUATION

9.1 INTRODUCTION AND BACKGROUND

In the proposed closed cycle Brayton system, the highest combination of stress and temperature occurs in the first row turbine blades. First stage stator vanes and blades are expected to operate at elevated temperatures for a system life in the range of 10,000 to 40,000 hours. The working fluid is an inert gas, helium, with equilibrium concentrations of various impurities. Based on past helium turbine design technology, from the Westinghouse closed Brayton turbomachinery development with the United States Maritime Administration,[1,2] and based on expected materials properties, it has been concluded that a turbine inlet temperature on the order of 927°C (1700°F) pushes but does not exceed the state-of-the-art for uncooled turbine blades and stators in inert gas. This conclusion regarding materials capability, was based on engineering extrapolation of materials properties data obtained in inert gas at lower temperatures and on properties data at comparable temperature in air for shorter test time periods. However, to demonstrate material performance feasibility, additional material testing at or near expected service conditions was necessary to confirm materials properties and to provide baseline data for the feasibility evaluation.

Historically, superalloy alloy development has been aimed at problems associated with aviation and land gas turbines where thermal, fatigue hot corrosion, and oxidation are the primary factors which limit component life. While creep-rupture behavior is an important design consideration in such systems, hot component life is limited to a large degree by materials compatibility with combustion products, including fuel impurities such as sulfur compounds and catalytic agents, vanadium pentoxide, from fuel processing. In the case of CCCBS turbine components, creep behavior is expected to be a primary design consideration. Minor amounts of active contaminants in the inert working fluid are expected to produce surface reactions which may or may not influence creep behavior.

The objective of the materials test program was to determine the feasibility of potential turbine materials to function under CCCBS operating conditions for the design life of the system. To achieve this objective, the creep rupture behavior of five selected alloys were evaluated at 982°C (1800°F) in air, in static ultra high purity helium (UHP He) and in a dynamic simulated CCCBS helium working fluid. Creep rupture properties were also compared to available published data obtained from the Mechanical Properties Data Center, Traverse City, Michigan. The five alloys chosen for evaluation were IN100, 713C, MAR M509, MA754 and LCM. A limited number of creep-rupture tests were carried out in air to characterize the creep rupture behavior of each particular heat of material obtained for evaluation. The LCM alloy was not tested in air due to its reactive nature with oxygen at elevated temperatures. Creep-rupture tests were conducted under a static ultra-high purity helium (UHP He -99.9999%) atmosphere to establish long term baseline data under test conditions which minimize environmental effects. Because superalloys, while under development, are normally tested in air for creep-rupture behavior, they are naturally optimized for use in an air environment. There exist data that indicate that an air test environment, particularly at elevated temperatures can have a beneficial or deleterious effect on creep-rupture behavior of certain superalloys.[3,4,5,6]

9.2 TEST EQUIPMENT AND PROCEDURES

Creep rupture tests were carried out in air, UHP He and simulated CCCBS helium working fluid. Creep tests in air were conducted in conventional lever arm units under static air environmental conditions. The air test equipment and procedures were conventional and routein in nature, thus a description is not included in this report. The static UHP He and dynamic simulated CCCBS environmental test equipment are considered to be unique, therefore a description of the test equipment and the test procedures used is included.

9.2.1 ULTRA HIGH PURITY HELIUM

9.2.1.1 TEST FACILITIES

Creep rupture testing was carried out in five ultra high vacuum creep test units modified for ultra high purity helium atmosphere operation. The creep

units are illustrated schematically in Figure 9-1 and are pictured in Figure 9-2. Ultra-high vacuum creep test operation of these units is described in detail elsewhere[7]. The cogent system characteristics which made these units ideally suited for ultra-high-purity helium atmospheric testing are:

- The all metal system construction utilizes crushable copper gasket seals which permits evacuation to pressures below 1×10^{-7} torr while the entire system is baked at 204°C (400°F). This operation removes adsorbed moisture and gases from all internal surfaces.
- The specimen is heated by radiation from a split tantalum resistance heating element insulated by tantalum radiation shields. Tantalum at temperatures above 538°C (1000°F) is an active "getter" of oxygen, thus the test specimen is exposed to an environment with a very low oxygen level.
- The specimen is deadweight loaded internally by weights contained in the system. External loads are transmitted to the specimen through a stainless steel bellow seal.
- Specimen strain is measured optically directly off the gage section. This feature plus deadweight loading eliminates systematic error.

9.2.1.2 HELIUM GAS ANALYSIS

Helium gas used for the creep testing atmosphere was Matheson Purity 99.9999% min. helium. Gas analysis was conducted using a one liter sample bottle which was attached to the system through a bakeable valve. The sample bottle, which was baked out under dynamic vacuum conditions, was permitted to equilibrate with the static helium environment within the test chamber. The helium in the sample bottle was analyzed using a concentration technique developed at the Westinghouse Research and Development Center[8,9]. The helium in the sample bottle is drawn through a liquid helium cooled freezeout trap which condenses out and effectively concentrates all gaseous impurities. The preconcentrated trapped gases are then warmed to room temperature. The resulting gas pressure in the cryogenic trap with a known volume is measured. The gases are then expanded into the inlet system of a mass spectrometer and analyzed quantitatively. Determination of water level is qualitative due to the limited size of the gas sample and difficulties which are inherent in the quantitative

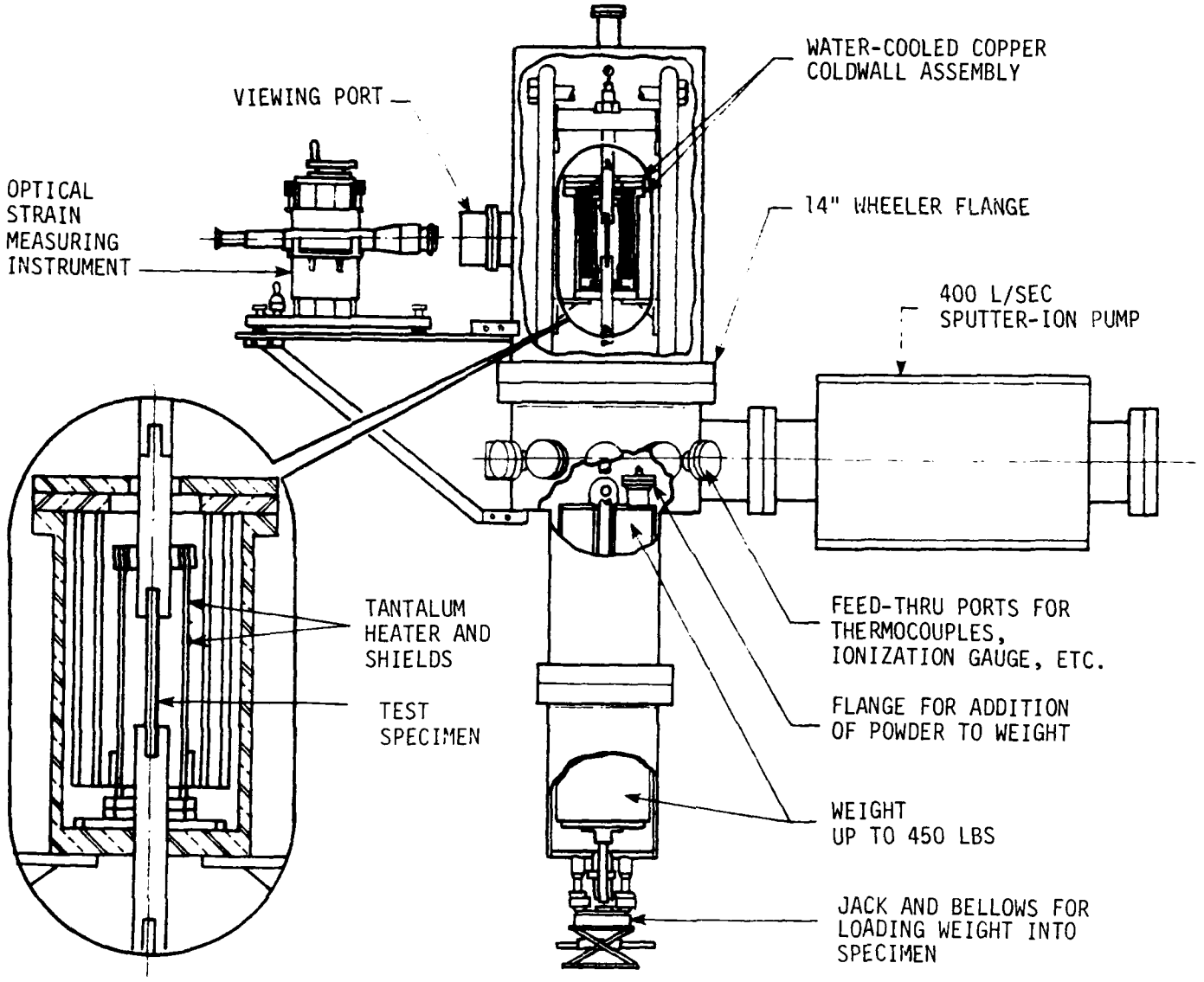

Figure 9-1. Schematic Diagram of Ultra-High-Purity Helium Creep Units

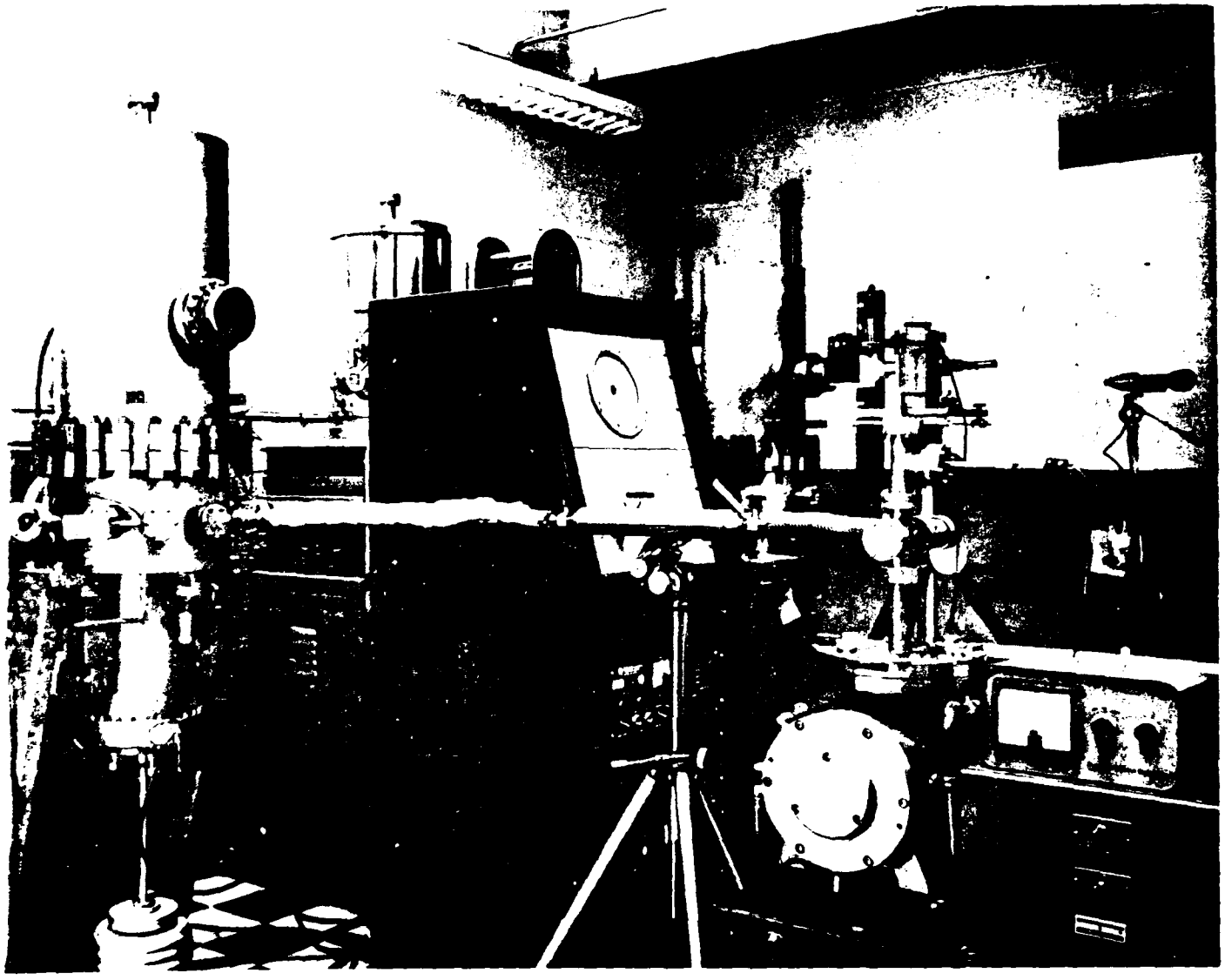

Figure 9-2. Photograph of Modified Ultra-High Vacuum Creep Units

analysis of water in the low ppm range. In all cases no distinction could be made between sample moisture level and mass spectrometer background which varied from the high ppb to the very low ppm level.

9.2.1.3 TEST PROCEDURE

A suitably prepared and thermocoupled test specimen was inserted into the test chamber shown previously in Figure 9-1. The grips were attached to the upper support member and weight train by means of pinned joints. The thermocouple leads were fed to the outside by means of a ceramic feedthrough assembly. Extreme care was exercised during loading of the system to prevent the introduction of any foreign matter, such as dirt, oil, etc., which would compromise system operation.

Personnel handled all hardware inside the vacuum envelope with lint-free gloves. After the necessary internal connections were made, the bell jar was put in place, all openings sealed, and the system evacuated. Pumpdown from atmospheric pressure was accomplished by means of a turbo-molecular pump to eliminate the possibility of contamination due to backstreaming of oil from the mechanical or diffusion pumps which employ organic pumping media. When the system pressure reached 1×10^{-5} torr the sputter ion pump was energized. After sufficient time to allow for pump outgassing and pump startup, the system was isolated from the turbo-molecular pump. After the ion pump startup, the system pressure decreased rapidly and after approximately one hour, was less than 1×10^{-6} torr. At that time the system was leak checked. After it was determined that the system was leak free, the system was baked to remove the adsorbed gas moisture from the walls of the test chamber. This was accomplished by enclosing the vacuum system within a two piece portable oven. The ion pump contains its own internal heater. Both pressure and temperature are used to control the amount of heat input during bakeout. During the initial portion of bakeout, a system pressure upper limit of 1×10^{-6} torr regulated the power input to the bakeout heaters. After removal of the major adsorbed gas load, the maximum temperature of the wall of the vacuum envelope is limited to approximately 204°C (400°F) to 260°C (500°F) by thermostats attached to the exterior surface of the vacuum system. After a bakeout of 12 - 24 hours, the system was cooled to room temperature and the bakeout oven removed. The system pressure after bakeout at room temperature was less

than 5×10^{-10} torr. At this point, the helium backfill system, illustrated in Figure 9-3, was attached to the test chamber through a bakeable microvalve. All lines were stainless steel, and all connections were made using crushable copper gasketed flanges. The gas lines and gas sampling bottle were fitted with trace heating tapes. The backfilling procedure consisted of attaching the fill lines to the evacuated test chamber, connecting the turbo-molecular pump to the system, and placing a gas sample bottle in the system. The lines between the helium supply bottle and the test chamber were heated along with the gas sample bottle to 149°C (300°F) while being evacuated by the turbo-molecular. A two to three hour bakeout was accomplished at a pressure of 1×10^{-6} torr or less, prior to release of the helium from the supply bottle into the backfill system and into the test chamber. The test chamber was filled to a pressure of 0.95 atmospheres. The gas sampling bottle valve was closed and the sample was removed for analysis.

Gas samples were taken at the beginning and at the conclusion of a creep test. Typical analytical results are reported in Table 9-1. Hydrogen was the most prominent active gas with concentration levels which varied from initial values of 0.35 ppm to maximum values as high as 4.0 at the end of testing. All other active gases were either not detected or were present in levels which were consistently less than 1.0 ppm.

The test specimen was heated to temperature; and once stabilized, the weight was applied. When internal loading was utilized, the weight was supported through a bellows assembly. A partial load of several hundred psi was maintained on the specimen at all times. As soon as the test temperature was reached and thermal equilibrium established, the total load was applied to the specimen by retracting the support platform. Measurements were made of the specimen gage length to establish the ℓ_0 at temperature. Periodically during the test duration in charge in ℓ_0, $\Delta\ell$ was measured to establish the time-elongation curve.

Creep strain was determined by direct measurement of the separation of fiducial scratches applied to the extremes of the uniform gage section of the test specimen. The separation of the fiducial marks was followed by a horizontal telescope which is moved vertically by a 12.7 micron (0.050 inch) pitch precision

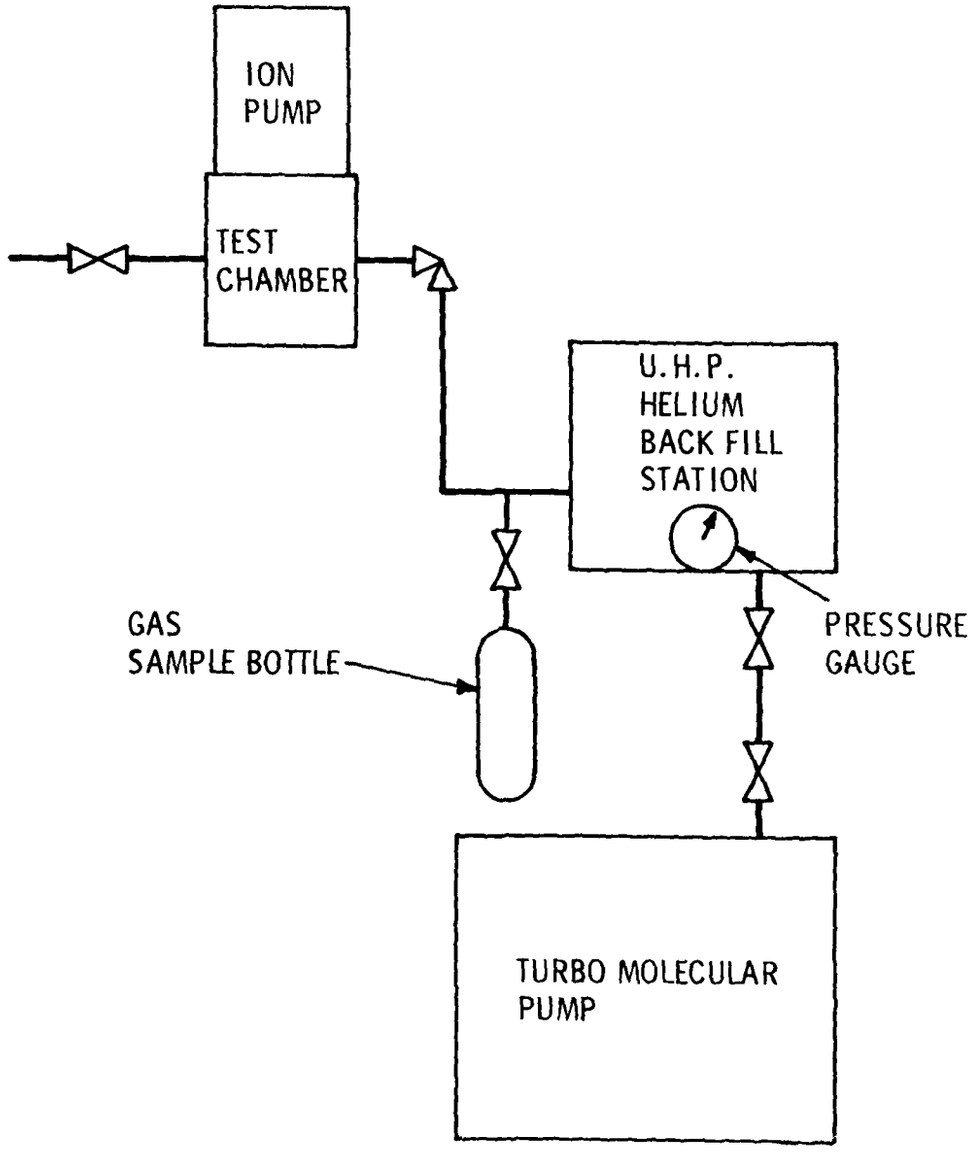

Figure 9-3. Schematic Diagram of Ultra-High Purity Helium Creep Test Unit with Helium Charging and Vacuum Evacuation Units in Place

TABLE 9-1

TYPICAL HELIUM GAS ANALYSIS

	Typical He Analysis (ppm)						
	H_2	O_2	N_2	CO	CO_2	THC	Ar
Final	1.0	0.04	0.9	ND	0.2	0.04	1.4
Initial	0.3	ND	0.07	ND	0.2	0.04	0.01
Initial	0.5	0.1	0.2	ND	0.4	0.10	0.01
Final	4.0	ND	ND	1.3	0.2	0.05	0.1
Initial	2.2	ND	ND	0.1	2.3	0.2	0.1

Final analyses were taken for tests run for >1000 hours. It must be noted that reported values at or below the 1 ppm level are at the limits of detectability and most likely represent background levels of the sampling and analytical equipment.

ND - Not Detected

THC - Total Hydrocarbons

micrometer screw and nut assembly. The readings are made with a vertical reference scale and 100 part drum equipped with a 10 part vernier. The instrument can be read to 0.01 microns (0.000050 inch).

Helium gas samples were also taken during and/or at the conclusion of the creep test. The helium backfill system (Figure 9-3) was reconnected to the test chamber and prepared as previously described. The test chamber valve was opened to allow the helium from the test system to enter the sample bottle. Sufficient time was allowed to permit pressure equilibration between the test chamber and sample bottle volume. After closing the valves to the test chamber and the sample bottle, the bottle was removed for analysis.

9.2.2 SIMULATED CCCBS HELIUM

Creep-rupture testing in simulated CCCBS helium working fluid was carried out in five lever arm test units equipped with a specially designed simulated CCCBS helium working fluid environmental supply system.

9.2.2.1 CREEP TEST FACILITIES

Creep testing in the simulated Compact Closed Cycle Brayton System (CCCBS) environment was performed in five creep units. Two units are displayed in Figure 9-4. Each unit consisted of a resistance wound radiation heater mounted so that the specimen was in the center of the hot zone. The creep chamber was a clear quartz tube with pyrex fused at each end; several transition zones separated the 100% quartz from the 100% pyrex. Crushable copper gasket seals were used in the metal-to-metal interfaces. The glass-to-metal seals were kovar. The thermocouple leads were introduced into the system through conventional vacuum feedthroughs. This permitted evacuation to pressures below 1×10^{-5} torr while the system was baked at 260 to 315°C (500 to 600°F). During baking absorbed moisture and gases from internal surfaces were removed. The specimen was deadweight loaded externally by way of a lever system; the load was transmitted to the specimen through a bellow seal. Molybdenum grips were used to hold the specimens in the hot zone. Strain was measured by a dial gage detecting lever arm motion. This measurement included deflections in the entire load train. This led to large indicated primary creep strains. However, secondary creep

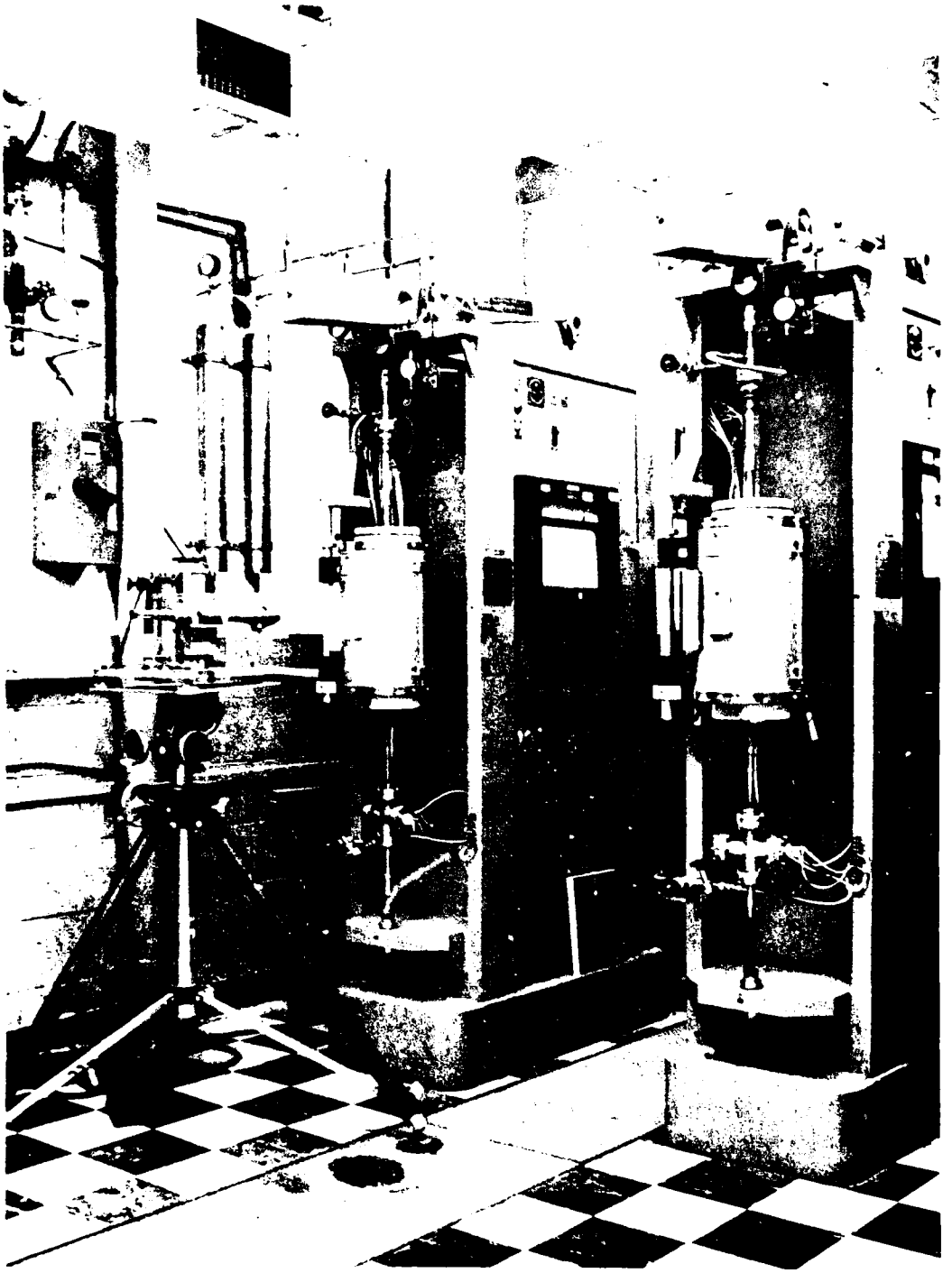

Figure 4-2. Stress Rupture Test Rack with Simulated

rate and rupture life were unaffected. Optical extensometers were also used to measure strain. However, difficulties in discerning fudicial marks on the specimen gage section caused this method of strain measurement to be less reliable.

9.2.2.2 TEST PROCEDURES

Extreme care was exercised during the preparation of the system to prevent the introduction of any foreign matter that could affect the operation of the system. Lint-free gloves were worn when internal parts were handled.

Thermocouples were attached to the test specimen at three places along the gage length. The specimen was connected to the load train by means of either button head of threaded joints. This assembly was then placed inside the quartz tube. The thermocouple leads were led out of the tube by way of a ceramic feedthrough assembly. The quartz tube was attached to the frame of the creep machine, and the load train was connected to the loading apparatus. The load train emerged from the tube through a bellow seal and was connected to the load by means of a threaded joint.

Evacuation of the creep chamber was accomplished by a mechanical and diffusion pump. The pressure was reduced to 1×10^{-5} to 1×10^{-6} torr. The system was checked for leaks. Once it was determined that the system had no leaks, the chamber was baked to remove adsorbed gases and moisture from the internal surfaces. This was accomplished by heating the chamber to 260 to 316°C (500 to 600°F) and then cooling to room temperature.

The test chamber was made a part of the impure helium loop. The test specimen was heated to temperature, and once thermal equilibrium was established, the load was applied by means of a lever assembly. Periodically during the creep test the change in length, $\Delta\ell$, was measured by a dial gage. To determine the strain-time curve, ℓ_o was taken to be the length of the gage section at room temperature.

9.2.2.3 SIMULATED CCCBS HELIUM ENVIRONMENTAL SUPPLY SYSTEM

Figure 9-5 is a schematic of the impure helium loop creating the CCCBS environment. In the actual system, five creep-chambers were arranged in parallel. For

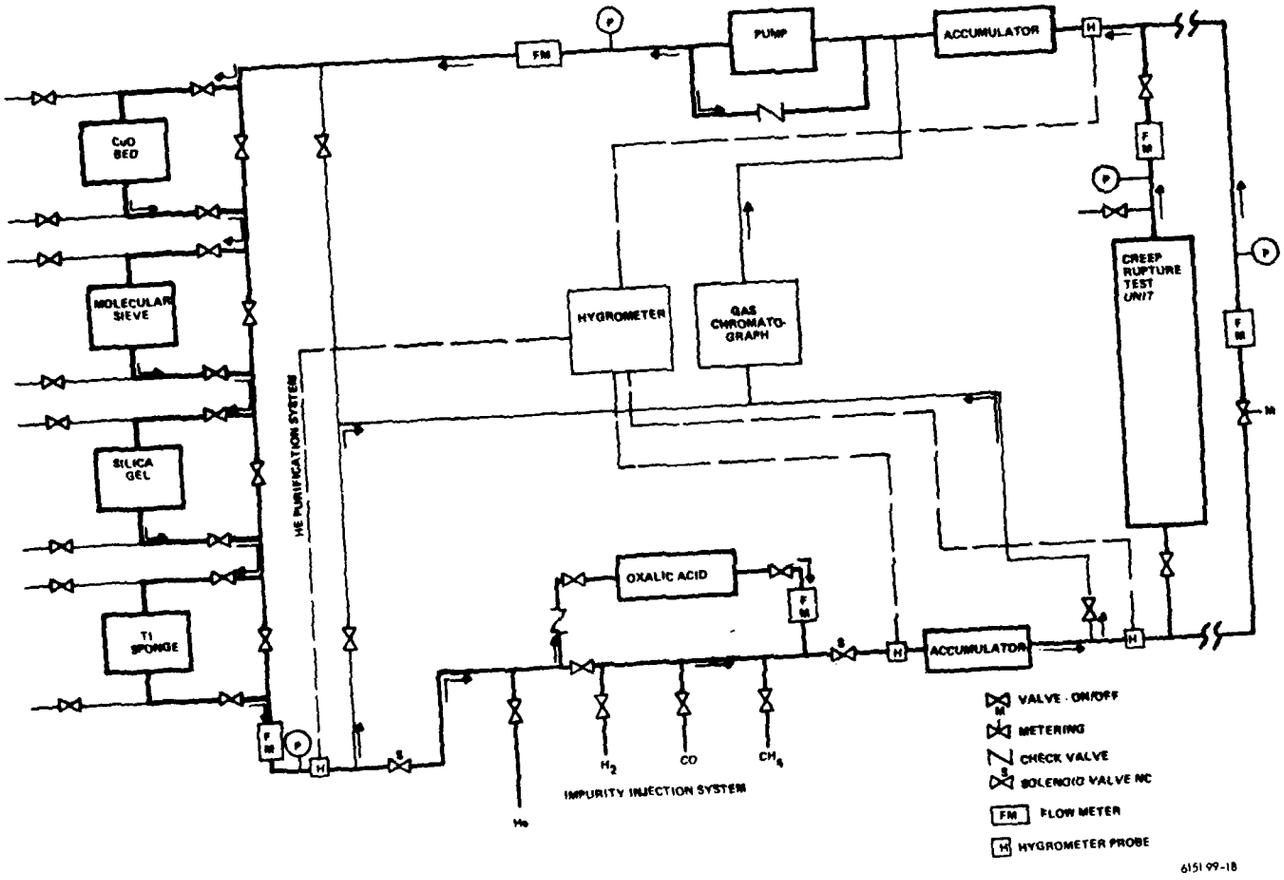

Figure 9-5. Schematic of CCCBS Helium Supply System

simplicity, only one is shown in the figure. A full flow purification system was utilized to remove all impurities from the recirculating helium. The desired levels of each impurity species in the helium was attained by an injection system prior to distribution of the helium gas to the test chambers. In this way, the species and concentration levels were precisely controlled.

The purification section of the loop consisted of a copper oxide bed operating at 371°C (700°F). The bed was filled with copper ribbon which was oxidized to CuO at 649°C (1200°F) by passing air through the bed. The CuO bed operating at 371°C (700°F) removed CO and H_2 by the following reaction:

$$CO + CuO \rightarrow Cu + CO_2$$

$$H_2 + CuO \rightarrow Cu + H_2O$$

After passing through the CuO bed, the helium gas was permitted to cool to ambient temperature prior to passing through a type 5A molecular sieve bed. The molecular sieve bed which was maintained at ambient temperature removed CO_2 and H_2O by adsorption. Following the molecular sieve bed was a silica-gel trap cooled by a refrigeration system to - 40°C(-40°F). The silica gel trap removed N_2, CH_4 and traces of CO, CO_2 and H_2O from the helium gas stream. The final step in the purification process was a titanium sponge bed operating at a temperature of 649°C (1200°F). Titanium is an active "getter" of oxygen at elevated temperatures. The calculated equilibrium partial pressure of oxygen over titanium at 1200°F is $< 1 \times 10^{-45}$ atmospheres. The oxygen level in the helium under flow conditions of 5 liters-per-minute through the titanium sponge bed was well below the limits of detectability.

The continuous injection of the impurity gases was accomplished through micro-flow rate needle valves. The gases were supplied by cylinders of high purity CO, CH_4, and H_2. In parallel to the impurity injection line was an oxalic acid bed to supply moisture to the carrier gas as required to maintain the desired level in the recirculating helium. The impurity injection system was isolated by two "normally closed" solenoid operated valves in the event of an electrical ou-age. This possibility was minimized as the system electrical power was supplied through an uninterruptable power supply (UPS). Accumulators

were used to smooth out pressure surges in the loop and to serve as a mixing chamber for blending impurities in the helium carrier gas. Quartz wool was included in the supply side accumulator for this purpose.

Helium was circulated by means of stainless steel bellows pump operating with an output pressure of 28 psig and a suction pressure of 5 psig. Helium flow was maintained at 5 liters per minute with a one liter per minute flow through each test chamber.

9.2.2.4 HELIUM GAS ANALYSIS

The identity and concentration level of impurities in the simulated CCCBS helium working fluid test environment was determined by a Varian Aerograph gas chromatograph, Model 2732. This instrument utilizes a helium ionization detector which makes it ideally suited for analyzing trace impurities in inert gases. A 457 cm (15 ft) 13 X MS column operating at 121°C (250°F) was used to separate the impurity constituents in the gas sample being analyzed. Calibration curves for H_2, CO and CH_4 were generated using helium doped with individual impurity species in the range of interest. The calibration curves were rechecked using a single helium source containing all of the impurity species at concentrations within the ranges of interest for each impurity species. This helium gas source was used to periodically check the calibration of the gas chromatograph during loop operations. Sampling lines permitted the helium stream to be analyzed after passing through the purification system, after the impurity injection system and after passing through the test chambers.

The moisture content of the recirculating helium was monitored by means of sensors located in the gas stream after the purification and impurity injection systems and prior to and after passing through the test chambers. The sensors were part of a Pannametric hygrometer and are essentially aluminum oxide capacitors. Water molecules adsorbed on the oxide structure in equilibrium with moisture in the gas stream determines the conductivity of the oxide capacitor. The impedance of the circuit thus providing a direct measurement of the water vapor partial pressure in the helium gas stream.

9.2.2.5 SELECTION OF SIMULATED CCCBS HELIUM COMPOSITION

The compatibility testing of CCCBS turbine materials for feasibility study requires an estimate of the likely impurity species and levels in the helium working fluid. In the absence of operational data from a full-size system, operational data from other similar systems must be utilized after appropriate considerations of their individual design peculiarities and modify this information on the basis of the design features of CCCBS.

A directly coupled gas cooled reactor with a graphite core represents the most stringent operating condition with respect to the CCCBS helium working fluid. The chemical nature of the hot graphite core significantly influences the character of the working fluid impurities and how the working fluid is treated. The reactivity of carbon at elevated temperatures produces an oxygen partial pressure in the helium working fluid on the order of 10^{-20} atmospheres or less. In helium-graphite systems, hydrogen, moisture, methane, carbon monoxide, carbon dioxide and nitrogen are the most common impurities. With the possible exception of nitrogen, all enter into a chemical relationship governed by thermodynamic and kinetic considerations. These relationships are discussed in detail by Everette for gas-cooled reactor systems[10]. The operating experiences of three prototype helium-cooled reactor systems were also reviewed. They are: Dragon, which operated at 20 MWth at a reactor outlet temperature of 738°C (1450°F); Peach Bottom, which operated at 115 MWth, at a reactor outlet temperature of 538°C (1000°F); and AVR, which operated at 46 MWth at a reactor outlet temperature of 850°C (1562°F) which was increased to 950°C (1742°F) in 1974. The operational experience of these systems were reviewed with the purpose of setting impurity levels in a dynamic helium environment for materials evaluation, primarily creep and stress rupture data generation, for high temperature reactor systems. The conclusions drawn by Everette as a result of the review of the operation of the above-mentioned systems are quoted directly as follows:

- To assess helium impurities likely to occur in operating reactors a considerable amount of reactor engineering design information and experience with operational prototype reactors must be taken into account.

- [illegible] ratios (H_2-H_2O, CO-CO_2, H_2-CH_4) are the most important [illegible] materials compatibility testing and can be estimated with [illegible] certainty since fundamentally the chemical balance is [illegible] hot graphite of the reactor core.

- Impurity levels are more difficult to assess but are of less importance than the ratios which determine oxidation and carburizing potentials. Estimates have been made for power reactor operation and recommendations made for compatibility testing of primary circuit materials.

Based on information developed as a result of the review, Everette recommended the following impurity levels for test loops supplying simulated systems environment for testing of high temperature gas-cooled reactors (HTR) materials used in direct cycle gas turbines.

	Micron-Atmospheres (μ-atmos)				
	H_2	H_2O	CO	CO_2	CH_4
HTR-GT	500	1.5	50	(1)*	50

*The CO_2 level should be allowed to find its own level in the loop through the water shift reaction.

The H_2/H_2O ratio is 333:1, CO/CO_2 ratio is 50:1, and the H_2/CH_4 ratio is also 10:1. Other material test programs, which are currently in progress or planned, are listed along with the impurity levels for the simulated reactor helium environment.

SIMULATED REACTOR HELIUM COMPOSITION OF VARIOUS MATERIALS TEST PROGRAMS

	(μ Atmos.)					
	H_2	H_2O	CO	CO_2	CH_4	Ref.
VHTR Materials Test Program:						
G.E. DCHT-NPH	400	2	40		20	11
CIIR - Oslo (Dragon) 1972 - 74	50 - 100	0.5-3	25-50	1	3 - 8	10, 12
Fiat - Italy After 1974	500	1.5	50	1	50	
Tokai Research Lab Jaeri, Japan	190- 220	2 - 4	90 - 110	2 - 3	5 - 6	13
General Atomics	1500	50	450	-	50	14
ORNL	275	10	15	-	25	15
KFA, Germany	500	1.5	15	-	20	16, 17

Based on the review of the data of Everette and the composition of simulated reactor helium used in other materials test programs around the world, it was concluded that the CCCBS materials test environment would operate in the following impurity ranges:

H_2 - 400 to 500 μ atmos.

H_2O - 1 to 3 μ atmos.

CO - 40 to 50 μ atmos.

CO_2 - permitted to establish equilibrium levels

CH_4 - 40 to 50 μ atmos.

9.3 ALLOY SELECTION, PROCUREMENT AND CHARACTERIZATION

9.3.1 ALLOY SELECTION

The alloys selected for the initial phase of the materials testing program are listed in Table 9-2. The first three alloys were selected on the basis of their commercial status and their particular applicability to the Compact Closed Brayton System requirements. Alloys 713LC, IN100 and MAR-M509 are commercially available alloys which have been used extensively in gas turbine applications over the past 10 to 15 years. Their history of metallurgical development and mechanical behavior is well documented. Thermal stability as determined by microstructural behavior on thermal exposure at elevated temperature is also well known and recorded. Alloy 713LC is one of a few nickel-base superalloys which does not contain cobalt as an intentional alloying addition. There are applications where cobalt is an objectionable alloying addition, and its presence is undesirable. IN100 is a "workhorse" turbine blade material designed to have a relatively low density combined with excellent creep resistance up to 1038°C (1900°F). The alloy has been successfully cast and utilized in a variety of shapes from turbine blades, vanes, and nozzles to integral wheels. Cobalt alloys are generally used as vanes, nozzles and other static hot structures

TABLE 9-2

SELECTED ALLOYS AND NOMINAL COMPOSITIONS

ALLOY	DENSITY (lbs/in^3)	COMPOSITION (wt. %)
1. Alloy 713LC	0.289	Ni-12Cr-4.5Mo-2Cb-5.9Al-0.6Ti-0.05C
2. IN100	0.280	Ni-10Cr-15Co-3Mo-4.7Ti-5.5Al-0.9V-0.18C
3. MAR-M509	0.320	Co-23.5Cr-10Ni-7.0W-3.5Ta-0.2Ti-0.5Zr-0.6C
4. MA 754	0.300	Ni-20Cr-0.5Ti-0.3Al-0.6Y_2O_3-0.05C
5. TZM	0.368	Mo-0.5Ti-0.08Zr-0.02C

because of their excellent hot corrosion (sulfidization) resistance. Cobalt alloys, however, are not generally used for rotating parts due to their lower creep and oxidation resistance compared to nickel-base alloys. MAR-M509 has good creep strength, resistance to thermal stressing, and resistance to crack propagation. The alloy can be used in the as-cast condition; no heat treatment is required. It can be successfully welded and joined both to itself and to many dissimilar metals by conventional techniques.

MA 754 is a recently developed nickel-chromium alloy produced by mechanical alloying which uniformly disperses yttrium oxide for dispersion strengthening at temperatures to the alloy is melting point. MA 754 exhibits excellent stress-rupture properties which are equivalent to or superior to cast alloys. MA 754 is currently being used as vanes in gas-turbine engines where high temperature strength is required. The superior creep-rupture properties of MA 754 provides high temperature growth potential for CCCBS turbine components.

TZM, a molybdenum-base alloy, is a refractory metal alloy which has demonstrated compatibility with inert gases at elevated temperatures and has superior creep strength at 982°C (1800°F) and above. TZM provides system growth to higher temperature capability.

9.3.2 PROCUREMENT

Alloy 713LC, IN100 and MAR-M509 were obtained as "as-cast" creep specimens from Jet Shapes, Inc., of Rockleigh, NJ. Alloy 713LC was purchased according to a Westinghouse specification, since no formal published specification for the alloy could be found in the open literature. The specification was modeled after AMS 5391 for alloy 713C. The only difference being a lower carbon level, 0.05 percent for the LC version vs 0.12 percent for the "C" alloy designation. IN100 specimens were cast according to AMS 5397 and MAR-M509 to a Pratt and Whitney specification, PWA 647E. Cast specimens were examined by x-ray analysis to insure sound porosity-free gage sections.

MA754 test material was procured from Huntington Alloys as solution annealed bar stock 8.9 cm x 3.2 cm by 12.7 cm (3-½ in. x 1-¼ in. by 5 in. long). No

specification exists at this time for this material. A Huntington data sheet supplied with the material indicated the solution annealing heat treatment to be ½ hour at 1316°C (2400°F) followed by air cooling.

The TZM test specimens were machined from forged and stress relieved material which was part of a NASA sponsored creep test program. Processing information and chemical analysis were supplied by TRW, Cleveland, OH, the contractor to NASA[18]. The TZM alloy was obtained from Climax Molybdenum of Michigan (now AMAX) in the form of 27.9 cm (11 inch) diameter disc forging. The material was vacuum arc-melted to 29.2 cm (11-½ in.) diameter ingot, extruded to a 15.9 cm (6-¼ in.) diameter, then upset forged to final size at 1204°C (2200°F) after heating to 1482°C (2700°F). The material was then stress relieved one hour at 1482°C (2700°F). Creep specimens were cut in a radial direction from the forged disc with the gage section parallel to the wrought microstructure. Chemical analyses of the test materials are given in Table 9-3.

9.3.2.1 MICROSTRUCTURE OF STARTING MATERIAL

The microstructures of the starting materials are shown in Figures 9-6, 9-7, 9-8, 9-9 and 9-10. Cross sections of the specimen gage sections of alloy 713LC and IN100 are shown to give an indication of the typical as-cast grain size. The microstructures shown at higher magnification are typical of cast superalloys. Alloy 713LC displays a dentritic type appearance. The low carbon modification of Alloy 713 resulted from desire to improve low temperature ductility by reducing massive MC formation during solidification. The resulting microstructure is relatively clean with some $M_{23}C_6$ located at the grain boundaries. MC and $M_{23}C_6$ are carbide phases which precipitate from the matrix and have a pronounced effect on mechanical properties. The microstructure of IN100 contains nodular gamma prime, γ', an intermetallic compound primarily Ni_3Al, throughout the matrix, white appearing particles, along with MC and $M_{23}C_6$ carbide phases. The MAR-M509 alloy is a cobalt-base alloy which contains $M_{23}C_6$ and MC phases. Tantalum, titanium and zirconium tend to dominate the monocarbide, MC. The $M_{23}C_6$ tends to form massive blocks in the interdendritic zones and at the grain boundaries.

The MA 754 alloy displayed a microstructure typical of oxide-dispersion strengthened material. In the transverse direction grains are irregular, while

TABLE 9-3

CHEMICAL ANALYSIS OF TEST MATERIAL*
(PERCENT)

Alloy	Heat No.	C	Mn	P	S	Si	Ni	Cr	Mo	Co	Fe	Ti	Al	B	Zr	Other
713LC	B553	.06	<.1	<.01	.003	<.1	bal.	11.4	4.0	.1	.05	.6	5.75	.015	.13	Cu-.04; Cb-1.99
IN 100	B747	.16	<.01	-	.004	.01	bal.	8.9	3.0	14.1	.2	.91	4.75	5.44	.001	V-.91
MAR-M509	B716	.621	.042	<.005	.005	.058	10.51	23.39	-	bal.	.408	.205	-	.0073	.467	Ta-3.47; W-7.24
MA 754**	DT007482-2	.02	-	-	-	-	bal.	20.0	-	-	-	.44	.3	-	-	Y_2O_3-.6
TZM	7502	.01	-	-	-	-	-	-	bal.	-	-	.5	-	-	.1	O_2-.002, N_2-.01; H_2-.001

* Certified analysis by supplier
** Typical analysis

Alloy 713LC, IN 100, and MAR-M509 supplied by Jet Shapes, Inc., MA 754 by INCO, and TZM by AMAX.

A

12 X

B

100 X

Figure 9-6. Microstructure of As-Cast Alloy 713LC

A

B

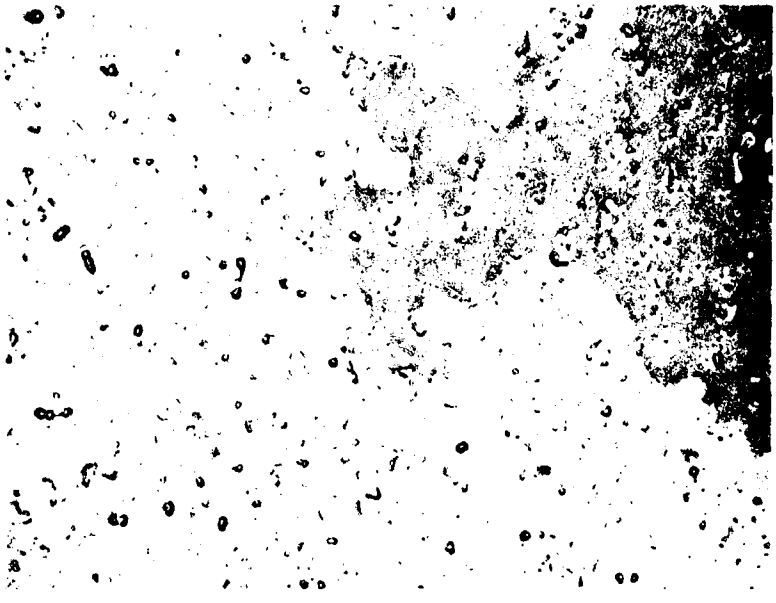

Figure 9-7. Microstructure of As-Cast IN100

A

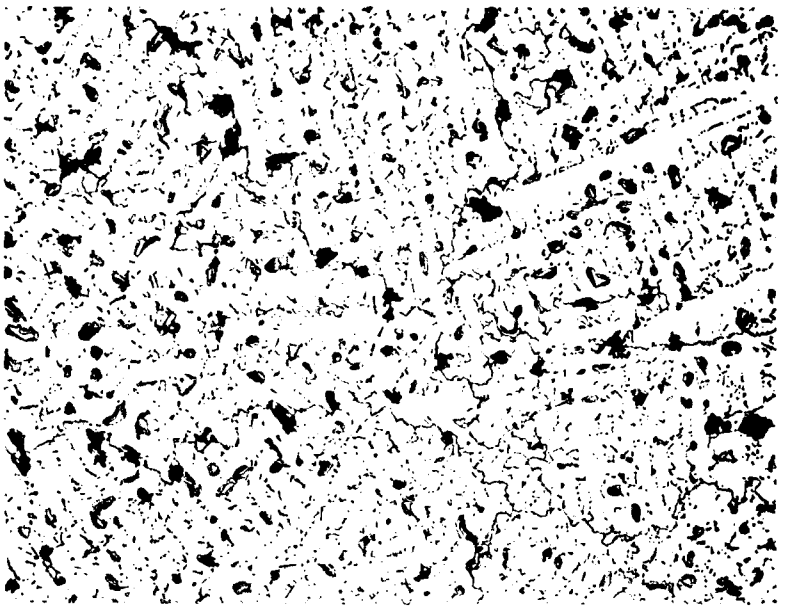

100 X

B

500 X

Figure 9-8. Microstructure of As-Cast MAR-M509

A
Transverse

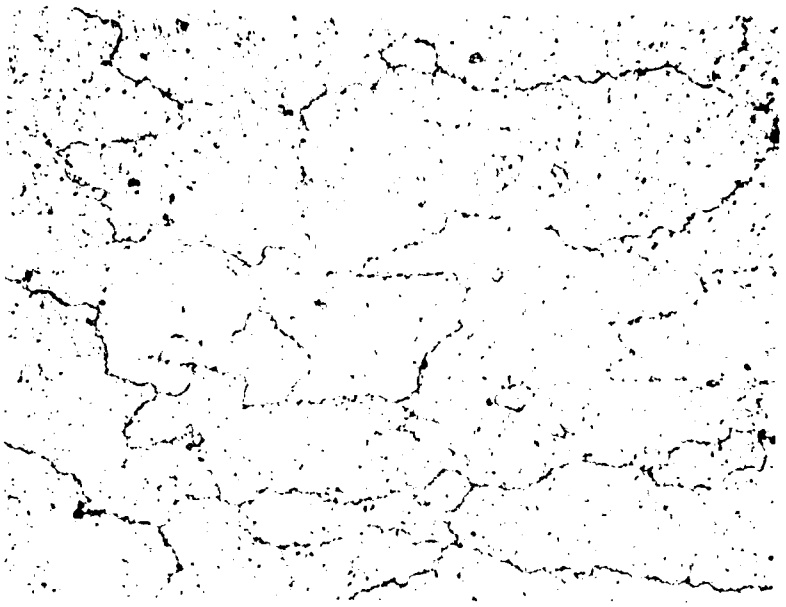

500 X

B
Longitudinal

500 X

Figure 9-9. Microstructure of MA 754

Longitudinal 100 X

Figure 9-10. Microstructure of Stress-Relieved TZM

in the longitudinal direction (parallel to working direction) the microstructure exhibited a large grain aspect ratio with interlocking grain boundaries pinned by finely dispersed Y_2O_3.

The TZM alloy exhibits a wrought microstructure with no evidence of recrystallization as a result of the stress relieve anneal. The test specimen blanks were cut parallel to the radii of "pancake" forging and thus exhibit a high aspect ratio wrought structure which resulted from the upset forging operation.

9.3.2.2 TEST SPECIMEN GEOMETRY

The creep-rupture test specimen geometries, which were used, are shown graphically in Figure 9-11. Actual test specimens are shown in Figure 9-12. The cast materials, Alloy 713LC, IN100 and MAR-M509, were received as cast-to-size specimens. The specimens had a nominal 0.64 cm (1/4 inch) diameter gage section 3.2 cm (1-¼ inch) long with ½-13 threaded ends. The as-cast specimens were machined to produce a round, uniform diameter along the gage length as shown by specimen 2 in Figure 9-12. These specimens were used for the air tests because the cross-sectional area was compatible with the load capacity of the lever arm test machines. For the deadweight loaded tests in ultra-high purity helium, the cross-sectional area of the gage section was reduced to a diameter of 4 mm (0.160 inch) as illustrated by specimen 1 in Figure 9-12. The gage diameter for each material was adjusted to accommodate the physical volume of the load required to achieve the desired stress levels and remain within the equipment limitations. Double shoulder-type creep specimens with differing gage diameters were used for the MA 754 and TZM materials as shown by specimens 3 and 4 in Figure 9-12. The MA 754 specimen gage diameter was 4.6 mm (0.180 inch), and the TZM specimen diameter was 2.5 mm (0.1 inch).

9.2.2.3 TENSILE PROPERTIES OF TEST MATERIALS

In order to more completely characterize the creep-rupture test materials, a limited number of tensile tests were conducted. The number of tensile tests conducted was dependent upon the availability of extra test specimens. The results are given in Table 9-4 along with test data from the alloy developer or other available services. Tests were conducted at room temperature and at 927°C

AS–RECEIVED
CAST SPECIMEN
CONFIGURATION

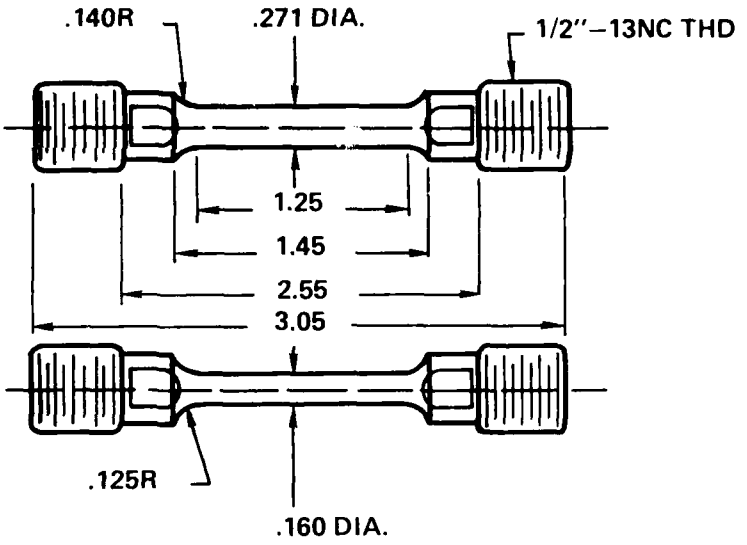

MODIFIED CAST
SPECIMEN
CONFIGURATION FOR
UHP–He TESTING

DOUBLE SHOULDER
SPECIMEN CONFIGURATION
FOR MA 754 AND TZM
UHP–He TESTING

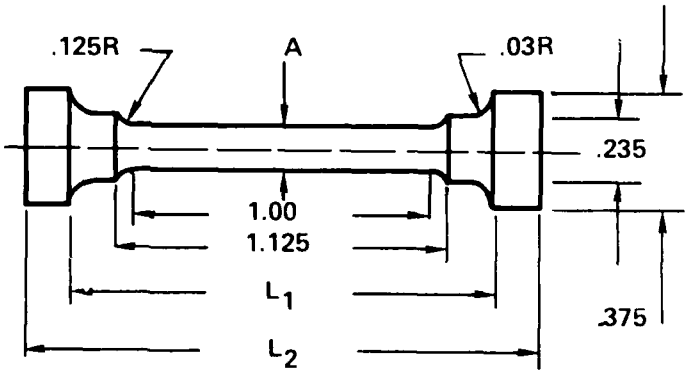

A	TZM	0.100
A	MA 754	0.179
L_1	TZM	1.25
L_1	MA 754	1.45
L_2	TZM	2.00
L_2	MA 754	2.25

Figure 9-11. Creep-Rupture Specimen Geometries for Various Test Materials

AD-A081 380 WESTINGHOUSE ELECTRIC CORP PITTSBURGH PA ADVANCED ENE--ETC F/G 20/13
COMPACT CLOSED CYCLE BRAYTON SYSTEM FEASIBILITY STUDY. VOLUME I--ETC(U)
AUG 79 R E THOMPSON, R L AMMON, R CALVO N00014-76-C-0706
UNCLASSIFIED WAES-TNR-237-VOL-2 NL

5 OF 6
AD A081 380

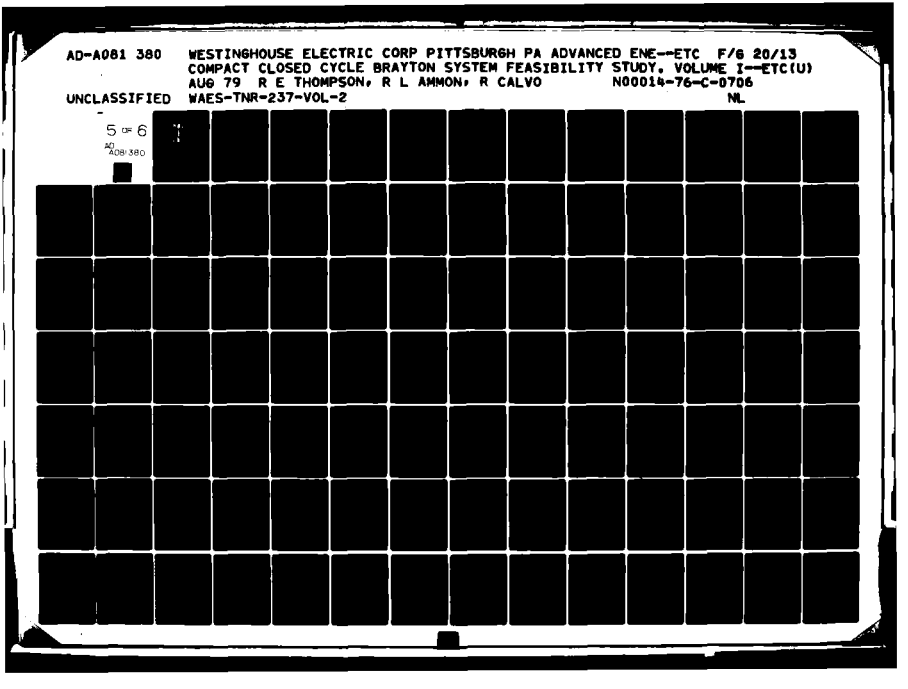

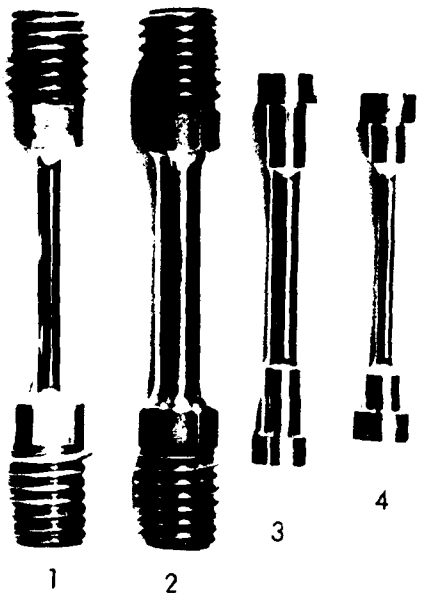

1. Ultra-high purity helium test specimen for as-cast Alloy 713LC, IN100 and MAR-M509 material.
2. Air test specimens for as-cast alloy 713LC, IN100 and MAR-M509.
3. MA 754 creep-rupture test specimen.
4. TZM creep-rupture test specimen.

Figure 9-12. Photographs of Creep-Rupture Test Specimens

TABLE 9-4

TENSILE PROPERTIES OF TEST MATERIALS

Material	Test Temp. (°C)	Test Temp. (°F)	0.02 Yield Strength (MPa)	0.02 Yield Strength (Ksi)	Ultimate Strength (MPa)	Ultimate Strength (Ksi)	Elong. (%)	R. A. (%)	Comment*
713LC	RT		830.2	(120.4)	1006.7	(146.0)	8.0	7.2	
	RT		856.4	(124.2)	1026.0	(148.0)	8.8	8.7	
	RT		751.6	(109.0)	894.4	(130.0)	15.3	20.9	INCO Data
	871	(1600)	606.1	(87.9)	706.7	(102.5)	8.3	7.2	
	927	(1700)	475.8	(69.0)	557.1	(80.8)	8.8	12.9	
	927	(1700)	490.2	(71.1)	588.1	(85.3)	11.2	17.8	
	927	(1700)	461.3	(66.9)	649.5	(94.2)	6.0	12.0	INCO Data
	982	(1800)	348.9	(50.6)	411.6	(59.7)	11.3	9.6	
IN 100	RT		868.1	(125.9)	974.3	(141.3)	8.8	15.2	
	RT		848.1	(123.0)	1013.6	(147.0)	9.0	11.0	
	871	(1600)	722.6	(104.8)	774.3	(112.3)	4.0	6.4	
	927	(1700)	595.7	(86.4)	654.3	(94.9)	4.8	4.8	
	927	(1700)	503.3	(73.0)	737.8	(107.0)	6.0	7.2	INCO Data
	982	(1800)	464.0	(67.3)	499.9	(72.5)	4.6	5.6	
MAR M509	RT		639.9	(92.8)	790.2	(114.6)	1.6	2.1	
	RT		420.6	(61.0)	820.5	(90.0)	6.0	-	W GTED
	871	(1600)	322.7	(46.8)	392.3	(56.9)	21.6	25.2	
	927	(1700)	273.7	(39.7)	312.3	(45.3)	21.6	32.7	
	927	(1700)	206.8	(30.0)	255.1	(37.0)	35.0	-	W GTED
	982	(1800)	224.1	(32.5	249.6	(36.2)	25.6	32.7	
MA 754	RT		673.0	(97.6)	995.6	(144.4)	21.0	31.7	
	927	(1700)	223.4	(32.4)	237.2	(34.4)	15.0	33.4	

*All data are for material evaluated on this current program, exept where noted.

Strain Rate - 0.05/min

W GTED - Westinghouse Gas Turbine Engine Division

INCO - International Nickle Corporation - Data Brochure

(1700°F) and at other elevated temperatures where possible. No tensile tests of TZM alloy were conducted.

9.4 CREEP-RUPTURE TEST RESULTS AND EVALUATION

Creep-rupture testing of five selected turbine materials was conducted in ultra-high purity helium and simulated CCCBS helium working fluid environment. Supplementary creep-rupture tests were also conducted in static air for Alloy 713LC, IN100, MAR-M509 and MA754. The test data generated during this program are listed in Table 9-5. A total of 40,035 test hours were accumulated in air, 76,583 hours in ultra-high purity helium, and 11,350 hours in a dynamic simulated CCCBS helium working fluid. Termination of the program by the customer prevented completion of the tests involving the dynamic simulated CCCBS helium working fluid environment. Test results for each alloy are described and evaluated individually in the following discussions.

9.4.1 ALLOY 713LC

Four creep-rupture tests of Alloy 713LC were conducted in ultra-high purity helium for a total of 5733 test hours. Test times ranged in duration from 269 to 3182 hours. Four air tests at corresponding stress levels were also conducted. One test in the dynamic simulated CCCBS environment was conducted at a stress of 117 MPa (17 ksi). The test results, rupture life vs stress level, are plotted in Figure 9-13. In order to provide a basis for comparison, a computer printout of creep-rupture data for Alloy 713LC was obtained from the Mechanical Property Data Center (MPDC), Traverse City, Michigan. The MPDC is a DOD supported materials information center. The Alloy 713LC printout contained data for 831 creep-rupture tests, which were carried out in air in the temperature range 732 to 1204°C (1350 to 2200°F). The data were gathered primaryly from government-sponsored programs. Of the 831 creep-rupture test results reported, 507 were carried out a 982°C (1800°F) at a stress level of 152 Mpa (22 ksi). These test conditions are apparently used for heat qualification. Only three tests of >10,000 hours were reported, and they were conducted at 816°C (1500°F) or lower. Sixteen creep-rupture tests of greater than 1000 hours were reported. These data illustrate the dearth of long-term high temperature creep-rupture data available in the open literature for a widely used, relatively old, commercial superalloy.

TABLE 9-5

CREEP-RUPTURE DATA FOR SELECTED CCCBS MATERIALS AT 930°C (1700°F)

Material	Test Atmos.	Stress (MPa)	Stress (ksi)	Time to % Strain (Hours) 0.5%	1.0%	3.0%	Total Strain (%)	Rupture Time (Hrs)	Reduction in Area (%)	Status
Alloy 713LC	UHP He	138	(20.0)	84	192	268	6.4	269	16.7	Completed
		138	(20.0)	260	495	691	8.0	755	22.0	Completed
		124	(18.0)	128	943	1522	4.8	1527	8.4	Completed
		103	(15.0)	1060	2500	3150	5.6	3182	10.2	Completed
	Air	138	(20.0)	212	395	572	9.6	623	25.8	Completed
		138	(20.0)	8	86	324	10.4	397	8.7	Completed
		124	(18.0)	29	119	405	9.6	476	8.3	Completed
		103	(15.0)	100	740	1870	5.6	1959	8.1	Completed
	CCCBS*	117	(17.0)	575	820	1130	8.0	1268	26.8	Completed
IN 100	UHP He	155	(22.5)	700	1170	1982	16.0	2272	17.6	Completed
		124	(18.0)	1217	-	-	-	1448	-	1
		110	(16.0)	3000	4300	7950	10.4	9452	34.5	Completed
	Air	207	(30.0)	8	70	211	6.4	271	6.7	Completed
		207	(30.0)	22	93	285	7.2	334	8.5	Completed
		172	(25.0)	1	7	490	7.2	685	4.3	Completed
		155	(22.5)	110	550	1130	7.2	1347	6.0	Completed
		124	(18.0)	1460	2890	2985	7.2	3110	12.1	Completed
		110	(16.0)	200	3800	4900	8.0	5244	16.1	Completed
	CCCBS*	124	(18.0)	1550	2000	2810	7.2	3338	23.7	Completed
		110	(16.0)	-	-	-	-	1316	-	1
		110	(16.0)	1000	2650	3920	13.5	6304	24.2	Completed
MAR M509	UHP He	103	(15.0)	2350	2440	2460	4.0	2537	0.1	Completed
		86	(12.5)	1900	5050	7900	12.8	11615	44.4	Completed
	Air	124	(18.0)	2	5	264	21.6	618	34.1	Completed
		103	(15.0)	1	570	1910	16.8	2507	19.6	Completed
		86	(12.5)	5	25	2750	7.2	4652	0.9	Completed
MA 754	UHP He	152	(22.0)	-	-	-	-	8751	-	1
		138	(20.0)	-	-	-	-	17626	-	Stopped
	Air	152	(22.0)	-	-	-	-	2100	-	2
		138	(20.0)	70	3480	15440	12.0	15712	10.4	Completed
	CCCBS*	165	(24.0)	20	100	230	5.0	289	9.2	Completed
		155	(22.5)	40	110	636	3.0	636	7.6	Completed
		155	(22.5)	100	600	1445	4.0	1445	1.9	Completed
		152	(22.0)	1	500	2640	4.4	2660	9.4	Completed
TZM	UHP He	414	(60.0)	220	425	1095	12.0	1483	98.0	Completed
		379	(55.0)	450	1010	2000	14.5	2256	98.0	Completed
		362	(52.5)	790	2000	5200	10.2	5592	76.0	Completed
		331	(48.0)	1850	4650	-	-	7818	-	Stopped

*Simulated CCCBS He Working Fluid, 400 to 500 μ atmos. H_2, 40 to 50 μ atmos. CH_4, 40 to 50 μ atmos. CO, 1 to 3 μ atmos. H_2O, CO_2 equilibrium levels.

1 Temperature Controller Malfunctioned

2 Specimen Failed in Grips

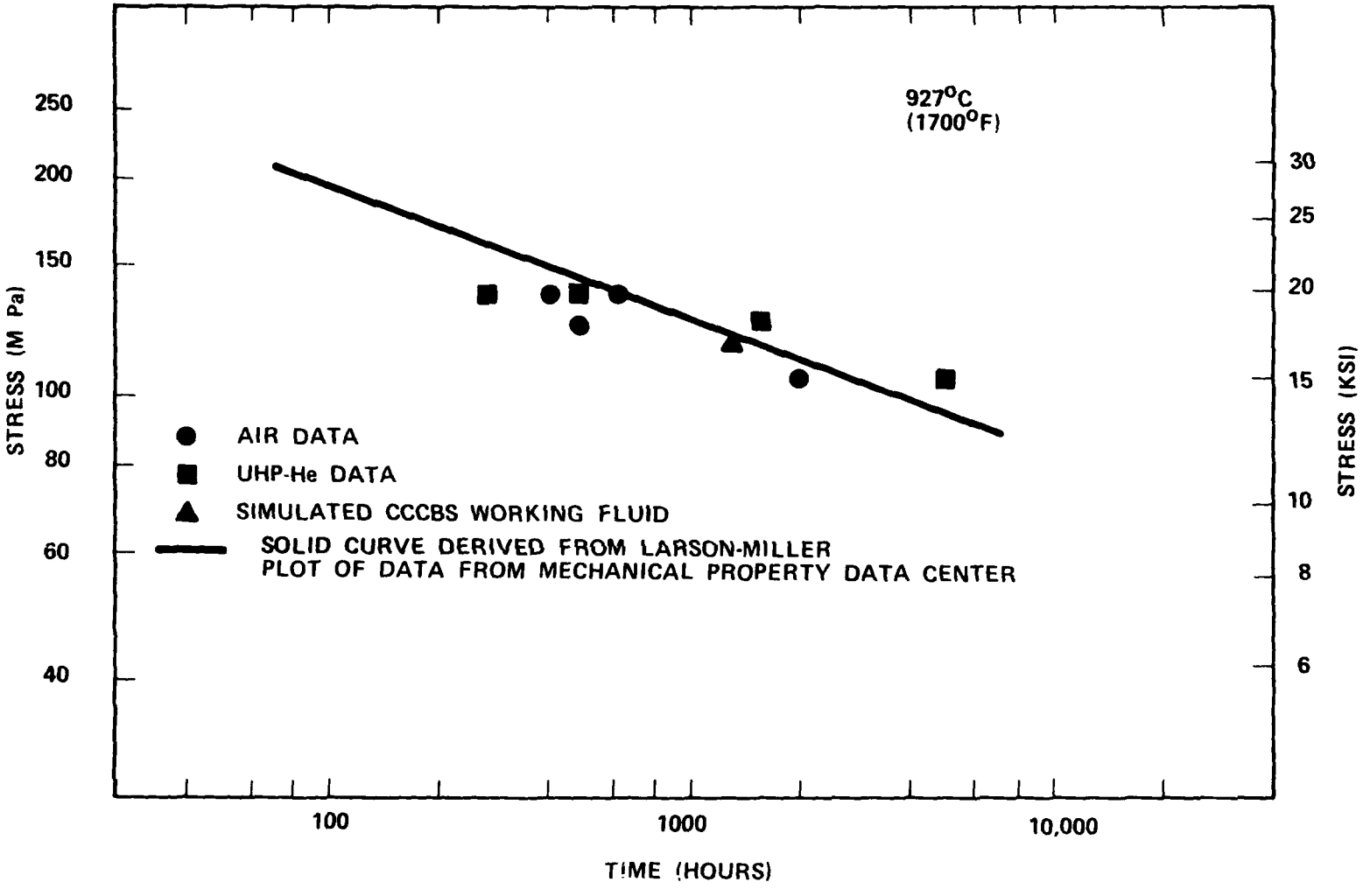

Figure 9-13. Creep-Rupture Life of Alloy 713LC

The solid reference curve in Figure 9-13 was generated from a Larson-Miller plot of the MPDC data. Logarithmic curve fit and linear regression analysis were used to produce a best-fit curve for 61 data points representing the rupture life of Alloy 713LC in the stress range 86 to 207 MPa (12.5 to 30 ksi) and test temperatures in the range 871 to 982°C (1600 to 1800°F). The air, ultra-high purity helium, and the CCCBS environment test data for material evaluated on this program compare favorably with the reference curve. At the 138 MPa (20 ksi) stress level, four tests were conducted, two under each environmental condition. The actual creep-rupture curves are shown in Figure 9-14. The specimens tested in ultra-high purity helium exhibited rupture times ranging from 269 to 755 hours with fracture strains of 6.4 and 8.0 percent, respectively. The two air tests had rupture times of 397 and 623 hours with slightly higher fracture strains of 10.4 and 9.6 percent. At the lower stress levels, Figures 9-15 and 9-16, the ultra-high purity helium tests exhibited significantly longer rupture times compared to tests conducted in air. The test results for both environmental conditions, however, fall within a reasonable scatter band, Insufficient test data prevent definitive conclusions to be drawn, although a trend to improved rupture life of Alloy 713LC in ultra-high purity helium appears as a possibility. Additional tests preferably at times of 10,000 hours or longer, are required to definitely establish the validity of the observed trend. The one simulated CCCBS helium working fluid environmental test had a rupture life of 1268 hours at a stress level of 117 MPa (17 ksi). This data point fell on the reference curve.

One additional comment regarding the stress-rupture behavior of Alloy 713LC relevant to CCCBS requirements involves the projected stress required to give a 10,000 hour rupture life. Initial data published by INCO in which a limited number of rupture tests of less than 3500 hours, indicated an extrapolated rupture life of 10,000 hours at a stress of slightly higher than 103 MPa (15 ksi) at 927°C (1700°F)[19]. Data from MPDC involving many more test results indicate that the extrapolated 10,000 hour rupture life may be closer to 83 MPa (12 ksi) at 927°C (1700°F). Actual creep-rupture behavior for long-term tests greater than a few thousand hours may be affected by air oxidation resulting in a reduced stress for 10,000 hour life.

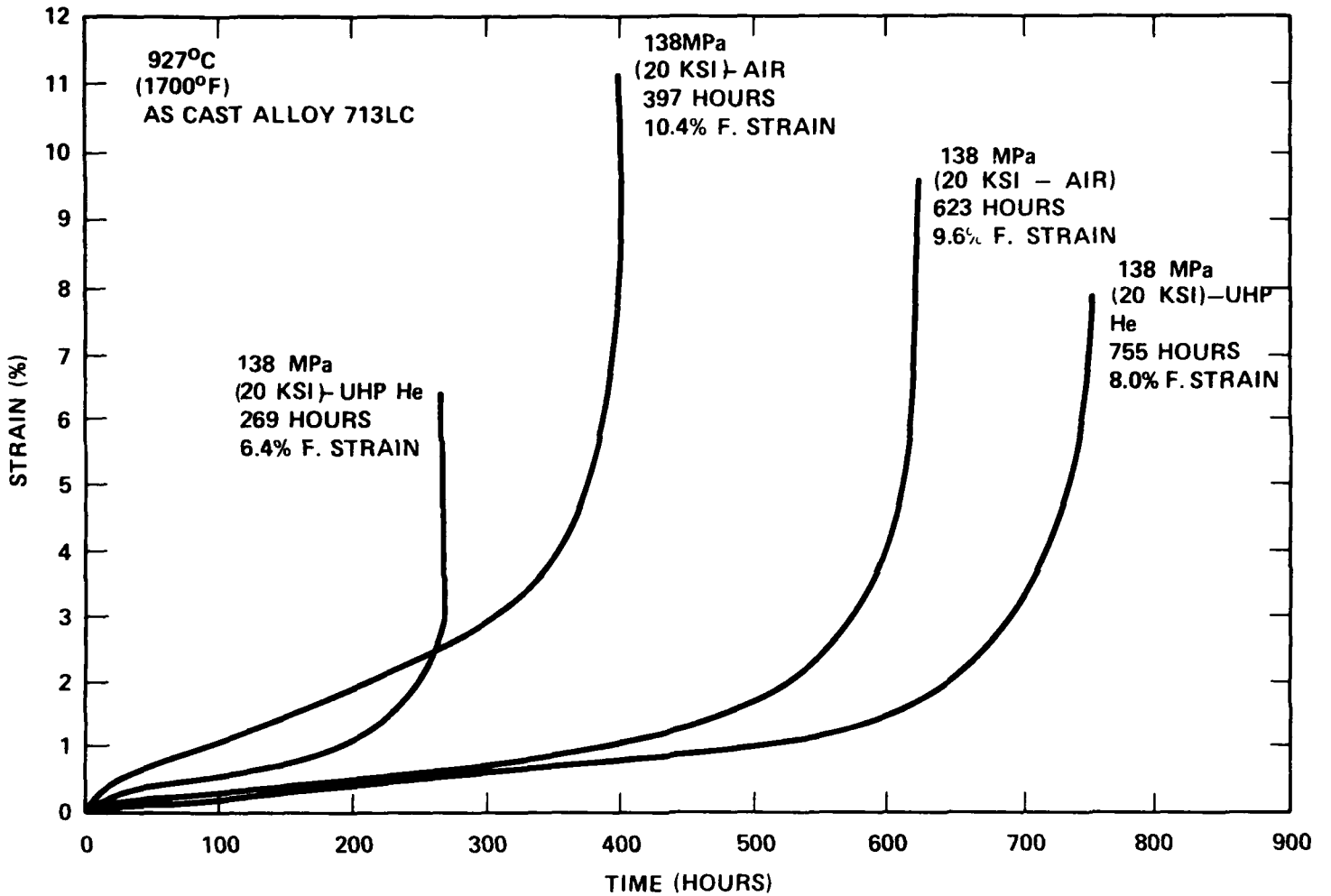

Figure 9-14. Creep-Rupture Curve for As-Cast Alloy 713LC

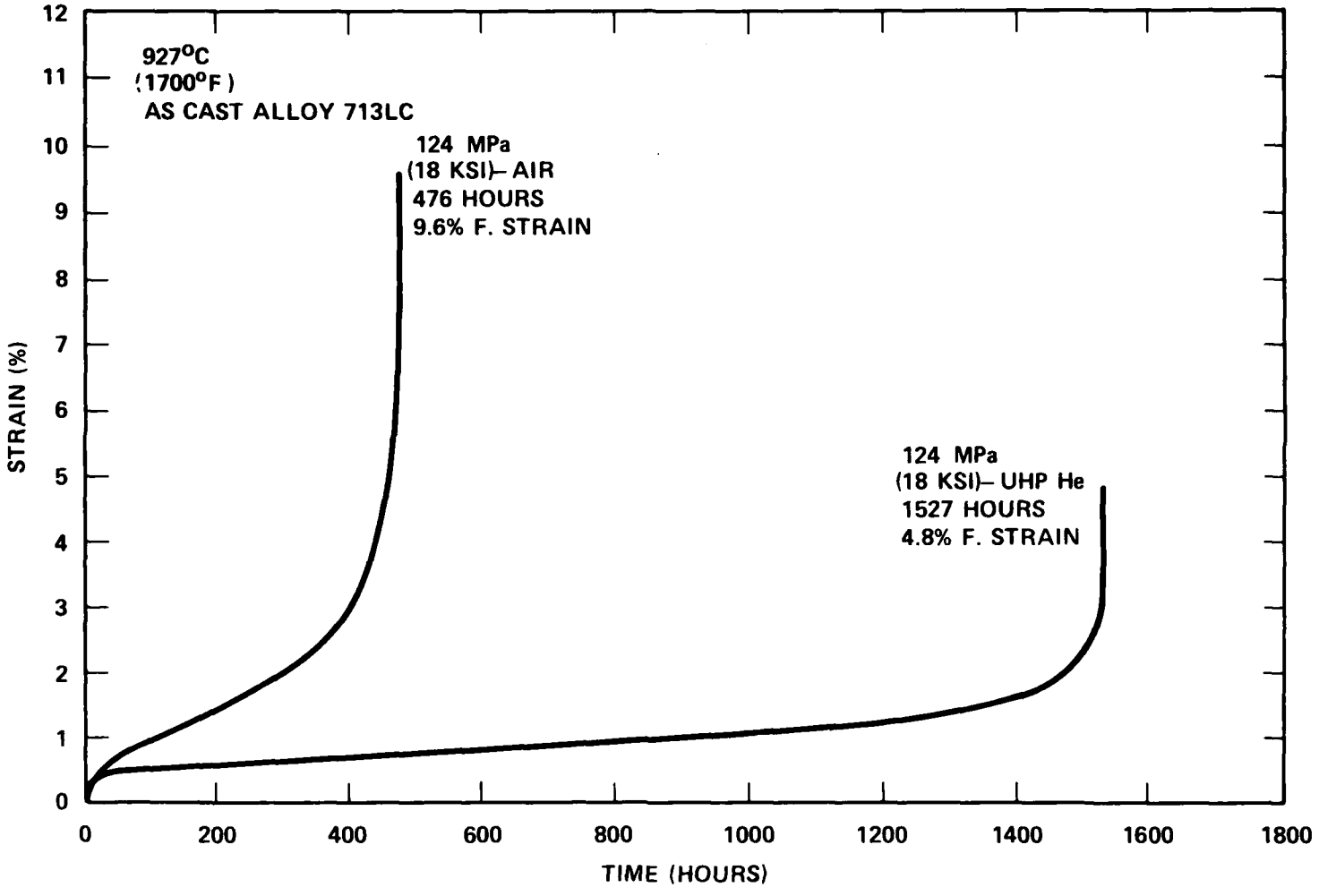

Figure 9-15. Creep-Rupture Curve for As-Cast Alloy 713LC

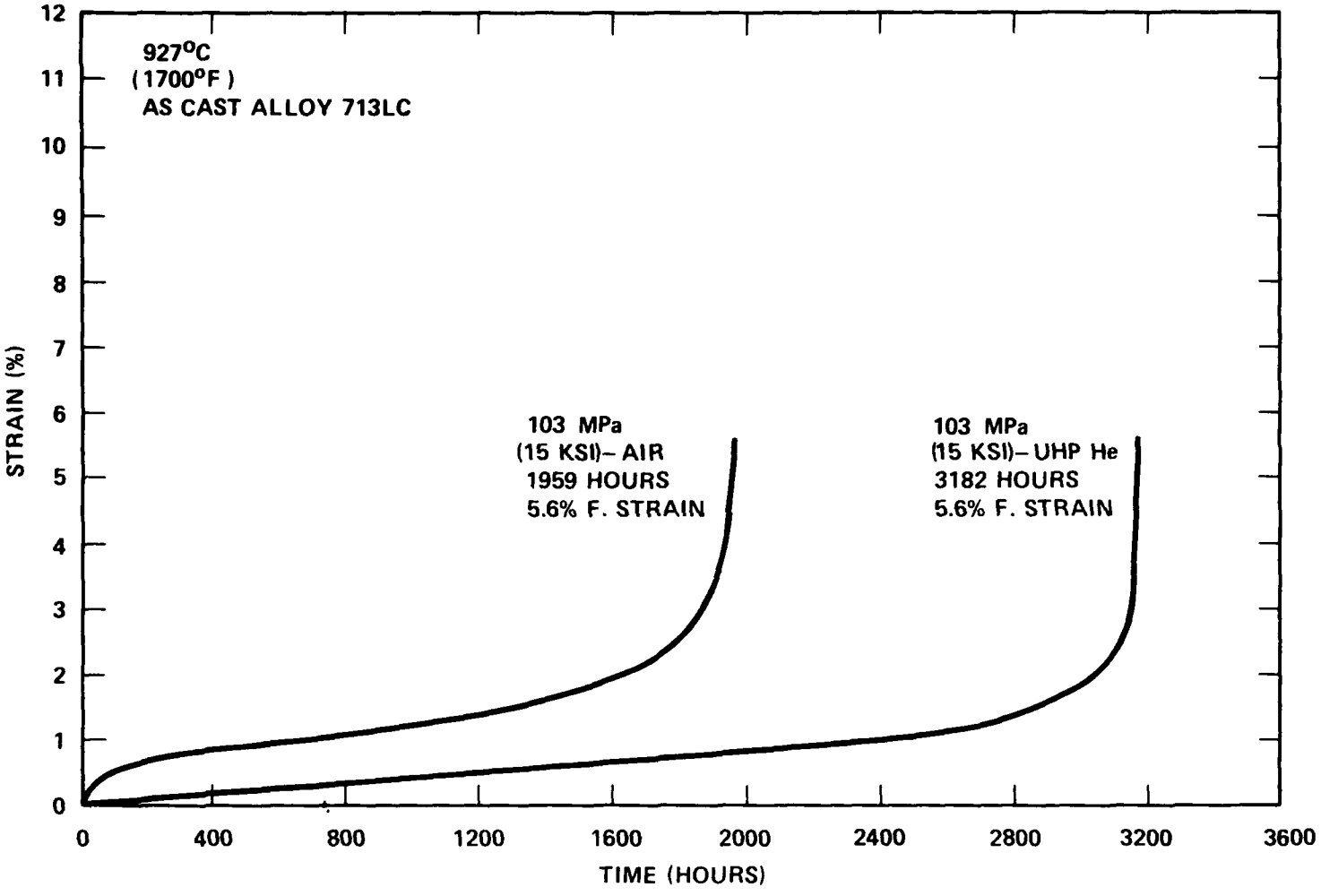

Figure 9-16. Creep-Rupture Curve for As-Cast Alloy 713LC

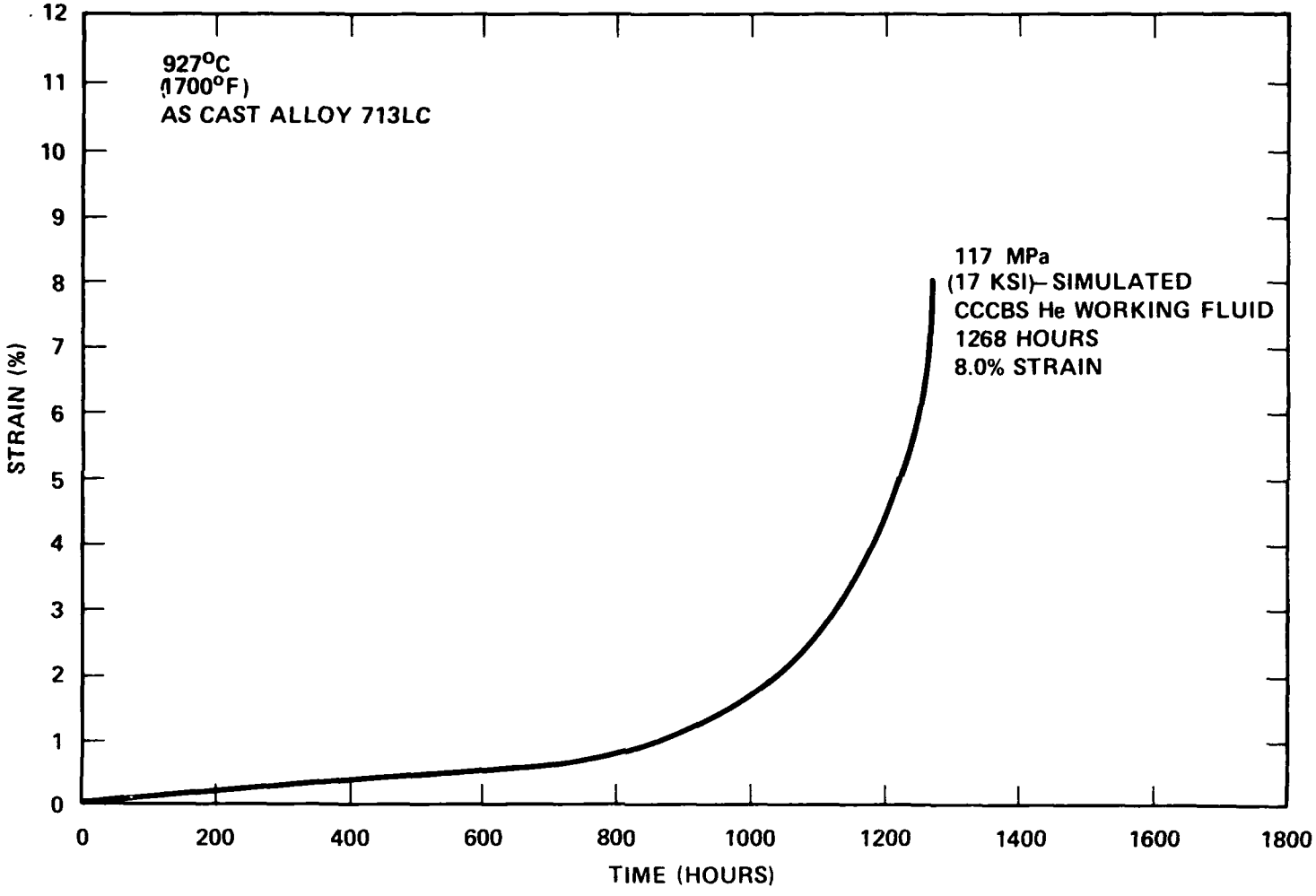

Figure 9-17. Creep-Rupture Curve for As-Cast Alloy 713LC

9.4.2 ALLOY IN100

A total of 12 IN100 creep-rupture tests were conducted including six in air, three in UHP-He, and three in CCCBS helium working fluid environment. One test in the CCCBS helium environment was in progress at the completion of the report period. The rupture life data are given in Figure 9-18. The reference curve was generated from a Larson-Miller plot of data received from the Mechanical Property Data Center. As pointed out in the discussion of Alloy 713LC, the number of long-term tests conducted at temperatures above 871°C (1600°F) was very limited. Of the 573 reported test results, only 22 tests of greater than 1000 hours were reported. There were no test results in the 871 to 982°C (1600 to 1800°F) test temperature range greater than 4700 hours. A total of 52 data points were used to develop a Larson-Miller curve from which the reference curve in Figure 9-18 was produced. The air data show excellent correlation with the reference data. Creep-rupture curves for tests conducted at 207 MPa (30 ksi) and 172 MPa (25 ksi) are shown in Figures 9-19 and 9-20. Creep-curves for tests conducted at 155 MPa (22.5 ksi) in air and UHP-He are shown in Figure 9-21. The rupture life in UHP-He was significantly higher than the air test results. Fracture strain was also significantly higher for UHP-He test, 16 vs 7.2 percent. At the 110 MPa (16 ksi) stress level, as shown in Figure 9-23, results were similar. The UHP-He test displayed significantly greater rupture life and moderately greater fracture strain. The rupture life of the two UHP-He tests that were completed exhibited rupture life that was significantly greater than the reference data base and for the air data generated from test specimens from the sam heat of material. Whether the behavior is a real environmental effect remains to be determined. One test involving the simulated CCCBS helium working fluid environment was completed; a second was still in progress at the end of the report period. The completed simulated CCCBS helium test was conducted at a stress level of 124 MPa (18 ksi). The creep-rupture curve for this test is shown in Figure 9-22, along with results for an air test at the same stress level. Rupture life and fracture strain for both tests were comparable. The CCCBS helium test, however, exhibited transition to third-stage creep at a much earlier time compared to the air test. This behavior may or may not be the result of environmental influence. Additional tests would be required to resolve this anomalous behavior.

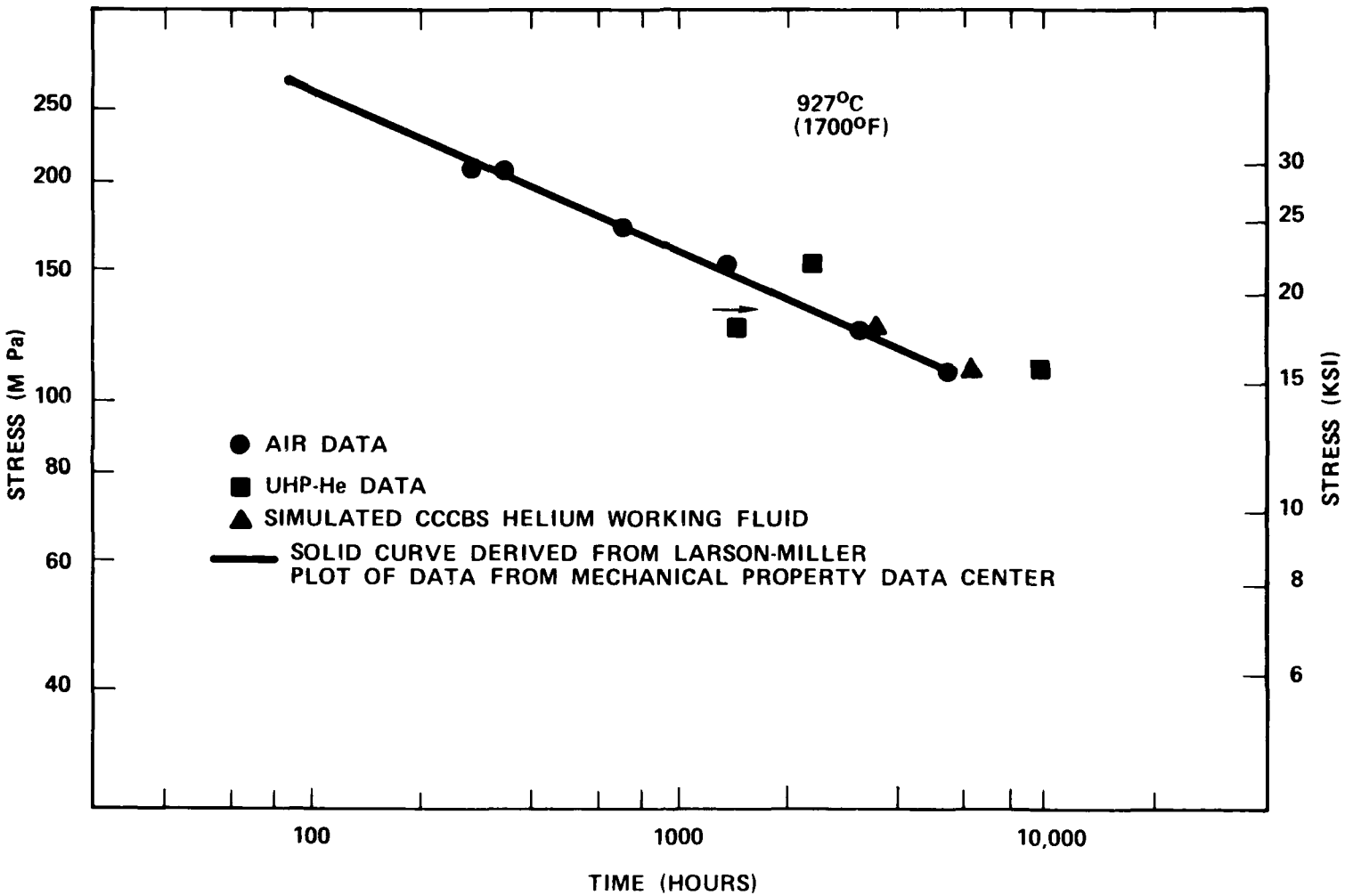

Figure 9-18. Creep-Rupture Life of As-Cast IN100

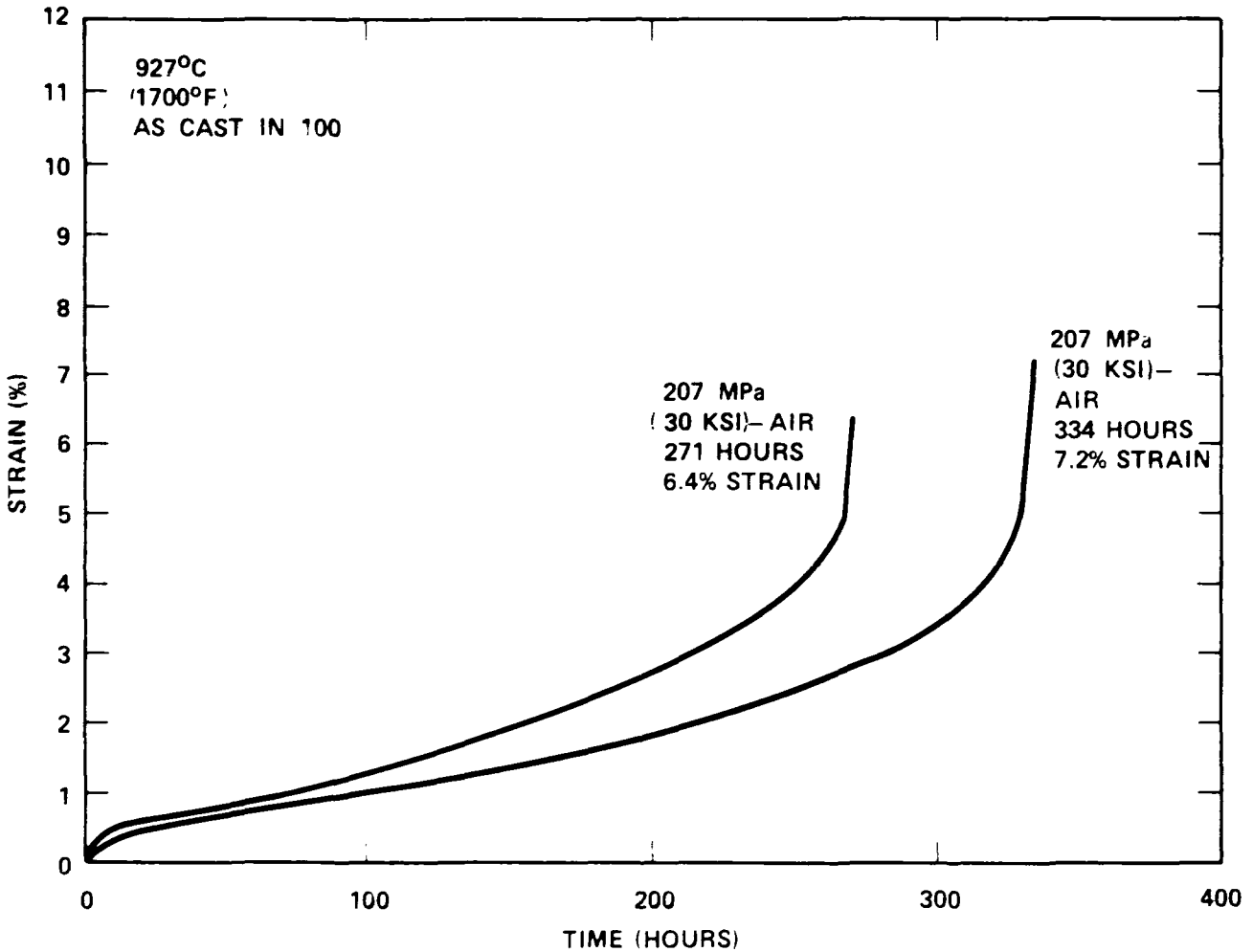

Figure 9-19. Creep-Rupture Curve for As-Cast IN100

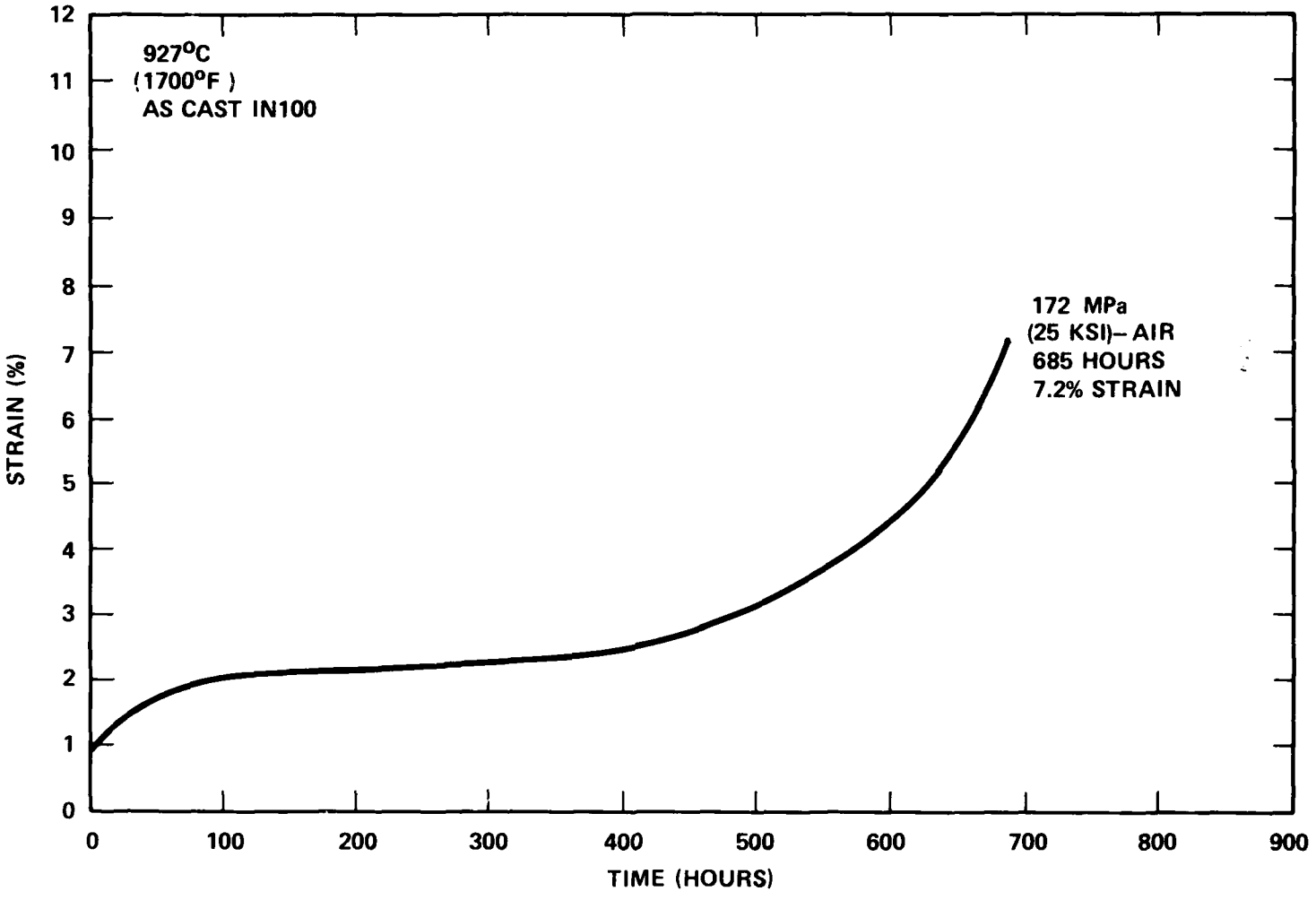

Figure 9-20. Creep-Rupture Curve for As-Cast IN100

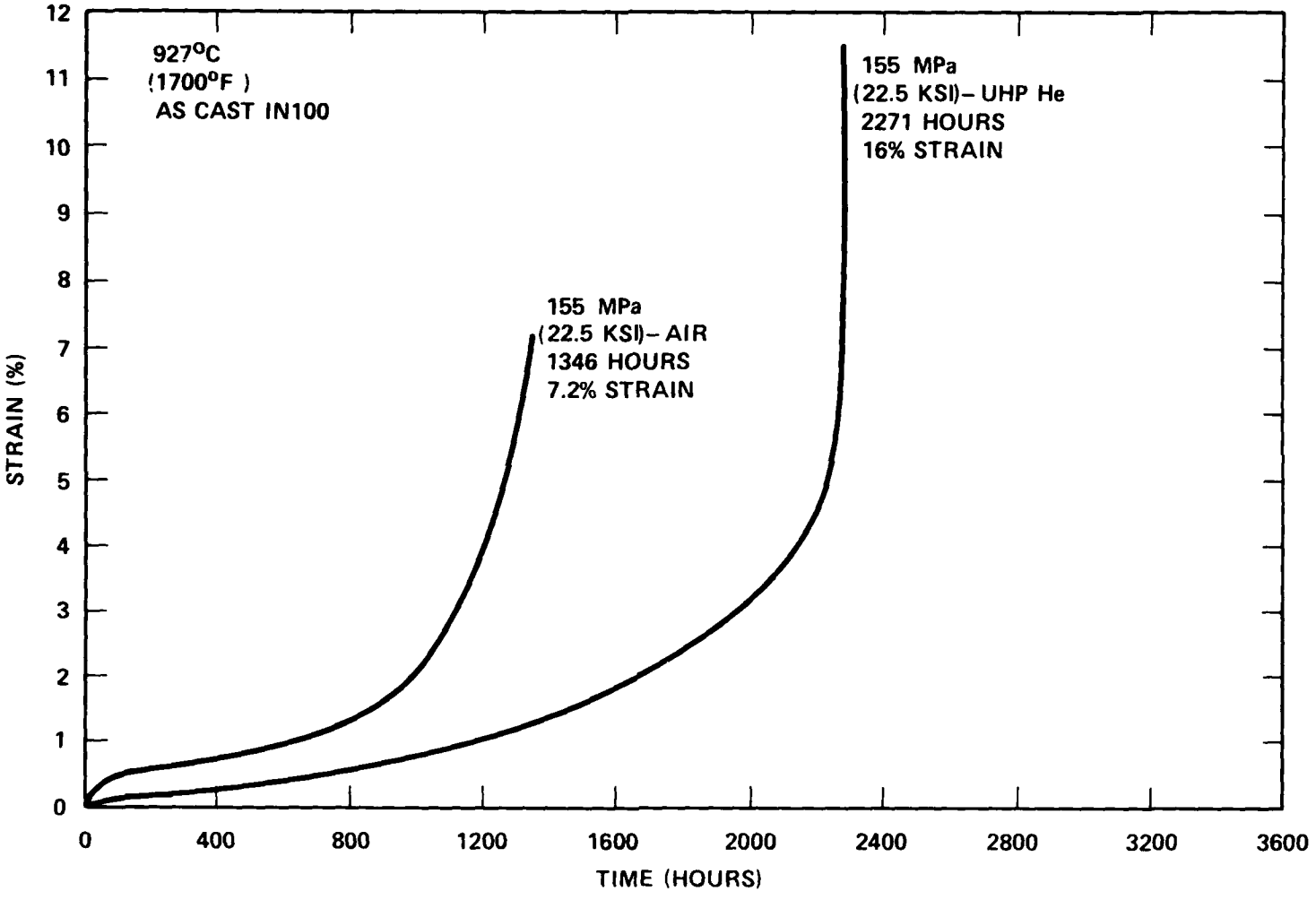

Figure 9-21. Creep-Rupture Curve for As-Cast IN100

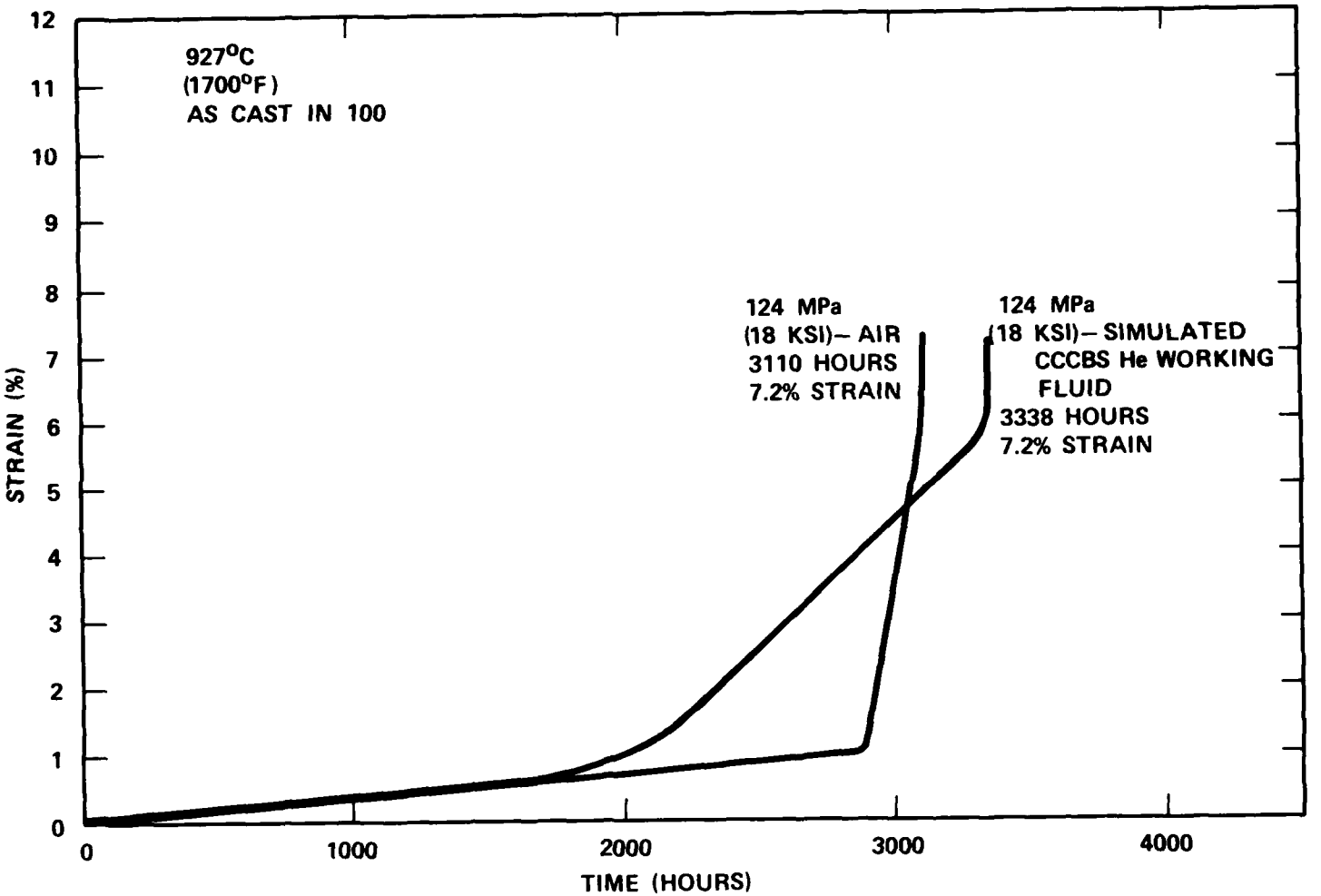

Figure 9-22. Creep-Rupture Curve for As-Cast IN100

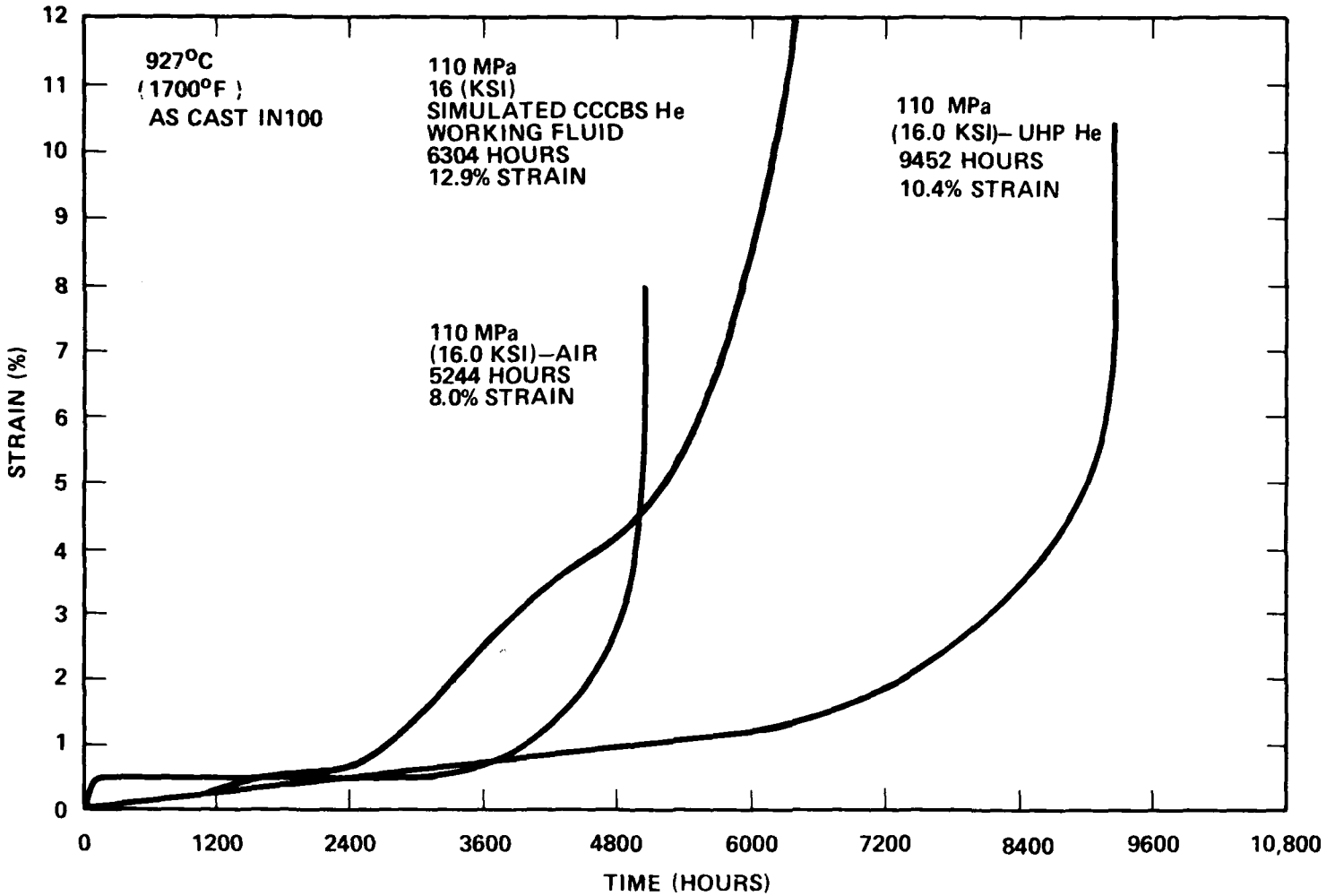

Figure 9-23. Creep Rupture Curve for As-Cast IN100

It should be noted that the reference curve in Figure 9-18 derived from MPDC data varies from other published data regarding the expected stress to produce 10,000 hour rupture life at 927°C (1700°F)[20]. The extrapolated stress to produce a 10,000 hour rupture life at 927°C (1700°F) is approximately 83 MPa (12 ksi).

9.4.3 ALLOY MAR-M509

A total of five creep-rupture tests of Alloy MAR-M509 were conducted, three in air and two in UHP-He. All tests were completed, and the data are shown in Figure 9-24. The reference curve was produced from MPDC data and represented 90 creep-rupture tests in the temperature range 871 to 1093°C (1600 to 2000°F). The longest test time reported was 3220 hours at 982°C (1800°F) at 70 MPa (10 ksi). The remainder of the reported tests were carried out at higher stress levels for test times of less than 800 hours in duration. The creep-rupture curves for the five tests reported here are given in Figures 9-25, 9-26 and 9-27. The air test curves exhibit an apparent strain on loading which was due to the method of strain measurement. Lever arm motion was measured with a dial gage, thus the total motion of the load train was included in the initial loading. In the UHP-He test, strain was measured directly off the gage section of the test specimen optically, therefore extraneous motion of the load train was not included in the strain on loading. The air data for this particular heat of MAR-M509 compares quite well with the MPDC derived curve. The curves in Figures 9-26 and 9-27 which illustrate creep behavior at a stress of 103 and 83 MPa (15 and 12.5 ksi), respectively, indicate a possible beneficial influence of the UHP-He test environment compared to air. At a stress of 103 MPa (15 ksi), the rupture life of each is essentially identical; however, the initiation of third stage creep occurs much later in the UHP-He test environment. At a stress level of 86 MPa (12.5 ksi), the secondary creep rate for the UHP-He test environment was 2.0×10^{-4} percent/hr whereas the secondary creep rate for the air test was 1.0×10^{-3}, a factor of five greater. While the limited data preclude conclusive proof as to the beneficial influence of UHP-He test environment over air, it can be stated that the UHP-He test environment does not produce a gross deleterious effect on the creep-rupture behavior of MAR-M509. MAR-M509 was not tested in the dynamic simulated CCCBS helium working fluid environment.

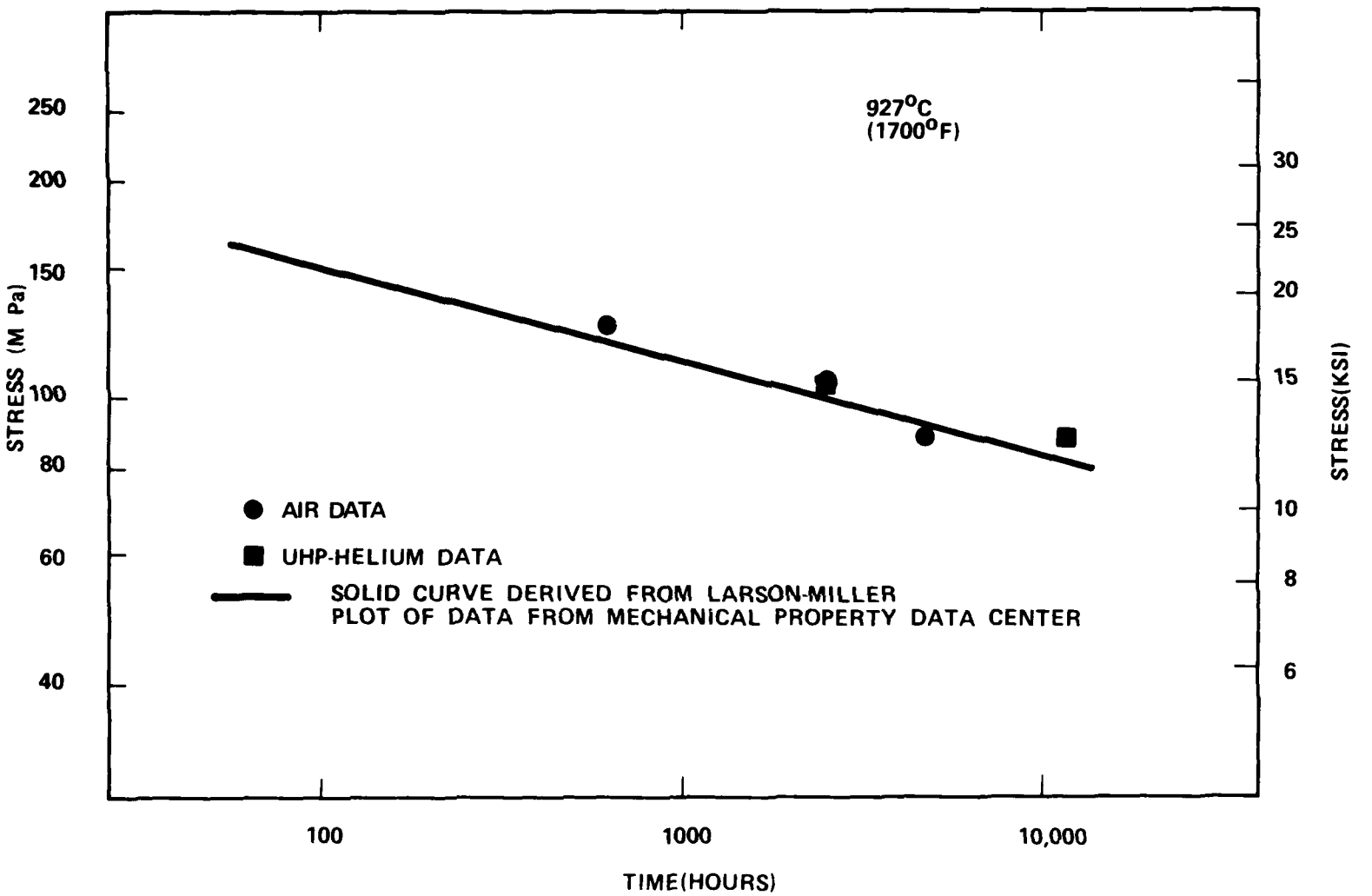

Figure 9-24. Creep Rupture Life of As-Cast MAR-M-509

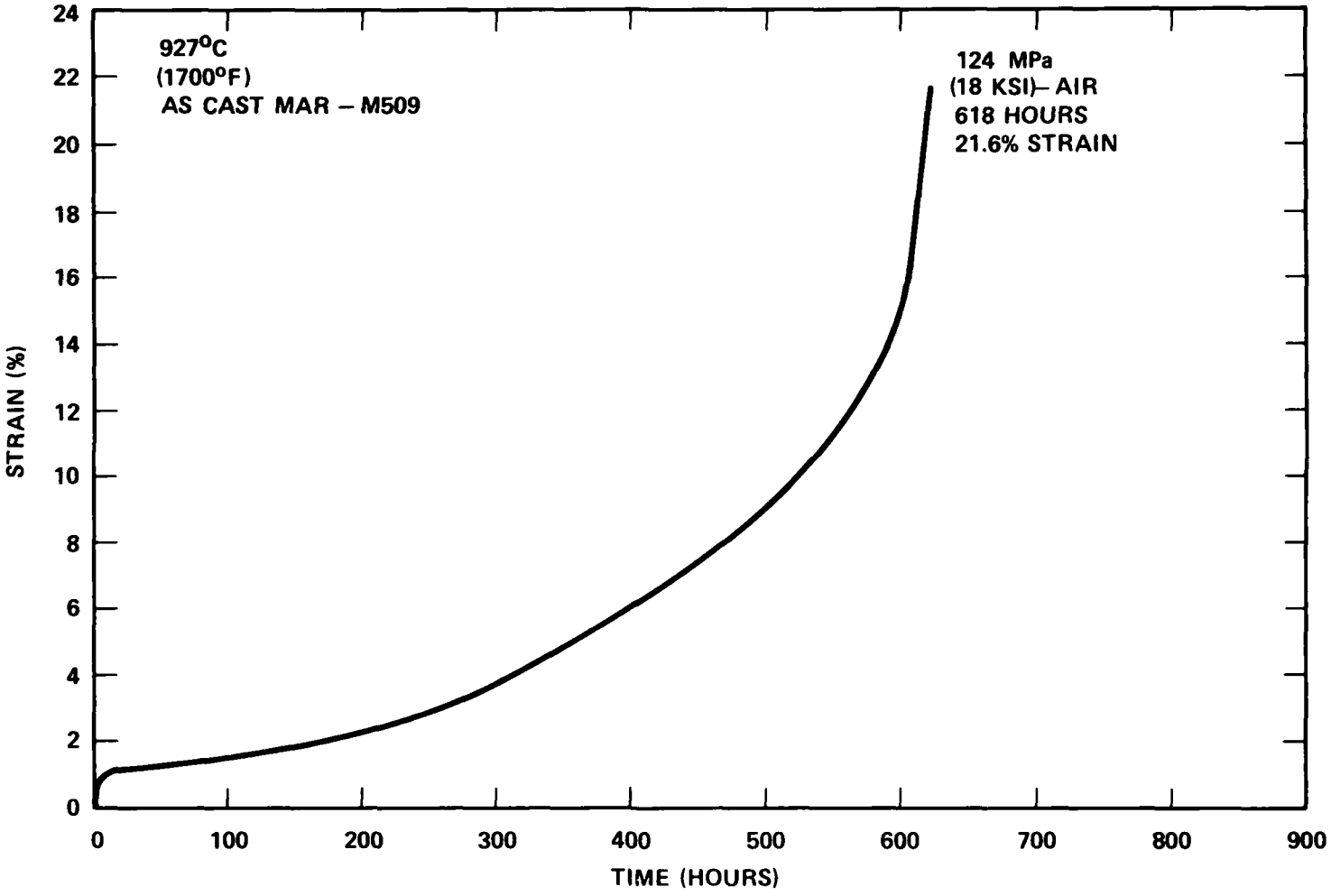

Figure 9-25. Creep-Rupture Curve for As-Cast MAR-M-509

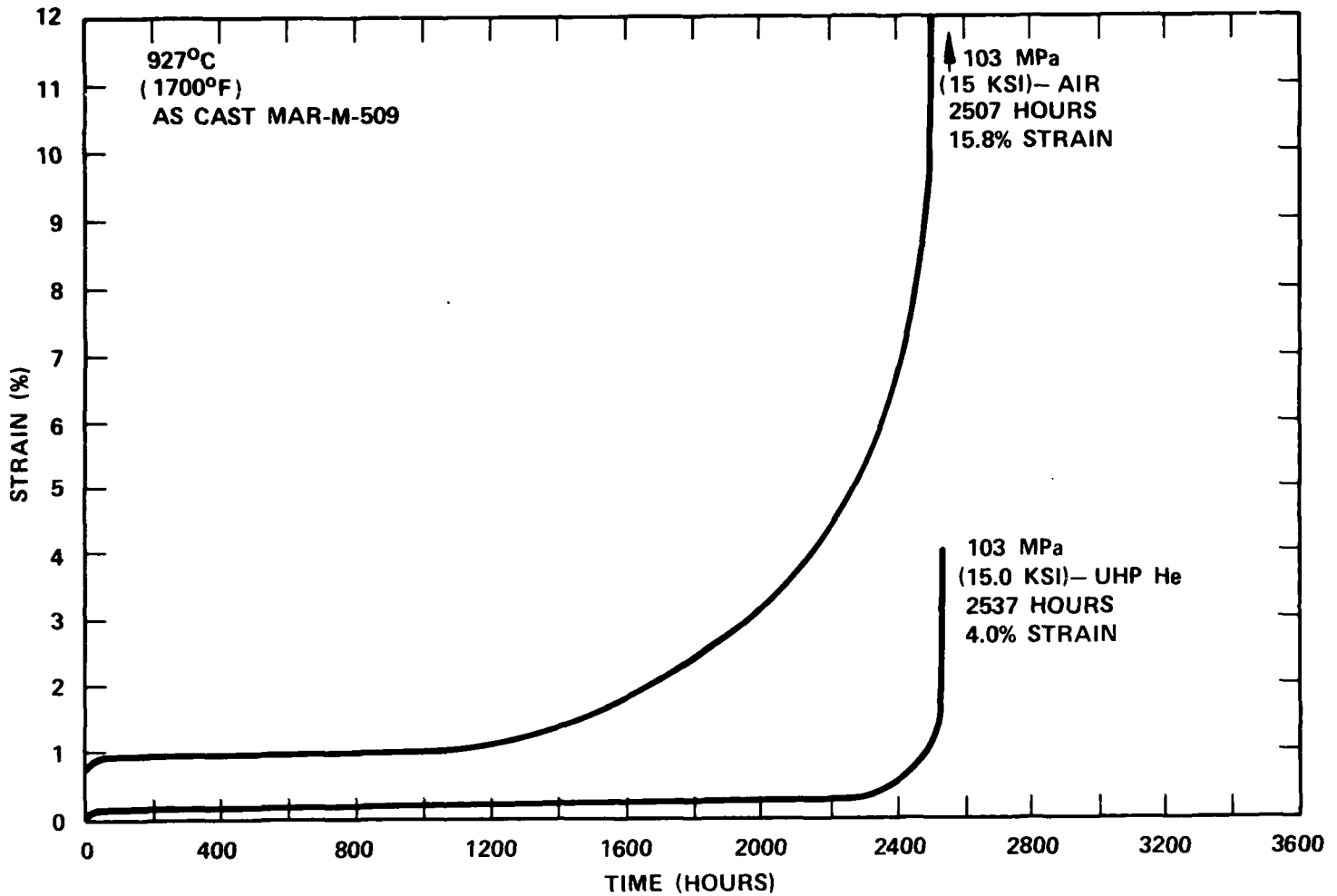

Figure 9-26. Creep-Rupture Curve for As-Cast MAR-M509

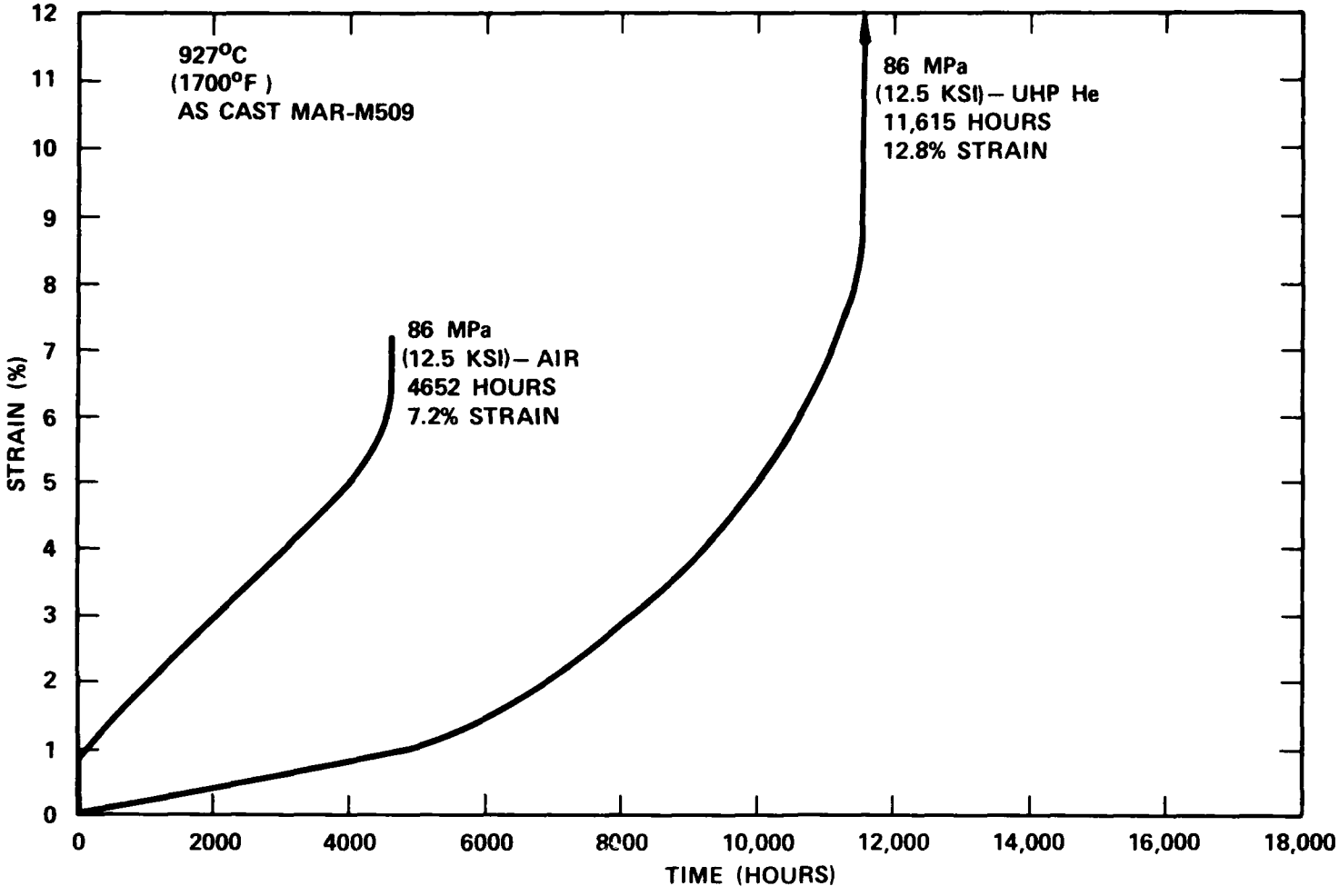

Figure 9-27. Creep-Rupture Curve for As-Cast MAR-M509

9.4.4 ALLOY MA754

A total of eight creep-rupture tests of MA754 were conducted, two in air, two UHP-He, and four in simulated CCCBS helium working fluid. The creep-rupture life data are given in Figure 9-28. The reference curve was produced from rupture life data at 1093°C (2000°F) published by INCO[22]. A Larson-Miller plot of the INCO data was used to obtain the reference curve in Figure 9-28. Creep curves are presented in Figures 9-29 through 9-31. Air tests were conducted at 152 and 138 MPa (22 and 20 ksi) stress levels. The 152 MPa (22 ksi) failed in the threaded portion of the specimen after 2100 hours while the 138 MPa (20 ksi) test fialed after 15,712 hours. Both air test results agreed quite well with the reference curve. The two UHP-He tests were conducted at the same stress levels.

The test at 152 MPa (22 ksi) was halted by a malfunctioning controller which overtemptured the specimen after 8751 hours. The test at 138 MPa (20 ksi) was stopped after 17,626 hours. Both specimens when halted exhibited no measurable strain. The 138 MPa (20 ksi) air test failed with 12 percent fracture strain and also produced three percent strain after 15,440 hours and 1.0 percent strain after 3480 hours. A potential effect of test environment is indicated. Four tests were conducted in the dynamic simulated CCCBS helium working fluid environment at stress ranging from 152 to 165 MPa (22 to 24 ksi). One test at 152 MPa (22 ksi) was still in progress at the end of the report period. While recognizing the short time duration of the CCCBS environmental creep-rupture tests, there appears to be no gross deleterious influence of the CCCBS test environment on the creep-rupture life of MA754 for those tests that were completed.

9.4.5 ALLOY TZM

A total of four TZM creep-rupture tests were conducted. Three were completed, and the fourth was stopped after 7818 hours. The creep-rupture life test data are given in Figure 9-32 and the creep curves for the completed tests are presented in Figure 9-33. The reference curve in Figure 9-32 was produced by the extrapolation of shorter term test results for stress relieved TZM generated at higher stress levels and temperatures under ultra-high vacuum test conditions[22]. No tests of TZM were conducted in air due to the incompatibility of molybdenum with oxygen at temperatures above 300°C (600°F). The UHP-He test

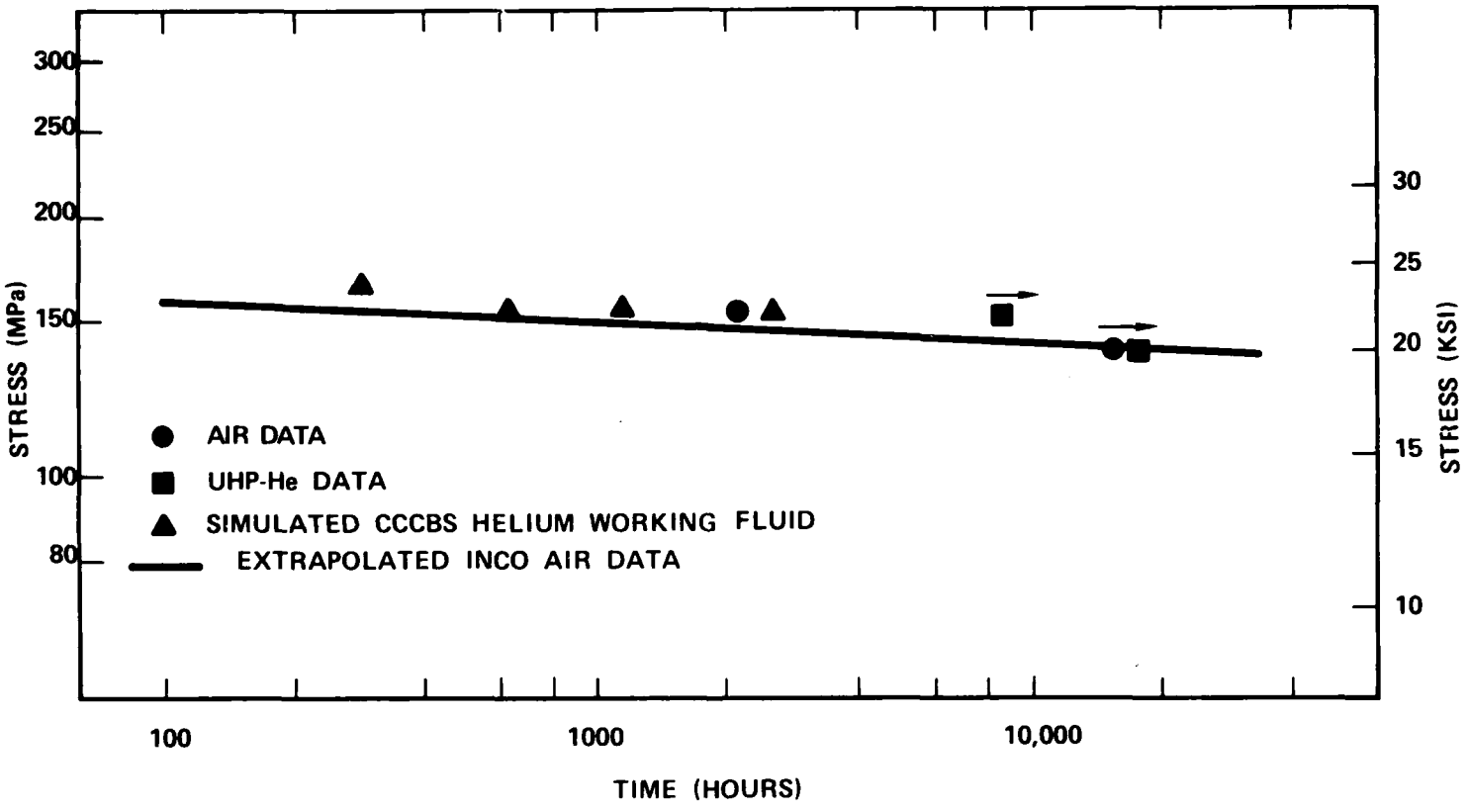

Figure 9-28. Creep-Rupture LIfe of MA754

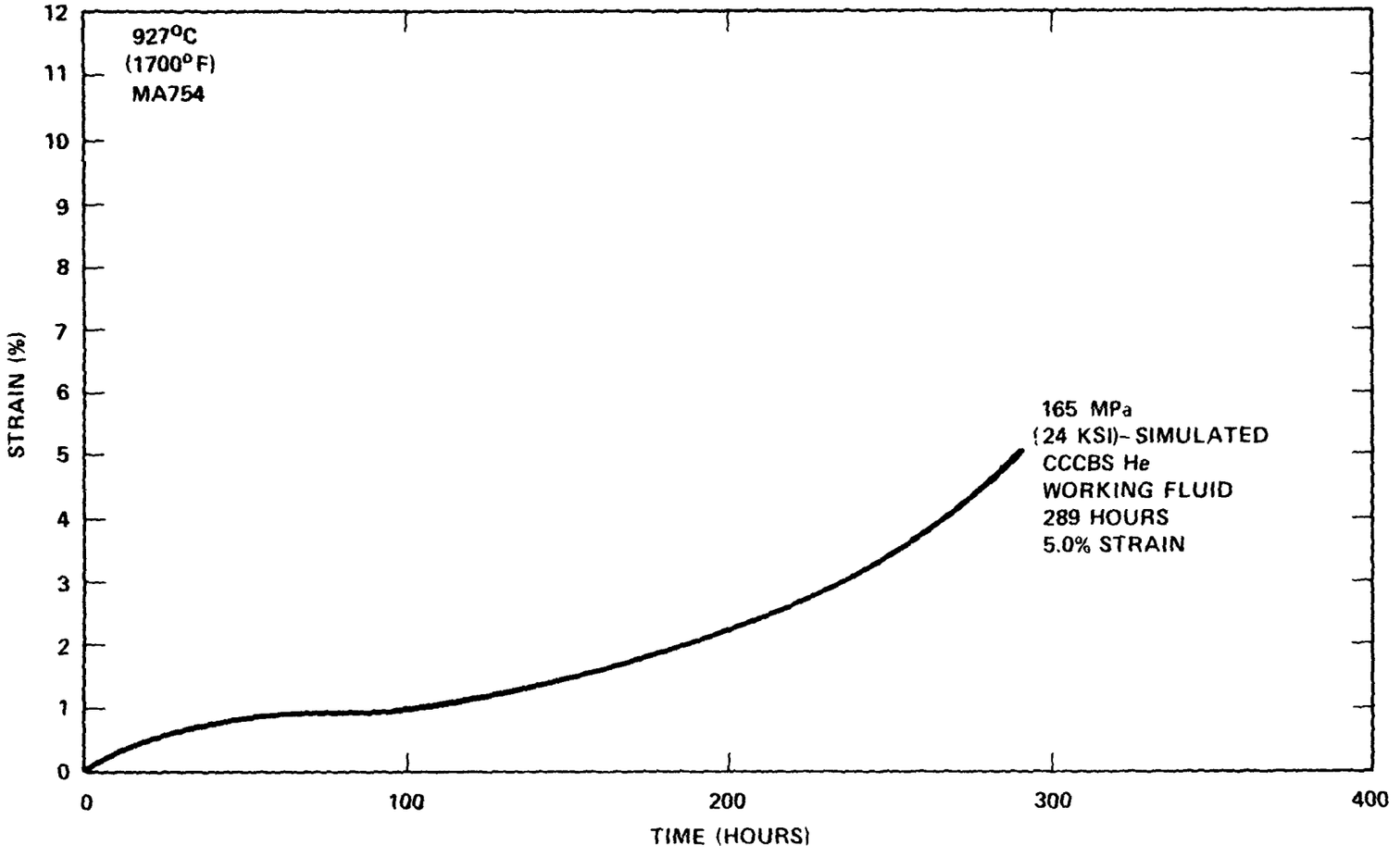

Figure 9-29. Creep-Rupture Curve for MA754

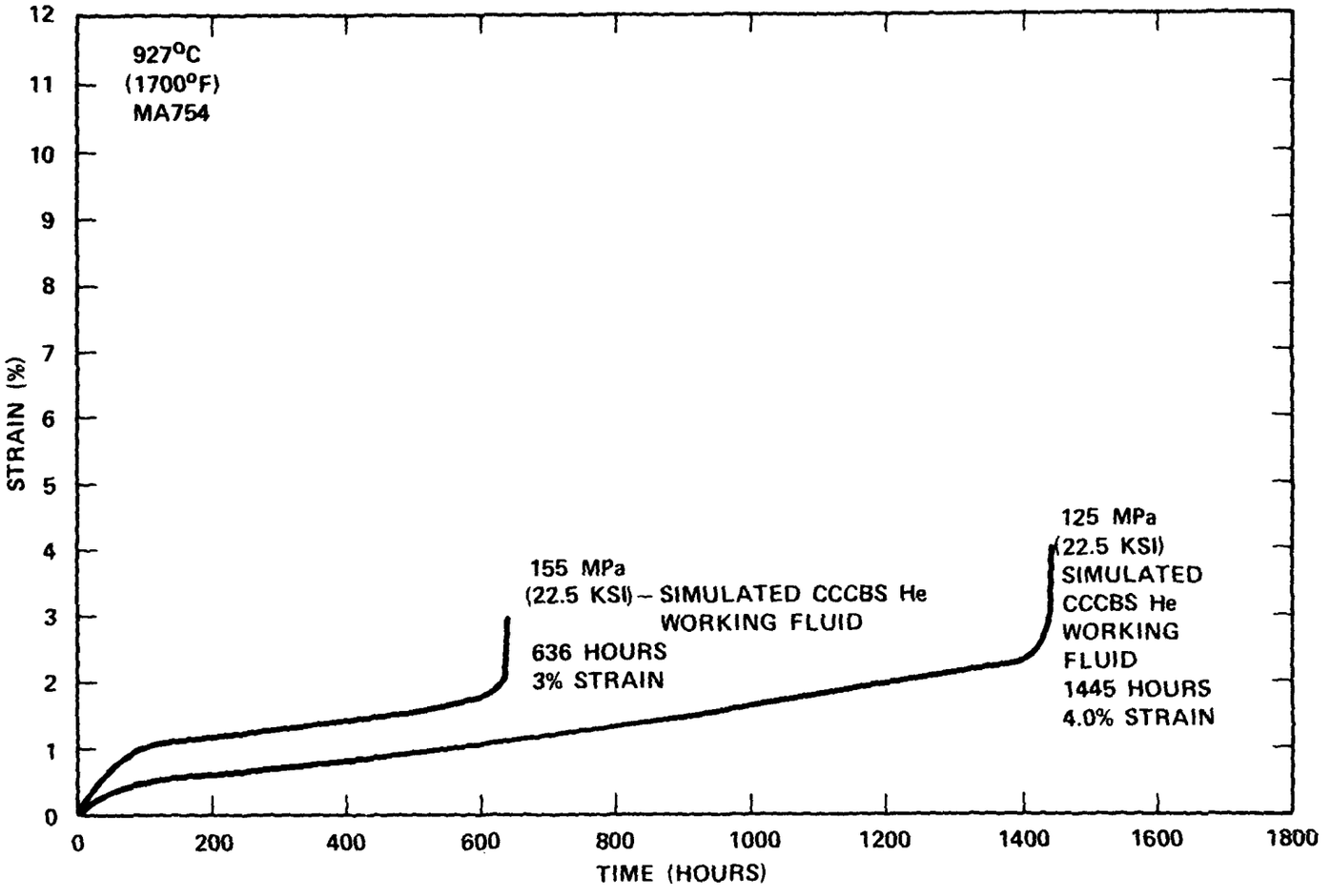

Figure 9-30. Creep-Rupture Curve for MA754

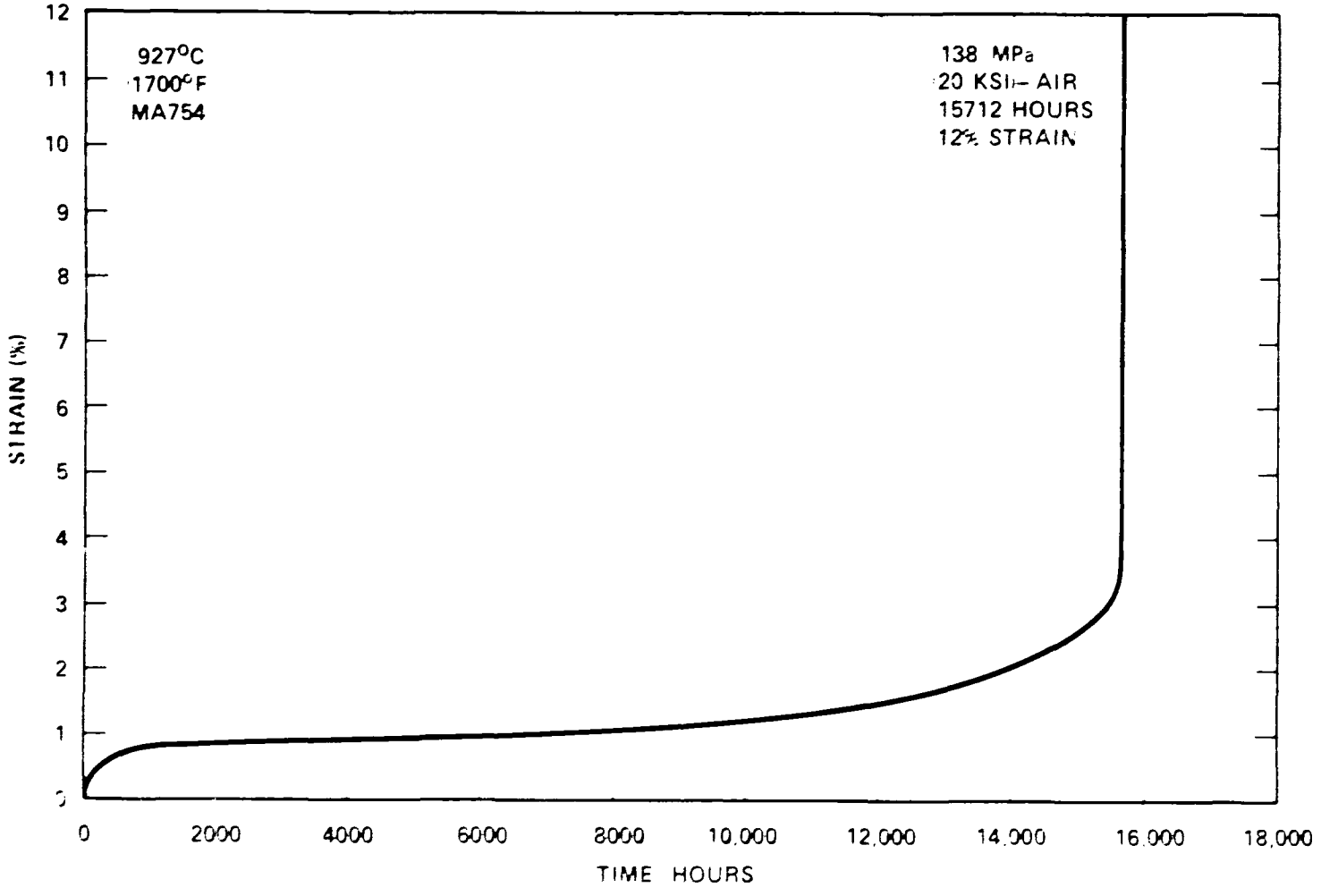

Figure 3-31. Creep-Rupture Curve for MA754

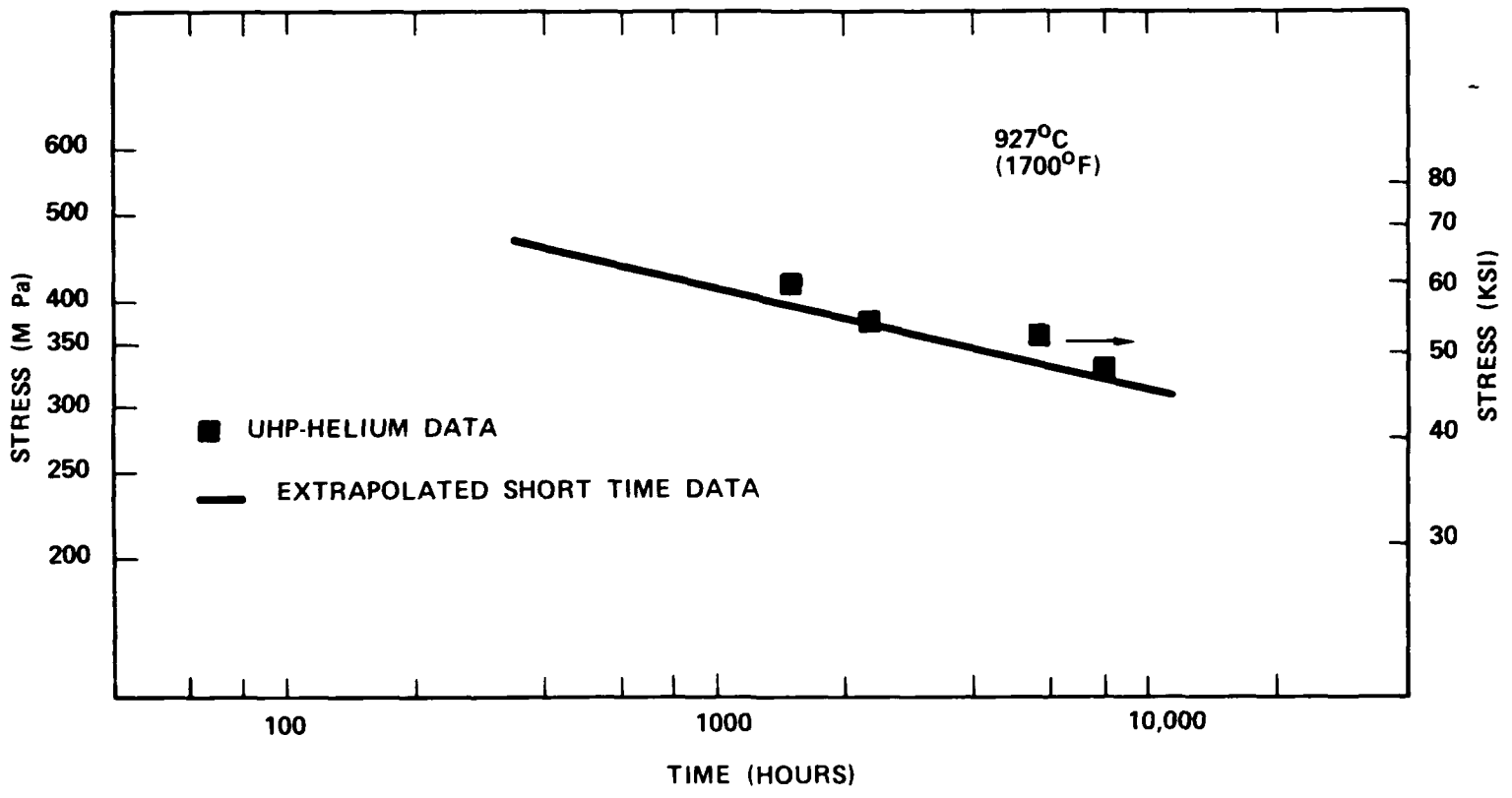

Figure 9-32. Creep-Rupture Life of Stress Relieved TZM

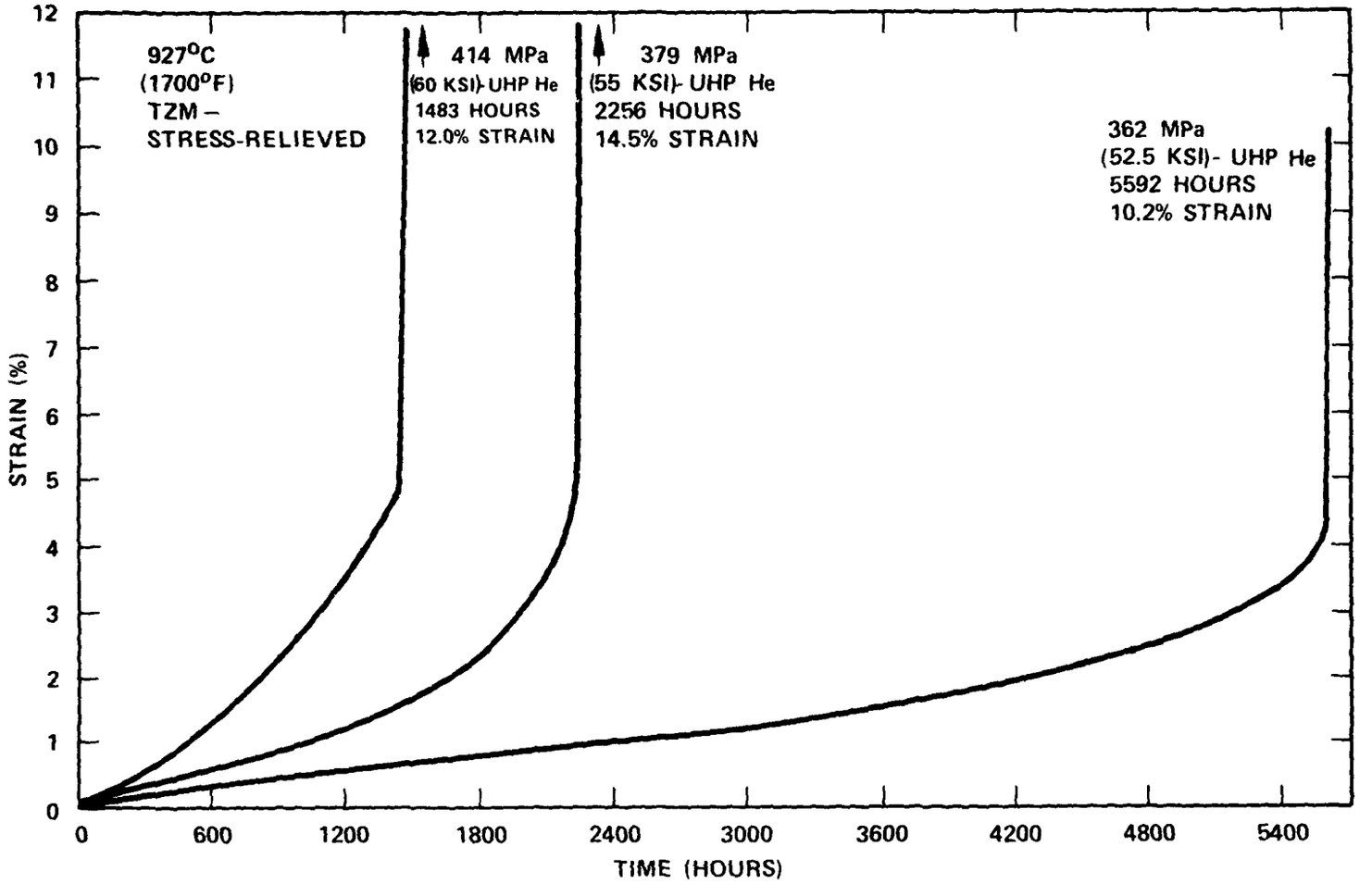

Figure 9-33. Creep-Rupture Life of Stress-Relieved TZM

results show good agreement with the reference curve, indicating that the UHP-He test environment was comparable to an ultra-high vacuum of 1×10^{-8} torr or better. TZM was not tested in the dynamic simulated CCCBS helium working fluid environment.

9.4.6 SUMMARY OF RESULTS

- Creep-rupture data obtained from the Mechanical Property Data Center for the three relatively standard gas turbine superalloys, 713LC, IN100 and MAR-M509, confirmed the dearth of published creep-rupture data that exists for materials at temperatures above 871°C (1600°F) and for test times greater than 1000 hours.

- The air test data at 927°C (1700°F) for Alloys 713LC, IN100 and MAR-M509 indicate that the materials evaluated in this program were typical of commercially available heats of the respective alloys. Air test data for MA754 appeared to agree with the limited available data supplied by the producer of the alloy.

- The ultra-high purity helium environmental creep-rupture test results indicated that all five materials were not adversely affected by the ultra-high purity helium test environment. Creep-rupture life times at 927°C (1700°F) were comparable to or exceeded life times for material tested in air. The TZM alloy being a refractory metal alloy was not tested in air due to reactivity with oxygen. TZM creep-rupture life data was comparable to extrapolated data obtained under ultra-high vacuum test conditions.

- Limited creep-rupture data obtained in a dynamic simulated helium working fluid containing 400 to 500 micro-atmospheres hydrogen, 40 - 50 micro-atmospheres carbon dioxide, 40 - 50 micro-atmospheres methane and 1 to 3 micro-atmospheres-moistures, at a test temperature of 927°C (1700°F) for three alloys, 713LC, IN100 and MA754, indicated no effect of the test environment on material rupture life for times up to 4000 hours.

  One test was conducted for Alloy 713LC, two for IN100, and four for MA754. Test times were less than 4000 hours, thus proof of compatibility for times greater than 10,000 hours was not obtained.

9.5 RECOMMENDED MATERIALS TEST PROGRAM FOR DEVELOPMENT OF THE CCCBS

As a result of the initial effort carried out under this feasibility study and the results that were derived, the following materials development program is recommended.

- Complete creep-rupture evaluation of initially selected turbine materials in simulated CCCBS helium working fluid. This series of creep-rupture tests was not completed as planned due to the reduction in scope of the feasibility study. A limited number of short-term tests were carried out involving two of the five materials under investigation. While gross degradation in the creep-rupture behavior of these materials was not observed, longer term tests of 10,000 hours or more is required to confirm compatibility with the CCCBS helium working fluid.

- Expand creep-rupture test program to include test temperatures in the range 815 to 982°C (1500 to 1800°F) to fully characterize material behavior at "off design" conditions. Stresses at the turbine blade root are expected to be much higher while temperatures are lower than those expected in the airfoil section of the blade.

- Expand creep-rupture test program to include newly developed turbine blade materials in the evaluation process. The MATE program (Materials for Advanced Turbine Engines) sponsored by NASA-LRC has identified a number of potential blade materials with increased creep-rupture strength in the temperature range of interest for the CCCBS. These materials are currently being evaluated for use in aviation gas turbine engines. These newly developed materials offer the same performance advantages to the CCCBS provided compatibility with the helium working fluid can be demonstrated.

- Investigate the effects of simulated CCCBS helium working fluid environment on fracture mechanic properties (crack growth rate), and low and high cycle fatigue behavior of selected turbine materials, These properties are particularly sensitive to surface conditions, thus any modification of the surface of structural components as a result of long-term thermal exposure to a CCCBS working fluid environment could result in a significant departure from expected behavior. These potential effects which cannot be inferred from creep-rupture behavior must be evaluated separately in order to completely characterize structural material behavior in the CCCBS operating environment.

- Investigate the effects of variations in individual contaminant levels in simulated CCCBS helium working fluid environment on corrosion and creep-rupture behavior of selected turbine materials. During "startup" and "shutdown" operations and at other times during the life of the CCCBS, it is not inconceivable that the level of impurity in the helium working fluid may diverge significantly from steady state levels. The impact of these "off design"

conditions on material mechanical property behavior must be investigated and characterized. This can be best accomplished by a systematic study of the effect of variations in concentration of individual and combinations of impurity species on the corrosion and mechanical behavior of selected candidate structural materials. A systematic study would provide a fundamental understanding of the gas-metal interactions involved and thus permit materials behavior to be predicted should actual large CCCBS working fluid composition vary from the anticipated composition.

- Conduct alloy optimization research directed specifically toward inert gas environment applications. As stated previously, super alloy development for gas turbine applications has been motivated by the needs of the aviation and land based gas turbine industry. The primary concern in these applications is compatibility with combustion products; i.e., resistance to oxidation and hot corrosion. The more benign CCCBS helium working fluid should permit a trade-off in alloy composition to meet the requirements of the CCCBS. The alloy optimization study should first look at modification of existing alloys systems for use in the CCCBS environment. However, a full-scale alloy development program beginning with a fundamentally new alloy base may be required. This requirement should become evident in the modification study of existing alloys.

- Generation of Design Data

  - Once a reference material has been selected for each CCCBS critical component, based on preliminary evaluations listed above, a testing program to generate statistical design data is required. This program can be carried out in conjunction with the detailed design phase and is intended to provide material design limitations under normal operating conditions and under faulted or off design conditions.

9.6 REFERENCES

1. F. J. Wall, Metallurgical Development for 1500°F MGCR Gas Turbine Maritime Gas-Cooled Reactor Project Engineering Report EC-193, February 1964.

2. F. J. Wall, Final Metallurgical Report of 1300°F MGCR Gas Turbine Maritime Gas-Cooled Reactor Project Engineering Report GTM-123, April 1961.

3. P. N. Chaku and C. J. McMahon, Jr., The Effect of an Air Environment on the Creep and Rupture Behavior of a Nickel-Base High Temperature Alloy, Metallurgical Transactions, Vol. 5, No. 2, February 1974, pp. 441.

4. R. Widmer and N. J. Grant, The Role of Atmosphere in the Creep-Rupture Behavior of 80 Ni-20 Cr Alloys, Journal of Basic Engineering, Transactions of the ASME, December 1960, pp. 882.

5. P. Shahinian and M. R. Acheter, Temperature and Stress Dependence of the Atmosphere Effect on a Nickel-Chromium Alloy, Transactions ASM 51, 1959, pp. 244.

6. P. Shahinian, Effect of Environment on Creep-Rupture Properties of Some Commercial Alloys, Transactions ASM 49, 1957, pp. 862.

7. R. W. Buckman and J. S. Heatherington, Apparatus for Determining Creep Behavior Under Conditions of Ultra-High Vacuum, The Review of Scientific Instruments, Vol. 37, No. 8, August 1966.

8. W. M. Hickam, Proceedings of the 9th Annual Conference of Mass Spectrometry, ASTM Committee E-14, Chicago, IL 346 (1966).

9. W. M. Hickam, Cryogenics Applied to Mass Spectrometric Trace Gas Analysis, Analytical Chemistry, Vol. 45, p. 315, February 1973.

10. M. R. Everette, Helium Impurity Levels for Compatibility Testing of HTR Primary Circuit Materials, D. P. Report 932, Dragon Project, May 1975.

11. Advanced Gas Cooled Nuclear Reactor Materials Evaluation and Development Program, DOE Contract EY-76-C-02-2975 A002, General Electric, Energy Systems Programs Department, Schenectady, NY.

12. L. W. Graham, et al, Environmental Conditions in HTRS and the Selection and Development of Primary Circuit Materials, International Symposium on Gas Cooled Reactors with Emphasis on Advanced Systems, Julich, Federal Republic of Germany, 13-17 October 1975.

13. T. Kondo, Annual Review of the High Temperature Metals Research for VHTR at JAERI, January 1977.

14. F. N. Mazandarany and P. L. Rittenhouse, Effects of Service Environments on the Behavior of HTGR Steam Generator Structural Materials, International Conference on Materials for Nuclear Steam Generators, September 9-12, 1975, Gatlinburg, TN, General Atomics Report GA-A13553.

15. C. R. Brinkman, et al, Application of Hastelloy X in Gas-Cooled Reactor Systems, ORNL/TM 5404, October 1975, Oak Ridge National Laboratory.

16. H. Schuster, W. Jakobeit, High Temperature Alloys for Power Conversion Loops of Advanced HTRs, International Symposium on Gas-Cooled Reactors with Emphasis on Advanced Systems, Julich, Federal Republic of Germany, 13 - 17 October 1975.

17. D. F. Lupton and U. Schmidt, The Stability of Surface Oxides on HTR Helium, Extended Abstracts, Vol. 78-2, Fall Meeting Electrochemical Society, Pittsburgh, PA, October 15 - 20, 1978.

18. J. C. Sawyers and E. A. Stiegerwald, Generation of Long Time Creep Data on Refractory Alloys at Elevated Temperatures, Final Report NASA Contract NAS3-2545, June 1967, TRW Cleveland, OH.

19. INCO Data Brochure, Alloy 713LC - Low Carbon Alloy 713C, Preliminary Data, July 1964 - 1M6-68-4290.

20. INCO Data Brochure, Engineering Properties of IN100 Alloy, 2M9-69-5073.

21. Huntington Alloys Data Sheet, Inconel Alloy MA754, 3M-9-75S-51.

22. R. L. Salley and E. A. Kovacevick, Materials Investigation, SNAP 50/SPUR Program, Creep-Rupture Properties of Stress Relieved TZM Alloy, Report APL-TDR-64-116, Part 1, Garrett Corporation, AiResearch Manufacturing Division, October 1964.

APPENDIX A

FINITE ELEMENT MODEL

APPENDIX A

FINITE ELEMENT MODEL

The finite element model global axes assumed in this study are shown in Figure A-2 and are X (fore and aft), Y (horizontal, perpendicular to X), and Z (vertical). The shaft axes of the pair of turbomachinery are symmetric about the X axis. The turbomachinery shafts, housing, and outer casings are modeled along a single axis as pipe and mass elements. Nodes 3 to 12 of Figure A-1 include the shafts and rotary masses. Nodes 13 to 21 and 34 include the shaft housing and stationary masses. Nodes 22 to 33 include the outer casing and masses of the precooler, intercooler, recuperator, and generator. The pair of turbomachinery have rigid coupling from the housing to the pedestal. These rigid elements are along the Y-axis of Figure 4-2. The flexibilities of the six degrees of freedom for the pedestal are spring constants modeled at the origin of the XYZ coordinate system shown on Figure A-2. Flow pipes come out of the turbomachinery housing and connect to the reactor vessel lower head as shown by nodes 41, 42, 141, and 142. The axes of the pair of turbomachinery are perpendicular to the paper at nodes 28 and 128. The six degrees of freedom for the reactor vessel lower bulkhead are modeled as springs between nodes 42 and 43 and 142 and 143. The reactor vessel, containment, and internals are shown by the modeling on Figure A-1, where nodes 43 and 54 are all along the Z-axis of Figure A-2. In Figure A-1, the reactor internals are comprised of nodes 44 to 49; the vessel is nodes 43, 44, 50, 51, and 52; and the reactor containment is modeled with nodes 53 and 54. This is the basic description of the reference design. The modified design for which some mode shapes are shown on Figures A-5, A-6, and A-7 eliminates the pedestal and the reactor and containment. The modified design is the pair of turbomachinery hanging from its flow pipes connected to the reactor lower head, which is assumed fixed at the flange of the lower head.

The model boundary conditions are:

$$UX_1 = UY_1 = UZ_1 = \omega X_1 = \omega Y_1 = \omega Z_1 = 0$$

$$UX_{33} = UY_{33} = UZ_{33} = \omega X_{33} = \omega Y_{33} = \omega Z_{33} = 0$$

$$UX_3 = UX_{21}$$

$$\omega Y_5 = UY_6 = UY_{19},\ UZ_5 = UZ_6 = UZ_{19}$$

$$UX_9 = UX_{10},\ UY_9 = UY_{10} = UY_{15},\ UZ_9 = UZ_{10} = UZ_{15}$$

$$UX_{12} = UX_{13},\ UY_{12} = UY_{13},\ UZ_{12} = UZ_{13}$$

$$UY_{17} = UY_{27},\ UZ_{17} = UZ_{27}$$

$$UY_{18} = UY_{29},\ UZ_{18} = UZ_{29}$$

$$UY_{22} = UY_{34},\ UZ_{22} = UZ_{34}$$

$$UX_{52} = UX_{53},\ UY_{22} = UY_{53}$$

$$UX_{54} = UY_{54} = UZ_{54} = \omega X_{54} = \omega Y_{54} = \omega Z_{54} = 0$$

where UA_b and ωA_b denote displacement and rotation in the A direction for node b, respectively.

The values of the material properties at temperature are taken from Reference (1).

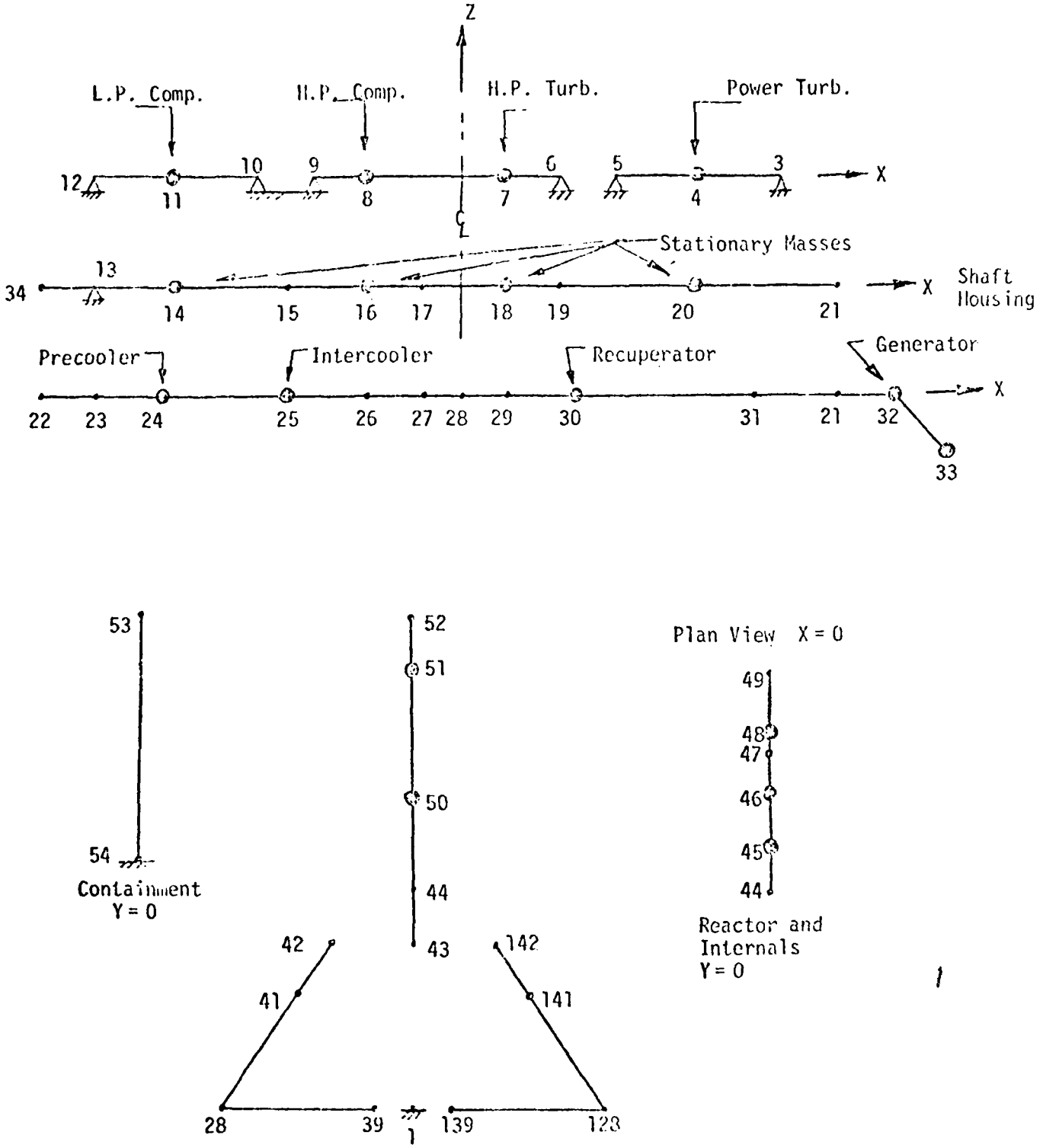

Figure A-1. Schematic of the Finite Element Model

MODE = 6 FREQ = 19

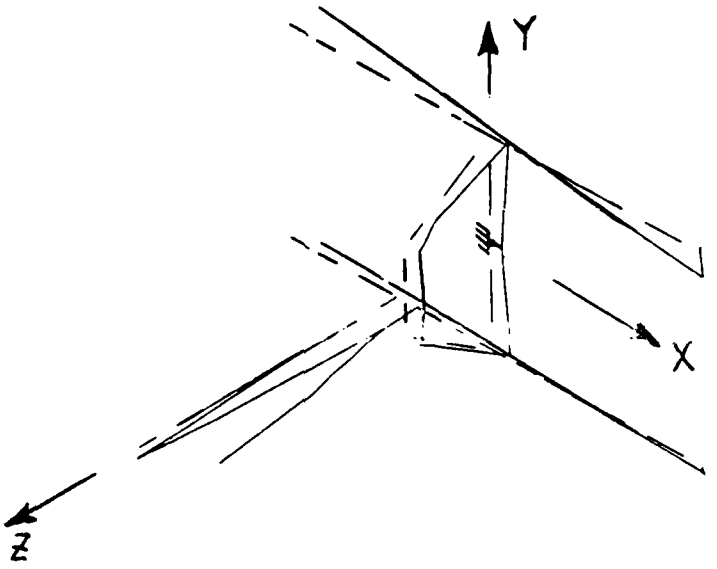

MODE SHAPES 63 DOOF RUN2 R A SMITH PLOT 6 DISPLOT

Figure A-2. Dominant X-Direction Mode Shape for the Reference Design

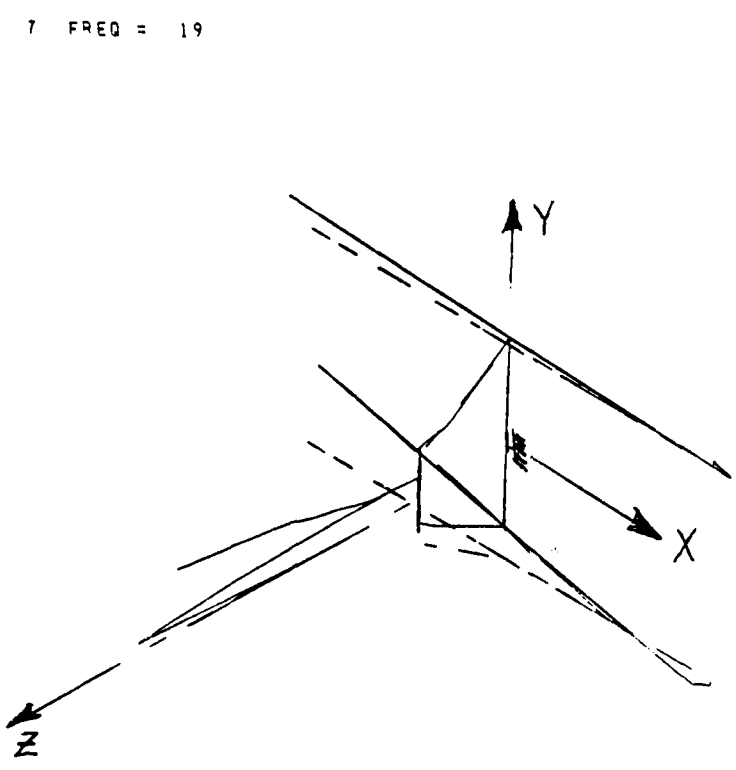

Figure A-3. Dominant Y-Direction Mode Shape for the Reference Design

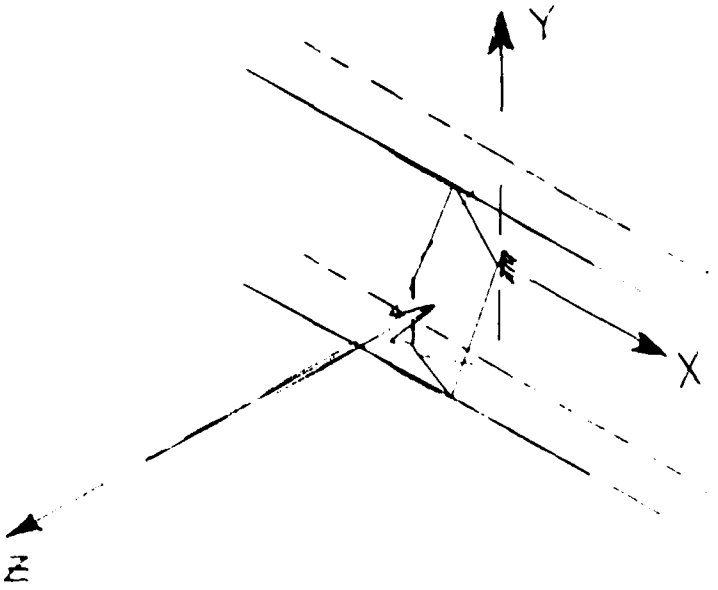

Figure A-4. Dominant Z-Direction Mode Shape for the Reference Design

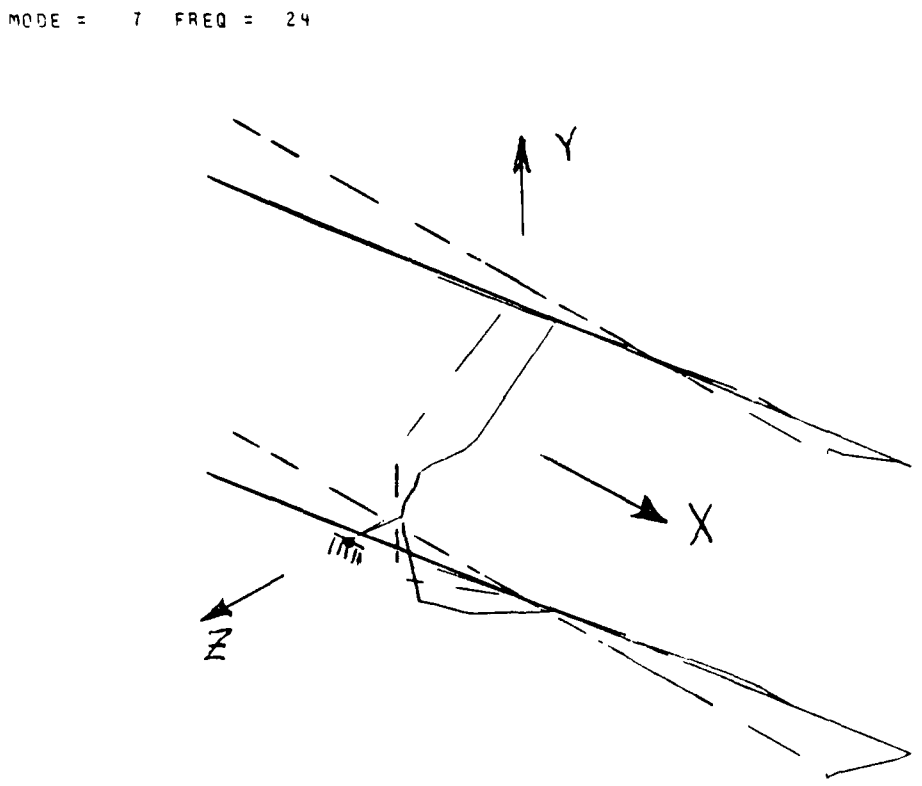

Figure A-5. Dominant X-Direction Mode Shape for the Modified Design

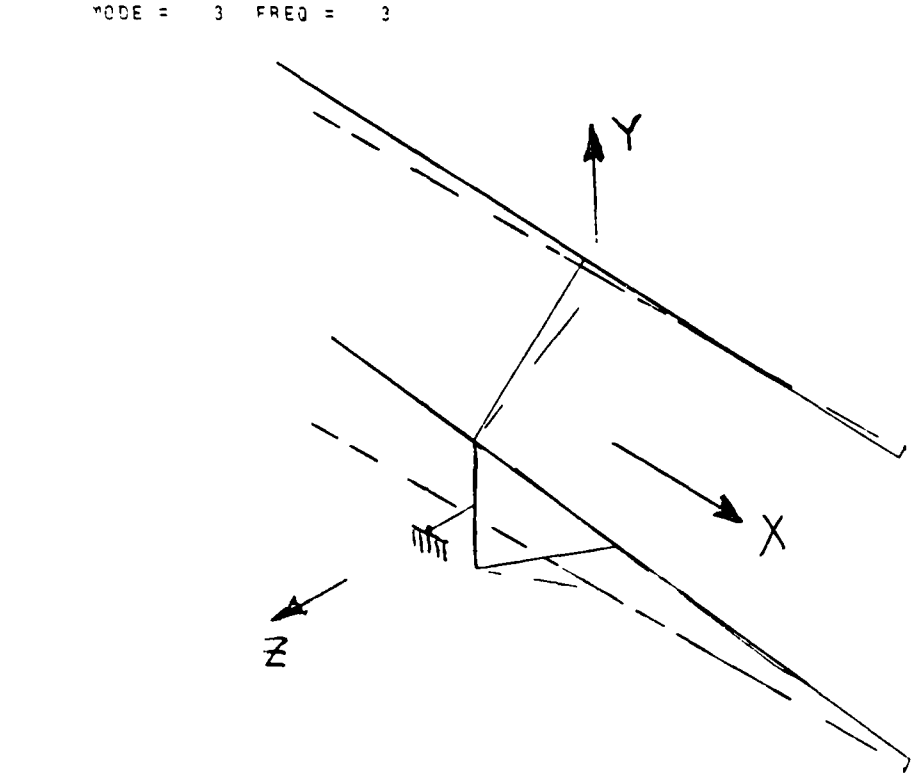

Figure A-6. Dominant Y-Direction Mode Shape for the Modified Design

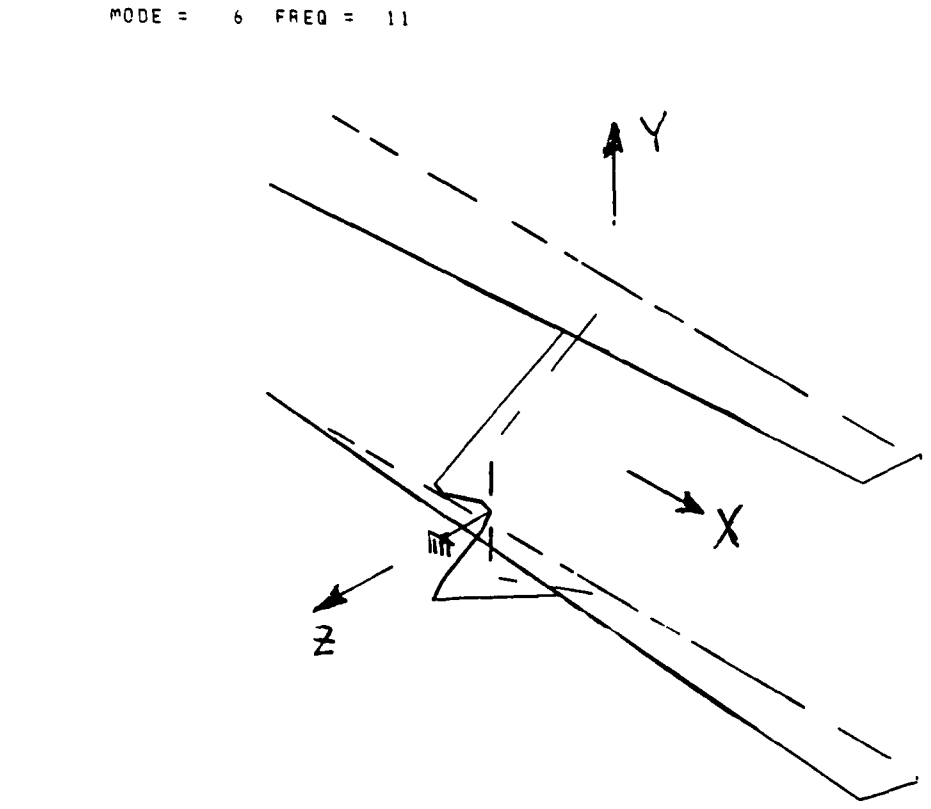

Figure A-7. Dominant Z-Direction Mode Shape for the Modified Design

```
AN3HA,T132,P6000,UANRAS,STMFA,      SMITH   WAES0 X5245
ACCOUNT(AN77119)
GET(OUTPUT,   ,AN,RASMITH,S       MODAL REDUCTION S)
ATTACH(DUM,    MODES3)
COPY(DUM,TAPE12)
REWIND(TAPE12)
FTN.
LGO.
$
      PROGRAM SHRED(INPUT,OUTPUT,TAPE5=INPUT,TAPE6=OUTPUT,TAPE12)
C                          ******
C       MODAL ANALYSIS FOR NAVY SHOCK ANALYSIS-NO REACTOR,NO PEDISTAL
C
      DIMENSION  JELTYP(99),DISP(600),TITLE(20),KEY(28),D(100)
     1,DISHED(6),UX(100),UY(100),UZ(100),DMASS(26),INUM(26),
     2WMASS(100),UXM(100),UYM(100),UZM(100),DM(100),NODD(26),NODE(100)
      P=3.14159
      G=386.
      READ(12)(TITLE(J),J=1,20),(DISHED(J),J=1,6),NUMNP,NUMEL,NITTER,
     1NUMDIS,NUMFOR,NUMPRS,NUMNPR,TIME,ITTER,ITIME,(KEY(J),J=1,28),
     2NUMTYP,(JELTYP(J),J=1,NUMTYP)
      DO10 I=1,NUMNPR
      WMASS(I)=0.0
   10 CONTINUE
      READ(5,1) MODES,MPNUM
    1 FORMAT(2I3)
      READ(5,2)((INUM(I),NODD(I),DMASS(I)),I=1,MPNUM)
    2 FORMAT(2I4,F8.0,2I4,F8.0,2I4,F8.0,2I4,F8.0,2I4,F8.0)
      DO 20 I=1,MPNUM
      K=INUM(I)
      WMASS(K)=DMASS(I)
      NODE(K)=NODD(I)
      WRITE(6,201)K,NODE(K),WMASS(K)
  201 FORMAT(2I4,F10.0)
   20 CONTINUE
      READ(12)
      READ(12)
      IRECD=KEY(2)+3*KEY(4)+KEY(10)+KEY(1)*KEY(4)
      DO 3 I=1,NUMEL
      READ(12)
    3 CONTINUE
      K7NP=KEY(7)*NUMNPR
      DO100 K=1,MODES
      SUMD=0.
      SUMX=0.
      SUMY=0.
      SUMZ=0.
      READ(12)FREQ,(DISP(J),J=1,K7NP)
      DO 30 I=1,NUMNPR
      IF(WMASS(I).EQ.0.0)GOTO30
      I1=1+KEY(7)*(I-1)
      I2=I1+1
      I3=I2+1
      UX(I)=DISP(I1)
      UY(I)=DISP(I2)
      UZ(I)=DISP(I3)
      D(I)=UX(I)*UX(I)+UY(I)*UY(I)+UZ(I)*UZ(I)
```

```
      UXM(I)=UX(I)*WMASS(I)
      UYM(I)=UY(I)*WMASS(I)
      UZM(I)=UZ(I)*WMASS(I)
      DM(I)=D(I)*WMASS(I)
      SUMD=SUMD+DM(I)
      SUMX=SUMX+UXM(I)
      SUMY=SUMY+UYM(I)
      SUMZ=SUMZ+UZM(I)
   30 CONTINUE
      WRITE(6,4)K,FREQ
    4 FORMAT(I3,10X,F10.3)
      PX=SUMX/SUMD
      PY=SUMY/SUMD
      PZ=SUMZ/SUMD
      WX=PX*SUMX/1000.
      WY=PY*SUMY/1000.
      WZ=PZ*SUMZ/1000.
      AK1X=(WX*
      AK1Y=(WY*
      AK1Z=(WZ*
      AK2X=6.*P*FREQ*(WX
      AK2Y=6.*P*FREQ*(WY
      AK2Z=6.*P*FREQ*(WZ
      CX=20.*
      CY=20.*
      CZ=20.*
      DX=CX*AK1X
      IF(AK2X.LT.AK1X)DX=CX*AK2X
      DY=CY*AK1Y
      IF(AK2Y.LT.AK1Y)DY=CY*AK2Y
      DZ=CZ*AK1Z
      IF(AK2Z.LT.AK1Z)DZ=CZ*AK2Z
      WRITE(6,5)WX,WY,WZ,PX,PY,PZ,DX,DY,DZ
    5 FORMAT(3F8.2,3F8.3,3F10.2)
      IF(DX.LT.6.0)DX=6.0
      IF(DY.LT.6.0)DY=6.0
      IF(DZ.LT.6.0)DZ=6.0
      DO 50 I=1,NUMNPR
      IF(WMASS(I).EQ.0.0)GO TO 50
      PX=PX+DX*UXM(I)
      PY=PY+DY*UYM(I)
      PZ=PZ+DZ*UZM(I)
      WRITE(6,6)I,NODE(I),WMASS(I),PX,PY,PZ
    6 FORMAT(I3,I4,F10.0,3F10.1)
   50 CONTINUE
  100 CONTINUE
      STOP
      END
```

See Ref. (2)

```
*
 44 20
   2   4   2548.   5   7   1462.   6   8    715.   9  11    873.  13  15  10818.
  15  17  13927.  17  19  25877.  19  21  18753.  20  22  10791.  38 104   2548.
  41 107   1462.  42 108    715.  45 111    873.  49 115  18212.  51 117  13927.
  53 119  25877.  55 121  18753.  56 122  10791.  34  42    180.  70 142    180.
*
```

REFERENCES

1) "WECAN, Westinghouse Electric Computer Analysis, User's Manual," Westinghouse Research Laboratories, Pittsburgh, Pa. 15235, April 9, 1976.

2) "Formulas for the Computation of Shock Design Values," Naval Research Laboratory Interim Report, 1976.

APPENDIX B

SUPPLEMENTS SECTION 8.3.1

HI TEMP HE TURB ROW 1 113 BLADES/ROW HUB SECTION
RADIUS = 8.4435
INLET ANGLE = 70.45
OUTLET ANGLE = 29.13
No. OF BLADES = 113

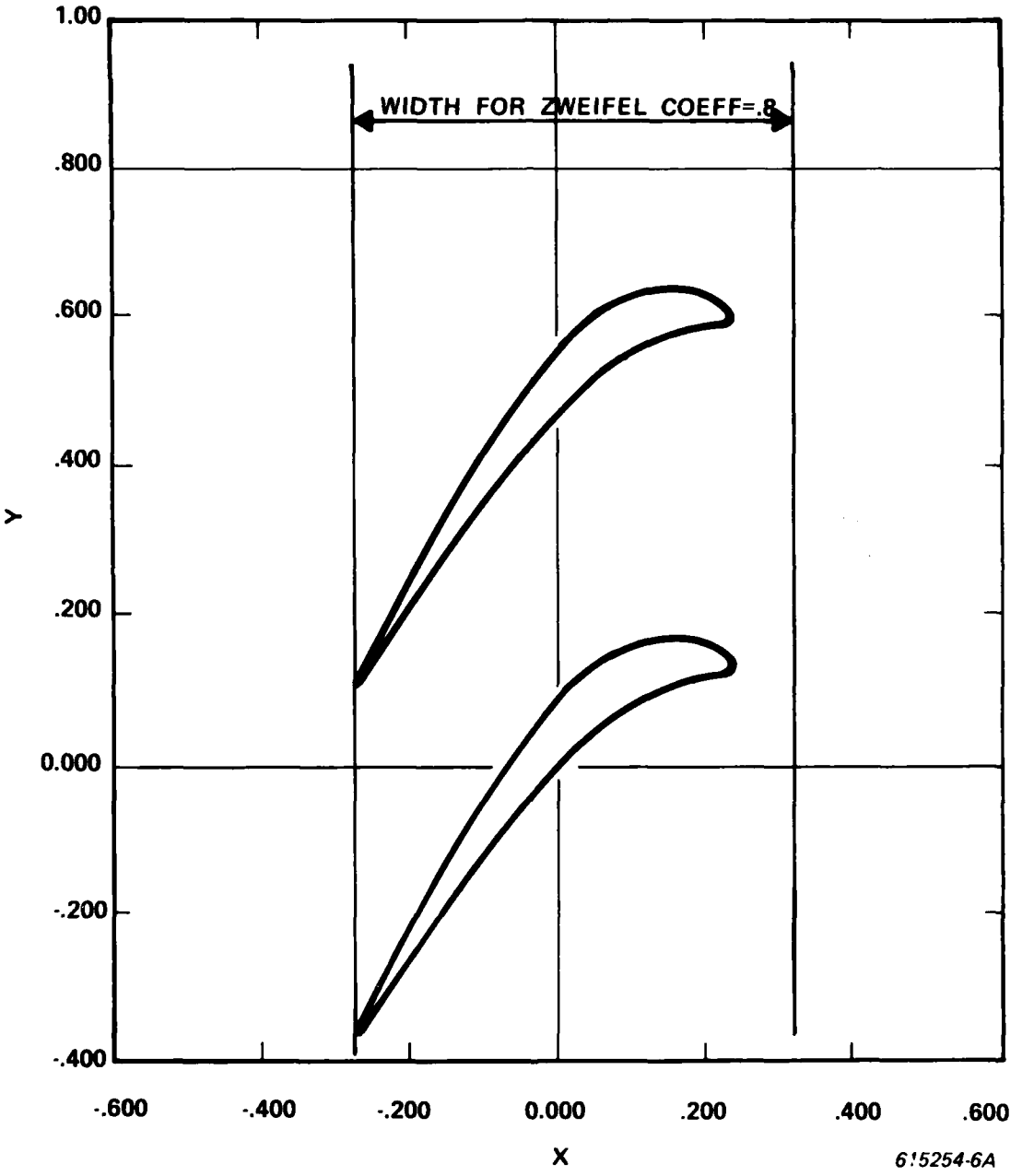

Figure B-1.

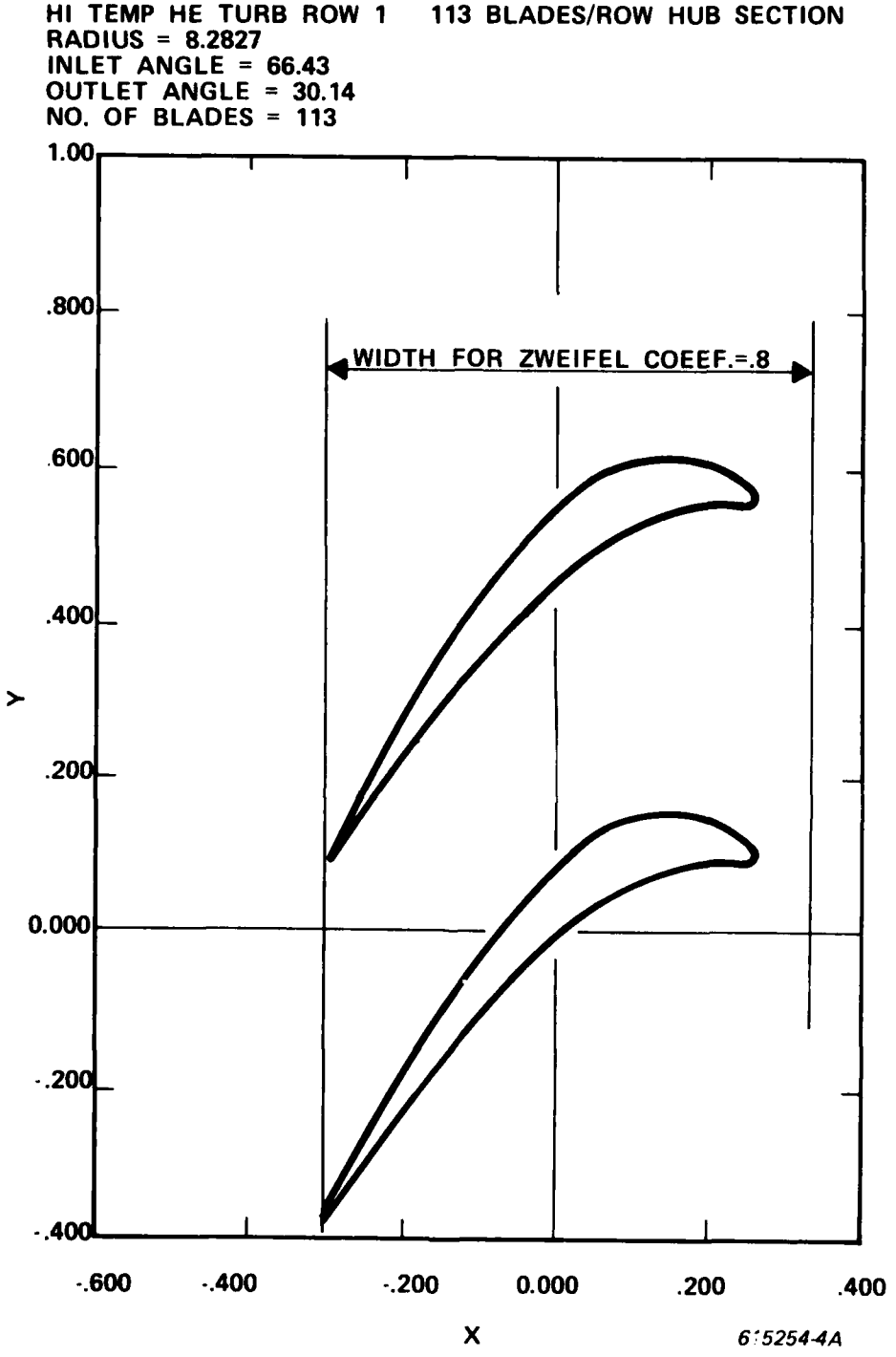
HI TEMP HE TURB ROW 1 113 BLADES/ROW HUB SECTION
RADIUS = 8.2827
INLET ANGLE = 66.43
OUTLET ANGLE = 30.14
NO. OF BLADES = 113
1.00
.800
.600
.400
.200
0.000
-.200
-.400
Y
WIDTH FOR ZWEIFEL COEEF.=.8
-.600
-.400
-.200
0.000
.200
.400
X
615254-4A

Figure B-2

HI TEMP HE TURB ROW 1 113 BLADES/ROW HUB SECTION
RADIUS = 8.1219
INLET ANGLE = 63.09
OUTLET ANGLE = 30.87
NO. OF BLADES = 113

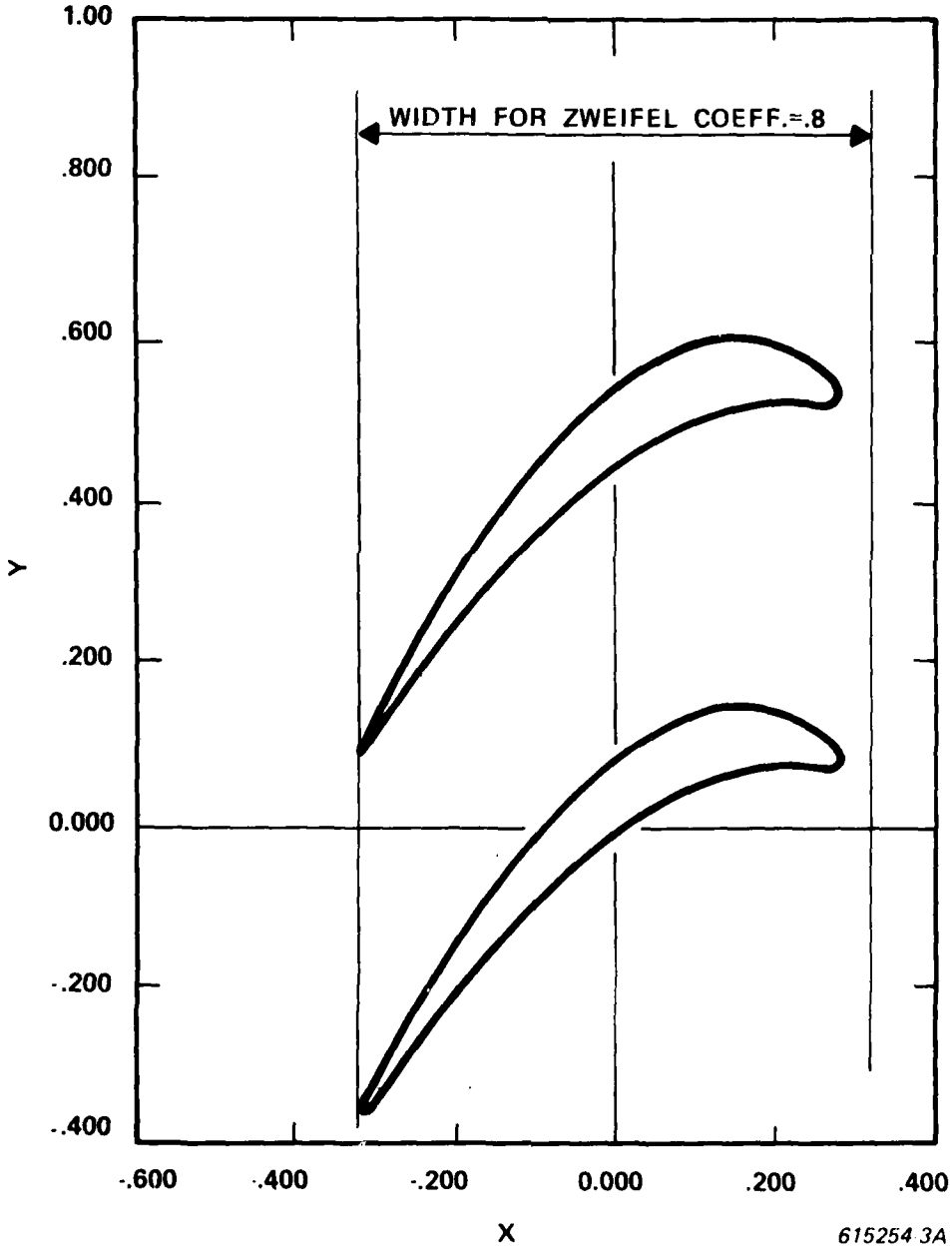

Figure B-3.

HI TEMP HE TURB ROW 1 113 BLADES/ROW HUB SECTION
RADIUS = 7.9511
INLET ANGLE = 50.31
OUTLET ANGLE = 31.34
NO. OF BLADES = 113

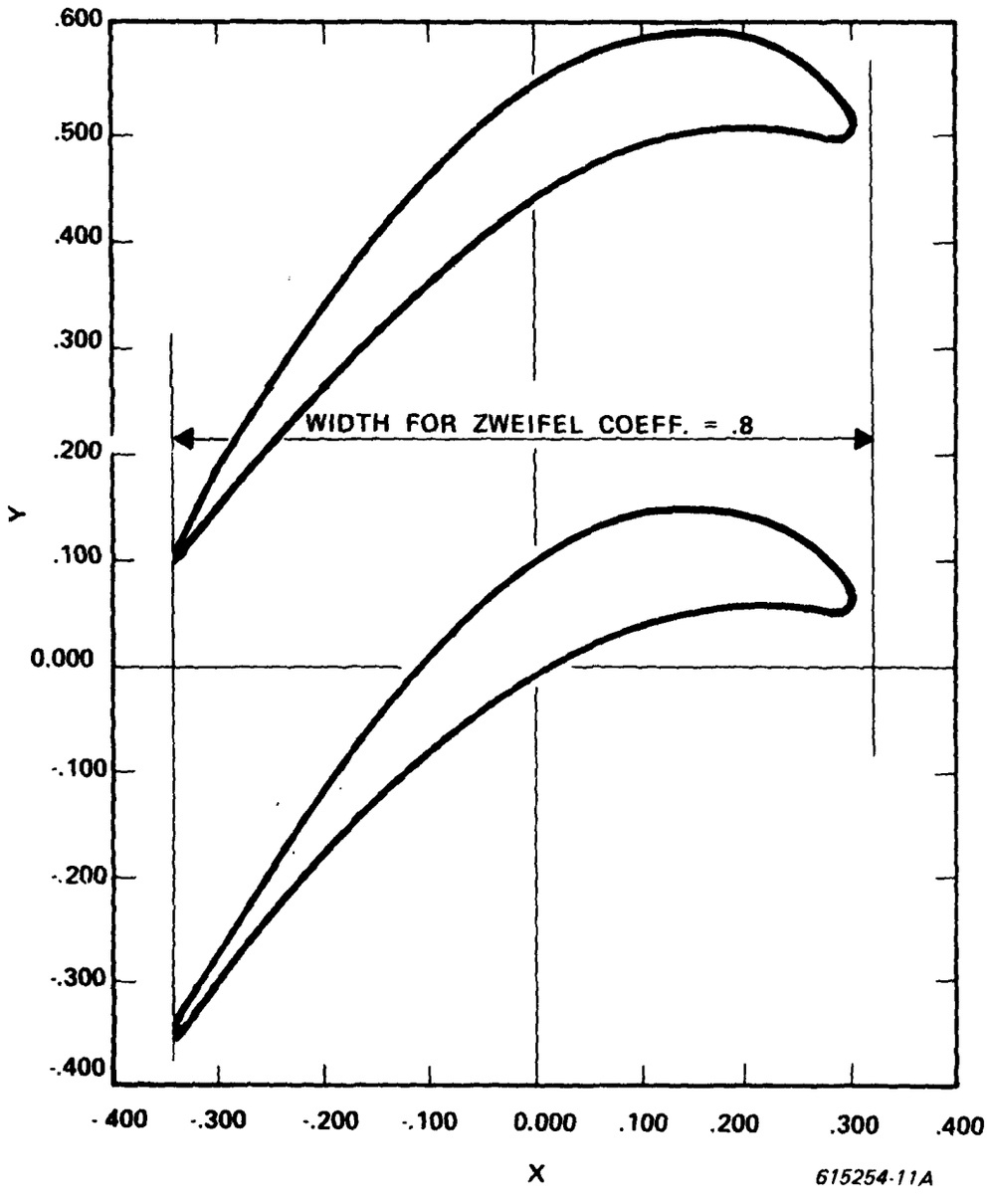

Figure B-4.

HI TEMP HE TURB ROW 1 113 BLADES/ROW HUB SECTION
RADIUS = 7.8003
INLET ANGLE = 57.96
OUTLET ANGLE = 31.63
NO. OF BLADES = 113

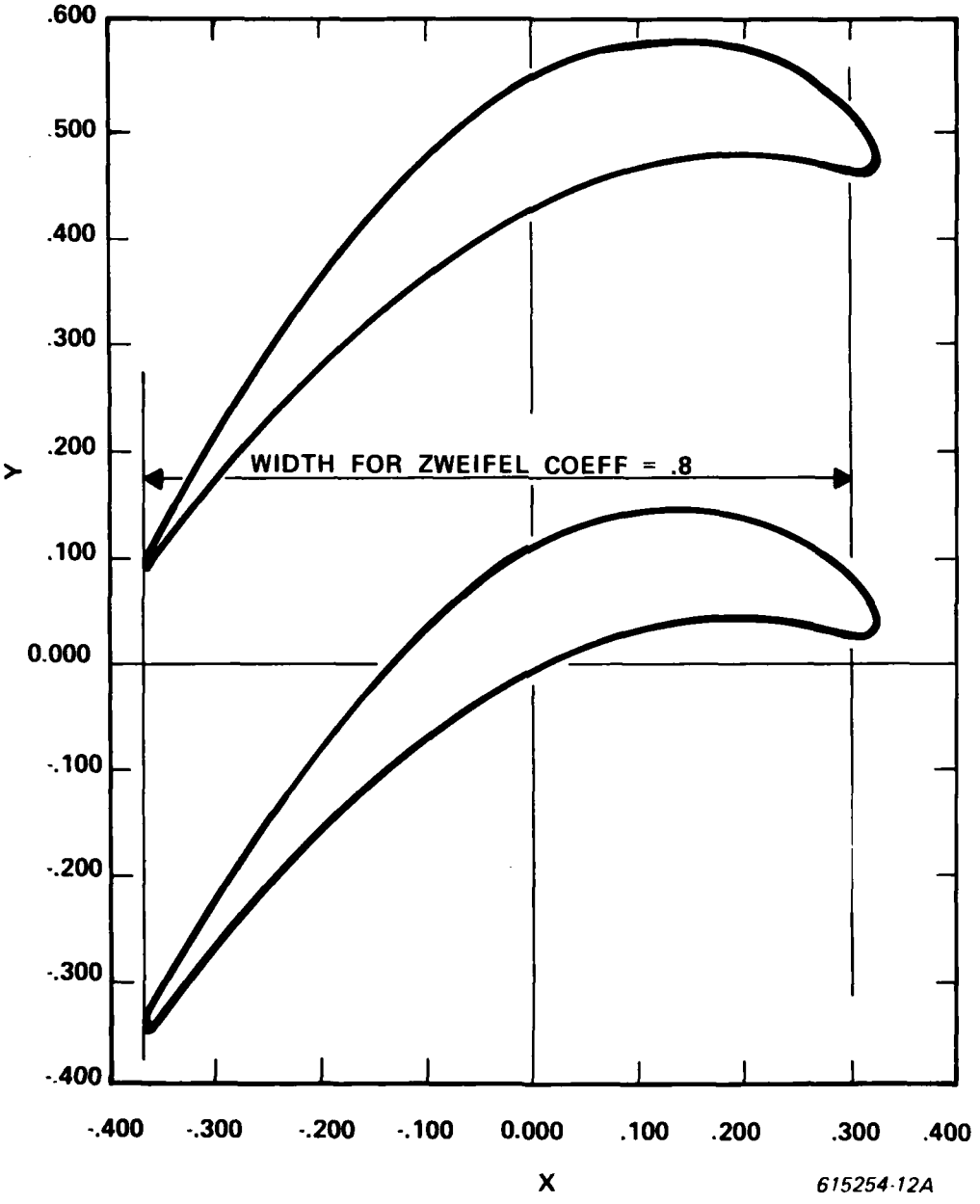

Figure B-5.

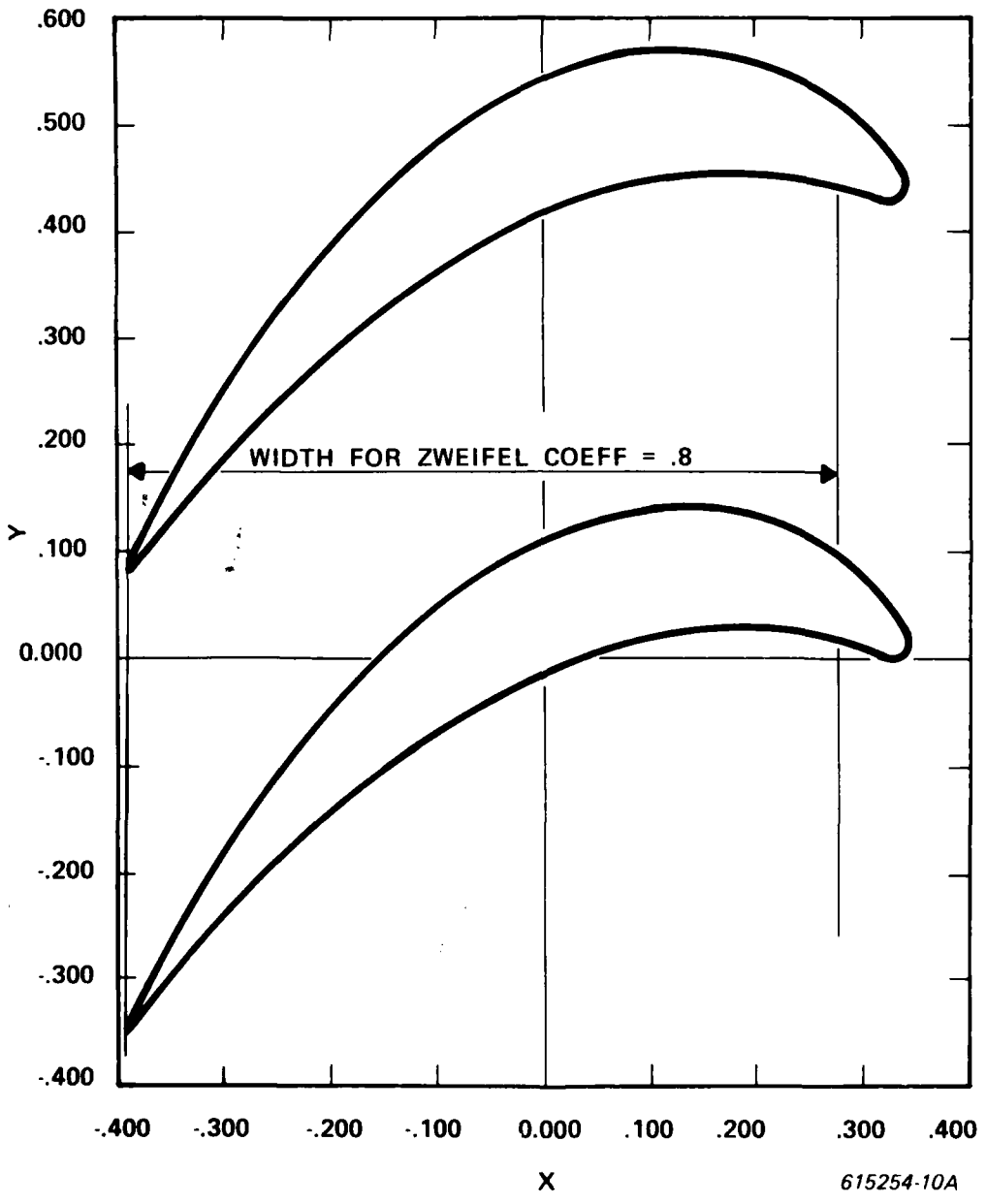
HI TEMP HE TURB ROW 1 113 BLADES/ROW HUB SECTION
RADIUS = 7.6395
INLET ANGLE = 55.96
OUTLET ANGLE = 31.76
NO. OF BLADES = 113
.600
.500
.400
.300
.200
.100
0.000
-.100
-.200
-.300
-.400
Y
WIDTH FOR ZWEIFEL COEFF = .8
-.400
-.300
-.200
-.100
0.000
.100
.200
.300
.400
X
615254-10A

Figure B-6.

HI TEMP HE TURB ROW 1 113 BLADES/ROW HUB SECTION
RADIUS = 7.4787
INLET ANGLE = 54.24
OUTLET ANGLE = 31.77
NO. OF BLADES = 113

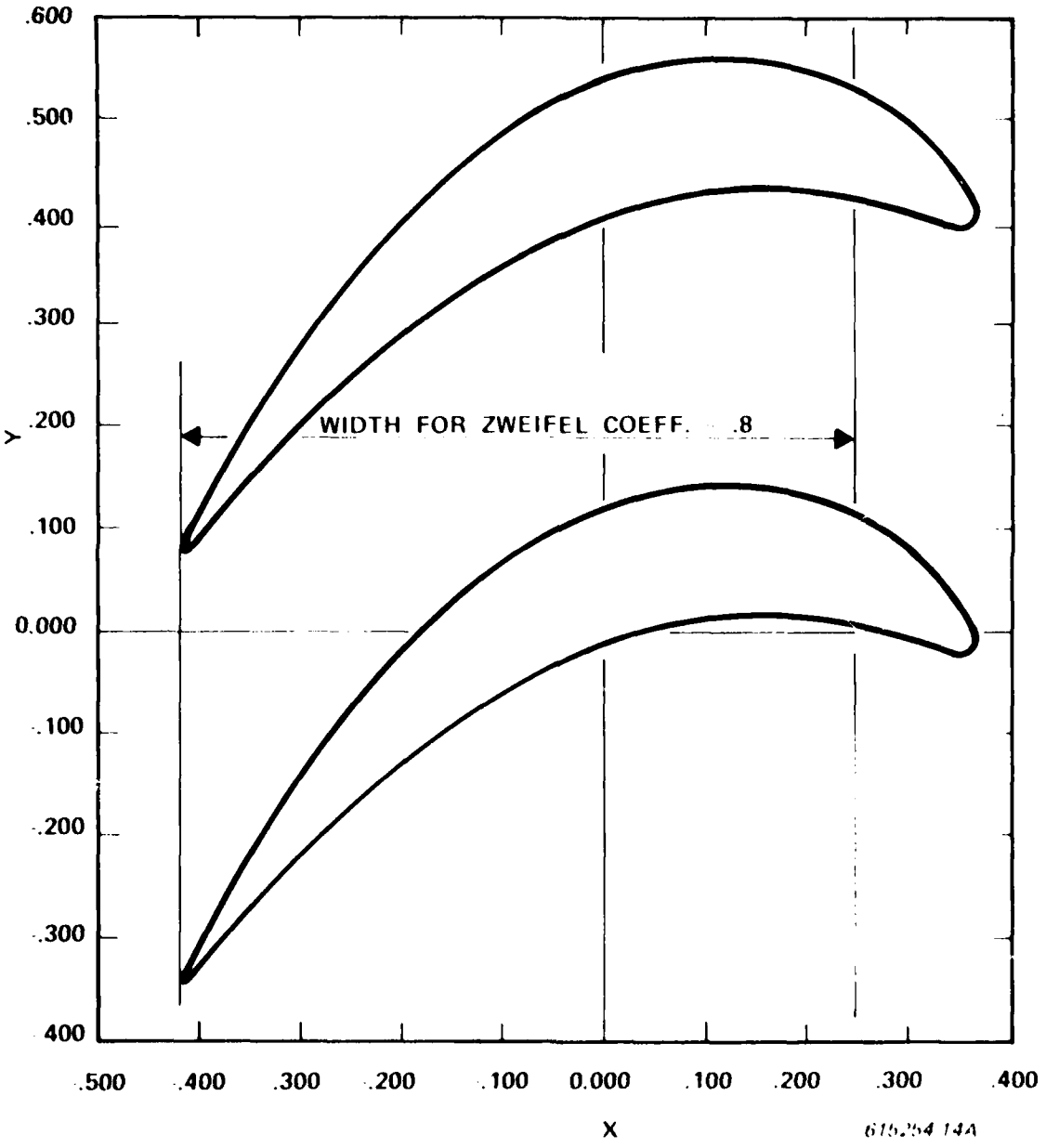

Figure B-7.

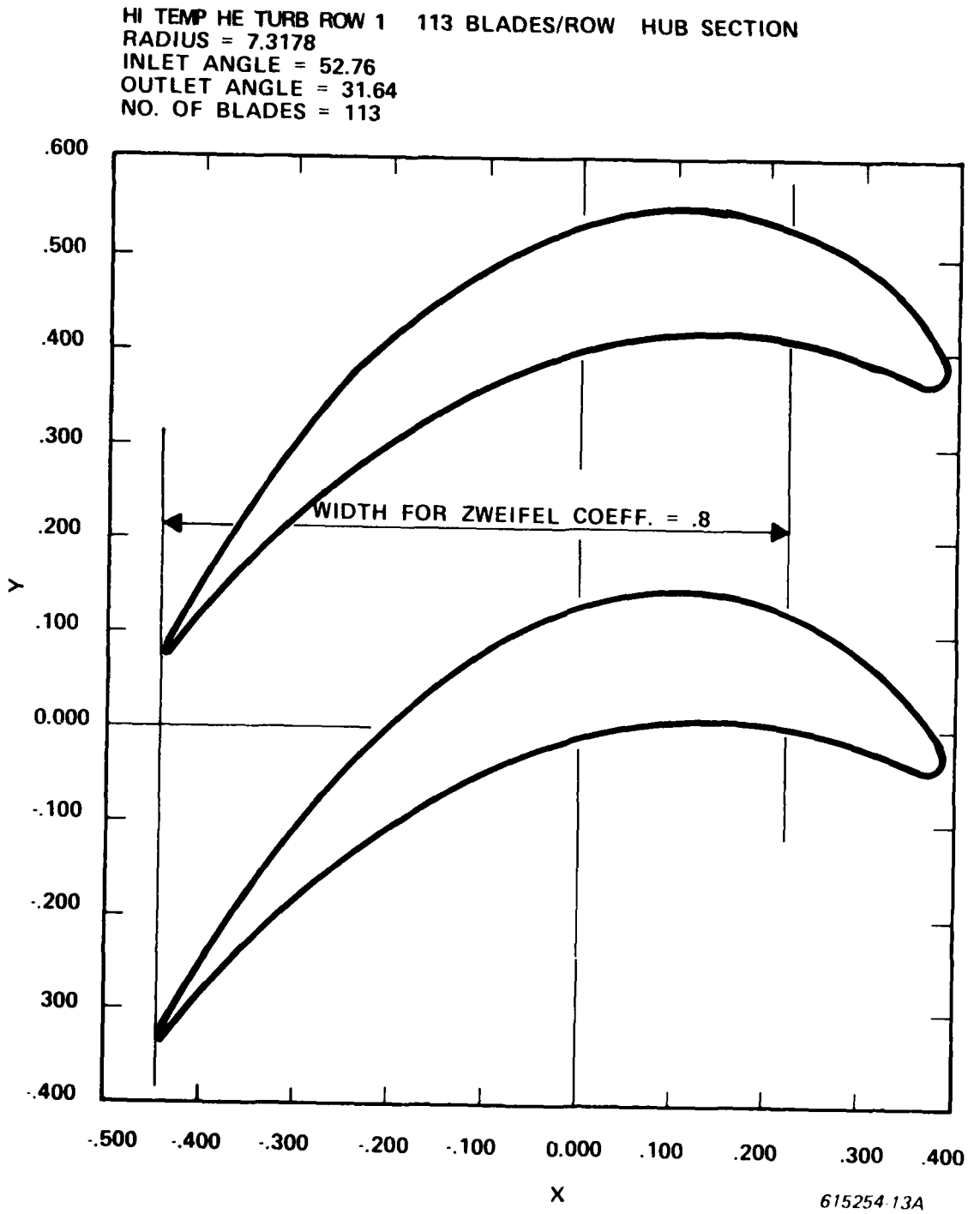
HI TEMP HE TURB ROW 1 113 BLADES/ROW HUB SECTION
RADIUS = 7.3178
INLET ANGLE = 52.76
OUTLET ANGLE = 31.64
NO. OF BLADES = 113
.600
.500
.400
.300
.200
.100
0.000
-.100
-.200
300
-.400
Y
WIDTH FOR ZWEIFEL COEFF. = .8
-.500
-.400
-.300
-.200
-.100
0.000
.100
.200
.300
.400
X
615254-13A

Figure B-8.

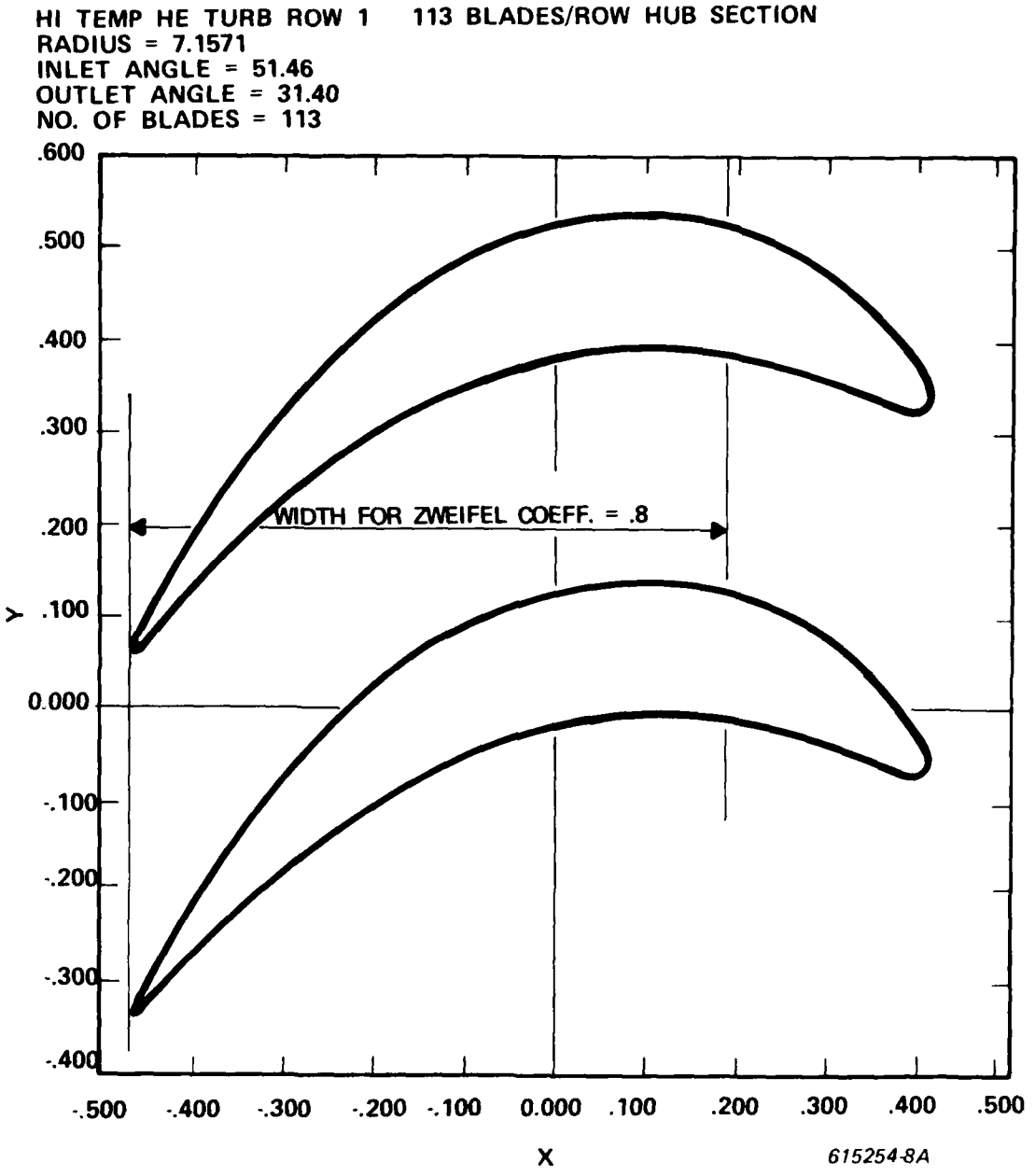
HI TEMP HE TURB ROW 1 113 BLADES/ROW HUB SECTION
RADIUS = 7.1571
INLET ANGLE = 51.46
OUTLET ANGLE = 31.40
NO. OF BLADES = 113
.600
.500
.400
.300
.200
.100
0.000
-.100
-.200
-.300
-.400
Y
WIDTH FOR ZWEIFEL COEFF. = .8
-.500
-.400
-.300
-.200
-.100
0.000
.100
.200
.300
.400
.500
X
615254-8A

Figure B-9.

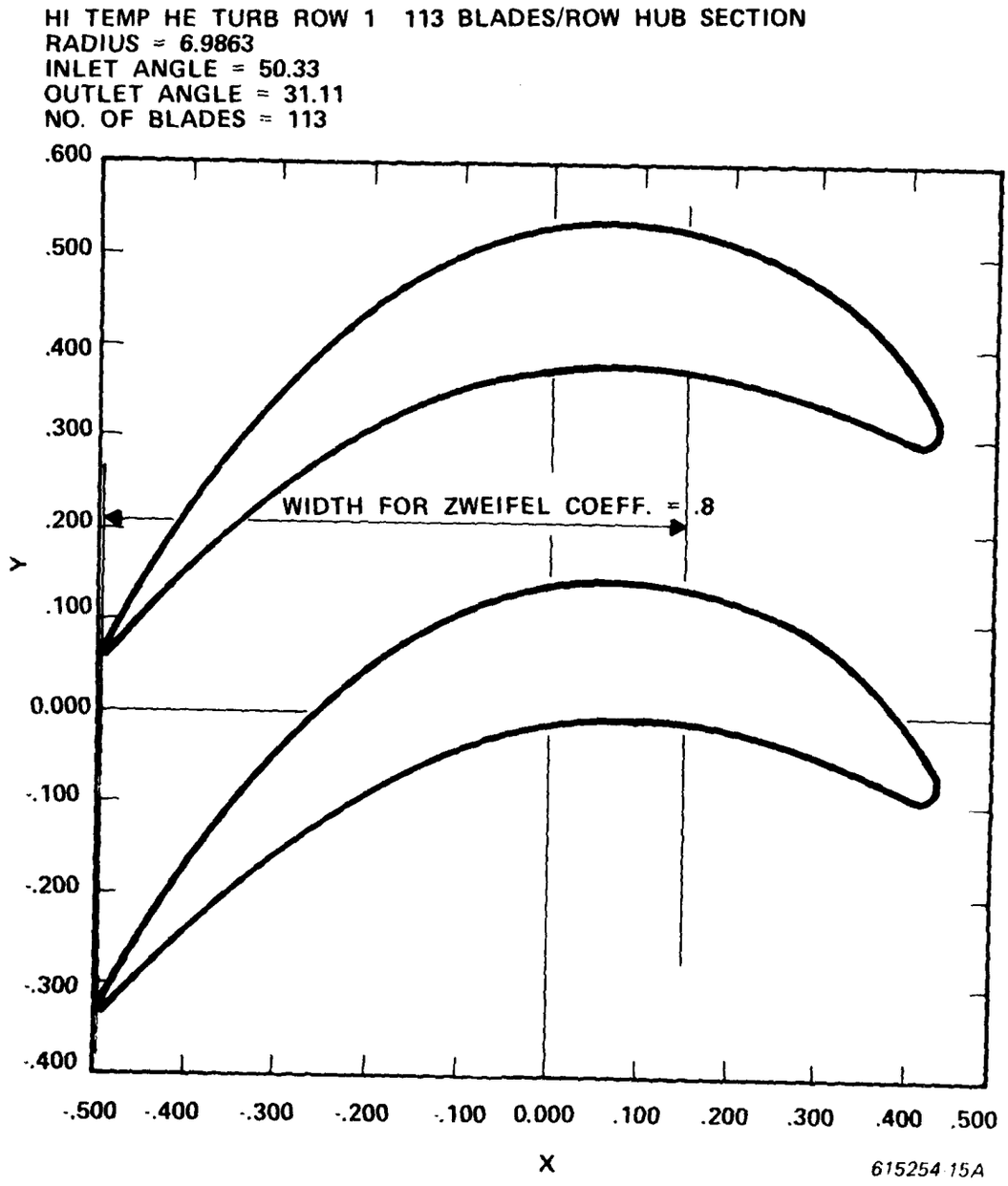
HI TEMP HE TURB ROW 1 113 BLADES/ROW HUB SECTION
RADIUS = 6.9863
INLET ANGLE = 50.33
OUTLET ANGLE = 31.11
NO. OF BLADES = 113
.600
.500
.400
.300
.200
.100
0.000
-.100
-.200
-.300
-.400
Y
WIDTH FOR ZWEIFEL COEFF. = .8
-.500 -.400 -.300 -.200 -.100 0.000 .100 .200 .300 .400 .500
X
615254 15A

Figure B-10.

HI TEMP HE TURB ROW 1 113 BLADES/ROW HUB SECTION
RADIUS = 8.8355
INLET ANGLE = 48.32
OUTLET ANGLE = 30.79
NO. OF BLADES = 113

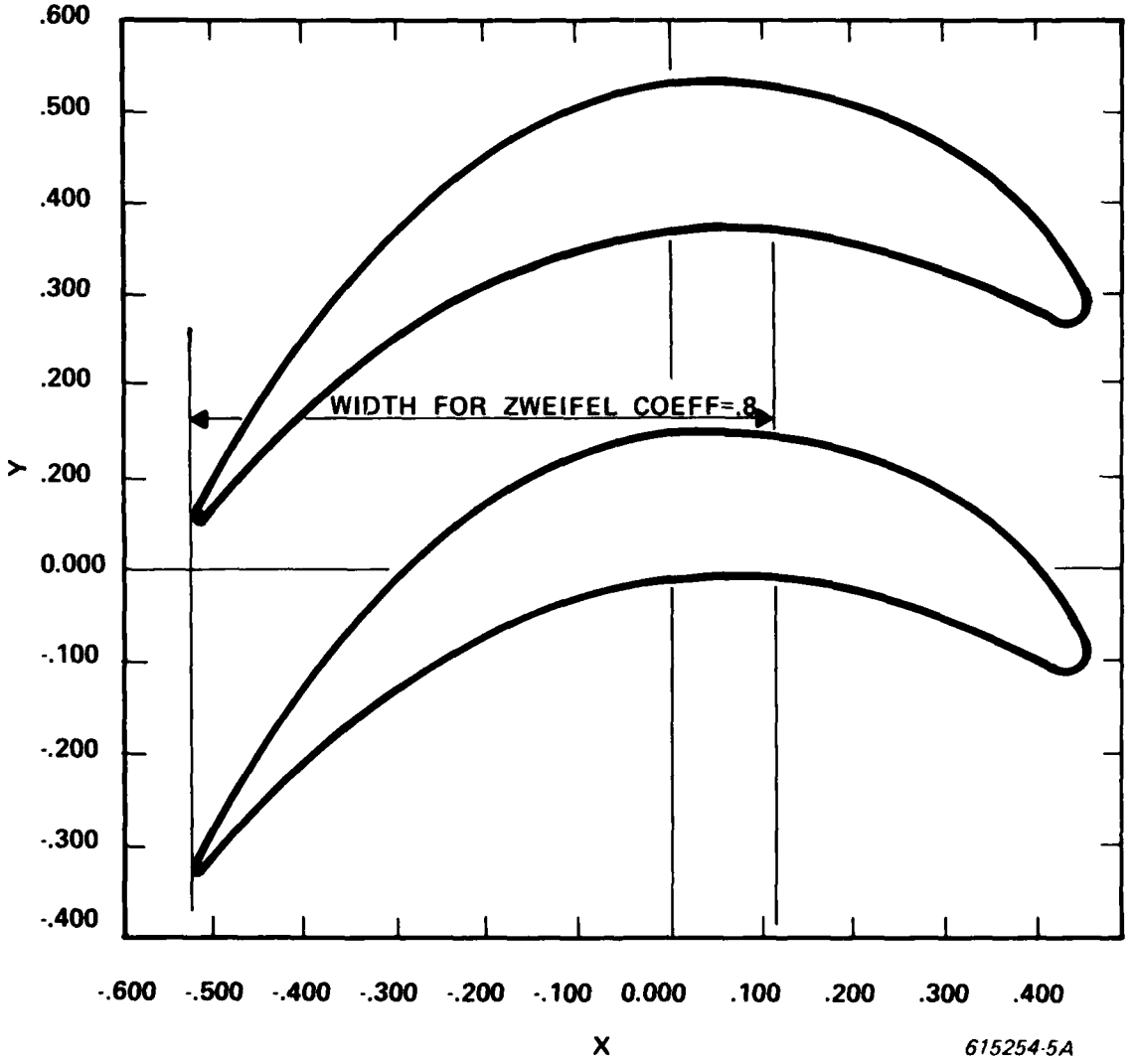

Figure B-11.

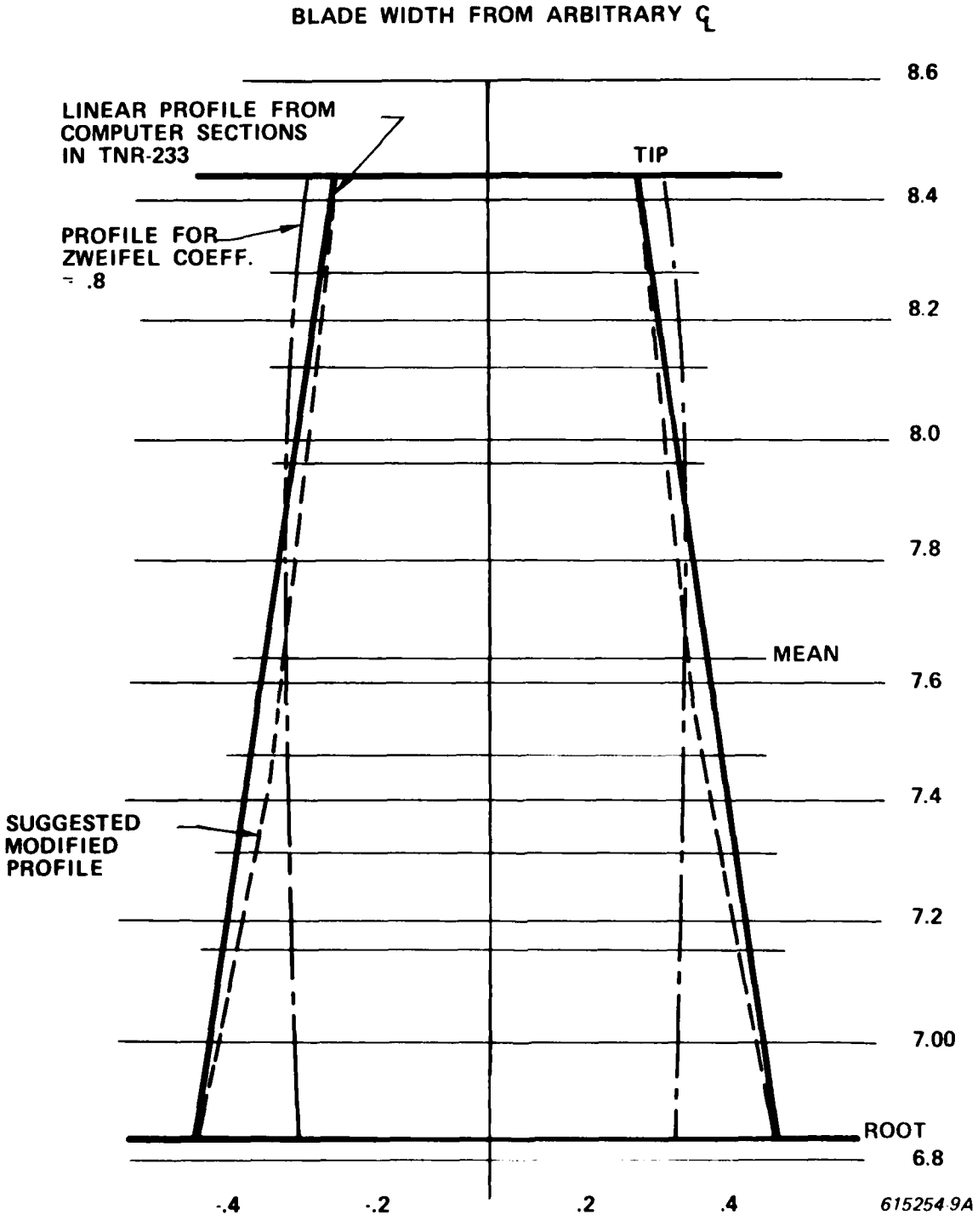

Figure B-12. Blade Width Profile Comparison (Scale 5X)

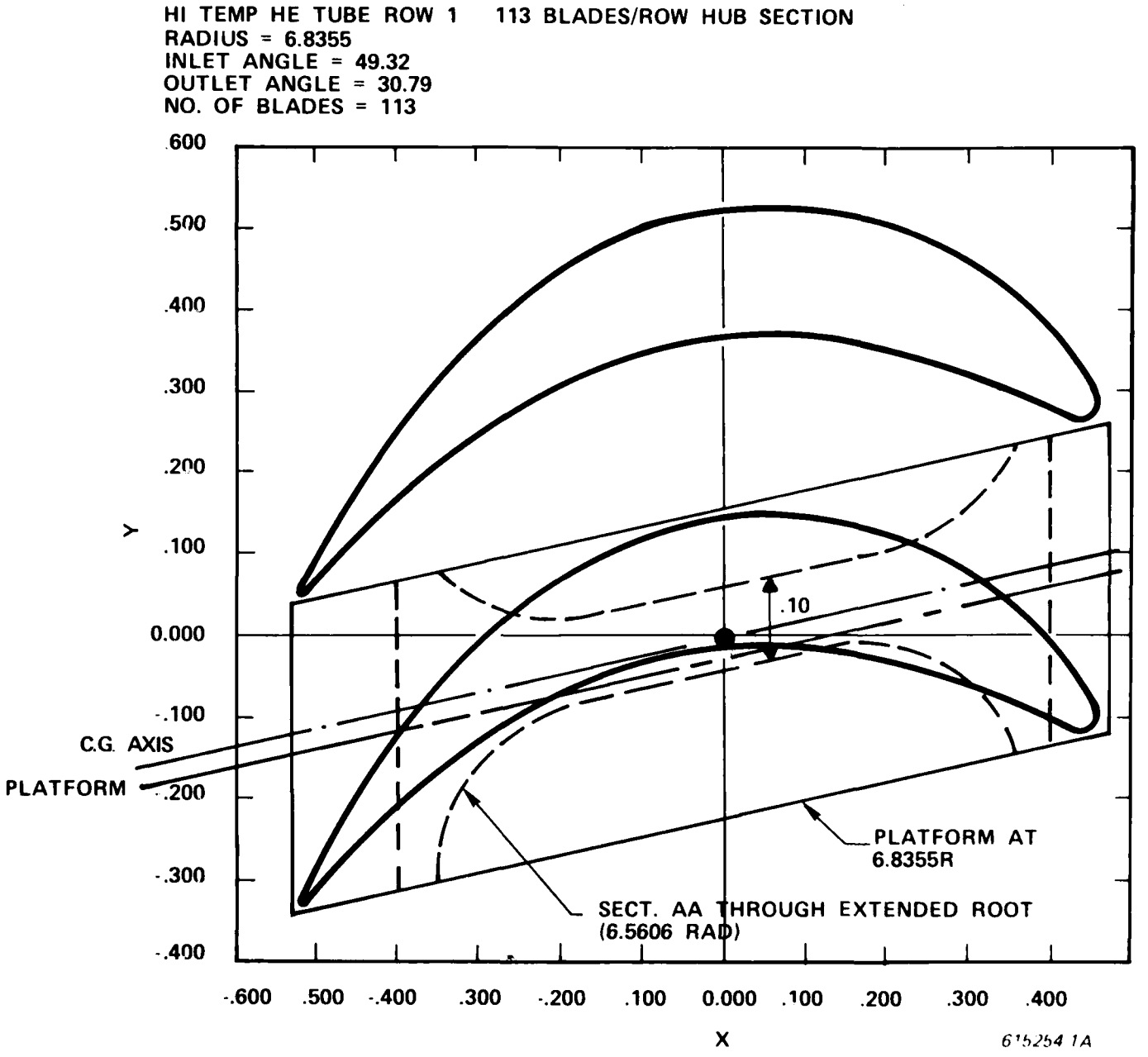
HI TEMP HE TUBE ROW 1 113 BLADES/ROW HUB SECTION
RADIUS = 6.8355
INLET ANGLE = 49.32
OUTLET ANGLE = 30.79
NO. OF BLADES = 113
.600
.500
.400
.300
.200
.100
0.000
-.100
-.200
-.300
-.400
Y
C.G. AXIS
PLATFORM
.10
PLATFORM AT
6.8355R
SECT. AA THROUGH EXTENDED ROOT
(6.5606 RAD)
-.600 .500 -.400 .300 -.200 .100 0.000 .100 .200 .300 .400
X
615254 1A

Figure B-13.

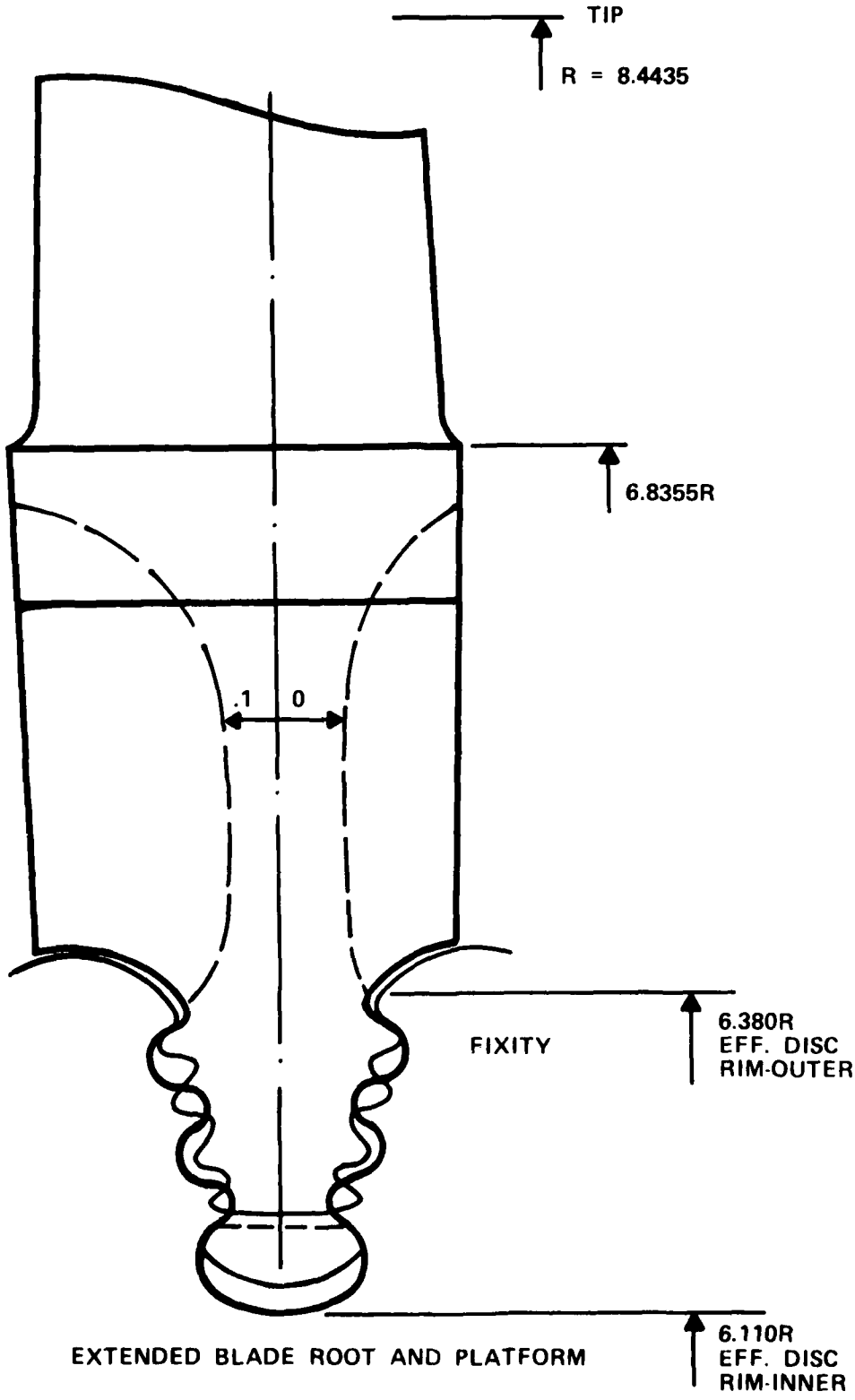
TIP
R = 8.4435
6.8355R
.1
0
FIXITY
6.380R
EFF. DISC
RIM-OUTER
EXTENDED BLADE ROOT AND PLATFORM
6.110R
EFF. DISC
RIM-INNER

Figure B-14.

MODIFIED EXTENDED BC ADL ROOT

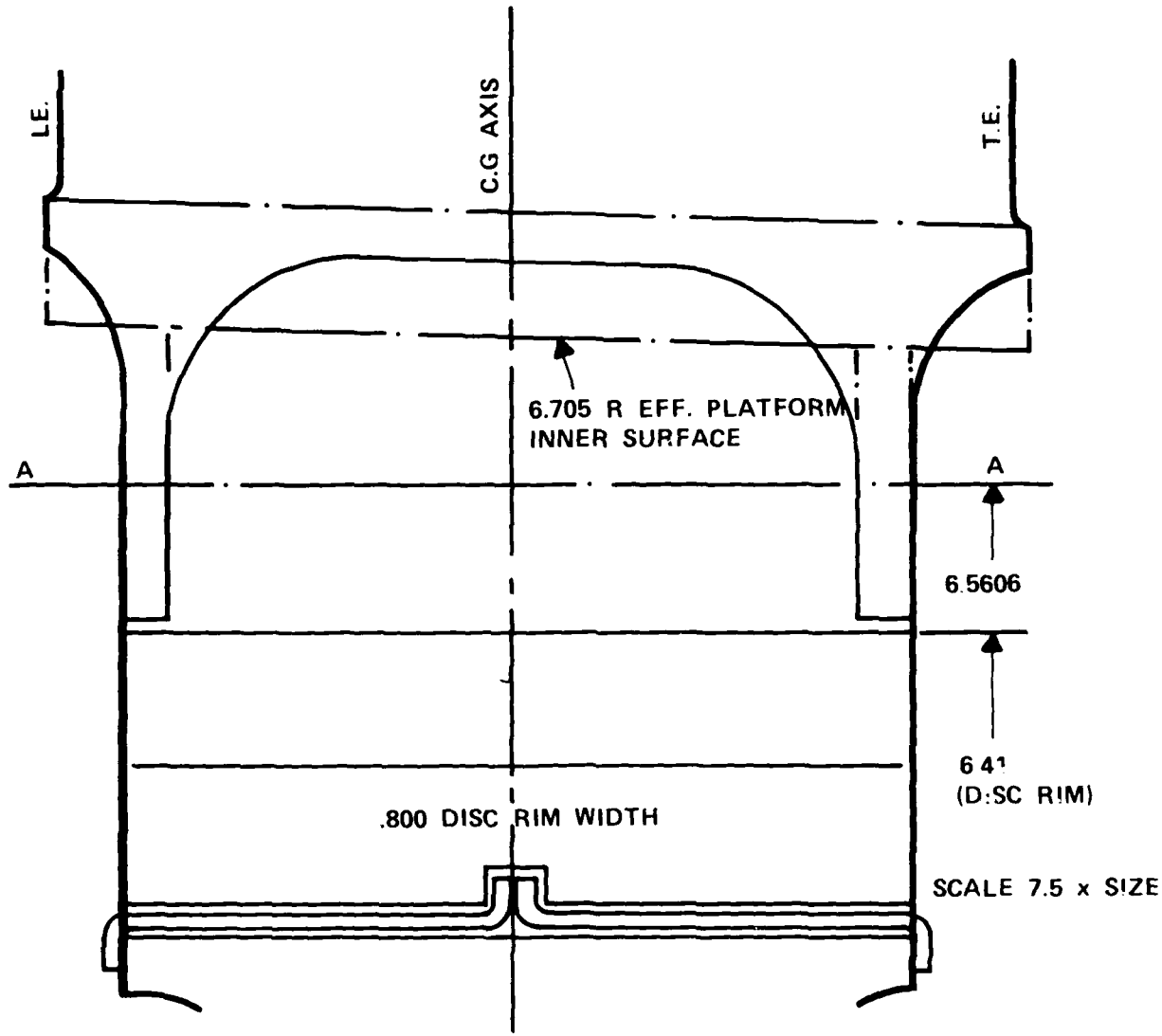

Figure B-15.

TABLE B-1

Calculate blade width for Zweifel coefficient of .8 for airfoil sections developed by Westinghouse Gas Turbine Division computer.

Radius	Pitch (t) = $\frac{2\pi R}{113}$	Inlet Angle β_1	Outlet Angle β_2	Cot β_1	Cot β_2	$\sin^2 \beta_2$	$b/t = 2.5 \sin^2\beta_2 (\cot \beta_1 + \cot \beta_2)$ $Z = 8$	Width (b)
8.4435	0.469	70.46	29.13	0.3549	1.7944	0.237	1.27346	0.5973
8.2827	0.461	66.43	30.14	0.4363	1.7223	0.252	1.36	0.627
8.1219	0.452	63.09	30.87	0.5075	1.6729	0.263	1.4336	0.648
7.9611	0.4427	60.31	31.34	0.57	1.642	0.271	1.499	0.663
7.8003	0.4337	57.96	31.63	0.627	1.624	0.275	1.548	0.671
7.6395	0.4248	55.96	31.76	0.676	1.615	0.277	1.587	0.674
7.4787	0.4158	54.24	31.77	0.720	1.614	0.277	1.616	0.672
7.3179	0.4069	52.76	31.64	0.760	1.623	0.275	1.638	0.667
7.1571	0.398	51.46	31.4	0.8	1.638	0.271	1.652	0.657
6.9963	0.389	50.33	31.11	0.829	1.657	0.267	1.659	0.646
6.8355	0.38	49.32	30.79	0.860	1.678	0.262	1.662	0.632

TABLE B-2

CENTRIFUGAL STRESS DISTRIBUTION FOR MODIFIED WIDTH PROFILE (DOTTED LINE)

Assume airfoil shapes are scaled from computed sections of TNR 233 and that section area is adjusted in proportion to width squared.

$\frac{\omega^2}{g} = \frac{1885^2}{386.4} = 9196$ Assume $\rho = 0.305$ 18,000 RPM = 1885 rads/sec = ω

	②	③	④	⑤	⑥	⑦	⑧	⑨	⑩	⑪
RADIUS	AREA FROM TNR 233	WIDTH FROM TNR 233	ADJUSTED WIDTH (DOTTED LINE)	ADJUSTED AREA ② x ④² / ③²	$\overline{\text{AREA}}$	ΔR	$\bar{R}$	Centrifugal force (lb) = $\overline{\text{area}} \times \Delta R \times .305 \times \bar{R} \times 9186$	Centr. Stress (psi) ⑨ / ⑤	Centr. Stress (psi) at .28 density ⑩ x .28/.305
AIRFOIL								Inc.	Σ	
8.4435	0.0320	0.51	0.51	0.0320						
8.2827	0.0385	0.55	0.54	0.0371	0.03455	0.1608	8.3631	130	130	3,504	3,216
8.1219	0.0456	0.60	0.57	0.0412	0.03915	0.1608	8.2023	145	275	6,675	6,128
7.9611	0.0532	0.65	0.605	0.0461	0.04365	0.1608	8.0415	158	433	9,393	8,623
7.8003	0.0615	0.7	0.64	0.0514	0.04875	0.1608	7.8807	173	606	11,790	10,824
7.6395	0.0704	0.74	0.67	0.0577	0.05455	0.1608	7.7199	190	796	13,795	12,664
7.4787	0.0798	0.79	0.72	0.0663	0.062	0.1608	7.5591	211	1007	15,189	13,944
7.3179	0.0899	0.84	0.776	0.0767	0.0715	0.1608	7.3983	239	1246	16,245	14,913
7.1571	0.1005	0.89	0.84	0.0895	0.0831	0.1608	7.2375	271	1517	16,950	15,560
6.9963	0.1118	0.93	0.906	0.1061	0.0978	0.1608	7.0767	312	1829	17,238	15,825
6.8355	0.1236	0.98	0.98	0.1236	0.1148	0.1608	6.9159	358	2187	17,694	16,243
PLATFORM										
6.8355	0.3797									
6.705	0.3725				0.3761	0.1305	6.7702	932	3119	8,373	7,687
EXTENDED ROOT										
6.705	0.128									24,367	22,370
6.350	0.128	Measured			0.128	0.355	6.5275	832	3951	30,867	28,337
AVG. CENT. AT OUTER FILLET IN BLADE ROOT (UNFACTORED)										
	0.12 (if 0.15 x .8 dimensions of P.4-81 of TNR 233 are retained)								3951	32,925	30,225
DISC RIM		$\frac{2 \times \pi \times 6.110}{113} \times 0.8$								
6.380	0.272	$\frac{2 \times \pi \times 6.245}{113} \times 0.8$ =			0.278	0.270	6.245	1315	5266	19,360	17,773
								AVG RADIAL STRESS AT RIM 6.11 R x 0.8 TH			
AVG CENT. AT INNER FILLET IN DISC (UNFACTORED)										
AREA = 0.8 x 0.2		SCALING MODIFIED = 0.160 SKETCH P.4-Ei TNR 233							5266	32,912	30,215

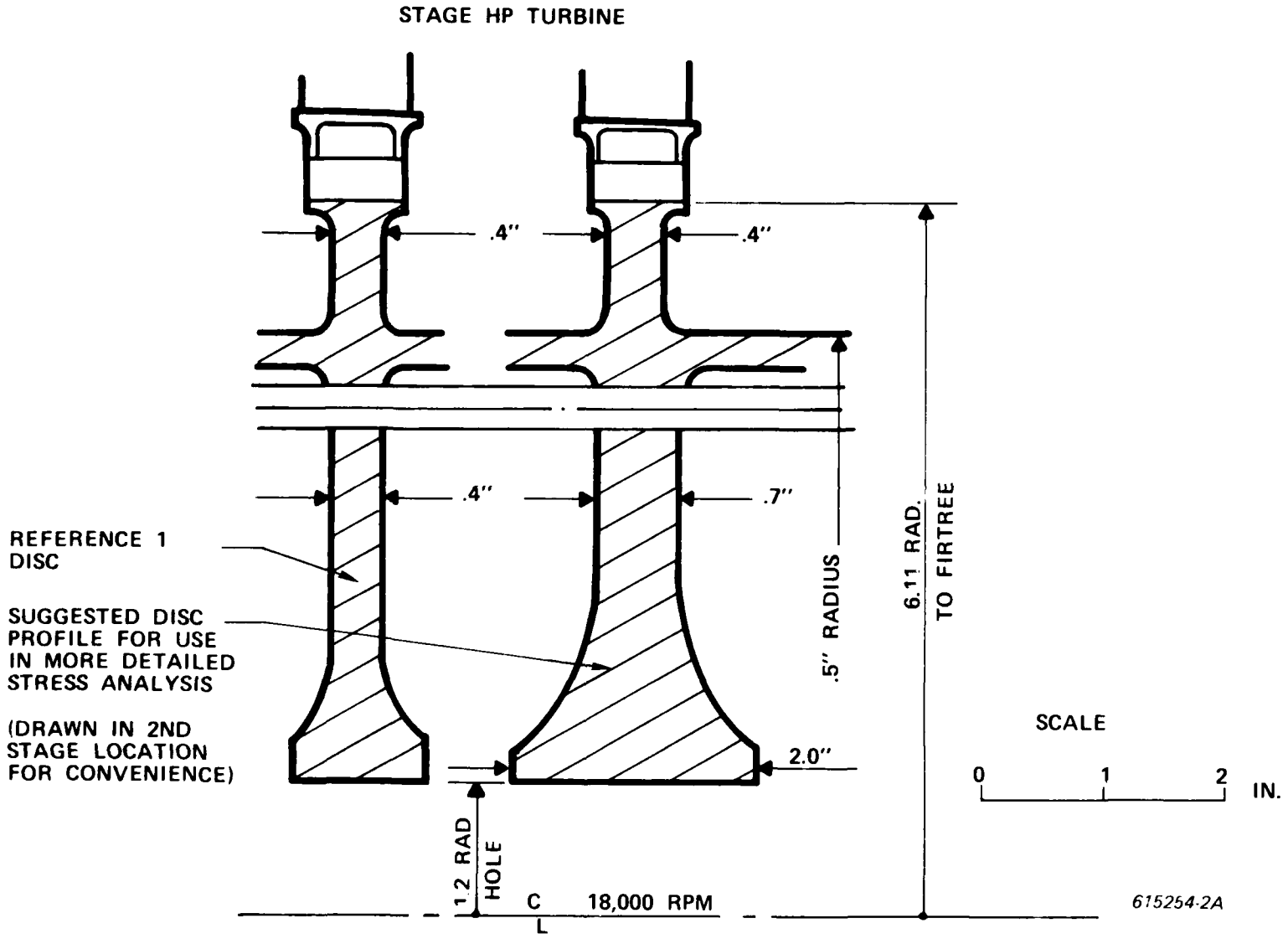
STAGE HP TURBINE
.4"
.4"
.4"
.7"
REFERENCE 1 DISC
SUGGESTED DISC PROFILE FOR USE IN MORE DETAILED STRESS ANALYSIS
(DRAWN IN 2ND STAGE LOCATION FOR CONVENIENCE)
.5" RADIUS
6.11 RAD. TO FIRTREE
2.0"
SCALE
0 1 2 IN.
1.2 RAD HOLE
C L
18,000 RPM
615254-2A

Figure B-16.

APPENDIX C

6000 RPM TURBINE

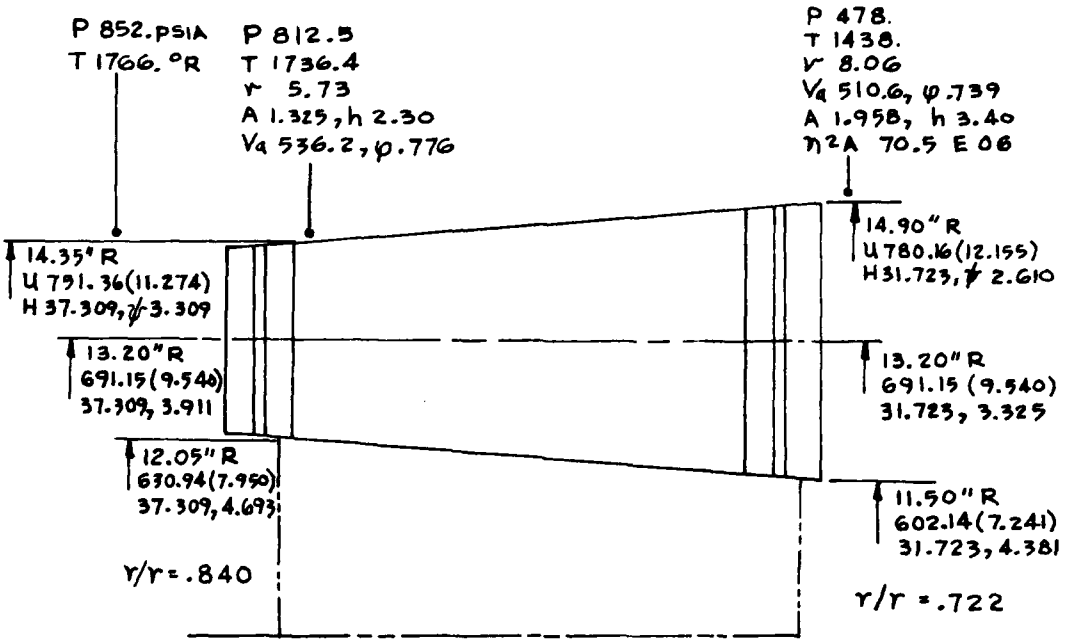

71400. shp * 1.018 = 72670. INTERNAL HP

H = 72670/124. pm/sec / 1.41485 hp/(BTU/sec) = 414.19 BTU/pm

$H_{STG\ Avg.}$ = 34.516 BTU/pm

FLOW PATH - 12 stgs - 6000 rpm

W 124. pm/sec

He properties

M = 4.

R = 386. f-p/pm/°R
= 12419. f p/sl/°R

cp = 1.25
= 31296. f p/SL/°R

$a/T^{1/2}$ = 143.539

γ = 1.6579

Figure C-1.

12 stg velocity triangles - 6000 rpm

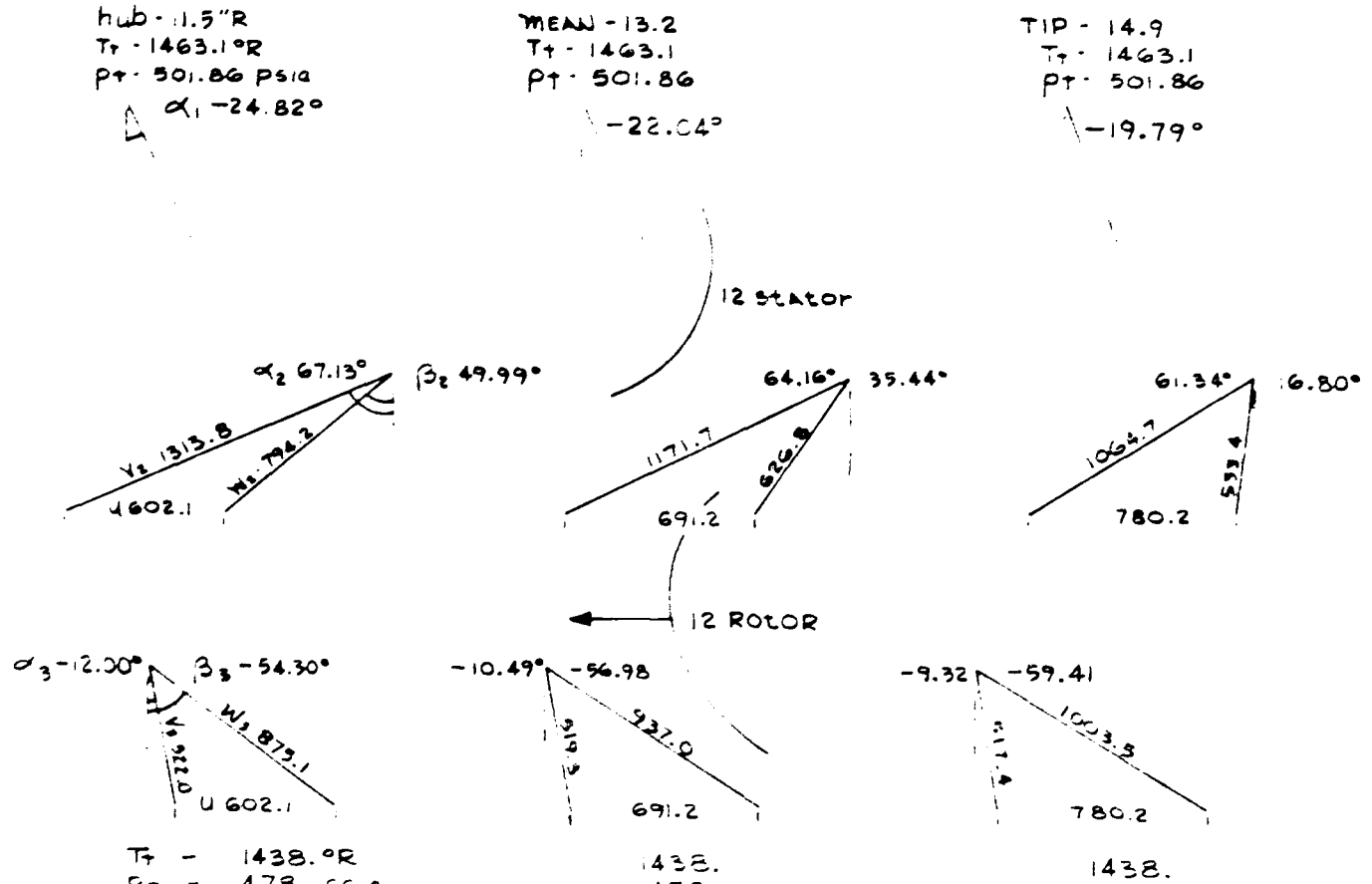

Tt -	1438.°R	1438.	1438.
pt -	478. psia	478.	478.
react -	.072	.26	.389
H/(U²/2)	4.38	3.33	2.61

TABLE C-I

STAGE DATA - 12 STAGE

	HUB	MEAN	TIP
R - radius - in	11.50	13.20	14.90
n - rpm		6000.	
u - fps	602.1	691.2	780.2
H - Btu/pm	31.723	31.723	31.723
$H/(u^2\ 2\ gj)$	4.382	3.325	2.610
$\Delta V_\theta = gjH/u$ - fps	1319.0	1149.2	1018.0
$r = \frac{W3^2 - W2^2}{W3^2 - W2^2 + V2^2}$	.072	.261	.389
w - pm/S		124.	
Tt, inlet - ^oR	1463.1	1463.1	1463.1
pt, inlet - psia	501.86	501.86	501.86
pt, exit - psia	478.0	478.0	478.0
T rotor blade - ^oF	986.	988.	990.

TABLE C-2

BLADING DATA - 12 STATOR VANE

	HUB	MEAN	TIP
R - radius	11.50	13.20	14.90
α_1, α_2 - flow angles	-24.82, 67.13	-22.04, 64.16	-19.79, 61.34
W - axial width	.706	.810	.914
s - pitch	.623	.7150	.8071
n - no. vanes		116.	
ζ - zweifel coefficient	.755	.828	.889
α_1' - inlet blade angle	-24.6	-22.3	-20.2
arc cos o/s - blade angle	.2271	.2974	.3720
T - trailing edge thickness	.015	.015	.015
T/O - blockage	.068	.052	.040
UCT - uncovered turning	10.3	-	12.8
Bow	.19	-	.24
A - cross-sectional area	.0973	.1110	.1246

NOTE - All blading dimensions in inches and deg.

DATE= 05/08/7
12STAT HELIUM TURBINE= WEDNESDAY 03 78

X	Y	PCT.OPENING	PCT.WIDTH FROM T.E.	THROAT	SURFACE LENGTH	RADIUS = 11.500 HOLE X	HOLE Y	HOLE D
-.3554	-.5303	.9461	0.0000		1.2049	0.0000	0.0000	0.0000
-.2855	-.3421	.8518	.0995		.9971	0.0000	0.0000	0.0000
-.2151	-.1733	.7830	.1992		.8142	0.0000	0.0000	0.0000
-.1447	-.0321	.7378	.2991		.6564	0.0000	0.0000	0.0000
-.0742	.0797	.7138	.3988		.5242	0.0000	0.0000	0.0000
-.0036	.1616	.7067	.4989		.4159	0.0000	0.0000	0.0000
.0670	.2130	.7150	.5988		.3283	0.0000	0.0000	0.0000
.1376	.2347	.7383	.6989		.2540	0.0000	0.0000	0.0000
.2084	.2277	.7788	.7992		.1823	0.0000	0.0000	0.0000
.2792	.1943	.8387	.8995		.1038	0.0000	0.0000	0.0000
.3501	.1364	.9197	1.0000		0.0000	0.0000	0.0000	0.0000
-.3557	-.5699			0.0000	1.0464	0.0000	0.0000	0.0000
-.2853	-.4344			.2353	.9054	0.0000	0.0000	0.0000
-.2144	-.3085			.2578	.7611	0.0000	0.0000	0.0000
-.1443	-.1954			.2947	.6278	0.0000	0.0000	0.0000
-.0738	-.0986			.3415	.5080	0.0000	0.0000	0.0000
-.0032	-.0211			.3888	.4031	0.0000	0.0000	0.0000
.0674	.0355			.4292	.3125	0.0000	0.0000	0.0000
.1380	.0717			.4592	.2330	0.0000	0.0000	0.0000
.2088	.0899			.4793	.1598	0.0000	0.0000	0.0000
.2794	.0938			.4926	.0889	0.0000	0.0000	0.0000
.3503	.0864			0.0000	0.0000	0.0000	0.0000	0.0000

CIRCLE PARAMETERS	R L	X L	Y L	R R	X R	Y R	
BETA L 22.8405	.0077	-.3480	-.5376	.0316	.3186	.1229	
BETA R 65.3546	X GAGING	-.1431	Y GAGING	-.0294			
GAGING .227085	PITCH	.622901	D/P	.364560	SIN=1 D/P	21.3805	

MECHANICAL PROPERTIES				TAN.ANG	-8.358677	STAGGER	43.277825
AREA .097348	M X	.000000	M Y	.000000	I X	.002914	
I Y .003225	I XY	.002703	I MIN	.000362	I MAX	.005777	
F Y 1392.841066	F X	1541.594958	F XY	1291.976380	ALPHA	46.647386	
BAR I X .002914	BAR I Y	.003225	BAR I XY	.002703	MAX THICK	.158917	
C MIN LE -.178894	C MAX LE	.308046	C MIN TE	-.123716	C MAX TE	-.629818	
Z MIN LE -.002024	Z MAX LE	.018753	Z MIN TE	-.002927	Z MAX TE	-.009172	
C MIN B .085634	C MAX B	.228729	Z MIN B	.004229	Z MAX B	.025257	
BAR S -.000403	BAR C	-.000805	BAR D	.000890	CHORD	.977741	
BAR X .000001	BAR Y	.000303	K	.000380	WIDTH	.705905	

DATE= 05/08/7
12STAT HELIUM TURBINE= WEDNESDAY 03 78

X	Y	PCT.OPENING	PCT.WIDTH FROM T.E.	THROAT	SURFACE LENGTH	RADIUS = 12.350 HOLE X	HOLE Y	HOLE D
-.3846	-.5482	.9519	0.0000		1.2519	0.0000	0.0000	0.0000
-.3088	-.3528	.8645	.1000		1.0410	0.0000	0.0000	0.0000
-.2329	-.1819	.7999	.2001		.8539	0.0000	0.0000	0.0000
-.1570	-.0380	.7573	.3002		.6913	0.0000	0.0000	0.0000
-.0813	.0767	.7342	.4002		.5537	0.0000	0.0000	0.0000
-.0054	.1612	.7271	.5003		.4400	0.0000	0.0000	0.0000
.0703	.2145	.7342	.6002		.3471	0.0000	0.0000	0.0000
.1460	.2375	.7552	.7001		.2675	0.0000	0.0000	0.0000
.2218	.2313	.7922	.8001		.1910	0.0000	0.0000	0.0000
.2975	.1982	.8477	.9000		.1081	0.0000	0.0000	0.0000
.3733	.1406	.9232	1.0000		0.0000	0.0000	0.0000	0.0000
-.3846	-.5804			0.0000	1.0965	0.0000	0.0000	0.0000
-.3088	-.4434			.2714	.9502	0.0000	0.0000	0.0000
-.2329	-.3157			.2962	.8017	0.0000	0.0000	0.0000
-.1571	-.2008			.3355	.6636	0.0000	0.0000	0.0000
-.0813	-.1010			.3842	.5387	0.0000	0.0000	0.0000
-.0055	-.0214			.4329	.4286	0.0000	0.0000	0.0000
.0703	.0368			.4741	.3330	0.0000	0.0000	0.0000
.1461	.0738			.5043	.2485	0.0000	0.0000	0.0000
.2218	.0924			.5246	.1703	0.0000	0.0000	0.0000
.2975	.0964			.5381	.0944	0.0000	0.0000	0.0000
.3733	.0892			0.0000	0.0000	0.0000	0.0000	0.0000

CIRCLE PARAMETERS	R L	X L	Y L	R R	X R	Y R	
BETA L 24.2491	.0078	-.3768	-.5496	.0324	.3409	.1262	
BETA R 66.5812	X GAGING	-.1464	Y GAGING	-.0202			
GAGING .261602	PITCH	.668942	D/P	.391069	SIN=1 D/P	23.0210	

MECHANICAL PROPERTIES				TAN.ANG	57.313970	STAGGER	41.843468
AREA .104195	M X	-.000039	M Y	-.000016	I X	.003596	
I Y .003586	I XY	.003176	I MIN	.000415	I MAX	.006767	
F Y 1279.900424	F X	1276.157172	F XY	1130.241830	ALPHA	44.952553	
BAR I X .003596	BAR I Y	.003586	BAR I XY	.003176	MAX THICK	.159932	
C MIN LE -.184123	C MAX LE	.330799	C MIN TE	-.130637	C MAX TE	-.654582	
Z MIN LE -.002255	Z MAX LE	.020455	Z MIN TE	-.003179	Z MAX TE	-.010337	
C MIN B .089955	C MAX B	.231753	Z MIN B	.004616	Z MAX B	.029197	
BAR S -.000490	BAR C	-.000945	BAR D	.001128	CHORD	1.025942	
BAR X -.000378	BAR Y	-.000156	K	.000427	WIDTH	.757894	

Figure C-3.

DATE= 05/04/77
12STAT HELIUM TURBINE= WEDNESDAY 03 78

X	Y	PCT.OPENING	PCT.WIDTH FROM T.E.	THROAT	SURFACE LENGTH	RADIUS = 13.200 HOLE X	HOLE Y	HOLE D
-.4134	-.5601	.9570	0.0000		1.2994	0.0000	0.0000	0.0000
-.3321	-.3635	.8755	.1004		1.0852	0.0000	0.0000	0.0000
-.2507	-.1905	.8148	.2009		.8940	0.0000	0.0000	0.0000
-.1694	-.0439	.7743	.3012		.7284	0.0000	0.0000	0.0000
-.0883	.0737	.7521	.4014		.5834	0.0000	0.0000	0.0000
-.0072	.1607	.7450	.5015		.4643	0.0000	0.0000	0.0000
.0737	.2161	.7510	.6014		.3660	0.0000	0.0000	0.0000
.1545	.2404	.7699	.7012		.2812	0.0000	0.0000	0.0000
.2353	.2349	.8040	.8009		.1998	0.0000	0.0000	0.0000
.3159	.2022	.8556	.9004		.1125	0.0000	0.0000	0.0000
.3965	.1448	.9262	1.0000		0.0000	0.0000	0.0000	0.0000
-.4135	-.5909			0.0000	1.1468	0.0000	0.0000	0.0000
-.3323	-.4525			.3085	.9954	0.0000	0.0000	0.0000
-.2511	-.3229			.3354	.8425	0.0000	0.0000	0.0000
-.1699	-.2053			.3767	.6996	0.0000	0.0000	0.0000
-.0889	-.1035			.4271	.5694	0.0000	0.0000	0.0000
-.0079	-.0217			.4770	.4541	0.0000	0.0000	0.0000
.0731	.0380			.5189	.3534	0.0000	0.0000	0.0000
.1540	.0759			.5494	.2640	0.0000	0.0000	0.0000
.2348	.0948			.5698	.1808	0.0000	0.0000	0.0000
.3155	.0989			.5835	.0999	0.0000	0.0000	0.0000
.3963	.0921			0.0000	0.0000	0.0000	0.0000	0.0000

CIRCLE PARAMETERS	R L	X L	Y L	R R	X R	Y R	
BETA L	25.6096	.0077	-.4056	-.5616	.0331	.3633	.1294
BETA R	67.7282	X GAGING	-.1497	Y GAGING	-.0127		
GAGING	.297391	PITCH	.714983	O/P	.415942	SIN=1 O/P	24.5786

MECHANICAL PROPERTIES				TAN.ANG	55.615841	STAGGER	40.537608
AREA	.111015	M X	-.000056	M Y	-.000023	I X	.004375
I Y	.003963	I XY	.003693	I MIN	.000471	I MAX	.007867
F Y 1191.	213311	F X 1070.	095247	F XY 997.	001176	ALPHA	43.405206
BAR I X	.004375	BAR I Y	.003963	BAR I XY	.003693	MAX THICK	.160886
C MIN LE	-.186923	C MAX LE	.353435	C MIN TE	-.137189	C MAX TE	-.680087
Z MIN LE	-.002692	Z MAX LE	.022260	Z MIN TE	-.003432	Z MAX TE	-.011568
C MIN B	.095080	C MAX B	.232366	Z MIN B	.004951	Z MAX B	.033858
BAR B	-.000591	BAR C	-.001103	BAR D	.001417	CHORD	1.074705
BAR X	-.000506	BAR Y	-.000210	K	.000474	WIDTH	.809884

DATE= 05/04/77
12STAT HELIUM TURBINE= WEDNESDAY 03 78

X	Y	PCT.OPENING	PCT.WIDTH FROM T.E.	THROAT	SURFACE LENGTH	RADIUS = 14.050 HOLE X	HOLE Y	HOLE D
-.4022	-.5720	.9615	0.0000		1.3474	0.0000	0.0000	0.0000
-.3353	-.3743	.8852	.1008		1.1299	0.0000	0.0000	0.0000
-.2685	-.1991	.8278	.2016		.9344	0.0000	0.0000	0.0000
-.1818	-.0498	.7892	.3021		.7617	0.0000	0.0000	0.0000
-.0954	.0707	.7678	.4024		.6133	0.0000	0.0000	0.0000
-.0090	.1602	.7606	.5026		.4888	0.0000	0.0000	0.0000
.0773	.2176	.7657	.6025		.3851	0.0000	0.0000	0.0000
.1629	.2432	.7829	.7021		.2950	0.0000	0.0000	0.0000
.2487	.2385	.8143	.8013		.2087	0.0000	0.0000	0.0000
.3342	.2061	.8625	.9008		.1169	0.0000	0.0000	0.0000
.4197	.1490	.9289	1.0000		0.0000	0.0000	0.0000	0.0000
-.4024	-.6013			0.0000	1.1973	0.0000	0.0000	0.0000
-.3558	-.4616			.3465	1.0409	0.0000	0.0000	0.0000
-.2692	-.3301			.3751	.8835	0.0000	0.0000	0.0000
-.1827	-.2103			.4181	.7357	0.0000	0.0000	0.0000
-.0961	-.1060			.4700	.6003	0.0000	0.0000	0.0000
-.0101	-.0219			.5211	.4797	0.0000	0.0000	0.0000
.0760	.0393			.5637	.3739	0.0000	0.0000	0.0000
.1619	.0780			.5945	.2795	0.0000	0.0000	0.0000
.2479	.0972			.6150	.1913	0.0000	0.0000	0.0000
.3336	.1015			.6290	.1054	0.0000	0.0000	0.0000
.4193	.0949			0.0000	0.0000	0.0000	0.0000	0.0000

CIRCLE PARAMETERS	R L	X L	Y L	R R	X R	Y R	
BETA L	26.9233	.0077	-.4345	-.5736	.0338	.3858	.1327
BETA R	68.7998	X GAGING	-.1531	Y GAGING	-.0067		
GAGING	.334256	PITCH	.761023	O/P	.439219	SIN=1 O/P	26.0541

MECHANICAL PROPERTIES				TAN.ANG	42.040470	STAGGER	39.345247
AREA	.117805	M X	-.000045	M Y	-.000019	I X	.005256
I Y	.004358	I XY	.004255	I MIN	.000529	I MAX	.009085
F Y 1094.	329801	F X 907.	435880	F XY 885.	895681	ALPHA	41.989260
BAR I X	.005256	BAR I Y	.004358	BAR I XY	.004255	MAX THICK	.161786
C MIN LE	-.193358	C MAX LE	.375913	C MIN TE	-.143410	C MAX TE	-.706295
Z MIN LE	-.002734	Z MAX LE	.024169	Z MIN TE	-.003686	Z MAX TE	-.012863
C MIN B	.097108	C MAX B	.239519	Z MIN B	.005446	Z MAX B	.037962
BAR B	-.000707	BAR C	-.001280	BAR D	.001764	CHORD	1.123958
BAR X	-.000382	BAR Y	-.000161	K	.000521	WIDTH	.861873

Figure C-4.

DATE= 05/08/7
12STAT HELIUM TURBINE= WEDNESDAY 03 78

X	Y	PCT.OPENING	PCT.WIDTH FROM T.E.	THROAT	SURFACE LENGTH	RADIUS = 14.900 HOLE X	HOLE Y	HOLE D
-.4710	-.5839	.9654	0.0000		1.3958	0.0000	0.0000	0.0000
-.3786	-.3850	.8938	.1011		1.1749	0.0000	0.0000	0.0000
-.2863	-.2077	.8393	.2021		.9750	0.0000	0.0000	0.0000
-.1942	-.0558	.8024	.3029		.7973	0.0000	0.0000	0.0000
-.1024	.0677	.7817	.4034		.6434	0.0000	0.0000	0.0000
-.0108	.1598	.7745	.5036		.5134	0.0000	0.0000	0.0000
.0804	.2192	.7787	.6034		.4042	0.0000	0.0000	0.0000
.1713	.2461	.7943	.7029		.3090	0.0000	0.0000	0.0000
.2621	.2421	.8234	.8022		.2177	0.0000	0.0000	0.0000
.3525	.2101	.8687	.9012		.1214	0.0000	0.0000	0.0000
.4429	.1533	.9312	1.0000		0.0000	0.0000	0.0000	0.0000
-.4713	-.6118			0.0000	1.2481	0.0000	0.0000	0.0000
-.3793	-.4707			.3853	1.0867	0.0000	0.0000	0.0000
-.2874	-.3374			.4151	.9247	0.0000	0.0000	0.0000
-.1955	-.2153			.4598	.7719	0.0000	0.0000	0.0000
-.1039	-.1085			.5130	.6312	0.0000	0.0000	0.0000
-.0124	-.0222			.5652	.5053	0.0000	0.0000	0.0000
.0789	.0406			.6085	.3944	0.0000	0.0000	0.0000
.1699	.0801			.6396	.2950	0.0000	0.0000	0.0000
.2609	.0996			.6602	.2018	0.0000	0.0000	0.0000
.3516	.1041			.6744	.1108	0.0000	0.0000	0.0000
.4424	.0978			0.0000	0.0000	0.0000	0.0000	0.0000

CIRCLE PARAMETERS		R L	X L	Y L	R R	X R	Y R
BETA L	28.1917	.0075	-.4635	-.5855	.0345	.4082	.1360
BETA R	69.8008	X GAGING	-.1567	Y GAGING	-.0020		
GAGING	.372032	PITCH	.807064	D/P	.460970	SIN=: D/P	27.4497

MECHANICAL PROPERTIES				TAN.ANG	-88.225767	STAGGER	38.252471
AREA	.124566	M X	-.000000	M Y	-.000001	I X	.006244
I Y	.004769	I XY	.004862	I MIN	.000589	I MAX	.010424
P Y	1017.330716	P X	777.141696	P XY	792.254893	ALPHA	40.890194
BAR I X	.006244	BAR I Y	.004769	BAR I XY	.004862	MAX THICK	.162611
C MIN LE	-.197480	C MAX LE	.398200	C MIN TE	-.149340	C MAX TE	-.733168
Z MIN LE	-.002981	Z MAX LE	.026178	Z MIN TE	-.003942	Z MAX TE	-.014218
C MIN B	.099059	C MAX B	.246158	Z MIN B	.005943	Z MAX B	.042348
BAR B	-.000839	BAR C	-.001477	BAR D	.002179	CHORD	1.173638
BAR X	-.000003	BAR Y	-.000009	K	.000568	WIDTH	.913862

Figure C-5.

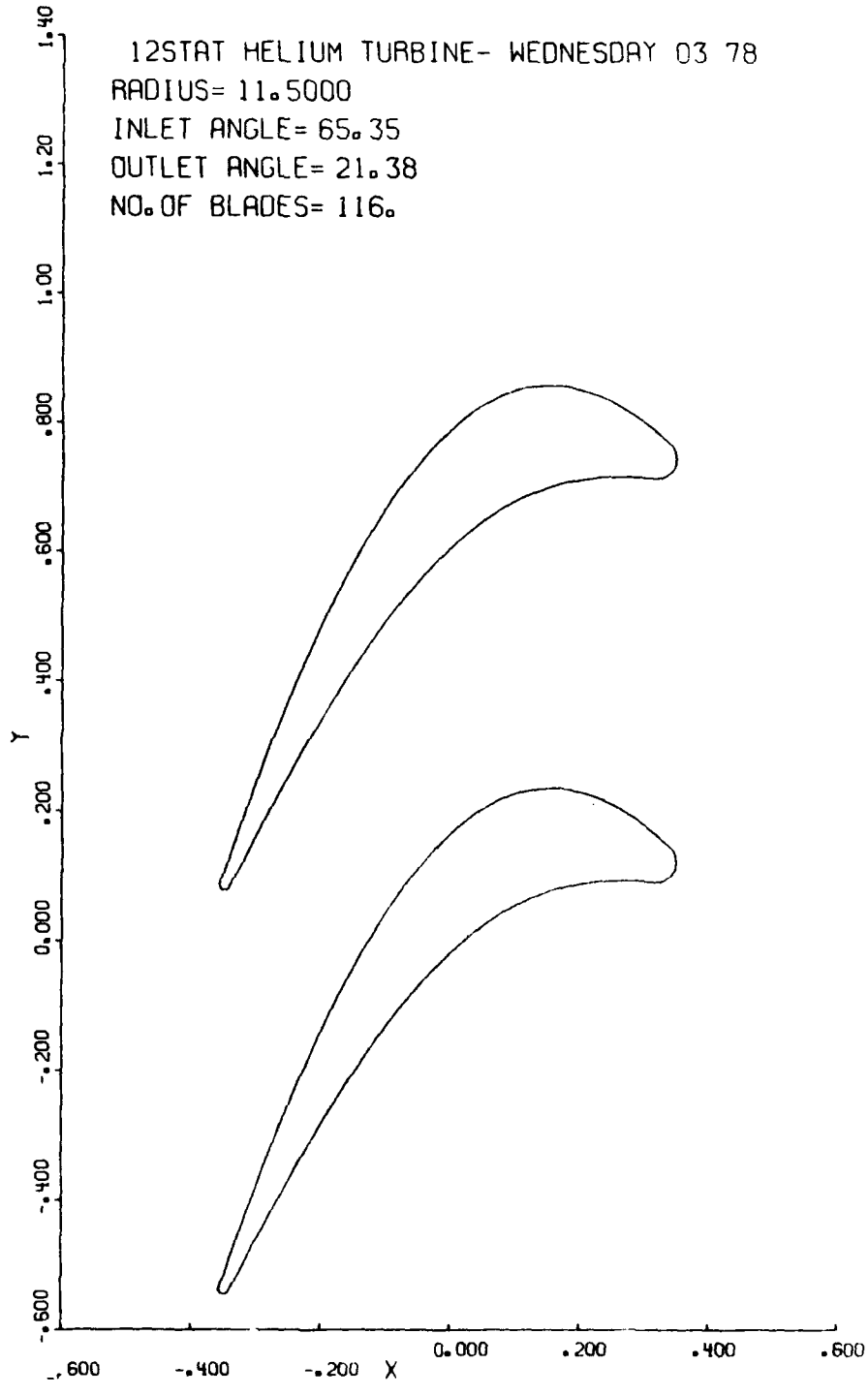
12STAT HELIUM TURBINE- WEDNESDAY 03 78
RADIUS= 11.5000
INLET ANGLE= 65.35
OUTLET ANGLE= 21.38
NO. OF BLADES= 116.
1.40
1.20
1.00
.800
.600
.400
.200
0.000
-.200
-.400
-.600
Y
-.600
-.400
-.200
0.000
.200
.400
.600
X

Figure C-6.

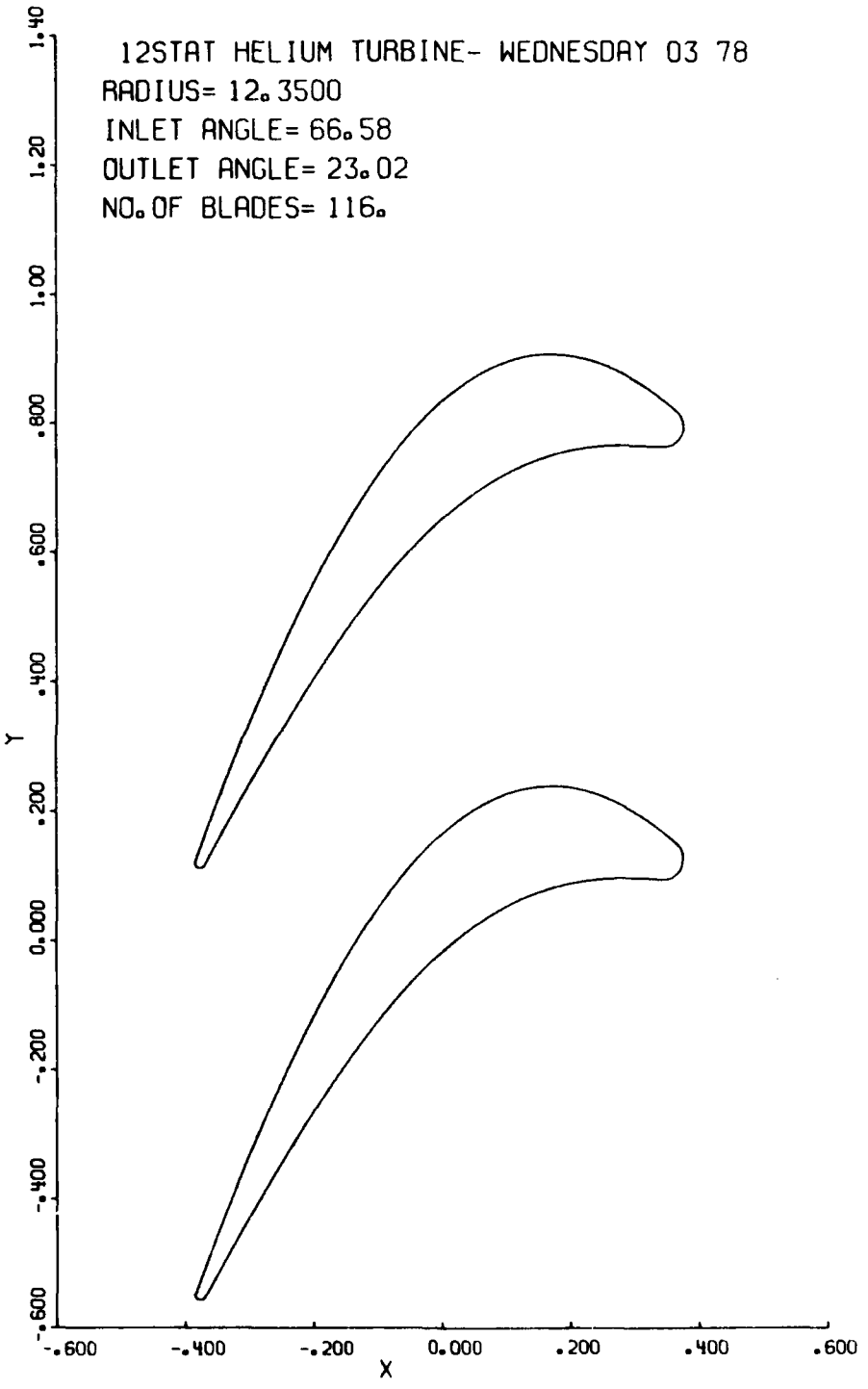
12STAT HELIUM TURBINE- WEDNESDAY 03 78
RADIUS= 12.3500
INLET ANGLE= 66.58
OUTLET ANGLE= 23.02
NO. OF BLADES= 116.
1.40
1.20
1.00
.800
.600
.400
.200
0.000
-.200
-.400
-.600
Y
-.600
-.400
-.200
0.000
.200
.400
.600
X

Figure C-7.

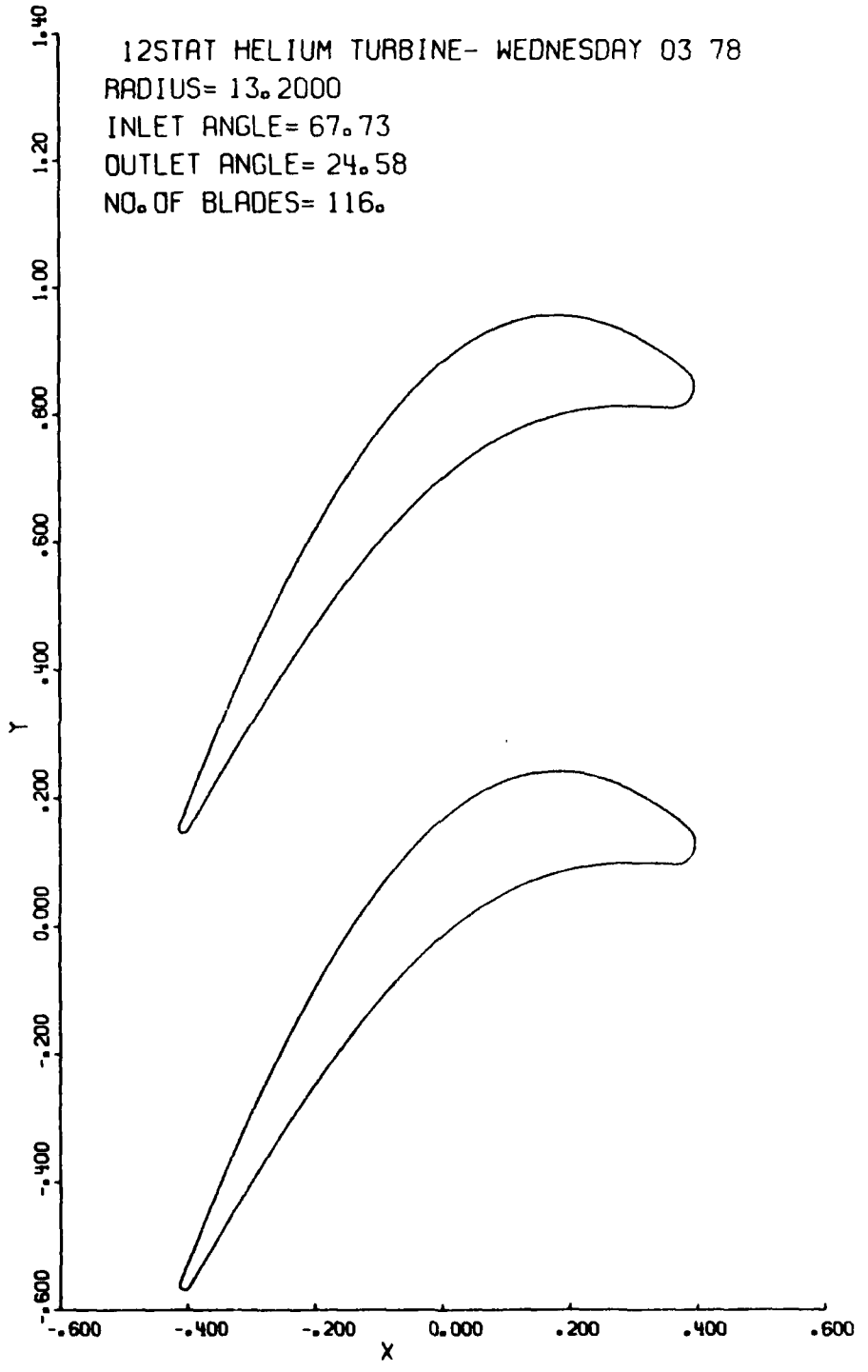
12STAT HELIUM TURBINE- WEDNESDAY 03 78
RADIUS= 13.2000
INLET ANGLE= 67.73
OUTLET ANGLE= 24.58
NO. OF BLADES= 116.
1.40
1.20
1.00
.800
.600
.400
.200
0.000
-.200
-.400
-.600
Y
-.600
-.400
-.200
0.000
.200
.400
.600
X

Figure C-8.

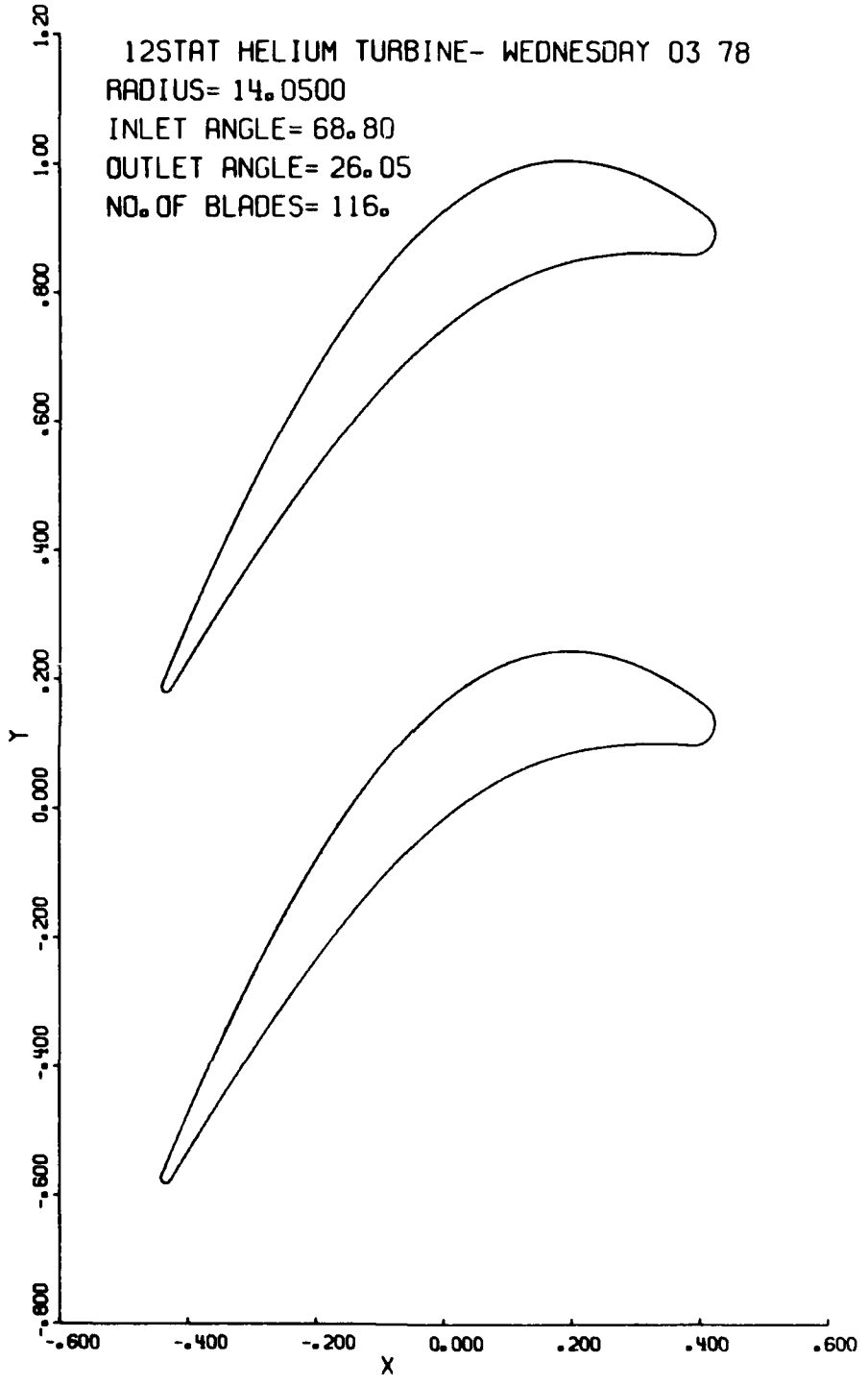
12STAT HELIUM TURBINE- WEDNESDAY 03 78
RADIUS= 14.0500
INLET ANGLE= 68.80
OUTLET ANGLE= 26.05
NO. OF BLADES= 116.
1.20
1.00
.800
.600
.400
.200
0.000
-.200
-.400
-.600
-.800
Y
-.600
-.400
-.200
0.000
.200
.400
.600
X

Figure C-9.

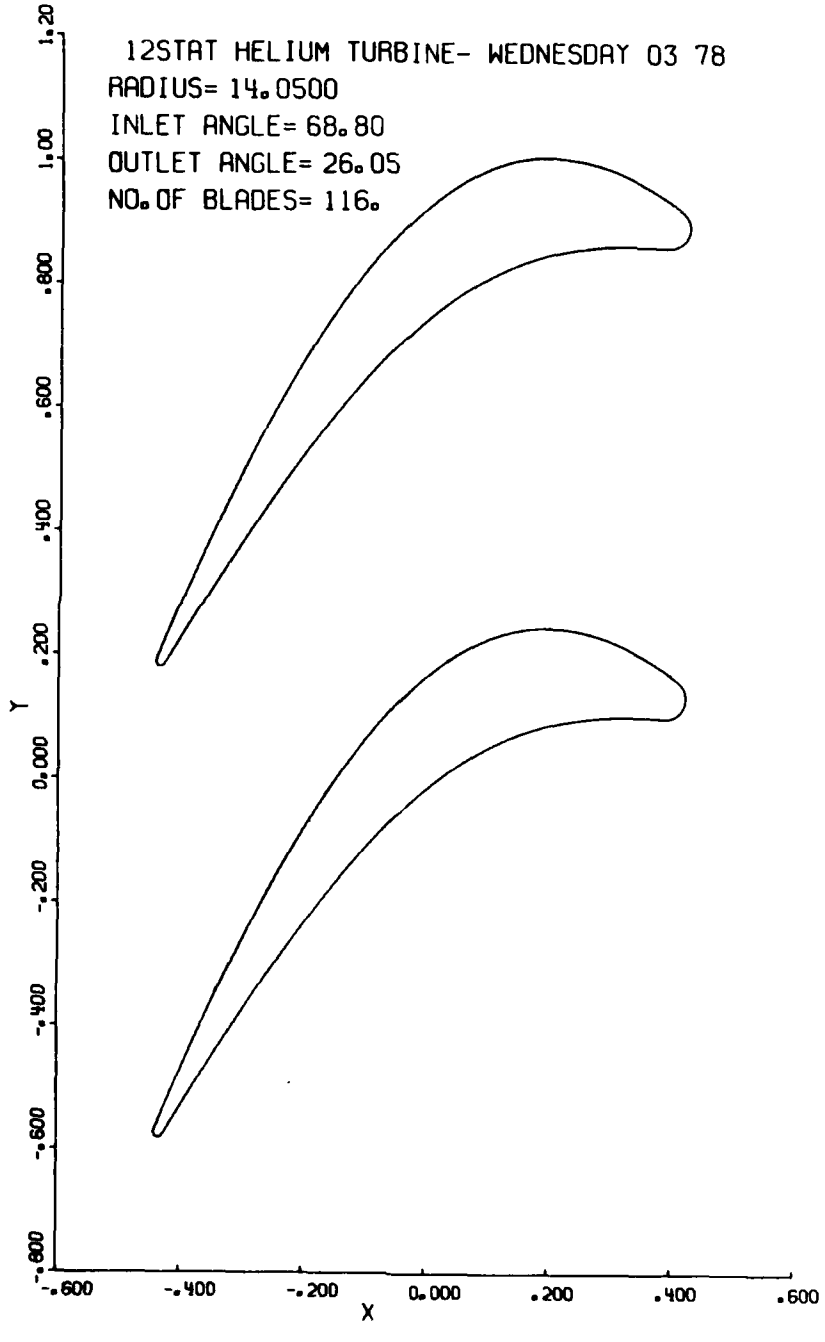
12STAT HELIUM TURBINE- WEDNESDAY 03 78
RADIUS= 14.0500
INLET ANGLE= 68.80
OUTLET ANGLE= 26.05
NO. OF BLADES= 116.
1.20
1.00
.800
.600
.400
.200
0.000
-.200
-.400
-.600
-.800
Y
-.600
-.400
-.200
0.000
.200
.400
.600
X

Figure C-9.

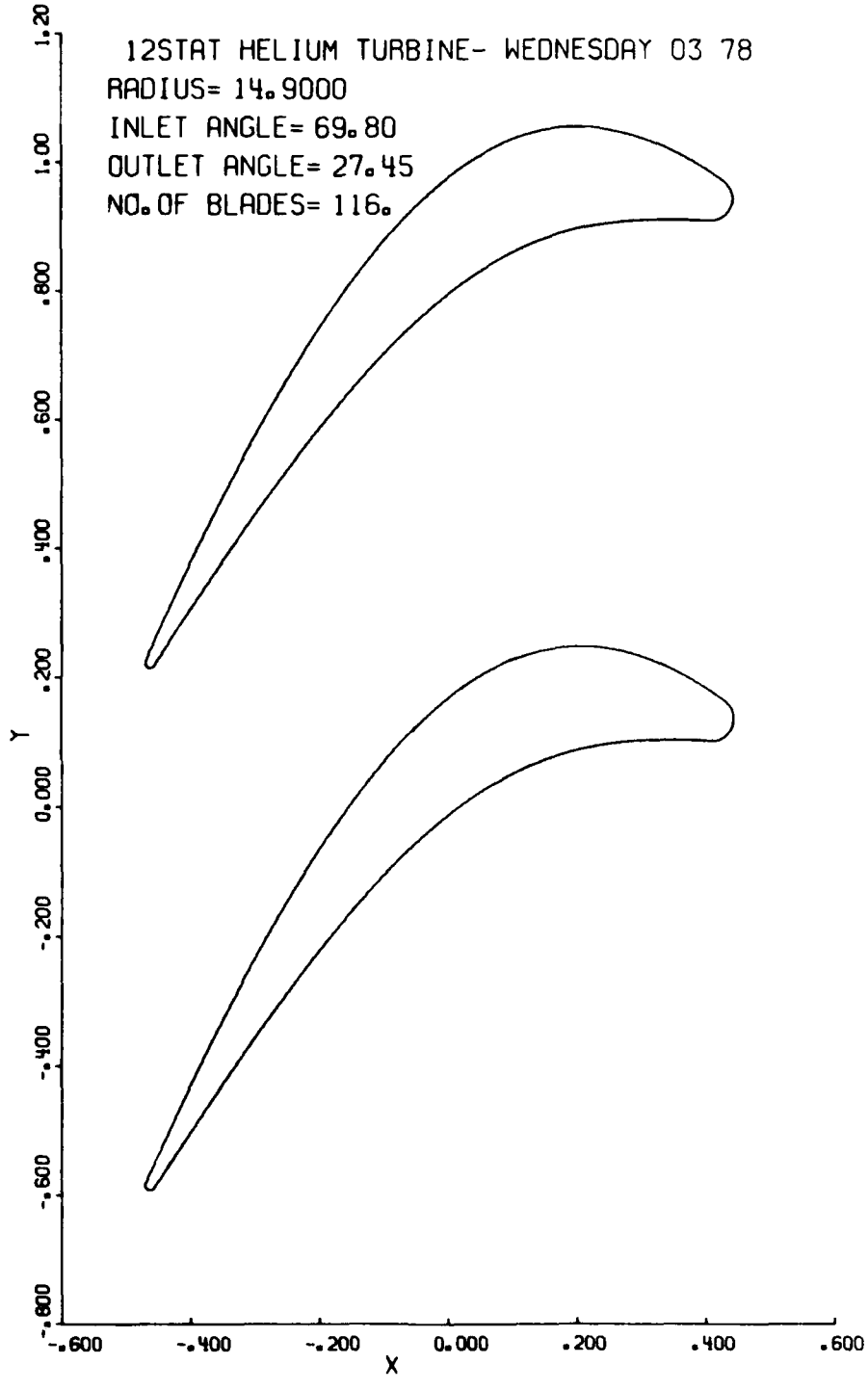
12STAT HELIUM TURBINE- WEDNESDAY 03 78
RADIUS= 14.9000
INLET ANGLE= 69.80
OUTLET ANGLE= 27.45
NO. OF BLADES= 116.
Y
X
1.20
1.00
.800
.600
.400
.200
0.000
-.200
-.400
-.600
-.800
-.600
-.400
-.200
0.000
.200
.400
.600

Figure C-10.

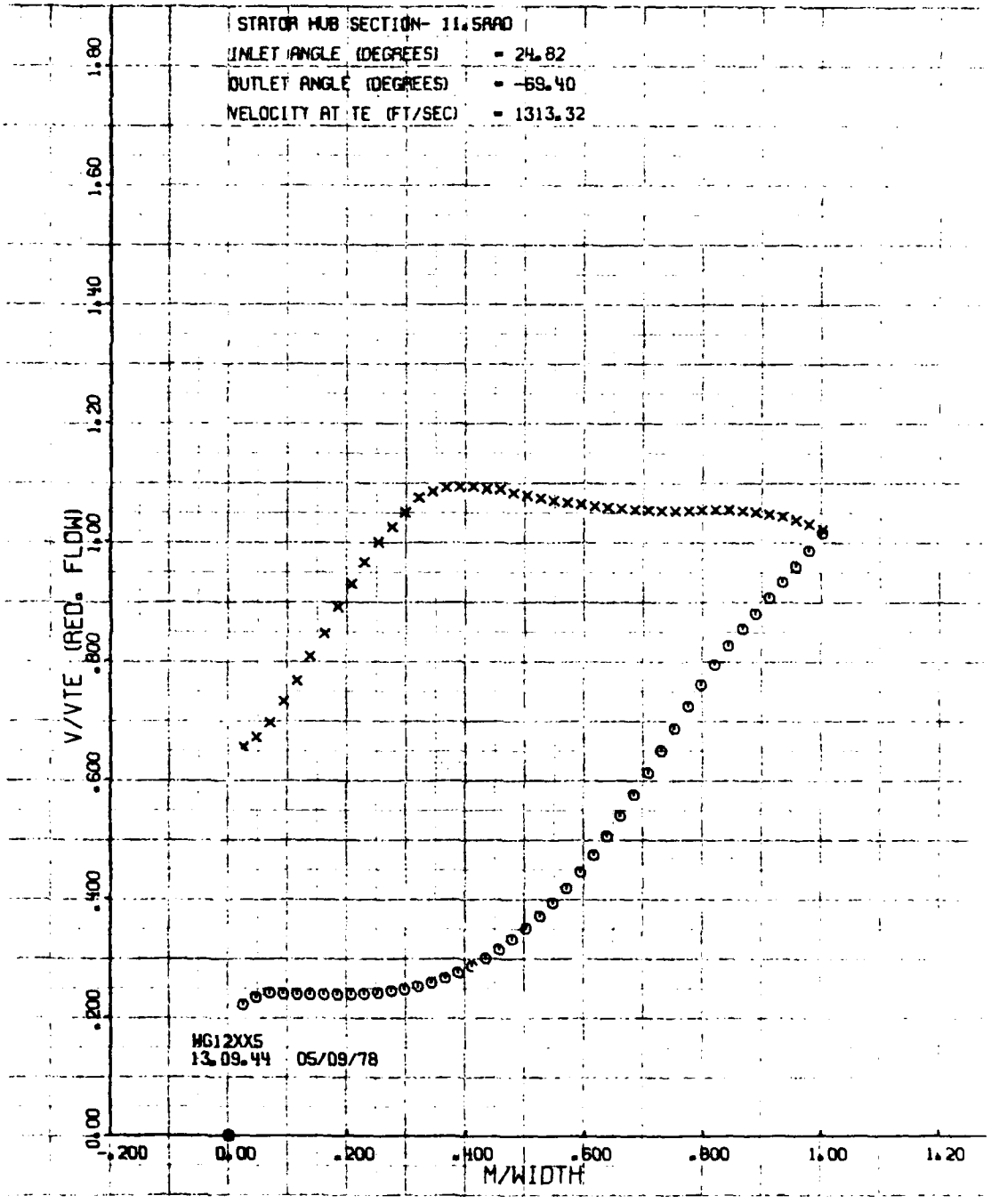
STATOR HUB SECTION- 11.5RAD
INLET ANGLE (DEGREES) = 24.82
OUTLET ANGLE (DEGREES) = -69.40
VELOCITY AT TE (FT/SEC) = 1313.32
V/VTE (REL. FLOW)
M/WIDTH
.000
.200
.400
.600
.800
1.00
1.20
1.40
1.60
1.80
-.200
0.00
.200
.400
.600
.800
1.00
1.20
WG12XX5
13.09.44 05/09/78

Figure C-11.

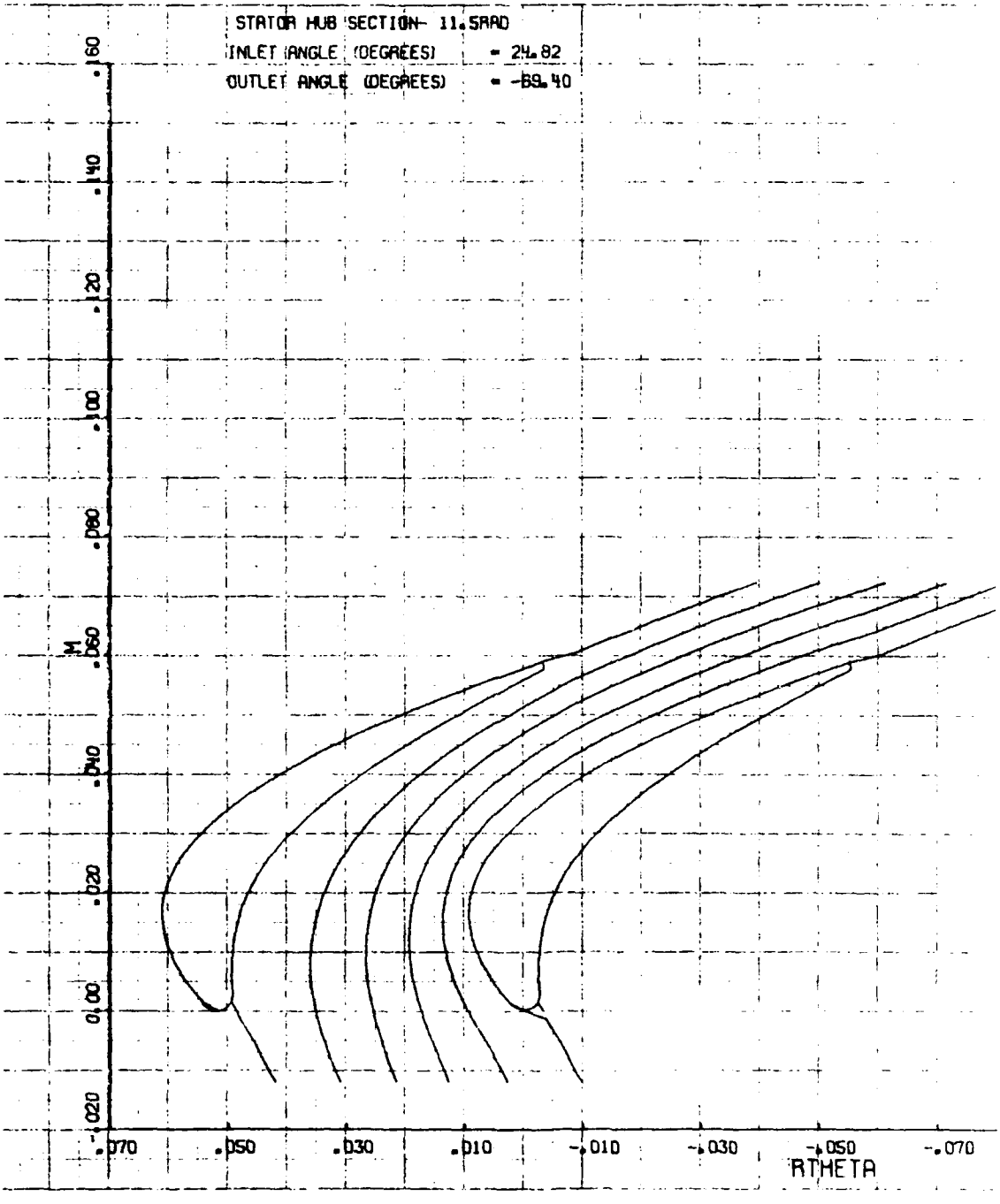
STATOR HUB SECTION- 11.5RAD
INLET ANGLE (DEGREES) = 24.82
OUTLET ANGLE (DEGREES) = -69.40
.160
.140
.120
.100
.080
.060
.040
.020
.000
-.020
M
.070
.050
.030
.010
-.010
-.030
-.050
-.070
RTHETA

Figure C-12.

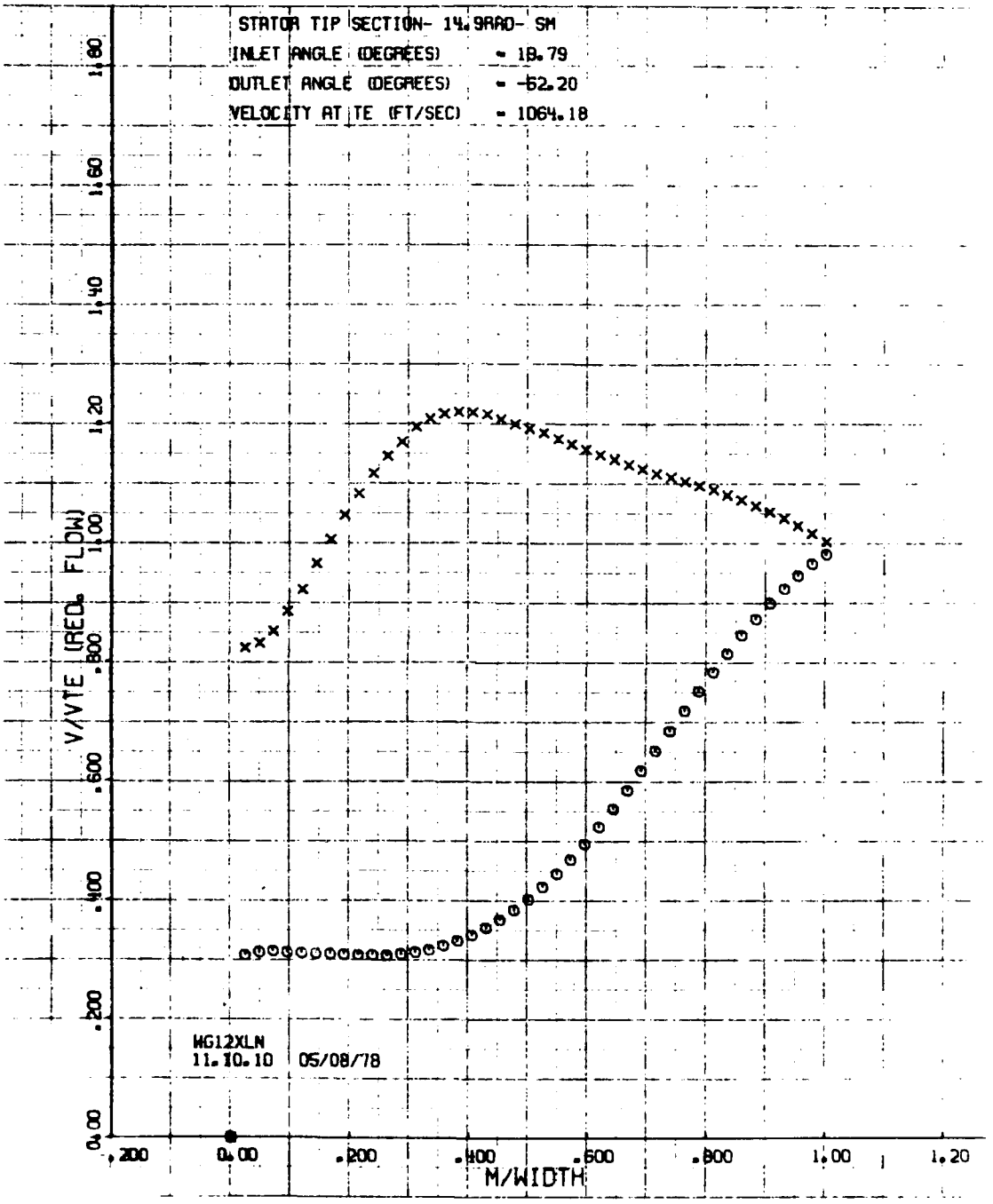
STATOR TIP SECTION- 14.9RAD- SM
INLET ANGLE (DEGREES) = 18.79
OUTLET ANGLE (DEGREES) = -62.20
VELOCITY AT TE (FT/SEC) = 1064.18
V/VTE (REL. FLOW)
M/WIDTH
WG12XLN
11.10.10 05/08/78

Figure C-13.

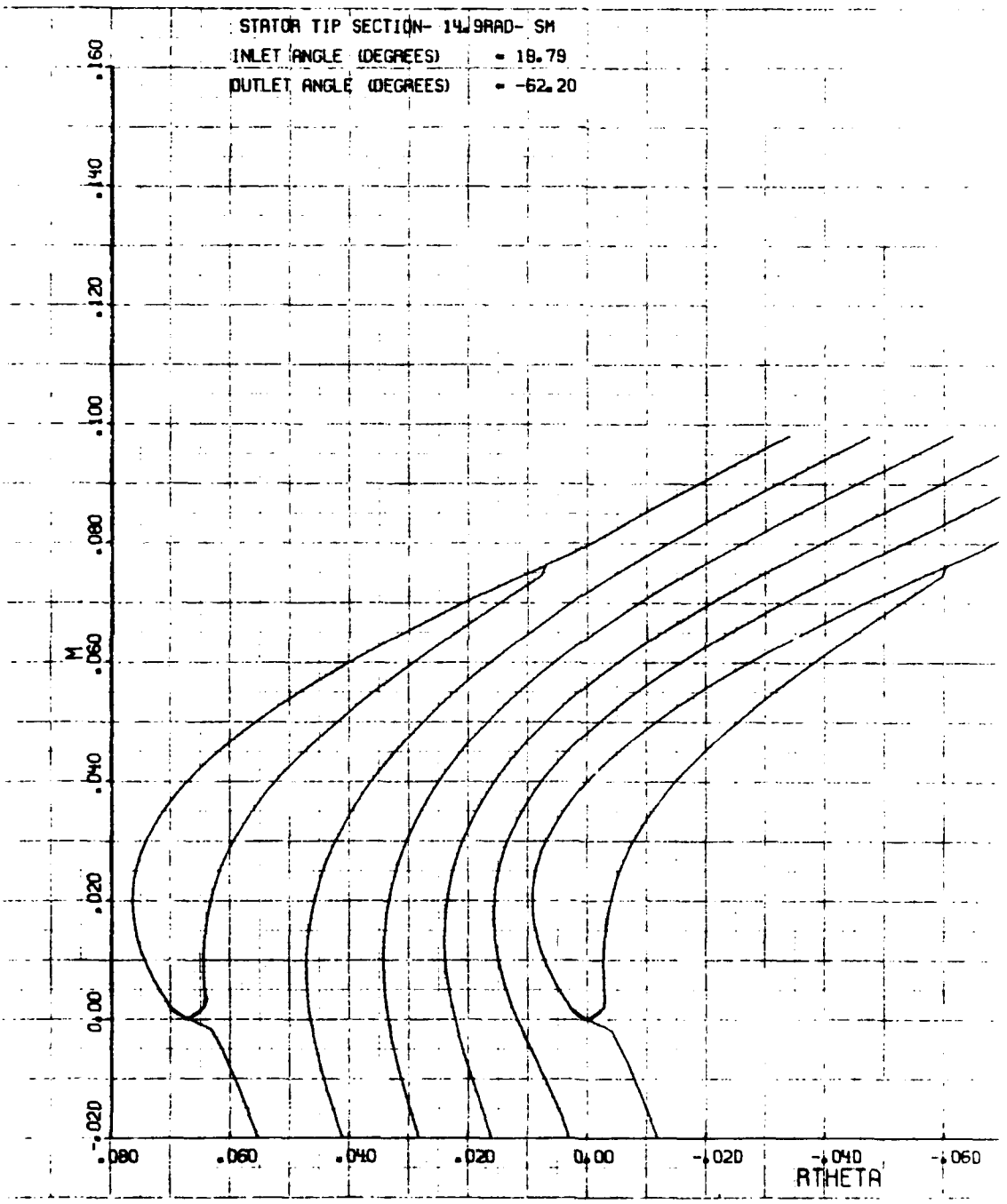
STATOR TIP SECTION- 14.9RAD- SM
INLET ANGLE (DEGREES) = 18.79
OUTLET ANGLE (DEGREES) = -62.20
M
.160
.140
.120
.100
.080
.060
.040
.020
0.00
-.020
.080
.060
.040
.020
0.00
-.020
-.040
-.060
RTHETA

Figure C-14.

TABLE C-3

BLADING DATA - 12 ROTOR BLADE

	HUB	MEAN	TIP
R - radius	11.50	13.20	14.90
β_1, β_2, - flow angles	49.99, -54.30	35.44, -56.98	16.80, -59.41
W - axial width	1.005	.9104	.8025
S - pitch	.5161	.5924	.6687
n - no. blades		140.	
ζ - zweifel coefficient	.903	.870	.860
β'_1 - blade inlet angle	47.8	41.7	19.6
arc cos o/s - blade angle	-56.24	-58.47	-60.70
O - throat	.2868	.3098	.3273
T - trailing edge thickness	.015	.015	.015
T/O - blockage	.052	.055	.046
UCT - uncovered turning	17.1	17.9	9.2
Bow	.42	.48	.35
A - cross-sectional area	.1532	.1264	.0860

NOTE - All blading dimensions in inches and deg.

DATE= 05/01/7
MONDAY MAY 01 78

12Rotor Blade

X	Y	PCT.OPENING	PCT.WIDTH FROM T.E.	THROAT	SURFACE LENGTH	RADIUS = 11.500 HOLE X	HOLE Y	HOLE D
-.5369	-.3221	.9587	0.0000		1.3386	0.0000	0.0000	0.0000
-.4295	-.1445	.8226	.1068		1.1291	0.0000	0.0000	0.0000
-.3221	-.0168	.7333	.2136		.9620	0.0000	0.0000	0.0000
-.2148	.0744	.6735	.3204		.8209	0.0000	0.0000	0.0000
-.1074	.1348	.6361	.4272		.6975	0.0000	0.0000	0.0000
.0000	.1664	.6185	.5340		.5852	0.0000	0.0000	0.0000
.0937	.1709	.6186	.6272		.4912	0.0000	0.0000	0.0000
.1874	.1519	.6342	.7204		.3954	0.0000	0.0000	0.0000
.2811	.1063	.6682	.8136		.2909	0.0000	0.0000	0.0000
.3748	.0272	.7263	.9068		.1681	0.0000	0.0000	0.0000
.4685	-.1000	.8240	1.0000		0.0000	0.0000	0.0000	0.0000
-.5369	-.3434			0.0000	1.1503	0.0000	0.0000	0.0000
-.4295	-.2361			.2930	.9999	0.0000	0.0000	0.0000
-.3221	-.1545			.2998	.8649	0.0000	0.0000	0.0000
-.2148	-.0941			.3064	.7416	0.0000	0.0000	0.0000
-.1074	-.0531			.3123	.6265	0.0000	0.0000	0.0000
.0000	-.0305			.3169	.5166	0.0000	0.0000	0.0000
.0937	-.0260			.3189	.4227	0.0000	0.0000	0.0000
.1874	-.0368			.3182	.3283	0.0000	0.0000	0.0000
.2811	-.0650			.3135	.2303	0.0000	0.0000	0.0000
.3748	-.1140			.3040	.1244	0.0000	0.0000	0.0000
.4685	-.1908			0.0000	0.0000	0.0000	0.0000	0.0000

CIRCLE PARAMETERS		R L	X L	Y L	R R	X R	Y R
BETA L	35.2577	.0075	-.5294	-.3240	.0365	.4320	-.1104
BETA R	42.1440	X GAGING	-.3247	Y GAGING	-.0193		
GAGING	.286799	PITCH	.516118	O/P	.555684	SIN-1 O/P	33.7578

MECHANICAL PROPERTIES				TAN.ANG	-11.426556	STAGGER	10.834023
AREA	.153265	M X	-.000017	M Y	-.000002	I X	.009516
I Y	.001366	I XY	.001468	I MIN	.001110	I MAX	.009772
P Y	877.519466	P X	125.989826	P XY	135.419759	ALPHA	9.909183
BAR I X	.009515	BAR I Y	.001366	BAR I XY	.001468	MAX THICK	.197678
C MIN LE	-.219661	C MAX LE	.406680	C MIN TE	-.235547	C MAX TE	-.577161
Z MIN LE	-.005052	Z MAX LE	.024029	Z MIN TE	-.004711	Z MAX TE	-.016931
C MIN B	.159575	C MAX B	.084207	Z MIN B	.006954	Z MAX B	.116047
BAR B	-.000461	BAR C	-.000803	BAR D	.001548	CHORD	1.028672
BAR X	-.000110	BAR Y	-.000010	K	.001318	WIDTH	1.005442

DATE= 05/01/7
MONDAY MAY 01 78

12 Rotor Blade

X	Y	PCT.OPENING	PCT.WIDTH FROM T.E.	THROAT	SURFACE LENGTH	RADIUS = 12.350 HOLE X	HOLE Y	HOLE D
-.5095	-.3392	.9546	0.0000		1.3004	0.0000	0.0000	0.0000
-.4076	-.1551	.8268	.1062		1.0880	0.0000	0.0000	0.0000
-.3057	-.0252	.7527	.2123		.9226	0.0000	0.0000	0.0000
-.2038	.0672	.7067	.3185		.7849	0.0000	0.0000	0.0000
-.1019	.1290	.6787	.4247		.6655	0.0000	0.0000	0.0000
.0000	.1632	.6643	.5308		.5577	0.0000	0.0000	0.0000
.0901	.1710	.6620	.6247		.4671	0.0000	0.0000	0.0000
.1801	.1561	.6713	.7185		.3756	0.0000	0.0000	0.0000
.2702	.1154	.6967	.8123		.2765	0.0000	0.0000	0.0000
.3603	.0422	.7475	.9062		.1602	0.0000	0.0000	0.0000
.4503	-.0775	.8448	1.0000		0.0000	0.0000	0.0000	0.0000
-.5095	-.3644			0.0000	1.1191	0.0000	0.0000	0.0000
-.4076	-.2511			.3111	.9695	0.0000	0.0000	0.0000
-.3057	-.1623			.3275	.8342	0.0000	0.0000	0.0000
-.2038	-.0954			.3433	.7122	0.0000	0.0000	0.0000
-.1019	-.0491			.3560	.6001	0.0000	0.0000	0.0000
.0000	-.0228			.3643	.4947	0.0000	0.0000	0.0000
.0901	-.0163			.3669	.4043	0.0000	0.0000	0.0000
.1801	-.0260			.3645	.3136	0.0000	0.0000	0.0000
.2702	-.0527			.3569	.2196	0.0000	0.0000	0.0000
.3603	-.0977			.3451	.1188	0.0000	0.0000	0.0000
.4503	-.1635			0.0000	0.0000	0.0000	0.0000	0.0000

CIRCLE PARAMETERS		R L	X L	Y L	R R	X R	Y R
BETA L	32.8434	.0063	-.5012	-.3411	.0370	.4133	-.0883
BETA R	43.9383	X GAGING	-.2836	Y GAGING	-.0020		
GAGING	.297627	PITCH	.554266	O/P	.536974	SIN-1 O/P	32.4779

MECHANICAL PROPERTIES				TAN.ANG	-13.600440	STAGGER	13.724282
AREA	.142396	M X	-.000032	M Y	.000010	I X	.008286
I Y	.001389	I XY	.001675	I MIN	.001004	I MAX	.008672
P Y	952.170736	P X	159.582154	P XY	192.465758	ALPHA	12.952080
BAR I X	.008246	BAR I Y	.001389	BAR I XY	.001675	MAX THICK	.187475
C MIN LE	-.215814	C MAX LE	.383208	C MIN TE	-.228592	C MAX TE	-.564682
Z MIN LE	-.004650	Z MAX LE	.022629	Z MIN TE	-.004390	Z MAX TE	-.015357
C MIN B	.150336	C MAX B	.109659	Z MIN B	.006676	Z MAX B	.079079
BAR B	-.000454	BAR C	-.000746	BAR D	.001315	CHORD	.994135
BAR X	-.000222	BAR Y	.000070	K	.001105	WIDTH	.959824

Figure C-15.

DATE= 05/01/7
MONDAY MAY 01 78
12 Rotor Blade

X	Y	PCT.OPENING	PCT.WIDTH FROM T.E.	THROAT	SURFACE LENGTH	RADIUS = 13.200 HOLE X	HOLE Y	HOLE D
-.4815	-.3698	.9531	0.0000		1.2525	0.0000	0.0000	0.0000
-.3852	-.1840	.8435	.1058		1.0414	0.0000	0.0000	0.0000
-.2889	-.0502	.7825	.2116		.8765	0.0000	0.0000	0.0000
-.1926	.0473	.7452	.3174		.7390	0.0000	0.0000	0.0000
-.0963	.1150	.7220	.4232		.6211	0.0000	0.0000	0.0000
.0000	.1558	.7088	.5290		.5163	0.0000	0.0000	0.0000
.0858	.1700	.7052	.6232		.4291	0.0000	0.0000	0.0000
.1715	.1624	.7119	.7174		.3428	0.0000	0.0000	0.0000
.2573	.1303	.7338	.8116		.2510	0.0000	0.0000	0.0000
.3431	.0685	.7801	.9058		.1450	0.0000	0.0000	0.0000
.4288	-.0345	.8704	1.0000		0.0000	0.0000	0.0000	0.0000
-.4815	-.3975			0.0000	1.0867	0.0000	0.0000	0.0000
-.3852	-.2768			.3295	.9368	0.0000	0.0000	0.0000
-.2889	-.1791			.3546	.7995	0.0000	0.0000	0.0000
-.1926	-.1036			.3787	.6771	0.0000	0.0000	0.0000
-.0963	-.0497			.3986	.5666	0.0000	0.0000	0.0000
.0000	-.0167			.4121	.4646	0.0000	0.0000	0.0000
.0858	-.0046			.4177	.3779	0.0000	0.0000	0.0000
.1715	-.0083			.4174	.2919	0.0000	0.0000	0.0000
.2573	-.0274			.4116	.2039	0.0000	0.0000	0.0000
.3431	-.0618			.4022	.1114	0.0000	0.0000	0.0000
.4288	-.1112			0.0000	0.0000	0.0000	0.0000	0.0000

CIRCLE PARAMETERS		R L	X L	Y L	R R	X R	Y R
BETA L	30.6651	.0085	-.4730	-.3716	.0367	.3922	-.0481
BETA R	48.2870	X GAGING	-.2449	Y GAGING	-.0010		
GAGING	.309703	PITCH	.592414	O/P	.522782	BIN=1 O/P	31.5190

MECHANICAL PROPERTIES							
AREA	.126421	M X	-.000013	TAN.ANG	-13.557453	STAGGER	18.876868
I Y	.001454	I XY	.001974	M Y	-.000003	I X	.006691
F Y	1147.416991	F X	249.260692	I MIN	.000793	I MAX	.007352
BAR I X	.006691	BAR I Y	.001454	F XY	338.421165	ALPHA	18.500669
C MIN LE	-.204789	C MAX LE	.357385	BAR I XY	.001974	MAX THICK	.174466
Z MIN LE	-.003873	Z MAX LE	.020571	C MIN TE	-.210855	C MAX TE	-.566386
C MIN B	.133512	C MAX B	.137119	Z MIN TE	-.003762	Z MAX TE	-.012980
BAR B	-.000455	BAR C	-.000680	Z MIN B	.005941	Z MAX B	.053616
BAR X	-.000102	BAR Y	-.000026	BAR D	.001074	CHORD	.969587
				K	.000815	WIDTH	.910365

DATE= 05/01/7
MONDAY MAY 01 78
12 Rotor Blade

X	Y	PCT.OPENING	PCT.WIDTH FROM T.E.	THROAT	SURFACE LENGTH	RADIUS = 14.050 HOLE X	HOLE Y	HOLE D
-.4531	-.4115	.9534	0.0000		1.2026	0.0000	0.0000	0.0000
-.3625	-.2282	.8683	.1057		.9964	0.0000	0.0000	0.0000
-.2719	-.0889	.8187	.2113		.8301	0.0000	0.0000	0.0000
-.1812	.0170	.7866	.3170		.6905	0.0000	0.0000	0.0000
-.0906	.0941	.7649	.4226		.5713	0.0000	0.0000	0.0000
.0000	.1448	.7514	.5283		.4673	0.0000	0.0000	0.0000
.0809	.1681	.7474	.6226		.3829	0.0000	0.0000	0.0000
.1618	.1704	.7541	.7170		.3017	0.0000	0.0000	0.0000
.2428	.1501	.7758	.8113		.2181	0.0000	0.0000	0.0000
.3237	.1041	.8197	.9057		.1248	0.0000	0.0000	0.0000
.4046	.0258	.8988	1.0000		0.0000	0.0000	0.0000	0.0000
-.4531	-.4409			0.0000	1.0603	0.0000	0.0000	0.0000
-.3625	-.3112			.3450	.9087	0.0000	0.0000	0.0000
-.2719	-.2033			.3778	.7677	0.0000	0.0000	0.0000
-.1812	-.1176			.4100	.6429	0.0000	0.0000	0.0000
-.0906	-.0541			.4375	.5321	0.0000	0.0000	0.0000
.0000	-.0120			.4577	.4320	0.0000	0.0000	0.0000
.0809	.0088			.4690	.3483	0.0000	0.0000	0.0000
.1618	.0153			.4745	.2671	0.0000	0.0000	0.0000
.2428	.0087			.4755	.1858	0.0000	0.0000	0.0000
.3237	-.0095			.4738	.1028	0.0000	0.0000	0.0000
.4046	-.0380			0.0000	0.0000	0.0000	0.0000	0.0000

CIRCLE PARAMETERS		R L	X L	Y L	R R	X R	Y R
BETA L	28.6876	.0082	-.4449	-.4132	.0350	.3696	.0127
BETA R	56.3622	X GAGING	-.2039	Y GAGING	-.0064		
GAGING	.320581	PITCH	.630562	O/P	.508406	BIN=1 O/P	30.5577

MECHANICAL PROPERTIES							
AREA	.107101	M X	.000002	TAN.ANG	-10.985238	STAGGER	25.935113
I Y	.001602	I XY	.002180	M Y	-.000018	I X	.005011
F Y	1530.951040	F X	489.412891	I MIN	.000539	I MAX	.006074
BAR I X	.005011	BAR I Y	.001602	F XY	666.127643	ALPHA	25.991102
C MIN LE	-.185435	C MAX LE	.337804	BAR I XY	.002180	MAX THICK	.157935
Z MIN LE	-.002906	Z MAX LE	.017979	C MIN TE	-.184537	C MAX TE	-.580909
C MIN B	.109092	C MAX B	.166147	Z MIN TE	-.002920	Z MAX TE	-.010455
BAR B	-.000444	BAR C	-.000628	Z MIN B	.004940	Z MAX B	.036555
BAR X	.000017	BAR Y	-.000165	BAR D	.000878	CHORD	.962328
				K	.000517	WIDTH	.857704

Figure C-16.

DATE= 05/01/7
MONDAY MAY 01 78

12 Rotor Blade

X	Y	PCT.OPENING	PCT.WIDTH FROM T.E.	THROAT	SURFACE LENGTH	RADIUS = 14.900 HOLE X	HOLE Y	HOLE D
-.4243	-.4621	.9548	0.0000		1.1605	0.0000	0.0000	0.0000
-.3394	-.2846	.8980	.1057		.9622	0.0000	0.0000	0.0000
-.2546	-.1387	.8584	.2115		.7934	0.0000	0.0000	0.0000
-.1697	-.0218	.8289	.3172		.6488	0.0000	0.0000	0.0000
-.0849	.0678	.8065	.4230		.5253	0.0000	0.0000	0.0000
.0000	.1309	.7919	.5287		.4194	0.0000	0.0000	0.0000
.0756	.1654	.7880	.6230		.3361	0.0000	0.0000	0.0000
.1513	.1797	.7963	.7172		.2589	0.0000	0.0000	0.0000
.2269	.1738	.8201	.8115		.1828	0.0000	0.0000	0.0000
.3025	.1473	.8632	.9057		.1024	0.0000	0.0000	0.0000
.3782	.0998	.9283	1.0000		0.0000	0.0000	0.0000	0.0000
-.4243	-.4923			0.0000	1.0492	0.0000	0.0000	0.0000
-.3394	-.3528			.3549	.8946	0.0000	0.0000	0.0000
-.2546	-.2334			.3940	.7480	0.0000	0.0000	0.0000
-.1697	-.1362			.4341	.6189	0.0000	0.0000	0.0000
-.0849	-.0616			.4698	.5058	0.0000	0.0000	0.0000
.0000	-.0083			.4982	.4055	0.0000	0.0000	0.0000
.0756	.0237			.5174	.3233	0.0000	0.0000	0.0000
.1513	.0439			.5322	.2450	0.0000	0.0000	0.0000
.2269	.0535			.5442	.1687	0.0000	0.0000	0.0000
.3025	.0558			.5554	.0930	0.0000	0.0000	0.0000
.3782	.0518			0.0000	0.0000	0.0000	0.0000	0.0000

CIRCLE PARAMETERS		R L	X L	Y L	R R	X R	Y R
BETA L	26.9290	.0076	-.4167	-.4637	.0303	.3479	.0846
BETA R	70.4366	X GAGING	-.1609	Y GAGING	-.0112		
GAGING	.327286	PITCH	.668710	O/P	.489429	SIN=1 O/P	29.3030

MECHANICAL PROPERTIES							
AREA	.086018	M X	-.000004	TAN.ANG	=0.407579	STAGGER	34.262952
I Y	.001790	I XY	.002157	M Y	-.000001	I X	.003442
P Y	2282.918216	F X	1187.025553	I MIN	.000306	I MAX	.004925
BAR I X	.003442	BAR I Y	.001790	F XY	1430.579401	ALPHA	34.520973
C MIN LE	-.157799	C MAX LE	.334569	BAR I XY	.002157	MAX THICK	.136449
Z MIN LE	-.001940	Z MAX LE	.014721	C MIN TE	-.153563	C MAX TE	-.606061
C MIN B	.083377	C MAX H	.184823	Z MIN TE	-.001993	Z MAX TE	-.008126
BAR B	-.000403	BAR C	-.000587	Z MIN B	.003671	Z MAX B	.026647
BAR X	-.000047	BAR Y	-.000010	BAR D	.000735	CHORD	.978754
				K	.000272	WIDTH	.802484

Figure C-17.

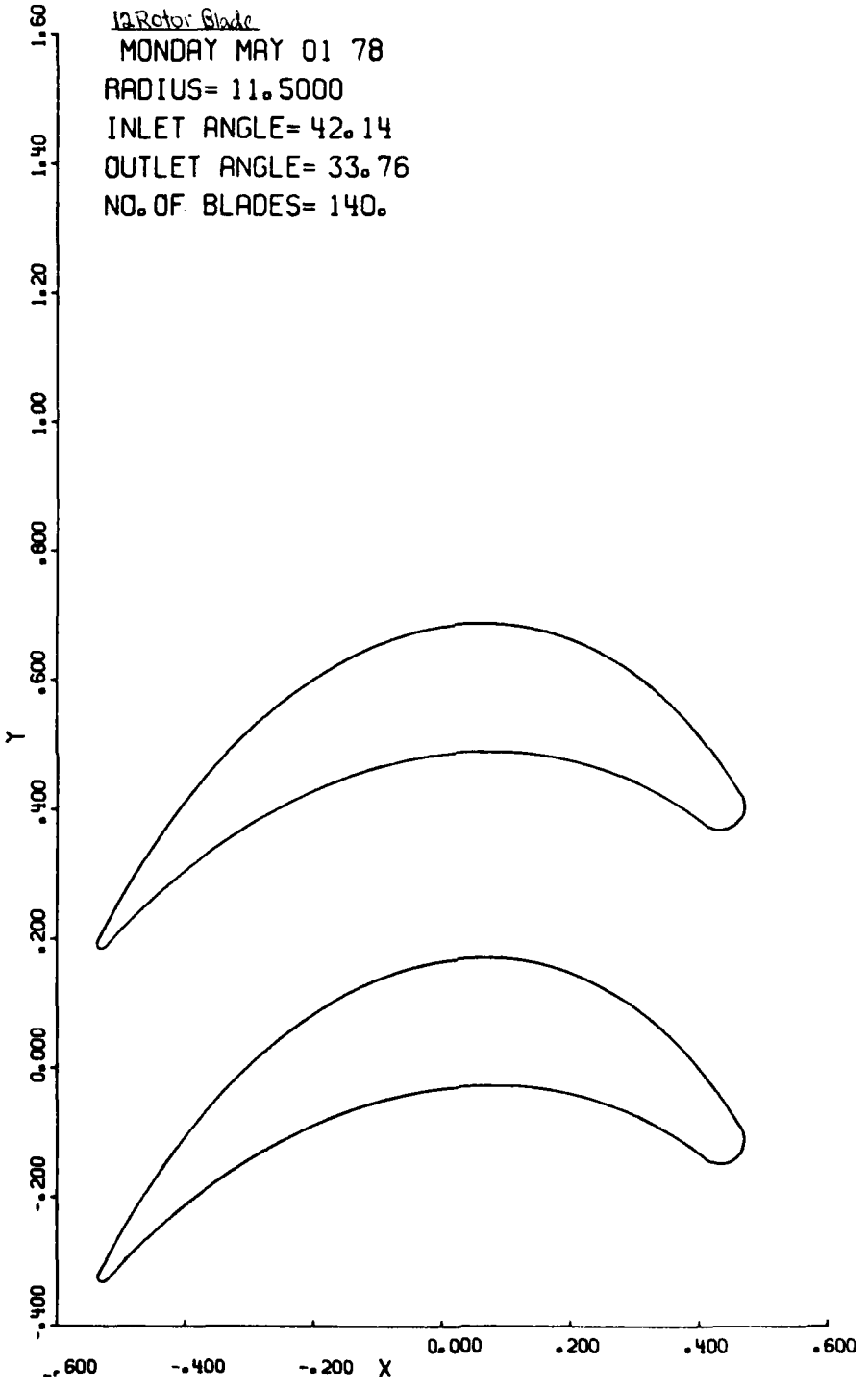
12 Rotor Blade
MONDAY MAY 01 78
RADIUS= 11.5000
INLET ANGLE= 42.14
OUTLET ANGLE= 33.76
NO. OF BLADES= 140.
1.60
1.40
1.20
1.00
.800
.600
.400
.200
0.000
-.200
-.400
Y
-.600
-.400
-.200
0.000
.200
.400
.600
X

Figure C-18.

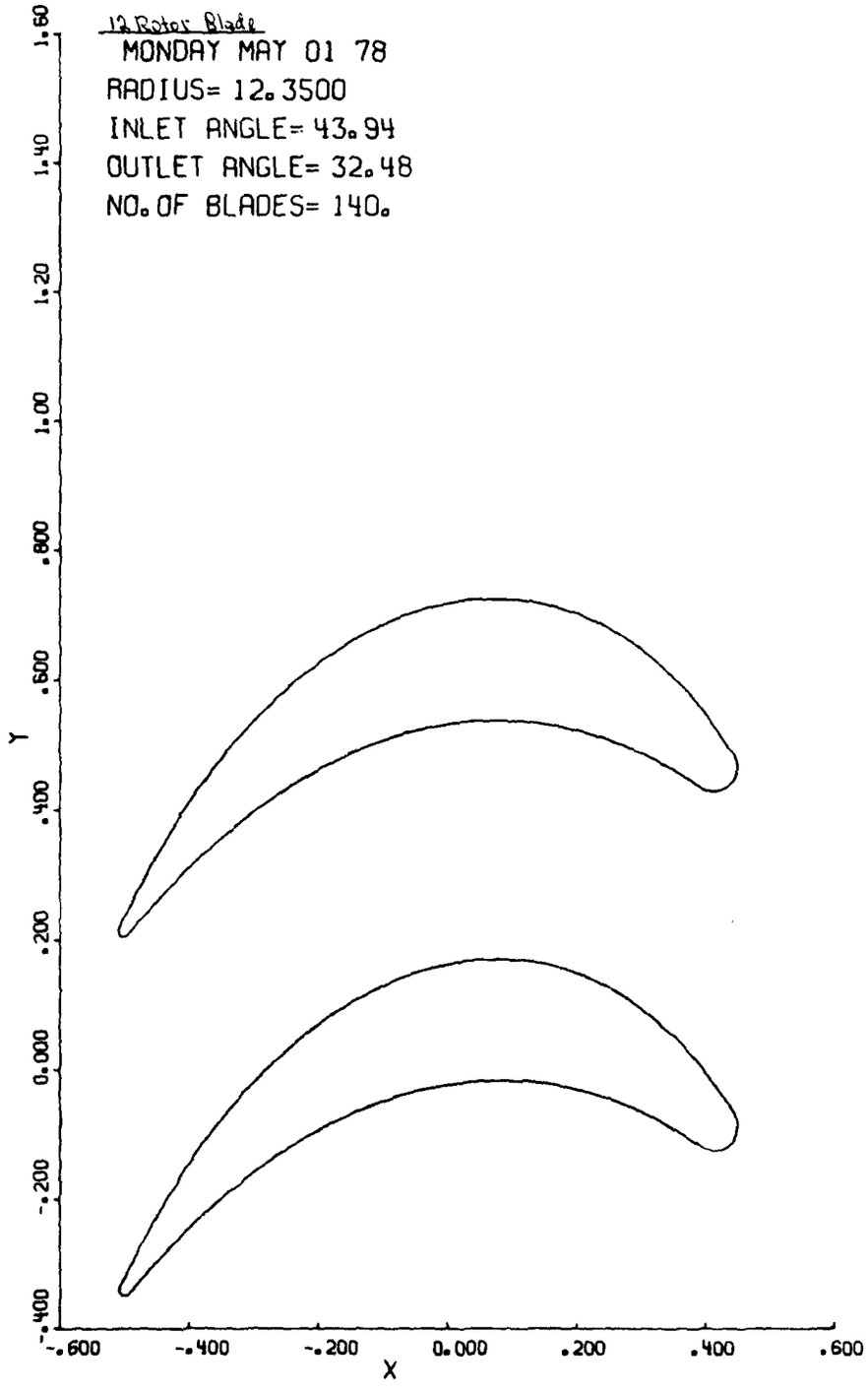
12 Rotor Blade
MONDAY MAY 01 78
RADIUS= 12.3500
INLET ANGLE= 43.94
OUTLET ANGLE= 32.48
NO. OF BLADES= 140.
1.60
1.40
1.20
1.00
.800
.600
.400
.200
0.000
-.200
-.400
Y
-.600
-.400
-.200
0.000
.200
.400
.600
X

Figure C-19.

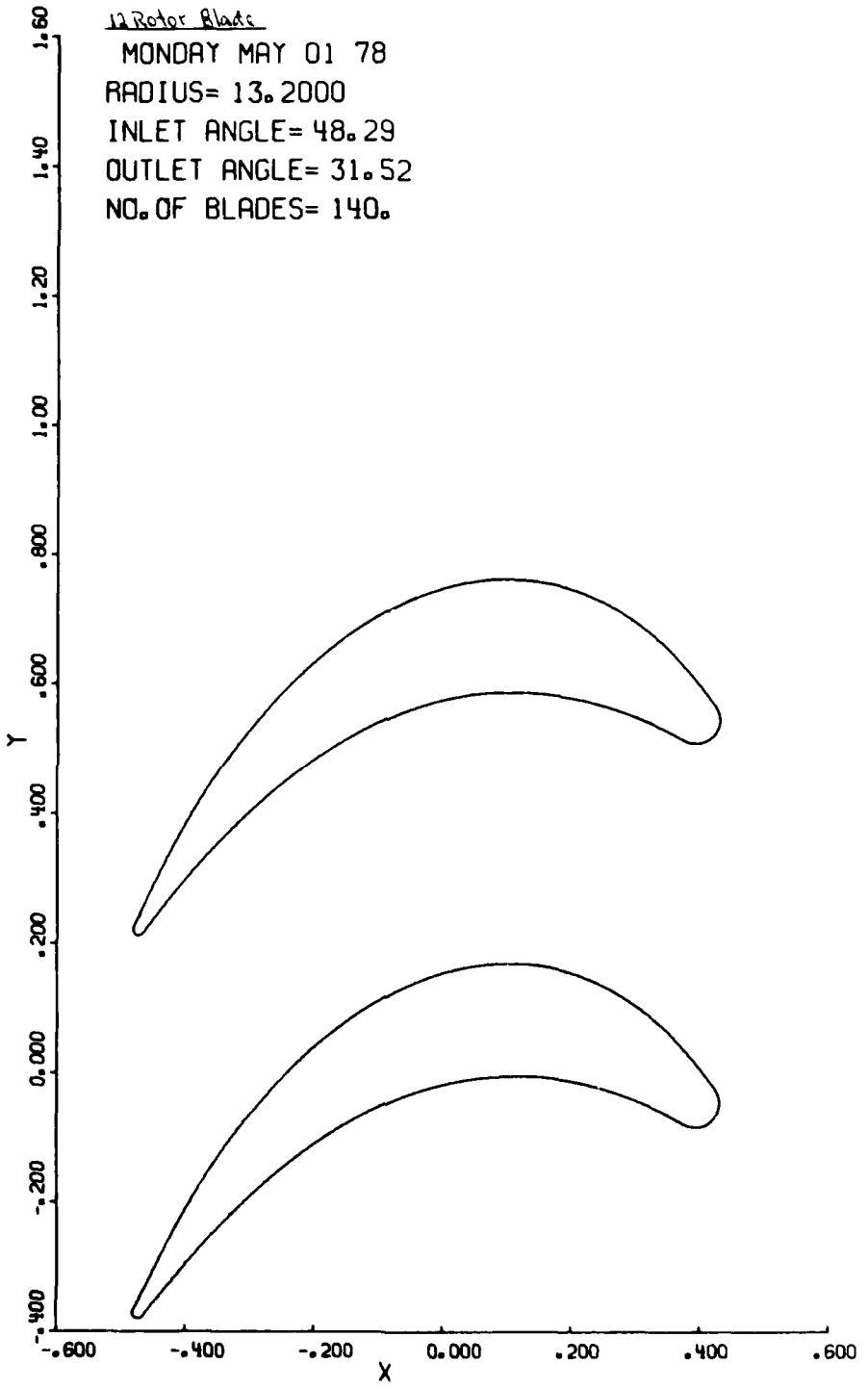
12 Rotor Blade
MONDAY MAY 01 78
RADIUS= 13.2000
INLET ANGLE= 48.29
OUTLET ANGLE= 31.52
NO. OF BLADES= 140.
1.60
1.40
1.20
1.00
.800
.600
.400
.200
0.000
-.200
-.400
Y
-.600
-.400
-.200
0.000
.200
.400
.600
X

Figure C-20.

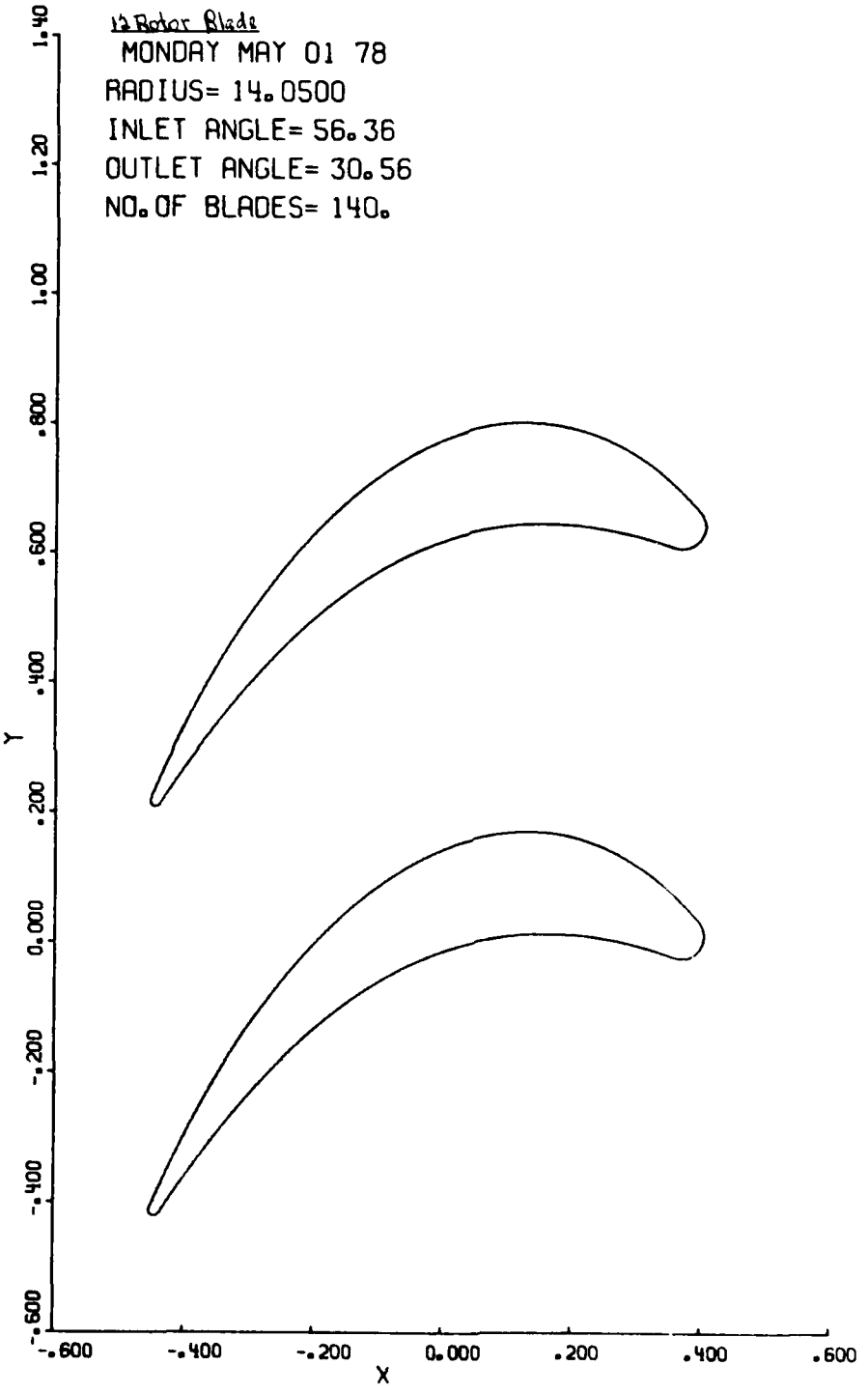
12 Rotor Blade
MONDAY MAY 01 78
RADIUS= 14.0500
INLET ANGLE= 56.36
OUTLET ANGLE= 30.56
NO. OF BLADES= 140.
1.40
1.20
1.00
.800
.600
.400
.200
0.000
-.200
-.400
-.600
Y
-.600
-.400
-.200
0.000
.200
.400
.600
X

Figure C-21.

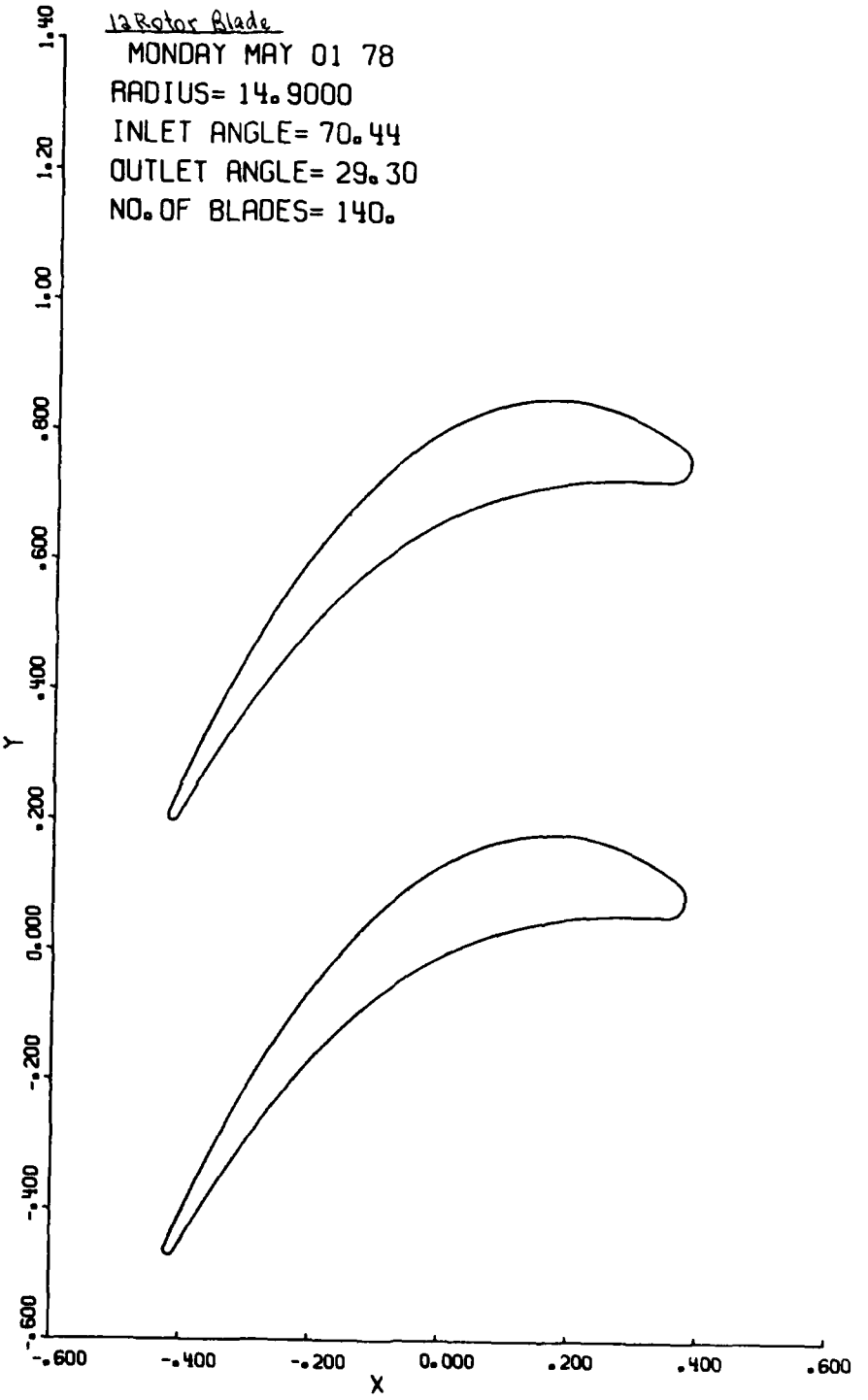
12 Rotor Blade
MONDAY MAY 01 78
RADIUS= 14.9000
INLET ANGLE= 70.44
OUTLET ANGLE= 29.30
NO. OF BLADES= 140.
1.40
1.20
1.00
.800
.600
.400
.200
0.000
-.200
-.400
-.600
Y
-.600
-.400
-.200
0.000
.200
.400
.600
X

Figure C-22.

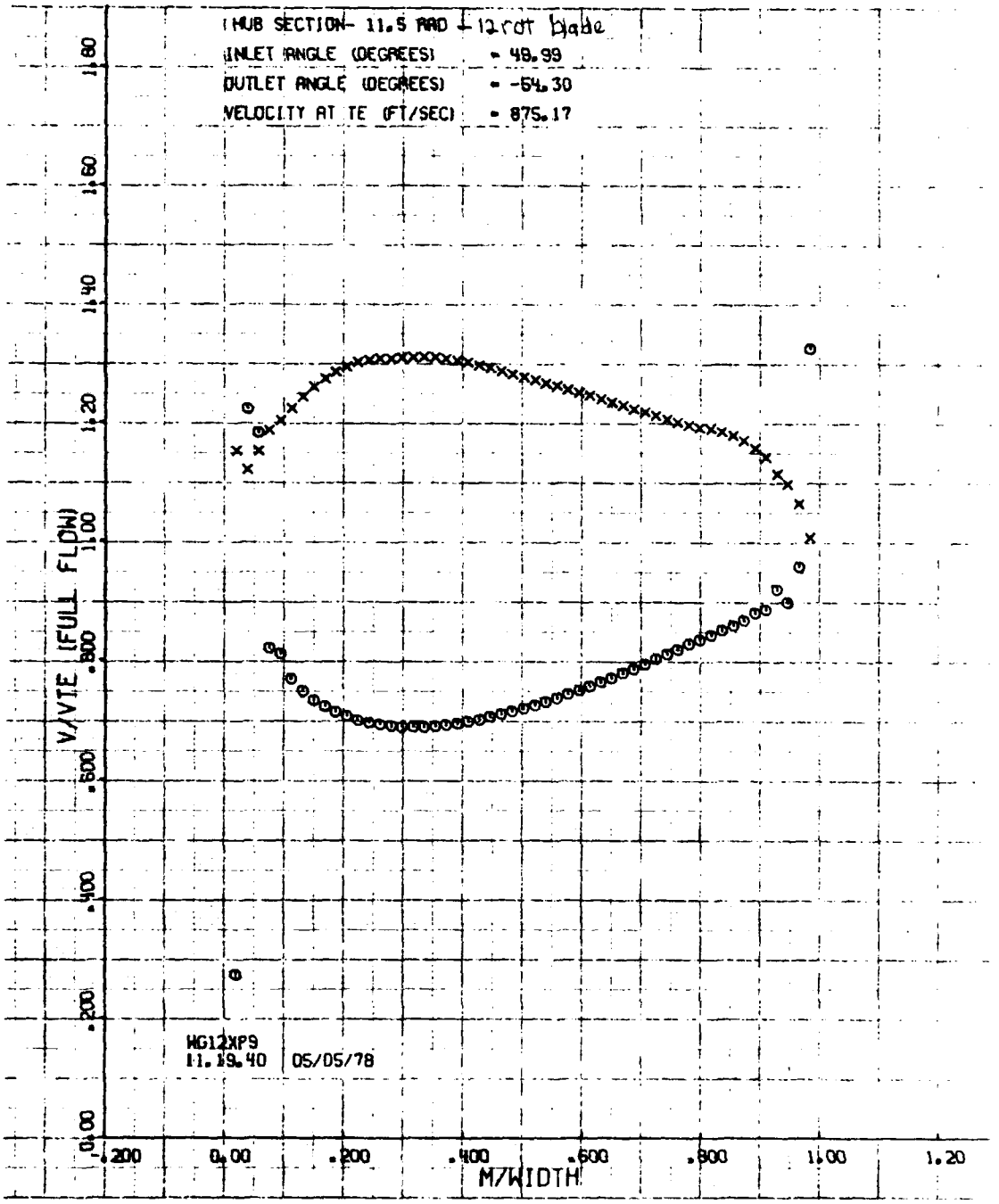
HUB SECTION- 11.5 RAD - 12rot blade
INLET ANGLE (DEGREES) = 48.99
OUTLET ANGLE (DEGREES) = -54.30
VELOCITY AT TE (FT/SEC) = 875.17
V/VTE (FULL FLOW)
M/WIDTH
WG12XP9
11.19.40 05/05/78

Figure C-23.

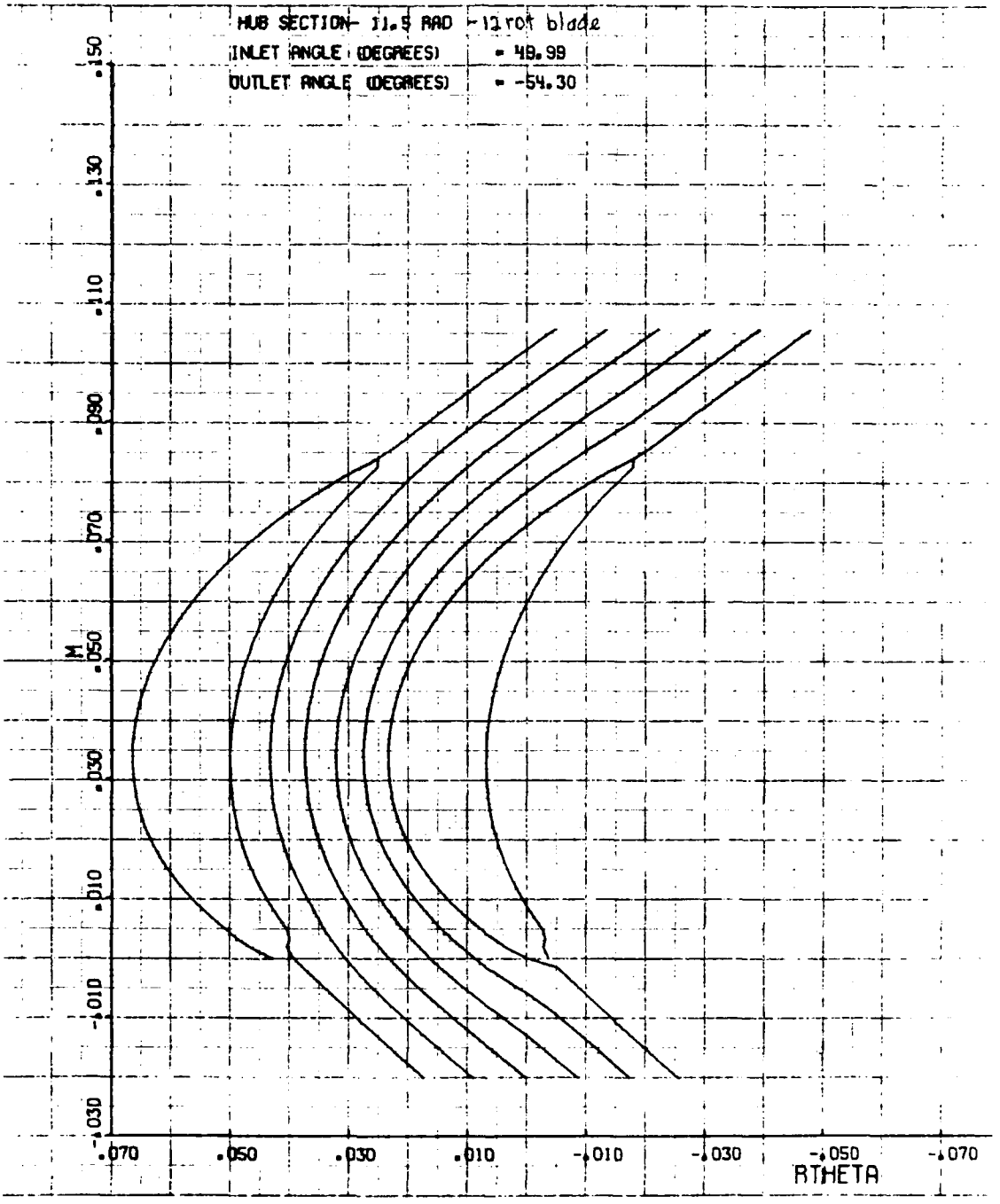
HUB SECTION- 11.5 RAD -12 rot blade
INLET ANGLE (DEGREES) = 49.99
OUTLET ANGLE (DEGREES) = -54.30
.150
.130
.110
.090
.070
.050
.030
.010
-.010
-.030
M
-.070
.050
.030
.010
-.010
-.030
-.050
-.070
RTHETA

Figure C-24.

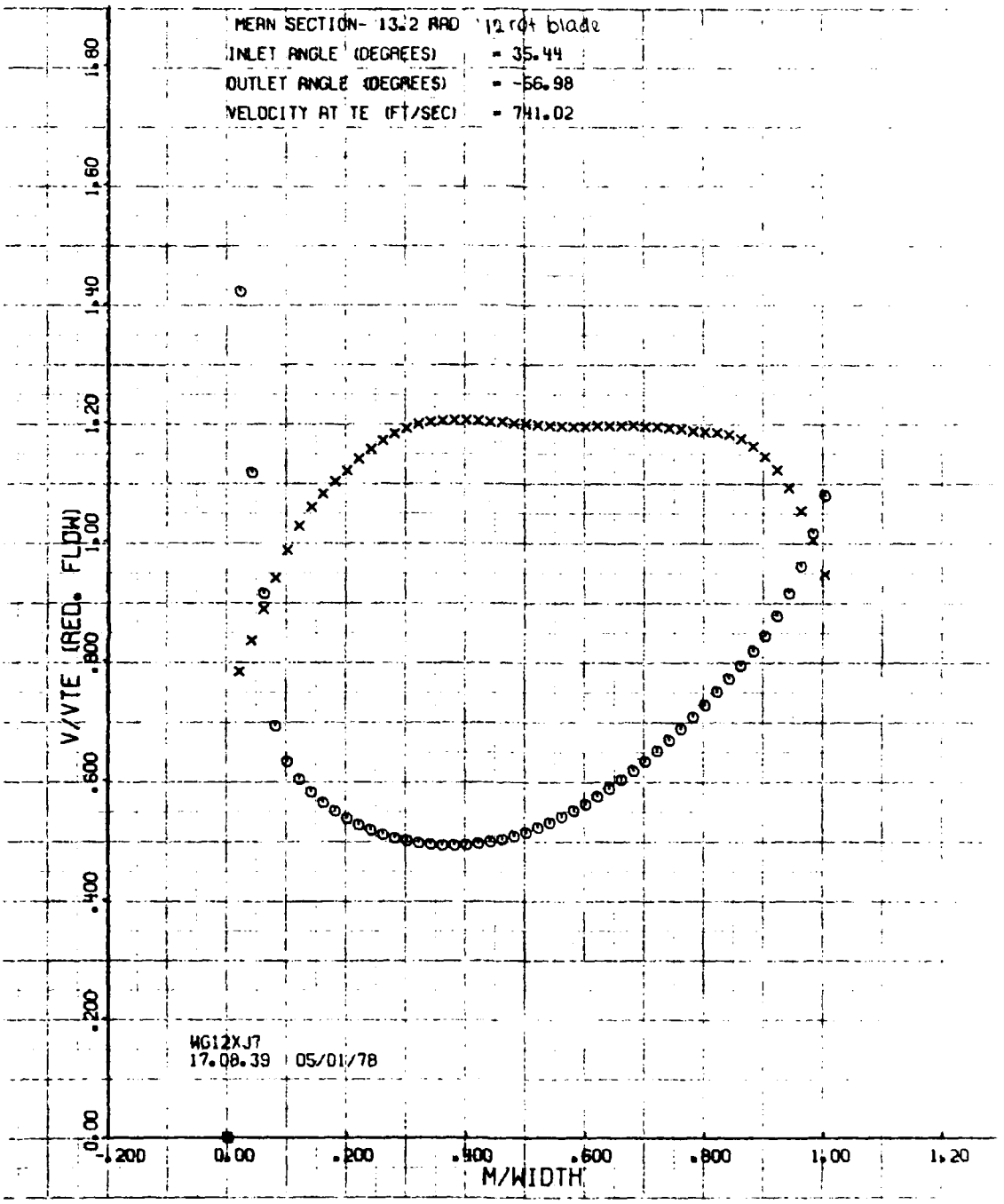
MEAN SECTION- 13.2 RAD 12 rpt blade
INLET ANGLE (DEGREES) = 35.44
OUTLET ANGLE (DEGREES) = -56.98
VELOCITY AT TE (FT/SEC) = 741.02
V/VTE (REL. FLOW)
M/WIDTH
MG12XJ7
17.08.39 05/01/78

Figure C-25.

AD-A081 380 WESTINGHOUSE ELECTRIC CORP PITTSBURGH PA ADVANCED ENE--ETC F/G 20/13
COMPACT CLOSED CYCLE BRAYTON SYSTEM FEASIBILITY STUDY, VOLUME I--ETC(U)
AUG 79 R E THOMPSON, R L AMMON, R CALVO N00014-76-C-0706
UNCLASSIFIED WAES-TNR-237-VOL-2 NL

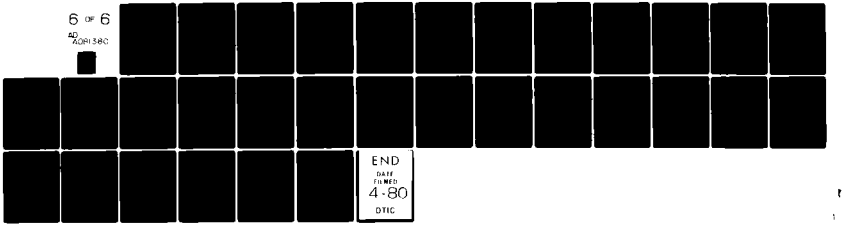

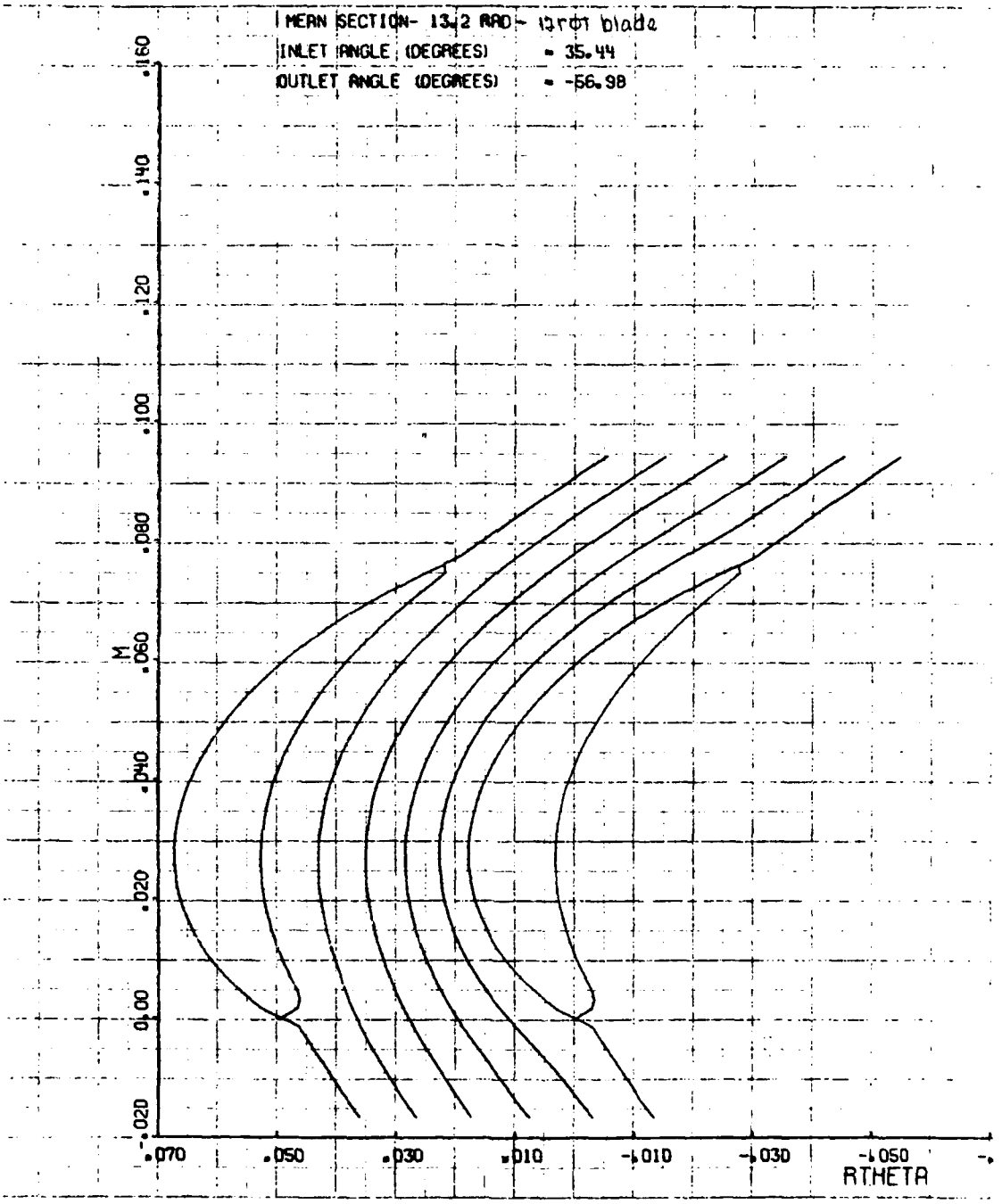
MEAN SECTION- 13.2 RAD - 12th blade
INLET ANGLE (DEGREES) = 35.44
OUTLET ANGLE (DEGREES) = -56.98
M
.160
.140
.120
.100
.080
.060
.040
.020
.000
-.020
.070
.050
.030
.010
-.010
-.030
-.050
RTHETA

Figure C-26.

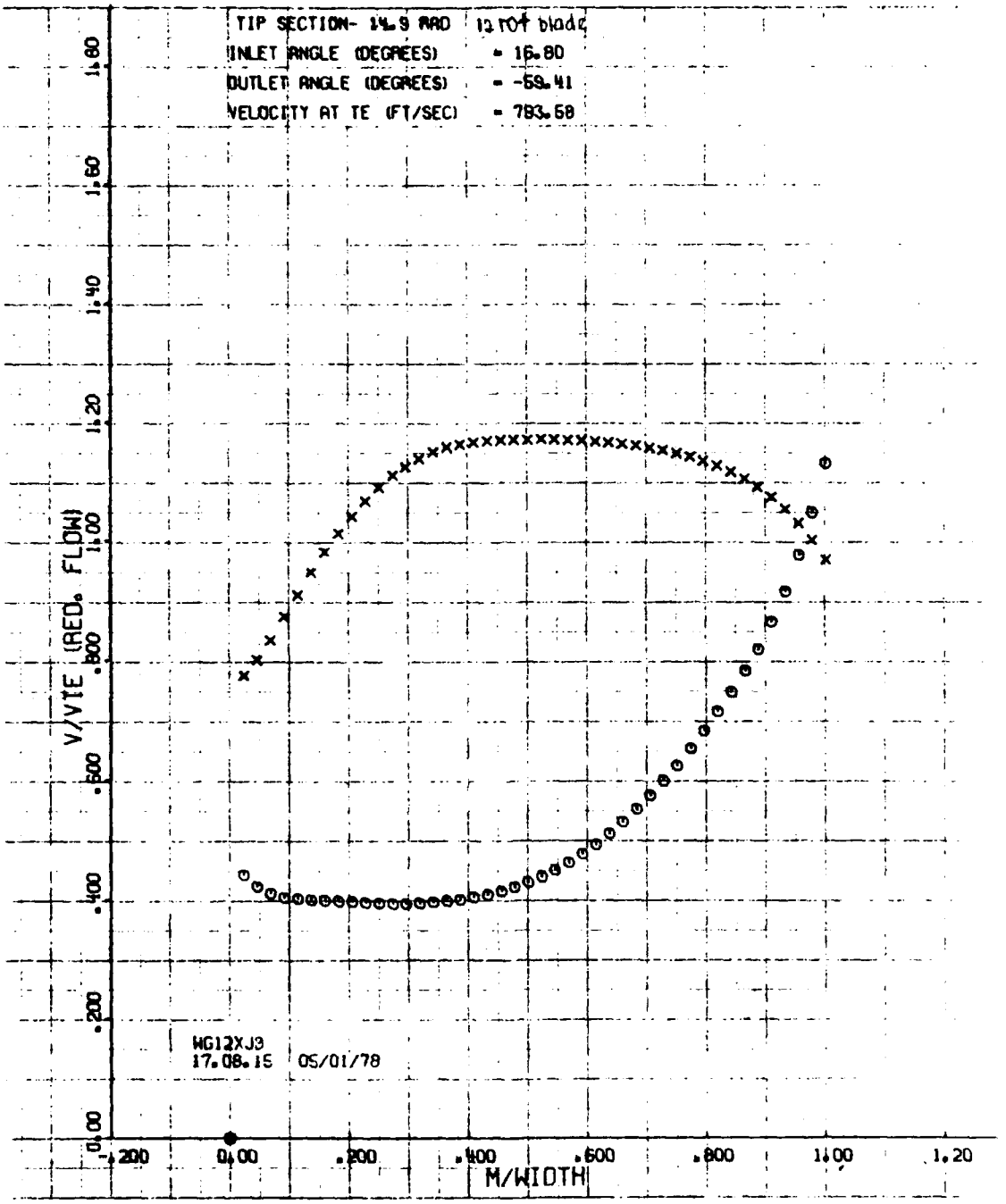
TIP SECTION- 14.9 RAD 12 FOT blade
INLET ANGLE (DEGREES) = 16.80
OUTLET ANGLE (DEGREES) = -59.41
VELOCITY AT TE (FT/SEC) = 783.58
V/VTE (RED. FLOW)
M/WIDTH
WG12XJ3
17.08.15 05/01/78

Figure C-27.

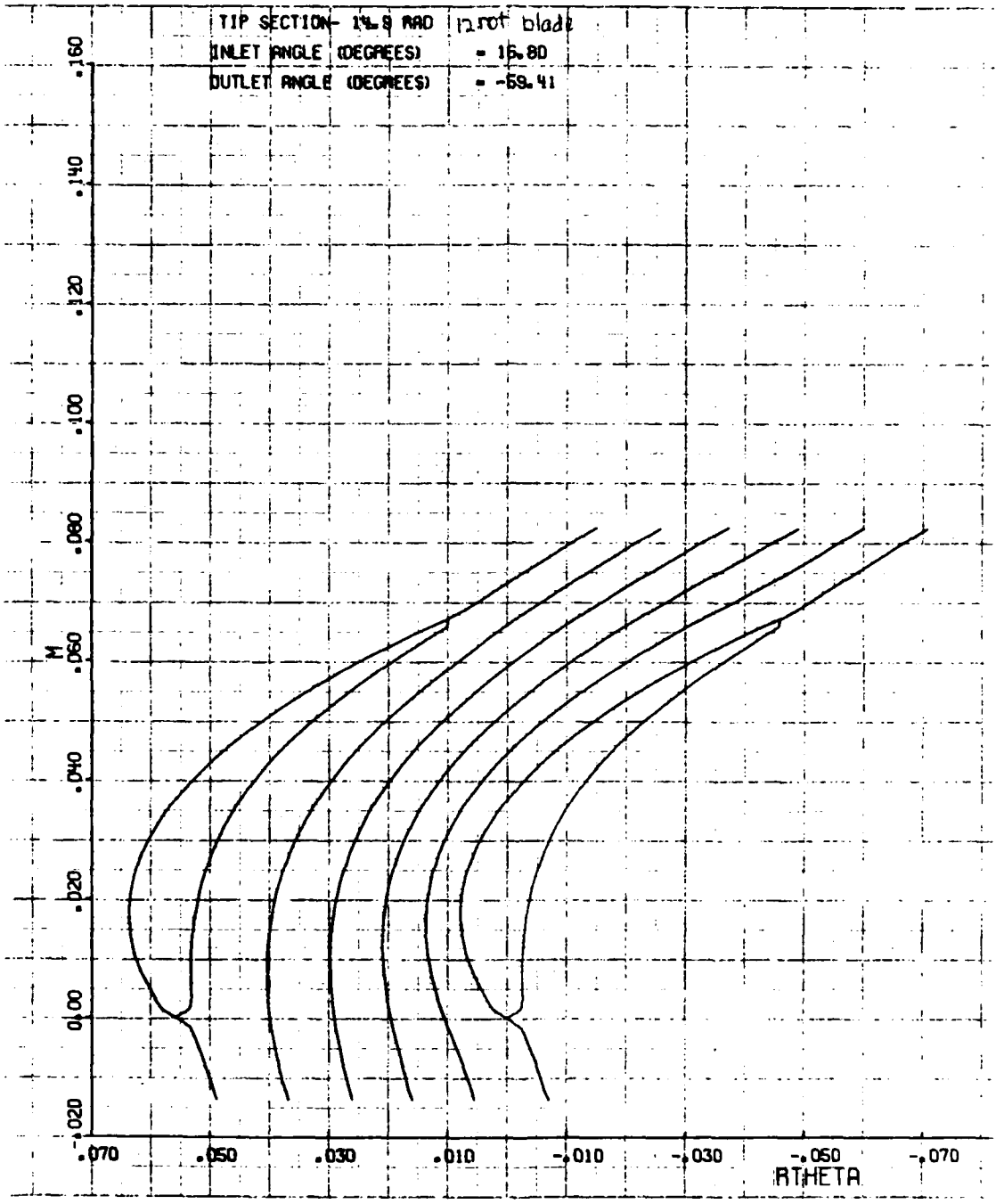
TIP SECTION- 14.9 RAD 12 rot blade
INLET ANGLE (DEGREES) = 16.80
OUTLET ANGLE (DEGREES) = -69.41
M
.160
.140
.120
.100
.080
.060
.040
.020
.00
-.020
.070
.050
.030
.010
-.010
-.030
-.050
-.070
RTHETA

Figure C-28.

TABLE C-4

MECHANICAL DATA

	HELIUM TURBINE 12 ROT BLADE	W251X 4 ROT BLADE
Rhub - in.	11.5	17.65
Rtip - in.	14.9	32.92
blade height - in.	3.4	15.27
η - rpm	6000.	5778.
uhub - fps	602.1	890.
utip - fps	780.2	1660.
Aannular - f^2	1.958	16.85
N^2 A * 10^{-6}	70.5	562.

APPENDIX D

9000 RPM TURBINE

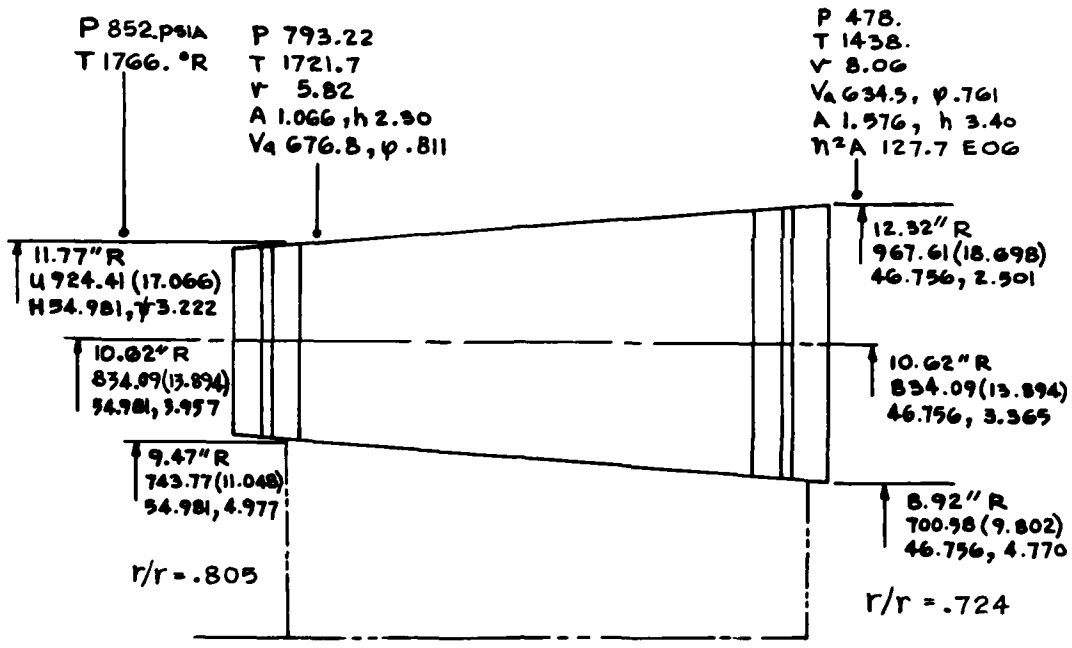

71400 shp

H = 71400./124 pm/sec/1.41485 hp/(Btu/sec) = 406.97 BTU/pm

$H_{STG\ Avg.}$ = 50.872 BTU/pm

FLOW PATH - 8 stgs. - 9000 rpm

W 124. pm/sec

He properties

M = 4.

R = 386. f-p/pm/°R
= 12419. fp/sl/°R

cp = 1.25
= 31296. f-p/sl/°R

$a/T^{1/2}$ = 143.539

γ = 1.6579

Figure D-1.

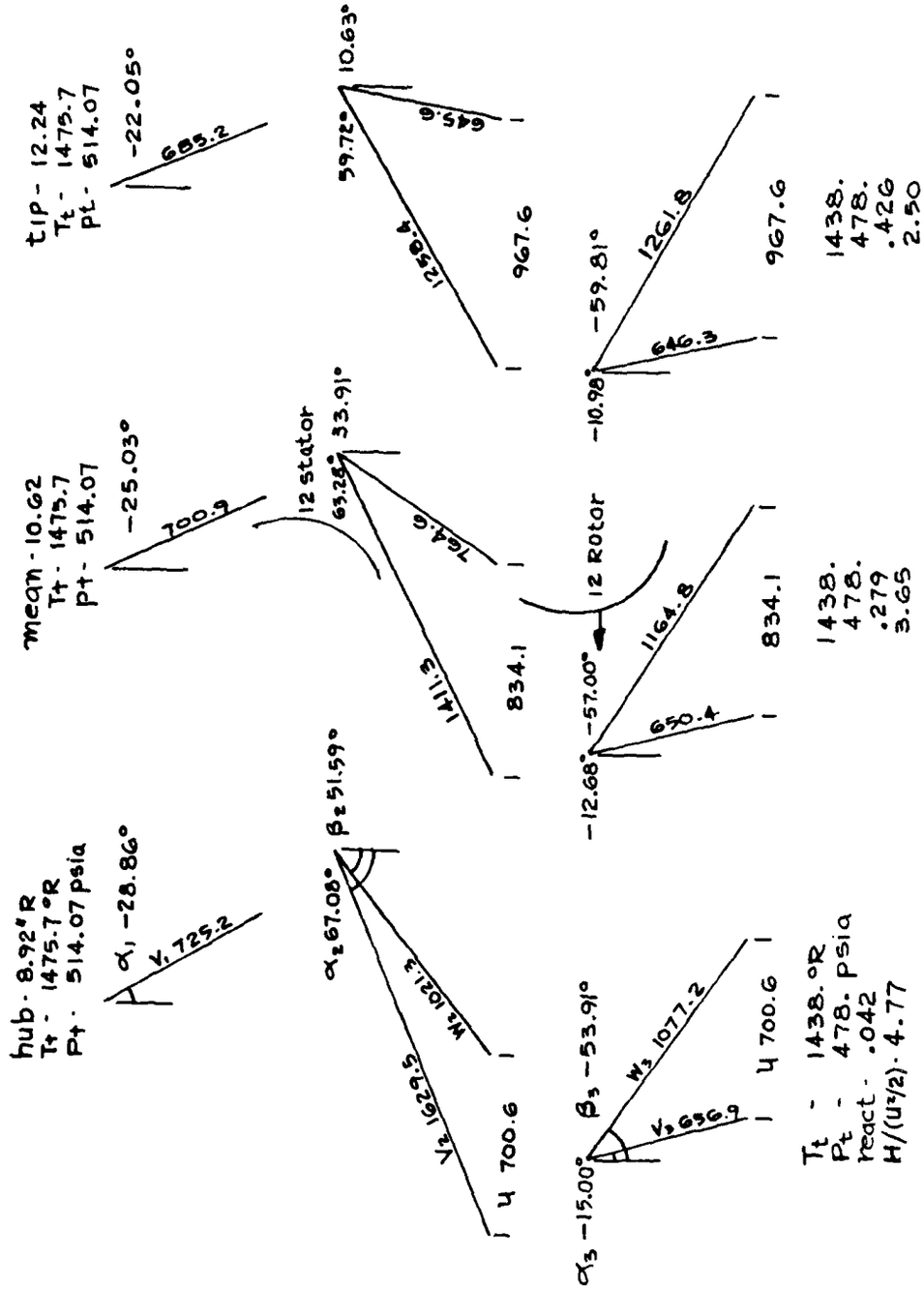

8th stg. Velocity triANGles - 9000 rpm

Figure D-2.

APPENDIX E

FIRST COMPRESSOR STAGE

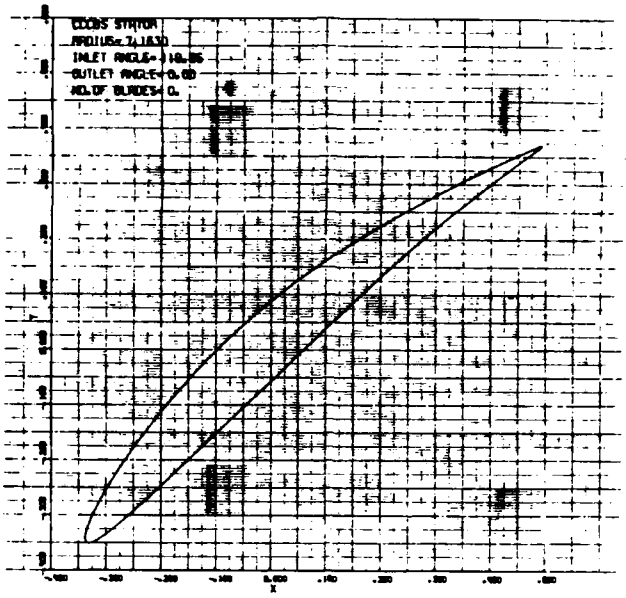
CCDS STATOR
INLET ANGLE= 116.86
OUTLET ANGLE= 0.00
NO. OF BLADES= 0.

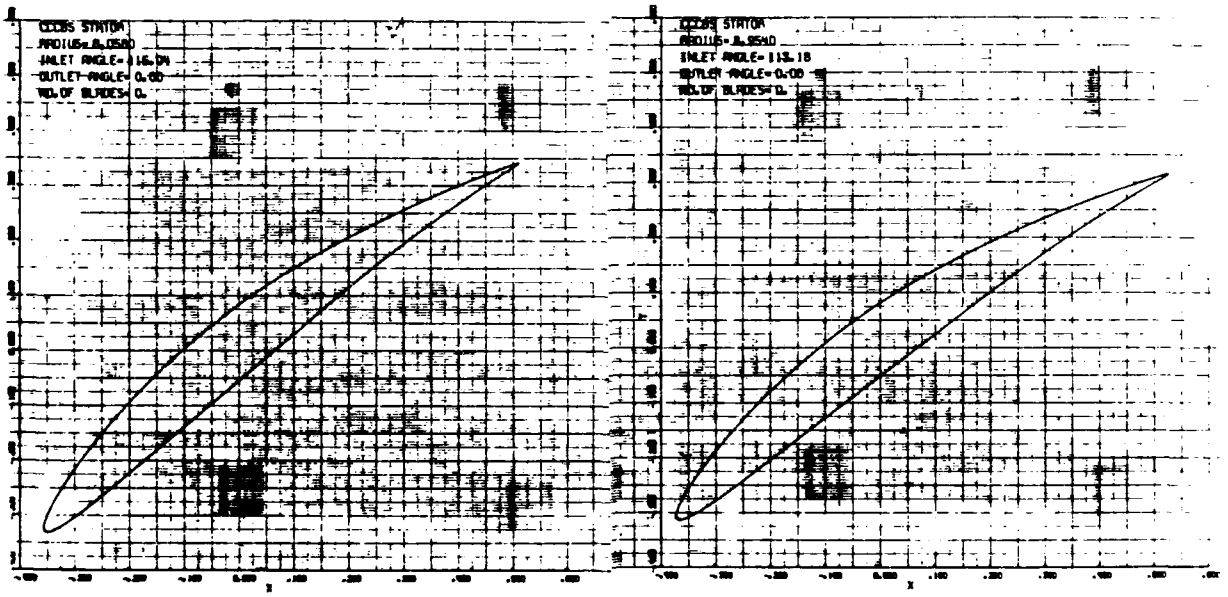
CCDS STATOR
INLET ANGLE= 116.74
OUTLET ANGLE= 0.00
NO. OF BLADES= 0.
CCDS STATOR
INLET ANGLE= 115.18
OUTLET ANGLE= 0.00
NO. OF BLADES= 0.

Figure E-1.

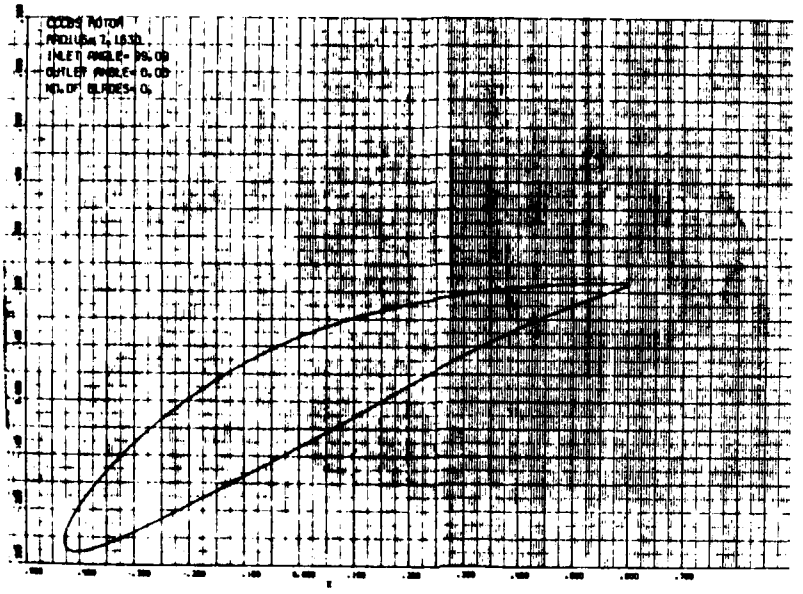
CCDBS ROTOR
OUTLET ANGLE= 0.00

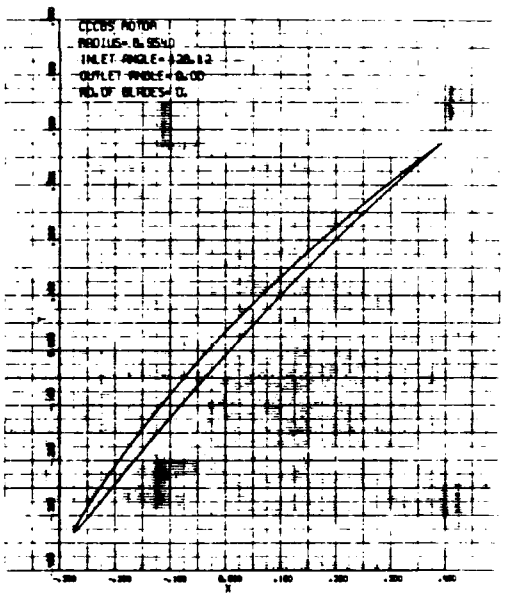
CCDBS ROTOR
OUTLET ANGLE= 0.00

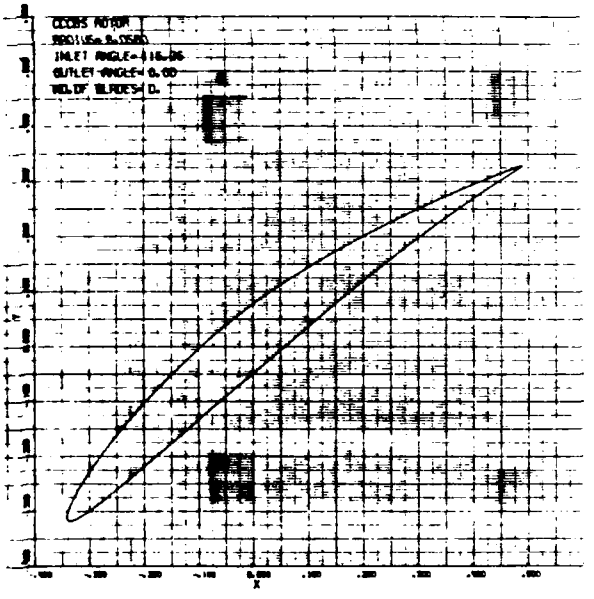
CCDBS ROTOR
OUTLET ANGLE= 0.00

Figure E-2.

```
LIST 100-140

00100 READ C4,V,G,N1,O1,P,F1,N                                    ext.
00110 DATA .094,367.5,127.9,1800 ,14,325,14,0.0,49
00120 READ T1,L1,C1,T2,L2,C2,T3,L3,C3,S,Q,H1,F,R
00130 DATA .160,1.134,32.63,.095,1.05,23.28,.030,.972,17.09,25.35,37.86,
00140 DATA 1.791,32000.00,.279
*RUN

LBU  27-MAR-78  13:25

AREA R          AREA M          AREA T
 .139068         7.07921E-2      1.91574E-2

SIGMA CF        FREQ            HARMONIC        ALL MAG
 19376.9         2497.52         8.32507         2.97632

FORCE T         FORCE P         SIGMA VIB       SIGMA TOT
 29.8182         25.908          11784.4         31161.3

ACT MAG         LBU             AR MEAN
 2.88987         .970954         1.70571

HUB CHORD       MEAN CHORD      TIP CHORD       NO.BLADES
 1.134           1.05            .972            49

C/P UNITS 5
*TEXT 110,0.0_.025
00110 DATA .094,367.5,127.9,18000,14.325,14,.025,49
*RUN                                                              ext.

LBU  27-MAR-78  13:27

AREA R          AREA M          AREA T
 .139068         7.07921E-2      1.91574E-2

SIGMA CF        FREQ            HARMONIC        ALL MAG
 19376.9         2429.23         8.09743         3.09545

FORCE T         FORCE P         SIGMA VIB       SIGMA TOT
 29.8182         25.908          11784.4         31161.3

ACT MAG         LBU             AR MEAN
 2.88987         .933589         1.70571

HUB CHORD       MEAN CHORD      TIP CHORD       NO.BLADES
 1.134           1.05            .972            49

C/P UNITS 4
*
```

```
TEXT 110,.025_.050
00110 DATA .094,367.5,127.9,18000,14.325,14,.050,49
*RUN                                                              ext.

LBU  27-MAR-78  13:28

AREA R          AREA M          AREA T
 .139068         7.07921E-2      1.91574E-2

SIGMA CF        FREQ            HARMONIC        ALL MAG
 19376.9         2363.7          7.87901         3.21956

FORCE T         FORCE P         SIGMA VIB       SIGMA TOT
 29.8182         25.908          11784.4         31161.3

ACT MAG         LBU             AR MEAN
 2.88987         .897598         1.70571

HUB CHORD       MEAN CHORD      TIP CHORD       NO.BLADES
 1.134           1.05            .972            49

C/P UNITS 4
*BYE
CP UNITS:  27.0
CONNECT TIME:  00:09
```

MARGIN ON T_e (15%)

FACTOR OF SAFETY ON ULTIMATE (1.25)

Figure E-3.

29 MARCH 78
[illegible]
CCBS LPC FIRST STAGE FINAL CHORDS

NACA DEVIATION

PROGRAM PW6187 - AN AERODYNAMIC ANALYSIS FOR CCBS LPC FIRST STAGE FINAL CHORDS

PRINTOUT OF INPUT DATA

NUMBER OF STATIONS	=	7
NUMBER OF STREAMLINES	=	7
MAXIMUM NUMBER OF ITERATIONS	=	50
INDICATOR FOR BOUNDARY LAYER CALCULATION	=	2
INDICATOR FOR STREAMLINE CHARACTERISTICS	=	0
NUMBER OF POINTS TO BE COMPUTED	=	1
INDICATOR FOR INPUT	=	0
INDICATOR FOR OUTPUT	=	0
PRESSURE RATIO PERCENT	=	,0050
PERCENT UNCONVERGED	=	,4000
STREAMLINE ADJUSTMENT FACTOR	=	,2000
ACCELERATION DUE TO GRAVITY	=	32,1740
JOULES EQUIVALENT	=	778,1200
GAS CONSTANT	=	386,0000
TOLERANCE FOR ITERATIVE SOLUTION	=	,0010
KINEMATIC VISCOSITY OF GAS	=	0,0000000
LINEAR DIMENSION SCALING FACTOR	=	12,0000

CONSTANTS DETERMINING SPECIFIC HEAT AT CONSTANT PRESSURE

CP0	=	1,2420
CP1	=	0,
CE1	=	1,0000
CP2	=	0,
CE2	=	2,0000
CP3	=	0,
CE3	=	3,0000
CP4	=	0,
CE4	=	4,0000

POINTS TO BE COMPUTED

POINT NO,	SPEED FACTOR	FLOW RATE	SEC, FLOW	P RATIO	BLK FACTOR	LOSS FACTOR
1	18000,0000	127,9000	0,00000	=0,0000	1,0000	1,5000

Figure E-4.

ANNULUS GEOMETRY SPECIFICATION

STATION NUMBER	AXIAL COORDINATE ON CENTERLINE	HUB RADIUS	CASING RADIUS	STATION ANGLE	COOLING FLOW	COOLING TEMP
1	10,00000	7,16300	8,95400	0,0000	0,0000	0,000
2	11,00000	7,16300	8,95400	0,0000	0,0000	0,000
3	12,00000	7,16300	8,95400	0,0000	0,0000	0,000
4	13,02500	7,16300	8,95400	0,0000	0,0000	0,000
5	13,25000	7,16300	8,95400	0,0000	0,0000	0,000
6	14,07500	7,16300	8,95400	0,0000	0,0000	0,000
7	15,00000	7,16300	8,95400	0,0000	0,0000	0,000

STATION THERMODYNAMIC DATA

STATION 1 NDATA= 1 NTERP=0 NMACH=0
BLOCKAGE=0,0000

RADIUS	TOTAL TEMPERATURE	TOTAL PRESSURE	WHIRL ANGLE
8,0580	560,000	458,000	0,00

STATION 2 FOLLOWS A BLADE PERFORMING THUS
NWORK=6 NLOSS=1 NDATA= 3 NTERP=0 NPUNCH=0 NMACH=0 NWREF= 0 NLREF= 1
BLOCKAGE= ,0100 SPEED= 0,0 WORK DONE FACTOR=1,0000 STAT LOSS MULT=1,000
REY FACT MULT=1,0000

RADIUS	DTWORK	DTLOSS	BLOCKAGE	LOSS MULT	SEC LOSS
7,1630	506,000	0,00000	0,0000	1,0000	0,0000
8,0580	449,800	0,00000	0,0000	1,0000	0,0000
8,9540	404,700	0,00000	0,0000	1,0000	0,0000

STATION 3 FOLLOWS A BLADELESS INTERVAL
BLOCKAGE= ,0150

STATION 4 FOLLOWS A BLADE DESCRIBED BY THE FOLLOWING
NDATA= 3 NTERP=1 NPUNCH=1 NMACH=0 NLREF= 1 IARC=1
IANG=0 IFORM=0 IFTRAN=0 IDEV=1 NBLADE= 49 IBL=
BLOCKAGE= ,0200 SPEED= 1,0 WORK DONE FACTOR=1,0000
TLOSS=1,0000 SHAPEK= 1,000 DEVM= 0,0000

RADIUS	CAMBER	STAGGER	SOLIDITY	T/C	A/C	M1 ANGLE	M2 ANGLE	LOS,MULT	ADD,DEVN.
7,1630	32,630	25,350	1,2350	,1600	,5000	0,000	0,000	1,0000	0,0000
8,0580	23,280	37,890	1,0160	,0950	,5000	0,000	0,000	1,0000	0,0000
8,9540	17,090	46,670	,8470	,0300	,5000	0,000	0,000	1,0000	0,0000

STATION 5 FOLLOWS A BLADELESS INTERVAL
BLOCKAGE= ,0250

STATION 6 FOLLOWS A BLADE DESCRIBED BY THE FOLLOWING
NDATA= 3 NTERP=1 NPUNCH=1 NMACH=0 NLREF= 1 IARC=1
IANG=0 IFORM=0 IFTRAN=0 IDEV=1 NBLADE= 48 IBL=
BLOCKAGE= ,0300 SPEED= 0,0 WORK DONE FACTOR=1,0000
TLOSS=1,0000 SHAPEK= 1,000 DEVM= 0,0000

RADIUS	CAMBER	STAGGER	SOLIDITY	T/C	A/C	M1 ANGLE	M2 ANGLE	LOS,MULT	ADD,DEVN.
7,1630	23,500	41,090	1,1670	,1000	,5000	0,000	0,000	1,0000	0,0000
8,0580	23,500	37,780	1,0370	,1000	,5000	0,000	0,000	1,0000	0,0000
8,9540	23,500	34,910	,9330	,1000	,5000	0,000	0,000	1,0000	0,0000

STATION 7 FOLLOWS A BLADELESS INTERVAL
BLOCKAGE= ,0300

STATION 7 DEFINES A DIFFUSER INLET
DIFFUSER EFFICIENCY =1,0000

1	18	44	0	2	127,90000
2	13	12	0	2	127,90000
3	7	7	0	2	127,90000
4	6	2	0	2	127,90000
5	3	0	0	2	127,90000
6	0	0	0	2	127,90000

Figure E-5.

PRINTOUT OF RESULTS FOR POINT 1

ITERATION 7

STATION 1 CP=1.242000 GAMMA=1.66503 GASR=386.0000 FLOW= 127.9000

FLOW DESCRIPTION

STRM LINE	RADIUS	VELOCITIES MERID	VELOCITIES TANGEN	PRESSURES TOTAL	PRESSURES TOTAL	PRESSURES STATIC	TEMPERATURES TOTAL	TEMPERATURES STATIC	MACH NO.	ANGLES WHIRL	ANGLES STRMLN	RADIUS OF CURV	RHO-VM	AXIAL LENGTH
1	7.1630	685.4	0.0	685.4	454.00	438.82	560.0	552.4	.2028	0.00	.51	0.0	203.095	10.000
2	7.3617	685.4	0.0	685.4	454.00	438.82	560.0	552.4	.2028	0.00	.40	0.0	203.098	10.000
3	7.7439	685.4	0.0	685.4	454.00	438.82	560.0	552.4	.2028	0.00	.19	0.0	203.101	10.000
4	8.1081	685.4	0.0	685.4	454.00	438.82	560.0	552.4	.2028	0.00	-.00	0.0	203.102	10.000
5	8.4566	685.4	0.0	685.4	454.00	438.82	560.0	552.4	.2028	0.00	-.20	0.0	203.101	10.000
6	8.7913	685.4	0.0	685.4	454.00	438.82	560.0	552.4	.2028	0.00	-.41	0.0	203.097	10.000
7	8.9540	685.4	0.0	685.4	454.00	438.82	560.0	552.4	.2028	0.00	-.51	0.0	203.094	10.000

STATION 2 CP=1.242000 GAMMA=1.66503 GASR=386.0000 FLOW= 127.8999

FLOW DESCRIPTION

STRM LINE	RADIUS	VELOCITIES MERID	VELOCITIES TANGEN	PRESSURES TOTAL	PRESSURES TOTAL	PRESSURES STATIC	TEMPERATURES TOTAL	TEMPERATURES STATIC	MACH NO.	ANGLES WHIRL	ANGLES STRMLN	RADIUS OF CURV	RHO-VM	AXIAL LENGTH
1	7.1720	700.2	505.4	863.5	454.00	430.05	560.0	548.0	.2565	35.82	.38	-223.4	204.986	11.000
2	7.3687	699.3	492.5	855.3	454.00	430.50	560.0	548.2	.2540	35.16	.30	-303.1	204.840	11.000
3	7.7473	698.7	468.3	841.1	454.00	431.26	560.0	548.6	.2497	33.83	.15	-642.5	204.900	11.000
4	8.1080	698.8	447.0	829.5	454.00	431.87	560.0	548.9	.2462	32.61	-.01	-14935.8	205.101	11.000
5	8.4531	698.9	428.8	820.0	454.00	432.37	560.0	549.2	.2433	31.53	-.16	676.4	205.275	11.000
6	8.7842	699.4	412.7	812.1	454.00	432.78	560.0	549.4	.2409	30.54	-.31	300.6	205.541	11.000
7	8.9450	700.0	405.1	808.8	454.00	432.95	560.0	549.5	.2399	30.06	-.38	223.4	205.751	11.000

PERFORMANCE OF MACHINE

STRM LINE	INLET THROUGH STATION PRESSURE RATIO	INLET THROUGH STATION DELTA T ON T	INLET THROUGH STATION EFFICIENCIES ISEN	INLET THROUGH STATION EFFICIENCIES POLY	STATION TO STATION PRESSURE RATIO	STATION TO STATION DELTA T ON T	STATION TO STATION EFFICIENCIES ISEN	STATION TO STATION EFFICIENCIES POLY	BLADE LOADINGS AVERAGE RADIUS	BLADE LOADINGS AXIAL	BLADE LOADINGS TANGEN
1	1.0000	0.0000	0.0000	0.0000	1.0000	0.0000	0.0000	0.0000	7.26635	-361.82	1003.5
2	1.0000	0.0000	0.0000	0.0000	1.0000	0.0000	0.0000	0.0000	7.55542	-348.69	1004.3
3	1.0000	0.0000	0.0000	0.0000	1.0000	0.0000	0.0000	0.0000	7.92685	-332.16	1003.9
4	1.0000	0.0000	0.0000	0.0000	1.0000	0.0000	0.0000	0.0000	8.28146	-317.71	1003.9
5	1.0000	0.0000	0.0000	0.0000	1.0000	0.0000	0.0000	0.0000	8.62132	-305.32	1004.5
6	1.0000	0.0000	0.0000	0.0000	1.0000	0.0000	0.0000	0.0000	8.86865	-296.52	1004.6
7	1.0000	0.0000	0.0000	0.0000	1.0000	0.0000	0.0000	0.0000	0.00000	0.00	0.0
	1.0000	0.0000	0.0000	0.0000	1.0000	0.0000	0.0000	0.0000	INTEGRATED VALUES		

INTEGRATED TOTAL TEMPS AT BLADE INLET
ABSOLUTE = 560.00 RELATIVE = 560.00

PERFORMANCE OF BLADING

STRM LINE	RADIUS OUTLET	RELATIVE ANGLE INLET	RELATIVE ANGLE OUTLET	RELATIVE MACH NO. IN	RELATIVE MACH NO. OUT	RELATIVE VELOCITY INLET	RELATIVE VELOCITY OUTLET	OMEGA INLET	INLET REL PRESSURE	TOTAL TEMP.	UZ	STAT PRES RISE COEF	SLOPE
1	7.17196	0.000	35.822	.2028	.2565	685.37	863.54	0.0000	454.00	560.0	0.0	-.578	.515
2	7.36871	0.000	35.157	.2028	.2540	685.38	855.27	0.0000	454.00	560.0	0.0	-.548	.196
3	7.74732	0.000	33.829	.2028	.2497	685.39	841.12	0.0000	454.00	560.0	0.0	-.498	.195
4	8.10805	0.000	32.605	.2028	.2462	685.39	829.54	0.0000	454.00	560.0	0.0	-.458	-.001
5	8.45309	0.000	31.552	.2028	.2433	685.39	819.99	0.0000	454.00	560.0	0.0	-.425	-.202
6	8.78425	0.000	30.545	.2028	.2409	685.38	812.13	0.0000	454.00	560.0	0.0	-.398	-.400
7	8.94505	0.000	30.061	.2028	.2399	685.36	808.76	0.0000	454.00	560.0	0.0	-.387	-.513

Figure E-6.

STATION 3 CP=1,242000 GAMMA=1,66503 GASR=386,0000 FLOW= 127,8999

FLOW DESCRIPTION

STRM LINE	RADIUS	VELOCITIES MERID	VELOCITIES TANGEN	PRESSURES TOTAL	PRESSURES STATIC	TEMPERATURES TOTAL	TEMPERATURES STATIC	MACH NO.	ANGLES WHIRL	ANGLES STRMLN	RADIUS OF CURV	RHO-VM	AXIAL LENGTH
1	7,1764	702,8	505,1	865,2	456,00	489,96	560,0	548,0	,2870	35,72	,25	-9271,6	205,608	12,000
2	7,3724	702,0	492,2	857,4	456,00	430,38	560,0	548,2	,2567	35,04	,23	1447,8	205,623	12,000
3	7,7492	702,4	468,2	844,1	456,00	431,10	560,0	548,5	,2506	33,68	,13	973,2	205,925	12,000
4	8,1080	703,0	447,0	833,0	456,00	431,69	560,0	548,8	,2473	32,45	,03	739,9	206,266	12,000
5	8,4911	703,2	428,9	823,7	456,00	432,18	560,0	549,1	,2445	31,38	-,08	829,7	206,470	12,000
6	8,7805	703,3	412,9	815,6	456,00	432,60	560,0	549,3	,2420	30,62	-,21	3282,6	206,630	12,000
7	8,9406	703,5	405,3	811,9	456,00	432,79	560,0	549,4	,2409	29,95	-,28	9271,6	206,733	12,000

PERFORMANCE ANALYSIS FOR BLADE ROW BETWEEN STATIONS 3 AND 4 ROTOR 1

STREAMLINE 1

BI= 41,783 CAM= 32,404 C/B=1,2304 T/C= ,1589 A/C= ,5000 INC= -,249 M1R= ,2788 IRF= 0,000 DRF= 9,59 DVA= ,1
DI= -,010 MIC= ,781 DM = 0,00 DEV= 9,77 D = ,388 WMN= ,0330 WMR= 0,000 WTP= 0,000 IWN= ,315 W = ,033
CI=-12,777 BI = 16,638 DP = ,396 DF = ,399 CM=-11,410 BM = 10,560 CRD= 1,133 REY= 2,07E+06

STREAMLINE 2

BI= 43,505 CAM= 30,357 C/B=1,1751 T/C= ,1446 A/C= ,5000 INC= -,022 M1R= ,2874 IRF= 0,000 DRF= 9,31 DVA= ,1
DI= -,001 MIC= ,785 DM = 0,00 DEV= 9,45 D = ,388 WMN= ,0322 WMR= 0,000 WTP= 0,000 IWN= ,313 W = ,032
CI=-11,942 BI = 15,077 DP = ,400 DF = ,399 CM=-11,460 BM = 10,121 CRD= 1,111 REY= 2,09E+06

STREAMLINE 3

BI= 46,816 CAM= 26,451 C/B=1,0819 T/C= ,1173 A/C= ,5000 INC= ,027 M1R= ,3049 IRF= 0,000 DRF= 8,59 DVA= ,1
DI= ,002 MIC= ,792 DM = 0,00 DEV= 8,70 D = ,383 WMN= ,0312 WMR= 0,000 WTP= 0,000 IWN= ,307 W = ,031
CI=-10,431 BI = 12,434 DP = ,401 DF = ,393 CM=-11,591 BM = 9,308 CRD= 1,075 REY= 2,15E+06

STREAMLINE 4

BI= 49,847 CAM= 22,919 C/B=1,0047 T/C= ,0913 A/C= ,5000 INC= -,226 M1R= ,3221 IRF= 0,000 DRF= 7,75 DVA= ,1
DI= -,018 MIC= ,800 DM = 0,00 DEV= 7,88 D = ,373 WMN= ,0307 WMR= 0,000 WTP= 0,000 IWN= ,297 W = ,030
CI= -9,087 BI = 10,320 DP = ,396 DF = ,380 CM=-11,743 BM = 8,644 CRD= 1,045 REY= 2,21E+06

STREAMLINE 5

BI= 52,024 CAM= 20,576 C/B= ,9343 T/C= ,0665 A/C= ,5000 INC= -,071 M1R= ,3386 IRF= 0,000 DRF= 7,14 DVA= ,0
DI= -,007 MIC= ,803 DM = 0,00 DEV= 7,23 D = ,366 WMN= ,0299 WMR= 0,000 WTP= 0,000 IWN= ,295 W = ,029
CI= -7,868 BI = 8,666 DP = ,388 DF = ,372 CM=-11,988 BM = 7,758 CRD= 1,012 REY= 2,25E+06

STREAMLINE 6

BI= 54,114 CAM= 18,336 C/B= ,8755 T/C= ,0427 A/C= ,5000 INC= -,163 M1R= ,3546 IRF= 0,000 DRF= 6,51 DVA= ,1
DI= -,020 MIC= ,808 DM = 0,00 DEV= 6,60 D = ,357 WMN= ,0295 WMR= 0,000 WTP= 0,000 IWN= ,288 W = ,029
CI= -6,725 BI = 7,213 DP = ,379 DF = ,361 CM=-12,147 BM = 7,120 CRD= ,986 REY= 2,30E+06

STREAMLINE 7

BI= 55,130 CAM= 17,244 C/B= ,8495 T/C= ,0311 A/C= ,5000 INC= -,280 M1R= ,3625 IRF= 0,000 DRF= 6,18 DVA= ,1
DI= -,037 MIC= ,810 DM = 0,00 DEV= 6,30 D = ,351 WMN= ,0295 WMR= 0,000 WTP= 0,000 IWN= ,283 W = ,029
CI= -6,177 BI = 6,547 DP = ,375 DF = ,355 CM=-12,191 BM = 6,850 CRD= ,974 REY= 2,32E+06

STATION 4 CP=1,242000 GAMMA=1,66503 GASR=386,0000 FLOW= 127,9050

FLOW DESCRIPTION

STRM LINE	RADIUS	VELOCITIES MERID	VELOCITIES TANGEN	PRESSURES TOTAL	PRESSURES STATIC	TEMPERATURES TOTAL	TEMPERATURES STATIC	MACH NO.	ANGLES WHIRL	ANGLES STRMLN	RADIUS OF CURV	RHO-VM	AXIAL LENGTH
1	7,1809	689,3	888,6	1124,6	481,81	440,19	573,9	555,6	,3324	52,20	,70	80,2	208,465	13,025
2	7,3769	692,4	870,6	1112,3	482,17	441,42	574,1	554,2	,3286	51,51	,46	84,3	205,719	13,025
3	7,7522	694,6	831,6	1083,5	482,36	443,63	574,2	555,4	,3197	50,13	,22	325,0	206,995	13,025
4	8,1094	692,3	792,4	1052,2	482,07	445,51	574,2	556,4	,3102	48,86	,09	1141,3	206,803	13,025
5	8,4903	697,0	749,5	1038,2	482,79	447,14	574,5	557,2	,3089	47,83	-,10	-564,6	208,654	13,025
6	8,7770	695,6	743,9	1018,4	482,07	448,63	574,7	558,0	,2998	46,92	-,44	-74,6	208,639	13,025
7	8,9361	692,5	730,5	1006,6	482,91	449,36	574,7	558,4	,2962	46,53	-,70	-40,2	207,913	13,025

Figure E-7.

PERFORMANCE OF MACHINE
****

STRM LINE	INLET THROUGH STATION PRESSURE RATIO	DELTA T ON T	EFFICIENCIES IBEN	POLY	STATION TO STATION PRESSURE RATIO	DELTA T ON T	EFFICIENCIES IBEN	POLY	BLADE LOADINGS AVERAGE RADIUS	AXIAL	TANGEN
1	1,0613	,0249	,9664	,9668	1,0613	,0249	,9664	,9668	7,27667	459,74	770,5
2	1,0620	,0252	,9657	,9661	1,0620	,0252	,9657	,9661	7,56269	539,63	783,8
3	1,0625	,0254	,9631	,9636	1,0625	,0254	,9631	,9636	7,92969	634,95	786,9
4	1,0618	,0253	,9595	,9600	1,0618	,0253	,9595	,9600	8,27968	729,71	797,8
5	1,0634	,0260	,9577	,9582	1,0634	,0260	,9577	,9582	8,61472	824,61	815,8
6	1,0638	,0262	,9549	,9554	1,0638	,0262	,9549	,9554	8,85854	886,53	816,6
7	1,0637	,0262	,9530	,9536	1,0637	,0262	,9530	,9536	0,00000	0,00	0,0
	1,0627	,0256	,9601	,9606	1,0627	,0256	,9601	,9606	INTEGRATED VALUES		

INTEGRATED TOTAL TEMPS AT BLADE INLET
ABSOLUTE = 560,00 RELATIVE = 567,76

PERFORMANCE OF BLADING
****

STRM LINE	RADIUS OUTLET	RELATIVE ANGLE INLET	OUTLET	RELATIVE MACH NO, IN	OUT	RELATIVE VELOCITY INLET	OUTLET	OMEGA INLET	INLET REL PRESSURE	TOTAL TEMP,	UR	STAT PRES RISE COEF	SLOPE
1	7,18091	-41,534	-19,150	,2788	,2157	938,34	729,64	,0312	458,32	562,1	1128,0	,361	,25
2	7,37694	-43,483	-22,599	,2874	,2215	967,56	749,94	,0304	480,59	563,2	1158,8	,365	,254
3	7,75225	-46,844	-29,067	,3049	,2345	1026,87	794,71	,0300	465,24	565,5	1217,7	,367	,171
4	8,10937	-49,621	-34,815	,3221	,2486	1085,08	843,19	,0302	469,94	567,8	1273,8	,361	,079
5	8,45034	-51,953	-38,677	,3386	,2630	1141,00	892,77	,0302	474,62	570,0	1327,4	,353	-,041
6	8,77699	-53,951	-42,384	,3546	,2772	1195,19	941,71	,0306	479,33	572,3	1378,7	,343	-,19
7	8,93609	-54,849	-44,188	,3625	,2842	1221,88	965,79	,0309	481,71	573,4	1403,7	,339	-,25

STATION 5 CP=1,242000 GAMMA=1,66503 GASR=386,0000 FLOW= 127,8931
****

FLOW DESCRIPTION
****

STRM LINE	RADIUS	VELOCITIES MERID	TANGEN	TOTAL	PRESSURES TOTAL	STATIC	TEMPERATURES TOTAL	STATIC	MACH NO,	ANGLES WHIRL	STRMLN	RADIUS OF CURV	RHO-VM	AXIAL LENGTH
1	7,1854	696,4	888,1	1129,8	481,81	439,82	573,9	553,4	,3340	51,82	,73	-36,3	207,066	13,250
2	7,3706	696,4	870,3	1114,6	482,17	441,25	574,1	554,1	,3295	51,33	,54	-107,7	206,883	13,250
3	7,7533	695,5	831,5	1084,0	482,36	443,59	574,2	555,3	,3199	50,09	,30	531,1	207,256	13,250
4	8,1098	693,3	792,4	1052,9	482,07	445,47	574,2	556,3	,3104	48,81	,16	239,9	207,112	13,250
5	8,4498	699,6	769,5	1040,0	482,79	447,02	574,5	557,1	,3064	47,72	-,08	142,5	209,418	13,250
6	8,7744	702,8	744,1	1023,6	482,87	448,29	574,7	557,8	,3014	46,63	-,44	61,9	210,714	13,250
7	8,9316	704,3	730,9	1015,0	482,91	448,81	574,7	558,1	,2988	46,06	-,73	36,3	211,299	13,250

PERFORMANCE ANALYSIS FOR BLADE ROW BETWEEN STATIONS 5 AND 6 STATOR 1
****

STREAMLINE 1
****

BI= 52,755 CAM= 23,514 C/B=1,1630 T/C= ,1000 A/C= ,5000 INC= -,937 MIR= ,3340 IRF= 0,000 DRF= 7,77 DVA= ,3
DI= -,052 MIC= ,811 DM = 0,00 DEV= 8,03 D = ,388 MMN= ,0361 MMR= 0,000 MTP= 0,000 INN= ,328 M = ,03
CI= -9,333 SI = 10,352 DP = ,434 DF = ,390 CMB=10,866 SM = 9,708 CRD= 1,094 REY= 2,42E+06

STREAMLINE 2
****

BI= 52,038 CAM= 23,520 C/B=1,1322 T/C= ,1000 A/C= ,5000 INC= -,706 MIR= ,3293 IRF= 0,000 DRF= 7,79 DVA= ,3
DI= -,042 MIC= ,808 DM = 0,00 DEV= 7,94 D = ,385 MMN= ,0349 MMR= 0,000 MTP= 0,000 INN= ,319 M = ,03
CI= -9,371 SI = 10,484 DP = ,420 DF = ,383 CMB=11,041 SM = 9,509 CRD= 1,094 REY= 2,39E+06

STREAMLINE 3
****

BI= 50,656 CAM= 23,517 C/B=1,0776 T/C= ,1000 A/C= ,5000 INC= -,568 MIR= ,3199 IRF= 0,000 DRF= 7,84 DVA= ,1
DI= -,037 MIC= ,804 DM = 0,00 DEV= 7,92 D = ,379 MMN= ,0328 MMR= 0,000 MTP= 0,000 INN= ,301 M = ,03
CI= -9,443 SI = 10,681 DP = ,400 DF = ,375 CMB=11,347 SM = 9,156 CRD= 1,094 REY= 2,33E+06

Figure E-8.

```
                                STREAMLINE  4
                                ************
BI= 48,364 CAM= 23,510 C/B=1,0302 T/C= ,1000 A/C= ,5000 INC=  =,550 MIR= ,3104 IRF= 0,000 DRF= 7,92 DVA=  ,1
DI=  =,039 MIC=   ,800 DM =  0,00 DEV=  8,00 D  =  ,374 MMN=  ,0310 MMR= 0,000 MTP= 0,000 IMN= ,283 M =  ,031
CI= =9,511 SI =  10,883 DP =  ,387 DF =  ,371 CM=-11,606 SM =  8,844 CRD= 1,094 REY= 2,26E+06

                                STREAMLINE  5
                                ************
BI= 48,275 CAM= 23,502 C/B= ,9868 T/C= ,1000 A/C= ,5000 INC=  =,552 MIR= ,3064 IRF= 0,000 DRF= 8,01 DVA=  ,0
DI=  =,042 MIC=   ,796 DM =  0,00 DEV=  8,02 D  =  ,369 MMN=  ,0295 MMR= 0,000 MTP= 0,000 IMN= ,276 M =  ,029
CI= =9,568 SI =  11,054 DP =  ,366 DF =  ,360 CM=-11,819 SM =  8,556 CRD= 1,094 REY= 2,24E+06

                                STREAMLINE  6
                                ************
BI= 47,235 CAM= 23,490 C/B= ,9523 T/C= ,1000 A/C= ,5000 INC=  =,601 MIR= ,3014 IRF= 0,000 DRF= 8,11 DVA=  ,0
DI=  =,049 MIC=   ,793 DM =  0,00 DEV=  8,10 D  =  ,365 MMN=  ,0282 MMR= 0,000 MTP= 0,000 IMN= ,267 M =  ,028
CI= =9,622 SI =  11,216 DP =  ,352 DF =  ,356 CM=-12,006 SM =  8,301 CRD= 1,094 REY= 2,20E+06

                                STREAMLINE  7
                                ************
BI= 46,729 CAM= 23,483 C/B= ,9356 T/C= ,1000 A/C= ,5000 INC=  =,670 MIR= ,2988 IRF= 0,000 DRF= 8,16 DVA=  ,0
DI=  =,056 MIC=   ,792 DM =  0,00 DEV=  8,16 D  =  ,362 MMN=  ,0276 MMR= 0,000 MTP= 0,000 IMN= ,262 M =  ,027
CI= =9,649 SI =  11,295 DP =  ,347 DF =  ,351 CM=-12,091 SM =  8,184 CRD= 1,094 REY= 2,18E+06

                STATION  6      CP=1,262000     GAMMA=1,66903     GASR=386,0000     FLOW=  127,9000
                **********

                FLOW DESCRIPTION
                ****************

STRM  RADIUS    ----VELOCITIES----    -PRESSURES-    TEMPERATURES    MACH    --ANGLES---    RADIUS   RHU-VM    AXIAL
LINE            MERID   TANGEN   TOTAL   TOTAL STATIC   TOTAL STATIC   NO,    WHIRL  STRMLN  OF CURV            LENGTH

  1   7,1899   676,5    514,8   850,1  480,28  456,30   573,9   562,3   ,2493   37,27    ,16   =161,2  204,796   14,075
  2   7,3852   682,9    504,6   849,1  480,73  456,80   574,1   562,5   ,2490   36,46    ,22   =141,4  206,887   14,075
  3   7,7580   687,3    482,4   839,7  481,08  457,65   574,2   562,9   ,2461   35,06    ,20   =196,6  208,474   14,075
  4   8,1128   684,5    459,3   824,3  480,93  456,34   574,2   563,2   ,2415   33,86    ,15   =314,8  207,816   14,075
  5   8,4506   676,1    448,4   828,1  481,73  456,92   574,5   563,5   ,2426   32,79    ,05   =1057,2  211,488   14,075
  6   8,7715   700,2    434,8   824,2  481,99  459,37   574,7   563,7   ,2414   31,84   =,09    248,9  212,849   14,075
  7   8,9271   700,2    427,5   820,4  481,97  459,56   574,7   563,8   ,2403   31,40   =,16    161,2  212,916   14,075

                PERFORMANCE OF MACHINE
                **********************

STRM  ------INLET THROUGH STATION------      --------STATION TO STATION-------    -------BLADE LOADINGS------
LINE  PRESSURE  DELTA T    EFFICIENCIES      PRESSURE  DELTA T    EFFICIENCIES     AVERAGE     AXIAL     TANGEN
        RATIO    ON T     ISEN    POLY        RATIO     ON T     ISEN    POLY     RADIUS

  1    1,0579    ,0249   ,9161   ,9150         ,9968  0,0000  0,0000  0,0000    7,28801    697,67   =750,4
  2    1,0589    ,0252   ,9173   ,9183         ,9970    ,0000**********          7,56903    681,27   =758,2
  3    1,0597    ,0254   ,9206   ,9215        1,0026   =,0000    ,0000   ,0000   7,93351    652,85   =760,2
  4    1,0593    ,0253   ,9212   ,9221         ,9976    ,0000**********          8,28077    629,56   =767,3
  5    1,0611    ,0260   ,9232   ,9241         ,9978    ,0000**********          8,61156    611,60   =779,3
  6    1,0616    ,0262   ,9231   ,9241         ,9980    ,0000**********          8,85116    595,47   =782,4
  7    1,0616    ,0262   ,9225   ,9834         ,9980  0,0000  0,0000  0,0000    0,00000      0,00      0,0

       1,0601    ,0256   ,9209   ,9218         ,9976    ,0000**********  INTEGRATED VALUES

          INTEGRATED TOTAL TEMPS AT BLADE INLET
          ABSOLUTE =  574,33      RELATIVE =  574,33

                PERFORMANCE OF BLADING
                **********************

STRM  RADIUS    RELATIVE ANGLE    RELATIVE MACH NO, IN   RELATIVE VELOCITY  OMEGA  INLET REL TOTAL   U2    STAT PRES SLOPE
LINE  OUTLET    INLET    OUTLET     OUT      INLET      OUTLET  INLET  PRESSURE  TEMP,          RISE COEF

  1   7,18987  51,818   37,270   ,3340   ,2493   1129,78  850,09  ,0364  481,81  573,9   0,0   ,392     ,311
  2   7,38524  51,332   36,459   ,3293   ,2490   1114,62  849,11  ,0351  482,17  574,1   0,0   ,380     ,304
  3   7,75801  50,089   35,064   ,3199   ,2461   1084,04  839,75  ,0329  482,36  574,2   0,0   ,363     ,326
  4   8,11293  48,814   33,868   ,3104   ,2415   1052,90  824,32  ,0311  482,07  574,2   0,0   ,352     ,214
  5   8,45060  47,723   32,790   ,3064   ,2426   1040,03  828,05  ,0296  482,79  574,5   0,0   ,333     ,052
  6   8,77152  46,634   31,840   ,3014   ,2414   1023,55  824,20  ,0283  482,97  574,7   0,0   ,320    =,197
  7   8,92714  46,060   31,404   ,2988   ,2403   1015,01  820,43  ,0277  482,91  574,7   0,0   ,315    =,311
```

Figure E-9.

STATION 7 CP=1,242000 GAMMA=1,66503 GASR=386,0000 FLOW= 127,8992

FLOW DESCRIPTION

STRM LINE	RADIUS	VELOCITIES MERID	VELOCITIES TANGEN	PRESSURES TOTAL	PRESSURES STATIC	TEMPERATURES TOTAL	TEMPERATURES STATIC	MACH NO.	ANGLES WHIRL	ANGLES STRMLN	RADIUS OF CURV	RHO=VM	AXIAL LENGTH
1	7,1899	673,7	514,8	847,9	480,28	576,42	573,9	562,4	,2486	37,38	0,00	0,0	203,990	15,000
2	7,3859	681,1	504,5	847,6	480,73	456,88	574,1	562,6	,2485	36,53	,08	0,0	206,386	15,000
3	7,7592	687,1	482,3	839,5	481,08	457,67	574,2	562,9	,2461	35,07	,08	0,0	208,388	15,000
4	8,1140	685,3	459,2	824,9	480,93	458,31	574,2	563,2	,2417	33,83	,07	0,0	208,025	15,000
5	8,4512	697,3	448,4	829,0	481,73	458,86	574,5	563,5	,2429	32,75	,08	0,0	211,820	15,000
6	8,7716	700,9	434,8	824,8	481,99	459,34	574,7	563,7	,2416	31,81	,01	0,0	213,067	15,000
7	8,9271	700,4	427,5	820,6	481,97	459,55	574,7	563,8	,2403	31,40	0,00	0,0	212,973	15,000

PERFORMANCE OF MACHINE

STRM LINE	INLET THROUGH STATION PRESSURE RATIO	INLET THROUGH STATION DELTA T ON T	INLET THROUGH STATION EFFICIENCIES ISEN	INLET THROUGH STATION EFFICIENCIES POLY	STATION TO STATION PRESSURE RATIO	STATION TO STATION DELTA T ON T	STATION TO STATION EFFICIENCIES ISEN	STATION TO STATION EFFICIENCIES POLY	BLADE LOADINGS AVERAGE RADIUS	BLADE LOADINGS AXIAL	BLADE LOADINGS TANGEN
1	1,0579	,0249	,9161	,9150	,9968	0,0000	0,0000	0,0000	7,28518	697,84	-749,12
2	1,0589	,0252	,9173	,9183	,9970	,0000	**********	**********	7,56949	681,37	-757,59
3	1,0597	,0254	,9206	,9215	1,0026	-,0000	,0001	,0001	7,93407	652,88	-760,35
4	1,0593	,0253	,9212	,9221	,9976	,0000	**********	**********	8,28118	629,48	-767,82
5	1,0611	,0260	,9232	,9241	,9978	,0000	**********	**********	8,61174	611,44	-780,01
6	1,0616	,0262	,9231	,9241	,9980	,0000	**********	**********	8,85118	595,31	-783,30
7	1,0616	,0262	,9225	,9234	,9980	0,0000	0,0000	0,0000	0,00000	0,00	0,00
	1,0601	,0256	,9209	,9218	,9976	,0000	**********	**********	INTEGRATED VALUES		

INTEGRATED TOTAL TEMPS AT BLADE INLET
ABSOLUTE = 574,33 RELATIVE = 574,33

7 0 0 0 2 127,90000

WITH DIFFUSER = MACHINE EFFICIENCY = ,9209 MACHINE PRESSURE RATIO = 1,0601

THE SOLUTION ABOVE IS CONVERGED
****

Figure E-10.

```
PM4111
ROHR
CCCBS ROTOR


TIME= 14,44,5 DATE= 05/08/7
PM4111
ROHR
CCCBS ROTOR

      THICK./CHORD =  ,1600          CAMBER = 32,6300          CHORD = 1,1340          TWIST = 25,3500
      T.E. LIMIT =  0,0000

      COORDINATES -AXES AT L.E.
        XS          YS          XP          YP
    0,0000      ,0118     0,0000     -,0062
     ,0019      ,0147      ,0095     -,0114
     ,0086      ,0237      ,0196     -,0155
     ,0208      ,0355      ,0359     -,0193
     ,0465      ,0546      ,0669     -,0232
     ,0734      ,0704      ,0967     -,0246
     ,1008      ,0844      ,1260     -,0251
     ,1568      ,1081      ,1834     -,0244
     ,2140      ,1273      ,2396     -,0225
     ,3305      ,1547      ,3499     -,0177
     ,4485      ,1687      ,4587     -,0125
     ,5670      ,1683      ,5670     -,0057
     ,6846      ,1528      ,6762      ,0034
     ,8004      ,1268      ,7872      ,0102
     ,9141      ,0925      ,9003      ,0123
    1,0255      ,0509     1,0157      ,0084
    1,0803      ,0271     1,0743      ,0043
    1,1346      ,0019     1,1334     -,0019

      ROTATED COORD.-AXES AT C.G.
        XS          YS          XP          YP
    -,4360      -,2635      -,4302      -,2798
    -,4375      -,2601      -,4194      -,2805
    -,4353      -,2491      -,4084      -,2797
    -,4293      -,2332      -,3921      -,2763
    -,4142      -,2049      -,3626      -,2665
    -,3967      -,1791      -,3349      -,2550
    -,3779      -,1548      -,3083      -,2429
    -,3375      -,1098      -,2567      -,2177
    -,2940      -,0675      -,2067      -,1919
    -,2005       ,0071      -,1091      -,1403
    -,0998       ,0703      -,0130      -,0891
     ,0075       ,1206       ,0820      -,0366
     ,1204       ,1570       ,1768       ,0184
     ,2361       ,1831       ,2742       ,0720
     ,3536       ,2007       ,3755       ,1224
     ,4721       ,2108       ,4814       ,1683
     ,5318       ,2128       ,5361       ,1897
     ,5916       ,2133       ,5922       ,2094

   CIRCLE PARAMETERS
      RL          XL          YL          RR          XR          YR          XLR         YLR         XRR         YRR
    ,0201       ,0201       ,0058       ,0024      1,1317       ,0007      -,4172      -,2604       ,5896       ,2110

    MECHANICAL PROPERTIES ABOUT L.E. AXES
    AREA        ,139068          IXX        ,000308          IYY        ,009340
    IXY         ,000198          IMIN       ,000304          ANGLE OF MIN. AXIS      1,2527
```

Figure E-11.

```
DATE= 05/08/7
PM4111
ROHR
CCCBS ROTOR
     SECTION  1  RADIUS =  7,163  ROTATION =  0,0000 DEG,  NO,OF BLADES =  0,  SL,FCTR = 0,0000  TYPE  1
     SECTION ANGLE =   0,0000
     INPUT COORDINATES      COORD,ABOUT N O,      ROTATED COORD,=N O,      FINAL COORD,=N O,          THROAT
          X         Y          X         Y          X         Y          X         Y
      =,4380    =,2635     =,4284    =,2608     =,4284    =,2608     =,4284    =,2608          0,0000
      =,4375    =,2601     =,4279    =,2573     =,4279    =,2573     =,4279    =,2573          0,0000
      =,4353    =,2491     =,4257    =,2464     =,4257    =,2464     =,4257    =,2464          0,0000
      =,4293    =,2332     =,4197    =,2305     =,4197    =,2305     =,4197    =,2305          0,0000
      =,4142    =,2049     =,4046    =,2022     =,4046    =,2022     =,4046    =,2022          0,0000
      =,3967    =,1791     =,3872    =,1764     =,3872    =,1764     =,3872    =,1764          0,0000
      =,3779    =,1548     =,3684    =,1521     =,3684    =,1521     =,3684    =,1521          0,0000
      =,3375    =,1094     =,3279    =,1066     =,3279    =,1066     =,3279    =,1066          0,0000
      =,2940    =,0675     =,2844    =,0648     =,2844    =,0648     =,2844    =,0648          0,0000
      =,2005     ,0071     =,1909     ,0098     =,1909     ,0098     =,1909     ,0098          0,0000
      =,0998     ,0703     =,0902     ,0730     =,0902     ,0730     =,0902     ,0730          0,0000
       ,0075     ,1206      ,0171     ,1234      ,0171     ,1234      ,0171     ,1234          0,0000
       ,1204     ,1570      ,1300     ,1597      ,1300     ,1597      ,1300     ,1597          0,0000
       ,2361     ,1831      ,2457     ,1858      ,2457     ,1858      ,2457     ,1858          0,0000
       ,3536     ,2007      ,3632     ,2034      ,3632     ,2034      ,3632     ,2034          0,0000
       ,4721     ,2108      ,4817     ,2136      ,4817     ,2136      ,4817     ,2136          0,0000
       ,5318     ,2128      ,5414     ,2156      ,5414     ,2156      ,5414     ,2156          0,0000
       ,5916     ,2133      ,6012     ,2160      ,6012     ,2160      ,6012     ,2160          0,0000
      =,4302    =,2798     =,4206    =,2771     =,4206    =,2771     =,4206    =,2771          0,0000
      =,4194    =,2805     =,4098    =,2778     =,4098    =,2778     =,4098    =,2778          0,0000
      =,4084    =,2797     =,3988    =,2770     =,3988    =,2770     =,3988    =,2770          0,0000
      =,3921    =,2763     =,3825    =,2735     =,3825    =,2735     =,3825    =,2735          0,0000
      =,3626    =,2665     =,3530    =,2638     =,3530    =,2638     =,3530    =,2638          0,0000
      =,3349    =,2550     =,3253    =,2523     =,3253    =,2523     =,3253    =,2523          0,0000
      =,3083    =,2429     =,2987    =,2402     =,2987    =,2402     =,2987    =,2402          0,0000
      =,2567    =,2177     =,2471    =,2150     =,2471    =,2150     =,2471    =,2150          0,0000
      =,2067    =,1919     =,1971    =,1892     =,1971    =,1892     =,1971    =,1892          0,0000
      =,1091    =,1403     =,0995    =,1376     =,0995    =,1376     =,0995    =,1376          0,0000
      =,0130    =,0891     =,0034    =,0864     =,0034    =,0864     =,0034    =,0864          0,0000
       ,0820    =,0366      ,0916    =,0339      ,0916    =,0339      ,0916    =,0339          0,0000
       ,1768     ,0184      ,1863     ,0211      ,1863     ,0211      ,1863     ,0211          0,0000
       ,2742     ,0720      ,2838     ,0748      ,2838     ,0748      ,2838     ,0748          0,0000
       ,3755     ,1224      ,3851     ,1252      ,3851     ,1252      ,3851     ,1252          0,0000
       ,4814     ,1683      ,4910     ,1710      ,4910     ,1710      ,4910     ,1710          0,0000
       ,5361     ,1897      ,5457     ,1924      ,5457     ,1924      ,5457     ,1924          0,0000
       ,5922     ,2094      ,6018     ,2121      ,6018     ,2121      ,6018     ,2121          0,0000

     CIRCLE PARAMETERS      R L          X L          Y L          R R          X R          Y R
     BETA L      48,4964    ,0201       =,4076       =,2576        ,0024        ,5992        ,2137
     BETA R      99,0890     X GAGING     0,0000      Y GAGING     0,0000
     GAGING    0,000000      PITCH      0,000000     O/P        0,000000     BIN=1 O/P    0,0000
     MECHANICAL PROPERTIES ABOUT ORIGINAL AXES       TAN,ANG   26,719510     STAGGER   25,350087
     AREA         ,139084     M X        =,001334     M Y        =,000378     I X          ,007638
     I Y          ,002132     I XY        ,003661     I MIN       ,000303     I MAX        ,009453
     P Y     2659,002423      P X      742,898218     P XY   1275,412368     ALPHA     26,543599
     BAR I X      ,007626     BAR I Y     ,002131     BAR I XY    ,003658     MAX THICK    ,181457
     C MIN LE    =,078958     C MAX LE    ,631519     C MIN TE   =,068407     C MAX TE    =,479765
     Z MIN LE    =,003842     Z MAX LE    ,014968     Z MIN TE   =,004435     Z MAX TE    =,019703
     C MIN B      ,105895     C MAX B     =,042739     Z MIN B     ,002865     Z MAX B     =,221173
     BAR B        ,000473     BAR C        ,000041     BAR D       ,001437     CHORD       1,134106
     BAR X       =,009593     BAR Y       =,002718     K           ,000997     WIDTH       1,029263
```

Figure E-12.

```
TIME= 14,44,5 DATE= 05/08/7
PM0111
ROMR
CCCBS ROTOR

      THICK,/CHORD =  ,0950          CAMBER = 23,2800          CHORD = 1,0500          TWIST = 37,8900
      T,E, LIMIT =   0,0000

      COORDINATES -AXES AT L,E,                              ROTATED COORD,-AXES AT C,G,
        XS        YS        XP        YP                      XS        YS        XP        YP
     0,0000    ,0052     0,0000    -,0040                   -,3496    -,3175    -,3440    -,3248
      ,0038    ,0084      ,0087    -,0063                   -,3486    -,3127    -,3372    -,3225
      ,0109    ,0136      ,0153    -,0083                   -,3462    -,3042    -,3292    -,3188
      ,0233    ,0206      ,0292    -,0101                   -,3407    -,2911    -,3171    -,3117
      ,0485    ,0320      ,0565    -,0115                   -,3278    -,2667    -,2948    -,2960
      ,0741    ,0415      ,0834    -,0116                   -,3134    -,2434    -,2735    -,2796
      ,1000    ,0499      ,1100    -,0111                   -,2981    -,2209    -,2528    -,2629
      ,1523    ,0642      ,1627    -,0093                   -,2657    -,1775    -,2122    -,2291
      ,2049    ,0758      ,2151    -,0071                   -,2312    -,1359    -,1723    -,1952
      ,3112    ,0925      ,3188    -,0025                   -,1577    -,0575    -,0932    -,1278
      ,4180    ,1012      ,4220     ,0016                   -,0787     ,0149    -,0143    -,0613
      ,5250    ,1013      ,5250     ,0057                    ,0057     ,0807     ,0644     ,0052
      ,6317    ,0925      ,6283     ,0103                    ,0953     ,1393     ,1432     ,0723
      ,7376    ,0772      ,7324     ,0129                    ,1883     ,1923     ,2237     ,1383
      ,8427    ,0566      ,8373     ,0122                    ,2839     ,2405     ,3069     ,2022
      ,9469    ,0312      ,9431     ,0076                    ,3817     ,2845     ,3932     ,2635
      ,9987    ,0166      ,9963     ,0039                    ,4315     ,3048     ,4375     ,2933
     1,0502    ,0011     1,0498    -,0011                    ,4818     ,3242     ,4827     ,3222

     CIRCLE PARAMETERS
        RL        XL        YL        RR        XR        YR        XLR       YLR       XNR       YRR
      ,0079     ,0079     ,0016     ,0012    1,0488     ,0002    -,3412    -,3156     ,4812     ,3227

      MECHANICAL PROPERTIES ABOUT L,E, AXES
      AREA      ,070792          IXX       ,000051          IYY       ,004076
      IXY       ,000061          IMIN      ,000050          ANGLE OF MIN, AXIS        ,8725

DATE= 05/08/7
PM0111
ROMR
CCCBS ROTOR
     SECTION  2  RADIUS =  8,058  ROTATION =  0,0000 DEG,  NO,OF BLADES =  0,  BL,FCTR = 0,0000  TYPE  1
     SECTION ANGLE =   0,0000
     INPUT COORDINATES      COORD,ABOUT N D,      ROTATED COORD,-N D,      FINAL COORD,-N D,       THRUST
        X         Y           X         Y           X         Y           X         Y
     -,3496    -,3175      -,3423    -,3127      -,3423    -,3127      -,3423    -,3127        0,0000
     -,3486    -,3127      -,3413    -,3079      -,3413    -,3079      -,3413    -,3079        0,0000
     -,3462    -,3042      -,3388    -,2994      -,3388    -,2994      -,3388    -,2994        0,0000
     -,3407    -,2911      -,3334    -,2863      -,3334    -,2863      -,3334    -,2863        0,0000
     -,3278    -,2667      -,3204    -,2618      -,3204    -,2618      -,3204    -,2618        0,0000
     -,3134    -,2434      -,3060    -,2386      -,3060    -,2386      -,3060    -,2386        0,0000
     -,2981    -,2209      -,2908    -,2160      -,2908    -,2160      -,2908    -,2160        0,0000
     -,2657    -,1775      -,2583    -,1727      -,2583    -,1727      -,2583    -,1727        0,0000
     -,2312    -,1359      -,2239    -,1311      -,2239    -,1311      -,2239    -,1311        0,0000
     -,1577    -,0575      -,1503    -,0527      -,1503    -,0527      -,1503    -,0527        0,0000
     -,0787     ,0149      -,0714     ,0198      -,0714     ,0198      -,0714     ,0198        0,0000
      ,0057     ,0807       ,0130     ,0856       ,0130     ,0856       ,0130     ,0856        0,0000
      ,0953     ,1393       ,1026     ,1441       ,1026     ,1441       ,1026     ,1441        0,0000
      ,1883     ,1923       ,1956     ,1971       ,1956     ,1971       ,1956     ,1971        0,0000
      ,2839     ,2405       ,2913     ,2454       ,2913     ,2454       ,2913     ,2454        0,0000
      ,3817     ,2845       ,3891     ,2894       ,3891     ,2894       ,3891     ,2894        0,0000
      ,4315     ,3048       ,4389     ,3096       ,4389     ,3096       ,4389     ,3096        0,0000
      ,4818     ,3242       ,4891     ,3290       ,4891     ,3290       ,4891     ,3290        0,0000
     -,3440    -,3248      -,3366    -,3200      -,3366    -,3200      -,3366    -,3200        0,0000
     -,3372    -,3225      -,3299    -,3176      -,3299    -,3176      -,3299    -,3176        0,0000
     -,3292    -,3188      -,3219    -,3140      -,3219    -,3140      -,3219    -,3140        0,0000
     -,3171    -,3117      -,3098    -,3068      -,3098    -,3068      -,3098    -,3068        0,0000
     -,2948    -,2960      -,2874    -,2912      -,2874    -,2912      -,2874    -,2912        0,0000
     -,2735    -,2796      -,2662    -,2747      -,2662    -,2747      -,2662    -,2747        0,0000
     -,2528    -,2629      -,2455    -,2580      -,2455    -,2580      -,2455    -,2580        0,0000
     -,2122    -,2291      -,2049    -,2242      -,2049    -,2242      -,2049    -,2242        0,0000
     -,1723    -,1952      -,1650    -,1903      -,1650    -,1903      -,1650    -,1903        0,0000
     -,0932    -,1278      -,0859    -,1230      -,0859    -,1230      -,0859    -,1230        0,0000
     -,0143    -,0613      -,0070    -,0564      -,0070    -,0564      -,0070    -,0564        0,0000
      ,0644     ,0052       ,0718     ,0101       ,0718     ,0101       ,0718     ,0101        0,0000
      ,1432     ,0723       ,1505     ,0772       ,1505     ,0772       ,1505     ,0772        0,0000
      ,2237     ,1383       ,2310     ,1431       ,2310     ,1431       ,2310     ,1431        0,0000
      ,3069     ,2022       ,3142     ,2070       ,3142     ,2070       ,3142     ,2070        0,0000
      ,3932     ,2635       ,4005     ,2683       ,4005     ,2683       ,4005     ,2683        0,0000
      ,4375     ,2933       ,4448     ,2981       ,4448     ,2981       ,4448     ,2981        0,0000
      ,4827     ,3222       ,4901     ,3270       ,4901     ,3270       ,4901     ,3270        0,0000
```

Figure E-13.

CIRCLE PARAMETERS		R L		X L		Y L		R R		X R		Y R
BETA L	40,7135	,0079		-,3338		-,3107		,0012		,4885		,3275
BETA R	116,2633	X GAGING		0,0000		Y GAGING		0,0000				
GAGING	0,000000	PITCH		0,000000		D/P		0,000000		BIN=1 D/P		0,0000
MECHANICAL PROPERTIES ABOUT ORIGINAL AXES						TAN,ANG		38,518628		STAGGER		37,884956
AREA	,070500	M X		-,000517		M Y		-,000341		I X		,002507
I Y	,001635	I XY		,001974		I MIN		,000050		I MAX		,004087
P Y	12319,001942	P X		8035,809961		P XY		9699,097067		ALPHA		38,774328
BAR I X	,002504	BAR I Y		,001633		BAR I XY		,001971		MAX THICK		,099761
C MIN LE	-,051820	C MAX LE		,585940		C MIN TE		-,041044		C MAX TE		-,454861
Z MIN LE	-,000960	Z MAX LE		,006975		Z MIN TE		-,001212		Z MAX TE		-,008985
C MIN B	,060348	C MAX B		-,037805		Z MIN B		,000824		Z MAX B		-,108104
BAR B	,000172	BAR C		,000071		BAR D		,000524		CHORD		1,050026
BAR X	-,007339	BAR Y		-,004837		K		,000155		WIDTH		,831424

```
TIME= 14,44,5 DATE= 05/08/7
PM4111
ROMR
CCCBB ROTOW
```

THICK,/CHORD = ,0300 CAMBER = 17,0900 CHORD = ,9720 TWIST = 46,6700
T,E, LIMIT = 0,0000

COORDINATES -AXES AT L,E,				ROTATED COORD,-AXES AT C,G,			
XS	YS	XP	YP	XS	YS	XP	YP
0,0000	,0014	0,0000	-,0013	-,2798	-,3353	-,2779	-,3371
,0045	,0029	,0052	-,0014	-,2778	-,3310	-,2742	-,3335
,0117	,0050	,0126	-,0014	-,2745	-,3243	-,2691	-,3281
,0237	,0081	,0249	-,0010	-,2685	-,3135	-,2610	-,3188
,0477	,0133	,0495	,0005	-,2558	-,2924	-,2453	-,2999
,0719	,0179	,0739	,0023	-,2425	-,2716	-,2298	-,2809
,0961	,0221	,0983	,0042	-,2290	-,2512	-,2144	-,2619
,1447	,0294	,1469	,0078	-,2009	-,2109	-,1837	-,2240
,1933	,0354	,1955	,0111	-,1720	-,1713	-,1528	-,1864
,2908	,0444	,2924	,0166	-,1116	-,0942	-,0903	-,1121
,3884	,0494	,3892	,0203	-,0483	-,0198	-,0265	-,0392
,4860	,0503	,4860	,0223	,0181	,0518	,0384	,0326
,5836	,0469	,5828	,0228	,0875	,1204	,1045	,1034
,6810	,0399	,6798	,0211	,1594	,1865	,1723	,1728
,7782	,0298	,7770	,0168	,2335	,2502	,2421	,2405
,8752	,0166	,8744	,0096	,3097	,3118	,3141	,3064
,9237	,0088	,9231	,0051	,3486	,3417	,3509	,3387
,9720	,0003	,9720	-,0003	,3879	,3710	,3883	,3705

CIRCLE PARAMETERS									
RL	XL	YL	RR	XR	YR	XLR	YLR	XRR	YRR
,0016	,0016	,0002	,0003	,9717	,0000	-,2779	-,3349	,3879	,3706

MECHANICAL PROPERTIES ABOUT L,E, AXES

AREA	,019157	IXX	,000002	IYY	,000945
IXY	,000010	I-IN	,000002	ANGLE OF MIN, AXIS	,6332

Figure E-14.

```
DATE= 05/08/7
PM4111
ROHR
CCCBS ROTOR
     SECTION  3  RADIUS =  8,954  ROTATION =  0,0000 DEG,  NO,OF BLADES =  0,  SL,FCTR = 0,0000  TYPE  1
     SECTION ANGLE =  0,0000
     INPUT COORDINATES      COORD,ABOUT N O,      ROTATED COORD,=N O,      FINAL COORD,=N O,          THROAT
        X          Y           X          Y          X          Y          X          Y
     =,2798     =,3353      =,2741     =,3298     =,2741     =,3298     =,2741     =,3298          0,0000
     =,2778     =,3310      =,2721     =,3254     =,2721     =,3254     =,2721     =,3254          0,0000
     =,2745     =,3243      =,2688     =,3187     =,2688     =,3187     =,2688     =,3187          0,0000
     =,2685     =,3135      =,2628     =,3079     =,2628     =,3079     =,2628     =,3079          0,0000
     =,2558     =,2924      =,2501     =,2868     =,2501     =,2868     =,2501     =,2868          0,0000
     =,2425     =,2716      =,2368     =,2661     =,2368     =,2661     =,2368     =,2661          0,0000
     =,2290     =,2512      =,2232     =,2456     =,2232     =,2456     =,2232     =,2456          0,0000
     =,2009     =,2109      =,1952     =,2053     =,1952     =,2053     =,1952     =,2053          0,0000
     =,1720     =,1713      =,1663     =,1657     =,1663     =,1657     =,1663     =,1657          0,0000
     =,1116     =,0942      =,1059     =,0887     =,1059     =,0887     =,1059     =,0887          0,0000
     =,0483     =,0198      =,0426     =,0143     =,0426     =,0143     =,0426     =,0143          0,0000
      ,0181      ,0518       ,0238      ,0574      ,0238      ,0574      ,0238      ,0574          0,0000
      ,0875      ,1204       ,0932      ,1260      ,0932      ,1260      ,0932      ,1260          0,0000
      ,1594      ,1865       ,1651      ,1921      ,1651      ,1921      ,1651      ,1921          0,0000
      ,2335      ,2502       ,2392      ,2558      ,2392      ,2558      ,2392      ,2558          0,0000
      ,3097      ,3118       ,3154      ,3173      ,3154      ,3173      ,3154      ,3173          0,0000
      ,3486      ,3417       ,3543      ,3472      ,3543      ,3472      ,3543      ,3472          0,0000
      ,3879      ,3710       ,3936      ,3766      ,3936      ,3766      ,3936      ,3766          0,0000
     =,2779     =,3371      =,2722     =,3316     =,2722     =,3316     =,2722     =,3316          0,0000
     =,2742     =,3335      =,2685     =,3279     =,2685     =,3279     =,2685     =,3279          0,0000
     =,2691     =,3281      =,2634     =,3225     =,2634     =,3225     =,2634     =,3225          0,0000
     =,2610     =,3188      =,2553     =,3132     =,2553     =,3132     =,2553     =,3132          0,0000
     =,2453     =,2999      =,2396     =,2943     =,2396     =,2943     =,2396     =,2943          0,0000
     =,2298     =,2809      =,2241     =,2753     =,2241     =,2753     =,2241     =,2753          0,0000
     =,2144     =,2619      =,2087     =,2563     =,2087     =,2563     =,2087     =,2563          0,0000
     =,1837     =,2240      =,1780     =,2185     =,1780     =,2185     =,1780     =,2185          0,0000
     =,1528     =,1864      =,1471     =,1808     =,1471     =,1808     =,1471     =,1808          0,0000
     =,0903     =,1121      =,0846     =,1066     =,0846     =,1066     =,0846     =,1066          0,0000
     =,0265     =,0392      =,0208     =,0336     =,0208     =,0336     =,0208     =,0336          0,0000
      ,0384      ,0326       ,0441      ,0382      ,0441      ,0382      ,0441      ,0382          0,0000
      ,1045      ,1034       ,1102      ,1090      ,1102      ,1090      ,1102      ,1090          0,0000
      ,1723      ,1728       ,1780      ,1783      ,1780      ,1783      ,1780      ,1783          0,0000
      ,2421      ,2405       ,2478      ,2460      ,2478      ,2460      ,2478      ,2460          0,0000
      ,3141      ,3064       ,3198      ,3120      ,3198      ,3120      ,3198      ,3120          0,0000
      ,3509      ,3387       ,3566      ,3443      ,3566      ,3443      ,3566      ,3443          0,0000
      ,3883      ,3705       ,3940      ,3761      ,3940      ,3761      ,3940      ,3761          0,0000

     CIRCLE PARAMETERS      R L          X L          Y L          R R          X R          Y R
     BETA L     34,8886     ,0016       =,2722       =,3294       ,0003        ,3936        ,3762
     BETA R    128,1203       X GAGING     0,0000     Y GAGING     0,0000
     GAGING     0,000000      PITCH       0,000000   O/P          0,000000     SIN=1 O/P    0,0000
     MECHANICAL PROPERTIES ABOUT ORIGINAL AXES       TAN,ANG   46,740382     STAGGER   46,669956
     AREA       ,019039       M X         =,000109   M Y         =,000106     I X          ,000435
     I Y        ,000512       I XY        ,000470    I MIN       ,000002      I MAX        ,000944
     F Y  210613,341259       F X  247696,409008     F XY 227340,276719       ALPHA     47,331311
     BAR I X    ,000435       BAR I Y     ,000511    BAR I XY    ,000469      MAX THICK    ,029163
     C MIN LE  =,034778       C MAX LE    ,543335    C MIN TE   =,024637      C MAX TE  =,426695
     Z MIN LE  =,000063       Z MAX LE    ,001737    Z MIN TE   =,000089      Z MAX TE  =,002211
     C MIN B    ,021860       C MAX B    =,034329    Z MIN B     ,000100      Z MAX B   =,027488
     BAR B      ,000032       BAR C       ,000023    BAR D       ,000103      CHORD        ,972004
     BAR X     =,005703       BAR Y      =,005570    K           ,000004      WIDTH        ,667724
```

Figure E-15.

```
PM4111
RUNR
CCCBS STATOR


TIME= 16.20.3 DATE= 05/08/7
PM4111
RUNR
CCCBS STATOR

      THICK./CHORD =  .1000          CAMBER = 23.5000          CHORD = 1.0940          TWIST = 41.0900
      T.E. LIMIT =   0.0000

      COORDINATES -AXES AT L.E.                                ROTATED COORD.-AXES AT C.G.
        XS          YS          XP          YP                  XS          YS          XP          YP
    0.0000      .0058     0.0000     -.0043                  -.3452      -.3507      -.3385      -.3583
     .0038      .0092      .0071     -.0069                  -.3445      -.3456      -.3315      -.3556
     .0112      .0148      .0161     -.0092                  -.3427      -.3365      -.3232      -.3514
     .0240      .0224      .0307     -.0113                  -.3380      -.3224      -.3109      -.3434
     .0503      .0346      .0591     -.0130                  -.3262      -.2960      -.2882      -.3260
     .0769      .0448      .0872     -.0133                  -.3128      -.2707      -.2669      -.3078
     .1039      .0538      .1149     -.0130                  -.2985      -.2462      -.2462      -.2894
     .1563      .0692      .1699     -.0115                  -.2675      -.1989      -.2058      -.2520
     .2132      .0816      .2244     -.0093                  -.2343      -.1534      -.1661      -.2146
     .3239      .0995      .3325     -.0047                  -.1626      -.0672      -.0877      -.1401
     .4354      .1087      .4398     -.0006                  -.0847       .0130      -.0095      -.0665
     .5470      .1087      .5470      .0038                  -.0006       .0804       .0684       .0073
     .6582      .0991      .6546      .0090                   .0896       .1523       .1461       .0819
     .7687      .0826      .7629      .0121                   .1837       .2124       .2257       .1555
     .8782      .0605      .8722      .0118                   .2807       .2677       .3082       .2271
     .9867      .0334      .9825      .0074                   .3804       .3186       .3942       .2963
    1.0906      .0178     1.0880      .0038                   .4312       .3423       .4384       .3300
    1.0942      .0012     1.0938     -.0012                   .4826       .3650       .4837       .3629

    CIRCLE PARAMETERS
      -L          XL          YL          RR          XR          YR          XLR         YLR         XRR         YRR
     .0349       .0089       .0018       .0013     1.0927      .0003      -.3359       .3479       .4820       .3633

      MECHANICAL PROPERTIES ABOUT L.E. AXES
      AREA      .080994          IXX       .000069          IYY       .005056
      IXY       .000077          IMIN      .000067          ANGLE OF MIN. AXIS        .8818
```

Figure E-16.

```
DATE= 05/08/7
PN4111
ROMR
CCC8S STATOR
     SECTION  1  RADIUS =  7,183  ROTATION =  0,0000 DEG,  NO,OF BLADES =  0,  SL,FCTR = 0,0000  TYPE  1
     SECTION ANGLE =   0,0000
     INPUT COORDINATES      COORD,ABOUT N O,      ROTATED COORD,-N O,     FINAL COORD,-N O,        THROAT
        X         Y           X         Y           X         Y           X         Y
     -,3452    -,3507      -,3378    -,3453      -,3378    -,3453      -,3378    -,3453          0,0000
     -,3445    -,3456      -,3371    -,3402      -,3371    -,3402      -,3371    -,3402          0,0000
     -,3427    -,3365      -,3353    -,3311      -,3353    -,3311      -,3353    -,3311          0,0000
     -,3380    -,3224      -,3306    -,3170      -,3306    -,3170      -,3306    -,3170          0,0000
     -,3262    -,2960      -,3188    -,2905      -,3188    -,2905      -,3188    -,2905          0,0000
     -,3128    -,2707      -,3054    -,2653      -,3054    -,2653      -,3054    -,2653          0,0000
     -,2985    -,2462      -,2911    -,2408      -,2911    -,2408      -,2911    -,2408          0,0000
     -,2675    -,1989      -,2601    -,1935      -,2601    -,1935      -,2601    -,1935          0,0000
     -,2343    -,1534      -,2270    -,1480      -,2270    -,1480      -,2270    -,1480          0,0000
     -,1626    -,0672      -,1552    -,0618      -,1552    -,0618      -,1552    -,0618          0,0000
     -,0847     ,0130      -,0773     ,0184      -,0773     ,0184      -,0773     ,0184          0,0000
     -,0068     ,0864       ,0068     ,0918       ,0068     ,0918       ,0068     ,0918          0,0000
      ,0896     ,1523       ,0970     ,1577       ,0970     ,1577       ,0970     ,1577          0,0000
      ,1837     ,2124       ,1910     ,2179       ,1910     ,2179       ,1910     ,2179          0,0000
      ,2807     ,2677       ,2881     ,2731       ,2881     ,2731       ,2881     ,2731          0,0000
      ,3804     ,3186       ,3878     ,3240       ,3878     ,3240       ,3878     ,3240          0,0000
      ,4312     ,3423       ,4386     ,3477       ,4386     ,3477       ,4386     ,3477          0,0000
      ,4826     ,3650       ,4899     ,3704       ,4899     ,3704       ,4899     ,3704          0,0000
     -,3385    -,3583      -,3311    -,3529      -,3311    -,3529      -,3311    -,3529          0,0000
     -,3315    -,3556      -,3241    -,3502      -,3241    -,3502      -,3241    -,3502          0,0000
     -,3232    -,3514      -,3158    -,3460      -,3158    -,3460      -,3158    -,3460          0,0000
     -,3109    -,3434      -,3035    -,3380      -,3035    -,3380      -,3035    -,3380          0,0000
     -,2882    -,3260      -,2809    -,3206      -,2809    -,3206      -,2809    -,3206          0,0000
     -,2669    -,3078      -,2595    -,3024      -,2595    -,3024      -,2595    -,3024          0,0000
     -,2462    -,2894      -,2388    -,2839      -,2388    -,2839      -,2388    -,2839          0,0000
     -,2058    -,2520      -,1984    -,2466      -,1984    -,2466      -,1984    -,2466          0,0000
     -,1661    -,2146      -,1587    -,2092      -,1587    -,2092      -,1587    -,2092          0,0000
     -,0877    -,1401      -,0803    -,1347      -,0803    -,1347      -,0803    -,1347          0,0000
     -,0095    -,0665      -,0021    -,0610      -,0021    -,0610      -,0021    -,0610          0,0000
      ,0684     ,0073       ,0758     ,0128       ,0758     ,0128       ,0756     ,0128          0,0000
      ,1461     ,0819       ,1534     ,0873       ,1534     ,0873       ,1534     ,0873          0,0000
      ,2257     ,1555       ,2331     ,1609       ,2331     ,1609       ,2331     ,1609          0,0000
      ,3082     ,2271       ,3156     ,2325       ,3156     ,2325       ,3156     ,2325          0,0000
      ,3942     ,2963       ,4016     ,3017       ,4016     ,3017       ,4016     ,3017          0,0000
      ,4384     ,3300       ,4458     ,3354       ,4458     ,3354       ,4458     ,3354          0,0000
      ,4837     ,3629       ,4911     ,3683       ,4911     ,3683       ,4911     ,3683          0,0000

     CIRCLE PARAMETERS       R L          X L          Y L          R R          X R          Y R
     BETA L      37,3181     ,0089      -,3285      -,3424       ,0013       ,4894       ,3687
     BETA R     119,3529       X GAGING    0,0000      Y GAGING    0,0000
     GAGING      0,000000      PITCH       0,000000    O/P         0,000000    SIN-1 O/P   0,0000
     MECHANICAL PROPERTIES ABOUT ORIGINAL AXES        TAN,ANG  41,792062      STAGGER  41,089955
     AREA        ,080576       M X        -,000596     M Y        -,000439     I X         ,002837
     I Y         ,002308       I XY       ,002491      I MIN       ,000067     I MAX       ,005071
     P Y     8306,661359       P X     6762,827632     P XY    7296,834596     ALPHA    41,980623
     BAR I X     ,002832       BAR I Y    ,002306      BAR I XY    ,002488     MAX THICK   ,109415
     C MIN LE   -,054559       C MAX LE    ,610428     C MIN TE   -,043678     C MAX TE   -,473251
     Z MIN LE   -,001232       Z MAX LE    ,008308     Z MIN TE   -,001539     Z MAX TE   -,010716
     C MIN B     ,065698       C MAX B    -,038962     Z MIN B     ,001023     Z MAX B    -,130156
     BAR B       ,000218       BAR C       ,000104     BAR D       ,000706     CHORD      1,094029
     BAR X      -,007391       BAR Y      -,005443     K           ,000213     WIDTH       ,828079
```

Figure E-17.

```
TIME= 16.2..3 DATE= 05/08/7
PHW111
ROHR
CCCRS STATOR

      THICK./CHORD =  .1000          CAMBER = 23.5000          CHORD = 1.0940          TWIST = 37.7800
      T.E. LIMIT =  0.0000

      COORDINATES =AXES AT L.E.                                  ROTATED COORD.=AXES AT C.G.
        XS        YS        XP        YP                        XS        YS        XP        YP
    0.0000      .0056   0.0000    =.0043                      =.3649    =.3302    =.3587    =.3382
      .0038     .0092     .0071   =.0069                      =.3639    =.3252    =.3514    =.3359
      .0112     .0148     .0161   =.0092                      =.3615    =.3162    =.3429    =.3322
      .0240     .0224     .0307   =.0113                      =.3560    =.3024    =.3302    =.3249
      .0503     .0346     .0591   =.0130                      =.3428    =.2786    =.3066    =.3086
      .0769     .0448     .0872   =.0133                      =.3279    =.2522    =.2843    =.2919
      .1039     .0538     .1149   =.0130                      =.3122    =.2280    =.2625    =.2747
      .1583     .0692     .1699   =.0115                      =.2788    =.1831    =.2200    =.2397
      .2132     .0816     .2244   =.0093                      =.2428    =.1396    =.1762    =.2047
      .3239     .0995     .3325   =.0047                      =.1662    =.0577    =.0956    =.1349
      .4354     .1087     .4398   =.0006                      =.0838    .0179     =.0133    =.0658
      .5470     .1087     .5470    .0038                       .0044    .0863     .0687     .0034
      .6582     .0991     .6546    .0090                       .0982    .1468     .1505     .0733
      .7687     .0826     .7629    .0121                       .1956    .2015     .2343     .1422
      .8782     .0605     .8722    .0118                       .2957    .2510     .3208     .2089
      .9867     .0334     .9825    .0074                       .3981    .2961     .4106     .2730
    1.0906      .0178   1.0380     .0038                       .4503    .3168     .4568     .3041
    1.0962      .0012   1.0938    =.0012                       .5028    .3365     .5039     .3344

    CIRCLE PARAMETERS
       WL        XL        YL        RR        XR        YR        XLR       YLR       XRR       YRR
      .0089     .0089     .0018     .0013    1.0927     .0003    =.3554    =.3279     .5022     .3349

      MECHANICAL PROPERTIES ABOUT L.E. AXES
      AREA      .080894          IXX       .000069          IYY       .005056
      IXY       .000077          IMIN      .000067          ANGLE OF MIN. AXIS          .8818


DATE= 05/08/7
PHW111
ROHR
CCCRS STATOR
      SECTION  2  RADIUS =  8.058  ROTATION =  0.0000 DEG.  NO.OF BLADES =  0.  SL.FCTR = 0.0000  TYPE  1
      SECTION ANGLE =   0.0000
      INPUT COORDINATES      COORD.ABOUT N.A.        ROTATED COORD.=N.A.       FINAL COORD.=N.A.          THROAT
         X         Y          X         Y             X         Y             X         Y
       =.3649    =.3302     =.3572    =.3252        =.3572    =.3252        =.3572    =.3252          0.0000
       =.3639    =.3252     =.3562    =.3202        =.3562    =.3202        =.3562    =.3202          0.0000
       =.3615    =.3162     =.3538    =.3112        =.3538    =.3112        =.3538    =.3112          0.0000
       =.3560    =.3024     =.3483    =.2974        =.3483    =.2974        =.3483    =.2974          0.0000
       =.3428    =.2786     =.3351    =.2716        =.3351    =.2716        =.3351    =.2716          0.0000
       =.3279    =.2522     =.3203    =.2472        =.3203    =.2472        =.3203    =.2472          0.0000
       =.3122    =.2286     =.3045    =.2236        =.3045    =.2236        =.3045    =.2236          0.0000
       =.2788    =.1831     =.2709    =.1781        =.2709    =.1781        =.2709    =.1781          0.0000
       =.2428    =.1396     =.2351    =.1346        =.2351    =.1346        =.2351    =.1346          0.0000
       =.1662    =.0577     =.1585    =.0527        =.1585    =.0527        =.1585    =.0527          0.0000
       =.0838     .0179     =.0761     .0229        =.0761     .0229        =.0761     .0229          0.0000
        .0044     .0863      .0121     .0913         .0121     .0913         .0121     .0913          0.0000
        .0982     .1468      .1059     .1519         .1059     .1519         .1059     .1519          0.0000
        .1956     .2015      .2033     .2065         .2033     .2065         .2033     .2065          0.0000
        .2957     .2510      .3034     .2560         .3034     .2560         .3034     .2560          0.0000
        .3981     .2961      .4058     .3011         .4058     .3011         .4058     .3011          0.0000
        .4503     .3168      .4579     .3218         .4579     .3218         .4579     .3218          0.0000
        .5028     .3365      .5105     .3415         .5105     .3415         .5105     .3415          0.0000
       =.3587    =.3382     =.3510    =.3332        =.3510    =.3332        =.3510    =.3332          0.0000
       =.3514    =.3359     =.3438    =.3309        =.3438    =.3309        =.3438    =.3309          0.0000
       =.3429    =.3322     =.3352    =.3272        =.3352    =.3272        =.3352    =.3272          0.0000
       =.3302    =.3249     =.3225    =.3199        =.3225    =.3199        =.3225    =.3199          0.0000
       =.3066    =.3088     =.2989    =.3038        =.2989    =.3038        =.2989    =.3038          0.0000
       =.2843    =.2919     =.2766    =.2869        =.2766    =.2869        =.2766    =.2869          0.0000
       =.2625    =.2747     =.2548    =.2697        =.2548    =.2697        =.2548    =.2697          0.0000
       =.2200    =.2397     =.2123    =.2347        =.2123    =.2347        =.2123    =.2347          0.0000
       =.1782    =.2047     =.1706    =.1997        =.1706    =.1997        =.1706    =.1997          0.0000
       =.0956    =.1349     =.0880    =.1298        =.0880    =.1298        =.0880    =.1298          0.0000
       =.0133    =.0658     =.0056    =.0608        =.0056    =.0608        =.0056    =.0608          0.0000
        .0687     .0034      .0764     .0084         .0764     .0084         .0764     .0084          0.0000
        .1505     .0733      .1582     .0783         .1582     .0783         .1582     .0783          0.0000
        .2343     .1422      .2420     .1472         .2420     .1472         .2420     .1472          0.0000
        .3208     .2089      .3285     .2139         .3285     .2139         .3285     .2139          0.0000
        .4106     .2730      .4183     .2780         .4183     .2780         .4183     .2780          0.0000
        .4568     .3041      .4644     .3091         .4644     .3091         .4644     .3091          0.0000
        .5039     .3344      .5116     .3394         .5116     .3394         .5116     .3394          0.0000
```

Figure E-18.

CIRCLE PARAMETERS	R L	X L	Y L	R R	X R	Y R
BETA L 40,6917	,0089	=,3477	=,3229	,0013	,5098	,3599
BETA R 116,0449	X GAGING 0,0000		Y GAGING 0,0000			
GAGING 0,000000	PITCH 0,000000		O/P 0,000000		BIN=1 O/P 0,0000	
MECHANICAL PROPERTIES ABOUT ORIGINAL AXES			TAN,ANG 38,482056		STAGGER 37,779956	
AREA ,080568	M X =,000619		M Y =,000403		I X ,003122	
I Y ,002023	I XY ,002444		I MIN ,000067		I MAX ,005071	
P Y 9145,222491	P X 5928,352758		P XY 7161,185566		ALPHA 38,670569	
BAR I X ,003117	BAR I Y ,002021		BAR I XY ,002441		MAX THICK ,109413	
C MIN LE =,054554	C MAX LE ,610418		C MIN TE =,043674		C MAX TE =,473258	
Z MIN LE =,001232	Z MAX LE ,008307		Z MIN TE =,001539		Z MAX TE =,010714	
C MIN B ,065690	C MAX B =,039354		Z MIN B ,001023		Z MAX B =,128847	
BAR B ,000222	BAR C ,000091		BAR D ,000706		CHORD 1,094029	
BAR X =,007683	BAR Y =,005005		K ,000213		WIDTH ,867776	

TIME= 16,20,3 DATE= 05/08/7
PH4111
ROHR
CCCBS STATOR

THICK,/CHORD = ,1000 CAMBER = 23,5000 CHORD = 1,0940 TWIST = 34,9100
T,E, LIMIT = 0,0000

COORDINATES =AXES AT L,E,				ROTATED COORD,=AXES AT C,G,			
XS	YS	XP	YP	XS	YS	XP	YP
0,0000	,0058	0,0000	=,0043	=,3809	=,3115	=,3751	=,3198
,0038	,0092	,0071	=,0069	=,3797	=,3065	=,3678	=,3179
,0112	,0148	,0181	=,0092	=,3769	=,2977	=,3591	=,3146
,0240	,0224	,0307	=,0113	=,3707	=,2842	=,3460	=,3080
,0503	,0346	,0591	=,0130	=,3562	=,2591	=,3217	=,2931
,0769	,0448	,0872	=,0133	=,3402	=,2355	=,2985	=,2773
,1039	,0538	,1149	=,0130	=,3232	=,2127	=,2759	=,2612
,1583	,0692	,1699	=,0115	=,2874	=,1689	=,2317	=,2284
,2132	,0816	,2244	=,0093	=,2495	=,1273	=,1883	=,1955
,3239	,0995	,3325	=,0047	=,1689	=,0493	=,1023	=,1299
,4354	,1087	,4398	=,0006	=,0828	,0220	=,0166	=,0650
,5470	,1087	,5470	,0038	,0087	,0860	,0688	=,0001
,6582	,0991	,6546	,0090	,1054	,1417	,1540	,0657
,7687	,0826	,7629	,0121	,2055	,1914	,2411	,1303
,8782	,0605	,8722	,0118	,3079	,2359	,3309	,1926
,9867	,0334	,9825	,0074	,4125	,2758	,4238	,2521
1,0406	,0178	1,0380	,0038	,4656	,2938	,4714	,2809
1,0942	,0012	1,0938	=,0012	,5190	,3109	,5200	,3087

CIRCLE PARAMETERS							
RL	XL	YL	RR	XR	YR	XLR	YLR	XRR	YRR
,0089	,0089	,0018	,0013	1,0927	,0003	=,3714	=,3097	,5183	,3093

MECHANICAL PROPERTIES ABOUT L,E, AXES

AREA	,080894	IXX	,000069	IYY	,005056
IXY	,000077	IMIN	,000067	ANGLE OF MIN, AXIS	,8818

Figure I-19.

```
DATE= 05/08/7
PM4111
ROHR
CCCRS STATION
     SECTION  3  RADIUS =  6,950  ROTATION =  0,0000 DEG,  NO,OF BLADES =  0,  SL,FCTR = 0,0000  TYPE  1
     SECTION ANGLE =  0,0000
     INPUT COORDINATES      COORD,ABOUT P O,      ROTATED COORD,PO,      FINAL COORD,PO,          THKRAT
        X         Y          X         Y           X         Y          X         Y
     -,3809    -,3115     -,3730    -,3069      -,3730    -,3069     -,3730    -,3069          0,0000
     -,3797    -,3065     -,3718    -,3019      -,3718    -,3019     -,3718    -,3019          0,0000
     -,3769    -,2977     -,3690    -,2930      -,3690    -,2930     -,3690    -,2930          0,0000
     -,3707    -,2842     -,3628    -,2796      -,3628    -,2796     -,3628    -,2796          0,0000
     -,3562    -,2591     -,3483    -,2545      -,3483    -,2545     -,3483    -,2545          0,0000
     -,3402    -,2355     -,3322    -,2309      -,3322    -,2309     -,3322    -,2309          0,0000
     -,3233    -,2127     -,3153    -,2081      -,3153    -,2081     -,3153    -,2081          0,0000
     -,2874    -,1689     -,2795    -,1643      -,2795    -,1643     -,2795    -,1643          0,0000
     -,2495    -,1273     -,2416    -,1227      -,2416    -,1227     -,2416    -,1227          0,0000
     -,1689    -,0493     -,1610    -,0447      -,1610    -,0447     -,1610    -,0447          0,0000
     -,0829     ,0220     -,0749     ,0267      -,0749     ,0267     -,0749     ,0267          0,0000
      ,0087     ,0860      ,0166     ,0906       ,0166     ,0906      ,0166     ,0906          0,0000
      ,1054     ,1417      ,1133     ,1464       ,1133     ,1464      ,1133     ,1464          0,0000
      ,2055     ,1914      ,2134     ,1960       ,2134     ,1960      ,2134     ,1960          0,0000
      ,3074     ,2359      ,3159     ,2405       ,3159     ,2405      ,3159     ,2405          0,0000
      ,4125     ,2758      ,4204     ,2804       ,4204     ,2804      ,4204     ,2804          0,0000
      ,4656     ,2938      ,4735     ,2985       ,4735     ,2985      ,4735     ,2985          0,0000
      ,5191     ,3109      ,5270     ,3155       ,5270     ,3155      ,5270     ,3155          0,0000
     -,3751    -,3198     -,3672    -,3152      -,3672    -,3152     -,3672    -,3152          0,0000
     -,3674    -,3179     -,3599    -,3132      -,3599    -,3132     -,3599    -,3132          0,0000
     -,3591    -,3146     -,3512    -,3100      -,3512    -,3100     -,3512    -,3100          0,0000
     -,3460    -,3080     -,3381    -,3033      -,3381    -,3033     -,3381    -,3033          0,0000
     -,3217    -,2931     -,3137    -,2885      -,3137    -,2885     -,3137    -,2885          0,0000
     -,2985    -,2773     -,2906    -,2727      -,2906    -,2727     -,2906    -,2727          0,0000
     -,2759    -,2612     -,2680    -,2566      -,2680    -,2566     -,2680    -,2566          0,0000
     -,2317    -,2284     -,2238    -,2238      -,2238    -,2238     -,2238    -,2238          0,0000
     -,1883    -,1955     -,1804    -,1909      -,1804    -,1909     -,1804    -,1909          0,0000
     -,1023    -,1299     -,0943    -,1253      -,0943    -,1253     -,0943    -,1253          0,0000
     -,0166    -,0650     -,0087    -,0604      -,0087    -,0604     -,0087    -,0604          0,0000
      ,0689    -,0001      ,0767     ,0045       ,0767     ,0045      ,0767     ,0045          0,0000
      ,1540     ,0657      ,1619     ,0703       ,1619     ,0703      ,1619     ,0703          0,0000
      ,2411     ,1303      ,2490     ,1349       ,2490     ,1349      ,2490     ,1349          0,0000
      ,3309     ,1926      ,3388     ,1972       ,3388     ,1972      ,3388     ,1972          0,0000
      ,4238     ,2521      ,4317     ,2567       ,4317     ,2567      ,4317     ,2567          0,0000
      ,4714     ,2809      ,4793     ,2855       ,4793     ,2855      ,4793     ,2855          0,0000
      ,5200     ,3087      ,5279     ,3133       ,5279     ,3133      ,5279     ,3133          0,0000

CIRCLE PARAMETERS        R L          X L          Y L          R R          X R          Y R
BETA L      43,6031      ,0089       -,3635       -,3051        ,0013        ,5262        ,3139
BETA R     113,1764        X GAGING    0,0000       Y GAGING     0,0000
GAGING      0,000000       PITCH       0,000000     O/P          0,000000     SIN=1 O/P    0,0000
MECHANICAL PROPERTIES ABOUT ORIGINAL AXES          TAN,ANG     35,612052     STAGGER     34,909959
AREA         ,080563       M X         -,000038     M Y          -,000372     I X          ,003363
I Y          ,001781       I XY        ,002377      I MIN        ,000067      I MAX        ,005070
P Y      9855,467865       P X      5221,278679     P XY      6965,882051     ALPHA       35,800534
BAR I X      ,003358       BAR I Y     ,001779      BAR I XY     ,002374      MAX THICK    ,109411
C MIN LE    -,054550       C MAX LE    ,610412      C MIN TE    -,043672      C MAX TE    -,473263
Z MIN LE    -,001232       Z MAX LE    ,008306      Z MIN TE    -,001539      Z MAX TE    -,014714
C MIN B      ,065679       C MAX B     -,039751     Z MIN B      ,001023      Z MAX B     -,127552
BAR B        ,000226       BAR C       ,000080      BAR D        ,000706      CHORD       1,094029
BAR X       -,007917       BAR Y       -,004613     K            ,000213      WIDTH        ,899886
```

Figure E-20.

DISTRIBUTION LIST

M. K. Ellingsworth (3)
Scientific Officer
Office of Naval Research
Code 473
800 N. Quincy Street
Arlington, VA 22217

Commander, Defense Contract Admin. (1)
Services District, Hartford
96 Murphy Road
Hartford, CT 06114

Director, Naval Research Lab. (6)
Attn: 2627
Washington, DC 20375

Office of Naval Research (6)
Department of the Navy
Attn: Code 102 IP
Arlington, VA 22217

Commanding Officer (1)
Office of Naval Research Branch Office
495 Summer Street
Boston, MA 02201

United States Naval Post Graduate School (1)
Dept. of Mechanical Engineering
Attn: Prof. Paul Pucci
Monterey, CA 93940

Defense Advanced Research Projects Agency (1)
Director of Tactical Technology
Attn: Dr. Robert Moore
1400 Wilson Blvd.
Arlington, VA 22209

Defense Advanced Research Projects Agency (1)
Attn: CAPT Cox
1400 Wilson Blvd.
Arlington, VA 22209

United States Coast Guard Research & Technology (1)
Attn: CAPT D. B. Flanagan
400 7th Street SW
Washington, DC 20590

DISTRIBUTION LIST

Dr. Larry W. Noggle (1)
ASD/XRD
Wright Patterson AFB
Dayton, OH 45402

Mr. James Remson (1)
Headquarters, Naval Material Command
(MAT) 033
Washington, DC 20360

Mr. Zel Levine, Director (1)
Office of Advanced Ship Development
Department of Commerce
Maritime Administration
Room 4610, Code 920
14th & E Streets, NW
Washington, DC 20230

Mr. Frank Welling (1)
Naval Sea Systems Command
Code 521, National Center No. 4
Washington, DC 20360

Mr. H. D. Marron (1)
Naval Sea Systems Command
Code 5231, National Center No. 4
Washington, DC 20360

Dr. Robert Allen (1)
David W. Taylor
Naval Ship Research & Development Center
Code 012
Bethesda, MD 20084

Dr. Earl Quandt (1)
David W. Taylor
Naval Ship Research & Development Center
Code 272
Annapolis, MD 21402

David W. Taylor (1)
Naval Ship Research & Development Center
Code 15 (2)
Bethesda, MD 20084

David W. Taylor (1)
Naval Ship Research & Development Center
Code 16 (2)
Bethesda, MD 20084

DISTRIBUTION LIST

Dr. F. R. Riddell (1)
Institute for Defense Analyses
Room 9A11
400 Army & Navy Drive
Arlington, VA 22202

Mr. Charles Miller (1)
Naval Sea Systems Command 03
Crystal City
National Center No. 3
Washington, DC 20360

United Technologies Research Center (1)
Attn: Dr. Simion C. Kuo
East Hartford, CT 06108

Mechanical Technology Incorporated (1)
Attn: Mr. Tom Ivsan
968 Albany-Shaker Road
Latham, NY 12110

General Atomic Company (1)
Attn: Dr. Leon Green
Suite 709
2021 K Street, NW
Washington, DC 20002

Colin F. McDonald (1)
General Atomic Company
P. O. Box 81608
San Diego, CA 92138

E. F. Brady (1)
Ingalls Shipbuilding
P. O. Box 149
Pascagoula, MS 39567

Thomas E. Duffy (1)
Solar Division of International Harvester
2200 Pacific Highway
P. O. Box 80966
San Diego, CA 92138

DISTRIBUTION LIST

C. J. Mole (1)
Westinghouse Electric Corporation
Research & Development Center
1310 Beulah Road
Pittsburgh, PA 15235

Defense Documentation Center (12)
Bldg. No. 5, Cameron Station
Alexandria, VA 22314